Industrial Instrumentation

Springer-Verlag London Ltd.

Tattamangalam R. Padmanabhan

Industrial Instrumentation

Principles and Design

With 429 Figures



Springer

Tattamangalam R. Padmanabhan, PhD
Amrita Institute of Technology and Science, Ettimadai, Coimbatore 641 105, India

ISBN 978-1-4471-1145-0

British Library Cataloguing in Publication Data
Padmanabhan, Tattamangalam R.
Industrial instrumentation : principles and design
1. Electronic instruments 2. Industrial electronics
I. Title
670.4'27
ISBN 978-1-4471-1145-0

Library of Congress Cataloging-in-Publication Data
Padmanabhan, Tattamangalam R., 1941-
Industrial instrumentation : principles and design / Tattamangalam R. Padmanabhan.
p. cm.
ISBN 978-1-4471-1145-0 ISBN 978-1-4471-0451-3 (eBook)
DOI 10.1007/978-1-4471-0451-3
1. Process control - Instruments. 2. Electronic instruments.
3. Measuring instruments. I. Title.
TS156.8.P18 1999 99-41995
629.8—dc21 CIP

Apart from any fair dealing for the purposes of research or private study, or criticism or review, as permitted under the Copyright, Designs and Patents Act 1988, this publication may only be reproduced, stored or transmitted, in any form or by any means, with the prior permission in writing of the publishers, or in the case of reprographic reproduction in accordance with the terms of licences issued by the Copyright Licensing Agency. Enquiries concerning reproduction outside those terms should be sent to the publishers.

© Springer-Verlag London 2000
Originally published by Springer-Verlag London Berlin Heidelberg in 2000
Softcover reprint of the hardcover 1st edition 2000

The use of registered names, trademarks, etc. in this publication does not imply, even in the absence of a specific statement, that such names are exempt from the relevant laws and regulations and therefore free for general use.

The publisher makes no representation, express or implied, with regard to the accuracy of the information contained in this book and cannot accept any legal responsibility or liability for any errors or omissions that may be made.

Typesetting: camera ready by author

69/3830-543210 Printed on acid-free paper SPIN 10736297

To

My Uma
My Prop

Preface

Barely 10 years back, Instrumentation was considered a queer mix of technology and practical skills. There were pneumatic schemes, hydraulic schemes, electro-pneumatic schemes, electro-hydraulic schemes and magnetic amplifier based schemes; electronic schemes were essentially apologies. A lot of skill and technical input went into the strip-chart recorder, the flapper-nozzle scheme and so on. The copper tube lines that carried the pneumatic supply and signals were as common in the industry as the electric power supply conduits. With the advent of electronic schemes, all these have become things of the past. Microprocessors have a knack of thrusting themselves everywhere – especially in instrumentation schemes. Quantities, which were, ignored (gas concentration) and those perceived as 'not measurable' (high temperature) have catapulted and fallen preys to sensors. On-line correction and compensation have become common with electronic schemes. Intensive calculations using sensor outputs – often on-line – have become the order of the day. Though the principles remain the same, the trend for on-line correction, compensation and information extraction is likely to continue unabated.

There is a clear-cut need for a book on industrial instrumentation, the stress being on electronics based state-of-the-art schemes. This need is addressed to by this book. In part I of the book the scope of an instrumentation scheme has been brought out through specific examples and 'what one looks for in an instrumentation scheme' identified. The functional modules that make up the scheme are identified. The role of each such module is dealt with in succeeding chapters. Despite the variety in the schemes and applications, there are certain common threads running through many of the schemes. These lead to the 'Generic Instrumentation schemes' which provide the basic framework for most of the instrumentation schemes. The structure and scope of such generic schemes built with the basic functional modules, are also discussed. Part II is devoted to schemes and applications. Instrumentation of the most common industrial physical variables is discussed in detail. Displacement, force and related quantities, temperature, pressure and flow are the major ones here. Wherever possible attempts have been made to identify the threshold level for sensing, full-scale accuracy and the like, and quantify them.

In the last chapter, an attempt has been made to identify an order and gradation in the complexity levels of instrumentation schemes. Subsequently, typical practical schemes of the more complex type are discussed.

Throughout, the stress has been on industrial instrumentation *per se*. As such analysis instrumentation, biomedical instrumentation and laboratory instruments – each a specialized area in its own right – have not been dealt with. To retain focus, Displays, which has become a vast area of its own, has been left out consciously. I

hope the book will be of use to the professionals in instrumentation as well as the academic community.

T. R. Padmanabhan, Ph.D.
Amrita Institute of Technology and Science
Ettimadai
Coimbatore
October 1999

Acknowledgements

I have honed my skills through the discussions with my erstwhile teachers and colleagues at the Electrical Engineering Department, Indian Institute of Technology Kharagpur, India. My associates in the industry over the last two decades at the Tata Iron & Steel Co. Ltd., Jamshedpur, Crompton Greaves Ltd., Mumbai and Premier Polytronics Ltd., Coimbatore, too have been helpful in many ways in this venture. I owe a lot to all of them. Ms Radhamani Pillai, Professor at Amrita Institute of Technology Coimbatore, has gone through the manuscript with diligence and has been instrumental for many changes to improve the clarity of expression, continuity and style. I thank her for her involvement. I am obliged to my friend Mr K N Easwaran who stooped to conquer 'Word' and mastered it for my sake; his eagle's eyes missed hardly any mistake in the edited text. Mr Oliver Jackson of Springer Verlag has been informal, prompt and helpful in many ways during this venture; I thank him for his involvement. I thank my family – my wife Uma, kids Ravi and Chandra and my late mother – who have put up with my apparent prolonged isolation on account of this effort.

Contents

Part I Principles and Components

1 Instrumentation Schemes Structure and Specifications 3
1.1 Introduction 3
1.2 Shop-Floor Compressor 3
1.3 Plastic Extrusion 3
1.4 Reaction Vessel 7
1.5 Characteristics of an Instrumentation Scheme 9
1.5.1 Accuracy 9
1.5.2 Precision 11
1.5.3 Errors and Correction 12
1.5.4 Sensitivity 13
1.5.5 Hysteresis 14
1.5.6 Resolution 15
1.5.7 Threshold and Dead Zone 15
1.5.8 Drift 15
1.5.9 Repeatability and Zero Stability 17
1.5.10 Range 17
1.5.11 Linearity 18
1.5.12 Input and Output Impedances 19
1.6 Instrumentation Scheme - Block Diagram 21
1.6.1 Primary Sensor 22
1.6.2 Secondary Sensor 23
1.6.3 Stages of Analog Signal Processing 23
1.6.4 Output 24
1.6.4.1 Display 24
1.6.4.2 Transmitter 24
1.7 Digital System 25
2 Secondary Transducers 29
2.1 Introduction 29
2.2 Unbalanced Wheatstone Bridge 30
2.2.1 Assumptions 30
2.2.2 Bridge Near Balance 30
2.2.3 Transducer Bridge Behaviour for Large ε Values 33
2.2.4 Transducer Bridge with Multiple Sensing Elements 36
2.2.4.1 Transducer Bridge with Diagonally Opposite Sensing Arms 36
2.2.4.2 Transducer Bridge with Adjacent Sensing Arms 37
2.2.4.3 Transducer Bridges with Four Sensing Arms 39
2.2.5 Unbalanced Bridges 39
2.3 AC Bridges 40
2.3.1 Possible Configurations 40
2.3.2 Sensitivity of Unbalanced AC bridges 43

2.3.3 Transducer with Off-Balance AC Bridge 46
2.3.4 Wein Bridge 47
2.3.5 Mutual Inductance Bridges 49
2.4 Oscillator Type of Transducers 51
2.4.1 Sensitivity of Oscillator Type Transducers 54
2.5 Feedback Type Transducers 54
3 Operational Amplifiers 56
3.1 Introduction 56
3.2 Ideal Opamp 56
3.3 Specifications of Opamps 57
3.3.1 Open Loop Gain 57
3.3.2 Gain Bandwidth Product 58
3.3.3 Phase Lag 58
3.3.4 Range of Output Voltage 59
3.3.5 Linearity 59
3.3.6 Input Currents 60
3.3.7 Offset Voltage (V_{os}) 61
3.3.8 Input Offset Voltage Drift 61
3.3.9 Input Offset Current and its Drift 62
3.3.10 Common Mode Rejection 62
3.3.11 Output Impedance 62
3.3.12 Slew Rate 63
3.3.13 Noise in Opamps 63
3.3.13.1 Schottky Noise (Shot Noise) 64
3.3.13.2 Flicker Noise (1/f Noise) 64
3.3.13.3 Popcorn Noise 65
3.3.13.4 Total Opamp Noise 65
3.4 Opamp Characteristics – Trade-offs 66
3.5 Characteristics of Typical Commercial Opamps 66
3.6 Opamp Selection 68
4 Linear Signal Processing 74
4.1 Introduction 74
4.2 General Considerations 74
4.3 Inverting Amplifiers 76
4.3.1 Analysis of the Non-ideal Amplifier 78
4.3.2 Noise in the Amplifier 82
4.3.3 Minimisation of Leakage Errors 85
4.4 Summing Amplifier 86
4.5 Current to Voltage Convertor 87
4.6 Integrator 87
4.7 Non-Inverting Amplifier 89
4.8 Buffers 90
4.9 Differentiator 91
4.10 Difference Amplifier 92
4.11 Adaptations of the Difference Amplifier 94
4.12 Instrumentation Amplifier 96
4.13 Isolation Amplifier 102
4.13.1 Schematic Arrangement 102
4.13.2 Transformer Type 103
4.13.3 Capacitance Coupled Type 104
4.13.4 Opto-coupled Type 105
4.13.5 Comparison 106

5 Active Filters.....107
5.1 Introduction.....107
5.2 Classification of Ideal Characteristics.....107
5.2.1 Low Pass Filter (LPF).....107
5.2.2 High Pass Filter (HPF).....108
5.2.3 Band Pass Filter (BPF).....109
5.2.4 Band Rejection Filter (BRF).....110
5.2.5 All Pass Filters.....110
5.3 Filter Requirements in Instrumentation Schemes.....111
5.4 Specifications of Practical Filters.....111
5.4.1 Low Pass Filter.....111
5.4.2 High Pass Filter.....114
5.4.3 Band Pass Filter.....114
5.4.4 Band Rejection Filters.....115
5.4.5 Narrow Band and Notch Filters.....116
5.5 Normalized LPF.....117
5.5.1 Butterworth Filter.....118
5.5.2 Chebyshev Filter.....119
5.5.3 Bessel / Thomson Filter.....121
5.5.4 Elliptic Filter.....122
5.5.5 Comparison.....123
5.6 Low Pass Filter Configurations.....125
5.6.1 Sallen and Key (S-K) LPF.....126
5.6.2 First Order Term.....128
5.6.3 Multiple Feedback Filter.....129
5.6.4 State Variable (S-V) Filter.....131
5.7 LPF Circuit Realizations.....135
5.8 High Pass Filters.....135
5.8.1 Filter Circuit Configurations.....136
5.8.1.1 Sallen and Key filter.....136
5.8.1.2 Multiple Feedback Filters.....139
5.8.1.3 State Variable Filter.....140
5.8.2 High Pass Filter Circuit Configurations.....141
5.9 Band Pass Filter.....141
5.9.1 Narrow Band Filter.....142
5.9.2 Narrow Band Filter Configurations and Realizations.....143
5.9.2.1 Sallen-Key Realization.....144
5.9.2.2 Multiple Feedback Realization.....146
5.9.2.3 State Variable Filter Realization.....148
5.9.2.4 Narrow Band Filter Circuit Realizations.....149
5.10 Band Rejection Filters.....149
5.10.1 Notch Filter.....150
5.10.2 Notch Filter Configurations and Realizations.....150
5.10.2.1 Notch Filters with Twin -T Networks.....150
5.10.2.2 Notch Filter with State Variable Scheme.....153
5.10.2.3 Notch Filter Circuit Realizations.....154
5.11 Switched Capacitor Filters.....154
6 Non-linear Signal Processing.....157
6.1 Introduction.....157
6.2 Modulation and Demodulation.....157
6.2.1 Amplitude Modulation and Demodulation.....158
6.2.1.1 Principles of Amplitude Modulation.....158

6.2.1.2 Practical Aspects of Amplitude Modulation 163
6.2.1.3 AM Demodulation 165
6.2.1.4 Effects of Harmonics in the Carrier 166
6.2.1.5 Circuit Schemes for AM Modulation and Demodulation 167
6.2.1.6 Multiplier Based AM Modulator 167
6.2.1.7 Simple Modulator with Analog Switch 169
6.2.1.8 Chopper Amplifier 169
6.2.1.9 Chopper Pair Using Analog Switch 172
6.2.1.10 Balanced Modulator 172
6.2.1.11 Balanced Modulator And Demodulator Using Analog Switch 174
6.2.1.12 Envelope Detector 174
6.2.2 Frequency Modulation 175
6.2.2.1 Principles of Frequency Modulation 175
6.2.2.2 Significant Bandwidth of the FM Wave 178
6.2.2.3 Practical Aspects of Frequency Modulation 179
6.2.2.4 Circuits for FM Modulation 181
6.2.2.5 Circuits for FM Demodulation 182
6.2.2.6 Phase Locked Loops 184
6.3 Non-linear Amplifiers 189
6.3.1 Piece-wise Linear Amplifier 189
6.3.2 Precision Rectifier 191
6.3.3 Logarithmic Amplifier 193
7 Noise and System Performance 196
7.1 Introduction 196
7.2 External Noise 196
7.2.1 Elimination / Minimization of Conducted Noise 197
7.2.2 Elimination / Minimization of Capacitively Coupled Noise 199
7.2.3 Elimination / Minimization of Inductively Coupled Noise 202
7.2.4 Comparison of Electrically and Magnetically Coupled Noise 205
7.3 Characterization of Random Signals 206
7.3.1 Amplitude Characteristics 207
7.3.2 Frequency Characteristics 208
7.3.3 Signals from Physical Systems 210
7.3.4 Equivalent Noise Bandwidth 213
7.3.5 Narrow Band Random Process 214
7.4 Internal Noise 215
7.4.1 Shot Noise 215
7.4.2 Thermal Noise 217
7.4.3 Flicker Noise 218
7.4.4 Contact Noise 219
7.4.5 Popcorn Noise 220
7.4.6 Total Noise 220
7.4.7 Minimization of Effects of Internal Noise 220
7.4.7.1 Effect of Noise Inside Feedback Loops 221
7.4.7.2 Amplifier Selection Depending on Signal Source 221
7.5 Performance of Modulation Systems in the Presence of Noise 227
7.5.1 Noise Performance of AM Systems 228
7.5.1.1 DSB-SC: 228
7.5.1.2 Envelope Detection 229
7.5.2 Noise Performance of FM Systems 231
8 Analog-Digital Interface 235
8.1 Introduction 235

8.2 Signal Conversion – Basics 236
8.2.1 Ideal Sampling 236
8.2.2 Practical Sampling 240
8.2.3 Quantization 241
8.2.4 Signal Reconstruction 243
8.3 Sampling Hardware 246
8.3.1 Analog Switch 246
8.3.1.1 Specifications of Analog Switches 248
8.3.2 Sample and Hold Operation 249
8.3.2.1 Hold to Sample Transition Errors 250
8.3.2.2 Sample Errors 251
8.3.2.3 Sample to Hold Transition Errors 251
8.3.2.4 Hold Interval Errors 252
8.3.2.5 Feedthrough Error 253
8.3.2.6 Other Errors 254
8.3.3 Sample-Hold Topologies 255
8.3.4 Multiplexing 257
8.4 Voltage References 261
8.4.1 Zener Based Reference 262
8.4.2 Band Gap Based Reference 263
8.5 Specifications of ADCs and DACs 263
8.5.1 Quantization Error 264
8.5.2 Conversion Rate 264
8.5.3 Accuracy 264
8.5.4 Offset Error 264
8.5.5 Gain Error 265
8.5.6 Linearity Error 266
8.5.6.1 Integral Non-linearity 266
8.5.6.2 Differential Non-linearity 267
8.5.7 Monotonicity 267
8.5.8 Dynamic Range 267
8.5.9 Sensitivity to Power Supply Variations 268
8.5.10 Temperature Coefficient 268
8.6 Digital to Analog Converters (DAC) 269
8.6.1 Current Based Conversion 269
8.6.2 Voltage Based Conversion 270
8.6.3 Microcomputer Interface 273
8.7 Analog to Digital Convertors 274
8.7.1 Dual Slope ADC 274
8.7.2 Successive Approximation Type of ADCs 277
8.7.3 Flash ADCs 278
8.7.4 Sub-Ranging ADC 279
8.7.5 Serial or Ripple ADC 281
8.7.6 Sigma Delta Converter 284
8.7.7 Microcomputer Interface 289
9 Digital Signal Processing for Instrumentation 291
9.1 Introduction 291
9.2 Handling LUTs 291
9.2.1 Direct Reading 292
9.2.2 Indirect Reading 294
9.2.3 Corrections for Parametric Changes 296
9.3 Digital Filters 296

9.3.1 Finite Impulse Response Filter 297
9.3.1.1 Linear Phase Filters 298
9.3.2 FIR Filter Design 299
9.3.2.1 Approach 1 299
9.3.2.2 Approach 2 302
9.3.3 Other Applications 303
9.3.3.1 Determination of Centroid 304
9.3.3.2 Edge Detection 304
9.3.3.3 Profile Detection 305
9.4 IIR filters 306
9.4.1 Design of IIR Filters 307
9.4.1.1 Approximation of Derivatives 307
9.4.1.2 Impulse Invariance 308
9.4.1.3 Other Methods 309
9.4.2 IIR Filter Realizations 319
9.5 Other Linear Operations 312
9.5.1 Derivatives and Integrals 313
9.5.2 Interpolation and Extrapolation 313
9.6 DFT and FFT 316
10 Generic Structures of Instrumentation Schemes 318
10.1 Introduction 318
10.2 Instrumentation Schemes Based on Resistance Sensors 318
10.2.1 Resistance as a Circuit Element 319
10.2.2 Circuit Configurations for Resistance Sensors 320
10.2.2.1 Wheatstone Bridge Type Sensor 320
10.2.2.2 Modifications of the Wheatstone Bridge 322
10.2.2.3 Self-Calibrating Schemes 327
10.3 Capacitance Transducers 328
10.3.1 Capacitance as a Circuit Element 328
10.3.2 Electrode Geometries and Capacitances. 330
10.3.2.1 Parallel Plate Capacitance 330
10.3.2.2 Concentric Cylinders 332
10.3.2.3 Parallel cylinders 332
10.3.2.4 Cylinder and Plane 333
10.3.3 Circuit Configurations 334
10.3.3.1 DC Circuits 334
10.3.3.2 Oscillators 335
10.3.3.3 Amplitude Modulated Schemes 336
10.3.3.4 Signal Threshold with Capacitance Sensors 337
10.3.4 Guard Ring and Shielding 338
10.4 Inductance Transducers 342
10.4.1 Inductance as a Circuit Element 342
10.4.2 Sensor Geometries and Inductances 346
10.4.3 Circuit Configurations 347
10.4.3.1 Oscillator Scheme 347
10.4.3.2 Bridge Schemes 347
10.4.3.3 Differential Transformer Scheme 349
10.5 Feedback Transducers 350

Part II Schemes

11 Displacement Instrumentation 355

11.1 Introduction 355
11.2 Potentiometers 355
11.2.1 Wire Wound Potentiometers 356
11.2.2 Conductive Plastic Potentiometer 357
11.2.3 Magneto-resistance Potentiometers 357
11.2.4 Comparison 358
11.2.5 Signal Processing with Pot Based Position Sensors 358
11.3 Differential Transformers 359
11.3.1 Signal Processing with Differential Transformers 362
11.3.2 Variants of the Differential Transformer 364
11.3.2.1 Resolvers 364
11.3.2.2 Microsyn 366
11.3.2.3 Variable Reluctance Transformer 367
11.3.3 Differential Inductance Transducers 369
11.4 Capacitance Transducers 370
11.4.1 Comparison of Inductance and Capacitance Type Sensors 371
11.5 Encoders 372
11.5.1 Principle of Electro-optic Encoder 373
11.5.2 Incremental Encoders 374
11.5.3 Design of Incremental Encoders 374
11.5.3.1 Approach 1 375
11.5.3.2 Approach 2 377
11.5.4 Encoder Disc / Strip 378
11.5.5 Absolute Encoders 379
11.5.6 Information from Encoder Output 380
11.5.6.1 Velocity 380
11.5.6.2 Surface Roughness 381
11.5.6.3 The Bearing Ratio Curve 381
11.6 Rotational Speed Transducers 382
11.6.1 Homopolar Generator 382
11.6.2 DC Tachogenerator 383
11.6.3 AC Tachogenerator 387
12 Force and Allied Instrumentation 388
12.1 Introduction 388
12.2 Principle of the Resistance Strain Gauge 388
12.3 Practical Considerations 389
12.3.1 Unbonded Metal Wire Gauge 389
12.3.2 Bonded Foil Gauge 390
12.3.3 Vacuum Deposited Foil Gauge 390
12.3.4 Sputter-Deposited Foil Gauge 390
12.3.5 Semiconductor SGs 390
12.3.6 Backing Material 391
12.3.7 Adhesive 391
12.3.8 Quantitative details 391
12.4 SG Patterns 392
12.5 Error Compensation with SG Bridges 396
12.6 Strain Gauge Signal Processing 399
12.7 Direct Measurement of Strain 400
12.8 Load Cells 403
12.8.1 Column Type Load Cells 403
12.8.2 Cantilever Type Load Cells 404
12.8.3 S Beam Type Load Cell 405

12.8.4 Thin Beam Load Cell 405
12.9 Piezo-Electric Sensors 407
12.10 Force Transducers 409
12.10.1 SG Based Force Sensors 409
12.10.2 LVDT Based Force Sensing 409
12.10.3 Force Balance System 410
12.11 Tension Sensing 411
12.12 Acceleration Transducers 412
12.12.1 Piezo-Electric Accelerometers and Vibration Sensing 414
12.13 Torque Transducers 416
12.13.1 Reaction Force Sensing 417
12.13.2 Direct Torque Sensing 418
13 Process Instrumentation I 420
13.1 Introduction 420
13.2 Temperature Scale 420
13.3 Conventional Methods of Temperature Sensing 421
13.4 Resistance Thermometer Detectors (RTD) 422
13.4.1 Unbalanced Wheatstone Bridge 422
13.4.2 Direct Conversion 423
13.4.3 Platinum 424
13.4.4 Copper 424
13.4.5 Nickel 425
13.4.6 Other RTDs 425
13.5 Thermistors 425
13.5.1 Temperature Sensing Using Thermistors 426
13.6 Semiconductor Temperature Sensors 427
13.7 Thermocouple Based Temperature Sensing 429
13.7.1 Basics of Thermocouples 429
13.7.2 Thermocouple Types 431
13.7.3 Junction 432
13.7.4 Thermocouple Outfit 432
13.7.5 Cold Junction Compensation 433
13.7.5.1 Approach 1 433
13.7.5.2 Approach 2 435
13.7.5.3 Approach 3 435
13.7.6 Extension Wires 436
13.7.7 Processing of Thermocouple Signals 436
13.8 Infra-Red Thermometry 441
13.8.1 Basics of Radiation 441
13.8.2 Emissivity 444
13.8.3 Methods of Sensing 445
13.8.3.1 Indirect Detection 445
13.8.3.2 Direct Detection 445
13.8.4 Optics 446
13.8.5 Indirect Methods - Thermal Detection 446
13.8.6 Direct Methods - Radiation Detection 449
13.8.6.1 Photoconductors 450
13.8.6.2 Photo-voltaic Sensor 451
13.8.6.3 Photo-emissive Sensors 454
13.8.7 Direct Method-Execution 454
13.8.7.1 Two-colour Method 454
13.8.7.2 Single Colour Pyrometer 457

13.8.8 Temperatures of Inaccessible Locations 457
14 Process Instrumentation II 460
14.1 Introduction 460
14.2 Pressure Instrumentation 460
14.2.1 Types of Pressure Measurement 460
14.2.2 Units of Pressure 461
14.2.3 Bourdon Tube and Bellows 461
14.2.4 SG Based Pressure Sensors 463
14.2.4.1 Diaphragm with Bonded SG 464
14.2.4.2 Diaphragm with Semiconductor SG 465
14.2.4.3 Application Considerations 466
14.2.5 Capacitance Type Pressure Transducers 466
14.2.6 Low Pressure Instrumentation 467
14.2.6.1 Pirani Gauge 467
14.2.6.2 Thermocouple Gauge 468
14.2.6.3 Ionization Gauges 468
14.3 Basics of Fluid Flow 470
14.3.1 Flow of Fluids 470
14.3.1.1 Flow of Gases 472
14.3.1.2 Viscosity of Gases 472
14.3.2 Density of Gases 473
14.3.3 Standard Conditions 475
14.3.4 Compensation 476
14.4 Flowmeters 477
14.4.1 Quantum Flow Measurement 478
14.4.2 Differential Pressure Measurement 478
14.4.2.1 Principle of the Differential Pressure Flowmeter 478
14.4.2.2 Orifice Plate 481
14.4.2.3 Other Differential Pressure Schemes 485
14.4.2.4 Venturi Meter 485
14.4.2.5 Flow Nozzle 486
14.4.2.6 Comparison 486
14.4.2.7 Elbowmeter 488
14.4.3 Magnetic Flowmeters 488
14.4.3.1 DC Magnetic Flowmeter 490
14.4.3.2 Pulsed Magnetic Flowmeter 490
14.4.3.3 Permanent Magnet Type Magnet Flowmeter 490
14.4.3.4 AC Magnetic Flowmeter 490
14.4.4 Vortex Flowmeter 492
14.4.5 Turbine Flowmeter 495
14.4.5.1 Vertical Impeller Type 495
14.4.5.2 Helical Impeller Type 495
14.4.6 Target Flowmeter 497
14.4.7 Coriolis Flowmeter 498
14.4.8 Ultrasonic Flowmeter 500
14.4.8.1 Transit Time Based Flowmeter 501
14.4.8.2 Doppler-Effect Based Flowmeter 503
14.4.9 Other Flowmeters 506
14.4.9.1 Variable Area Flowmeters 507
14.4.9.2 Capillary Type Flowmeters 507
14.4.9.3 Pitot Tube 507
14.4.9.4 Positive Displacement Flowmeters 507

14.4.9.5 Thermal Flowmeters 508
14.4.9.6 Bypass Flowmeters 508
14.5 Level Instrumentation 509
14.5.1 Level Transducer with Differential Pressure Sensing 509
14.5.2 Capacitance Based Level Sensors 509
14.5.2.1 Capacitance Sensors for Conducting Liquids 510
14.5.2.2 Capacitance Sensor for Non-conducting Liquids 510
14.5.3 Other Types of Level Gauges 512
14.5.3.1 Displacement Type Level Sensor 513
14.5.3.2 Ultrasonic Level Sensor 513
14.5.3.3 Gamma Ray Level Sensor 514
15 Process Instrumentation III 516
15.1 Introduction 516
15.2 pH Instrumentation 516
15.2.1 Basic Ideas of pH Value 516
15.2.2 Measurement of Electrode Potentials 518
15.2.3 Glass Electrode 519
15.2.4 Reference Electrode 519
15.2.4.1 Calomel Electrode 520
15.2.4.2 Silver- Silver Chloride Electrode 520
15.2.5 Buffers 520
15.2.6 Signal Processing 521
15.3 Humidity Sensing 521
15.3.1 Basic Ideas of Humidity 521
15.3.2 Humidity Measurement by Dew Point Sensing 522
15.3.3 Humidity Measurement Using Lithium Chloride 523
15.3.4 Other Methods 523
15.3.4.1 Pope Cell 524
15.3.4.2 Electrolytic Sensor 524
15.4 Gas Sensors 524
15.4.1 Ceramic Sensors 525
15.4.1.1 Circuit Scheme 525
15.4.2 IR Sensors 526
15.5 Gas Analysis 526
15.5.1 Thermal Conductivity Measurement 527
15.5.2 Interferometer 529
15.6 Radiation Based Instrumentation 530
15.6.1 Photo-Detectors – Principles 530
15.6.1.1 Equivalent Circuit 533
15.6.1.2 V – I characteristics 534
15.6.1.3 Constructional Variants 536
15.6.1.4 Spectral Response 537
15.6.1.5 Noise Characteristics 538
15.6.1.6 Response Time 539
15.6.1.7 Effect of Temperature Changes 540
15.6.2 Circuits with Photo-diodes 540
15.6.3 Radiation Sensor Arrays with CCDs 542
15.6.3.1 CCD Array 543
15.6.3.2 Sensing Array 545
15.6.3.3 Pixel Sensitivity 546
15.6.3.4 Interface with CCD 547
15.6.3.5 Anti-Blooming and Exposure Control 549

15.6.3.6 Types of Detector Arrays 549
15.6.3.7 Application Example 552
15.6.3.8 CCD Signal Processing 554
15.7 Instrumentation Based on Magnetics 556
15.8 Flux Gate Magnetometer 556
15.8.1 High Current Measurement 558
15.8.2 Current Sensing Using Hall Effect Device 560
16 Typical Instrumentation Schemes 564
16.1 Introduction 564
16.2 Categorization of Instrumentation Schemes 564
16.2.1 Level 0 564
16.2.2 Level 1 565
16.2.3 Level 2 565
16.2.4 Level 3 566
16.2.5 Level 4 566
16.2.6 Level 5 567
16.2.7 Level 6 567
16.2.8 Level 7: Schemes with Information Extraction 567
16.2.9 Level 8: Specialized Schemes 567
16.2.10 Level 9: Composite Instrumentation Systems 568
16.3 Typical instrumentation Schemes 568
16.3.1 Optically Powered Remote Instrumentation Scheme 568
16.3.2 Fibre Length Distribution 570
16.3.2.1 Fibre Length Distribution and Related Indices 571
16.3.2.2 Fibrogram 574
16.3.2.3 Principle of Measurement 576
16.3.2.4 Circuit Scheme 577
16.3.2.5 Parameters and Ranges 577
16.3.2.6 Optical Source and Detection 578
16.3.2.7 Sequence of Operations 580
16.3.3 Power Analyzers 581
16.3.3.1 Schematic Arrangement 582
16.3.3.2 Electrical Quantities of Interest 582
16.3.3.3 Sensors 583
16.3.3.4 Operational Details 583
16.3.4 Instrumentation for a Blast Furnace 588
16.3.4.1 Blast Furnace 589
16.3.4.2 Blast Furnace Chemistry 590
16.3.4.3 Flow of Materials 593
16.3.4.4 Blast Furnace and Accessories 594
16.3.4.5 Blast Furnace Process Description 599
16.3.4.6 Functions of the Instrumentation Scheme 600
16.3.4.7 Investigative Studies 601
16.3.4.8 Quantities for Instrumentation 602
16.3.4.9 Computations 603
16.4 User Configurable Instrumentation Scheme 605
16.4.1 Signal Conditioning Unit 605
16.4.2 Data Acquisition Card 606
16.4.3 Software 606
16.4.4 Drivers 606
16.4.5 Utilities 607
16.4.5.1 Data Analysis 607

16.4.5.2 System Analysis.....607
Appendix A 611
Appendix B 614
Appendix C 618
Appendix D 619
Appendix E 627
Appendix F 628
References 631
Index 637

Part I

Principles and Components

1 Instrumentation Schemes Structure and Specifications

1.1 Introduction

An instrumentation scheme senses a well identified physical variable, quantifies it uniquely and converts it into a suitable form – mostly an electrical form. At this stage, it may be used for display for further processing or for guiding a closely related activity in a related process. This broadly – though loosely – forms the scope of an instrumentation scheme. We will examine a few typical but practical schemes to bring out the role of different modules that make up an instrumentation scheme. To a certain extent, this helps us appreciate the need for an in-depth study and understanding of the different modules and their characteristics. The discussion is limited to such details as help our task on hand.

1.2 Shop-Floor Compressor

Most machine shops which do fabrication or machining and allied activities, use compressed air. It serves a variety of purposes ranging from that of an energy source to a cleaning agent. Normal compressors and compressed air supply lines operate within a limited pressure range. Safety considerations limit the upper value while the need for satisfactory working of various implements/tools using the pressure line as an energy source, require the pressure to be above a certain set value. Apart from restricting the pressure within these two limits, rarely does the need arise to measure or to regulate it precisely. The compressor is normally fitted with an air pressure indicator; it displays the air pressure. A few dominant widely spaced marks and a red mark to indicate the upper safe limit for pressure, characterise the display, or the pressure indicator. The accuracy of measurement and display together may not be better than 10%! If the compressed air supply line is too long, additional pressure indicators may be fitted along the pressure line at selected points. The basic function of the indicator is to display the magnitude of pressure – often a rough estimate suffices. However, it is necessary that the indicator is robust and functions reliably.

1.3 Plastic Extrusion

Consider a more involved application – that of the plastic extrusion process with multiple measurements. Figure 1.1 shows one typical scheme for extrusion of PVC films [Woebcken]. Raw material is available in the form of pellets, in a bin of the extruder. The pellets are heated, melted and extruded in the form of a fine film. The

T. R. Padmanabhan, *Industrial Instrumentation*
© Springer-Verlag London Limited 2000

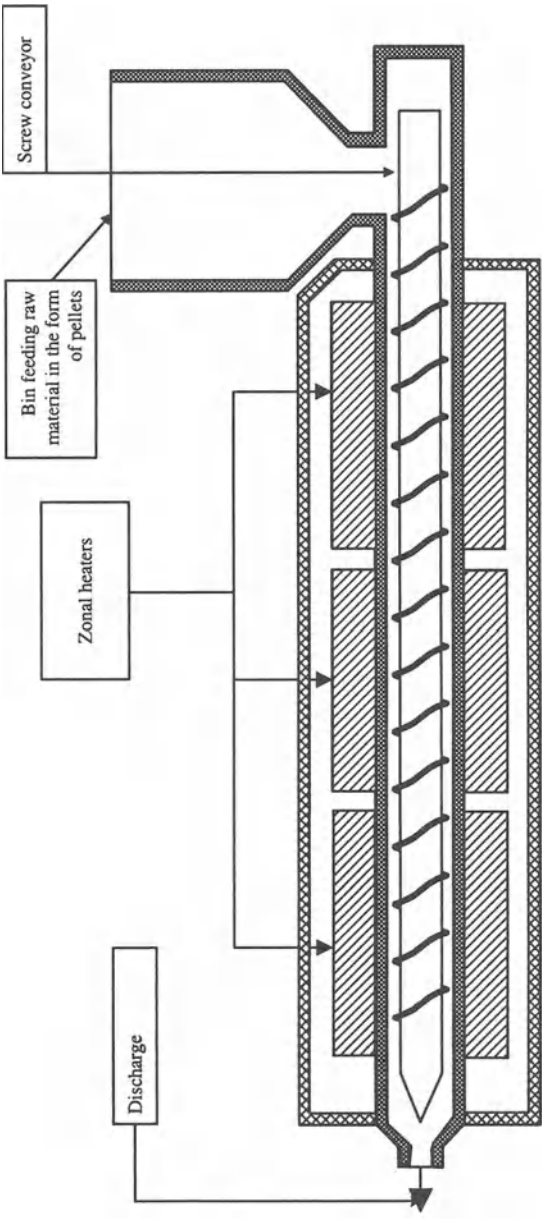


Figure 1. 1 Simplified schematic arrangement of a single screw plastic extruder.

pellets are fed into the bin as and when the material level in the bin goes below a minimum desired mark. Such feeding, being infrequent is done manually. The bin opens into a screw conveyor. The opening of the bin is adjusted to suit the desired production rate. The screw conveyor has heaters distributed along its length. Due to external heating, the pellets fed at one end melt. The melt is pushed forward by the screw conveyor. The opening of the bin is adjusted to suit the desired production rate. The length of the barrel and heating profile together ensure that the melt is homogeneous and of the right constituency. The barrel may have vents to allow trapped air, volatile matter in the melt and any water vapour present, to escape. In some cases due to the excessive friction at the screw conveyor, and the viscous nature of the melt, there may be excess heating. To counter its effects, The screw and barrel may be cooled by external cooling water. This may be necessary at the delivery end of the screw. Finally, the material is delivered at the outlet nozzle to the extruder. The production rate is decided by the speed of the screw and the opening level at the bin end of the screw. The system will have facility for the following measurements: -

⇒ Measurement of temperature at selected points along the barrel.
⇒ Measurement of inlet and outlet water temperatures (if water-cooling is provided).
⇒ Measurement of water flow rate if water-cooling is provided.
⇒ Measurement of speed of screw.
⇒ Measurement of heater current and screw-drive-motor current.

The simplest and economic conveyors may not have all the above facilities; but as the size of the scheme increases and quality requirements become stringent, these may get added. The system may have facilities to set different temperatures in different zones and to adjust the screw speed. As the plant becomes more sophisticated, such settings may be fed from a PC and updated at suitable intervals. The overall instrumentation and control scheme can be as shown in Figure 1.2.

The scheme has been made sufficiently sophisticated and elaborate. It can cater to the use of a variety of raw materials and ensure a high level of quality and consistency of quality. Measurement of temperature is central to the operation of the scheme. The desired temperature may range from 60°C to 300°C at different zones and at different times. The closer the temperatures are measured and regulated, the better the quality of the product; material wastage too will be reduced. Temperature measurement may be desired to an accuracy of 0.5% (1.5°C) of full scale. This may have to be done under all environmental conditions. Consider the use of (Iron-Constantine) thermocouples for the measurement of temperature. The main problems that may be encountered here are: -

⇒ low signal levels – in the mV range
⇒ need for cold junction compensation (to eliminate the errors due to environmental temperature changes)
⇒ need to protect the thermocouples from corrosion *etc.*,

The millivolt-level signal cannot be used directly. It has to be amplified early enough retaining the 'fidelity of the signal'. Amplifier noise, drift, pick-up in transmission *etc.*, are problems that need careful addressing during the design and commissioning stage. The signal has to be amplified through a difference amplifier, preferably an instrumentation amplifier. It has to be filtered to eliminate contamination by noise at undesirable frequencies. Such filtering has to be effective

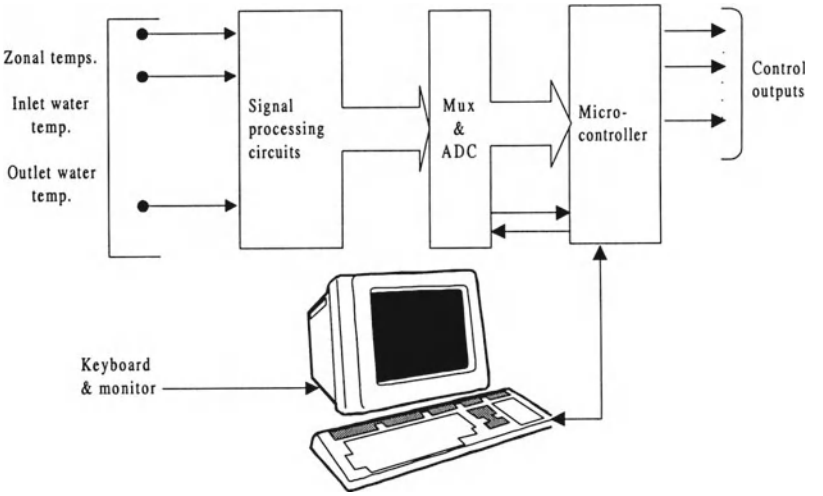


Figure 1.2 Instrumentation and control scheme for plastic extrusion process

against aliasing error at the ADC stage. The keyboard is rather primitive but well defined in its functions. Broadly, it serves two purposes: -

⇒ Commands to start the process, stop the process, change the set values *etc.*, can be given from the keyboard.

⇒ The process status can be called up from the keyboard and observed.

One can see that the keyboard has become an integral part of the system.

The display too has become much more sophisticated here compared to the previous case. One thing to be appreciated here is the possibility to display all parameters *etc.*, in the same format and structure, and on the same screen. This is said to add to the operator's comfort. The earlier alternative was to provide dedicated meters, instruments and other displays for each variable separately. As long as the number of quantities to be displayed remains small, these are manageable.

Now-a-days cold junction compensation is done through well-established techniques. Protection of the sensors and associated cabling from corrosion calls for a careful study of the environment and process, identifying possible sources of corrosion and contamination and using a suitable protection procedure. In an application of this type, careful selection and layout of the schemes, is only half the story. Effective control (especially temperature control) is essential for satisfactory working of the plant. Consider one challenging problem encountered here. The heaters are normally arranged in segments for effective temperature control. With this, a desired temperature profile along the screw can be effectively ensured. Further the response will be faster than with a single heater. An increase in the heater current in one segment, will directly increase the heat input to that segment and hence its temperature. It will also increase the temperatures of the two adjacent segments though only to a limited extent. Such increase takes place with associated time delays. An interference of this sort complicates the control problem. If the heat input to any segment is to be changed, its effect on adjacent segments must be judged beforehand and suitably accounted for. Similarly the effect of the adjacent zones on this, have to be made allowance for. Thus, no segment can be controlled

for its temperature separately. One has to have a thermal model of the system and any change in heat input *etc.*, has to be brought about only with the help of this model. The extent to which the model represents system dynamics and the effectiveness with which it is used, decides how closely the temperature profile (temporal as well as spatial) follows the desired one. Modelling and carrying out the temperature regulation with it calls for extensive on-line computing.

Provision of a computer for on-line computing along with the sensor outputs opens up other possibilities, which are of the 'value addition' type. One can do a regular energy balance. All process-related data and production information can be stored in structured formats. These can be used to provide trending, history *etc.* Such extracted information can be of use in taking financial decisions as well.

In contrast to the previous example, the present one opens up many new dimensions of instrumentation schemes. Accuracy in measurement, suitable signal processing, effective neutralisation of threshold and environmental effects, on-line computation are all aspects calling for attention. One can no longer take refuge in simplicity. As the sophistication called for increases, one can fruitfully exploit the same to generate more useful information from the system. This bootstrapping ('You-kick-me-up-and-I-kick-you-up') syndrome is typical of today's technical development scenario.

1.4 Reaction Vessel

Instrumentation for a reaction vessel is more complex and demanding than the previous one of extrusion. Basically, two or more constituents in the form of liquids are input to the vessel in measured quantities. A reaction takes place in the vessel under controlled conditions to produce the desired output. Figure 1.3 shows a typical reaction vessel. A and B are two inputs. Another input, designated as C, is given as a catalyst to facilitate or hasten the reaction. At the end of the reaction, the resulting quantities are drained off the outlet D. The process can take various forms depending upon the chemical reactions and parameters guiding them.

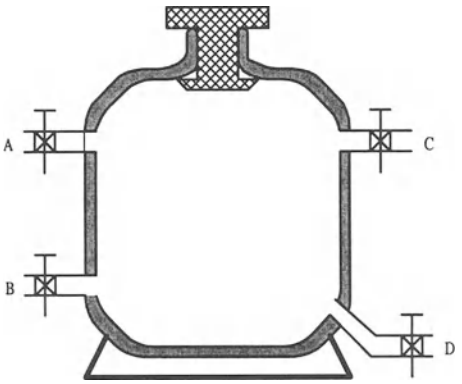


Figure 1.3 A reaction vessel

A typical sequence of the reaction process and allied activities can be on the following lines: -

⇒ Input measured quantities of the constituents A and B into the reaction vessel and close the respective inlet valves.

⇒ Heat or churn the vessel at a predetermined rate. Often heating is done by passing superheated steam through heater tubes set for the purpose. The heating may have to be done in a controlled manner so that the temperature follows a desired profile. Steam may have to be circulated through one or more pipes for this purpose.

⇒ In some cases, it may be necessary to churn the contents of the vessel to ensure efficient mixing or to provide centrifugal action for separation purposes. Such churning too may have to follow defined profiles. Speed control is provided for the concerned driving motor.

⇒ The catalyst has to be added as a measured quantity or at a measured rate.

⇒ The reaction has to be monitored clearly and closely. The temperature, pressure, pH value, colour, viscosity – all these are possible candidates for measurement. From a prior knowledge of these, the status of reaction is gauged. Note that this is an indirect estimation process.

⇒ Based on the observations above, the level of completion of the reaction is gauged. On possible completion of the reaction as decided using an index, the resulting constituents are drained off.

All the above steps – done in the desired sequence – constitute one 'batch' of the process. Incidentally, at this stage the catalyst too can be recovered. This may constitute another process, which is not discussed here. From the foregoing brief discussion, one can identify the variables to be measured: -

⇒ Temperature and flow-rate of individual input constituents

⇒ Temperature and flow-rate of the catalyst.

⇒ Weight of the reaction vessel before filling it and that at different stages of the batch process. This is to find the weights of the constituents filled, weights of the various constituents at the various stages *etc.*,

⇒ Temperature inside the reaction vessel possibly at a few selected locations.

⇒ Pressure, pH value, viscosity, colour *etc.*, – whichever can be used as an index of the progress of the reaction or whichever can be a constituent of a composite index of the progress of reaction.

There are processes, especially some producing specific organic compounds, which call for close monitoring of the process conditions. They call for abrupt stopping of the reaction by chilling, reducing the pressure, fast addition of stabilisers *etc*. Such steps may have to be taken to ensure the quality of the product, maximising throughput or purely from safety considerations. All these point to a need for fast and precise measurement of the concerned variables.

In yester years, the measured variables used to be displayed locally or at convenient panels. The process control decisions used to be manual. Expert operators and timely decisions were essential. Misjudgements possible at various stages affected the quality and the quantity of the product. The advent of powerful computers at economic rates has changed the scene dramatically. The processes concerned are modelled on the PC with sufficient elaboration. The control action for each of the variables is carried out by the PC. Human intervention, when the process is active, is rarely called for. Change in the settings done before

commencing the process or after its completion, are perhaps the sole occasions for human intervention.

The type and number of variables to be measured here, has increased substantially compared to the previous example. Measurement results are to be properly 'interwoven' and the process status elicited therefrom. From such information, the process progress has to be monitored and the next course of action guessed. Settings may have to be continuously decided. Exceptional situations are to be handled. Over and above this, the process status has to be presented to the operating personnel in meaningful and intelligent formats. To put it loosely, human intervention and decision-making need be only at a high level. The nitty-gritty of the process is taken care of by the instrumentation and control system. No doubt, all such systems, despite their high level of automation, have facilities for manual over-runs. These may be invoked only in an emergency.

1.5 Characteristics of an Instrumentation Scheme

Through the foregoing examples, we brought out what an instrumentation scheme encompasses. What is expected of an instrumentation scheme and how to quantify them? We address ourselves to this question in a generalised and rather abstract manner [Draper]. A variety of characteristics and yardsticks is in use to evaluate an instrumentation scheme [Considine, Neubert, Platt]. All these may not be relevant in all the situations. Depending on the application, a selected set will be in focus and only this matters in deciding the performance of the scheme. Hence only this restricted set of characteristics will be specified. The choice is often evident depending on the variables measured and the application concerned.

1.5.1 Accuracy

In any situation, a measured quantity has a true value. It can be expressed in numbers – true in the environment used for the measurement. Thus we may say, 'the true value of the variable (e.g., a displacement or an elongation) is such and such, at the specified conditions (e.g., atmospheric temperature, pressure, physical location of measurement, time of measurement and the like)'. The result of the measurement yields another number – again in the same units. Accuracy refers to the closeness of the two, rather the deviation of the measured value from the true value. Formally,

$$\text{accuracy}\ (\%) \quad = \quad \frac{\text{True value - Reading}}{\text{Reference value}} \times 100 \qquad (1.1)$$

The denominator used for normalising – 'Reference value' – is a specified true value, often the full-scale value. Reference to 'truth' requires all 'ifs' and 'buts' to be spelt out! All the environmental conditions that have a bearing on the physical variable being measured, are to be specified. Ideally, the measurement is carried out along with that of all the physical variables that constitute the environment. Under such specified environmental conditions, the variable under discussion has a true value. The reference here is to these two quantities.

If all the environmental factors that have a say here, are known and they can be quantified. The true value may perhaps be 'known' and can form the reference; however, in most situations, not all these factors are known. Some of the known factors are not quantified. Both these prevent the true value being known. One can only gauge the true value here as best as possible and specify accuracy in terms of it. Needless to say, 'assessed true value' has to be much closer to the 'true value' compared to the reading. Only then, the specified accuracy has a credibility or meaning. Figure 1.4 depicts the quantities in abstract terms. *OA* is the true value. *OB* is the reading in a measurement and *AB* represents the deviation between the two.

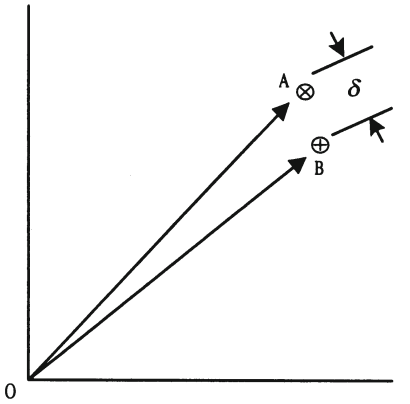


Figure 1.4 Determination of the accuracy. *OA* is the true value. *OB* is the read value. *AB* is the deviation signifying accuracy.

$$\text{Accuracy (\%)} = \frac{OA - OB}{OA} \times 100 \tag{1.2}$$

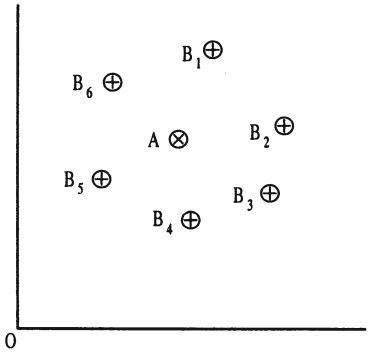


Figure 1.5 Dispersion of the reading around the true value. B_1, B_2, B_3 *etc.*, are the different readings.

One may carry out the measurement of the same physical quantity under identical environmental conditions; OB_1, OB_2, *etc.*, represent these readings in Figure 1.5. Established statistical procedures can be used to define how well the readings from the measurements carried out, approach the true value. These are not

of direct significance to an instrumentation scheme. But, a calibration carried out to ascertain the closeness of the measured value to the true value as above, goes a long way in establishing the fidelity or credibility or reliability of an instrumentation scheme.

1.5.2 Precision

Precision signifies clarity or sharpness of a measurement. It is closely related to accuracy. A clear understanding of precision and its difference from accuracy is essential. These are better illustrated through a few tangible examples. A displacement may be measured using a normal laboratory linear scale and expressed as 13.1 mm. Possibly, we mean that the reading lies between 13.0 mm and 13.1 mm (Often this is expressed as 13.1_1).

$$\text{precision in measurement (\%)} = \frac{0.1}{13.1} \times 100\ \% = 0.77\ \%. \quad (1.3)$$

The same measurement can be carried out using a vernier scale and expressed as 13.14 mm. Possibly, we mean that the reading lies between 13.135 mm and 13.145 mm. The reading can be expressed as 13.14_5 mm where the suffix 5 signifies the extent of indecision. The precision may be expressed as

$$\text{precision in measurement (\%)} = \frac{0.005}{13.14} \times 100\% = 0.038\ \%. \quad (1.4)$$

If need arises, the same measurement may be carried out with the help of a travelling microscope. The reading may be 13.142_1, where the '1' represents the indecision in the measurement. The corresponding precision is

$$\text{precision in measurement (\%)} = \frac{0.0001}{13.142} \times 100\ \% = 0.00077\ \% \quad (1.5)$$

The precision in measurement in the above three cases, increases in the same order in which they are presented. Such an improvement in precision does not necessarily imply increase in accuracy. Consider a (hypothetical) situation wherein the graduated scale of the travelling microscope introduces an error – say the travelling microscope is used at an elevated temperature where its performance is not guaranteed; the error due to this may be 0.1 %. Despite the high level of precision in the measurement tools used and the method of measurement, the accuracy attainable is rather poor.

Take a more obvious example in Electronics. Twenty bit A/D converters have become common place. Precision possible here is 1ppm (1 in 10^6). The conversion may be carried out using a 5V reference. If the reference value itself drifts by say 0.1 %, the measured value is accurate only to this extent; still, the precision attainable is 1ppm. A few possible situations are depicted in Figure 1.6. The following are noteworthy here: -

⇒ The precision required, in the method of measurement adopted, has to be as good as the accuracy that is desired.

⇒ An improvement in precision does not imply improvement in accuracy.

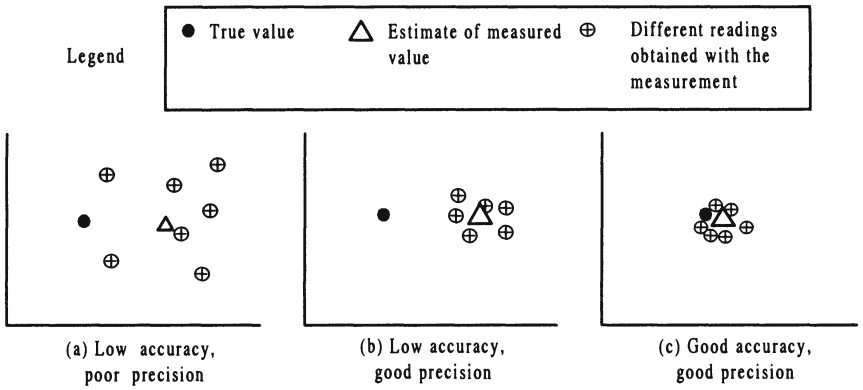


Figure 1.6 Relationship between precision and accuracy

Accuracy and precision are mutual chasers. An improvement or radical innovation in technology may lead to an improvement in the precision attainable in a measurement. This is inevitably followed by attempts to improve accuracy. This may involve direct as well as indirect methods of compensation. Many such situations will be discussed in the following chapters. The reverse situation is also quite common. A process may demand a more accurate measurement, perhaps to cater to more stringent quality requirements. This necessarily calls for an improvement in the precision of measurement, which motivates further development.

1.5.3 Errors and Correction

Formal definition of error and correction in line with accuracy is in order.

$$\begin{aligned} \text{True value} &= \text{Reading} + \text{Correction} \\ \therefore \text{Correction} &= \text{True value} - \text{Reading} \\ \text{Error} &= -\text{Correction} \\ &= \text{Reading} - \text{True value} \\ \%\ \text{Error} &= \frac{\text{Reading - True value}}{\text{Reference value}} \times 100 \end{aligned} \tag{1.6}$$

The error in a measurement can be due to various reasons. Errors due to the method of measurement and the errors used in the tools for measuring, cause 'systematic' errors. The illustrations, considered to bring out the difference between precision and accuracy, are of this category. They invariably lead to poor accuracy despite the high level of precision available. Errors like parallax error are caused by ignorance or carelessness on the part of the user. They are not systematic but are 'gross errors'. In general, other errors are termed 'random'. The unpredictability and lack of repeatability of these make them random. Error due to hysteresis in a deciding component, drift in a component value, *etc.*, all these contribute to random errors. If we measure a quantity repeatedly, readings will differ from one another. They will be spread out around an 'expected value'. The extent to which they are spread out is

a measure of the randomness associated with the measurement. These are dealt with in a later chapter.

1.5.4 Sensitivity

Sensitivity is the ratio of the change in output to the change in the input *i.e.*, the change in the variable being measured. To be precise, it is the slope of the curve relating the input variable to the output at the point representing the measurement. Figure 1.7 illustrates this. When the input variable has value x_0, the corresponding output value is y_0. As the input changes by a small value δx, the output changes by a corresponding amount δy. The ratio $\delta y/\delta x$ represents the sensitivity, approximately. The actual sensitivity at x_0 – designated as S – is defined as,

$$S = \lim_{\delta x \to 0} \frac{\delta y}{\delta x} = \left.\frac{dy}{dx}\right|_{x=x_0} \tag{1.7}$$

One can define a DC sensitivity separately; but it is not of much practical use. Depending on the nature of the sensor used, the sensitivity may change with changes in the input variable – hence the need to have sensitivity defined as here.

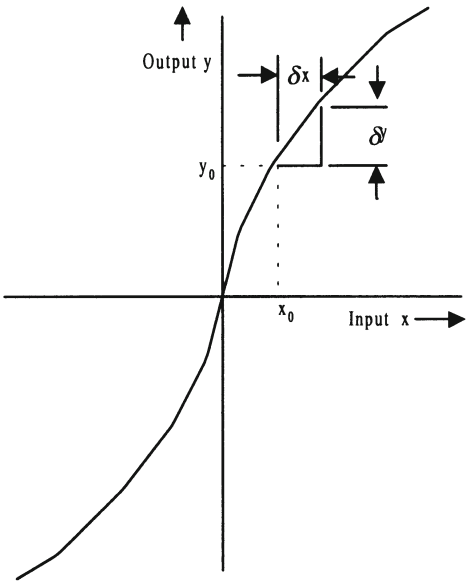


Figure 1.7 Illustration of sensitivity

In any instrumentation scheme, the primary sensing element [See Sec.1.6.1] plays a crucial role – that of conversion of the quantity being measured to a different form. It is essential that this conversion be done with the highest possible sensitivity. One can apparently increase sensitivity at a later stage, by amplification. Increase in noise content and reduction in the signal to noise ratio is inevitable in any such signal modification process. This is the primary factor calling for the use

of as high a sensitivity as possible, at the first stage itself. In other words, sensitivity is a key factor in the selection of the primary sensor. One gives more weight to increasing sensitivity than to decreasing complexity, cost *etc.*, that ensue.

1.5.5 Hysteresis

The input-output characteristic of a typical sensor is shown in an exaggerated form in Figure 1.8. *A*, *B*, *C*, *etc.*, represent various operating points on the characteristic.

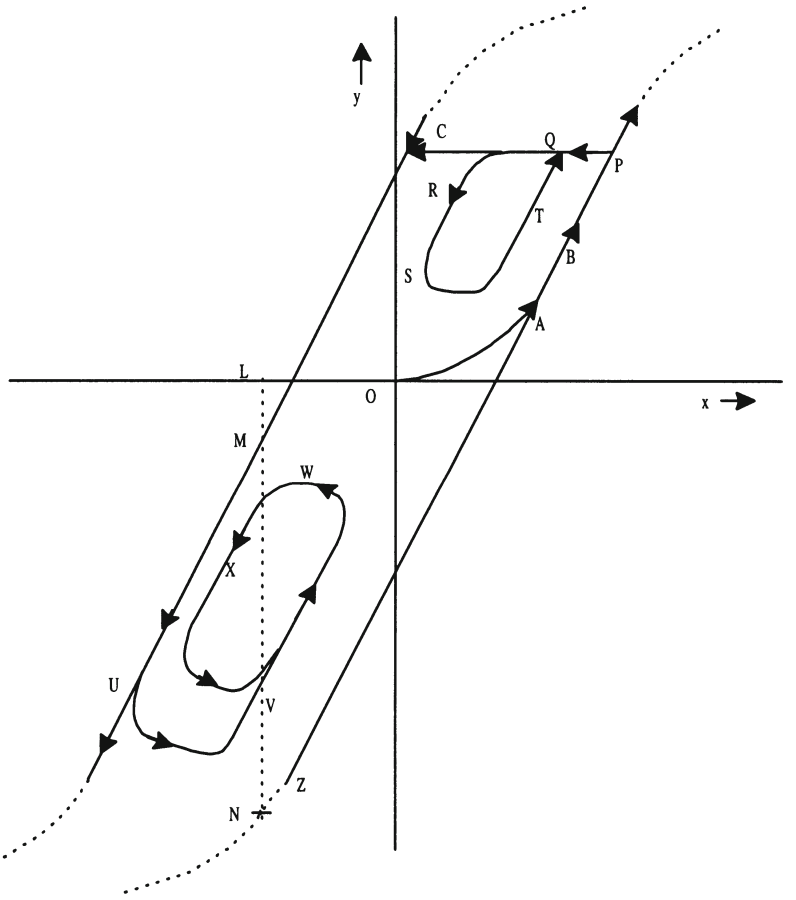


Figure 1.8 Input-Output relationship of a sensor showing hysteresis

Consider the sensor with zero input. The expected input-output situation is depicted by point *O*. Starting from here if we increase the input, the output increases until point *A*. Thereafter output follows changes in input, as long as input is increased monotonically – this is represented by the segment *OABP* of the characteristic and indicated by the arrows on the characteristic. At point *P*, the input stops increasing and decreases – again monotonically; the portion *PQRS* represents this portion of

the characteristic. Starting from *S*, the input increases once again until point *Q* when the input-output curve joins the earlier one. Hereafter, the input is decreased until point *C*. Further decrease in input is followed by a corresponding decrease in output until point *U* is reached. Starting with *U*, the input increases and decreases as represented by the segment *UVWXV* of the characteristic. On the whole, the output appears to follow changes in input in an undefined manner. However, as mentioned earlier, the relationship is shown in an exaggerated manner to bring home the point. Throughout, the output follows the input but with an 'inertia'. The input-output relationship here is characterised by the following: -

⇒ It always lies in the band decided by *ZP* and *CU*. The uniqueness of the input-output relation is limited by the width of the band.

⇒ At any input value, the output is decided mainly by the magnitude of the input, plus an amount decided by the history of the input-output changes. Thus for input *OL*, the output may lie anywhere between *LM* and *LN*.

The phenomenon discussed here is called 'Hysteresis'. In many situations, it is the inertia of the materials concerned at the molecular level, which manifests itself in this form. By a proper selection of materials and pre-treatment, the effect of hysteresis can be reduced. Although it cannot be eliminated, its effect can be made insignificant in an instrumentation scheme.

1.5.6 Resolution

Resolution refers to the smallest discernible change in the input *i.e.*, the smallest change in the input that manifests itself as a perceptible change in the output that can be felt. Take the example of displacement measurement with the travelling microscope. A reading obtained was 13.142mm. A change in displacement by 0.000 02 mm cannot be detected by the travelling microscope. The change has to be at least 0.000 1 mm to be sufficient to be detected by the travelling microscope. Here the resolution is 0.000 1 mm. One can see that the resolution of an instrumentation scheme has to be at least as good as its precision. Resolution is a primary factor in deciding precision. But it is possible for a scheme to have a very good resolution but not so good a precision. Again, taking the example of the travelling microscope, with time and continued use, its parts may wear out; the graduation and optics may still be good. This is a typical case of good resolution but not a matching level of precision. With new instrumentation schemes, such situations do not arise; the two will be matched. Rarely does one use an element of better resolution than called for, by the requirement of precision. However, in retrofit situations this is possible.

1.5.7 Threshold and Dead Zone

Threshold represents the smallest input change from the zero value that makes an output change discernible. Referring to Figure 1.9 (a), the physical variable may be considered to be at zero initially, represented by point *O*. The input may increase upto *OP* in the positive side without causing any change in the output. Only after it exceeds the level *OP*, does the output start increasing. The input *OP* is the 'threshold level' of the input. Similarly *ON* is the threshold level in the negative

side. In practice, the input-output relationship of a sensor may not follow the clearly linearly segmented characteristic represented by *RNOPQ*. The practical situation is shown in Figure 1.9 (b). *OT* in the positive side and *OV* in the negative side represent the output corresponding to the resolution. In the region shown shaded, for all inputs, output will be interpreted as zero. The actual input-output curve may follow the bold dotted line. The threshold is represented by point *S* in the positive side (and *U* in the negative side).

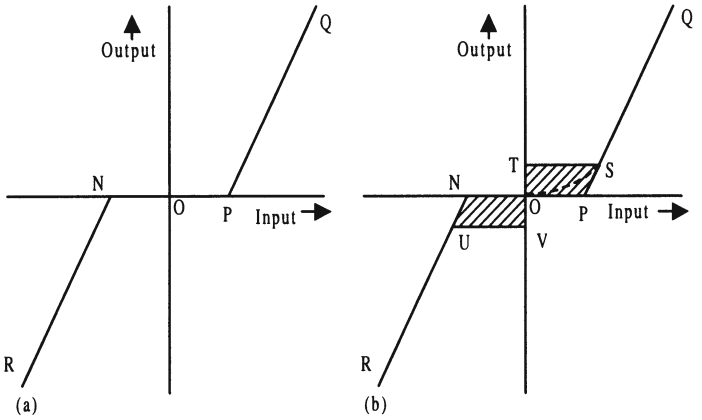


Figure 1.9 Threshold and dead zone in the input-output characteristic: (a) Idealised situation. (b) Practical situation.

The total range of input, over which the output remains zero (*NOP*), is the 'dead zone'. If the input goes through a transition from a large negative value to a large positive value or *vice versa*, as it sweeps through NOP, the output remains frozen at zero. The elements/devices using the output perceive the input as suddenly going frozen. Hence the term 'dead zone' to describe this range. Static friction, Hysteresis *etc.*, contribute to this effect.

1.5.8 Drift

With the physical variable remaining unchanged, the measured reading may go on shifting randomly – called 'Drift'. Such a drift at the zero value of the variable is called 'zero drift'. Zero drift can be broadly due to two reasons.

The sensor may respond to changes in other quantities, apart from the variable of interest. One or more of these may change, though the measured variable may remain unchanged, resulting in the drift. A typical example is a gas sensor (e.g., CO sensor), which is to respond to changes in the concentration of the concerned gas in air. The sensor is often sensitive to changes in the concentration of other gases like hydrogen and moisture. Changes in the environmental conditions under which the sensor functions, also cause such drift.

A second cause is drift due to some undesirable change or effect associated with the sensor itself. As an example, consider a strain gauge bridge. It is intended to sense changes in the strain of objects. The same is converted into an output through

a Wheatstone bridge. If one or more of the resistances of the bridge change, the same cause an output even in the absence of a strain; this forms a drift in the bridge output.

1.5.9 Repeatability and Zero Stability

Consider a sensor giving an output for a specific level of the physical variable being sensed. It will give a specific output reading. The same condition can yield a slightly different reading on repeating the measurement. Repeatability refers to the closeness of all such readings. It may be expressed as a percentage as,

$$\% \text{ repeatability} = \frac{\text{Maximum value of reading - Minimum value of reading}}{\text{Maximum value of reading + Minimum value of reading}} \times 100$$

$$= \frac{\text{Maximum deviation from average}}{\text{Average value}} \times 100 \qquad (1.8)$$

The measurement process along with its environment comes within the scope of repeatability. The measurement is to be done for the same value of the physical variable under the same set of conditions next time and every time. But precision is essentially restricted to the fidelity of the reading *per se.* How precisely can it be defined?

'Zero stability' is a concept closely allied to repeatability as well as dead zone and threshold. It refers to how stable the zero value remains. Stability can be expressed with respect to changes in any one of the parameters affecting the variable or their combinations. Typically, it can be zero stability with respect to ambient temperature variations, change in power supply or stability with respect to time.

Often the instrumentation scheme is used as the sensing element of a control or regulating system. A physical variable may have to be regulated and kept steady at one value. In such cases, zero stability attains importance.

1.5.10 Range

The active span of an instrumentation scheme is its range. Ideally one may aim at a range of $-\infty$ to $+\infty$ (or 0 to $+\infty$ as the case may be) but accommodating such wide ranges is not practically possible; further with a wide range, accuracy and resolution suffer. These have to be grossly sacrificed. In all cases, the application concerned will call for a limited range only. The range of the sensor will be made slightly wider than what is necessary for the application, to ensure that the full requirement is always met. With a variable like temperature or pressure, different applications call for different ranges. In each case, the resolution and accuracy has to be kept up too. Sensors are designed to cater to each such range separately. Further, one may use different principles of transduction in different ranges.

In contrast, instrumentation schemes for vibration, noise *etc.*, are often used for indication purposes only. A high level of accuracy, especially at the full-scale end, may not be called for here. Such instrumentation schemes are characterised by very wide ranges. Often to accommodate the wide range, a logarithmic scale is used for the output.

1.5.11 Linearity

The basic function of a sensor is to convert the value of a physical variable to a more easily useable and standard form. The magnitude of the physical variable and the output of the sensor should have a one-to-one relationship. *i.e.*, every value of the variable must have one and only one output value from the sensor. Conversely, every output from the sensor must correspond to one and only one value of the physical variable. A few typical possible characteristics conforming to these conditions are shown in Figure 1.10.

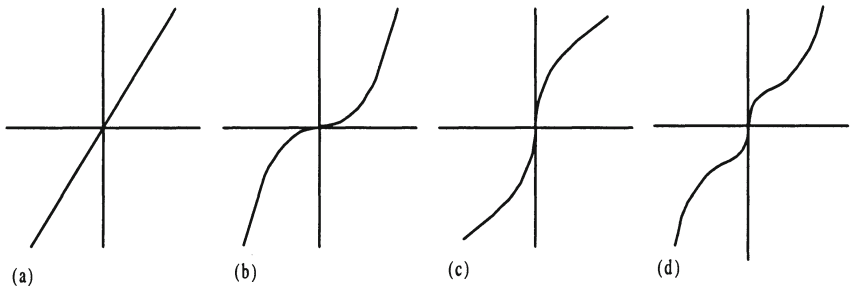


Figure 1.10 A few possible input-output characteristics of sensors. (a) Linear (b) Hard spring (c) Soft spring (d) Combination of soft and hard springs.

A sensor, having any one of these or similar characteristics, will satisfy all specifications laid down in terms of the characteristics discussed so far. However, the characteristic shown in Figure 1.10 (a) is 'linear' and is preferable in most cases. Linearity is a measure of the steadiness of sensitivity throughout the active range. Specifically a linear relationship will have d*y*/d*x* (Figure 1.7) constant over the whole range. Deviation from this value makes the characteristic non-linear. Referring to Figure 1.11, the extent of such deviation may be expressed as,

$$\% \text{ non-linearity} = \frac{|y_0 - k \times x_0|}{x_0} \times 100 \tag{1.9}$$

where

⇒ x_0 = the value of the physical variable where nonlinearity is expressed,
⇒ k = the 'best' fit slope of the sensor characteristic and
⇒ y_0 = the numerical variable of the sensor output at x_0.

k – representing the slope of the best-fit straight line – can be defined in various ways. We have used a value without getting into details (We may hasten to add here that there is no universally accepted definition of nonlinearity. However, the above one suffices for our purposes). Although we used the instantaneous slope to define linearity, it is not used to define departure from linearity, *i.e.*, nonlinearity. Often we estimate the nonlinearity at full scale or the maximum nonlinearity within a specified range. One of these is used as the criterion for departure from linearity.

Departure from linearity is undesirable on the following counts: -

⇒ When the sensor forms part of a control loop, the control system may exhibit unexpected behaviour syndromes – hanging, oscillations *etc.*, are typical of these.

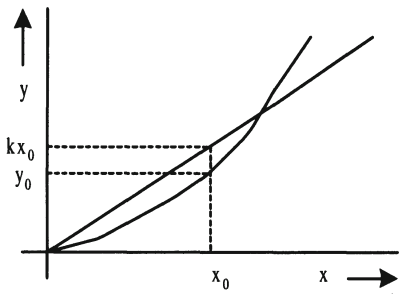


Figure 1.11 Definition of non-linearity

⇒ If the sensor output is used for direct analogue display, the display scale appears non-uniform (a non-uniform scale gives the impression of lack of accuracy – even when the non-uniform graduations are resorted to, for improving accuracy!)

⇒ If the sensor output is converted to digital form, through an ADC, the quantisation levels change with the signal level. This is obviously undesirable.

⇒ Often the sensor output is used for further signal processing and computational work. To avoid errors here, linearising has to be done in analogue form (before ADC) or digital form (using LUTs). This is an additional overhead in the scheme.

In some situations, departure from linearity is introduced intentionally: -

⇒ One selected segment of the sensor characteristic may have to be intentionally zoomed in contrast to others.

⇒ A portion of the sensor characteristic may not be significant. It may be suppressed by intentional scale distortion.

A wide scale range can be accommodated by using a suitable non-linear input-output characteristic.

1.5.12 Input and Output Impedances

'Observer' influences the measurement in any sensing process. Here the source is disturbed due to the 'Observer' absorbing energy from it, which is inherent in the sensing process. This is termed 'loading' of the source. Obviously, the loading has to be kept low enough to avoid affecting the process perceptibly. One yardstick is the precision of the measurement itself. The loading has to be so low that the change in the magnitude of the physical variable being measured will be smaller than the precision level expected (at least by one order). If the sensed quantity were an electrical voltage, we say that the 'input impedance has to be as high as possible'. Consider the equivalent circuit of Figure 1.12. The physical variable being sensed is represented by its equivalent circuit – of ideal voltage source V_s and internal resistance R_s across terminals A and B. The sensor is represented by its equivalent circuit of load resistance R_L. The block marked as S is an idealised sensor of zero internal impedance. The two together have terminals CD. When C and D are connected across A and B, we get sensed voltage V_o as,

$$V_o = V_s \times \frac{R_L}{R_s + R_L}$$
$$= V_s \frac{1}{1+(R_S / R_L)} \quad (1.10)$$

Table 1.1 Change in load-resistance versus error due to loading

R_s/R_L	1 %	0.1 %	0.01 %	0.001 %
Change in V_o	1 %	0.1 %	0.01 %	0.001 %

Table 1.1 shows percentage change in V_o due to loading for a few selected values of R_s/ R_L. One can see that both are of the same order. If the loading is 0.1 %, the error due to it is also 0.1 %. In other words, if we expect a precision in the measurement of say 0.1 %, the error due to loading has to be kept (one order less) down to 0.01 %, which means R_L > 10,000 R_s. Decrease in R_L beyond this level (*i.e.*, level compatible with the demands of precision), is not advisable. It makes the sensor sensitive and vulnerable to disturbing noise sources, which affect it adversely in other respects.

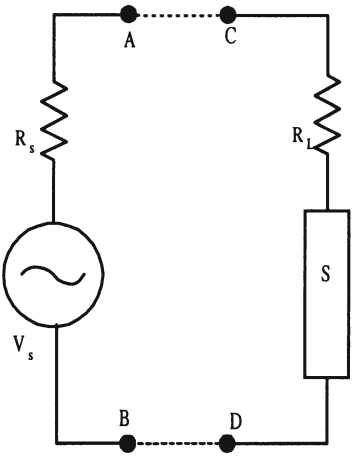


Figure 1.12 Equivalent circuit of a source and load

So far, we have been discussing loading of the source by the sensor of the instrumentation scheme. The reverse situation arises at the output side of the instrumentation scheme. Loading of the devices connected to the instrumentation scheme at its output side, affects the output. This also affects the precision of the instrumentation scheme. The loading has to be kept as low as possible. For this, the output impedance of the instrumentation scheme (assumed to be a voltage type output), has to be low enough. With R_s as its internal resistance and R_L as the load resistance, to attain a precision of 0.1 % (say) we must ensure that,

$$R_s < \frac{R_L}{10{,}000} \tag{1.11}$$

Again, for the reasons cited earlier, we should ensure that this ratio is not larger than is necessary. When the instrumentation scheme is loaded by more than one device tapping the variable (this is often the case), all the loads are connected together.

Sometimes the demand that the loading by the sensor be kept low, becomes too tall an order! Considerations of economy, lack of availability of such sensors, the required precision becoming too restrictive to be directly achieved (as with calibration in Standards Laboratories) *etc.*, can be the reasons. Two courses of action are possible here: -

⇒ Compute the actual degree of loading and compensate the reading externally.

⇒ Use a feedback based self-balancing scheme to keep down the loading.

The former scheme is simpler and economic. But the loading of the source is not acceptable in many situations. These call for resorting to the latter method, despite it being more elaborate, sophisticated and costly.

1.6 Instrumentation Scheme - Block Diagram

Many criteria to specify and evaluate instrumentation schemes have been discussed so far. Depending on the application, one or more of these become dominant and the scheme has to be tailored to satisfy them [Considine, Rangan]. When a single criterion dominates to the near exclusion of all others, the instrumentation scheme will be simple – as was the case with the example of the pressure gauge considered earlier. The complexity increases with more stringent requirements and with the number of criteria to be met. Such instrumentation schemes will have different functional blocks.

Figure 1.13 shows a fairly comprehensive instrumentation scheme in block diagram form. The physical variable to be sensed is embedded in the environment. Other variables, which can affect the measurement namely, the changing ambient conditions, corrosive or reactive nature of the constituents, hazardous and extremely unfavourable operating conditions and combinations or sum total of all these make up the environment. The primary sensor senses the physical variable concerned. Along with the rest of the instrumentation scheme, it 'distils' the variable *per se* and offers it in the desired form. Each block in the figure plays its role in the process.

The aim is to perform the instrumentation action conforming to the specifications. These specifications are quantified using all or some of the performance criteria, already discussed. Often, one block plays a heightened role *vis-à-vis* one or more of the performance criteria, and may be accentuated at the expense of another less important one.

An overview of each block and its role are in order here. An in-depth study of each is left to the following chapters. We may hasten to add here that all instrumentation schemes are not necessarily structured as rigidly or elaborately as brought here. The instrumentation scheme 'architecture' (if we may call it so!), is essentially decided by the sum total of the application requirements.

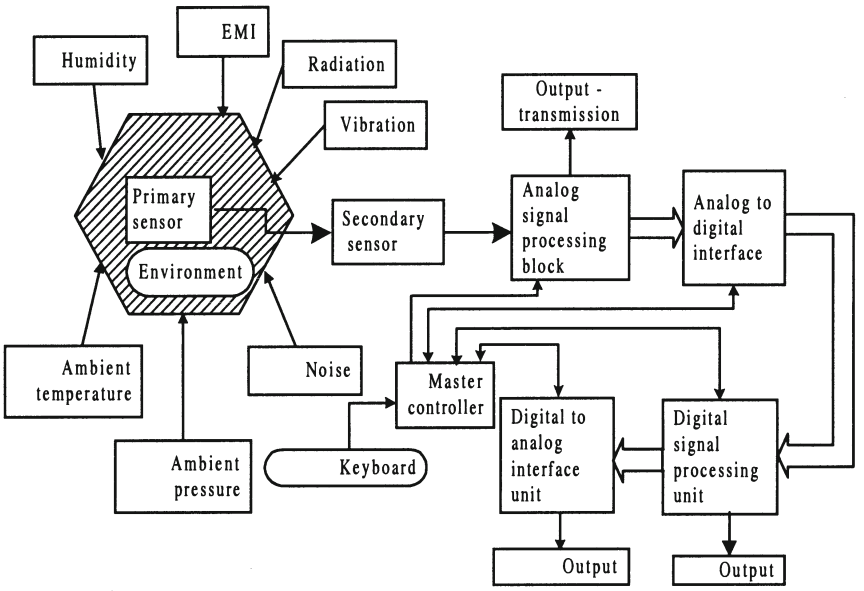


Figure 1.13 Block diagram of a comprehensive instrumentation scheme

1.6.1 Primary Sensor

Signals can be easily and effectively, processed when in the electrical form. There are only a few sensors which can convert the value of a physical variable directly into one of the electrical quantities – like a current, a voltage, a frequency, the amplitude of a carrier and so on. Thermocouple and Hall-effect sensor are typical examples. When this is not feasible, the physical variable to be sensed is converted into an intermediate variable and subsequently into an electrical form. The first conversion is carried out by the 'Primary Sensor' and the second (where the need arises), by the 'Secondary Sensor'. Displacement, *R, L, C etc.*, are the common intermediate variables. The primary sensor senses the physical variable and provides its value in another form. For all purposes, this replica is used as a measure of the physical variable – for control, display and all decision-making processes involving the physical variable. The need for fidelity need not be stressed here. In case other variables in the process or the environment affect the physical variable output beyond allowable limits, their effects may be compensated suitably. The requirements of the primary sensor are: -

⇒ It should have as high a sensitivity as possible. All subsequent processing stages may introduce definite noise into the signal. At each stage, the noise has a certain minimum value. Its relative contamination can be kept small only by having the highest possible sensitivity at the first stage (signal source) itself.

⇒ Its precision level has to be at least one order better than the precision expected of the overall instrumentation scheme. This requires that the combined effect of hysteresis, dead zone *etc.*, has to be compatibly low.

⇒ Under extremes of ambient conditions specified, the sensor characteristic has to be repeatable. The repeatability has to be better than the precision expected.
⇒ Sensitivity of the primary sensor to other variables and changes in ambient conditions, have to be one or two orders lower than that for the primary variable being measured. When this is not possible, such response to other variables is separately compensated.
⇒ It should not disturb the functioning of the main process. *i.e.*, loading due to it should be sufficiently small.
⇒ It should merge with the environment of the physical variable.
⇒ It should be small in size and should not jut into the process or out into the open, unduly.

1.6.2 Secondary Sensor

Whenever the primary sensor produces an output other than voltage or current, the same is in the form of a change in displacement or change in an electrical quantity like *R, L, C, Q, f*. Such changes are to be transformed into a voltage, or a current change. This transformation is the function of the secondary sensor. In many cases, the secondary sensor will be a part of the primary sensor (e.g., resistance thermometer) in which case the two cannot be separately configured. The secondary sensor uses a well-known circuit configuration like a Wheatstone bridge, one of the AC bridges, an oscillator circuit and so on. With the widespread availability of quality opamps, the secondary sensor often uses a subsequent signal processing stage as part of itself with certain attendant advantages. The input-output relation of the secondary sensor can be well defined to facilitate good design and engineering. All components, which have a bearing on the input-output relation, are carefully selected. Component-tolerances, accuracy, dimension, ageing-characteristic are all given due consideration. All these are necessary due to the low signal levels. Normally, the secondary sensor is externally powered. The circuit configuration will be chosen – if possible – to ensure that the power supply variations have only a secondary effect on the performance of the secondary sensor.

The secondary sensor is normally composed of a number of circuit elements. This makes room for compensating for the adverse effects of other variables, ambient changes *etc.*, associated with sensing. The approach here is to 'nip any disturbance in the bud '.

1.6.3 Stages of Analog Signal Processing

The electrical signals, from the primary or the secondary sensors, are 'weaklings' due to the following reasons: -

⇒ The signal level or magnitude is quite small
⇒ The signal power level is low; *i.e.*, if it is a voltage, its source impedance may not be low enough; if it is a current signal, its source impedance may not be high enough.
⇒ The signal may be in amplitude or frequency modulated form.
⇒ The signal may be biased or available only with a DC offset.

⇒ In case of modulated signals, a steady carrier may be present.
⇒ The signal may be contaminated by an undesirable signal (like the sensor responding to an extraneous variable).

The signal requires further processing in respect of each of the above, to bring it up to 'respectable' levels or more acceptable forms. All such processing has to be done with the aid of analog processing circuitry. Table 1.2 lists out the processing techniques and the specific functions carried out by each. A few observations are in order here: -

⇒ A DC instrumentation scheme is used as such only if the performance expectations are not stringent or other considerations dictate the choice. Otherwise, wherever possible the amplitude-modulated AC instrumentation scheme is more common.
⇒ The frequency-modulated scheme is used essentially with capacitance type sensors. Rarely do other schemes use frequency modulation (e.g., use of quartz crystal to sense small temperature variations).
⇒ Though crude (but ingenious) pulse modulation schemes were in use in the past, they are rarely used now-a-days.
⇒ The chopper amplifier is listed as a separate DC amplifier. It is an 'Amplitude Modulated' scheme. When used as part of a DC amplifier, it is termed a 'Chopper'; whenever the secondary sensor is part of a modulation scheme, it is termed an 'Amplitude Modulator'.
⇒ Developments in electronics, in recent years, have ushered in a variety of new circuits and techniques, considered impractical earlier. As a result, many instrumentation schemes considered too costly or unwieldy to be practical so far, are coming into vogue. The trend will continue. To that extent, the blocks listed in Table 1.2 may undergo changes – some may get merged with others, others may become more comprehensive and new ones may emerge.

1.6.4 Output

In analog instrumentation schemes, the signal – after analog processing – is output. The output can be in the form of a display or it may be transmitted in a suitable form. In more involved schemes, the signal may be converted into digital form and processed further before being output.

1.6.4.1 Display

In comparatively simpler instrumentation scheme, the processed analog signal is directly displayed. In others too, it may be locally displayed in analog or digital form and simultaneously processed further and / or transmitted. The final display takes a variety of forms and shapes depending on cost, context and application.

1.6.4.2 Transmitter

The process being sensed and the point of use of the concerned variables are often at a distance. There is a need to transmit the sensed signal over the distance extending over a few metres to a few kilometres. Before the advent of digital links (like RS232), such transmission was done in analog form. Specific and well-established formats were in use here. 0 – 5V and 4 – 20 mA are such. These

continue to be in vogue. When using an instrumentation scheme to conform to these, the signal is to be processed to get an output in the desired format and be capable of driving the load at the other end of the transmission.

1.7 Digital System

A digital scheme is characterised by speed, precision and processing capabilities. For a given volume demand of an instrumentation scheme, one can optimise the scope of the digital system as a trade off between economy and complexity. At the simplest level a digital scheme for an instrumentation scheme is characterised by: -

⇒ An ADC to convert the analog signal into equivalent digital form.
⇒ A microprocessor based computer to acquire the samples of the signal and do necessary processing
⇒ A dedicated keyboard for manual input into the system
⇒ A display for output
⇒ Perhaps a controller (to give out necessary control commands to regulate a process) may be integral to the scheme.
⇒ The digital signal may be converted back into analog form. This may facilitate display or control action.

As the complexity increases, a variety of solutions is possible: -

⇒ A comprehensive dedicated scheme may be designed. This is justified only if the volume justifies it or if the scheme is so specialised that standard modules do not fall in line to form a scheme.
⇒ At the other extreme end, one may bring out standardised modules, put them together and work with necessary software packages. Such a 'screw-driver' assembled scheme is well suited for one-of-a-type of solution.
⇒ In between the above two extremes, one has a variety of choices and alternatives. We do not intend to dwell into them here.
⇒ Many schemes incorporate some level of data logging and user friendly and meaningful displays.
⇒ Advent of DSPs has added a new dimension to the schemes. One is able to extract information from the streams of signal samples. On-line spectral analyses, feature extraction through image processing *etc.*, are typical examples of these. Control strategy and other decision-making processes can be based on such information.

Table 1.2 Different analogue processing circuits and their role in instrumentation schemes

Category	Type of processing	Primary function	Secondary functions / remarks
DC Amplifier	Single ended amplifier	Amplify single ended DC signals	Low loading of signal source. Provides low impedance output voltage or high impedance output current. Introduces desired (removes undesired) DC offset if and when necessary. Low pass filtering.
	Difference amplifier	Amplify floating input. Remove DC offset	-do-
	Instrumentation amplifier	-do-	-do- Suppresses common mode / interfering pick ups.
	Buffer	Low loading of source provides output signal with low source impedance	
	Chopper amplifier	Amplifies very low level signals	Amplification with very low noise addition. Band limiting. Easiness to handle / process subsequently.
		On-line calibration.	-do- Removing effects of ambient changes and other variables.
AC Amplifier	Wideband	Amplification of signal / modulated carrier.	Low loading of source. Provides low impedance output. Suppresses DC and avoids zero drift. Automatic nulling. Filtering.
	Narrowband	Amplification of modulated carrier	-do-

Table 1.2 (Continued)

Category	Type of processing	Primary function	Secondary functions / remarks
AC amplifiers	Buffer	Low loading of source provides output signal with low source	
Modulator	Amplitude modulation.	Provides a carrier whose amplitude is modulated by the signal	Avoid effect of drift. Reduce contamination of signal by noise. Suppressed carrier DSB is most common in instrumentation schemes.
	Frequency modulation	Provides a carrier whose frequency is modulated by the signal	-do- Excellent but somewhat costly scheme. Modulation is integral with the secondary signal.
Demodulator	Amplitude demodulator	Retrieves the signal from the modulated carrier.	These are required for chopper amplifiers also.
	FM demodulator	-do-	
Filter	Lowpass.	Suppress unwanted spectral components.	Noise reduction. Removal of specific interference.
		Anti-aliasing	Intentional band limiting before sampling. Minimising sampling error before sampling / multiplexing
	Bandpass	Suppress unwanted spectral components.	

Table 1.2 (Continued)

Category	Type of processing	Primary function	Secondary functions / remarks
Filter (Continued)	Narrowband	Extract the modulated carrier.	Same function for the modulated signal as a low pass filter does for a DC signal.
	Notch filter	Eliminate selected known interfering component.	
Others	Linearisation	Rectification of characteristic	Improvement in accuracy
	Shaping of characteristic	Restriction of active range of use.	Improve accuracy in a restricted range of interest.
	Multiplication	Modulation / demodulation of AM signal	
		Generation of a product signal.	
	Division	Normalising	Done only indirectly; rarely done directly.
		Nullifying the effects of undesirable variable.	-do-

2 Secondary Transducers

2.1 Introduction

Many transducers produce a corresponding change in a parameter value like resistance, inductance capacitance or mutual inductance, resonant frequency or the circuit Q value. Such changes are to be converted into equivalent voltage values (or current in some cases) before further processing. The 'Secondary Transducer' plays this role [Draper *et al.*, Neubert]. Three aspects are common to all secondary transducers: -

⇒ The secondary transducer produces an output voltage, which is a function of the change in the parameter concerned. Thus for example with resistance transducers, the output voltage V_o takes the form

$$V_o = \Delta R\, f(R, \Delta R) \tag{2.1}$$

where

- R is the resistance of the sensor
- ΔR is the change in resistance representing change in the physical variable being measured and
- f is a single valued function of R, ΔR and other quantities of the transducer.

The above equation shows that $V_o = 0$ for

$$\Delta R = 0 \tag{2.2}$$

and at least for small values of ΔR, it is linearly related to R.

⇒ The primary sensing element is often made one arm of a bridge. The bridge is operated near its balance to realise the above type of input-output relation. Wheatstone bridge is widely used with resistance type of sensors. One of the common and simple AC bridges is used with the other sensors.

⇒ The bridge is energised with a suitable supply. A stabilised DC supply is used with Wheatstone bridges. An amplitude and frequency stabilised AC supply is used with the AC bridges. If the magnitude of DC voltage or AC voltage changes, it affects V_o directly and causes a drift in the sensitivity. Hence the need to stabilise the supply.

Since the operation of DC and AC bridges, close to their balance conditions, are central to the secondary transducer, these are analysed first. Subsequently the generic features of various transducers are discussed. There are secondary transducer configurations not conforming to the above bridge types. The main ones amongst these are discussed subsequently.

T. R. Padmanabhan, *Industrial Instrumentation*
© Springer-Verlag London Limited 2000

2.2 Unbalanced Wheatstone Bridge

The apparently simple Wheatstone bridge is used in many instrumentation schemes. In a typical situation, one or more elements – say R_1 – is selected to change depending on the physical variable being sensed. With proper selection of the operating conditions for the bridge, its output voltage V_0 becomes a measure of the physical quantity being sensed. A closer look at the analysis of the operating conditions of the bridge, gives us a better insight into its working. With that the static characteristics and their inter-relations can be understood better [Harris].

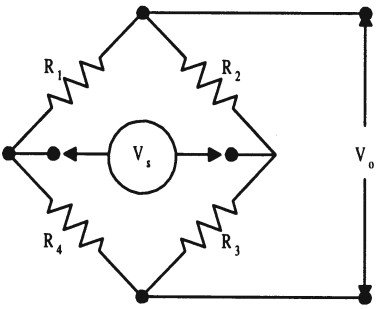


Figure 2.1 Wheatstone bridge

2.2.1 Assumptions

We assume certain ideal conditions to facilitate understanding of the scheme (Figure 2.1).

- ⇒ All resistors are ideal resistances. They do not possess residual inductance or capacitance.
- ⇒ The supply voltage V_s is constant.
- ⇒ The output impedance of the source is zero so that for all load conditions, V_s remains constant.
- ⇒ The output V_0 is not loaded by the following device connected to it, *i.e.*, the load current drawn by the load connected at V_0 is zero.

2.2.2 Bridge Near Balance

With the above assumptions we have,

$$\frac{V_0}{V_s} = \left(\frac{R_1}{R_1 + R_2} - \frac{R_4}{R_3 + R_4} \right) \tag{2.3}$$

Under balanced conditions,

$$V_0 = 0 \tag{2.4}$$

$$\therefore \frac{R_1}{R_1 + R_2} = \frac{R_4}{R_3 + R_4} \tag{2.5}$$

Let us consider an infinitesimal imbalance by increasing R_1 to $R_1 + \varepsilon$.

$$\frac{V_o}{V_i} = \frac{R_1 + \varepsilon}{R_1 + \varepsilon + R_2} - \frac{R_4}{R_3 + R_4} \tag{2.6}$$

Substituting from Equation 2.5, assuming $\varepsilon << R_1$ and simplifying we get,

$$\frac{V_o}{V_s} \approx \frac{\varepsilon}{R_1 + R_2}\left(1 - \frac{R_1}{R_1 + R_2}\right) \tag{2.7}$$

$$= \frac{a}{(1+a)^2}\frac{\varepsilon}{R_1} \tag{2.8}$$

where,

$$a = \frac{R_2}{R_1} = \frac{R_3}{R_4} \tag{2.9}$$

From Equation 2.8 we get,

$$\frac{V_o/V_s}{\varepsilon/R_1} = \frac{a}{(1+a)^2} \tag{2.10}$$

$[a/(1+a)^2]$ is a non-dimensional quantity. It is the ratio of the fractional change in the bridge output to the fractional change in the resistance. It is called the 'Sensitivity' of the sensor [See Section 1.5.4]. Sensitivity is one of the basic characteristics of a sensor. It has to be as repeatable and as large as possible. One aims to make the signal stand out as much as possible. The physical variable being measured, is transformed into an equivalent electrical form by the bridge of Figure 2.1. The signal representing the variable is at the least contaminated form here. Every further processing (amplification, filtering, modulation, demodulation, *A/D* conversion, *D/A* conversion *etc.,* to be discussed in the ensuing chapters) will add noise and other corrupting signals to it. *ipso facto,* one must have as high a sensitivity for the bridge as possible to reduce the effect of noise added subsequently. If we introduce the term S for sensitivity, we have,

$$S = \frac{a}{(1+a)^2} \tag{2.11}$$

We can see from Equation 2.11 that for very low values of a ($a << 1$) and for very high values of a ($a >> 1$), the sensitivity is small and S attains a maximum value in between. Differentiating S with respect to a

$$\frac{dS}{da} = \frac{(1+a)^2 - 2(1+a)a}{(1+a)^2} \tag{2.12}$$

$$\frac{dS}{da} = 0 \tag{2.13}$$

when,

$$(1+a)^2 - 2(1+a)a = 0$$

i.e.,

$$1 + a = 0 \tag{2.14}$$

This condition is physically not realisable; hence, it is not discussed any further here.

or,

$$a = 1 \tag{2.15}$$

Hence, S takes an extremum value for $a = 1$. By checking the sign of d^2s/dA^2 at $a = 1$, one can verify that S is a maximum at this point. Substitution of Equation 2.15 in Equation 2.11 gives the maximum value of S as,

$$S_{max} = 1/4 \tag{2.16}$$

Table 2.1 Values of S for different a values

a	0.01	0.03	0.1	0.3	1.0	3.0	10.0	30.0
S	0.0098	0.0283	0.0826	0.1775	0.25	0.1785	0.0826	0.0283

Table 2.1 gives the values of S for a range of a. The same have been plotted in Figure 2.2. One can see the following: -

⇒ S is a maximum at $a = 1$ and the maximum value of S is 0.25.

⇒ S reduces rapidly as a departs from this optimum value.

⇒ The value taken by S for any given value of a, is the same as for the corresponding $(1/a)$. In effect this means that if the bridge is balanced with $R_2 = 10R_1$, its behaviour for small variations, is similar to that with the bridge when balanced with $R_2 = R_1/10$ and similar small variations are considered.

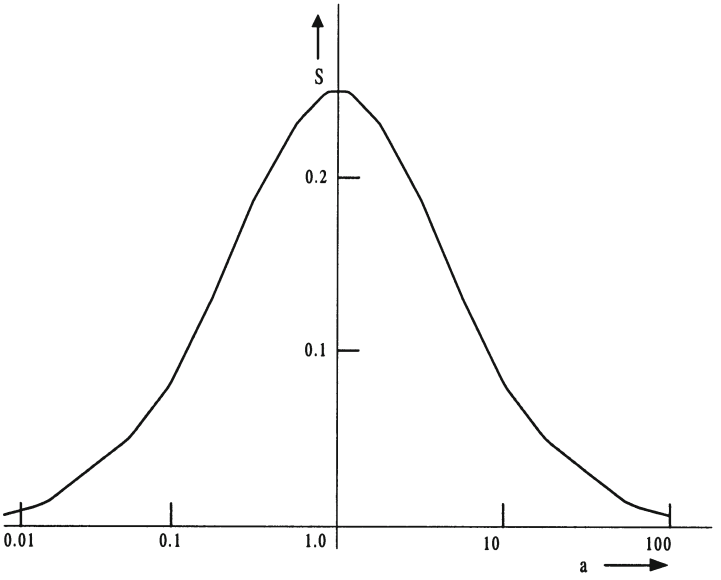


Figure 2.2 Nature of variation of sensitivity S of the unbalanced Wheatstone bridge with the bridge ratio a. The bridge has a single sensing element.

The analysis thus far, leads to the following of practical importance: -

⇒ Whenever possible, the transducer bridge is operated with $a = 1$, *i.e.*, the undeviated values of the four individual arms being equal to one another. This ensures maximum output from the scheme.

⇒ If the above is not possible, use a value of the ratio a as close to unity as possible. This ensures the maximum output from the scheme under the given conditions and subject to the practical constraints.

⇒ Operating the bridge close to $a = 1$, has another benefit associated with it – not evident from the analysis thus far. Consider increasing the value of a steadily. One way to do this is to keep $R_1 = R_4 = R$ constant and increase R_2 and R_3 such that they are equal. One can see that the output impedance of the bridge increases steadily. In the extreme case as $R_2 = R_3 \rightarrow \infty$, the output impedance becomes $2R$. Contrast it with the case when $a = 1$ with all the resistances being equal – the output impedance here is R. If the output impedance increases, the same imposes an increasing constraint on the input impedance of the following stage.

At this stage it appears that one can keep $a = 1$ throughout and still operate with increasing resistances. This case leads to a worse situation than the one above. Thus one may keep $R_1 = R_2 = 100$ (say) but increase R_3 and R_4 such that $R_3 = R_4$. This satisfies the condition $a = 1$ throughout. The output impedance increases more rapidly. It $\rightarrow \infty$ as $R_3 = R_4 \rightarrow \infty$. Hence, such increase becomes impracticable.

It is pertinent to point out here that in practice, transducer bridges are mostly operated with quiescent condition $R_1 = R_2 = R_3 = R_4 = R$. One strays off from this only when inevitable. From Equation 2.10, one can further see that any change in the supply voltage causes a proportionate change in the output. In other words, the scheme responds to the desired changes in R_1 (due to the change in the physical parameter being measured); in addition, it responds to changes in V_s as well. By sensing V_o, one cannot relate any portion of it as being exclusively due to changes in R_1 or changes in V_s. Hence any change in V_s causes an error in the output. Three courses of action are possible here: -

⇒ Keep V_s sufficiently stabilised. Hence, changes in V_o will be due to changes in R_1 only.

⇒ Always measure the ratio of V_o to V_s. This ratiometric measurement compensates for changes in V_s.

⇒ Carry out corrections – on-line – to the output to account for changes in V_s. This can be carried out, if the pattern of changes in V_s are clearly known beforehand and the same can be used for such compensation.

Depending on the context, one or another of the above three methods is adopted to minimise the error due to changes in V_s.

2.2.3 Transducer Bridge Behaviour for Large ε Values

The bridge behaviour for large ε is analysed here for the specific case, where all the bridge-arm-resistance values are close to each other. The more general case leads to cumbersome algebra but yields no additional information of relevance to us. The substitution,

$$R_2 = R_3 = R_4 = R$$

and

$$R_1 = R + \varepsilon \tag{2.17}$$

in Equation 2.6 and algebraic simplification yields,

$$\frac{V_o}{V_s} = \frac{\varepsilon/R}{2[2+(\varepsilon/R)]} \tag{2.18}$$

The (V_o/V_s)characteristic according to Equation 2.18 is shown sketched in Figure 2.3.

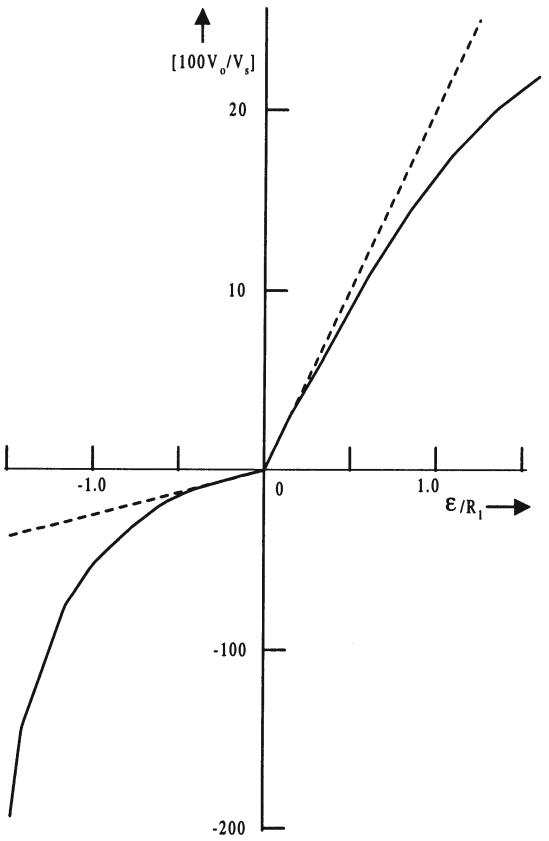


Figure 2.3 Input-output characteristic of unbalanced Wheatstone bridge for large values ε/R_1. Note the difference in the scales of the output, for positive and negative values of the input. The dotted lines show the initial slope, *i.e.*, the characteristic for very low values of input.

A few observations are in order here: -

⇒ Firstly, the input- output relationship is no longer linear.

⇒ Secondly, the input-output characteristic is asymmetric; *i.e.*, the change in the output, for a given change in the input in the positive direction, is different from that in the negative direction. This may not be of any consequence in some cases, while in other situations it may not be desirable. [1]

[1] The control loops involving such transducer bridges may sometimes lead to strange behaviour – this may be in terms of the system settling at an undesirable point or bursting into undesirable (asymmetric) oscillations.

Values of ε/R beyond (say) 0.2, are too large to be of any practical utility in transducer bridges. Therefore, the severity in the non-linearity or substantial reduction in sensitivity in such cases need not be dealt with in greater detail. Restricting ourselves to the lower ranges of ε/R, two issues warrant further attention: -

$\Rightarrow$ Can we reduce the non-linearity?

$\Rightarrow$ Can we bring about symmetry in the characteristic?

To address these questions and for other reasons as well, we revert to Equation 2.18 in the form,

$$\frac{V_o}{V_s} = \frac{\varepsilon}{4R}\left(1+\frac{\varepsilon}{2R}\right)^{-1} \tag{2.19}$$

Resorting to Binomial expansion of Equation 2.19,

$$\frac{V_o}{V_s} = \frac{\varepsilon}{4R}\left(1-\frac{\varepsilon}{2R}+\frac{\varepsilon^2}{4R^2}-\frac{\varepsilon^3}{8R^3}+\frac{\varepsilon^4}{16R^4}\ldots\right) \tag{2.20}$$

Considering only the first order differences

$$\frac{V_o}{V_s} = \frac{\varepsilon}{4R} \tag{2.21}$$

Accounting for second order differences also,

$$\frac{V_o}{V_s} = \frac{\varepsilon}{4R}\left(1-\frac{\varepsilon}{2R}\right) \tag{2.22}$$

Equation 2.22 shows that the departure from initial slope is of the same order as ε/R. It is possible to use the transducer bridge over the whole range in which ε/R and V_o/V_s are related such that they have a one to one relationship. Specifically for every ε/R, we should have one and only one V_o/V_s. This, as we saw earlier, is a wide range. The practically usable range is much more restricted. Normal practice is to restrict the use over a range of ε/R, where the relation can be considered linear. (Rarely does one trespass this limit, and resort to involved linearisation). To get an idea of the range, we may say that the full-scale accuracy aimed at is (say) 0.2 %. Various factors may contribute to this. We may assume (without sound basis!) that the assumption of linear relationship contributes to (say) 20 % of this *i.e.*, 0.04 %. From Equation 2.22 we get,

$$\left(\frac{\varepsilon}{2R}\right)_{\max.} = \frac{0.04}{100}$$

$$\therefore \left(\frac{\varepsilon}{R}\right)_{\max} = 0.08\% \tag{2.23}$$

The permissible range will increase or decrease, to the extent we relax or restrict the value of 0.04 % above (See Figure 2.4). If we relax it to 0.08 %, the limit of useful range of ε/R extends to 0.16 percentage. Nevertheless one can see that the maximum change of ε/R which can be meaningfully permitted, is restricted to 0.1 % to 0.2 %. Apart from linearity, there are other factors too, which impose such restrictions. However, chances are that the most severe one is due to the deviation from linearity.

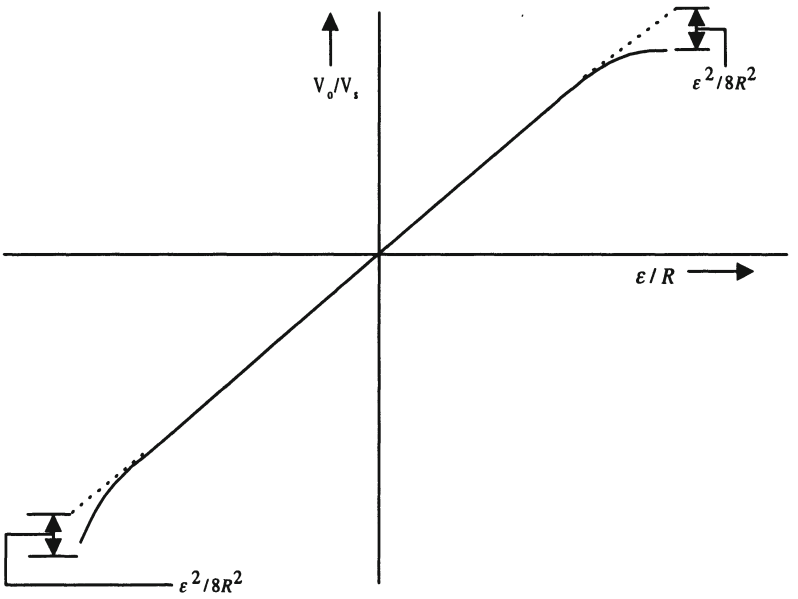


Figure 2.4 Non-linearity in the sensitivity characteristic of the unbalanced Wheatstone bridge with a single sensing arm.

2.2.4 Transducer Bridge with Multiple Sensing Elements

Transducer bridges of the type under discussion can be used with adjacent arms, opposite arms or all the four arms with changing R values. Such combinations serve mainly two purposes: -

⇒ Increase in bridge sensitivity.

⇒ Compensation for changes due to one or more types of environmental disturbances.

We extend the analysis of the above sections, to these cases as well. To avoid involved algebra, we restrict ourselves to the case of ε/R being equal in all the cases. (One cannot rule out unequal ε values in different branches in a practical situation. Analysis of this case is too intractable to provide meaningful information).

2.2.4.1 Transducer Bridge with Diagonally Opposite Sensing Arms

Referring to Figure 2.1, we consider R_1 and R_3 as varying by the same amount while R_2 and R_4 remain constant. Thus substituting,

$$R_1 = R_3 = R + \varepsilon \tag{2.24}$$

$$R_2 = R_4 = R \tag{2.25}$$

in Equation 2.6 and simplifying,

$$\frac{V_o}{V_s} = \frac{\varepsilon}{2R+\varepsilon} = \frac{\varepsilon}{2R}\left(1+\frac{\varepsilon}{2R}\right)^{-1} \tag{2.26}$$

Or

$$S = \frac{1}{2}\left(1+\frac{\varepsilon}{2R}\right)^{-1} \tag{2.27}$$

Binomial expansion of Equation 2.26 gives,

$$\frac{V_o}{V_s} = \frac{\varepsilon}{2R}\left(1-\frac{\varepsilon}{2R}+\frac{\varepsilon^2}{4R^2}-\frac{\varepsilon^3}{8R^3}+\frac{\varepsilon^4}{16R^4}\ldots\right)^{-1} \tag{2.28}$$

Two factors are noteworthy here: -

⇒ S here is twice that when we use a single element for transduction (Compare with Equation 2.16). This increase is to be expected.

⇒ The non-linearity factor remains the same as in the single element case. Hence, the useful range remains unaltered.

There are situations, where R_1 and R_3 change simultaneously, in opposite directions and the effect of this can be fruitfully made use of. Substituting,

$$R_1 = R+\varepsilon \tag{2.29}$$

$$R_3 = R-\varepsilon \tag{2.30}$$

$$R_2 = R_4 = R \tag{2.31}$$

in Equation 2.6 and simplifying,

$$\frac{V_o}{V_s} = -\frac{1}{4}\frac{(\varepsilon/R)^2}{1-\frac{1}{4}\left(\frac{\varepsilon}{R}\right)^2} \tag{2.32}$$

Doing binomial expansion and retaining only the first two terms,

$$\frac{V_o}{V_s} = -\frac{1}{4}\left(\frac{\varepsilon}{R}\right)^2\left[1+\frac{1}{4}\left(\frac{\varepsilon}{R}\right)^2\right] \tag{2.33}$$

Two factors are to be noted here: -

⇒ To a first order, the effects of changes in the two resistors R_1 and R_3 neutralise each other. Thus if we take the full-scale value of ε/R to be 0.001 (0.1%), S = 0.000 000 25 which is quite negligible. Thus, the scheme can be used to neutralise the effect of undesirable changes, provided one can manage to have R_1 and R_3 change in opposite senses.

⇒ V_o/V_s being a function of $(\varepsilon/R)^2$, the symmetry of the characteristic around the origin is lost. However, this appears to be of academic interest only.

2.2.4.2 Transducer Bridge with Adjacent Sensing Arms

Two cases arise here. The case when both are affected in the same manner is considered first. Substituting,

$$R_1 = R_4 = R + \varepsilon \tag{2.34}$$

$$R_2 = R_3 = R \tag{2.35}$$

in Equation 2.3 and simplifying,

$$V_0 = 0$$

The bridge remains balanced throughout. *i.e.*, effects of changes in R_1 are fully nullified by the effect of changes in R_4 and *vice versa*. This is a widely used method of compensating for the effects of disturbing environmental changes in the bridge.

Consider the second case *i.e.*, R_1 and R_4 changing in opposite directions. Substituting once again,

$$R_1 = R + \varepsilon \tag{2.36}$$

$$R_4 = R - \varepsilon \tag{2.37}$$

$$R_2 = R_3 = R \tag{2.38}$$

in Equation 2.3 and simplifying,

$$S = \frac{V_o/V_i}{\varepsilon/R} = \frac{1}{2}\left[1 - \left(\frac{\varepsilon}{2R}\right)^2\right]^{-1} \tag{2.39}$$

Comparing with Equation 2.27, we find that for small values of ε/R, the sensitivity remains the same. This is to be expected. Second-order changes and their effects may be considered using binomial expansion of Equation 2.39. This gives,

$$S = \frac{1}{2}\left[1 + \left(\frac{\varepsilon}{2R}\right)^2 + \left(\frac{\varepsilon}{2R}\right)^4 + \left(\frac{\varepsilon}{2R}\right)^6 + \ldots\right] \tag{2.40}$$

Two aspects of the above relationship – apart from sensitivity – are significant: -

⇒ The non-linear term is due to $(\varepsilon/2R)^2$. Contrast this with the earlier cases in Equation 2.20 and Equation 2.28, where it was due to ε/R. This expands the linear range of the bridge substantially. With an ε/R of 0.001, contribution of the non-linear term to error is only 0.000 001. In other words, if we want to limit the effect of non-linearity to 0.16 %, we have,

$$\left(\frac{\varepsilon}{2R}\right)^2 = 0.0016$$

$$\therefore \frac{\varepsilon}{R} = 0.08 = 8\% \tag{2.41}$$

Thus, even for 8 % of ε/R, the non-linearity contribution remains at 0.16 %.

⇒ The characteristic has symmetry with respect to the origin. The asymmetry with the characteristic, earlier, is removed. The symmetrical characteristic is more acceptable, and avoids certain undesirable behaviour characteristics, when the transducer-bridge forms part of a closed loop system.

Due to the better characteristics of this mode [See Figure 2.5], the transducer bridges are operated in this mode whenever the situation permits. A typical example is that of a strain gauge bridge where the adjacent arms are used to sense tensile and compressive strains from the same source. As mentioned earlier, increased sensitivity, wider useful range and a symmetrical characteristic are its advantages.

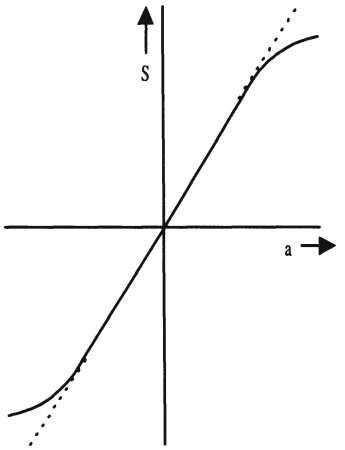


Figure 2.5 Input-output characteristic of a Wheatstone-bridge-type-sensing-bridge, with two adjacent sensing arms. The dotted line represents the extension of the linear characteristic used for small inputs.

2.2.4.3 Transducer Bridges with Four Sensing Arms

Although various combinations are possible, only one case is of importance here - that of the opposite arms changing in the same manner and the adjacent arms in the opposite manner all simultaneously. Only this case is considered.
Substituting,

$$R_1 = R_3 = R + \varepsilon \tag{2.42}$$

$$R_2 = R_4 = R - \varepsilon \tag{2.43}$$

in Equation 2.3 and simplifying,

$$S = 1 \tag{2.44}$$

The following are noteworthy here:

- ⇒ Sensitivity is a constant for all values of ε/R. Non-linear or asymmetric terms are absent. Hence, the input-output relationship is linear throughout.
- ⇒ Sensitivity S is equal to 1. The sensitivity level is conspicuously higher than in all the previous cases. This is also a definite gain.

Whenever the application permits, the transducer-bridge is arranged with all the four arms responding to the changes in the input variable. A typical common application is in strain gauge bridges. One pair of diagonally opposite arms may sense tensile strain, while the other pair senses compressive strain. Combining all the four elements in a bridge in this manner leads to the best possible strain gauge system of the resistance type.

2.2.5 Unbalanced Bridges

Sometimes the transducer bridges are operated under highly unbalanced conditions. A typical application can be one where a transducer has a high bias in the output, which has to be neutralised. Further, such neutralisation has to be effective over a range of variation of an environmental quantity like temperature. A brief discussion

of the unbalanced bridge is in order here. Referring once again to Figure 2.1, Equation 2.3 gives the bridge output voltage for any set of bridge resistance values. From one set of quiescent conditions, let R_1 increase to $R_1 + \varepsilon$, all the other resistances and the supply voltage remaining unaltered. Let the increase in output voltage due to this be δV_o. We have,

$$\frac{V_0 + \delta V_0}{V_s} = \frac{R_1 + \varepsilon}{R_1 + \varepsilon + R_2} - \frac{R_4}{R_3 + R_4} \tag{2.45}$$

Using this along with Equation 2.3 we get,

$$\frac{\delta V_0}{V_s} = \frac{R_1 + \varepsilon}{R_1 + \varepsilon + R_2} - \frac{R_1}{R_1 + R_2} \tag{2.46}$$

Using binomial expansion and assuming $\varepsilon << R_1$, Equation 2.46 simplifies to

$$\frac{\delta V_0}{V_s} = \frac{R_2 \varepsilon}{(R_1 + R_2)^2}\left(1 - \frac{\varepsilon}{R_1 + R_2}\right) \tag{2.47}$$

Retaining only the first order term in ε/R_1, Equation 2.47 can be recast as,

$$\frac{\delta V_0 / V_s}{\varepsilon / R_1} = \frac{R_1 R_2}{(R_1 + R_2)^2} \tag{2.48}$$

Equation 2.3 gives the steady state unbalanced voltage. Equation 2.48 gives the change in the unbalanced output voltage. Note that the fractional change is decided by R_1 and R_2 only. R_3 and R_4 do not affect this. Normal practice is to select R_1 and R_2 to provide the necessary δV_0. Subsequently R_3 and R_4 are selected to make V_0 have the desired level. Thus the output bias can be neutralised by R_3 and R_4 selection after the change in it is neutralised by choice of R_1 and R_2. Here R_1 has to be made to change depending on the same environmental parameter that affects the basic transducer [See Section 13.7.5 for one application].

2.3 AC Bridges

The arms of an AC bridge can be composed of resistances, capacitances, inductances, mutual inductances and their combinations. The frequency of supply also enters as a parameter. Further the unbalance brought about by the physical variable and its change can be in terms of amplitude and phase. All these contribute to a variety of possibilities. However practical considerations limit the choice possible for use as a transducer bridge to a few selected combinations only [Harris]. Hence, we focus attention only on these.

2.3.1 Possible Configurations

Referring to Figure 2.6, when the bridge is balanced,

$$V_o = 0 \tag{2.49}$$

With,

$$Z_1 = R_1 + jX_1 \tag{2.50}$$

$$Z_2 = R_2 + jX_2 \tag{2.51}$$

$$Z_3 = R_3 + jX_3 \tag{2.52}$$

$$Z_4 = R_4 + jX_4 \tag{2.53}$$

under balanced conditions, we get,

$$\frac{R_1 + jX_1}{R_2 + jX_2} = \frac{R_4 + jX_4}{R_3 + jX_3} \tag{2.54}$$

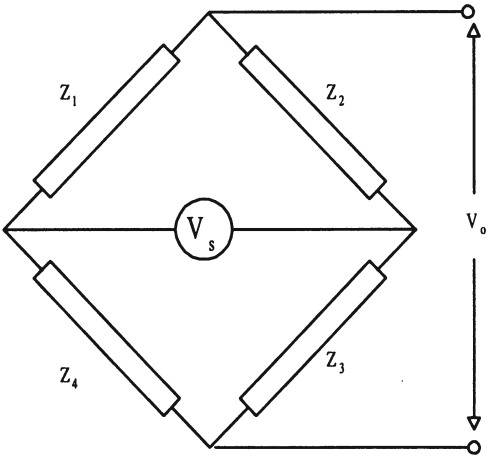


Figure 2.6 Four arm bridge

In general, the equality can be satisfied in infinite ways. Each impedance can have different phase angles and satisfy balance conditions. However, angles other than 0° or 90°, call for at least two elements to be used in the concerned arm. Since it does not offer any specific benefits, despite the increase in the number of components, complexity and cost, the same is avoided (except in rare cases as mentioned below). Thus, two arms at least will be pure resistances or reactance's. There are only a few possibilities conforming to this: -

⇒ Z_1 and Z_2 are pure resistances – R_1 and R_2 – and their ratio is a pure number.

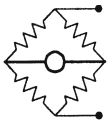
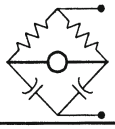
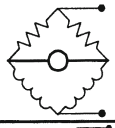
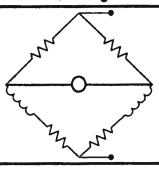
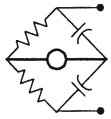
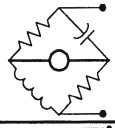
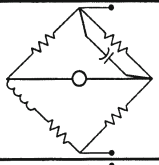
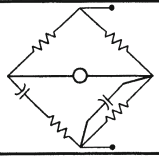
⇒ Z_1 is a resistance R_1 and Z_2 a pure reactance or *vice versa*. Further, pure inductances are not realisable in practice. Hence, choice of Z_2 is restricted to that of a capacitance. Here the ratio Z_1/Z_2 is purely imaginary with positive or negative sign.

⇒ Since pure inductances are not realisable in practice, bridge configurations involving them are modified to suit their series resistances also. These are, possibly, the only cases using complex ratios for the bridge.

Table 2.2 shows the bridge configurations under all the above categories. Apart from the above, one may use mutual inductance bridges also. These are treated separately. Bridges in 2nd and 5th rows of the table, are the same; the supply and the output terminals have been interchanged. This changes the ratio from a purely real number to a purely imaginary one. The imaginary ratio configuration offers better sensitivity. Despite this, the real ratio configuration is preferred, since it is more

advantageous from circuit point of view. The configuration in 4th row is also of this type. Its counterpart with complex ratio is not listed separately in the table.

Table 2.2 Classification of 4-arm type AC bridges

Sl. No	Type of ratio	Bridge configuration	Balance conditions	Remarks
1	Real number		$\frac{R_1}{R_2} = \frac{R_4}{R_3}$	Wheatstone bridge configuration; rarely used as an AC bridge
2	Real number		$\frac{R_1}{R_2} = \frac{C_3}{C_4}$	Used for capacitance transducers
3	Real number		$\frac{R_1}{R_2} = \frac{L_4}{L_3}$	Not practical due to the inductances not being ideal
4	Real number		$\frac{R_1}{R_2} = \frac{R_4}{R_3} = \frac{L_4}{L_3}$	Used for inductance transducers
5	Imaginary number		$R_1C_2 = R_4C_3$	Can be used for capacitance transducers; but the scheme of Sl. No. 2 above preferred
6	Imaginary number		$R_1R_3C_2 = L_4$	Not practical due to the inductances not being ideal
7	Complex ratio		$\frac{R_1}{R_2} = \frac{R_4}{R_3}$ $R_1R_3C_2 = L_4$	Can be used with inductance transducers
8	Real number		$R_1 = 2R_2$; $R_4 = R_3$ $C_3 = C_4 = C$	Used for frequency transducers - Wein bridge

2.3.2 Sensitivity of Unbalanced AC bridges

The bridge configuration is shown in Figure 2.6. The output voltage under unbalanced conditions is

$$V_o = \left(\frac{Z_1}{Z_1 + Z_2} - \frac{Z_4}{Z_3 + Z_4} \right) V_s \tag{2.55}$$

Let

$$Z_1 = Z_0 \tag{2.56}$$

correspond to the balance condition and let

$$Z_1 = Z_0 + \delta Z \tag{2.57}$$

and

$$a = \frac{Z_3}{Z_4} = \frac{Z_2}{Z_0} \tag{2.58}$$

Substituting in Equation 2.55 and simplifying with the assumption $\delta Z << Z_0$,

$$\frac{V_o}{V_s} = \frac{a}{(1+a)^2} \left[\frac{\delta Z}{Z_0} - \frac{1}{1+a} \left(\frac{\delta Z}{Z_0} \right)^2 \right] \tag{2.59}$$

Retaining only the first degree term in Equation 2.59,

$$\frac{V_o}{V_s} = \frac{a}{(1+a)^2} \frac{\delta Z}{Z_0} \tag{2.60}$$

$$\therefore S = \frac{V_o / V_s}{\delta Z / Z_0} = \frac{a}{(1+a)^2} = \frac{1}{a + 2 + (1/a)} = \frac{1}{T} \tag{2.61}$$

S is a maximum when $\frac{a}{(1+a)^2}$ is a maximum, *i.e.*, when

$$T = 2 + a + \frac{1}{a} \tag{2.62}$$

is a minimum. Let

$$a = \alpha \exp^{[j\theta]} \tag{2.63}$$

Substitution in Equation 2.62 and simplification gives,

$$T = 2 + \left(\alpha + \frac{1}{\alpha} \right) \cos\theta + j \left(\alpha - \frac{1}{\alpha} \right) \sin\theta \tag{2.64}$$

T being a complex function of two variables, derivation of maximum sensitivity conditions is cumbersome here. Two specific cases are considered:

Case 1: θ is a constant and α is varied.

When $\alpha = 1$, T is a real quantity given by,

$$T_0 = 2 + 2\cos\theta \tag{2.65}$$

Equation 2.64 shows that for every other value of α, Real part of $T > T_0$ and the imaginary part is non-zero. Hence T_0, given by Equation 2.65, represents the minimum value of T. Further, T_0 itself is minimum and equal to zero, when $\theta = \pi$ radians. This corresponds to infinite sensitivity of the bridge.

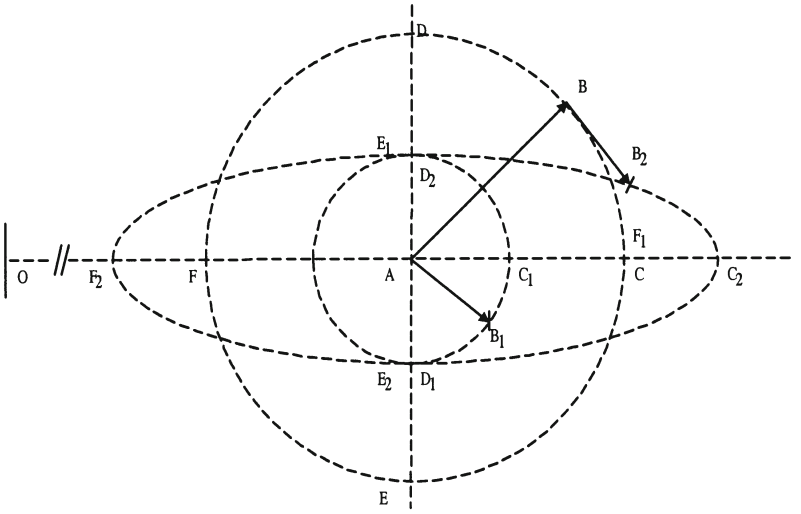


Figure 2.7 Locus of S as the phase angle of a is varied over the full range with its magnitude remaining constant.

Case 2: α is a constant and θ is varied.

The phasor diagram and the loci for a specific α value are shown in Figure 2.7 where,

$$OA = 2 \tag{2.66}$$

$$AB = \alpha \exp^{[j\theta]} \tag{2.67}$$

$$AB_1 = BB_2 = \frac{1}{\alpha} \exp^{[-j\theta]} \tag{2.68}$$

$$OB_2 = T \tag{2.69}$$

The x and y co-ordinates of T are,

$$x_T = 2 + \left(\alpha + \frac{1}{\alpha}\right)\cos\theta \tag{2.70}$$

$$y_T = \left(\alpha - \frac{1}{\alpha}\right)\sin\theta \tag{2.71}$$

The locus of T is obtained by eliminating θ from Equation 2.70 and Equation 2.71. This gives,

$$\left(\frac{x-2}{\alpha + (1/\alpha)}\right)^2 + \left(\frac{y}{\alpha - (1/\alpha}\right)^2 = 1 \tag{2.72}$$

This is the equation of an ellipse with $[\alpha + 1/\alpha]$ and $[\alpha - 1/\alpha]$ as the major and minor axes respectively. As θ varies from 0 to 2π radians,

$\Rightarrow$ the locus of B is a circle of radius α with centre at A;

$\Rightarrow$ the locus of B_1 is a circle of radius $(1/\alpha)$ with centre at A and

$\Rightarrow$ the locus of B_2 is an ellipse $B_2C_2E_2F_2D_2$.

T is a minimum at F_2 for which,

$$\theta = \pi \tag{2.73}$$

$$T_{min} = 2 - \alpha - \frac{1}{\alpha} \tag{2.74}$$

For

$$\alpha = 1 \tag{2.75}$$

$$T_{min} = 0 \tag{2.76}$$

This corresponds to

$$S \rightarrow \infty \tag{2.77}$$

which has already been considered in Case 1 above. Ideally for $\theta \rightarrow 180°$, we get $S \rightarrow \infty$. The sensitivity increases to very high levels. This corresponds to the use of a capacitance and an inductance in adjacent arms of the bridge and the bridge working under resonance conditions. Any slight variation in the value of the capacitance, inductance or the frequency upsets resonance. The sensitivity decreases abruptly. The situation is not desirable from a transducer point of view. Hence, the scheme is not of any practical utility.

The detailed analysis on the lines of the Wheatstone bridge done earlier, is not attempted here. This is to avoid repetition and the complexity in algebra without any new significant results. However the following are noteworthy: -

⇒ The sensitivity of the bridge for any complex ratio, is higher than that with a real ratio. For any given angle θ, the maximum sensitivity is

$$S_{max} = \frac{1}{2 + 2\cos\theta} \tag{2.78}$$

> ¼ (The sensitivity for the corresponding Wheatstone bridge).

For,

$$\theta = 90° \tag{2.79}$$

$$|S|_{max} = \frac{1}{2} \tag{2.80}$$

⇒ The non-linearity (to a first order) is introduced by the term involving $(\delta Z / Z_0)^2$ in Equation 2.59. Through an analysis done on the same lines as in Section 2.2 with the Wheatstone bridge, one can conclude that the maximum permissible range for $(\delta Z / Z_0)$ is 0.1 % to 0.2 % (*i.e.*, without affecting the linearity).

⇒ If two adjacent arms of the bridge have sensors in differential mode, the impedance of one increases from Z_i to $(Z_i + \delta Z)$, while the impedance of the other decreases to $(Z_0 - \delta Z)$. The result is an increase in the sensitivity by 100%. Such a configuration is often in use.

⇒ Transducer bridges with sensors in diagonally opposite arms, or in all the four arms, are rarely used.

⇒ The output voltage of the bridge is a modulated carrier.

- Its frequency is the same as that of the bridge-supply frequency.
- Its amplitude is proportional to the amplitude of the bridge-supply voltage, sensitivity and the percentage change in the sensing impedance.
- The phase angle of the output voltage is the sum of the phase angles of the sensitivity and the ratio $(\delta Z / Z_0)$.

2.3.3 Transducer with Off-Balance AC Bridge

The AC bridge configurations, used so far, operate close to the balance conditions. At input zero, the output is also zero. The schemes operate as double sideband modulators with suppressed carrier. A simpler alternative is to operate the bridge at definite off-balance conditions. The bridge scheme shown in Figure 2.8 is typical.

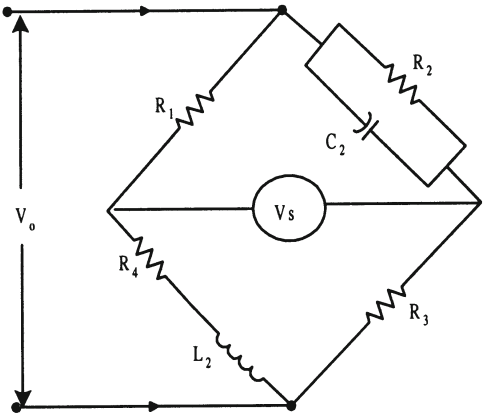


Figure 2.8 A typical off-balance AC bridge

Since the bridge is not balanced, we get V_0 at the same frequency as the input with definite amplitude. C_2 or L_4 can be the sensor. In either case, the bridge behaviour is similar. Taking L_4 as the sensor, let L_0 correspond to the zero input conditions. If L_4 increases, V_0 also increases in amplitude. If L_4 decreases, the amplitude of V_0 decreases correspondingly. The normal practice is to use an envelope detector and get a DC voltage proportional to the amplitude of V_0 [See Section 6.2.1]. As L changes, the magnitude of this voltage also changes correspondingly. Another DC voltage – constant in magnitude (bias suppression voltage) – is subtracted from this such that under zero input conditions the net output is zero. The difference voltage is a true replica of the input. The corresponding instrumentation scheme is shown in block diagram form in Figure 2.9. The waveforms, at key points, are also shown sketched.

This is done here to draw attention to certain working aspects of the scheme: -

- ⇒ The scheme is comparatively simple in concept and design. Its costs are also low.
- ⇒ The output is formed as the difference between two DC voltages (block D in Figure 2.9). The bridge output amplitude (block B), changes with input supply. To neutralize the corresponding error, the DC compensation voltage too can be made proportional to the input to the bridge. Despite this, these two voltages need not track each other sufficiently closely. This is a new source of error and drift, which is not present in the bridges considered so far. The precision possible with the bridge, is correspondingly lower. (Note that with the other bridges, change in input does not affect the zero but affects the sensitivity. Here change in the input affects the zero as well as the sensitivity).

The arrangement is useful for some low-cost instrumentation schemes where high accuracy is not demanded.

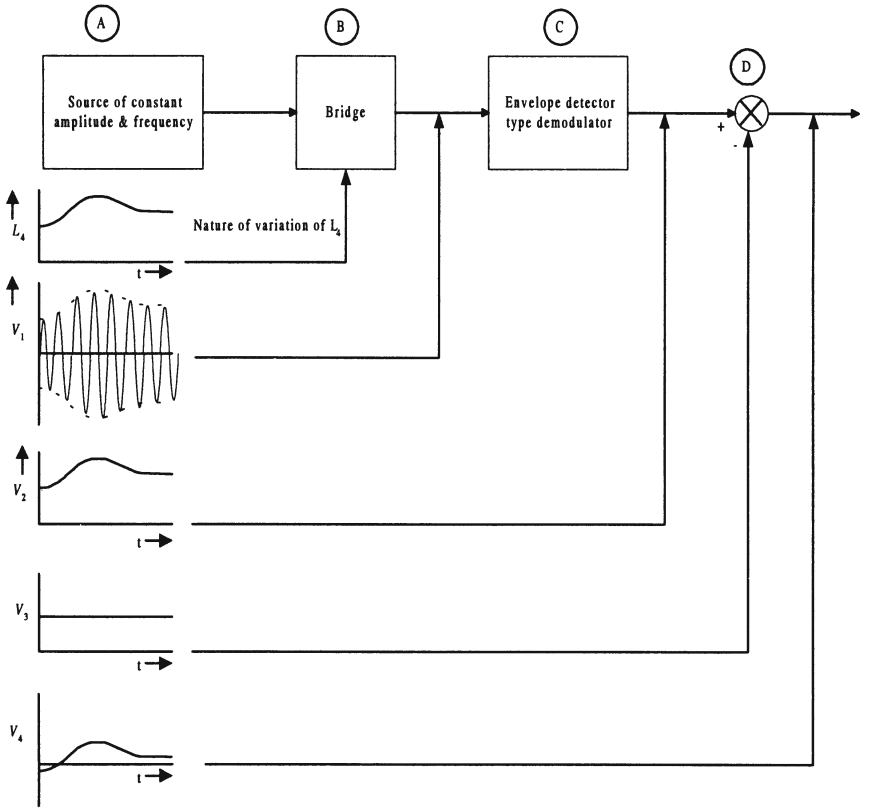


Figure 2.9 Unbalanced AC bridge type sensor with associated signal processing circuit blocks.

2.3.4 Wein Bridge

The Wein bridge is well suited to detect frequency deviations. Due to its out of the way nature, a separate analysis is in order. The bridge is shown in Figure 2.10.
For the bridge we have,

$$\frac{V_o}{V_s} = \frac{R_1}{R_1 + R_2} - \frac{Z_4}{Z_4 + Z_3} \tag{2.81}$$

where Z_3 and Z_4 are the impedances of the respective branches. The component values are normally chosen such that,

$$R_1 = 2R_2 \tag{2.82}$$

$$C_3 = C_4 = C \tag{2.83}$$

and,

$$R_3 = R_4 \tag{2.84}$$

Substituting these in Equation 2.81 and simplifying we get,

$$\frac{V_o}{V_s} = \frac{1}{3} - \frac{jRC\omega}{1 - R^2C^2\omega^2 + j3RC\omega} \tag{2.85}$$

For,

$$\omega = \omega_0 \tag{2.86}$$

Such that

$$RC\omega_0 = 1 \tag{2.87}$$

Equation 2.85 shows that the bridge is balanced and

$$V_o = 0 \tag{2.88}$$

For other values of ω, the bridge output can be obtained from Equation 2.85. Substituting,

$$\omega = \omega_0 + \delta\omega \tag{2.89}$$

in Equation 2.85, doing binomial expansion and retaining only the terms involving the lower powers of δω,

$$\frac{V_o}{V_s} = j\frac{2}{9}\frac{\delta\omega}{\omega_0} - \frac{4 - j3}{27}\left(\frac{\delta\omega}{\omega_0}\right)^2 \ldots \tag{2.90}$$

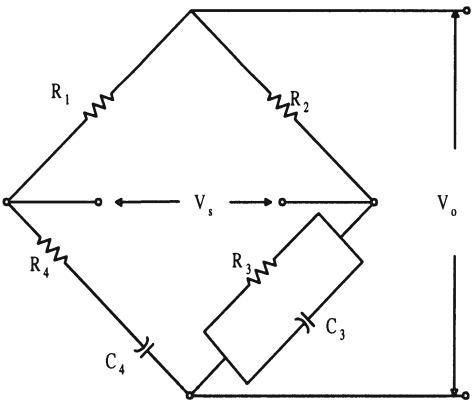


Figure 2.10 Wein bridge for frequency sensing

The magnitude of the output voltage is proportional to the frequency deviation if $\delta\omega << \omega_0$. The output voltage is in quadrature to the input. Its phase reverses as the frequency deviation reverses sign. These factors are to be considered (during demodulation), when the bridge output is processed further, to extract a signal proportional to the frequency deviation.

The sole sensing application of the Wein bridge is in sensing frequency deviations – and not in sensing the *R* and *C* values. Here, it is essential that the matching of the resistances and capacitances is done, to one or two orders of precision, better than that required of frequency deviation. This restricts the application mostly to the 50-to-100 Hz band of frequencies.

2.3.5 Mutual Inductance Bridges

Special high permeability cores like Permalloy, Mumetal *etc.*, have become available in recent years. One can have transformers with very low magnetising current, high core loss and tight coupling between the windings. These can be successfully used to form transducers. Consider a bridge shown in Figure 2.11 (a), where *AB* and *AD* are two inductances wound on the same core. The equivalent circuit of the bridge where the coupled set of inductances is replaced by an equivalent set of three inductances, without coupling, is shown in Figure 2.11 (b). With the use of special cores mentioned, coupled with good winding practice, one can get a very good coupling between the two sides. Z_1 and Z_2 are the impedances in the other two arms of the bridge. Both of these should be of the same type and have the same phase angle (at balance). One possible configuration of the bridge is shown in the figure.

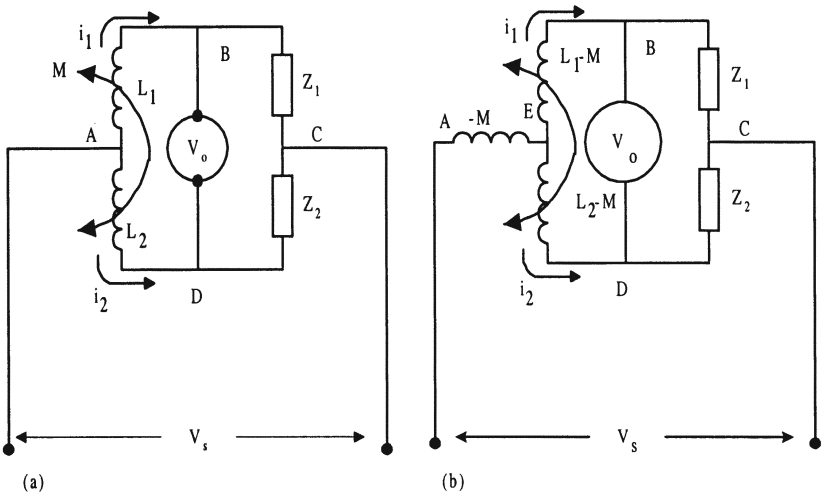


Figure 2.11 Inductively coupled ratio arm bridge. (a) Bridge circuit (b) Equivalent circuit of the bridge without the mutual coupling.

For the bridge we have,

$$V_{AC} = i_1 L_1 s + i_1 R_1 - i_2 M s + i_1 Z_1 \tag{2.91}$$

$$= i_2 L_2 s + i_2 R_2 - i_1 M s + i_2 Z_2 \tag{2.92}$$

where M is the mutual inductance between the two sides and s is the Laplace variable. At balance we have,

$$\frac{Z_1}{R_1 + j\omega(L_1 - M)} = \frac{Z_2}{R_2 + j\omega(L_2 - M)} \tag{2.93}$$

$\Rightarrow$ The bridges of the type under discussion are called 'Inductively Coupled Ratio Arm Bridges'. In all inductively coupled ratio arm bridges, the coupling coefficient will be 0.999 or better. Hence the voltage drops across self-inductances L_1 and L_2, will be practically neutralised due to the drop in

M. The net voltage drop across AD and AB will be respective resistance drops.

⇒ Due to the use of high μ cores like permalloy, $j\omega L_1$, $j\omega L_2$ and $j\omega M$ will be very large compared to R_1 and R_2. From Equation 2.93 we have,

$$\frac{Z_1}{Z_2} = \frac{R_1 + j\omega(L_1 - M)}{R_2 + j\omega(L_2 - M)} \tag{2.94}$$

Let,

$$L_1 = cN_1^2 \tag{2.95}$$

$$L_2 = cN_2^2 \tag{2.96}$$

and

$$M = kcN_1N_2 \tag{2.97}$$

N_1 and N_2 are the number of turns used for L_1 and L_2 respectively. c is a constant and k – the coefficient of coupling between the windings – is another constant. Further, the same winding wire is used to form the two inductances L_1 and L_2. Thus, we have,

$$R_1 = dN_1 \tag{2.98}$$

and,

$$R_2 = dN_2 \tag{2.99}$$

where d is another constant. Substitution of these in Equation 2.94 and the use of the fact that $k >> 0.999$ leads to,

$$\frac{Z_1}{Z_2} = \frac{N_1}{N_2} \tag{2.100}$$

Thus, the two branch impedances are in the same ratio as the respective number of turns.

⇒ The two resistance drops are equal. Since only these two resistance drops contribute to V_{AB} and V_{AD}, these two are equal. Hence once the turns ratio is selected, the two voltage drops, the current divisions, bridge balance *etc.*, are all governed by it. The circuit parameters like core inductance, resistance (and their variations due to temperature changes), *etc.*, do not affect the bridge operations.

⇒ $V_{AB} = V_{AD} = i_1R_1 = i_2R_2$. These voltages are quite small compared to $V_{BC} = V_{DC}$. Hence, if point A is grounded or kept near ground potential, points B and D are also close to ground potential. Thus, the currents through stray capacitances, leakage currents and effects of inter-turn capacitances are all reduced substantially. Further by adopting bifilar windings and a graded winding arrangement, potentials of corresponding points of the two halves of the winding, track each other very closely. This symmetry ensures equality or proportionality of the leakage currents as the case may be, in the two halves. All these factors contribute to the precision of the bridge substantially.

⇒ At balanced conditions, the core operates at zero flux level. Thus, the high initial permeability of the core decides the inductance values throughout the operation. This also contributes to the high value of coupling between the two halves.

For small deviations from balance, the analysis is easy. The voltage drop across AB and AD being very small, the full supply voltage appears across the impedances Z_1 and Z_2. Hence,

$$I_1 = \frac{V_s}{Z_1} \tag{2.101}$$

$$I_2 = \frac{V_s}{Z_2} \tag{2.102}$$

For small changes in Z_1 (or Z_2), the current remains unaffected. Hence, the output voltage due to a change δZ in Z_1 from balance becomes,

$$V_o = I_1 \delta Z = V_s \frac{\delta Z}{Z_1} \tag{2.103}$$

$$\therefore S = \frac{V_o / V_s}{\delta Z / Z_1} = 1 \tag{2.104}$$

The bridge offers unit sensitivity (Contrast it with a sensitivity of ¼ in the Wheatstone bridge case). Once again, the sensitivity is independent of the other circuit parameters.

One can operate the bridge with the inductively coupled arms on the detector side. The behaviour and analysis are similar to the case above. One can also use one set of coupled inductances on the supply side as here and another on the detector side. Such a configuration is successfully used in precision measurements. However the scheme is not in vogue in instrumentation schemes - perhaps size, complexity and hence the higher-cost, are the deterrents.

2.4 Oscillator Type of Transducers

The bridge type transducers considered thus far, provide an amplitude modulated output. They require a separate and suitable source of AC supply. An alternate approach in vogue uses frequency modulation. An FM scheme is attractive at least for the following to two reasons: -

- ⇒ Whenever the basic sensor is of the inductive or of the capacitive type, it can be directly incorporated into the oscillator circuit.
- ⇒ Once frequency modulated, the signal information is intact. An FM signal is amplified, transmitted, and processed with much less effect on signal to noise ratio as compared to an AM signal. This has been a primary motivating factor in the adoption of FM as compared to AM.

With the FM scheme, the signal transducer and the modulator are integral in nature. The inductance or capacitance, which is the sensor, forms one arm of an *LC* tank circuit around which the oscillator is built. The oscillators are of the Hartley, Colpitts or of the tuned *LC* tank circuit type[2]. The frequency of oscillation is

[2] Many other types of oscillator circuits are in vogue [Terman, Tietze *et al.*,]; they are not used with transducers – presumably their lower sensitivity is the main deterrent.

decided by the *LC* tank circuit. All the configurations used are of one of the two types in Figure 2.12.

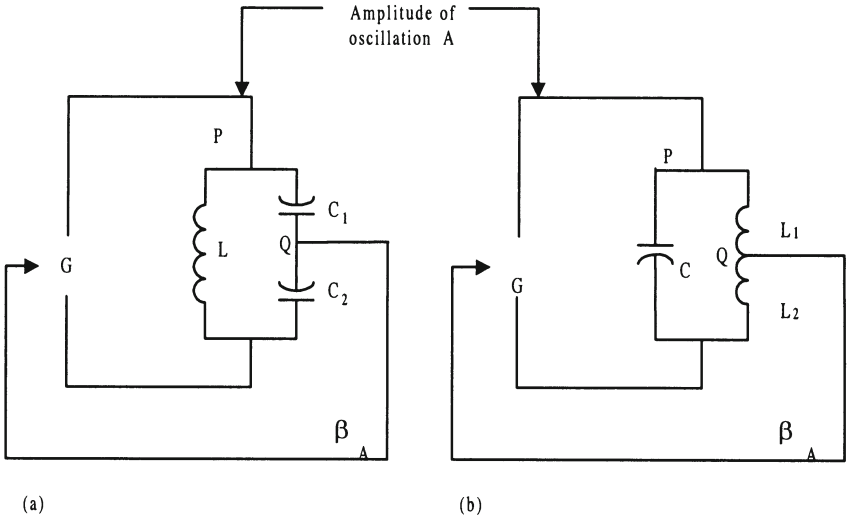


Figure 2.12 Two types of circuit configurations used with oscillator type of transducers

The tank circuit voltage has an amplitude of oscillation *A* at point *P*. A fraction of this (appearing across *L* or *C* as the case may be) is tapped at *Q*. This is amplified by amplifier of gain *G* and fed back to the tank. The arrangement is regenerative in nature and the oscillations build up. As the amplitude of oscillation increases beyond a limit, the amplifier gain reduces and stabilises the oscillation. A treatment of oscillator theory to facilitate circuit design of the secondary transducer, is too detailed to be dealt with, here [Minorsky]. Nevertheless, we highlight the major issues involved to bring them into focus: -

⇒ With an ideal *LC* tank, the oscillations are self-sustaining in nature. However, due to the dissipation – mainly in *L* – the oscillations will be damped out. The role of the amplifier is to make up for this power loss and thus sustain the oscillation. Power rating of the amplifier is decided by the circuit *Q*. Quality components are used for the tank circuit to minimise the power loss and hence the strain on the amplifier.

⇒ The amplifier gain is a function of the oscillator amplitude. As the amplitude builds up, the gain reduces. The oscillation stabilises when

$$\beta = \frac{1}{G(A)} \tag{2.105}$$

where

β – fraction of the output fed back – is the feedback factor
A is the amplitude of oscillation at the amplifier output and
G is the gain of the amplifier – an inverse function of *A*.

⇒ As the circuit *Q* improves, the power loss in the tank circuit reduces. In general, this reduces the power rating required of the amplifier. However, as *Q* increases the amplitude stability of the oscillator is adversely affected. The

speed of response of the transducer too reduces. Hence, one strikes a compromise and does not use a Q better than 10 to 30.

⇒ The frequency of oscillation is given by

$$f = \frac{1}{2\pi}\frac{1}{\sqrt{LC}} \tag{2.106}$$

where L and C are the total inductance and capacitance in the tank circuit. If the amplifier gain changes, to a first order of approximation, only the amplitude of oscillation is affected. Similarly change in the power supply voltage can affect the oscillator amplitude but the frequency is affected only to a less extent.

⇒ Specifically if the gain G changes by δG, the change in frequency has the form,

$$\delta f = kf\left[\left(\frac{\delta G}{G}\right)^2\right] \tag{2.107}$$

where k is a constant and f [ ] signifies a function of the argument. A 1% change in the gain affects the frequency by 0.01%. However gain stabilisation is highly desirable (Note that change in gain affects the oscillator amplitude). For the same reasons, the power supply voltage is to be stabilised too.

⇒ With today's transistor amplifiers, the gain may be decided by h_{fe} (or the forward transconductance as the case may be) and other circuit parameters. h_{fe} is a function of the junction temperature and operating conditions. With changes in these, the oscillator amplitude can drift. Hence the amplifier configuration chosen has to be such that the gain is a function of a ratio of element values and hence stable.

⇒ With inductive transducers, the zero-signal input-inductance will be in the mH range. The zero-signal frequency will be in the kHz range. Change in the position, orientation *etc.*, of any metal or metallised component in the vicinity, can affect the inductance and cause error. Care should be taken to eliminate such possibilities.

⇒ With capacitance transducers, the frequency is in the MHz range – this is because the zero-input capacitance is in the pF range. An adverse effect of this, is the possibility of the capacitance getting affected substantially even with small changes in the transducer orientation, geometry *etc.* Circuit layout, engineering, grounding *etc.*, has to be done with extreme care.

⇒ With capacitance type sensors, due to the low value of the capacitances involved, the amplifier-input capacitance comes into fray in determining the frequency of oscillation. Since this can change from unit to unit, consistency in performance is the victim. Such cases warrant selection of amplifiers and matching them to the sensor capacitance on a unit by unit basis.

⇒ The amplifier output is used directly to feed the tank circuit. If a load is connected to the output, it gets added to the tank circuit in parallel. In turn, it affects the amplitude of oscillation. It may also affect the frequency, if the load is reactive in nature. Changes in load if any, manifest as corresponding changes in the oscillator output frequency and amplitude. To avoid this, a separate load tap is to be provided on the oscillator. One solution is to separate the load block from the oscillator block; this decouples the load from the oscillator completely.

2.4.1 Sensitivity of Oscillator Type Transducers

The sensitivity can be obtained directly from the expression relating the frequency to the circuit L and C values. The output is the frequency here (and not the amplitude of the oscillator output); hence, one has to relate the change in the sensor characteristic (δL or δC as the case may be) to the resultant change in the frequency. Differentiation of Equation 2.106 with respect to L and simplification gives,

$$\frac{\ddot{a}f}{f} = \frac{1}{2}\frac{\ddot{a}L}{L} \tag{2.108}$$

$$\therefore S = \frac{\delta f/f}{\delta L/L} = -\frac{1}{2} \tag{2.109}$$

Proceeding in a similar manner we get the sensitivity for the capacitance transducer as,

$$S = \frac{\delta f/f}{\delta C/C} = -\frac{1}{2} \tag{2.110}$$

In both cases, the sensitivity is twice that of the Wheatstone bridge with one sensing arm (Note the negative sign in both the cases).

2.5 Feedback Type Transducers

The resolution of a conventional well-designed instrumentation scheme is decided *prima facie* by the accuracy of the primary transducer. There are situations where the primary transducer is comparatively crude and direct amplification, compensation or other signal processing activities do not ensure a satisfactory instrumentation scheme. However by an ingenious feedback scheme, the function of the primary transducer itself can be replicated and good overall precision achieved [Neubert].

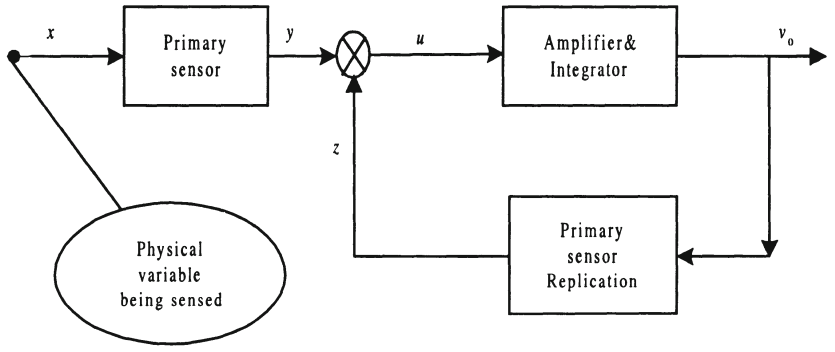


Figure 2.13 Block diagram schematic of a feedback transducer

Figure 2.13 shows the feedback transducer schematic in block diagram form. x represents the physical variable being sensed by the primary transducer. Its output y may be in the form of a voltage, a current or in any other form. It is compared with a feedback variable z and the difference is processed further. If the difference is a voltage or a current, it is amplified and integrated directly. If it is in some other form, the transducer converts it into an equivalent output voltage V_o. V_o is amplified, integrated and fed back. In the former arrangement, the fed-back signal z is subtracted from y. Only the difference is processed. In the latter case, V_o is used as the input to a block, which simulates the role of the primary transducer. The replication – due to its vicinity to the primary transducer – is affected in the same fashion as the primary transducer.

Under normal working conditions,

$$u = y - z \tag{2.111}$$

the difference signal will be identically equal to zero. If non-zero, the same will be integrated and the output V_o will continuously increase or decrease depending on whether it is positive or negative. Through the feedback path this is converted into corresponding increase or decrease in z. The integration action continues until u becomes zero. Hence under normal working conditions,

$$z = y \tag{2.112}$$

Since the replication is affected in the same manner as the primary transducer due to the extraneous agencies, V_o becomes a faithful electrical equivalent of the physical variable under measurement.

Current measurement using Hall effect, self-balancing potentiometer used with thermo-couples *etc.*, are typical examples of feedback transducers. The following observations are in order here: -

- ⇒ Feedback type transducers are more complex than direct or open-loop type transducers.
- ⇒ The speed of response of the feedback type transducer, is one order lower than that of the open-loop type.
- ⇒ The feedback type transducer is used only in such situations where the open loop type is otherwise unsuitable. Typically, it overcomes one or two limitations of the open-loop type transducers.

3 Operational Amplifiers

3.1 Introduction

Circuit schemes using discrete active components and detailed design procedures for each, are available in literature [Design of each analog processing block separately using discrete components, is not done any longer]. The opamp has become central to all such design. The versatility of the opamp as a functional module, its economic availability, numerous units meeting different stringent specifications - all these have contributed to its widespread use as the central unit for analog signal processing. With such a key role played by the opamp, its characteristics and limitations warrant a detailed discussion [Graeme, Wait *et al.*].

3.2 Ideal Opamp

The ideal opamp is shown as a block in Figure 3.1. It has two inputs termed 'Inverting' and 'Non-inverting' respectively. Signs ' – ' and ' + ' specify these. The opamp gain is shown as A. The output is V_o.

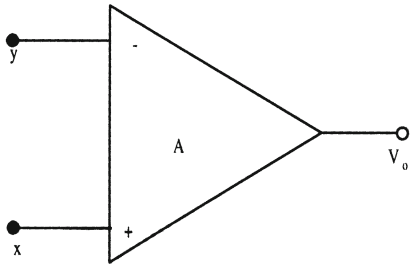


Figure 3.1 Ideal opamp - block diagram representation

The relation connecting the two inputs and the output is given by

$$V_o = A(x - y) \tag{3.1}$$

where y and x are given as inputs at the inverting and non-inverting input leads respectively. The 'ideal conditions' warrant some elaboration: -

- ⇒ The gain is infinitely large.
- ⇒ The bandwidth of gain extends to the full frequency spectrum (0 to ∞ Hz).
- ⇒ The phase shift introduced by the opamp is zero at all the frequencies.
- ⇒ V_o can take up any value dictated by the gain and the difference $x - y$.

T. R. Padmanabhan, *Industrial Instrumentation*
© Springer-Verlag London Limited 2000

⇒ There is a linear relationship between V_o and $x - y$.
⇒ For all values of inputs x and y, the current drawn at the respective inputs is zero *i.e.*, the input impedance is infinite.
⇒ If x and y increase or decrease equally, the output remains unaffected.
⇒ The output impedance is zero; if a load resistance is connected to V_o, it remains unchanged.
⇒ If $x - y$ is zero, despite the infinite gain, the output remains zero.
⇒ The noise voltage and the noise current, introduced by the opamp, are zero.

Due to its professed infinite gain, the opamp is rarely used in the open loop form shown. Feedback in one or more forms is provided. The type of feedback provided and circuit configurations used, differ from application to application. These will be discussed in sufficient detail in the ensuing chapters.

The practical opamp differs from the ideal one in all respects listed earlier. In one opamp some selected parameters may come closer to their respective abstractions at the expense of others. In another, a different set of parameters may be close to their ideal values. A variety of such trade-offs is possible. Depending on the specific application, – *i.e.*, the functional module desired – the opamp has to be selected. Opamps are specified in terms of a set of performance parameters, which are essentially measures of the abstractions above. Significance of these performance specifications, trade-offs involved in realizing them and the importance of each *vis-à-vis* individual application, form the subject matter of the present chapter.

3.3 Specifications of Opamps

The first stage of an opamp – at the input side – is a difference amplifier stage. Subsequent stages do level translations and impedance conversion, to provide output at low impedance and centred around zero volts. The first stage is critical *vis-à-vis* all input specifications. It provides the maximum gain and in many respects, the opamp performance is decided by it. The subsequent stages do the padding up (They too amplify!). However, this is too simplistic a model to be of use in design, discussions *etc*. Suffice it to say that the input stage is the key stage (and to some extent the output stage too). The final stage provides a low impedance output. Further, it provides linear output changes over the full range of inputs.

3.3.1 Open Loop Gain

The total loop gain is the product of gains of individual stages. Normally, only the order of the gain (or its minimum value) matters and not it's exact magnitude. The advantages of high gain are the following: -

⇒ Closed loop gain accuracy is better maintained.
⇒ Error due to input offset voltage is more effectively reduced.
⇒ Output impedance is reduced.
⇒ Closed loop input-output characteristic is more linear.

The disadvantages of a high gain due to more stages are: -

⇒ More time delay to respond from input to output.

⇒ More phase shift from input to output.

⇒ Tendency for instability and oscillatory behaviour of the closed loop configuration.

The open loop gain is normally specified in dB, which represents the gain of the opamp at low frequencies. Open loop gain changes with load, ambient temperature and supply voltage; but such changes will not affect the open loop gain by more than a factor (say) of 10. Gain mostly increases by 0.5 % to 1.0 % per degree Celsius of change in operating temperature; it changes by less than 2 % for every percentage change in supply voltage. Opamp manufacturers continuously strive to increase gain by refinements, new and ingenious circuit configurations and so on. Typically, an opamp will have three stages in cascade, making up the gain.

3.3.2 Gain Bandwidth Product

For a given amplifier configuration, gain and bandwidth are inversely related. An increase in gain is achieved only at the expense of bandwidth. The Gain-Bandwidth product (usually referred to as 'GBW') is a good measure of the quality of an amplifier. The same holds good for the opamp also. An increase in GBW is brought about only by a technological improvement or a circuit innovation. The frequency-versus-gain characteristics of opamps have the forms shown in Figure 3.2. The gain is high at low frequencies; for compensated opamps, it rolls off at a steady slope beyond 10Hz to 100 Hz (characteristic B). For uncompensated types of opamps, the gain remains high up to much higher frequencies and rolls off abruptly (characteristic A). At the gain cross-over frequency f_c (normally in the MHz range) the gain drops down to unity – GBW is f_c MHz. The opamp will be normally used for signal processing in the closed loop configuration, up to an upper frequency limit of only about $f_c/1000$ to $f_c/100$. This ensures stable and accurate operation.

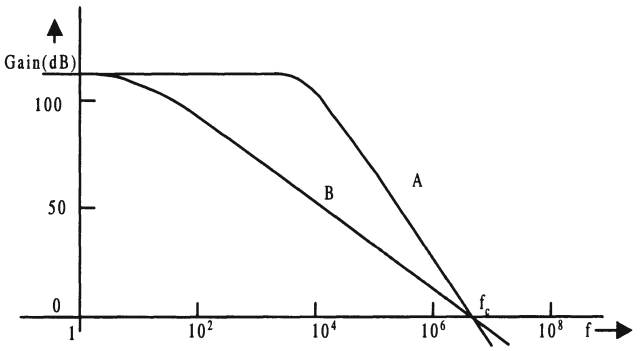


Figure 3.2 Frequency versus gain characteristic of an opamp: A is the characteristic of an uncompensated opamp and B that of a compensated one.

3.3.3 Phase Lag

The phase lag introduced by each stage of the opamp increases steadily with frequency. Hence, the overall phase lag also increases. Since the opamp is operated in closed loop fashion, the phase lag has to be kept in check to avoid instability or

oscillations. At the gain cross over frequency – *i.e.*, at f_c – the phase lag has to be less than 180°. Put another way, the gain should not fall steeper than 12 dB/decade in the vicinity of the cross over. This is acceptable only for configurations, which do not use external circuit elements causing additional phase lag in the feedback loop. With such configurations, the opamp lag has to be lower; this in turn restricts the bandwidth of operation further.

3.3.4 Range of Output Voltage

The output stage of any analog signal-processing block must have the provision for signal swings, up to the highest and down to the lowest levels. In the positive direction, normally, it extends up to 1V below the supply voltage; similarly, in the negative direction, it extends down to 1V above the supply voltage. Some opamps have a wider range ('rail-to-rail' operation). But at higher levels of the output voltage, the input-output relationship gets distorted. At input and intermediate stages, the output voltage swing is more restricted, and hence it is critical.

3.3.5 Linearity

The ideal input-output characteristic of an opamp will be linear over the whole range of inputs shown by line 'A' in Figure 3.3. But, since the output cannot

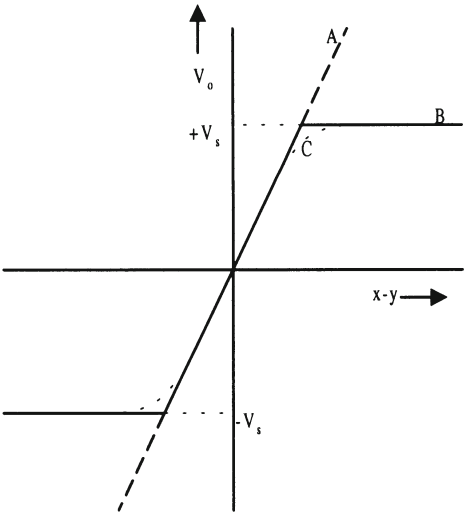


Figure 3.3 Ideal and actual input-output characteristics of the opamp. A shows the ideal characteristic, B shows an acceptable alternative to the ideal and C the actual characteristic.

exceed the power supply levels of the opamp in either direction, an acceptable alternative to the ideal is the characteristic shown as 'B'. Here, the characteristic is linear in either direction until it attains the respective power supply level shown here as $+V_s$ and $-V_s$. In practice, this is not achieved. The corners of the

characteristic are well rounded off as shown by the characteristic 'C'. As the signal levels handled increase, the gain value decreases; this is the main contributor to the flattening of the characteristic.

When the opamp is working in closed loop fashion, the characteristic is pronouncedly linear – *i.e.,* the closed loop gain essentially remains constant. As the closed loop gain approaches the open loop gain, deviation of the characteristic from linearity increases. Thus, there is a need to use as high a value, of the ratio of open loop gain to closed loop gain, as possible. Most of today's opamps have gains in excess of 10^5. Linearity of the characteristic is mostly ensured to 0.1 % precision, over the full output voltage range, for closed loop gain values up to 100.

3.3.6 Input Currents

The input currents fix the operating points of the opamp suitably. More formally, they represent the currents required to be sourced or sunk at the two input leads, to ensure a zero output under zero differential input conditions (*i.e.*, $x - y = 0$). The magnitude and range of variations of input-currents form an important specification of any opamp. With the voltage type of signals being processed – as is the case mostly – the input currents (called 'bias currents' and termed i_b), should be as low as possible. This is needed at least on three counts: -

⇒ i_b is drawn from the signal source or the preceding signal processing stage. This loads the source. There is a need to keep the source loading as low as possible [See Section 1.5.12]. Such loading can be reduced only by selecting an opamp with low i_b or by comparatively involved and skilled additional design. Normally, the latter is avoided.

⇒ i_b values cause voltage drops in impedances in the inverting and non-inverting sides at the input. If the impedances in the two sides are equal and the currents – i_{b1} and i_{b2} – in the two halves are also equal, then the two voltage drops are also equal; $(x - y)$ remains unaffected. However, both x and y increase or decrease by the same amount causing an additional Common Mode input. This may lead to an error, whose magnitude is decided by Common Mode Rejection Ratio (CMRR) [See Section 3.3.10]. Inequality in the two i_b values, or the two impedances or their combination – all these can cause a spurious difference mode signal; *i.e.,* $(x - y)$ may be altered. The error due to this is much higher than that due to the common mode input .

⇒ As the i_b level increases, the noise current level also increases at the input. Its effect gets magnified in circuits having comparatively higher impedances at the inputs of opamps.

Opamp manufacturers adopt three approaches to reduce i_b.

⇒ At the input stage of the opamp (BJT type), use a difference amplifier stage with low values of collector current (i_c). In turn, i_b also reduces. This has two deleterious effects. Firstly, the higher values of the collector resistances used to achieve this, result in higher levels of noise voltage. Secondly, due to these higher values of resistances and low i_c levels, the drive currents available for the following stage (including the current required to charge the input capacitances of the following stage), also reduce. This affects the opamp response speed adversely. The bandwidth and the slew rate drop down conspicuously.

⇒ An alternative is to go for an improved technology. 'Super high β' transistors can be used at the input stage. These keep down i_b but retain i_c at high enough levels. The corresponding collector resistances are not unduly high. Thus, voltage noise level and speed are not adversely affected.

⇒ A second alternative is to use FETs at the input stage. Due to their very nature, i_b is reduced substantially. The offset current (I_{os}) also reduces, but its drift with temperature may remain. Due to the difficulty of matching the FETs in the IC form, the voltage offset can be substantial. The GBW product and the slew rate are not sacrificed despite the reduction in i_b.

3.3.7 Offset Voltage (V_{os})

Due to the asymmetry in different stages and shift in the operating points from desired levels, opamps require a definite amount of $(x - y)$ value (difference in inputs) to be maintained to make the output zero. This difference in the inputs is referred as offset[3]. In an AC coupled amplifier and other configurations, the offset is not a serious problem. But in DC coupled cases (as is the case with many instrumentation schemes), the offset voltage causes an error in the measurement. This warrants minimization of the offset voltage.

The offset can be high as soon as the opamp is powered up. As the thermal transients associated with the opamp and concerned equipment settle, the offset may settle down to specified values.

3.3.8 Input Offset Voltage Drift

An amplifier trimmed for offset at one temperature may not retain the zero level at other temperatures. With care, the trimming circuit can compensate for temperature variations also but this is at the expense of simplicity and cost. Such temperature changes can be external (ambient) or internal owing to the temperature gradient in the die itself. As far as the user circuit is concerned, the effect appears as a random drift in the output (which has a perceptible correlation with the ambient temperature). The offset drift is not a problem in AC coupled amplifiers or circuit schemes but it has enough nuisance value in DC coupled schemes (as is the case with many instrumentation schemes). Looked another way, good long term V_{os} stability *vis-à-vis* an instrumentation scheme, implies that the instrumentation scheme recalibration can be correspondingly infrequent.

Improvements in the precision and the circuit geometries and processes reduce drift. Thus improvements in technology have resulted in opamps of sufficiently lower drift levels. Some opamps starting with the classic 741, and its subsequent pin to pin replacements, provide for offset adjustments to be done at one circuit point of the input stage. With such adjustments the offset can be trimmed and reduced by one order.

One can add a pre-amplifier stage externally at the opamp-input stage and trim off the offset. This adds to the cost of the scheme substantially but improves

[3] In BJT opamps, this can be due to the difference in V_{be} values and the difference in the loads of the two halves of the input. In FET input opamps it is mainly due to the difference in the characteristics of the two input FETs.

performance. As an alternative, one can reduce offset by an intentional asymmetry introduced at the input and adjusted by trial and error. This low-cost low-quality solution lacks in product repeatability.

3.3.9 Input Offset Current and its Drift

The difference in the two input bias currents, is the input offset current (I_{os}). The offset current itself is of the same order as the bias current. The bias currents and hence the offset currents change with temperature. This change is conspicuous with FETs where the bias current doubles for every 10°C rise in temperature. Since the bias current levels in FET input (and MOS) opamps are small, designs with them use larger values of resistances. Due to lack of care in design or selection of components, the opamp drift may adversely affect the circuit behaviour. Changes in ambient temperature, temperature gradient in the chip die *etc.*, all these directly contribute to such deterioration in performance.

3.3.10 Common Mode Rejection

The opamp is expected to respond to only the difference between the two inputs x and y. If x and y both change by the same amount [Such equal inputs at x and y are referred to as 'Common Mode (CM)' inputs.], the output has to remain unchanged. In practice, such CM changes in input can have unequal effects in the circuit of the opamp. Eventually this can cause a change in the output. Thus, a CM input causes an output as if it is due to a difference between x and y. The 'Common Mode Rejection Ratio (CMRR)' characterises this as

$$CMRR = 20\log\left(\frac{2v_o}{x+y}\right) \tag{3.2}$$

CMRR may range from 40 dB for simple opamps, to 150 dB (minimum) for good quality opamps. Use of constant current sources and judicious use of current mirrors, improves the CM performance of opamps.

Some circuit configurations like inverting amplifiers are characterised by low CM input. For these, a high CMRR is not essential. However, buffers, non-inverting amplifiers *etc.*, see a high CM input.

3.3.11 Output Impedance

The output impedance of opamps is normally in the range of hundreds of ohms. Mostly, opamp-based signal processing is done up to the final power stage of an instrumentation scheme, but not at the final stage itself. Hence, the output current or power to be delivered by an opamp in a circuit is small and the output impedance is not a deterrent – provided, it is not unduly high. Further, due to the feedback configurations adopted, effective output impedance is reduced by the feedback factor.

Output impedance becomes a factor to be considered only under two conditions.

⇒ Some low cost configurations use the opamp to drive the final load directly. Here, a low output impedance is desirable.

⇒ With capacitive loads, a low output impedance is desirable to ensure a hard drive. Otherwise, the output rise will be sluggish.

If the output impedance of the opamp is reduced under hard drive conditions, the power supply drain can be high. It can cause a dip in the power supply and affect opamp performance adversely.

3.3.12 Slew Rate

Slew rate is the maximum rate at which the output of an opamp can change. Normally it is of the order of 1V per μs. It is an index of the performance of the opamp. The current drive capacity of the final stage, the resistance values used in the preceding stages and the type and quality of transistors used – all these affect the slew rate. A high slew rate is desirable for two types of situations: -

⇒ When the load at the opamp output is capacitive and a fast enough response is required.

⇒ When the opamp is used in a configuration to handle fast changing signals. The fastest rate of change of signal that the opamp can handle is decided by the slew rate.

A low output impedance is a prerequisite to get a high slew rate (but not *vice versa*). To obtain a high slew rate, every stage of the opamp has to be fast enough – *i.e.,* the drive capacity at every stage has to be high. The stage impedances have to be low and the currents high. The resulting supply current is high. The bias currents are also high. High drive capability at each stage results in an increase in bandwidth. In general, opamps with high slew rates have correspondingly high bandwidths. The current offsets are also high. Hence low drift and high bandwidth are conflicting requirements. Due to the reduced stage resistance values, the stage gains also reduce. Thus, higher slew rates are obtained at the expense of gain.

Enough care has to be exercised in the designs using high slew rate amplifiers. With capacitive loads the output may get overloaded. Similarly, care is called for, in designs involving fast rising signals and slew-rate-limited opamps. When the input rises faster than what the opamp can cope up with, spike voltages can appear at the opamp input terminals. These may load the source unduly and may even distort it.

3.3.13 Noise in Opamps

Every semiconductor component generates noise. In an opamp such noise is mainly due to the transistors and other p-n junctions at the input stage. Although such units in subsequent stages also generate noise, the effect of these on opamp performance is much smaller and hence negligible. The internal resistance elements also generate noise but these are too small in comparison and negligible. The equivalent circuit in Figure. 3.4 is a simplified working model of the opamp with its generated noise. The noise can be represented as a voltage noise (v_n) getting added in series at the input and a current noise (i_n) in parallel. The practical opamp with inputs A and B is replaced by an ideal opamp with C and D as input terminals. The noise voltage and current are added prior to it, to represent the actual opamp. The points C and D being fictitious – representing idealisations – are not accessible. All external connections to the opamp are made at points A and B only. Hence in any application the noise voltage and current enter the fray and cause corresponding

errors. The extent of error in each case depends on the circuit configuration used. These will be discussed in detail in the following chapter. If a signal source is connected in series between A and B, the voltage noise v_n gets added in series. In this respect its role is similar to the offset voltage V_{os}. Further, if the resistance of the source (R_s) is large, it causes a voltage drop R_s i_n through it. The same gets added in series with v_n. If R_s is small, to that extent, the noise R_s i_n is also small. Hence from the point of view of reducing current induced noise, it is desirable to keep R_s low. But often input configurations may dictate otherwise.

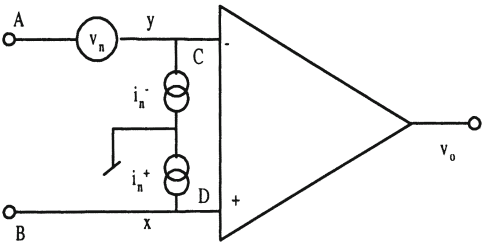


Figure 3.4 Opamp model inclusive of the internal noise

The externally connected resistances generate their own noise. These get added to the noise shown here. They are discussed in the following chapter in detail.

The presence of noise in opamps is a *fait accompli*; and one has to live with it. However, in any configuration of use of an opamp, one or two aspects of the signal only will be highlighted at the expense of others. For example, in an AC amplifier, a signal of a limited and specified bandwidth is amplified at the expense of others. By properly restricting the bandwidth to this range, noise outside this range is practically suppressed. A brief discussion of the nature of noise and its power spectral density *versus* frequency are in order here.

3.3.13.1 Schottky Noise (Shot Noise)

Schottky noise (also known as the shot noise) is a current noise, due to random spurts in the current, through the junctions in the transistors. All such Schottky noise gets added to the noise current shown as i_n in Figure. 3.4. The noise power is equally distributed in the band of interest. (Compare with Johnson noise in resistors in the next chapter). Further, the noise power is proportional to the current through the junction. The equivalent noise current is given by,

$$I_n^2 = 32.5\times10^{-8}\, IB \tag{3.3}$$

where

- I is the current through the device in pA.
- I_n is the rms value of the noise current in pA.
- B is the bandwidth of interest in Hz.

$$\therefore I_n = 5.4\times10^{-4}\sqrt{IB} \tag{3.4}$$

3.3.13.2 Flicker Noise (1/f Noise)

Flicker noise dominates at frequencies below 100 Hz or thereabout. It is thought to be the result of imperfect surface conditions of semiconductor devices. The noise power density, at any frequency, is inversely proportional to the frequency. The total flicker noise power (P) over a frequency band f_1 to f_2 is obtained as

$$P = \int_{f_1}^{f_2} \left[\frac{k}{f}\right] df \tag{3.5}$$

$$= k \ln\left(\frac{f_2}{f_1}\right) \tag{3.6}$$

where k is the constant of proportionality.

The flicker noise power over each decade can be seen to be constant. With a typical flicker noise of $1\mu V$ over a decade, over 9 decades upto 1Hz (say), we get the total noise voltage as $\sqrt{9\times1} = 3\mu V$. Note that 10^{-9} Hz = 30 years. Thus, though the flicker noise appears to increase with decrease in frequency, its total contribution to error over the nine decades from 10^{-9} to 10^{0}, will be substantially lower than the contribution due to the various extraneous factors [See also Section 7.4].

3.3.13.3 Popcorn Noise

Some transistors – especially in ICs – exhibit sudden spurt change in h_{fe}. These cause corresponding spurt change and hence noise in the transistor current – called the 'Popcorn Noise'.

3.3.13.4 Total Opamp Noise

⇒ All the above noise components are independent. Hence the total noise can be obtained as an equivalent rms noise as:-

$$I_n^2 = \bar{i_n^2} = \bar{i_1^2} + \bar{i_2^2} + \bar{i_3^2} + \ldots\ldots \tag{3.7}$$

where

- I_n is the total equivalent noise,
- $\bar{i_n^2}$ represents the mean square value of the total noise
- $\bar{i_1^2}$, $\bar{i_2^2}$, $\bar{i_3^2}$ represent the mean square value of noise from source 1, source 2 and source 3 respectively; and so on.

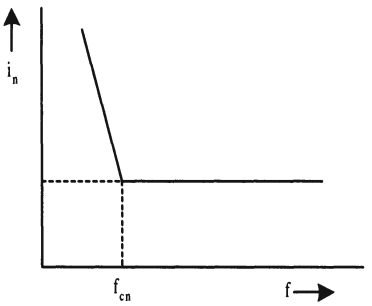


Figure 3.5 Nature of total noise spectral density of an opamp

Considering the current noise, the flicker noise dominates at low frequencies and the other noises – all put together – dominate at higher frequencies. When combined, the total noise spectral density has the form shown in Figure 3.5. It is characterised by a corner frequency f_{cn} and a steady value of noise power spectral

density beyond f_{cn}. Lower the value of the corner frequency, the better will be the noise performance of the opamp.

3.4 Opamp Characteristics – Trade-offs

The major characteristics of opamps were discussed in the last section. These are normally quantified through respective specifications. Some of these refer to the input side, some others to the output side and the rest to the overall performance. In general, if one demands stringent specifications in respect of one characteristic, it can be done only at the expense of another. These are highlighted through the matrix in Table 3.1. If two characteristics are directly related, – *i.e.,* when one increases, the other also increases – the same is indicated by a '++' sign in the corresponding cell. A '––' sign at the cell implies that the concerned characteristics are inversely related, – *i.e.,* when one increases, the other decreases. A '–' or a '+' symbol indicates that the concerned variables are similarly related but the relationship is rather weak. The following observations are in order here: -

⇒ The GBW and slew rate are directly related; increase of one, directly results in a corresponding increase of the other.

⇒ Increase in GBW or slew rate is achieved only with a corresponding increase in the supply current. Often it is accompanied by a larger V_{os} too. The offset voltage drift also may increase.

⇒ Any increase of input impedance reduces the bias currents as well as the bias current drift; but it increases the voltage noise and adversely affects the slew rate as well as the GBW.

⇒ Any increase in output voltage swing affects the GBW and the slew rate adversely.

Observations :-

- The input and output side specifications are generally independent.
- Supply Current (I_s) is generally an output side specification, since the major part of the supply current flows through the output stage.
- Since all the stages have a say in the Slew Rate (SR) and the Gain-Bandwidth product (GBW), these are closely related to the input and output side specifications.
- The tabular presentation here refers to one technology and one state of technology. Thus, it cannot be used to compare opamps 741 and OP07 or OP07 (BJT) and TL 08 [FET input]

3.5 Characteristics of Typical Commercial Opamps

A wide variety of opamps with different trade-offs in their specifications, is available commercially. A few have been selected and listed in Table 3.2 with their key specifications. The selection shows at a glance the variety in specifications and trade-offs possible. The following observations are in order here: -

Table 3.1 Qualitative relationships of opamp characteristics :- A '++' sign in a square means that both are directly related; a '—' sign in a square means that they are inversely related. A '+' sign means that they are directly related but the relationship is rather weak; similarly a '–' sign means that they are inversely related but the relationship is rather weak.

	V_{os}	I_b	dV_{os}/dT	dI_b/dT	SR	GBW	v_n	i_n	Z_i	Z_o	I_s	Linearity	V_o swing
V_{os}													
I_b									—				
dV_{os}/dT	++												
dI_b/dT		++											
SR	++	+	++	+									
GBW	++	++	++	++	++								
v_n	++				—	—							
i_n		+		+	++	++							
Z_i		—			—	—	++						
Z_o					—	—							
I_s					++	++				—			
Linearity					–	+				++	+		
V_o swing					—	—				—		—	

⇒ LM 741 is the old workhorse. It is a BJT version; it may still be used in the 'run of the mill' applications, due to its popularity and wide user base. Many later opamps and newer introductions are pin-to-pin compatible with it.
⇒ OP07 is a BJT opamp – an improved version of LM 741, the improvement being in terms of technology. It can be seen to be better in all respects. The improvement in offset and drift characteristics is marked.
⇒ LM 607 is an improvement on OP07; the input bias currents are less but the input-stage collector currents are maintained, thanks to the use of 'super β' transistors at the input stage. GBW is sustained but input current noise is reduced.
⇒ TL 081 and LF 356 are FET input versions. The input currents and impedances are one or two orders better than those of their BJT counterparts. Both are pin-to-pin replacements for 741. LF 356 is better in terms of input characteristics.
⇒ LH 4118G is a BJT opamp with high bandwidth. It is tailored to radio frequency applications; hence, the limited input performance is not a deterrent.
⇒ LMC 6061 is a CMOS amplifier. Its power consumption is extremely low. It is specifically tailored for use in battery powered instruments.

3.6 Opamp Selection

Design of an analog functional block today is a three-step process: -

⇒ Understanding the functional requirements and constraints of the application,
⇒ Selecting one or more opamps required and
⇒ Building the circuit for the application using the selected opamps and necessary additional components.

The first task is essentially that of selection of the sensor, dealt with in later chapters. The third, again, is discussed in detail in the following chapters. When it comes to selection, the opamp, due to its flexibility and variety, is treated as a black box by most designers. A selection with some amount of minimal reasoning may be workable in some cases, but for best results, a careful selection procedure on the following lines, is warranted. (Note that in today's scenario, the price of opamp is not a primary consideration): -

⇒ Examine the signal to be handled by the opamp *vis-à-vis* the signal level, its source impedance, its bandwidth of interest and precision. Identify the deciding requirements.
⇒ Match the above deciding requirements with respective opamp characteristics. Short-list the opamps suitable for the targeted application.
⇒ Accessibility and the function desired restrict the selection further.
⇒ Make a final selection taking the output side and other factors into consideration.

A variety of signal-processing applications is discussed in the following chapters. These as well as many of the sensor applications and instrumentation schemes discussed later, make extensive use of opamps. A set of common applications which figure frequently in instrumentation, their specific

characteristics and the relevant specifications of opamps to be considered for selection, are given in Table 3.3.

Table 3.2 Key specifications of a few selected opamps

IC feature	Type of opamp						
	LM 741	OP 07	LM 607	TL 081	LF 356	LH 4118G	LMC 6061
Max. input offset voltage (μV) at 25°C, $R_s < 10k\Omega$	5000	75	60	15000	2000	5000	350
V_{os} drift - μV/°C	15	2.5	0.6	10	5	10	1.0
I_{os} at 25°C -nA (Max.)	200	2.8	2.8	0.1	0.01		0.01
I_{os} drift at 25°C -pA/°C	500	50	3				
I_b at 25°C - nA (Max.)	500	3	3	0.2	0.05	25000	0.1 #
Input resistance - at 25°C & ± 20V (max.) supply: (MΩ)	3	20	2	10^6	10^6		10^6
CMRR ($R_s < 10k\Omega$) dB (min.)	70	110	116	70	85	50	75
Slew rate - at 25°C Unity gain - V/μs	0.5	0.1	0.4	13	10	2000	0.02

Normally much less

Table 3.2 (Continued)

IC feature	Type of opamp						
	LM 741	OP 07	LM 607	TL 081	LF 356	LH 4118G	LMC 6061
Voltage gain - V/mV Min. at 25°C	20	150	2000	25	50	0.30	400
GBW (MHz)	0.5	0.6	1.0	4	4	55	0.1
Supply current - at 25°C - max.: (mA)	2.8	8	1.5	2.8	10		0.024
Input noise Voltage (θ_{np-p})-max. - μV at 25°C		0.6	0.5				
θ_n at 25°C density max. - f = 10 Hz = 100 Hz =1000 Hz nV/√ Hz		 18 13 11	 18 10 8	 50 28 25	 15 12		 83
Input noise current at 25°C - i_{np-p} (pA) 0.1 Hz - 10 Hz		30	14	≈ 0	≈ 0	≈ 0	≈ 0
Input noise current density - pA/√ Hz f = 10 Hz = 100 Hz = 1000 Hz		 0.80 0.23 0.17	 0.32 0.14 0.12	 0.01	 0.01 0.01		 0.0002

Table 3.3 Applications and opamp requirements for them

Applica-tion	Characteristics	opamp specifications of primary consideration
Thermo-Couple	Low output voltage ▪ Low source impedance ▪ Remote accessibility & possibility of signal contamination ▪ Low signal bandwidth	High open loop gain ▪ Low V_{os} & low i_{os} ▪ Input impedance need not be very high; i_b need not be low; high CMRR ▪ Use instrumentation type opamp ▪ Slew rate & bandwidth are not primary considerations
Resistance thermometer	Low output voltage ▪ Low source impedance ($\approx$ 100 Ω) ▪ Floating input ▪ Low bandwidth	High open loop gain ▪ Low V_{os}, low i_{os} & low drift ▪ Input impedance > 1 MΩ ▪ High CMRR ▪ Difference/ Instrumentation amplifier configuration ▪ Slew rate & bandwidth are not primary considerations
Strain gauge (Instrument)	Low output voltage ▪ Low source impedance ($\approx$ 100 Ω) ▪ Floating input ▪ Bandwidth $\approx$ 1khz ▪ Battery operation	High open loop gain ▪ Low V_{os}, low i_{os} & low drift ▪ Input impedance > 1 MΩ ▪ High CMRR ▪ Difference/ Instrumentation amplifier configuration ▪ GBW of 5Mhz or more ▪ Micropower opamp is required
Photo-diode I R detector-DC mode	Short circuit operation preferred ▪ Source impedance $\approx$ 10 kΩ ▪ Bandwidth of the order of 10 kHz	Low V_{os}, low i_{os} & low i_b ▪ Input impedance > 10 MΩ ▪ GBW of 10 MHz or more
Photo-diode IR detector-Chopper mode	Need for frequent standardisation ▪ Low effective signal level ▪ Bandwidth $\approx$ 10 kHz	High slew rate ▪ High gain ▪ GBW of 10 MHz or more
Electrode potentials	Medium output voltage ▪ Slowly changing signals ▪ Low bandwidth ▪ High output impedance Battery operation	Open loop gain need not be very high ▪ Good long term drift stability ▪ GBW need not be high (100 khz is okay) ▪ Input impedance > 1000 MΩ ▪ Micro-power opamp

Table 3.3 (Continued)

Application	Characteristics	opamp specifications of primary consideration
Piezo-electric sensor, Ultrasonics vibration measurement	Medium output voltage ▪ AC coupled ▪ High output impedance ▪ Bandwidth ≈ 100 kHz	Open loop gain need not be very high ▪ V_{os} & its drift are not considerations ▪ Input impedance > 1000 MΩ ▪ High GBW
Acoustic noise measurement. Moving coil microphone.	Low output voltage ▪ Bandwidth up to 30 kHz ▪ No cable pick-up ▪ AC coupling ▪ Output impedance ≈ 100 Ω	High open loop gain ▪ GBW to be high ▪ Single-ended amplifier configuration ▪ Offset and drift are not primary considerations ▪ Input impedance > 100 kΩ
Low pass filter	Amplification from DC onwards ▪ Low bandwidth ▪ Wide output voltage range ▪ Good output drive capability (Low output impedance)	Low V_{os}, low i_{os} ▪ GBW & slew rate are not primary considerations ▪ Full output voltage swing, linearity ▪ Low output impedance ▪ Short circuit protected
Bandpass filter ▪ Notch filter	High signal bandwidth ▪ AC coupling ▪ Wide output voltage range ▪ Good output drive capability (Low source impedance)	High GBW, high slew rate ▪ V_{os} , i_{os} & their drift are not primary considerations ▪ Full output voltage swing ▪ Low output impedance ▪ Short circuit protected
Modulators & demodulators	Wide bandwidth ▪ Stability ▪ Source impedance not high ▪ Good DC performance ▪ Wide output voltage range	Wide bandwidth , high slew rate ▪ Steady gain drop-off with frequency ▪ Input impedance >100kΩ ▪ Low V_{os}, low drift ▪ Full output voltage swing
Strain gauge (system)	Low output voltage ▪ Floating input ▪ Bandwidth ≈ 1khz ▪ Likely contamination by noise in transmission, ground loop *etc.*	High open loop gain ▪ Low V_{os}, low i_{os} & low drift ▪ High CMRR ▪ Difference/ Instrumentation amplifier configuration ▪ GBW > 5 MHz ▪ Low noise amplifier ▪ Instrumentation type opamp

4 Linear Signal Processing

4.1 Introduction

Amplification and filtering are common linear processing activities. Opamps are universally used for these. Most amplifiers do a certain amount of filtering and most filters do a certain amount of amplification too. A variety of circuit configurations has evolved over the years tailored to specific amplification or filtering needs [Franco, Graeme, Gray and Meyer]. These have become almost universal. We discuss the commonly encountered functional requirements for signals and the well-accepted circuits used to meet them. Details and precautions specific to any circuit are discussed then and there. Noise and allied aspects common to all applications are discussed in detail only with the first configuration.

4.2 General Considerations

Opamps are available in compensated and uncompensated versions [See Figure 4.1]. In uncompensated opamps, the open loop gain remains sufficiently high over the whole bandwidth and may drop abruptly with frequency. Such amplifiers are to be used with external compensating capacitors as recommended by the manufacturer (Due to the steep drop of gain with frequency, the amplifier oscillates in any feedback configuration, if not compensated externally). With the choice of such a capacitor, the designer can tailor the closed loop frequency response and the speed of response to his specific needs. The compensated opamps are internally compensated. Their gain drops with frequency from about 100 Hz. At the gain crossover frequency, the phase shift is well below 180° (The gain drops at less than 12 dB/decade). Normal feedback configurations do not cause any oscillation with these opamps. The closed loop performance will be limited due to the pre-ordained gain-frequency characteristic. If necessary, one can restrain the closed loop performance further by external feedback. Whenever a high speed operation or selective gain at a comparatively high frequency is desired, the uncompensated opamp is preferred. Care is to be exercised in selecting compensation to get desired performance without sacrificing stability.

Opamps are not inherently protected against input over-voltages. Whenever the designer is sure that no external over-voltage or voltage spikes can appear at the input, the opamp can be used as such; but in the likelihood of such spikes, the opamp has to be protected. Figure 4.2 shows the commonly used protective circuit. If the input signal at x or y exceeds the positive supply V^+ by 0.7V, then diode D_4 or D_1, as the case may be, conducts and clamps the input concerned to $(V^+ + 0.7V)$.

Similarly, the negative excursions of the input are limited to $(V^- - 0.7V)$ by diodes D_3 or D_2 as the case may be. The price paid for the protection is an increase in cost and a deterioration in performance. The diode leakage paths reduce input

T. R. Padmanabhan, *Industrial Instrumentation*
© Springer-Verlag London Limited 2000

impedance of the opamps substantially (this is especially true of FET input opamps). The diode capacitances can affect the high frequency performance of the opamps severely. They may even affect the opamp stability in certain configurations.

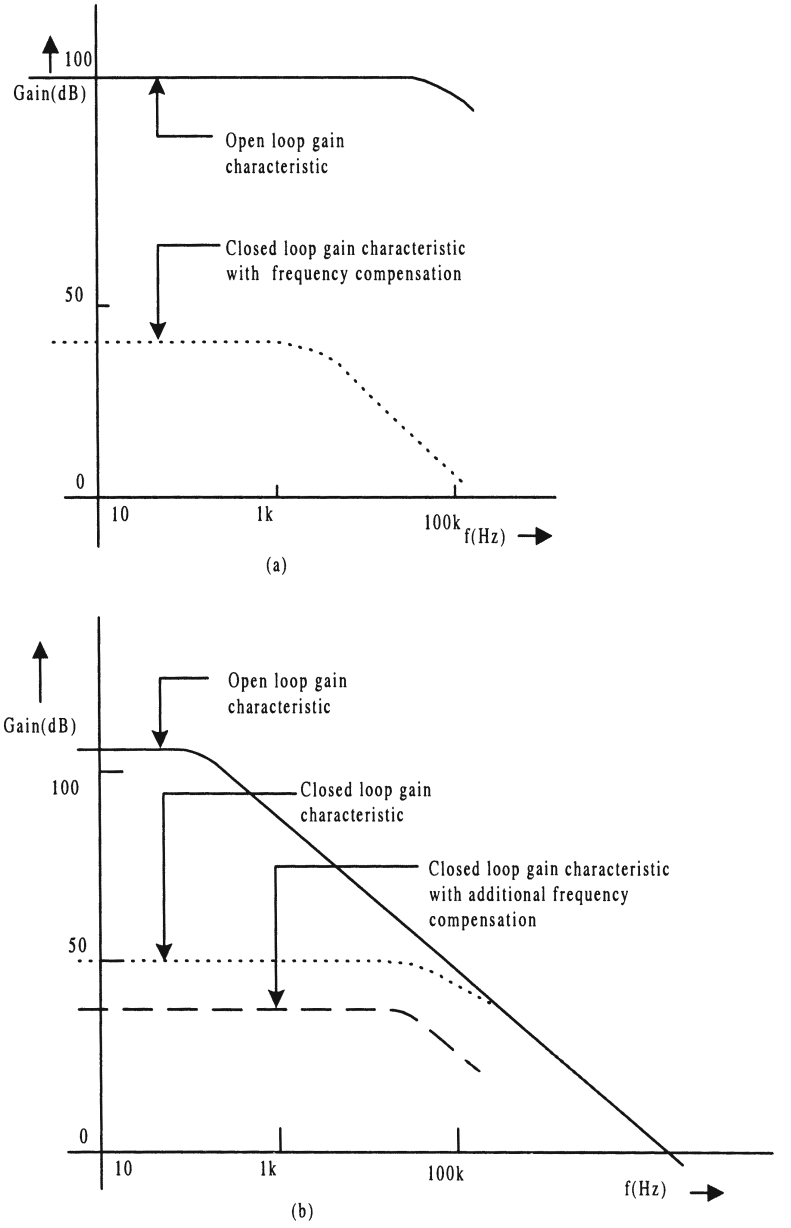


Figure 4.1 Gain characteristics of opamps with and without feedback: (a) Uncompensated opamp (b) Internally compensated opamp.

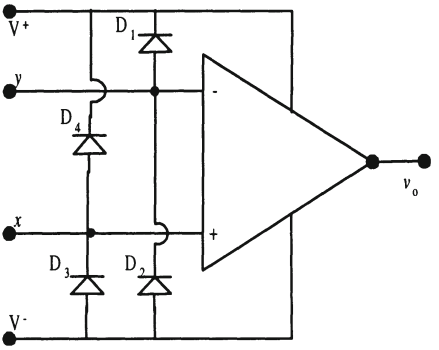


Figure 4.2 An opamp with the protection diodes at the input

FET input opamps have input impedance levels of 10^{12} ohms. One prefers them for applications where the input impedance required is of this level. However, with the ordinary circuits and PCBs, the leakage paths from inputs to the power supplies, can have same impedance levels. This can hamper circuit performances severely. Temperature changes too can affect such leakage currents (Even high quality epoxy PCBs are susceptible). Two 30mm tracks with 0.1mm separation, can have a leakage of 200 pA. Cleaning of boards and epoxy or silicone coating, are essential to keep these in check. Proper ground rings around input leads divert the leakage currents [See Section 4.2.3].

4.3 Inverting Amplifiers

The inverting amplifier with an ideal opamp is shown in Figure 4.3. For ideal conditions the input currents are zero. Referring to the figure,

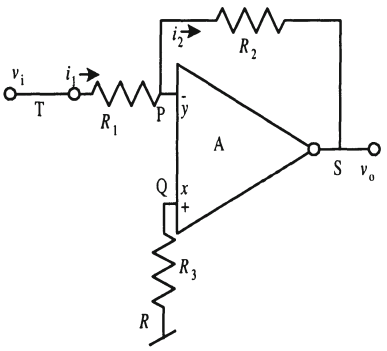


Figure 4.3 An inverting amplifier

$$(x-y)A = v_o \tag{4.1}$$

Or

$$x-y = \frac{v_o}{A} \tag{4.2}$$

The gain values are normally in excess of 10^4. Thus for v_o within the range of the supply voltages, $(x-y)$ will be quite small. This is true of all opamp configurations that maintain the opamp in the active region of operation through feedback. This gives the identity,

$$x = y \tag{4.3}$$

With zero current through R_3, point Q being at ground potential, R is also at ground potential. Therefore,

$$x = y = 0 \tag{4.4}$$

Current through R_1, *i.e.*,

$$i_1 = \frac{v_i}{R_1} \tag{4.5}$$

Since the opamp does not draw any current, this current is fully diverted through R_2.

$$\therefore i_2 = i_1$$

$$v_o = -i_2 R_2$$

$$= -\frac{R_2}{R_1} v_i \tag{4.6}$$

Thus the amplifier gain for closed loop configuration is $(-R_2 / R_1)$.

The above derivation assumes the open loop gain of the opamp to be infinite. One can estimate the error due to definite gain values. Referring to Figure 4.3, we have,

$$x - y = \frac{v_o}{A} \tag{4.7}$$

With $x = 0$,

$$y = -\frac{v_o}{A} \tag{4.8}$$

$$i_1 = \frac{v_i - y}{R_1}$$

$$= \frac{v_i + (v_o/A)}{R_1} = i_2 \tag{4.9}$$

$$\text{Voltage drop in } R_2 = i_2 R_2 \tag{4.10}$$

$$= \frac{v_i + (v_o/A)}{R_1} R_2 \tag{4.11}$$

Eliminating i_1, i_2 and y from the above set of equations,

$$v_o = -\frac{R_2}{R_1}\left[\frac{1}{1+\frac{1}{A}\left(1+\frac{R_2}{R_1}\right)}\right] v_i \tag{4.12}$$

Normally an inverting amplifier is used with gain greater than 1. As long as $(R_2/R_1) << A$, we have,

$$(R_2/R_1 A) << 1$$

$$\therefore v_o \approx -\frac{R_2}{R_1} v_i \tag{4.13}$$

To get 0.1 % accuracy in the relationship of Equation 4.13, from Equation 4.12

$$\frac{1}{A}\left(1+\frac{R_2}{R_1}\right) < 0.001$$

or

$$\frac{R_2}{R_1} < 0.001A \tag{4.14}$$

Taking the low frequency open loop gain to be > 10^5 (as with most opamps),

$$\frac{R_2}{R_1} < 100 \tag{4.15}$$

Since the gain value can change by one or two orders depending on the operating conditions, the error estimate here, has to be based on the minimum value of gain. Normally opamp based amplifiers are not designed with closed loop gain values higher than about 100, as it has been indicated by the inequality (4.15). The tolerances in resistance values also affect the closed loop gain directly.

Input impedance of the amplifier is R_1 since point P is at virtual ground. Common mode input is 0 volts, since points P and Q are at 'virtual ground' – *i.e.*, at ground potential without being directly grounded.

4.3.1 Analysis of the Non-ideal Amplifier

We considered the effect of definite opamp gain on the input-output relationship. Similarly we discuss the effects of offset voltage, current and drift. Subsequently we attempt an insight into the noise performance of the opamp. This approach, (rather than considering all the imperfections together) makes the discussion much less cumbersome but equally effective. Figure 4.4 shows the equivalent circuit of a practical opamp in terms of an ideal one. B and D represent the inverting and the non-inverting inputs of an ideal opamp and P and Q, those of a practical one. V_{os}, i_{b+} and i_{b-} are the offset voltage and the bias currents at the two inputs respectively. Consider the effect of the bias currents first. ($i_{b+} \times R_3$) is the voltage appearing at Q and [$i_{b-} \times (R_1 \,||\, R_2)$] is the voltage appearing at P. It is customary to make,

$$R_3 = \frac{R_1 R_2}{R_1 + R_2} \tag{4.16}$$

This nullifies the effects of the two bias currents if they are equal. Any mismatch between the bias currents, is the offset current i_{os}. This causes a voltage difference between P and Q. In effect it appears as an offset voltage equal to ($i_{os} \times R_3$) and adds to V_{os}.

$$\text{Effective offset voltage} = V_{os} + i_{os} R_3 \tag{4.17}$$

D and B – being the non-inverting and inverting input points of the ideal opamp – are at virtual ground. With $v_i = 0$ (zero input conditions),

$$\text{potential of point Q} = V_{os} + i_{os} R_3 \tag{4.18}$$

$$\therefore V_o = \left(V_{os} + i_{os}R_3\right)\left(1+\frac{R_2}{R_1}\right)$$

$$= V_{os}\left(1+\frac{R_2}{R_1}\right)+i_{os}R_2 \qquad (4.19)$$

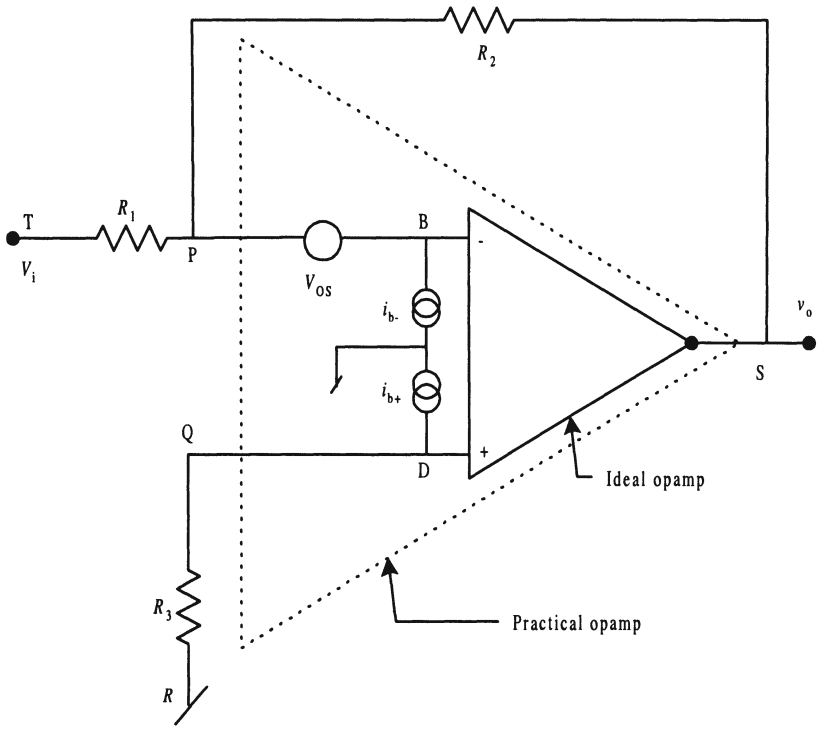


Figure 4.4 The practical opamp represented in terms of an ideal opamp along with offset currents and voltage. With this representation, the inverting amplifier of Figure 4.3 is considered for analysis.

Observations: -

- ⇒ V_{os} is amplified by the gain of the stage – hence the need to keep V_{os} low especially in high gain stages.
- ⇒ As R_2 increases the output error due to i_{os} increases. Hence the need to keep R_2 low. If R_2 is reduced, R_1 too is to be reduced correspondingly to keep the ratio R_2/R_1 constant; this affects the input impedance adversely. Hence, R_2 cannot be reduced beyond a limit. The need to keep i_{os} low, need hardly be emphasised further!
- ⇒ As the temperature at which the opamp operates drifts, V_{os} and i_{os} change causing a drift in the output V_o.
- ⇒ With FET input opamps, i_{b+} and i_{b-} are very low. i_{os} also reduces to corresponding levels. The offset error is essentially due to V_{os}.

$\Rightarrow$ With BJT input opamps, relative contribution of V_{os} and i_{os} to the total error in output, depends on the magnitude of these two quantities as well as the resistance values used in the scheme.

The error due to the offset voltage and current together can be nullified by returning R_3 to an adjustable voltage as shown in Figure 4.5. This can be adjusted so that $V_o = 0$ at zero input signal conditions. Such adjustment is cumbersome and warranted only in high precision work. The zeroing of error in this manner is valid only at the temperature of adjustment. As the operating temperature drifts, the output V_o also drifts correspondingly, although the drift here is lower than that in the case of Figure 4.3.

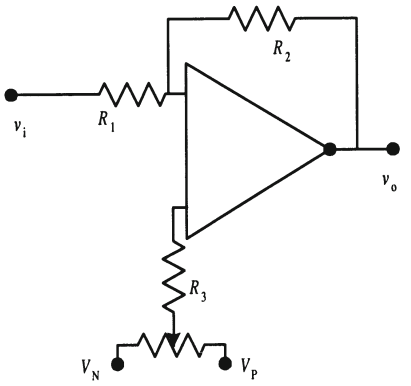


Figure 4.5 Inverting amplifier with the facility for output nulling

Two more issues warrant discussion here. For large values of R_2 as may happen with FET input opamps, the shunting effect of stray capacitances at the non-inverting input may become dominant. Potential of point P drops down with frequency. The output may swing more to restore balance leading to overdrive and instability. To avoid this, R_2 has to be shunted by a suitable capacitor C_2 and closed loop gain at higher frequencies, reduced as in Figure 4.6. For such fast-enough roll-

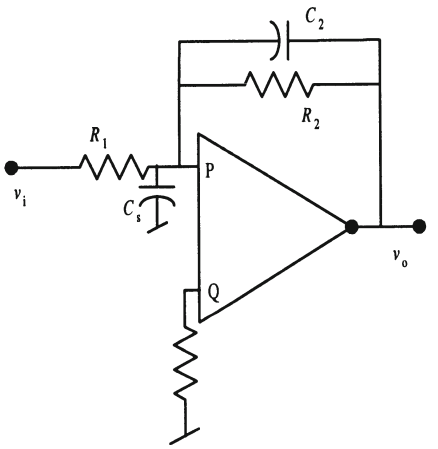


Figure 4.6 Stabilisation of high gain inverting amplifier by frequency limiting.

off, one has to ensure that $C_2R_2 > C_sR_1$ where C_s is the stray capacitance from the inverting input to ground. Such shunting of R_2 is called for, when R_2 is greater than (about) 10KΩ. Here, one sacrifices closed loop gain at higher frequencies for the sake of stability.

A second problem arises when the opamp drives a capacitive load (e.g., a cable). Here v_o reduces at high frequencies and affects stability adversely. A commonly used approach to alleviate this, is to segregate the capacitive load from the feedback / gain determining loop – at least at the higher frequencies. A circuit scheme for this is shown in Figure 4.7. R_3 of the order of 100 Ω and C_2 of the order of 10 pF are used. At low frequencies, $C_LR_3\omega << 1$. Hence the loading effect of C_L is negligible and the gain G becomes,

$$G = \frac{R_2}{R_1[1+(R_2+R_3)C_2s]}$$

Further with $R_3 << R_2$,

$$G \approx \frac{R_2}{R_1} \tag{4.20}$$

At high frequencies where the loading of the potential divider R_2-R_3 by $(1/C_L\omega)$ is not negligible, the gain is $(1/C_2R_1s)$. The capacitor C_2 provides sufficient attenuation to ensure stability at all frequencies. For satisfactory operation, ensure that $C_2R_2\omega > 10$ at the gain cross over frequency.

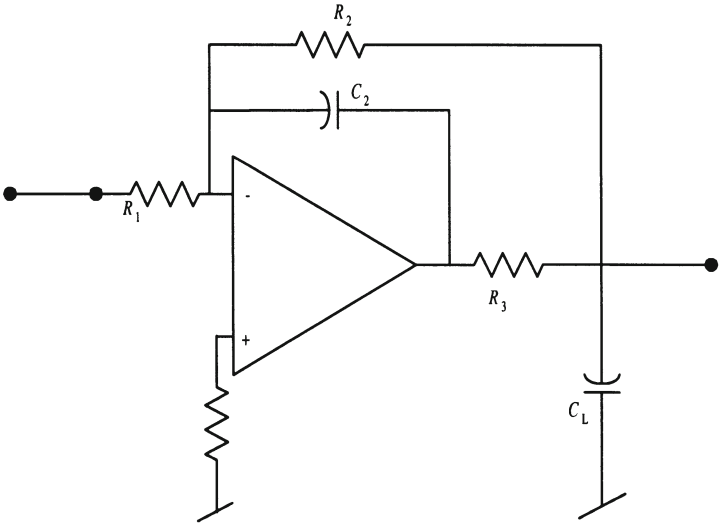


Figure 4.7 Inverting amplifier modified to drive capacitive loads

In both cases cited above, the loop gain is reduced by extraneous or undesirable elements. Whenever this happens, the opamp may try to restore balance and get into an unstable mode. The way out is a judicious modification of the basic circuit to neutralise the effect of the disturbing element. In the process, one may have to sacrifice performance.

4.3.2 Noise in the Amplifier

The noise generated internally in the amplifier has been discussed in the last chapter. The total noise in the amplifier is calculated accounting for the noise in the input circuit resistors – in addition to the internal noise. This is done here for the inverting amplifier (Some concepts, of random noise discussed in Chapter 7, are used here). Subsequently a specific example is considered to get a quantitative idea of the noise levels.

Different types of noise in opamps have already been dealt with in Section 3.3.13. If the individual components are known separately, one can substitute the frequency values of interest and compute individual noise contributions. Similar calculations can be made, if the noise corner frequency and the noise-density figure in the flat region of the spectrum are known. More often, the opamp data sheets give the total noise-density figures at selected frequencies only. One can use a piece-wise linear approach here to estimate the individual noise levels and all these can be combined to get the total noise.

When an opamp is used in any specific circuit configuration, the noise introduced by the resistances used in the circuit are additional to all the above which are internal to the amplifier. Such noise has a constant power spectral density over the full range of frequencies of interest [See Section 7.4.2]. At room temperature, this noise has the form

$$E_j^2 = 1.64\times10^{-20} R(f_u - f_l) \text{ volt}^2 \tag{4.21}$$

where

⇒ R is the resistance in ohms

⇒ f_u & f_l are the upper and the lower frequency limits considered and

⇒ E_j is the rms. noise voltage introduced by the resistance.

All the individual noise components in the opamp – current as well as voltage type – and the thermal noise above are mutually uncorrelated. Hence the total rms. noise voltage can be obtained as,

$$E^2 = \sum E_{ni}^2 + R_e \sum I_{ni}^2 \tag{4.22}$$

where

⇒ E_{ni} is the rms. value of the output of the i^{th} noise voltage source,

⇒ I_{ni} is the rms. value of the output of the i^{th} noise current source,

⇒ R_e is the equivalent source resistance and

⇒ E is the rms. value of the total noise.

If the noise components in different frequency segments are obtained separately, they are all uncorrelated and can be combined in a similar manner.

The noise-amplitude density distribution is Gaussian in nature. For the Gaussian noise, the peak-to-peak signal is within 6 times the rms. value for 99.73% of the time [Carlson, Davenport and Root]. This is taken as the customary peak-to-peak noise v_{np-p}.

$$v_{np-p} = 6\sqrt{E^2} \text{ volts} \tag{4.23}$$

Let us consider the specific example of an inverting amplifier (Figure 4.3) having a gain of 12 with,

$$R_1 = 10\text{k}\Omega \tag{4.24}$$

$$R_2 = 120\text{k}\Omega \tag{4.25}$$

and

$$R_3 = (R_1 || R_2) \tag{4.26}$$

$$= 9.2\text{k}\Omega \tag{4.27}$$

R_2 is shunted by C_2 to give a 20 dB/decade cut-off with a corner frequency of 1kHz. The opamp used is OP07. From the Data Sheet [National] we have,

$$v_{np-p} \text{ for the 0.1Hz to 10Hz range} = 0.6\mu\text{V} \tag{4.28}$$

$$\text{The corresponding rms. noise voltage } E_{n1} = 0.1\mu\text{V} \tag{4.29}$$

$$E_{n1}^2 = 0.01\mu\text{V}^2 \tag{4.30}$$

$$\text{The noise-voltage density } e_n \text{ at 10 Hz} = 18.0\,\text{nV}/\sqrt{\text{Hz}} \tag{4.31}$$

Similarly,

$$e_n \text{ at 100 Hz} = 13.0\,\text{nV}/\sqrt{\text{Hz}} \tag{4.32}$$

$$e_n \text{ at 1 kHz} = 11.0\,\text{nV}/\sqrt{\text{Hz}} \tag{4.33}$$

Using the piece-wise linear approach, the total mean square voltage noise over the 10Hz to 1kHz band E_{n2}^2 is,

$$E_{n2}^2 = 18^2(30-10) + 13^2(300-30) + 11^2(1000-300)\,\text{nV}^2 \tag{4.34}$$

$$= 0.137\,\mu\text{V}^2 \tag{4.35}$$

Combining E_{n1} and E_{n2},

$$E_{n2}^2 = E_{n1}^2 + E_{n2}^2 \tag{4.36}$$

$$= 0.01 + 0.137 \tag{4.37}$$

$$= 0.147\mu\text{V}^2 \tag{4.38}$$

For a 20dB/decade cut-off, the contribution of all the frequencies beyond the cut-off frequency, is equivalent to increasing the noise bandwidth by 1.57 [See Section 7.3.4]. With this correction,

$$\text{Mean square noise} = 0.147 \times 1.57\,\mu\text{V}^2$$

$$= 0.231\mu\text{V}^2 \tag{4.39}$$

From the Data Sheet,

$$\text{Input noise current in the 0.1Hz to 10Hz band} = 30\text{ pA peak-to-peak} \tag{4.40}$$

$$\therefore \text{ corresponding rms. noise current } I_{n1} = 5\text{ pA rms.} \tag{4.41}$$

$$\text{The noise current density } i_n \text{ at 10 Hz} = 0.80\,\text{pA}/\sqrt{\text{Hz}} \tag{4.42}$$

$$i_n \text{ at 100 Hz} = 0.23\,\text{pA}/\sqrt{\text{Hz}} \tag{4.43}$$

$$i_n \text{ at 1 k Hz} = 0.17\,\text{pA}/\sqrt{\text{Hz}} \tag{4.44}$$

Using the piece-wise linear approach, the total mean square current noise over the 10 Hz to 1 kHz band I_{n2}^2 is,

$$I_{n2}^2 = 0.80^2(30-10) + 0.23^2(300-30) + 0.17^2(1000-300)\,\text{pA}^2$$

$$= 47.3\,\text{pA}^2 \tag{4.45}$$

Combining this with Equation 4.41, we get the total rms. noise current I_n as,

$$I_n^2 = I_{n1}^2 + I_{n2}^2$$
$$= 25 + 47.3\ \text{pA}^2 \quad (4.46)$$
$$= 72.3\ \text{pA}^2 \quad (4.47)$$

Including the correction for 20 dB/decade cut-off,

$$I_n^2(\text{corrected}) = 72.3 \times 1.57\ \text{pA}^2$$
$$= 113.5\ \text{pA}^2 \quad (4.48)$$

$$\text{Total equivalent series resistance on input side} = R_3 + (R_1 || R_2)$$
$$= 18.4\ \text{k}\Omega \quad (4.49)$$

$$\text{Thermal noise due to resistance up to 1 kHz} = 1.64 \times 10^{-20} \times 18.4 \times 10^3 \times 10^3\ \text{volt}^2$$
$$= 30.2 \times 10^{-14}\ \text{volt}^2 \quad (4.50)$$

Including the correction for 20 dB/decade cut-off,

$$\text{Thermal noise (corrected)} = 30.2 \times 10^{-14} \times 1.57\ \text{volt}^2$$
$$= 47.4 \times 10^{-14}\ \text{volt}^2 \quad (4.51)$$

From Equations 4.39, 4.48, 4.49 and 4.51,

$$\text{Total noise} = (0.231 \times 10^{-12}) + (113.5 \times 10^{-24} \times 18.4 \times 10^3) + (47.4 \times 10^{-14})\ \text{volt}^2$$
$$= 0.705 \times 10^{-12}\ \text{volt}^2 \quad (4.52)$$
$$\text{rms. value of total noise} = 0.84\ \mu\text{V} \quad (4.53)$$
$$\text{Peak-to peak value of noise voltage} = 0.84 \times 6\ \mu\text{V}$$
$$= 5.04\ \mu\text{V} \quad (4.54)$$

Observations: -

⇒ The above computations are based on the noise figures given in the Data Sheet. Being typical values, they give an idea of the noise level to be expected rather than any precise quantitative figures.

⇒ Noise in the amplifier output due to common mode input, power supply ripple, interference from various sources – all these add as extraneous noise to the signal. In a well-designed and engineered scheme, contributions due to all these together may be one order higher than the noise voltage. Thus for the example here, all such noise together may amount to 50μV.

⇒ Signal threshold – *i.e.*, the minimum signal change that can be detected – is of the same order as the noise; here it is of the order of 50 μV.

⇒ The minimum attainable indecision in measurement and error, the best attainable accuracy and precision *etc.*, are all of this order.

⇒ Thus if the full scale signal level at the amplifier input is 10mV, the best attainable accuracy is given by

$$\text{Best attainable accuracy} = \frac{50}{10{,}000} \times 100\%$$
$$= 0.5\ \% \quad (4.55)$$

The signal threshold level, accuracy *etc.*, may be improved by reducing the all round noise level. The different possibilities of reducing the noise here, are: -

- Reduction of thermal noise – which is the most dominant here – by reducing the resistances (if the signal source impedance is low enough).
- Reduction of amplifier bandwidth, if the system permits the same.
- Use of the opamp at lower noise levels, like operation at a substantially lower temperature; or use of opamps having lower inherent noise levels.

It must be stressed here that any conspicuous reduction of noise level can be achieved only by very careful design and engineering measures; this includes reduction of power supply ripple, possible interferences *etc.* All these entail rapid increase in cost. Similar calculations can be made with other opamps and other amplifier configurations also.

4.3.3 Minimisation of Leakage Errors

In the inverting amplifier, both inverting and non-inverting inputs are near ground potential. With good quality opamps, the leakage currents to the inputs can be a source of error. As mentioned earlier, this is especially true of FET input opamps. The problem is to be tackled at two levels. By proper care in circuit layout, cleanliness and masking, the leakage current levels are to be minimised. Further, by judicious measures, a substantial part of the leakage currents may be diverted. In normal opamps the inverting and non-inverting input leads are adjacent to each other. They remain at the same potential. A separate PCB track-guard ring can surround the two inputs and the same can be returned to a selected point. The potential of this point has to be close to that of the inverting and non-inverting inputs – this avoids currents from the open leads to the guard ring. The return point selection has to be such that the diversion of guard ring current to this point does not cause any error. Figure 4.8 shows the guard ring layout and connection for an inverting amplifier.

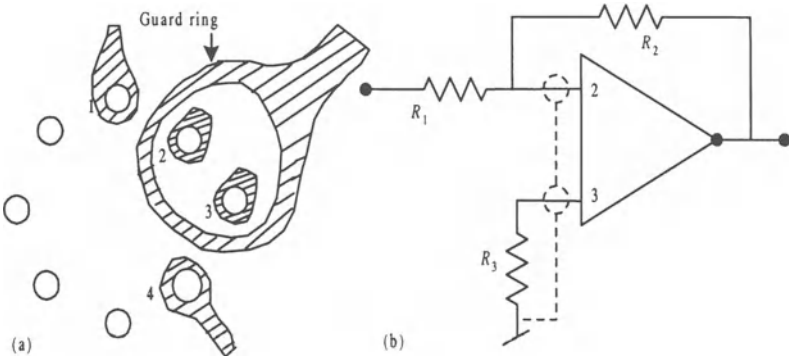


Figure 4.8 Minimisation of leakage currents and its effects in an inverting amplifier: (a) PCB layout details around the opamp and (b) Circuit with guard ring connection.

In Figure 4.8 (a), the guard ring surrounds the input leads completely. Further, it is returned to ground separately and directly as seen in Figure 4.8 (b). One can see that the guard ring current does not affect the currents in R_1, R_2 and R_3. If the leads to R_1, R_2 and R_3 are long, the guard ring should be extended on either side of these leads, to divert leakages there.

4.4 Summing Amplifier

Weighed sum of a set of analog signals can be obtained with the circuit shown in Figure 4.9 which is an extension of the inverting amplifier of Figure 4.3.

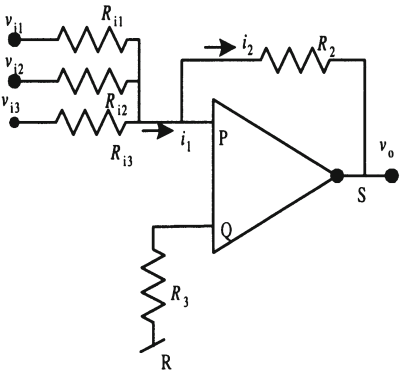


Figure 4.9 Summing amplifier

Under ideal conditions,

$$V_P = V_Q = 0 \tag{4.56}$$

The total current i_1 flowing into point P from the input side is,

$$i_1 = \frac{v_{i1}}{R_{i1}} + \frac{v_{i2}}{R_{i2}} + \frac{v_{i3}}{R_{i3}} \tag{4.57}$$

The input current into the opamp at point P being zero,

$$i_1 = i_2 \tag{4.58}$$

P being at virtual ground potential,

$$v_o = -i_2 R_2 \tag{4.59}$$

Eliminating i_1 and i_2 from the above set of equations,

$$v_o = -R_2\left(\frac{v_{i1}}{R_{i1}} + \frac{v_{i2}}{R_{i2}} + \frac{v_{i3}}{R_{i3}}\right) \tag{4.60}$$

Equation 4.60 shows that the output is a weighted sum of all the inputs.

Observations: -

- ⇒ By properly selecting R_{i1}, R_{i2}, R_{i3} *etc.*, different weight to individual inputs can be achieved.
- ⇒ Difficulties associated with component layout and errors due to increased leakage, limit the number of inputs at a stage to 2 or 3.
- ⇒ R_3 is selected as the equivalent parallel resistance connected at the inverting input terminal P. *i.e.,*

$$R_3 = (R_2 \parallel R_{i1} \parallel R_{i2} \parallel R_{i3}) \tag{4.61}$$

  This is once again to minimise the error due to bias currents.

- ⇒ R_2 is shunted by a suitable capacitance and the opamp bandwidth restricted. The considerations are the same as with the inverting amplifier – stabilisation against effect of leakage capacitance and restriction of error due to noise.

⇒ Guard ring may be provided and the same grounded, as was done with the inverting amplifier mentioned above – to minimise error due to leakage.
⇒ If the load is capacitive, the circuit may be modified as shown in Figure 4.7 to offer a suitable output drive.
⇒ Since both the inputs are at ground potential, the common mode voltage seen by the circuit is zero.
⇒ Offset, drift and noise considerations are similar to those of the inverting amplifier.

4.5 Current to Voltage Convertor

The inverting amplifier can be directly adapted to serve as a current to voltage converter as shown in Figure 4.10. Point P being at virtual ground, the current measured is 'grounded' and not loaded into a series resistance.

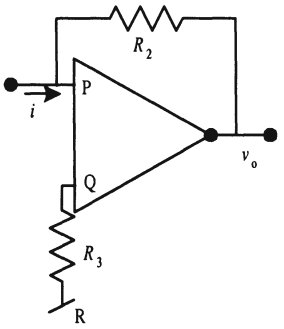


Figure 4.10 Current to voltage convertor

$$v_o = -iR_2 \tag{4.62}$$

Taking the current source to be of infinite resistance, R_3 is made equal to R_2 to minimise error due to the opamp input bias current.

⇒ Shunting of R_2 for stability, bandwidth limiting and noise reduction can be done as with the inverting amplifier.
⇒ Discussions regarding noise, drift *etc.*, which are done with the inverting amplifier, are all valid here. R_2 is the sole resistance connected at P – this is the only difference.
⇒ R_2 should be made only as high as is essential for the subsequent processing. Higher values increase gain error, thermal noise, offset drift *etc.*

4.6 Integrator

The integrator circuit built around an opamp is as shown in Figure 4.11. Under normal operating conditions with $V_P = V_Q = 0$ we have,

$$i_1 = \frac{v_i}{R_1} \tag{4.63}$$

$$= i_2 \tag{4.64}$$

$$\therefore V_o = -\frac{V_i}{R_1 C_2 s} \tag{4.65}$$

Expressing this in the equivalent time domain form,

$$v_o = -\frac{1}{R_1 C_2}\int v_i dt \tag{4.66}$$

$[1/R_1C_2]$ decides the rate of integration. R_1 and R_3 are made equal to avoid offset due to the bias currents.

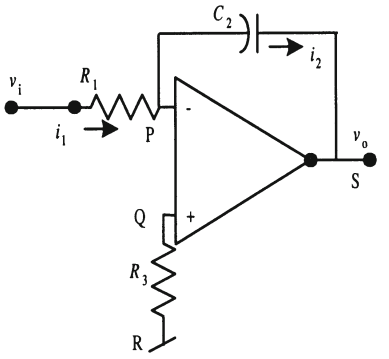


Figure 4.11 Integrator circuit

Observations: -

⇒ For large changes in v_i, the rate at which v_o can rise, is limited by the slew rate. Under such conditions, integration is not perfect.

⇒ As v_o approaches the supply voltage levels, the output can get distorted due to limited gain levels or saturation of the opamp.

⇒ Common mode voltage seen by the opamp is zero.

⇒ In the operation of the integrator, possibly offset causes the maximum error. Considering the voltage and current offsets, we get the input-output relationship of the integrator as,

$$v_o = -\frac{1}{R_1 C_2}\int v_i dt - \frac{1}{R_1 C_2}\int v_{os} dt - \frac{1}{C_2}\int i_{os} dt \tag{4.67}$$

⇒ One uses as large a value of C_2 as is practical to reduce the effect of offset current. As C_2 increases, the stage gain reduces. Further physical size restricts C_2 to 0.1μF or so. As C_2 increases, the leakage through it can cause error in v_o.

⇒ Increase of R_1 increases noise level.

⇒ One can return point R to an adjustable voltage and trim the offset to zero. However this requires unit to unit adjustment and does not eliminate drift due to temperature changes.

⇒ Even with zero input, in course of time v_o will go into positive or negative saturation due to leakage, drift *etc.* It can be avoided by shunting C_2 by a large enough R_2. With this change, the integrator is effective only below the

corner frequency of $1/(2\pi C_2 R_2)$. Alternately one may provide a separate reset circuit for the output. It may be activated when necessary. If the integrator is part of a closed loop scheme, such modifications are not necessary.

The functions of a summer and an integrator can be combined with circuit of Figure 4.12. Here (under ideal conditions) we have,

$$v_o = -\frac{1}{R_{i1}C_2}\int v_{i1}dt - \frac{1}{R_{i2}C_2}\int v_{i2}dt \tag{4.68}$$

v_1 and v_2 are weighted with $1/R_{i1}$ and $1/R_{i2}$ respectively and the sum is integrated. Effects of offset, drift, slew rate *etc.*, are as discussed earlier.

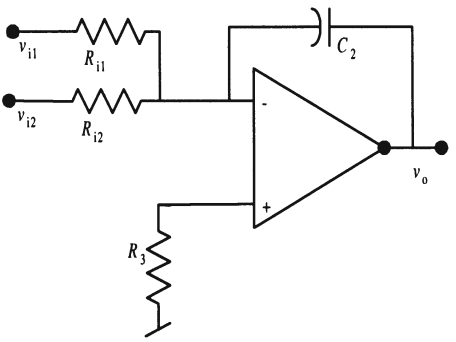


Figure 4.12 Circuit combining summer and integrator

4.7 Non-Inverting Amplifier

The non-inverting amplifier is shown in Figure 4.13. Through analysis as in the earlier sections we get,

$$v_o = \left(1+\frac{R_2}{R_1}\right)v_i \tag{4.69}$$

Even though v_i is fed through R_3, the latter does not enter the gain expression. Though it appears that one can increase R_1 and R_2 arbitrarily, there are trade-offs involved. The standing current through R_1 and R_2 should be high (at least ten times) compared to the bias current. This is to keep drift low. Further increase of R_1 or R_2 increases the thermal noise levels directly. Both these put an upper limit on R_1 and R_2. R_3 is selected to be equal to $(R_1 \parallel R_2)$ to avoid offset due to bias currents. The input impedance of the circuit is very high. For the same reason, if the input is left open, output can get saturated. This can be a problem when multiplexers precede the amplifier.

The common mode signal seen by the opamp is v_i (This is a distinct departure from the earlier schemes, where the common mode input seen by the opamp has been consistently zero.). Hence, opamps selected for non-inverting amplifier must have a high CMRR to keep errors, due to common mode signals, low. The output swing is limited by the common mode input; the swing limit becomes more constraining even at low gain levels (Contrast this with the inverting amplifier). R_2

may be shunted by a suitable capacitance C_2 to limit active bandwidth. This also avoids any stability problems due to stray capacitance at the inverting terminal.

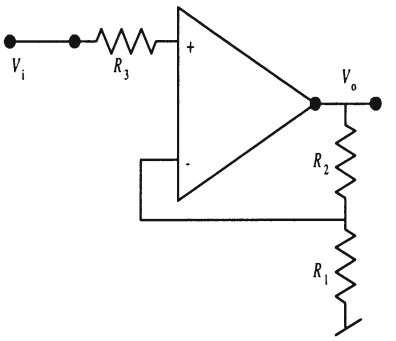


Figure 4.13 Non-inverting amplifier circuit

The non-inverting amplifier configuration is selected whenever the amplification required is of the non-inverting type and (or) the signal source impedance is high. The resistance values used for R_1, R_2 and R_3 are as high as is permissible. To keep drift errors and noise in check, opamps with low i_b and low current noise are selected.

4.8 Buffers

In the non-inverting amplifier configuration of Figure 4.13, if $R_1 \rightarrow \infty$ the gain becomes unity. This is the 'buffer' shown in Figure 4.14. The value of R_2 is selected to be equal to the source resistance to avoid offset current error. The buffer has the highest input impedance of all opamp configurations. It is used as a buffer between two stages whenever the source side cannot be loaded and the load side impedance is not high enough.

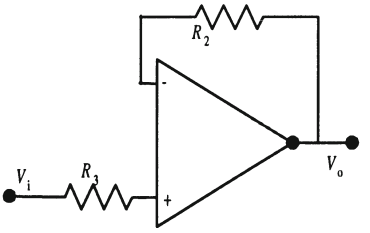


Figure 4.14 Buffer circuit

If the input signal swings faster than what the opamp output can cope up with its limited slew rate, a difference voltage appears at the opamp input. The signal source may be loaded and distorted under these conditions, especially if the signal source impedance is low. A definite value of R_3 is introduced to limit source loading under these conditions. In turn, R_2 is to be increased to match it. Other constraints due to the common mode input, i_b *etc.*, discussed with the non-inverting amplifier above, hold good here also.

4.9 Differentiator

The ideal differentiator circuit is shown in Figure 4.15 (a). The input-output relationship is given by,

$$V_o = R_2 C_1 s V_i \tag{4.70}$$

Expressing this in the equivalent time domain form,

$$v_o = R_2 C_1 \frac{dv_i}{dt} \tag{4.71}$$

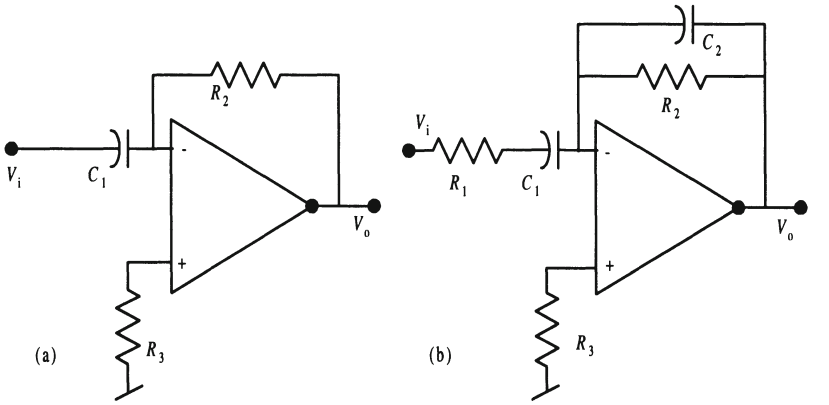


Figure 4.15 Differentiator circuits: (a) Ideal differentiator (b) Practical differentiator with limited bandwidth.

Due to its very nature, the scheme boosts up high frequency noise and causes erratic output swings. It is never used as such. If a differentiator is unavoidable, the modified differentiator of Figure 4.15 (b) may be used. It differentiates the low frequency signals but provides a 6 dB/octave high frequency cut off. We get the input-output relation for the scheme as,

$$\frac{V_o}{V_i} = -\frac{R_2}{(1+R_2C_2s)}\frac{C_1 s}{(1+R_1C_1s)}$$

$$= -\frac{R_2C_1s}{(1+R_2C_2s)(1+R_1C_1s)} \tag{4.72}$$

From the above we have for small s (*i.e.*, $s << [1/R_2C_2]$ & $s << [1/R_1C_1]$),

$$\text{Gain} = -R_2C_1s \tag{4.73}$$

$$\therefore f_1 = \frac{1}{2\pi R_2 C_1} \tag{4.74}$$

For large values of s (*i.e.*, $s >> [1/R_2C_2]$ & $s >> [1/R_1C_1]$),

$$\frac{V_o}{V_i} = -\frac{1}{R_1C_2s} \tag{4.75}$$

$$f_3 = \frac{1}{2\pi R_1 C_2} \tag{4.76}$$

We get maximum gain and range for the differentiator if the two corner frequencies $(1/2\pi C_1R_1)$ and $(1/2\pi C_2R_2)$ coincide; this gives,

$$f_2 = \frac{1}{2\pi R_1 C_1} = \frac{1}{2\pi R_2 C_2} \tag{4.77}$$

The Bode plot for the approximate differentiator is shown in Figure 4.16. The frequencies f_1, f_2 and f_3 are also shown marked in Figure 4.16. f_4 is the unity gain cross-over frequency for the open loop gain. For differentiation to be effective at frequency f_1, the following condition is to be satisfied.

$$f_1 << f_2 << f_4 \tag{4.78}$$

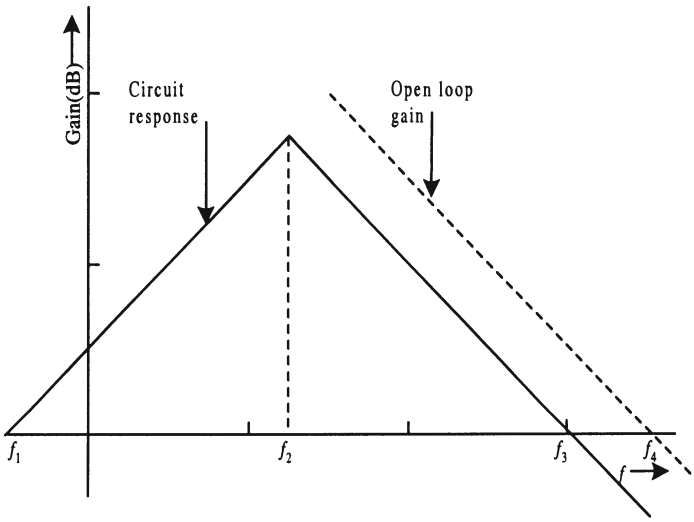


Figure 4.16 Frequency response of the practical differentiator shown in Figure.4.15 (b)

4.10 Difference Amplifier

A number of basic circuit configurations are available to amplify the difference between two signals. Figure 4.17 shows a low cost scheme built around a single opamp. The resistance ratios in the two halves are kept equal. With ideal conditions,

$$v_Q = \frac{R_2}{R_1 + R_2} x$$

$$= v_P \tag{4.79}$$

$$i_1 = \frac{y - v_Q}{R_1} \tag{4.80}$$

$$v_o = v_Q - i_1 R_2 \tag{4.81}$$

Eliminating i_1 and v_Q from the above set of equations,

$$v_o = \frac{R_2}{R_1}(x - y) \tag{4.82}$$

Thus the scheme amplifies the difference $(x - y)$ by (R_2 / R_1).

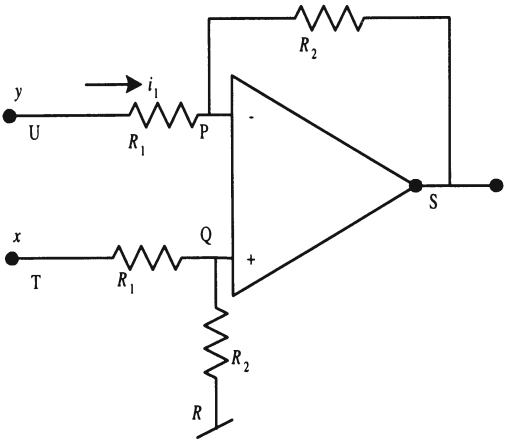


Figure 4.17 Difference amplifier circuit

Observations: -

⇒ The opamp sees a common mode voltage of $\{(x + y)\ R_2\}/\{2(R_1 + R_2)\}$. Opamps with a high CMRR should be selected for the configuration.

⇒ The resistances in the two halves are to be well matched. Any mismatch causes a differential output error of the same order. Thus, if R_1 connected to the non-inverting input x increases by δR_1, we get,

$$\text{Output error} = \frac{x}{R_1 + R_2}\frac{R_2}{R_1}\delta R_1 \tag{4.83}$$

⇒ A difference in the stray capacitances at the two inputs affects common mode rejection severely. The two R_2's may be shunted by selected equal capacitances to alleviate the problem. Stability and noise performance also improve due to this; but the effective bandwidth reduces.

⇒ The input impedances at the two inputs differ. The input impedance at the inverting input is R_1; that at the non-inverting input is $R_1 + R_2$.

⇒ The signal sources at the two inputs can typically take the form shown in Figure 4.18; v_p and v_n are the two voltages whose difference is to be amplified. The common point is shown as grounded. The common mode signal $(x + y) / 2$ [which is the same as $(v_p + v_n) / 2$] should not exceed the specified limits.

⇒ There are occasions when the junction point of v_p and v_n – J in Figure 4.18 – is floating and is not accessible. The scheme is well suited to amplify such signals. However, due to the high common-mode impedance, the circuit can easily pick up high common mode noise that can saturate the amplifier and even damage it. The input circuit should be fully shielded and the shield well grounded to ward off such spurious pick-ups.

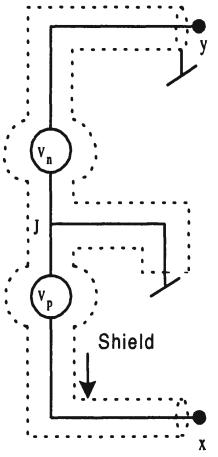


Figure 4.18 Shielding of difference amplifier inputs

Drift and noise performance can be analysed on the same lines, as was done with the inverting amplifier.

4.11 Adaptations of the Difference Amplifier

The basic difference amplifier has been adapted in a number of ways for transducer applications, especially for the resistance transducer. Some common schemes are discussed here. The basic difference amplifier scheme has been redrawn in Figure 4.19. Both the inputs are connected together to a well-stabilised supply V^+.

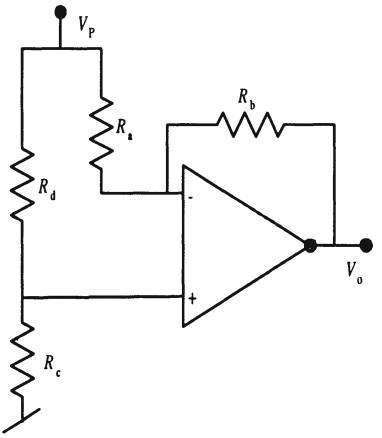


Figure 4.19 Commonly used adaptation of the difference amplifier for a resistance transducer

The resistances have been redesignated as R_a, R_b, R_c and R_d. In a resistance transducer these can form the four arms of the bridge. At balance we have,

$$\frac{R_d}{R_c} = \frac{R_a}{R_b} \tag{4.84}$$

Further, zero drift due to bias currents demands that,

$$R_d = R_a \tag{4.85}$$

and

$$R_c = R_b \tag{4.86}$$

Various possibilities of operation exist: -

⇒ With $R_a = R_b = R_c = R_d$, as zero signal condition, we have a unity ratio bridge. One can have one arm, two adjacent arms, two diagonally opposite arms or all four arms as transducer elements. We get the same output voltages as described in Section 2.2.4. But the outputs here are referred to the zero potential and can be loaded without buffering and without losing sensitivity. However, the scheme does not provide amplification.

⇒ Amongst the alternatives here for the single sensor case, R_c is the best suited to be the sensor, since one end of R_c is grounded.

⇒ $(R_c/R_d) = (R_b/R_a)$ can be made greater than 1, to amplify the transducer output. Here, R_a and (or) R_d will be the sensor(s) element(s). Both ends of the sensor are floating, which may not be acceptable always.

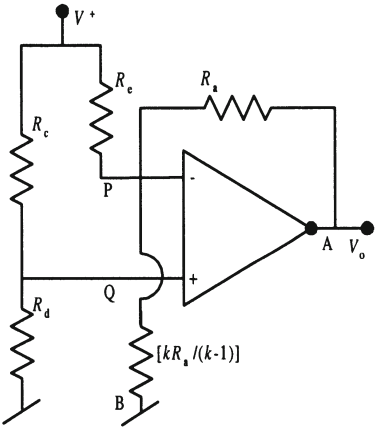


Figure 4.20 Another adaptation of the difference amplifier for a resistance transducer

⇒ A modification of the above scheme is shown in Figure 4.20. Note the ratio of the resistances selected. The scheme provides a gain of k. k can be typically in the range of 10 to 100. Normally, $R_c = R_d = R_a$. The fourth arm can be made up of an identical resistance in series with $R_a/(k-1)$. R_c, R_d and R_a can be the transducer resistors in any combination.

⇒ The basic difference amplifier as well as all its modifications considered, have two drawbacks:

- Mismatches in the resistances cause an output error. Difficulty to match the resistances better than 0.1 % results in error of the same order. Hence, the scheme is not suitable for precision work.
- The amplifier loads the inputs.

The circuit shown in Figure 4.21 is a difference amplifier using a modification of the non-inverting amplifier concept. Under normal working conditions,

$$V_P = V_Q \quad (4.87)$$

$$\text{Drop across } R_1 = x - y \quad (4.88)$$

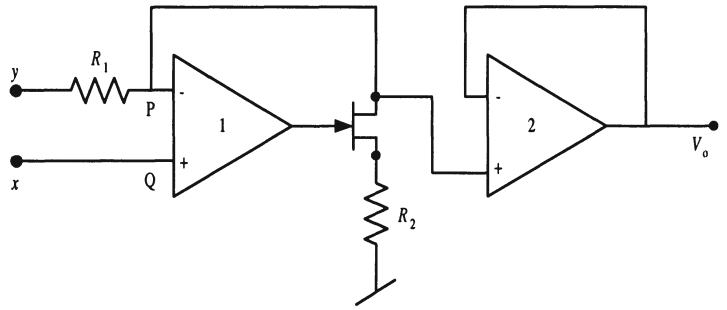


Figure 4.21 Modification of the non-inverting amplifier to function as a difference amplifier

Current through R_1 is $(x - y) / R_1$. The opamp biases the FET such that the full current passes through R_2. Drop across R_2 is $R_2 (x - y) / R_1$. The second opamp (2) acts as a buffer and prevents loading of R_2. The input current drawn from the signal source x is zero while that from y is decided by R_1. The tolerances and mismatch in the resistances affect only the stage gain. They do not cause any error. This is a conspicuous advantage of the arrangement, but it is at the cost of the additional components used.

4.12 Instrumentation Amplifier

The difference amplifier is well suited to amplify the difference between two signals. However, it has three limitations: -

⇒ The amplifier draws a definite set of currents from the signals and loads them to that extent.

⇒ The common mode rejection is decided by the tolerance in a set of resistances. It may not exceed 60 dB even though the CMRR of the amplifier may be 100 dB or more.

⇒ The practical gain values cannot exceed 100 or so.

The 'Instrumentation Amplifier' addresses these issues and performs better in some other respects as well. It is characterised by: -

⇒ Extremely high input impedances.

⇒ Low bias and offset currents.

⇒ Little performance deterioration even if source impedance changes.

⇒ Possibility of independent reference levels for source and amplifier.

⇒ Very high common mode rejection so that noise, pick-ups and effects of ground drops are minimised despite long sensor leads.

Instrumentation amplifiers are ideally suited for resistance transducers, thermo-couples *etc.* The basic instrumentation amplifier circuit is shown in Figure 4.22. All the components, except the resistance 2 R_G, are normally inside one monolithic IC.

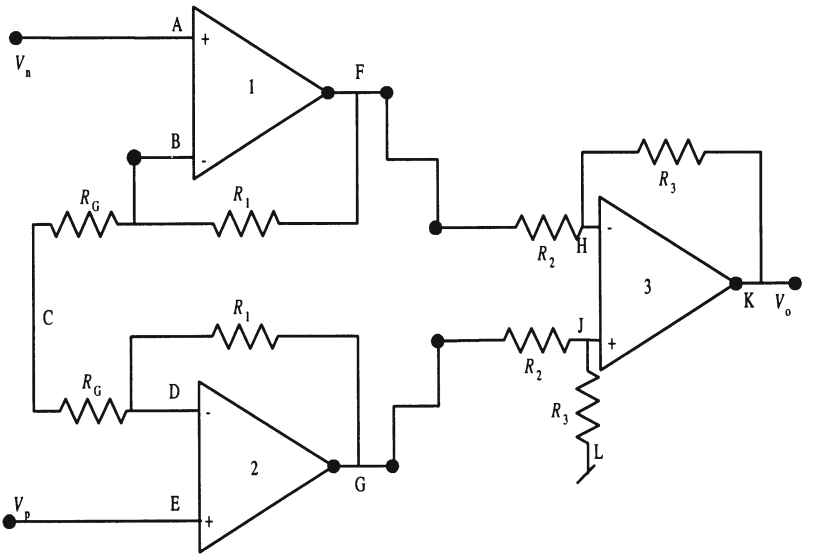


Figure 4.22 Three opamp based instrumentation amplifier

Amplifiers 1 and 2 are identical in characteristics. Being in the same IC, tracking of resistance pairs R_1, R_2 and R_3 is quite close. The amplifiers around opamp 1 and opamp 2, function as non-inverting amplifiers for differential mode input, and buffers for common mode input. The amplifier around opamp 3 is a difference amplifier. Analysis of the amplifier is considerably simplified by considering the common mode and the difference mode signals separately. Consider first a purely difference mode signal,

$$v_p = u \text{ volts} \tag{4.89}$$

$$v_n = -u \text{ volts} \tag{4.90}$$

both referred to the ground (0 V). Considering opamp 1,

$$V_B = -u \text{ volts} \tag{4.91}$$

For opamp 2,

$$V_D = +u \text{ volts} \tag{4.92}$$

Voltage across D and B, *i.e.*, resistance $2R_G$ = $2u$ volts (4.93)

Since point B is at $-u$ volts and point D is at $+u$ volts, point C remains at zero volts; *i.e.*, for difference mode signals, opamp 2 along with R_1 and R_G around it acts as a non-inverting amplifier.

$$\therefore v_G = \left(1+\frac{R_1}{R_G}\right)u \tag{4.94}$$

Further, the input impedance for v_P is very high.

In the same manner, opamp 1 along with R_1 and R_G functions as a non-inverting amplifier.

$$\therefore v_F = -\left(1+\frac{R_1}{R_G}\right)u \tag{4.95}$$

Here, the negative sign is due to the nature of input at point A as represented by Equation 4.90. Here again, the input impedance for V_n is very high.

$$\therefore v_G - v_F = 2\left(1+\frac{R_1}{R_G}\right)u \tag{4.96}$$

Opamp 3 with the pairs of resistances R_2 and R_3 functions as a difference amplifier with gain (R_3/R_2) [See Section 4.10].

$$\therefore v_o = (v_G - v_F)\frac{R_3}{R_2} \tag{4.97}$$

Combining Equation 4.96 and Equation 4.97 and using the fact that the input is $2u$,

$$\text{the total gain of the scheme} = \frac{v_o}{2u} \tag{4.98}$$

$$= \left(1+\frac{R_1}{R_G}\right)\frac{R_3}{R_2} \tag{4.99}$$

The overall gain of the instrumentation amplifier is built up in two stages. It is customary to use as high a gain as possible at the first stage and limit the second stage gain to a nominal value of 1 or 2 or of that order.
Now consider the common mode signal:

$$\text{Let} \quad v_p = v_n = w \text{ volts} \tag{4.100}$$

$$v_B = v_D = w \text{ volts} \tag{4.101}$$

The current through link BD is zero. The link can be considered as open.

$$V_F = V_G = w \text{ volts} \tag{4.102}$$

Opamps 1 and 2 function as unity gain buffers. Opamp 3, with the resistances around it, once again functions as a difference amplifier. With V_F and V_G being equal, $V_o = 0$.

The common mode impedance is also high. The input stages provide only unity gain to the common mode signal in contrast to a gain of $[1 + (R_1/R_G)]$, for the difference mode signal. This itself forms a substantial improvement in common mode performance.

Observations: -

- ⇒ Good-quality instrumentation amplifiers have become available in single IC form. They are preferred to instrumentation amplifiers built around identical opamps.
- ⇒ Difference mode gain can be adjusted by adjusting 2 R_G. This does not directly affect common mode performance.
- ⇒ Consider a mismatch between the two R_1's. As far as the common mode input w is concerned, opamps 1 and 2 act as unity gain buffers, and potentials of points F and G remain at w volts and the net output is still zero.
- ⇒ Consider the differential input. The mismatch in the two R_1's cause different amplifications for $+u$ at E and $-u$ at A. The common mode part of it is ignored by the amplifier around opamp 3. The difference-mode part gets

amplified. The net effect is to change only the gain for the difference-mode signal. This is in contrast to the previous difference amplifier, where a mismatch in the resistances generates a difference-mode output with a common-mode input resulting in a reduction in CMRR.

⇒ Mismatches in R_2 or R_3 cause common mode error but its effect is subdued on two counts:

- Firstly, the difference mode signal is substantially amplified in the first stage itself so that the relative magnitude of the error is reduced.
- Secondly, all the gain is normally arranged in the first stage and the difference stage works mostly at unity gain.

⇒ All environmental factors such as changes in ambient temperature, supply voltage *etc.*, affect the components symmetrically and hence do not cause any error. This is due to the matched components being physically close to each other in one package. The gain may be affected to an incremental extent only.

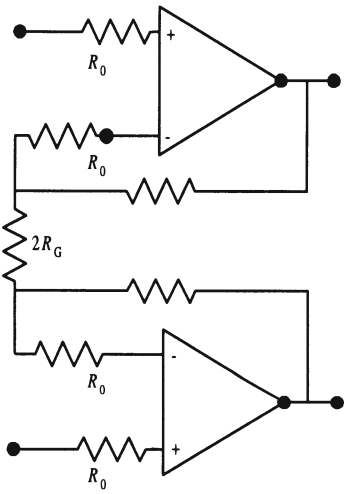


Figure 4.23 Modifications to the instrumentation amplifier to compensate for the lead resistances of R_G

⇒ As the gain increases to 1000, the value of resistance $2R_G$ may typically reduce to 10 – 40 ohms. The lead and solder joint resistances may add to it. R_G may be selected with a low temperature coefficient but the additional lead resistances may contribute to error. This is avoided by going in for the 4-terminal version of R_G as shown in Figure 4.23. Here the current and the voltage leads of R_G are separated. To compensate for resistances R_0 on either side of R_G, equal resistances are put in series with the input leads A and E of Figure 4.22.

⇒ If the inputs are prone to high voltage spikes or fast and large swings, which opamps 1 and 2 cannot cope up with, due to their limited slew rate, the opamps may be protected using back-to-back connected diodes at their inputs as shown in Figure 4.24. This reduces the input impedance values substantially and also limits the bandwidth.

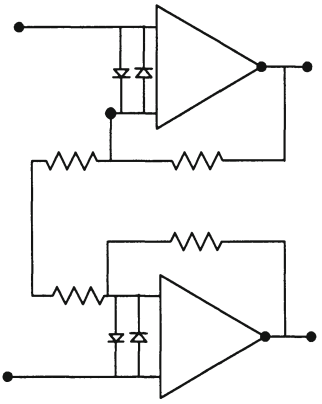


Figure 4.24 Modifications to the instrumentation amplifier to protect it against voltage spikes at the input side.

⇒ Some remote sensors are characterised by high source impedance and a local common mode different from the common mode seen by the instrumentation amplifier. The resulting potential gradients along the sensor leads can cause loading of the signal. This can be different in the two halves causing a common mode error. To avoid this, the sensor leads are enclosed in a screen. The screen is connected to the common voltage derived from the outputs of opamps 1 and 2 as shown in Figure 4.25. The common mode voltage is available at the junction of R_C's. It is buffered and the screen connected to the buffer. Leakage current to the screen is diverted to the buffer. The potential difference between the sensor leads and the screen is very low, since the screen is maintained at the common mode voltage. Thus, leakage current between the leads and the screen is eliminated.

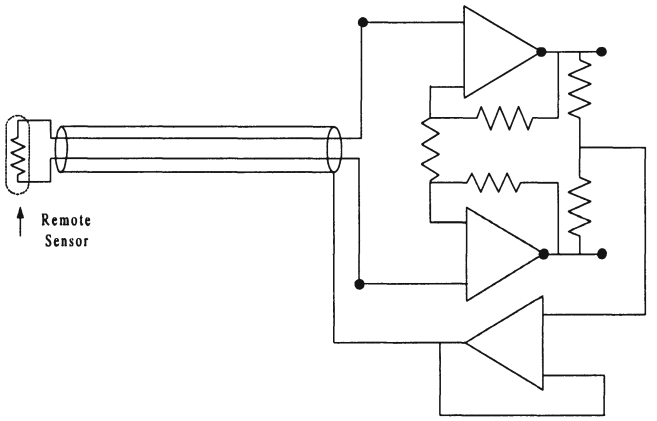


Figure 4.25 Instrumentation amplifier with remote sensors: Compensation for errors due to common mode voltage.

⇒ The output offset can be trimmed to zero by returning point L in Figure 4.22 to the output of a buffer as shown in Figure 4.26. It provides for an offset adjustment range of ±15mV. The resistance seen by the instrumentation

amplifier at the buffer output should be very low or it may cause mismatch of R_3's and affect CMRR adversely.

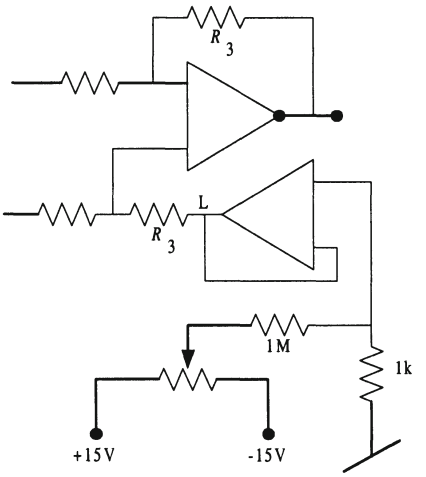


Figure 4.26 Modifications to the instrumentation amplifier in Figure 4.22 to trim the output offset to zero

⇒ Commercial instrumentation amplifiers are available with built-in $2R_G$ values. Three or four values are provided to correspond to gains of x1, x10, x100 and x1000. One has to short only the appropriate pins externally to get the desired gain. This makes the instrumentation amplifier compact without any external components. The instrumentation amplifier may even be kept close to the sensor.

Depending on the devices, technology and design, instrumentation amplifiers are available to different specifications. Table 4.1 gives representative specifications and typical applications.

Table 4.1 Instrumentation amplifiers – their key specifications and potential applications

Technology	Max. offset voltage (μV)	Max. offset voltage drift (V/°C)	Input bias current (nA) max.	Specific characteristics	Typical application
BJT	50	0.3	2	High accuracy	Thermocouple; Resistance bridge; transducer
FET input	500	5	0.02	High speed Low input bias current	Piezo- sensor
FET input	5000	10	10^{-5} nA	Very high input impedance	Electrometer; pH measurement
CMOS	50	0.5	5	Very low powe consumption (400μA drain)	Battery powered Instrumen-tation

4.13 Isolation Amplifier

Situations exist where the transducer signal to be amplified or processed is electrically at a high voltage and cannot be processed directly. Measurement of current in high voltage lines is an example. ECG and other similar biomedical instruments represent a reverse situation where the signal source is to be fully isolated and protected from the utility power supply based processing circuitry at comparatively much higher potential levels. 'Isolation Amplifiers' are used in these situations to faithfully transfer a signal across a high potential barrier. Ground loops formed in industrial environments involving thermocouple, RTD *etc.*, are also broken by such isolation amplifiers.

4.13.1 Schematic Arrangement

A generalized version of the isolation amplifier is shown in Figure 4.27. It functions through three isolated blocks – A is the signal input block, B the signal output block and C the power supply block. Block C accepts external input power and through an oscillator, isolation transformer and rectifiers, powers blocks A and B. Thus isolation of power supply to each block is ensured. Ports P_1 and P_2 do this power transfer function. The modulator in the input block modulates the signal. The modulated carrier is transmitted across the potential barrier through an isolation transformer or a coupling capacitor. The carrier is demodulated at the output block, amplified and output. The oscillator output is used as the carrier for modulation as well as the reference carrier for demodulation. Local availability of the reference carrier makes the DSC-SC scheme as the obvious choice for modulation and demodulation [See Section 6.2.1].

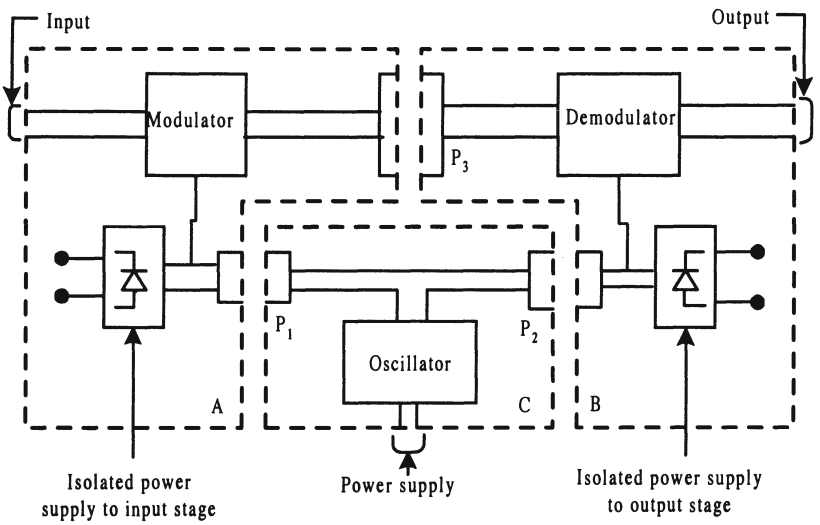


Figure 4.27 Isolation amplifier – general scheme

Power supply necessary for the input and output blocks, is transferred through dedicated ports P_1 and P_3. The modulated signal is transferred from the input to the output block through a third dedicated port P_3. This is the most general three-port scheme of the isolation amplifier. It requires the use of at least one transformer for the power transfer.

Observations: -

⇒ The isolation amplifiers in use today, are miniaturised hybrid blocks from specialised suppliers. One needs to know only its functional details and adapt it to the application. The isolation amplifier need not be designed from scratch.

⇒ The isolation function requires one port to be used to couple the modulated signal across. This is the minimum required; if such a single port is provided in the isolation amplifier, isolation of the power supplies has to be done externally. Such a scheme is the most cost-effective and simplest. More often, the isolation amplifier is powered on one side of the barrier – input or output side. Power to other side is transferred through a transformer. This forms the 'two port' scheme.

⇒ Separate non-committed amplifiers are often provided in the input and output sides. With these, the signal can be processed before and after the barrier in various configurations built around the opamps.

⇒ Often the isolation amplifier has a separate power supply output at the signal block. This facilitates excitation of the sensors without resorting to any additional power supplies.

⇒ The oscillator frequency may range from 50 to 500 kHz depending on the type of the isolation amplifier. Correspondingly, the small signal bandwidth can extend from 0 to 8 kHz at an oscillator frequency of 50 kHz and from 0 to 80 kHz at an oscillator frequency of 500 kHz.

⇒ The demodulated signal has a ripple content at twice the carrier frequency. This forms the main noise introduced by the isolation amplifier. If necessary, this may be reduced further using an external filter at the output side – this limits the bandwidth and the slew rate of the isolation amplifier.

Three types of isolation amplifiers are available: -

⇒ Transformer type

⇒ Capacitance coupled type

⇒ Opto-coupled type

Features of each are discussed here.

4.13.2 Transformer Type

In the transformer coupled isolation amplifier, the modulated output is coupled to the output side using a transformer. Figure 4.28 shows the scheme in block diagram form for a three port isolation amplifier. The transformer T_1 transfers power from block C to blocks A and B. The transformer T_2 couples the modulated signal across the barrier. It is normally of the toroidal core type with windings on either side – the other blocks are as described earlier. Use of the three-port scheme ensures very good isolation amongst the three blocks. Transformer coupled isolation amplifier is the earliest and most widely used of the instrumentation amplifiers.

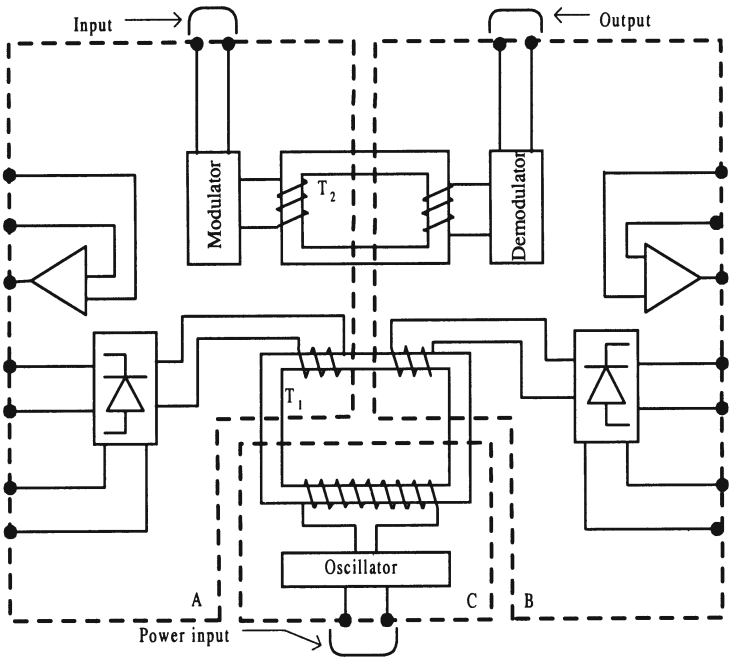


Figure 4.28 Transformer type isolation amplifier

4.13.3 Capacitance Coupled Type

Here the modulated output is coupled to the output side through coupling capacitors (Figure 4.29) which are in the 1 to 3 pF range. The capacitors are formed by the respective electrodes extended in the form of metallic spirals close to each other. These are directly deposited in the substrate and hermetically sealed. Normally the capacitor coupled instrumentation amplifiers are of the two-port type.

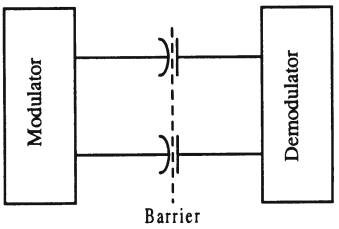


Figure 4.29 Capacitively coupled isolation amplifier

Frequency or pulse width modulation is used with the capacitively coupled isolation amplifiers. The carrier frequency is in the MHz range – hence capacitance of 1 to 3 pF suffices for coupling. The modulation scheme calls for much wider bandwidth for transmission across the barrier than the amplitude modulation

scheme. Hence, despite the carrier in the MHz range, signal bandwidth is in the 50 kHz range but gain accuracy is one order better than that with the transformer coupled versions.

4.13.4 Opto-coupled Type

Isolation amplifiers are being realised with the help of opto-couplers also. The transfer characteristic of opto-couplers does not exhibit repeatability or consistency to a level that justifies their direct use in isolation amplifiers. Hence they are used only in a feedback mode and the input signal is replicated in an indirect manner. (This is akin to the feedback transducer scheme in Section 10.5).

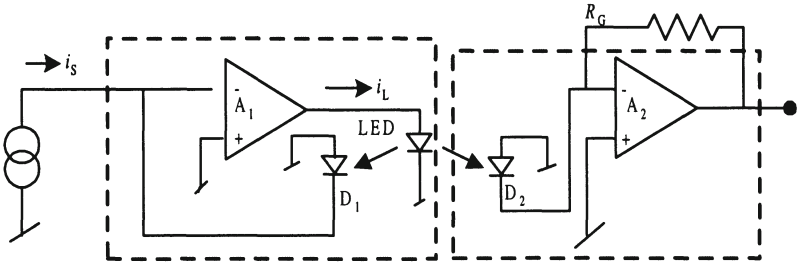


Figure 4.30 Optocoupler type isolation amplifier

The basic scheme is shown in Figure 4.30. It is built around an Opto-coupler with one LED and two detector diodes - D_1 and D_2. The diodes are identical in their characteristics and are identically positioned with respect to the LED. Any current i_L through the LED results in the same amount of radiation (from it) falling on the detector diodes D_1 and D_2. Hence, the currents induced in D_1 and D_2 are also identical. In the presence of the external signal current i_s, opamp A_1 drives a current through the LED until the current through the detector diode D_1 matches i_s (neglecting the bias current of A_1). An identical current is induced through diode D_2 also. The current amplifier around opamp A_2, converts this into an output voltage V_o. Referring to the figure, we have,

$$V_o = -i_s R_G \tag{4.104}$$

R_G is normally selected externally to provide the desired gain. Optical matching of D_1 and D_2 is achieved through laser trimming.

Observations: -

- ⇒ Although the current to light intensity characteristic of the LED and incident radiation to output current characteristic of the detector diodes are non-linear, overall transfer function is linear due to the feedback scheme employed.
- ⇒ The bias currents of the opamps A_1 and A_2 have to be low compared to the measuring current.
- ⇒ The basic operation described here is unipolar in nature. It is converted to bipolar form by suitable circuit modifications.

⇒ A separate power transfer port is to be added to the unit to provide isolated supplies on either side.
⇒ Voltage input signals are to be converted to current signal form and then used for amplification.

4.13.5 Comparison

⇒ In general, all three types are suitable for all applications. The transformer coupled isolation amplifier is the most widely used probably due to historical reasons.
⇒ The opto-coupled isolation amplifier uses the minimum number of components and is most cost effective. Transformer and capacitor coupled units increase in cost in that order.
⇒ Opto-isolated type offer lowest isolation voltage (800 V continuous) between the input and output. Transformer coupled type offers 1200 V and capacitance coupled ones offer 2200 V respectively. Of course, in each case the high-end versions offer improved isolation levels.
⇒ The isolation resistance levels are of the order of 10^{10}, 10^{12} and 10^{12} ohms for the transformer coupled, opto-coupled and capacitance coupled versions respectively. The corresponding capacitance values are of the order of 10 pF, 3 pF and 3 pF respectively.
⇒ Gain stability and non-linearity are best for capacitance coupled versions – 0.005 % – and on par for the other two – 0.02 %.

All the three types are essentially similar in all other respects.

5 Active Filters

5.1 Introduction

Filters are essential building blocks of instrumentation schemes; they serve a variety of purposes at different locations in the scheme: -

- ⇒ Band limiting and improving the signal to noise ratio
- ⇒ band limiting before sampling to minimize aliasing errors
- ⇒ picking out a frequency component or suppressing a selected frequency component from a signal
- ⇒ restricting the band of frequencies retained after modulation or demodulation

5.2 Classification of Ideal Characteristics

Filters can be of five broad categories. Ideal characteristics of each are discussed here.

5.2.1 Low Pass Filter (LPF)

The LPF passes all the low frequency components in the input signal but suppresses the high frequency components. The gain characteristic of an ideal LPF is as shown in Figure 5.1 (a). It has a constant definite value from 0 to a definite frequency – ω_c – but is zero thereafter. The frequency range 0 to ω_c is called the 'passband' of the filter. The ideal phase shift characteristic shown in Figure 5.1 (b), has the phase shift changing linearly with frequency in the passband; there is no restriction in the phase characteristic outside the passband. The need for the ideal phase characteristic is not apparent at the outset. If we give an input signal,

$$v_i(t) = f(t) \tag{5.1}$$

to a filter, the best output that can be expected is

$$v_o(t) = f(t - \tau) \tag{5.2}$$

where τ is a constant time delay introduced by the filter.

The transfer function of a constant time delay function is

$$G(s) = e^{-s\tau} \tag{5.3}$$

The frequency response of the delay function is

$$|G(j\omega)| = 1 \tag{5.4}$$

$$\angle G(j\omega) = -\omega\tau \text{ radians} \tag{5.5}$$

T. R. Padmanabhan, *Industrial Instrumentation*
© Springer-Verlag London Limited 2000

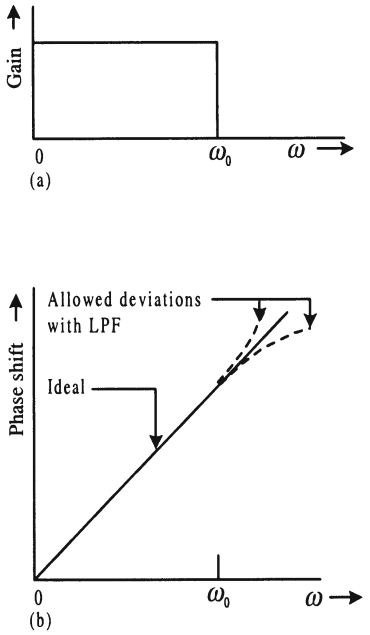


Figure 5.1 Frequency response of ideal low pass filter: (a) Gain characteristic (b) Phase shift characteristic

The phase shift characteristic of Equation 5.5 is a linear function of frequency as shown in Figure 5.1 (b). Taking a lead from Equations 5.4 and 5.5, we may expect an ideal low pass filter to satisfy the following conditions: -

⇒ Unity gain (or any other definite gain) within the passband
⇒ Zero gain beyond the passband
⇒ Linear phase shift characteristic within the passband conforming to Equation 5.5 and
⇒ No specific constraint on phase shift outside the passband

The ideal gain and phase characteristics are not physically realizable in practice. Practical filter realizations approximate these to different degrees using different criteria.

5.2.2 High Pass Filter (HPF)

The HPF is the dual of the LPF. It suppresses all frequency components up to ω_c but passes those beyond ω_c. The ideal gain characteristic of an HPF is shown in Figure 5.2. The gain is zero for all frequencies up to ω_c. For frequencies $\omega > \omega_c$, the gain is a constant. HPF applications do not seem to demand any specific phase characteristics (Hence normally no ideal phase characteristic is considered). Once again, the ideal gain characteristic is not physically realizable. Practical filters approximate this to different degrees using different criteria.

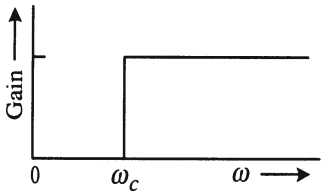


Figure 5.2 Frequency response characteristic (gain) of ideal high pass filter

5.2.3 Band Pass Filter (BPF)

A Bandpass filter passes a selected band of frequency components through but suppresses those on either side. The gain characteristic of an ideal BPF – shown in Figure 5.3 (a) – has

$$\text{Gain} = 0 \quad \text{for } \omega > \omega_{ch} \text{ and} \tag{5.6}$$

$$\text{Gain} = 0 \quad \text{for } \omega < \omega_{cl} \tag{5.7}$$

$$\text{Gain} = A \quad \text{for } \omega_{cl} \leq \omega \leq \omega_{ch} \tag{5.8}$$

$$\omega_o = \frac{\omega_{cl} + \omega_{ch}}{2} \tag{5.9}$$

where ω_o, ω_{cl} and ω_{ch} are the centre frequency, the lower cut-off frequency and the upper cut-off frequency respectively of the filter. When used with double sided modulation systems, the ideal phase characteristic has to be linear with frequency [See Figure 5.3 (b)] – ω_0 being the frequency at which the phase lag is zero. If used with single sideband systems, the lower half of the characteristic (ω_{cl} to ω_0) or its upper half (ω_0 to ω_{ch}), forms the ideally desired one [See Section 6.2.1].

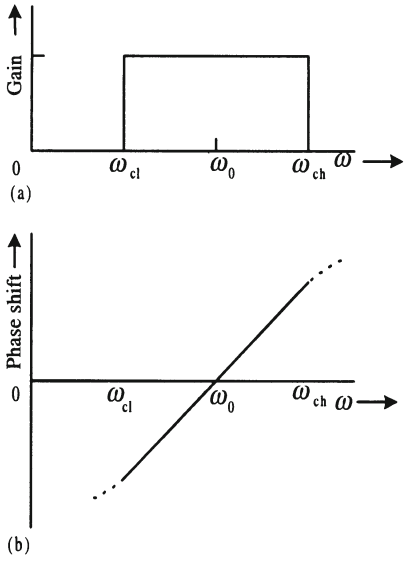


Figure 5.3 Frequency response characteristics of ideal bandpass filter: (a) Gain characteristic (b) Phase shift characteristic

When ω_{cl} and ω_{ch} are sufficiently close to ω_o such that

$$\omega_{ch} - \omega_{cl} = \Delta\omega << \omega_o \tag{5.10}$$

the BPF is called a 'Narrow Band Filter'.

Although the ideal BPF and the narrow band filters are similar in characteristics, their practical realizations are markedly different. Hence they are discussed separately. As with LPF and HPF, practical realizations of BPF and narrow band filters approximate the ideal filters to different degrees.

5.2.4 Band Rejection Filter (BRF)

The BRF rejects all signal components in the specified frequency band. The ideal BRF characteristic is shown in Figure 5.4.

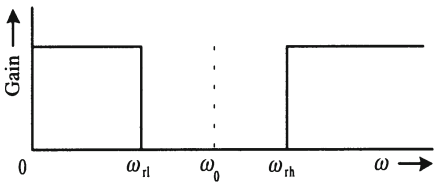


Figure 5.4 Frequency response (gain) characteristic of ideal band rejection filter

Its gain is such that,

$$\begin{aligned} \text{Gain} &= A \quad \text{for } \omega < \omega_{rl} \ \ \& \ \ \omega > \omega_{rh} \\ &= 0 \quad \text{for } \omega_{rl} \le \omega \le \omega_{rh} \end{aligned} \tag{5.11}$$

$$\omega_o = \frac{\omega_{rh} + \omega_{rl}}{2} \tag{5.12}$$

where ω_0, ω_{rl} and ω_{rh} are the centre frequency, the lower cut-off frequency and the upper cut-off frequency respectively of the filter. Applications which call for the use of a BRF, seem to impose restrictions only on the gain characteristic and not on the phase characteristic. If ω_{rl} and ω_{rh} are close *to* ω_0, such that

$$\omega_{rh} - \omega_{rl} = \Delta\omega << \omega_o \tag{5.13}$$

the BRF rejects a narrow band of frequencies around ω_0. Such a filter is termed a 'Notch Filter'. The ideal characteristics of the BRF and the notch filter are similar. However practical realizations are quite different. As with other filters, practical BRFs approximate the ideal ones to different degrees.

5.2.5 All Pass Filters

All pass filters are of a special category. They offer a phase shift for signals over a selected band of frequencies; but the gain remains the same over the whole frequency range. Thus they modify only the phase response. All pass filters are used in tandem with other filters to modify the phase versus frequency characteristic of the overall filter and bring it in line with a prescribed characteristic.

5.3 Filter Requirements in Instrumentation Schemes

Filters used in instrumentation schemes are of two broad categories. Those used directly at the outputs of sensors and those at individual signal processing stages. The signal processing stages are for modulation, demodulation and allied activities. Some types of filters are required prior to such processing and others after the processing. The need and scope of these will be dealt with later. Filters serve the following purposes: -

⇒ Cut off the unnecessary frequency bands and (hopefully) improve the signal to noise ratio.

⇒ Suppress specific frequency components e.g., carrier in a modulated sensor output, power frequency pick-up *etc.*

⇒ In an ADC, minimize aliasing errors by filtering before sampling (anti-aliasing filter).

⇒ To highlight a selected frequency component. The same may yield some specific information about the physical variable being measured.

In general, the sensors used to measure the common variables like temperature, pressure, flow *etc.*, give out low frequency outputs. Normally LPF are used with them. The filter output should be a faithful reproduction of the nature of time variation of the input signal; one may perhaps allow only a definite time delay. In such cases, the phase shift versus frequency characteristic and its specifications too, will be significant. For sensors that measure acoustic noise, vibration *etc.*, the sensor output is not used directly. The amplitude spectral characteristics being more important here, information extracted from the output in terms of the amplitudes of individual frequency components, is used. Only the amplitude response and its specifications – but not the time domain or phase shift characteristics – matter here.

5.4 Specifications of Practical Filters

Different specifications are used to judge the closeness of practical filter characteristics to the ideal one. Such specifications can be in terms of the frequency, the time response characteristics or a combination of both.

5.4.1 Low Pass Filter

Amongst filters, the LPF has the most varied of specifications. It can be in terms of gain characteristic, phase characteristic or time response or a combination of these. The gain characteristic is specified in terms of quantities indicated in Figure 5.5: -

⇒ Passband ripple represents a narrowly specified band within which the gain in the passband must lie.

⇒ Stopband attenuation is the minimum attenuation acceptable for all frequencies in the stopband.

⇒ Cut-off frequency – ω_c – is the largest frequency in the passband at which the gain lies within the permissible passband ripple.

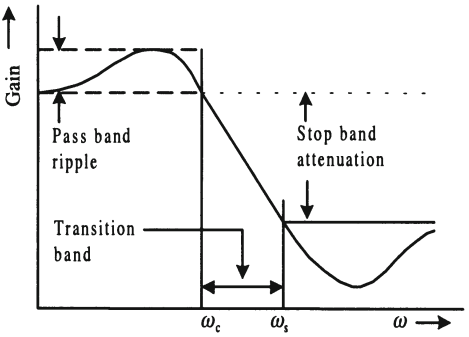


Figure 5.5 Frequency response (gain) specifications of low pass filter

⇒ The stopband frequency – ω_s – is the lowest frequency at which the attenuation reaches the specified value.

⇒ The transition band is $\omega_s - \omega_c$; *i.e.*, the frequency band over which the gain is lower than the minimum acceptable in the passband but higher than the maximum acceptable in the stopband.

For the filter,

⇒ the passband ripple should be as low as possible,

⇒ the stopband attenuation should be as high as possible and

⇒ the transition band should be as narrow as possible.

These being conflicting requirements, one has to strike a balance in realizing the filter.

The phase response of a typical LPF is shown in Figure 5.6. As mentioned earlier, the ideal phase response curve is linear, the phase lag increasing steadily from 0Hz onwards; the increase continues at least up to the end of the passband. In a practical situation, the maximum deviation from linearity – designated as 'δ' – can be the yardstick of linearity. Normally the phase characteristic specification is not rigidly quantified – presumably due to the fact that the phase characteristic is not of direct use. It is used only as a measure of uniformity or non-uniformity of the time delay introduced by the filter.

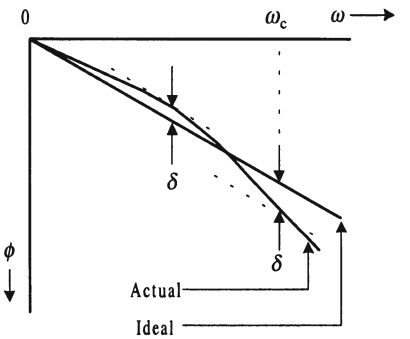


Figure 5.6 Phase shift specifications of low pass filter

The time response of the LPF is specified mostly in terms of the step response. Unit step input and typical response are shown sketched in Figure 5.7. All the parameters normally used to specify the step response, are also indicated in the figure: -

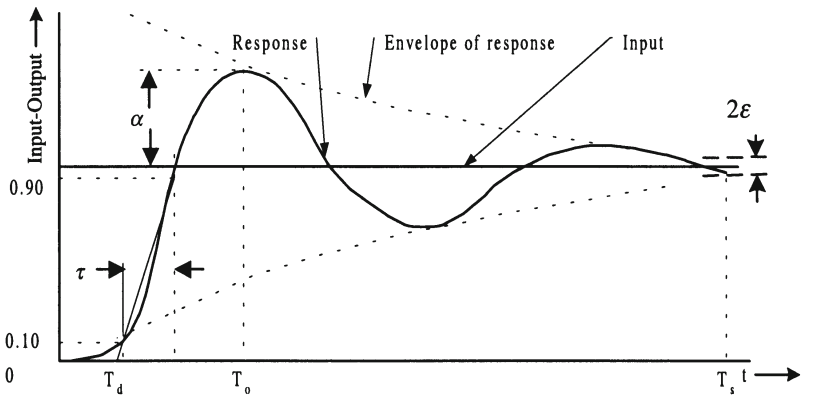


Figure 5.7 Step response specifications of low pass filter

⇒ 'τ' is the rise time. It represents the time taken for the response to increase from 0.1 to 0.9 during the initial rise. Sometimes, the inverse of the slope of the response when it reaches 0.5, or at the inflection point, is taken as the rise time.

⇒ 'α' is the first maximum overshoot – the extent by which the output overshoots the unit step input for the first time.

⇒ 'T_0' is the time for the first maximum overshoot.

⇒ 'T_d' is the delay time. It is a measure of the time for the system to 'rise up'. It is the point of intersection of the straight line joining the points representing 0.10 and 0.90 on the output curve, with the time axis.

⇒ 'T_s' is the settling time. It is the time taken for all the transients associated with the unit step response to die down to within ±5 % of the steady state value. Sometimes the settling is considered to within 3 % or 1 % also.

⇒ 'ε' is the steady state error. It is the extent to which the output fails to reach the input value even after all the transients die down.

The best filter will have all the above parameters as zero or each of them as low as possible. The conflicting nature of the requirements calls for a compromise, at least in some of the specifications. For all linear filters (which are the only ones considered here) specifications in terms of frequency response invariably imply corresponding specifications in terms of time response. This is due to the close correlation between the two responses. However, the correlation is used as a basis for relating specifications in the two planes – only to establish thumb rules or serve as a rough guide.

Filters meeting frequency response criteria are poor in time response and *vice versa* (good correlation it is!). Hence, depending on the context of application, only the frequency response specifications or only the transient response specifications are considered for the filter design.

5.4.2 High Pass Filter

HPF are specified normally only in terms of their gain characteristics. A typical response curve is shown sketched in Figure 5.8. The parameters that characterize the response are also indicated. The response and the parameters can be compared with their counterparts in the case of the LPF considered above. All the parameters here have the same significance as their corresponding counterparts in the LPF case.

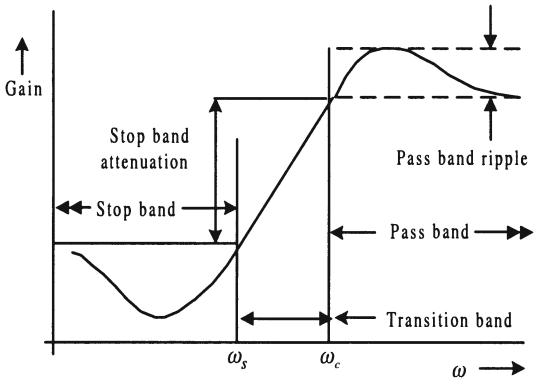


Figure 5.8 Frequency response (gain) specifications of high pass filter

⇒ Passband ripple specifies the maximum deviation permissible, in the passband gain.
⇒ Stopband attenuation is the minimum attenuation acceptable in the stopband.
⇒ Cut-off frequency – ω_c – is the lowest frequency at which the gain (*i.e.*, the minimum specified gain in the passband) lies within the specified passband ripple.
⇒ The stopband frequency – ω_s – is the largest frequency at which the gain lies below the minimum specified value.
⇒ The transition band $\omega_c - \omega_s$, is the band of frequencies over which the gain is lower than the minimum permissible in the passband but higher than the maximum permissible in the stopband.
⇒ The best filter is characterized by
- minimum passband ripple
- minimum transition bandwidth
- largest stopband attenuation

Practical filter realizations strike different levels of balance amongst these conflicting requirements.

5.4.3 Band Pass Filter

BPF are normally specified in terms of their gain and phase characteristics. Typical characteristics are shown sketched in Figure 5.9. The gain response is specified in terms of two sets of parameters.

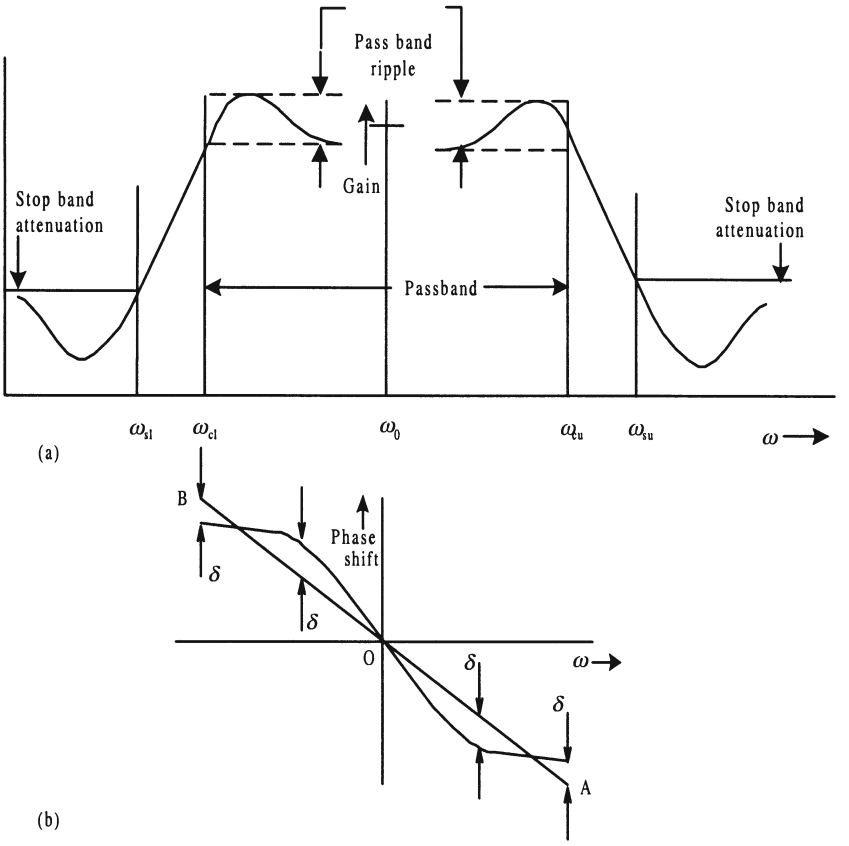


Figure 5.9 Frequency response specifications of band pass filter: (a) Gain characteristic (b) Phase shift characteristic

⇒ the upper cut-off frequency – ω_{cu}, the upper stopband frequency – ω_{su}, the upper transition band – $(\omega_{su}-\omega_{cu})$, passband ripple and minimum attenuation, are all identical to their LPF counterparts.

⇒ The lower cut-off frequency – ω_{cl}, lower stopband frequency – ω_{sl}, lower transition band – $(\omega_{cl}-\omega_{sl})$, passband ripple and minimum attenuation, are all identical to their HPF counterparts.

The phase response, desired and specified, depends on the expected function of the filter. When used with double sideband systems, an odd symmetric characteristic is desired. The maximum acceptable deviation from linearity – δ – may be specified. When the filter is used with single sideband schemes that use the upper sideband, the portion OA is specified; when used with the single sideband schemes that use the lower sideband, the portion OB is specified.

5.4.4 Band Rejection Filters

Gain characteristic of a typical BRF is shown in Figure 5.10. BRF are normally specified in terms of their gain characteristic only. The lower cut-off characteristic

specifications are identical to those of the LPF and the upper cut-off characteristic specifications to those of the HPF.

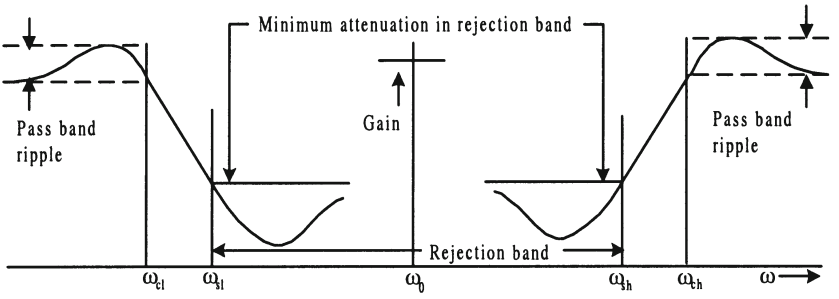


Figure 5.10 Frequency response (gain) specifications of band rejection filter

5.4.5 Narrow Band and Notch Filters

The narrow band and notch filters are special cases of the BPF and BRF respectively. Their bandwidths are small compared to their centre frequencies. Figures 5.11 (a) & (b) show the respective gain characteristics.

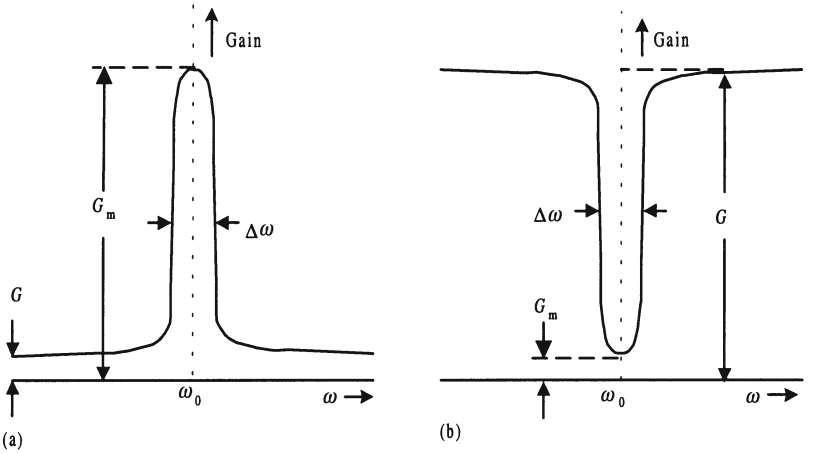


Figure 5.11 Frequency (Gain) response characteristics of (a) narrow band filter and (b) notch filter

For the narrow band filter

$\Rightarrow$ ω_0 is the centre frequency

$\Rightarrow$ G_m is the gain at the centre frequency

$\Rightarrow$ G is the gain at a frequency far away from ω_0. Normally it may be the gain at (ω_0/10) and (10 ω_0).

$\Rightarrow$ $\Delta\omega$ is the narrow band over which the gain lies above 0.707 G_m.

Normally ω_0, $\Delta\omega$ and the ratio (G_m / G) are specified. (G_m / G) is a measure of the relative boost to the selected band while $\Delta\omega$ is a measure of the sharpness of the

filter. Apart from specifying the magnitudes of ω_0, $\Delta\omega$ and (G_m / G), the tolerances on ω_0 and (G_m / G) as well as their stability with time, are specified.
For the notch filter

⇒ ω_0 is the centre frequency
⇒ G_m is the gain at the centre frequency
⇒ G is the gain at a frequency far away from ω_0. Normally it may be the gain at $(\omega_0 / 10)$ or $(10\omega_0)$.
⇒ $\Delta\omega$ is the narrow band over which the gain lies below 0.707 G_m.

As with the narrow band filter, ω_0, $\Delta\omega$ and the ratio (G_m / G) are specified. (G_m / G) is a measure of the relative rejection level to the selected band. $\Delta\omega$ is a measure of the sharpness of the filter. Apart from specifying the magnitudes of ω_0, $\Delta\omega$ and (G / G_m), the tolerance on ω_0 and (G_m / G) as well as their stability with time, are specified.

5.5 Normalized LPF

The LPF, HPF and the BPF can be studied in detail on a common basis [Huelsman]. Specifically we can investigate in detail the LPF with unit cut-off frequency – called the 'Normalized LPF'. The same can be scaled to get an LPF with any desired cut-off frequency. The HPF and BPF can be obtained from the LPF by a suitable frequency transformation. We discuss the different filter realizations in vogue with the normalized LPF as the basis. Aspects of design specific to any other filter, will be discussed separately subsequently. The normalized LPF has the filter transfer function of the form

$$G(s) = \frac{Z(s)}{P(s)} \tag{5.14}$$

where

⇒ $G(s)$ is the filter transfer function
⇒ $Z(s)$ is a polynomial in s of degree m
⇒ $P(s)$ is a polynomial in s of degree n and
⇒ n, m are positive integers with $m < n$.

The magnitude of the gain of the filter $|G(j\omega)|$ at any frequency ω, can be expressed as

$$|G(j\omega)|^2 = [G(s)G(-s)]_{s=j\omega} \tag{5.15}$$

where $j\omega$ has been substituted for s in Equation 5.14. The gain response characteristic of the normalized LPF is shown sketched in Figure 5.12. Its passband extends from 0 to 1 rad/s. For $s = j\omega$, with $0 < \omega < 1$ (passband),

$$1-\varepsilon < |G(j\omega)| < 1+\varepsilon \tag{5.16}$$

where ε is the allowable tolerance in gain in the passband. For

$$\omega > \omega_s = 1+\delta_s \tag{5.17}$$

$$|G(s)|_{s=j\omega} \leq A_s \tag{5.18}$$

where

⇒ ω_s is the stopband starting frequency

$\Rightarrow \delta_s$ is the width of the transition band and
$\Rightarrow A_a$ is the minimum attenuation required in the stopband.

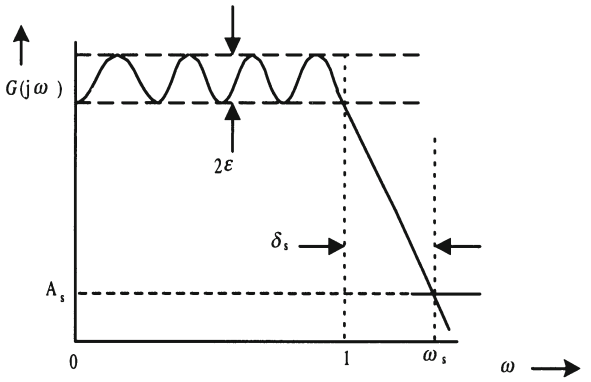


Figure 5.12 Frequency gain characteristic of the normalized low pass filter

Filter transfer functions in other forms too are possible. The 'ratio-of-polynomials' form used here has been well studied. Methods of realizing filters in this form are also well documented. Due to these reasons, filter circuit realizations in this form are in wide use. Four types of realizations of filters in ratio-of-polynomials form are in common use. We study these in greater detail here. With the normalized LPF, in three of these cases, the filter transfer function takes the form

$$G(s) = \frac{1}{P(s)} \tag{5.19}$$

i.e., the filter transfer function has only definite poles and no definite zeroes. These are the Butterworth, Chebyshev and the Bessel/Thomson forms. For these, the degree of the polynomial $P(s)$ is the order of the filter. For an n^{th} order filter, the eventual cut-off rate is $20n$ dB / decade. In the fourth case – the elliptic Filter – the filter is realized as a ratio of two polynomials.

5.5.1 Butterworth Filter

An n^{th} order Butterworth filter has n poles. The corresponding polynomial – called the Butterworth polynomial – can be obtained from Equations 5.15 and 5.20 [Heulsman]. All the poles lie on the unit circle in the left half plane. The pole configurations for a few low order Butterworth filters are shown in Figure 5.13.
The gain characteristic of the filter has the form

$$|G(j\omega)| = \frac{1}{\sqrt{1+\omega^{2n}}} \tag{5.20}$$

Observations: -

$\Rightarrow$ The gain is unity at zero frequency and falls off steadily as ω increases.
$\Rightarrow$ Once the order of the filter is decided, the Butterworth filter is uniquely fixed.

⇒ At $\omega = 1$, the gain is -3db. The -3db cut-off frequency is 1. In the passband, the lowest gain is at 1 rad/*s*.

⇒ The gain characteristic has zero slope at $\omega = 0$. All derivatives of the gain-function up to the n^{th}, are zero at $\omega = 0$; the filter characteristic is 'maximally flat' at $\omega = 0$.

⇒ The attenuation increases rapidly beyond $\omega = 1$. The final attenuation rate is $20n$ dB / decade.

⇒ Normally the Butterworth filter is realized as a series of second order sections followed by a first order section (if necessary). All these are connected in tandem.

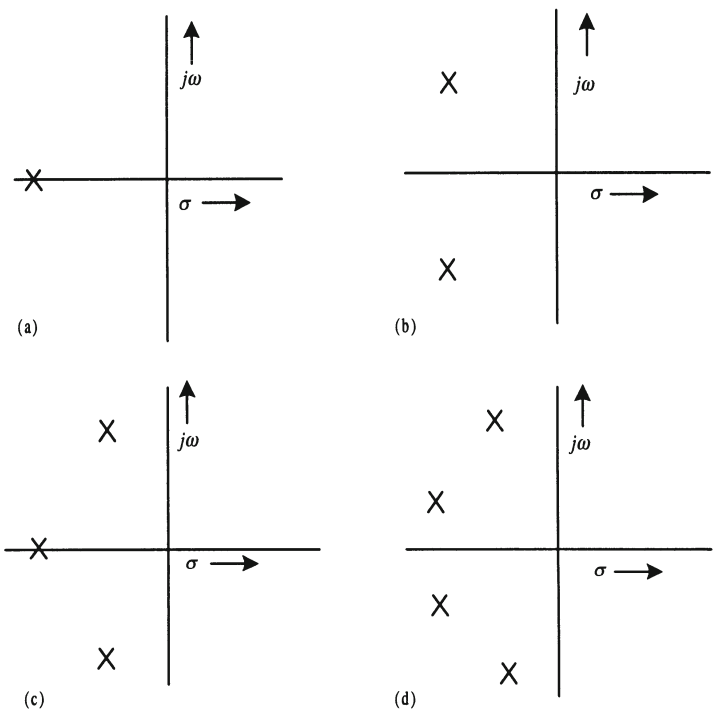


Figure 5.13 *s*-plane pole configurations of Butterworth filter for different orders (n): (a) $n = 1$ (b) $n=2$ (c) $n=3$ (d) $n = 4$

5.5.2 Chebyshev Filter

An n^{th} order Chebyshev filter has n poles. All the poles lie on an ellipse – in the left half plane as shown in Figure 5.14. The Chebyshev filter restricts the passband gain to a restricted slot around the mean gain value. The cut-off characteristics are similar to those of the Butterworth filter. As we increase the order of the filter, the number of times the gain characteristic swings within the restricted slot in the passband, increases – *i.e.*, the number of maxima and minima for the gain in the passband increases.

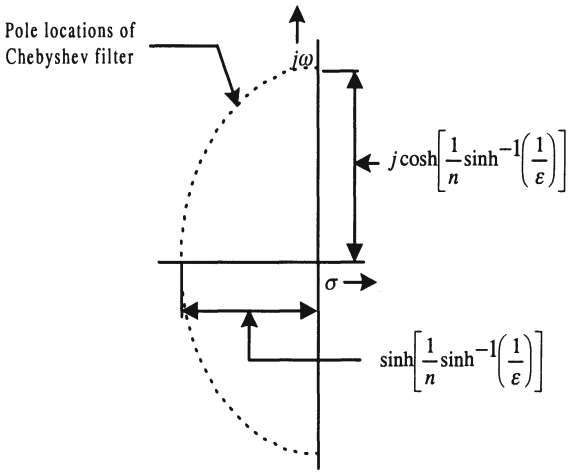


Figure 5.14 Pole locations of Chebyshev filter

The coordinates of the poles of the filter are given by,

$$s = \pm\sin\left[(2k+1)\frac{\pi}{2n}\right]\sinh\left(\frac{1}{n}\sinh^{-1}\frac{1}{\varepsilon}\right) \pm j\cos\left[(2k+1)\frac{\pi}{2n}\right]\cosh\left(\frac{1}{n}\sinh^{-1}\frac{1}{\varepsilon}\right) \quad (5.21)$$

where ε is the passband tolerance. Alternately one can use the Chebyshev polynomials

$$T_n(\omega) = \cos\left[n\cos^{-1}(\omega)\right] \quad (5.22)$$

and obtain the passband gain function $|G(j\omega)|$ from

$$|G(j\omega)|^2 = \frac{1}{1+\varepsilon^2 T_n^2(\omega)} \quad (5.23)$$

Equations 5.22 and 5.23 can be used along with Equation 5.15 to obtain $G(s)$. Note that the polynomials $T_n(\omega)$ are fixed once the order of the filter is fixed. A few low order Chebyshev polynomials are given in Table 5.1. For a given n, for each value of ε, we get different filter polynomials $P(s)$ and hence $G(s)$. The order of the filter and the number of filter stages, are determined by the gain specified at ω_s – the stopband frequency. If this gain is A_s, we get from Equations 5.22 and 5.23 the relation,

$$n \geq \frac{\cosh^{-1}\left(\frac{1}{\varepsilon}\sqrt{\frac{1}{A_s^2}-1}\right)}{\cosh^{-1}\omega_s} \quad (5.24)$$

n is to be chosen as the smallest positive integer that satisfies the above condition. If the stopband frequency ω_s, is very large compared to the cut-off frequency ω_c.
i.e.,

$$\omega_s >> \omega_c$$

one can use the approximate relationship

$$n \geq \ln\frac{\omega_s}{\omega_c} \tag{5.25}$$

A practical approach is to evaluate the smallest integral value of n satisfying Equation 5.25 and if necessary, correct it to satisfy Equation 5.24.

Observations: -

⇒ The Chebyshev polynomials are obtained by minimizing the maximum error between ideal and realized passband gain values. To this extent, the passband characteristic is better than that of the Butterworth filter.

⇒ The Chebyshev filter polynomial is determined uniquely if n and ε are known. The value of n is decided from the minimum attenuation that can be tolerated in the stopband. ε is specified as a criterion – maximum permissible deviation from the ideal gain.

⇒ The cut-off frequency ω_c, is the frequency beyond which the gain is less than the value $(1-\varepsilon)$.

⇒ The eventual cut-off rate is $20n$ dB/ decade – same as that with the Butterworth filter.

⇒ The filter is realized as a series of second order sections and (if necessary) a first order section. All these sections are connected in tandem to form the total filter.

⇒ Forming the Chebyshev filter polynomials and factorising them is more cumbersome than doing the same with the Butterworth filter polynomial. However, with the availability of extensive tabular data, this is no longer perceived as a problem.

Table 5.1 Chebyshev polynomials

n	0	1	2	3	4
$T_n(\omega)$	1	ω	$2\omega^2-1$	$4\omega^3-3\omega$	$8\omega^4-8\omega^2+1$

5.5.3 Bessel / Thomson Filter

The third commonly used form of filter, uses the Bessel polynomials as $P(s)$ in Equation 5.19. The first two Bessel polynomials are

$$B_0 = 1 \tag{5.26}$$

$$B_1 = s+1 \tag{5.27}$$

Subsequent Bessel polynomials are obtained from these, using the recursive formula

$$B_n = (2n-1)B_{n-1} + s^2 B_{n-2} \tag{5.28}$$

where B_n is the Bessel polynomial of order n.

Observations: -

⇒ The attractive characteristic of Bessel filters, is their linear frequency versus phase relationship.

⇒ Gain characteristics, cut-off rate *etc.*, are similar to the Butterworth filter and the Chebyshev Filter. The cut-off rate near the cut-off frequency is poorer than that of the Butterworth filter.

⇒ The filter is realized as a set of second order cascaded sections and (if necessary) an additional first order section.

5.5.4 Elliptic Filter

The simplest Elliptic filter transfer function has the form

$$G(s) = H\frac{s^2 + a_0}{s^2 + b_1 s + b_0} \tag{5.29}$$

For the case $a_0 > b_0$, it yields an LPF. Typical gain characteristic of a lowpass type elliptic filter is shown sketched in Figure 5.15. More such sections can be cascaded to obtain elliptic filters of higher orders.

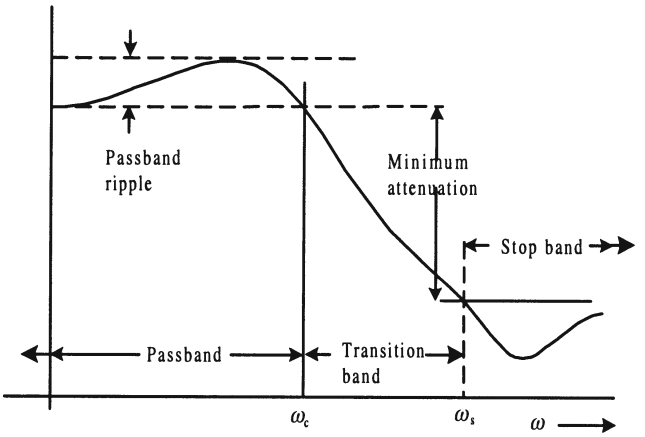


Figure 5.15 Frequency response (Gain) characteristic of low pass elliptic filter

Observations: -

⇒ Elliptic filters use 'Biquads' – ratio of two polynomials – of the type in Equation 5.29 to obtain the overall filter transfer function. A pair of zeroes on the imaginary axis and a pair of suitably positioned poles in the left half plane characterize each biquad.

⇒ The elliptic filter provides the steepest cut-off amongst all the filters, but its phase response is poor.

⇒ Unlike the other three filters, the gain does not drop down to zero with frequency; but it lies below a minimum specified value in the whole of the stopband.

⇒ Coefficients of the polynomials of the biquads of the type in Equation 5.29 are decided by trial and error. One approach is to iteratively arrive at the coefficient values to satisfy the set of given frequency response specifications.

5.5.5 Comparison

A brief qualitative comparison of the four types of filters is given in Table 5.2. Details of the transfer functions for Butterworth, Chebyshev and Bessel filters up to the fourth order are given in Table 5.3. In the case of the Chebyshev filter only – two representative cases have been considered. Detailed tables and response comparison are available in literature [Heulsman, Ludeman]. The elliptic filter stands out due to the different approach to filter realization. The variety in its combinations makes room for an equal variety in the transfer functions. One set of third and fourth order transfer functions of elliptic filters [Wait *et al.*] is also included in the table.

Table 5.2 A qualitative comparison of different types of low pass filters.

Filter type	Passband	Stopband	Gain roll-off	Phase linearity	Design complexity	Remarks
Bessel	Monotonic	Monotonic	Poor	Best	Less	All pole; Linear phase shift
Butterworth	Monotonic	Monotonic	Good	Better	Least	All pole; Maximally flat
Chebyshev	Rippled	Monotonic	Better	Good	More	All pole
Elliptic	Rippled	Rippled	Best	Poor	Most	Cascaded biquads

Some other aspects of the different filter realizations are noteworthy here: -

⇒ With Butterworth and Chebyshev filters, any improvement in the sharpness of cut-off is achieved only by compromising overshoot and settling time. In other words increase in the order of the filter results in increased ringing.

⇒ Again with Butterworth and Chebyshev filters, the delay time in step response increases with the order of the filter; but rise time remains essentially unaltered. With the Bessel filter the rise-time, for a given delay-time, decreases with increase in the filter order.

⇒ The step response of Bessel filter is essentially free of ringing which is not the case with the others.

⇒ The transition band roll-off of the elliptic filter can be adjusted independently of the passband ripple. To that extent, the design is more flexible. But as we try to increase the sharpness of roll-off, the stopband gain and passband ripple increase. One can increase the filter order (and hence complexity) to keep these down.

⇒ Elliptic filter approaches the 'Brick wall' type of filter gain characteristic but its phase response deviates most from linear. It is suitable for two types of applications: -

- In signals representing acoustic noise, vibration *etc.*, the relative amplitude spectral distribution is important. But the phase information is not important. In filtering these and keeping off unwanted spectral components, elliptic filter is useful.

Table 5.3 Normalized low pass filter transfer functions of Butterworth, Bessel, Chebyshev and Elliptic filters. In all the cases, the zero frequency gain has been normalized to 1. In the case of the elliptic filter, the minimum attenuations in the stop band are 34.5 dB and 51.9dB for the third and fourth order cases respectively[Wait et al]

Type of filter		Second order	Third order	Fourth order
Butterworth	Q(s)	1	1	1
	P(s)	$s^2+1.414s+1$	s^3+2s^2+2s+1	$S^4+2.613s^3+3.414s^2+2.613s+1$
Bessel (1s delay)	Q(s)	3	15	105
	P(s)	s^2+3s+3	$s^3+6s^2+15s+15$	$s^4+10s^3+45s^2+105s+105$
Chebyshev ε =0.509, 1dB	Q(s)	1.103	0.716	0.379
	P(s)	$s^2+1.0198+1.103$	$s^3+1.253s^2+1.535s+0.716$	$s^4+1.197s^3+1.717s^2+1.025s+0.379$
Chebyshev ε = 1.0, 3 dB	Q(s)	0.708	0.491	0.276
	P(s)	$s^2+0.645s+0.708$	$s^3+0.988s^2+1.238s+0.491$	$s^4+0.953s^3+1.454s^2+0.743s+0.276$
Elliptic Pass band ripple = 1dB; $\omega_s = 2.0$	Q(s)	--	$0.115(s^2+5.513)$	$0.00285(s^4+28.823s^2+111.29)$
	P(s)	--	$s^3+0.974s^2+1.335s+0.456$	$s^4+0.946s^3+1.594s^2+0.776s+0.317$

- After AM or FM, a restricted frequency band around the carrier which carries the full signal information, is to be extracted and all other components effectively filtered out. If (the modulated band/carrier frequency) ratio is small (< 0.1), elliptic filter can be considered for filtering. This is because over a sufficiently narrow frequency range, phase linearity is maintained.

⇒ Most instrumentation signals require the nature of their time variation to be retained through all processing stages. Bessel filter is ideally suited for this since it provides linear phase shift φ versus ω relationship in the passband.

⇒ Butterworth filter provides a good compromise when the gain and phase response – both matter. Hence, it is preferred whenever the requirement for a good gain or phase characteristic is not conspicuously dominant.

Most application situations call for one or another type of filter. Often the choice is made without much difficulty or detailed or in-depth examination of trade-off. In case an application demands gain and phase characteristics with narrow tolerances, one can have recourse to one of two alternatives: -

⇒ Start with a ratio of polynomials, do detailed analysis and simulation with the help of a PC and arrive at the best filter. This need not conform to any of the above four types.

⇒ Use combinations of second order filter sections to obtain the desired gain characteristic. Subsequently use an all pass filter to modify the phase characteristic as desired.

Normally each first order term of a filter is realized around one opamp. Each second order term is realized using one or three opamps. Since the cost or size of the opamp is not a primary constraint, one does not impose any *prima facie* restrictions on the number of stages. Deterioration in noise performance, accuracy, overall drift and possible overall loop stability seem to be the deciding factors.

5.6 Low Pass Filter Configurations

All the filter transfer functions discussed so far are characterized by

⇒ Unit cut-off frequency.

⇒ Ratios of polynomials as transfer functions

⇒ Polynomial expressions composed of factors of the form $(s + a)$ and $(s^2 + 2\xi\omega_k s + \omega_k^2)$.

If we substitute s with (s/ω_n), these polynomials become $[(s + a\omega_n)/\omega_n]$ and $[(s^2 + 2\xi\omega_n\omega_k s + \omega_n^2\omega_k^2)/\omega_n^2]$ respectively. The substitution amounts to frequency scaling by ω_n. In addition, we introduce a scaling factor H to represent the passband gain. Thus, the simple normalized second order LPF transfer function

$$G(s) = \frac{1}{s^2 + 2\xi s + 1} \tag{5.30}$$

becomes

$$G(s) = \frac{H\omega_n^2}{s^2 + 2\xi\omega_n s + \omega_n^2} \tag{5.31}$$

As a result of this scaling, the cut-off frequency (and all other characteristic frequencies used for design) increases by ω_n. The filter remains similar in all other

respects. All discussions regarding the normalized LPF are equally applicable to this generalized LPF with this frequency-scaling factor. Realizations of the LPF discussed here are for this more general case.

A variety of circuits is available in literature to realize the filters [Franco, Huelsman]. Three widely used configurations are discussed here. The second degree factor in the numerator – whenever present – and the denominator are conveniently taken in the form $(s^2 + 2\xi\omega_n s + \omega_n^2)$, where ω_n is the undamped natural frequency, $-\xi\omega_n \pm \omega_n\sqrt{1-\xi^2}$ form the pole pair and ξ is the damping factor. Realizing a second order LPF is equivalent to realizing an active circuit with a second order transfer function with the above pole pair.

5.6.1 Sallen and Key (S-K) LPF

The S-K filter circuit is shown in Figure 5.16. A non-inverting opamp based amplifier is the sole active element in the filter realization.

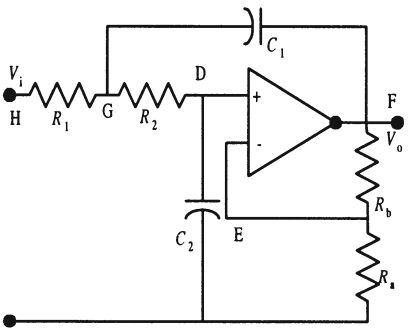


Figure 5.16 Sallen-Key realization of second order low pass filter section

Referring to the figure, under normal operating conditions we have

$$V_o = V_F = V_D\left(1+\frac{R_b}{R_a}\right)$$

$$= kV_D \tag{5.32}$$

where k is the gain of the amplifier.

$$V_G = V_D(1 + R_2C_2s) \tag{5.33}$$

Substitution from Equation 5.32 yields

$$V_G = \frac{V_F}{k}(1 + R_2C_2s) \tag{5.34}$$

$$\text{Current through } R_1 = \frac{V_i - V_G}{R_1}$$

$$= C_1s(V_G - V_o) + \left(\frac{V_G - V_D}{R_2}\right) \tag{5.35}$$

considering junction G.

Substituting for V_G, V_F and V_D in terms of V_o from the above set of equations, rearranging terms and simplifying we get,

$$\frac{V_o}{V_i} = \frac{\dfrac{k}{R_1R_2C_1C_2}}{s^2 + \left(\dfrac{1}{R_1C_1} + \dfrac{1}{R_2C_1} + \dfrac{1-k}{R_2C_2}\right)s + \dfrac{1}{R_1R_2C_1C_2}} \tag{5.36}$$

Apart from the two resistors deciding the gain factor k in Equation 5.32, we have four additional circuit elements here; a variety of combinations of practical values of these can be used to realize the quadratic term in Equation 5.36. Three cases in common use, are of specific interest.

Case 1: -

Choose

$$R_1 = R_2 = R \tag{5.37}$$

and

$$C_1 = C_2 = C \tag{5.38}$$

Substituting in Equation 5.36,

$$\frac{V_o}{V_i} = \frac{k/R^2C^2}{s^2 + [(3-k)/RC]s + \left(1/R^2C^2\right)} \tag{5.39}$$

Identifying the coefficients with those of Equation 5.31, we get,

$$\omega_n = \frac{1}{RC} \tag{5.40}$$

$$\xi = (3-k)/2 \tag{5.41}$$

With $1< k < 3$, all complex root possibilities can be realized. For any given ω_n, C can be selected to be a convenient and commonly available value and R calculated from Equation 5.40. For example, if

$$\omega_n = 628.4 \text{ rad / s (100 Hz)}$$

with

$$C = 47 \text{ nF}$$

We get

$$R = 33.86 \text{ k } \Omega.$$

k can be chosen to suit the ξ required.

Case 2: -

Let

$$k = 1 \tag{5.42}$$

$$R = R_1 = \frac{R_2}{n} \tag{5.43}$$

and

$$C = C_1 = \frac{C_2}{m} \tag{5.44}$$

Substituting in Equation 5.36

$$\frac{V_o}{V_i} = \frac{1/nmR^2C^2}{s^2 + [m(n+1)/mnRC] + 1/\left(nmR^2C^2\right)} \tag{5.45}$$

Identifying the coefficients with those of Equation 5.31,

$$\omega_n^2 = \frac{1}{mnR^2C^2} \tag{5.46}$$

$$2\xi\omega_n = \frac{m(n+1)}{mnRC} \tag{5.47}$$

$$\therefore \omega_n = \frac{1}{RC\sqrt{mn}} \tag{5.48}$$

$$\xi = \frac{m(n+1)}{2\sqrt{mn}} \tag{5.49}$$

Convenient values are selected for C_1 and C_2 (*i.e.*, m). R and n are decided subsequently by identifying the polynomial coefficients – as was done with case 1 above.

Case 3: -

Let

$$C_1 = C_2$$

$$R_a = R_b \tag{5.50}$$

$R_a = R_b$ makes the choice easy; the gain value can be precisely adjusted. $C_1 = C_2$ makes the choice easy from the point of view of manufacture. We have,

$$\frac{V_o}{V_i} = \frac{2k/R_1R_2C^2}{s^2 + (s/R_1C) + \left(1/R_1R_2C^2\right)} \tag{5.51}$$

Identifying the coefficients with those of Equation 5.31, the expressions for ω_n and ξ can be obtained. A convenient selection may be made for C. Subsequently R_1 is decided to give necessary damping. Using these and the coefficient of s^0, R_2 is decided.

5.6.2 First Order Term

First order term in the filter is realized using a simple opamp based circuit as shown in Figure 5.17. Its transfer function is

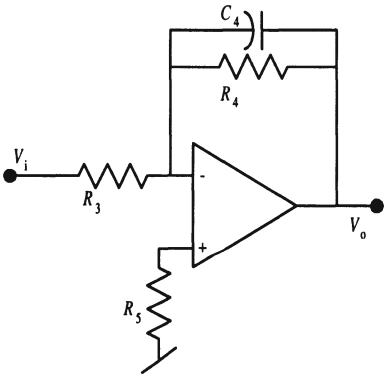


Figure 5.17 Circuit realization of first order term in LPF

$$\frac{V_o}{V_i} = -\frac{R_4}{R_3}\frac{1}{1+R_4C_4s}$$

$$= -\frac{1}{R_3C_4}\frac{1}{s+[1/R_4C_4]} \qquad (5.52)$$

The corner frequency of the first order term in Equation 5.52 decides R_4 C_4. C_4 is selected to be the same as in the second order terms. R_4 is decided by comparing the coefficients of s^0. The overall filter gain can be adjusted by a proper selection of R_3.

Observations: -

⇒ The S-K filter realization is comparatively insensitive to opamp characteristics and their variations.

⇒ The resistance ratios and the capacitance ratios are close to unity. This is one advantage of the S-K realization.

⇒ The ω_h and ξ values of the complex poles characterize each quadratic term of the filter. A fair level of independence between expressions deciding these two, makes the design easier.

⇒ When realizing the quadratic terms with low ξ values, the component values are quite sensitive to changes in ξ.

⇒ The common mode signal appearing at the opamp inputs in Figure 5.16, restrict the output swing.

5.6.3 Multiple Feedback Filter

The S-K filter section (Figure 5.16) is realized around a non-inverting amplifier. The opamp output is fed back to one junction point of the passive network. The multiple feedback arrangement provides an alternate and equally popular configuration. It is built around an inverting amplifier; the feedback is to two points of the passive network. The LPF version of the multiple feedback type filter is shown in Figure 5.18. The conductance values G_1, G_3 and G_4 are used here instead of the respective resistance values to simplify algebra.

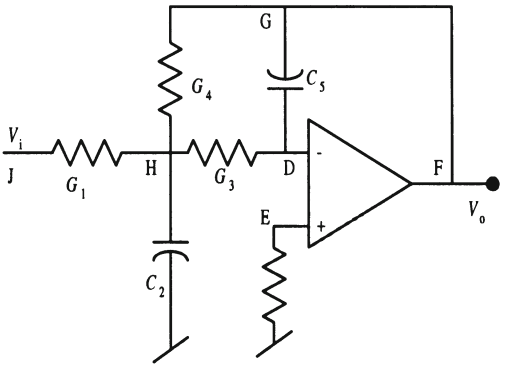


Figure 5.18 Multiple feedback circuit realization of second order LPF section

Under normal operating conditions (*i.e.*, as long as the opamp is in the active region)

$$V_D = V_E = 0 \tag{5.53}$$

Summing the currents at H to zero, we get

$$V_H [G_1 + C_2 s + G_3 + G_4] = V_i G_1 + V_o G_4 \tag{5.54}$$

Summing the currents at D to zero, we get

$$V_H G_3 + V_o C_5 s = 0 \tag{5.55}$$

Elimination of V_H from the above equations, rearrangement and subsequent simplification, lead to

$$\frac{V_o}{V_i} = -\frac{G_1 G_3 / C_2 C_5}{s^2 + [(G_1 + G_3 + G_4)s / C_2] + (G_3 G_4 / C_2 C_5)} \tag{5.56}$$

Equation 5.56 does not allow easy selection of components. We follow an approach that yields reasonable ratios of resistances and capacitances.

Identifying terms of Equation 5.56 with those of the filter in the normalized form of Equation 5.31

$$\omega_n^2 = \frac{G_3 G_4}{C_2 C_5} \tag{5.57}$$

and

$$H\omega_n^2 = \frac{G_1 G_3}{C_2 C_5} \tag{5.58}$$

$$2\xi\omega_n = \frac{1}{C_2}(G_1 + G_2 + G_4) \tag{5.59}$$

Dividing Equation 5.58 by Equation 5.57

$$H = \frac{G_1}{G_4} \tag{5.60}$$

Equation 5.57 gives

$$\omega_n = \sqrt{\frac{G_3 G_4}{C_2 C_5}} \tag{5.61}$$

Substitution from Equation 5.60 and Equation 5.61 in Equation 5.59 and simplification gives

$$2\xi = \left[(H+1)\sqrt{\frac{G_4}{G_3}} + \sqrt{\frac{G_3}{G_4}}\right]\sqrt{\frac{C_5}{C_2}} \tag{5.62}$$

If we treat $[G_3/G_4]$ as a parameter, 2ξ in Equation 5.62 is a minimum for

$$\frac{G_3}{G_4} = H + 1 \tag{5.63}$$

Correspondingly

$$\xi|_{min} = \sqrt{H+1}\sqrt{C_5/C_2} \tag{5.64}$$

Substituting from Equations 5.63 and 5.64 in Equation 5.61 and simplifying we get

$$\omega_n = \frac{G_4}{C_2} \tag{5.65}$$

Values of H close to unity yield component ratios also close to unity. Equation 5.64 shows that for $\xi \leq 1$, $C_5 < C_2$. The step by step design procedure is as follows: -

⇒ Select C_2. From Equation 5.65 calculate G_4 (R_4).
⇒ Select C_5 such that $(C_2/2) > C_5 > (C_2/10)$.
⇒ From Equation 5.64 calculate H.
⇒ From Equation 5.60 and Equation 5.63 compute $G_1(R_1)$ and G_3 (R_3) respectively. This completes the design.

H can be varied to a limited extent by altering C_5 values.

Observations: -

⇒ The multiple feedback filter provides a signal inversion (unlike the S-K configuration).
⇒ A specified DC gain (*i.e.*, gain in the passband) can be realized here.
⇒ Sensitivity of the filter to opamp gain changes is low.
⇒ For the same level of gain, sensitivity to changes in component value is lower with the multiple feedback configuration compared to that with others.
⇒ The maximum-to-minimum component ratios are higher here compared to the S-K realization.
⇒ The multiple feedback scheme is well suited for $\xi > 0.05$.
⇒ Being an inverting amplifier configuration, the common mode signal at the inputs, is zero. Correspondingly, a larger output swing is possible.

5.6.4 State Variable (S-V) Filter

The 'State Variable Filter' essentially follows the configuration used to simulate transfer functions in the analog computer of earlier years. S-V filter circuits normally use three opamps – two of them function as integrators and the third as a summer. Two slightly different configurations are used here.

Configuration 1: -

Figure 5.19 shows the circuit. All resistances except three are selected to have equal values – each of R ohms. Both capacitances are taken to have equal values of C Farads.

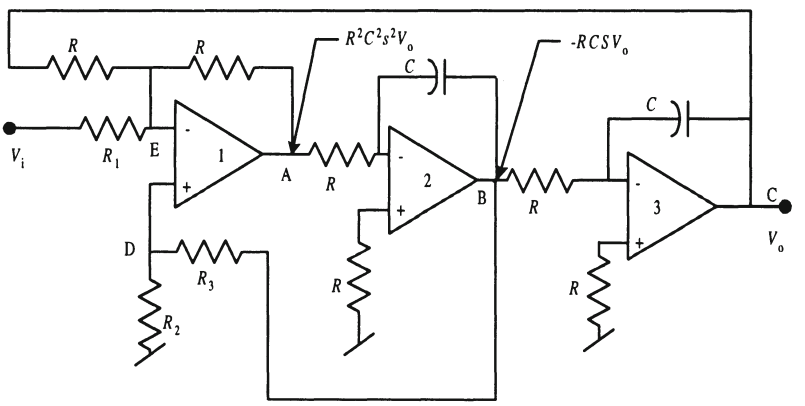


Figure 5.19 State variable circuit realization of second order LPF section – configuration 1

Let

$$R_2/(R_2+R_3) = k \tag{5.66}$$

Since opamps 2 and 3 are configured as integrators, signals at points B and A are proportional to the first and second derivatives of V_o respectively. Hence

$$V_B = -RCs\,V_o \tag{5.67}$$

$$V_A = R^2C^2s^2V_o \tag{5.68}$$

$$V_D = kV_B = -kRCsV_o \tag{5.69}$$

$$V_E = V_D$$

Summing the currents at point E

$$\frac{V_i}{R_1}+\frac{V_o}{R}+\frac{V_A}{R} = V_E\left(\frac{1}{R_1}+\frac{1}{R}+\frac{1}{R}\right) \tag{5.70}$$

Eliminating V_A, V_B, V_D and V_E from the above set of equations and simplifying

$$\frac{V_o}{V_i} = -\frac{1}{RR_1C^2}\,\frac{1}{s^2+\frac{k}{C}\left(\frac{1}{R_1}+\frac{2}{R}\right)s+\frac{1}{R^2C^2}} \tag{5.71}$$

Identifying the coefficients with those of the normalized form of Equation 5.31

$$\omega_n = \frac{1}{RC} \tag{5.72}$$

$$2\xi\omega_n = \frac{k}{C}\left(\frac{1}{R_1}+\frac{2}{R}\right) \tag{5.73}$$

and

$$H = \frac{R}{R_1} \tag{5.74}$$

From the above equations we have,

$$\xi = k\left(\frac{H}{2}+1\right) \tag{5.75}$$

Design Procedure: -

⇒ Select a convenient C value.

⇒ Using the above C value and known ω_n, calculate R from Equation 5.72.

⇒ Using Equation 5.74, select R_1 to give the required H value.

⇒ From known H and ξ values, calculate k from Equation 5.75.

⇒ From known k and Equation 5.66, calculate (R_2/R_3). Select R_2 and R_3 suitably.

One distinct advantage of the SV filter and the configuration, is the near total independence of selection of different component values. This is in marked contrast to the earlier configurations.

Configuration 2: -

This configuration – shown in Figure 5.20 – differs from the last one, only in respect of feeding of V_i; further, it has one resistance less. Apart from R_1 and R_2, all other resistances are taken as R ohms. Both capacitances are taken as C farads.

Signals at points A and B can be directly identified as proportional to the first and the second derivatives of V_o respectively.

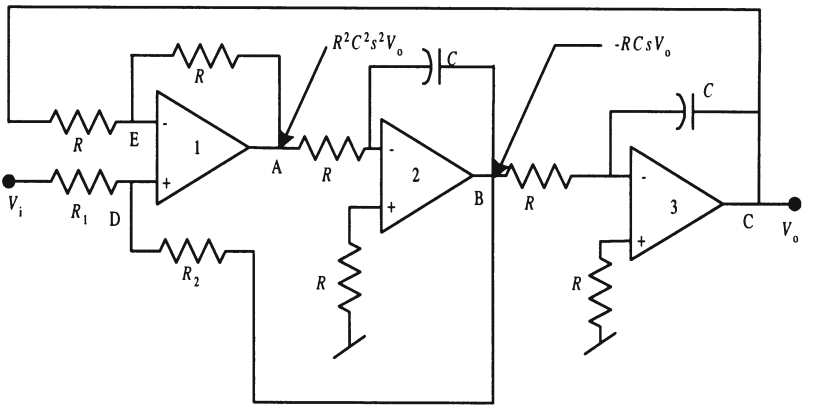


Figure 5.20 State variable circuit realization of second order LPF section - configuration 2

Referring to Figure 5.20,

$$V_D = \frac{R_2}{R_1+R_2}V_i - \frac{R_1RCs}{R_1+R_2}V_o$$

$$= V_E \tag{5.76}$$

Equating the currents at E to zero

$$\frac{V_o}{R} + \frac{R^2C^2s^2}{R}V_o = \frac{2}{R}\left(\frac{R_2}{R_1+R_2}V_i - \frac{R_1RCs}{R_1+R_2}V_o\right) \tag{5.77}$$

Rearranging and simplifying the above equation

$$\frac{V_o}{V_i} = \frac{H\omega_n^2}{s^2 + 2\xi\,\omega_n + \omega_n^2} \tag{5.78}$$

where

$$\omega_n^2 = \frac{1}{R^2C^2} \tag{5.79}$$

$$2\xi\omega_n = \frac{2R_1}{RC(R_1+R_2)} \tag{5.80}$$

From the above two equations

$$\xi = \frac{R_1}{R_1+R_2} = 1-k \tag{5.81}$$

where

$$\frac{R_2}{R_1+R_2} = k \tag{5.82}$$

$$H = \frac{2R_2}{R_1+R_2} = 2k \tag{5.83}$$

The above design equations are simple; each specifies one set of component values. Once ξ is known, k and H are also decided. The gain H cannot be fixed independently.

Design procedure: -

⇒ Select a convenient value of C.

⇒ From known ω_n and Equation 5.79, calculate the value of R.

⇒ With known ξ, select convenient values for R_1 and R_2 to satisfy Equation 5.80. Equation 5.82 and Equation 5.83 automatically decide k and H values.

Here also, we have near complete independence of selection of component values. The resistances around opamp 1 can be made different and a desired DC gain obtained but the simplicity of the expressions is no longer retained.

Observations: -

⇒ The S-V Filter has three opamps and more number of components than the other two circuits.

⇒ Since the integration is done in two stages, we get simpler expressions and independence of adjustment in parameters.

⇒ Due to the distinct integration stages, v_o, dv_o/dt and d^2v_o/dt^2 can be combined in suitable proportions to realize other types of filters also. This makes the SV filter quite versatile and easy to design.

⇒ Sensitivity of the filter to component value variations is low. Filter sections with very low values of ξ can be effectively realized.

⇒ The independence of adjustment allows us to reduce component spread to the desired level. To a great extent this was already done in the circuits discussed above by making capacitances and a set of resistance values common.

The component values for second order LPF realizations of different types of filters are given in Table 5.4. The filter cut-off frequency is taken as 100Hz in each case. Similar values can be obtained for higher order filters as well.

Table 5.4 Second order LPF realizations of different types for ω_c = 628 rad/s [f = 100 Hz]. All the capacitance values are in nF and the resistance values in kilo-ohms.

Filter circuit type							
Sallen-Key: case 1	Filter type	C		R	k		H
	Butterworth	47		33.9	1.586		625 000
	Bessel	47		19.8	1.268		1500 000
	Chebyshev [ε =0.509, 1dB]	47		32.3	1.95		849 000
Multiple feedback:	Filter type	C_2	C_5	R_1	R_3	R_4	H
	Butterworth	110	22	5.8	4.14	14.5	1.5
	Bessel	110	22	3.03	2.2	8.36	2.76
	Chebyshev [ε =0.509, 1dB]	110	22	5	10.1	13.8	0.368
State variable: configuration 2	Filter type	C	R	R_1	R_2	k	H
	Butterworth	47	33.2	33	13.7	0.293	0.586
	Bessel	47	19.8	33	215	0.133	0.267
	Chebyshev [ε =0.509, 1dB]	47	32.3	33	30.1	0.477	0.954

5.7 LPF Circuit Realizations

The component values for LPF circuit realizations considered so far are given in Table 5.4. All these have the nominal cut-off frequency = 628.4 rad/s (100 Hz) which is typical of many process variable transducers. Some general observations are in order here: -

⇒ In each case the number of combinations of R and C values possible, is infinite. Keeping down the component value spread low and imposing equality restrictions, reduce the choice substantially. The circuit values chosen and used are a few amongst these.

⇒ The DC specifications (offset voltage, offset current and drift) are given primary importance in the selection of opamps for the LPF.

⇒ In some cases the equivalent resistances connected to the inverting and non-inverting input leads of the opamp can be equalized and drift due to bias current difference reduced. This is not possible in all the cases.

⇒ In the process of filter realization, one may be able to achieve a signal gain also; but realizing the gain is to be considered of secondary importance compared to the filtering. If necessary, a separate gain stage may be added by adding another opamp-based unit. Incidentally, all odd order filters use one first order section, which can be used for gain adjustment too (*Vide* Section 5.6.2).

⇒ Higher order filters are realized by cascading first and second order sections. A careful ordering of sequencing of sections yields some incidental benefits. Normally, filters for instrumentation require gain, cut-off frequency and slew-rate values to be lower compared to the relative specifications of the opamps used. Hence, signal swings can be allowed at all opamp stages without impairing their quality. In these situations, the filter sections may be cascaded with the highest DC gain section in the beginning and the lowest DC gain section at the end. This minimizes the signal-to-noise ratio through the filter. However, there may be occasional situations where the filter gain, the bandwidth or the signal slew-rate may be quite demanding of the opamp. In such situations, the highest gain section may be kept last to avoid signal distortion.

⇒ When realizing higher order filters, the individual second order sections can be of different types; thus for sections with $\xi < 0.3$, S-V filter sections may be used to take advantage of the reduced sensitivity of component values to ξ here. For sections with $\xi > 0.3$, S-K or the multiple feedback filter sections can be used.

⇒ Many other filter circuit realizations are available in literature. One or another type cannot be universally recommended. Widespread use is the only justification for singling out the three types here for detailed discussion.

5.8 High Pass Filters

Consider a typical normalized second order LPF transfer function

$$G(s) = \frac{1}{s^2 + as + 1} \tag{5.84}$$

This has a nominal cut-off frequency of 1 rad /s and a ξ of $a/2$. If we substitute s by $1/s'$, we get

$$G(s') = \frac{s'^2}{s'^2 + as' + 1} \tag{5.85}$$

This is the normalized filter transfer function of an HPF with cut off frequency of 1rad/s. The infinite-frequency gain is unity and the zero-frequency gain zero. As the frequency increases through 1 rad/s, the gain increases according to the cut off rate of the function. The same holds good of higher order filters also. All the discussions regarding the four filter forms in Section 5.4 are equally valid here subject to the same transformation.

The normalized transfer function can be scaled up or down in frequency by substituting s/ω_n for s'. With this scaling and the use of the passband gain H, the normalized HPF takes the form

$$G(s) = \frac{Hs^2}{s^2 + 2\xi\omega_n s + \omega_n^2} \tag{5.86}$$

All the discussions of Section 5.5 are valid here – subject to the transformation and scaling.

5.8.1 Filter Circuit Configurations

The low pass filter was realized using resistances and capacitances as passive elements. High pass filters too are realized in this manner. Every LPF circuit configuration can be used in an HPF configuration by

⇒ replacing all resistances in the passive part of the circuit by capacitances and

⇒ replacing all capacitances in the passive part of the circuit by resistances.

The only exceptions are the resistances whose ratios decide the gains; normally these resistances are retained.

5.8.1.1 Sallen and Key filter

The HPF configuration of the S-K filter is shown in Figure 5.21.

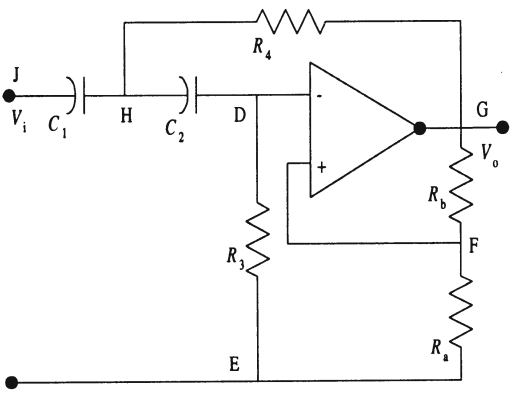


Figure 5.21 Sallen-Key circuit realization of second order HPF section

Let

$$k = 1+\frac{R_b}{R_a} \tag{5.87}$$

$$V_F = \frac{V_o}{k} = V_D \tag{5.88}$$

Equating currents at junction D

$$\frac{V_D}{R_3}+V_D C_2 s = V_H C_2 s \tag{5.89}$$

Equating currents at junction H

$$V_H\left(C_1 s + C_2 s + \frac{1}{R_4}\right) = V_i C_1 s + V_D C_2 s + \frac{V_o}{R_4} \tag{5.90}$$

Eliminating V_D and V_H from the above set of equations, rearranging terms and simplifying

$$\frac{V_o}{V_i} = \frac{ks^2}{s^2+\left[\frac{1}{C_1R_4}(1-k)+\frac{1}{C_2R_3}+\frac{1}{C_1R_3}\right]s+\frac{1}{C_1C_2R_3R_4}} \tag{5.91}$$

Case 1: -

With

$$C_1 = C_2 = C \tag{5.92}$$

and

$$R_3 = R_4 = R \tag{5.93}$$

Equation 5.91 becomes

$$\frac{V_o}{V_i} = \frac{ks^2}{s^2+\left(\frac{3-k}{RC}\right)s+\frac{1}{R^2C^2}} \tag{5.94}$$

Identifying coefficients with those of Equation 5.86

$$\omega_n = \frac{1}{RC} \tag{5.95}$$

$$\xi = \frac{3-k}{2} \tag{5.96}$$

$$H = k \tag{5.97}$$

With $1 < k < 3$, all complex root possibilities can be realized. The design procedure is straightforward: -

⇒ Select a convenient C value.
⇒ For the required ω_n, calculate R value from Equation 5.95.
⇒ From the given ξ, calculate k from Equation 5.96.
⇒ H is automatically fixed.

Case 2: -

With

$$k = 1 \tag{5.98}$$

$$R = R_3 = \frac{R_4}{n} \tag{5.99}$$

and

$$C = C_1 = \frac{C_2}{m} \tag{5.100}$$

Equation 5.91 becomes

$$\frac{V_o}{V_i} = \frac{s^2}{s^2 + 2\xi\omega_n s + \omega_n^2} \tag{5.101}$$

where

$$\omega_n = \frac{1}{RC\sqrt{mn}} \tag{5.102}$$

and

$$\xi = \frac{(m+1)}{2}\sqrt{\frac{n}{m}} \tag{5.103}$$

Design procedure: -

A variety of choices is possible.

⇒ Let $C_1 = C_2$ and $m = 1$.

⇒ With known ξ, calculate n from Equation 5.103.

⇒ Select a convenient value for C.

⇒ Substitute C and ω_n in Equation 5.102 and calculate R.

⇒ Here the capacitances are constrained to be equal. The passband gain is unity.

Case 3: -

With

$$R_3 = R_4 = R \tag{5.104}$$

and

$$R_a = R_b \tag{5.105}$$

$$k = 2 \tag{5.106}$$

Equation 5.91 becomes

$$\frac{V_o}{V_i} = \frac{2s^2}{s^2 + \frac{s}{RC_2} + \frac{1}{R^2C_1C_2}} \tag{5.107}$$

$$\omega_n = \frac{1}{R\sqrt{C_1C_2}} \tag{5.108}$$

$$\xi = \frac{1}{2}\sqrt{\frac{C_1}{C_2}} \tag{5.109}$$

Design procedure: -

⇒ Select a convenient C_2 value

⇒ From Equation 5.109 calculate C_1 using the known value of ξ.

⇒ Calculate R from Equation 5.108 using the known values of all the other quantities therein.

Here the passband gain is unity.

For small values of ξ, C_1 / C_2 ratio increases unduly. Component range also increases. Further capacitors are available only in limited values. One may not be able to get the C_1 value desired. These make the approach rather impractical.

5.8.1.2 *Multiple Feedback Filters*

The HPF using the multiple feedback configuration is shown in Figure 5.22.

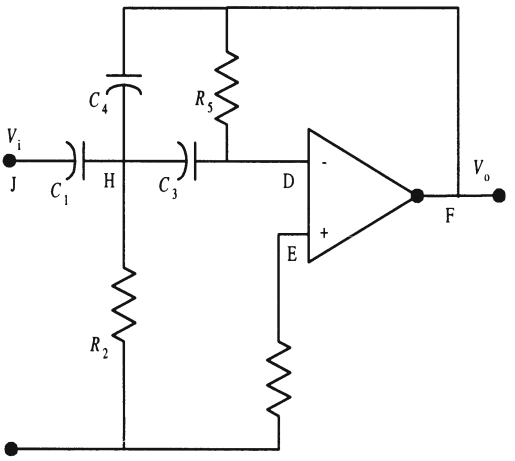


Figure 5.22 Multiple feedback circuit realization of second order HPF section

Equating currents at junction D,

$$\frac{V_o}{R_5} = -V_H C_3 s \tag{5.110}$$

Equating currents at junction H

$$V_H\left(C_1 s + \frac{1}{R_2} + C_3 s + C_4 s\right) = V_i C_1 s + V_o C_4 s \tag{5.111}$$

Eliminating V_H from the above two equations and simplifying

$$\frac{V_o}{V_i} = -\frac{C_1 s^2 / C_4}{s^2 + \frac{1}{R_5}\left(\frac{C_1}{C_3 C_4} + \frac{1}{C_3} + \frac{1}{C_4}\right)s + \frac{1}{R_2 R_5 C_3 C_4}} \tag{5.112}$$

One case simplifies component selection. Choose

$$C = C_1 = C_3 \tag{5.113}$$

With this, Equation 5.112 becomes

$$\frac{V_o}{V_i} = -\frac{s^2 C / C_4}{s^2 + \left(\frac{2}{C_4} + \frac{1}{C}\right)\frac{s}{R_5} + \frac{1}{R_2 R_5 C C_4}} \tag{5.114}$$

Identifying coefficients with those of Equation 5.86

$$C_4 = \frac{C}{H} \tag{5.115}$$

$$\omega_n^2 = \frac{1}{R_2 R_5 C C_4} \tag{5.116}$$

$$2\xi\,\omega_n = \frac{2C + C_4}{R_5 C C_4} \tag{5.117}$$

From the above two equations we get

$$\omega_n = \frac{1}{\sqrt{R_2 R_5 C C_4}} \tag{5.118}$$

$$\xi = \frac{1}{2}\left(2\sqrt{H} + \frac{1}{\sqrt{H}}\right)\sqrt{\frac{R_2}{R_5}} \tag{5.119}$$

Design procedure: -

⇒ Select $C = C_1 = C_2$ to be a convenient value.
⇒ For specified H, calculate C_4 from Equation 5.115.
⇒ Calculate R_2 R_5 from Equation 5.116 from known C_1 C_4 and specified ω_n.
⇒ Calculate R_2 / R_5 from Equation 5.119 and specified ξ and H.
⇒ From known R_2 R_5 and R_2 / R_5 calculate R_2 and R_5.

Note that H is to be selected such that C_4, which is calculated using Equation 5.115, is one of the available values. Hence, it is preferable to select C_4 and compute H from Equation 5.115. Component spread is kept limited by selecting H close to unity.

5.8.1.3 State Variable Filter

Consider the S-V filter configuration 1 of Figure 5.19. The transfer function is (Equation 5.71)

$$\frac{V_o}{V_i} = -\frac{1}{RR_1C^2} \frac{1}{s^2 + \frac{k}{C}\left(\frac{1}{R_1} + \frac{2}{R}\right)s + \frac{1}{R^2C^2}} \tag{5.71}$$

If the output is taken at point A instead of point C, we get

$$\frac{V_o}{V_i} = -\frac{1}{RR_1C^2} \frac{R^2C^2s^2}{s^2 + \frac{k}{C}\left(\frac{1}{R_1} + \frac{2}{R}\right)s + \frac{1}{R^2C^2}} \tag{5.120}$$

This is the HPF transfer function. The design procedure is identical to that with LPF. This holds good for configuration 2 also.

Observations: -

The S-K and multiple feedback schemes use circuit configurations, which can cause oscillations. This is due to the use of capacitors at the input side – akin to the differentiator. Unlike this with the S-V filter configuration, two opamps function as integrators and the third as a summer and all are stable. This makes the S-V filter the most attractive of the lot. Design of the S-V filter is as straightforward as was

explained in Section 5.6.4. Component adjustment relations are fairly independent of each other.

5.8.2 High Pass Filter Circuit Configurations

Butterworth, Chebyshev or Elliptic filter configurations can be used to realize HPFs. Table 5.5 gives the circuit parameter values for the configurations considered so far. The cut off frequency is taken as 100 Hz in all the cases. Since the S-V filter circuit parameters remain the same as those considered in Table 5.4 for the LPF case, they are not reproduced here.

Table 5.5 Second order HPF realizations for ω_c = 628 rad/s [f = 100 Hz]. All the capacitance values are in nF and the resistance values in kilo-ohms.

Filter circuit type					
Sallen-Key: case 1	Filter type	C	R	k = H	
	Butterworth	47	33.9	1.586	
	Chebyshev	47	34.7	1.955	
Multiple feedback:	Filter type	C_1=C_3=C_4	R_2	R_5	H
	Butterworth	47	16	71.9	1
	Chebyshev	47	12	98.8	1

Observations: -

⇒ HPF by itself requires the circuit to function with a definite gain above the crossover frequency of the opamps used. This can lead to oscillations or unstable operation. This is normally avoided by limiting the passband to a frequency above the highest frequency of interest, but well below the crossover frequency of the opamps used. This cut-off frequency is kept well above the highest frequency of interest so that the nature and rate of cut-off are not critical. It can be realized by connecting a small capacitance between the output and the inverting input of the concerned opamp.

⇒ Situations calling for handling signals beyond an upper limit of frequency are rare. Hence the use of HPF *per se* is also rare; this is all the more true of instrumentation signals. For this reason also, the use of a BPF is preferred to that of an HPF.

5.9 Band Pass Filter

It is possible to obtain the BPF transfer function directly from the LPF transfer function. The substitution to be used is

$$s = \frac{p}{\alpha} + \frac{\beta}{p} \tag{5.121}$$

where α and β are constants and p a normalized frequency variable. Consider a first order section of a low pass filter of the form

$$G(s) = \frac{a}{s+a} \tag{5.122}$$

This has unit gain in the passband and a 3 dB cut off frequency of a rad/s. The substitution for s from Equation 5.121 gives

$$G(p) = \frac{a}{\frac{p}{\alpha}+\frac{\beta}{p}+a}$$

$$= \frac{a\alpha p}{p^2+a\alpha\, p+\alpha\beta} \tag{5.123}$$

$F(p)$ is a bandpass filter with $\sqrt{\alpha\beta}$ as the centre frequency and – 20 db/decade cut-off rate on either side. We also find that the single pole transfer function $G(s)$ of Equation 5.122 is transformed into a 2 pole transfer function of Equation 5.123. The transformation of a second order term on these lines, leads to a fourth order term. To generalize, the order of a BPF is twice that of its LPF or HPF counterpart. This is essentially due to combining an LPF and an HPF into one filter. The transformation using Equation 5.121 leads to polynomials that are again to be factorized; they are not easily tractable either. The more common approach to BPF realization is of two types: -

⇒ When the passband required is of the same order as that of the centre frequency of the filter, the BPF is a wideband filter. Such wideband BPF are realized by cascading suitable LPF and HPF [See the observations in the preceding section].

⇒ When the bandwidth required is small compared to the centre frequency of the filter, the BPF is a narrowband filter. Narrowband filters are realized directly.

Situations calling for the use of wideband BPF are not very common. As mentioned above, whenever necessary, they are realized by cascading an LPF and an HPF. These have been discussed already in sufficient detail. Only the narrow band BPF is considered here for more detailed discussion.

5.9.1 Narrow Band Filter

The simplest normalized narrow band filter has the transfer function

$$G(s) = \frac{H\omega_n s}{s^2+2\xi\omega_n s+\omega_n^2} \tag{5.124}$$

Substituting $s = j\omega$ in Equation 5.124 and simplifying

$$|G(j\omega)|^2 = \frac{H}{4\xi^2+\left(\frac{\omega_n}{\omega}-\frac{\omega}{\omega_n}\right)^2}$$

$$= \frac{H}{\left(\frac{\omega_n}{\omega}\right)^2+\left(\frac{\omega}{\omega_n}\right)^2+2\left(2\xi^2-1\right)} \tag{5.125}$$

$|G(j\omega)|$ in Equation 5.125 is a maximum at $\omega = \omega_n$

$$|G(j\omega)|_{\omega=\omega_n} = \frac{H}{2\xi} \tag{5.126}$$

The phase lag ϕ at any frequency is given by

$$\tan\varphi = \frac{2\xi}{\left(\frac{\omega}{\omega_n}\right)-\left(\frac{\omega_n}{\omega}\right)} \tag{5.127}$$

Substitution with $\omega = \omega_n + \delta\omega$ and simplification with $\delta\omega << \omega_n$ gives

$$\tan\varphi \approx \frac{\xi}{\delta\omega/\omega_n}\left(1+\frac{\delta\omega}{2\omega_n}\right) \tag{5.128}$$

With $\varphi = (\pi/2)+\varepsilon$ and for $\varepsilon << (\pi/2)$

$$\tan\varphi \approx \frac{1}{\varepsilon}\left(1-\frac{\varepsilon^2}{3}\right) \tag{5.129}$$

Equating the above two expressions for tan φ and retaining only the first degree terms in $\delta\omega$ and ε

$$\varepsilon \approx \frac{\delta\omega/\omega_n}{\xi} \tag{5.130}$$

The 3 dB cut-off frequency ω_c can be obtained from Equation 5.124 as satisfying the relation

$$2\xi = \left|\frac{\omega_n}{\omega_c}-\frac{\omega_c}{\omega_n}\right| \tag{5.131}$$

After simplification this yields two values of ω_c as

$$\omega_c = \omega_n\left(\sqrt{1+\xi^2}+\xi\right) \tag{5.132}$$

and

$$\omega_c = \omega_n\left(\sqrt{1+\xi^2}-\xi\right) \tag{5.133}$$

From Equations 5.132 & 5.133 the passband $\Delta\omega$ is obtained as

$$\Delta\omega = 2\xi\,\omega_n \tag{5.134}$$

Observations : -

- ⇒ The gain attains a maximum value of $(H/2\xi)$ at $\omega = \omega_n$.
- ⇒ As ω departs from ω_n in either direction, the gain decreases. For large departures from ω_n, the gain drops at 20 dB/decade in either direction.
- ⇒ Equations 5.131 and 5.132 show that the passband is not symmetrical about the centre frequency ω_n. The filter response is depicted in Figure 5.23. The asymmetry in the characteristic is of the order of ξ.
- ⇒ The phase lag at $\omega = \omega_n$ is 90°. As ω deviates from ω_n, the change in phase lag from 90° is proportional to the frequency deviation $\delta\omega$. Again, this is true of small deviations only.

5.9.2 Narrow Band Filter Configurations and Realizations

The narrowband filter considered here is the simplest one. (It is the counterpart of the first order section of LPF or HPF. Hence it has the same form. Alternatives in

realization as Butterworth, Chebyshev forms *etc.*, do not exist). It can be realized as a circuit in S-K, multiple feedback or state variable form.

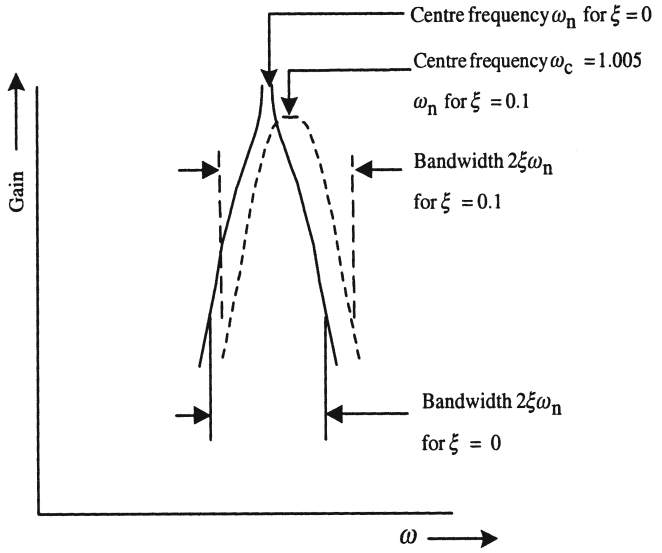


Figure 5.23 Gain response characteristic of the narrow band filter close to the centre frequency

5.9.2.1 Sallen-Key Realization

The S-K Narrow band filter circuit is shown in Figure 5.24. The impedance C_2 connected from point H to ground is a new addition (compare with Figures 5.16 & 5.21 for LPF and HPF respectively).

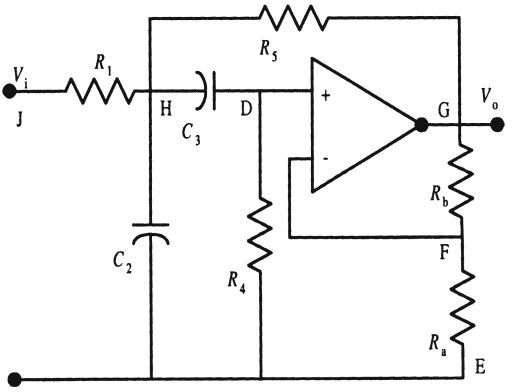


Figure 5.24 Sallen-Key circuit realization of Narrow band filter

Let

$$k = 1 + \frac{R_b}{R_a} \tag{5.135}$$

$$\therefore \; V_D = V_F = \frac{V_o}{k} \tag{5.136}$$

Equating the currents at D to zero

$$V_H C_3 s = V_D\left(\frac{1}{R_4} + C_3 s\right) \tag{5.137}$$

Equating the currents at H to zero

$$V_H C_3 s = V_D\left(\frac{1}{R_4} + C_3 s\right) \tag{5.138}$$

Eliminating V_D and V_H from the above set of equations, rearranging terms and simplifying

$$\frac{V_o}{V_i} = \frac{ks/C_2R_1}{s^2 + \left(\frac{1}{R_4C_3} + \frac{1}{R_4C_2} + \frac{1}{R_1C_2} + \frac{1}{R_5C_2} - \frac{k}{R_5C_2}\right)s + \left(\frac{1}{R_1} + \frac{1}{R_5}\right)\frac{1}{R_4C_2C_3}} \tag{5.139}$$

The filter realization is simplified in two cases of interest: -

Case 1: -

With

$$R = R_1 = R_4 = R_5 \tag{5.140}$$

and

$$C = C_2 = C_3 \tag{5.141}$$

Equation.5.139 simplifies to

$$\frac{V_o}{V_i} = \frac{ks/RC}{s^2 + \left(\frac{4-k}{RC}\right)s + \frac{2}{R^2C^2}} \tag{5.142}$$

Comparison with Equation 5.124 gives

$$\omega_n^2 = \frac{2}{R^2C^2} \tag{5.143}$$

$$2\xi\omega_n = \left(\frac{4-k}{RC}\right) \tag{5.144}$$

$$\therefore \omega_n = \frac{\sqrt{2}}{RC} \tag{5.145}$$

$$\xi = \frac{4-k}{\sqrt{8}} \tag{5.146}$$

$$H = \frac{k}{\sqrt{2}} \tag{5.147}$$

Design procedure: -

⇒ Select a suitable value for C.
⇒ For given ω_n, calculate R from Equation 5.145.
⇒ For given ξ, calculate k from Equation 5.146.
⇒ Calculate H from Equation 5.147.

Note that H cannot be independently adjusted here. For ξ <<1, (as is the case with narrow band filters), k is close to 4 and H is close to 2.8. All values of $0 < \xi < 1$, can be realized with $4 > K > (4 - \sqrt{8})$.

Case 2: -

With

$$k = 3 \tag{5.148}$$

$$C = C_2 = C_3 \tag{5.149}$$

and

$$R = R_4 = R_5 \tag{5.150}$$

Equation 5.139 becomes

$$\frac{V_o}{V_i} = \frac{ks/CR_1}{s^2 + \frac{s}{R_1 C} + \left(\frac{R}{R_1} + 1\right)\frac{1}{R^2 C^2}} \tag{5.151}$$

Identifying coefficients with those of Equation 5.124

$$\omega_n = \frac{1}{RC}\sqrt{\frac{R}{R_1} + 1} \tag{5.152}$$

$$\xi = \frac{R}{2R_1}\frac{1}{\sqrt{\frac{R}{R_1} + 1}} \tag{5.153}$$

$$H = 6\xi \tag{5.154}$$

Design procedure: -

⇒ Select a suitable value for C.
⇒ For known ξ, compute R/R_1 from Equation 5.153.
⇒ With ω_n known and using the value of R/R_1 obtained above, compute R from Equation 5.152.
⇒ Compute R_1, from known R and R/R_1
⇒ Compute H from Equation 5.154.

H value is not independently selectable. For low ξ value, H is also low. As ξ increases, the spread in resistance values also increases almost by the same extent.

5.9.2.2 Multiple Feedback Realization

The circuit is shown in Figure 5.25.

Equating currents at D, we get

$$\frac{V_o}{R_5} + V_H C_3 s = 0 \tag{5.155}$$

Equating currents at H, we get

$$V_H\left(\frac{1}{R_1} + \frac{1}{R_2} + C_3 s + C_4 s\right) = \frac{V_i}{R_1} + V_o C_4 s \tag{5.156}$$

Substituting

$$C = C_3 = C_4$$

and eliminating V_H from the Equations 5.155 & 5.156, rearranging terms and simplifying

$$\frac{V_o}{V_i} = -\frac{s/R_1C}{s^2 + \frac{2}{CR_5}s + \left(\frac{1}{R_1} + \frac{1}{R_2}\right)\frac{1}{R_5C^2}} \tag{5.157}$$

Identifying coefficients with those of Equation 5.124

$$\xi = \frac{1}{\sqrt{R_5\left(\frac{1}{R_1} + \frac{1}{R_2}\right)}} \tag{5.158}$$

$$\omega_n = \frac{1}{CR_5\xi} \tag{5.159}$$

$$H = \frac{R_5\xi}{R_1} \tag{5.160}$$

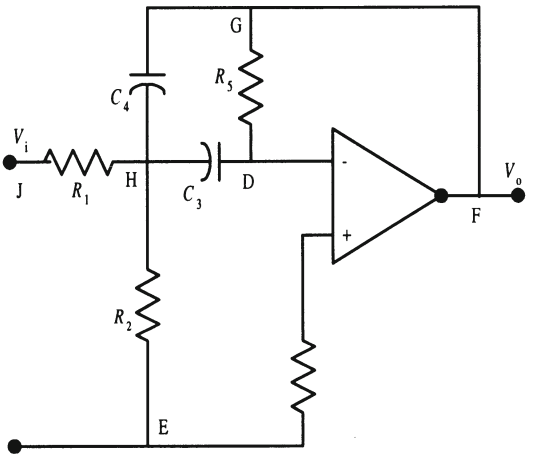


Figure 5.25 Multiple feedback circuit realization of narrow band filter

Design procedure: -

⇒ Select a convenient C value.

⇒ From previously known ξ and ω_n, and selected C, calculate R_5 from Equation 5.159.

⇒ From Equation 5.160, calculate R_1 for desired H.

⇒ From Equation 5.158, calculate the last unknown quantity R_2.

Once again, the centre frequency gain is not independently selectable. As long as its value is not critical, we can impose the condition $R_1 = R_2 = R$.

With this

$$\omega_n = \frac{1}{RC\xi} \tag{5.161}$$

$$\xi = \sqrt{\frac{R}{2R_5}} \tag{5.162}$$

$$H = \frac{1}{2\xi} \tag{5.163}$$

The filter realization equations are simpler here.

5.9.2.3 State Variable Filter Realization

Consider the State Variable configuration in Figure 5.19. The transfer function of the LPF is [Equation 5.71]

$$\frac{V_o}{V_i} = -\frac{1}{RR_1C^2} \frac{1}{s^2 + \frac{k}{C}\left(\frac{1}{R_1} + \frac{2}{R}\right)s + \frac{1}{R^2C^2}} \tag{5.164}$$

If the output is taken at point B instead of point C in Figure 5.19, we get

$$\frac{V_o}{V_i} = -\frac{1}{R_1C} \frac{s}{s^2 + \frac{k}{C}\left(\frac{1}{R_1} + \frac{2}{R}\right)s + \frac{1}{R^2C^2}} \tag{5.165}$$

Identifying the coefficients of Equation 5.165 with those of Equation 5.124, we get

$$\omega_n = \frac{1}{RC} \tag{5.166}$$

$$H = \frac{R}{R_1} \tag{5.167}$$

$$\xi = \frac{k}{2}(H+2) \tag{5.168}$$

Design procedure: -

⇒ Select a convenient value for C.

⇒ From known ω_n and Equation 5.166, decide R.

⇒ From known H value, decide R_1 using Equation 5.167 (or *vice versa*).

⇒ From known ξ, decide k from Equation 5.168.

Apparently, H and k values can be selected independently. But from practical considerations, one cannot restrict k (being ratio of resistances) to values below about 0.1. For values of ξ of the order of 0.1, which is the case for narrow band filters, H will be restricted to values close to unity.

The configuration of Figure 5.20 can be used in a similar manner leading to an alternate realization of the filter. With either S-V configuration, the selection of component values is easier as compared to the S-K or multiple feedback configurations.

Observations: -

⇒ Narrow band filters are generally used for two purposes – to extract a specific frequency component from a signal or to extract a narrow band of interest (which carries the information), around a carrier. For the former case, only gain may be of importance. For the latter, gain as well as the phase shift characteristic matter.

⇒ Centre frequencies and ξ values are normally very sensitive to component parameter changes. The problem aggravates as ξ decreases. Hence it is necessary to use as high a value of ξ, as can be accommodated

⇒ If the required ξ decreases below 0.05 or so, cascading two sections with ξ_1 and ξ_2, to provide an overall $\xi = \xi_1\ \xi_2$, is better. This improves stability substantially.

⇒ When cascading two narrow band filters to reduce ξ, a slight detuning will improve flatness characteristic and performance at the expense of a slight increase in ξ [Terman, Tietze *et al*].

5.9.2.4 Narrow Band Filter Circuit Realizations

Table 5.6 gives the component values for the narrow band filter circuit configurations discussed above for a specific case. The S-V filter circuit components are not reproduced since they remain the same as with the LPF.

Table 5.6 Narrow band filter realizations for $\omega c = 6283$ rad/s and $\xi = 0.05$. All capacitance values are in nF and the resistance values – except R in the multiple feedback circuit – in kilo-ohms.

Sallen-Key circuit	$C = 47$; $R = 4.82$; k = 3.86; $R_a = 10$; $R_b = 28.6$
Multiple feedback circuit	$C = 4.7$; $R = 169$ ohms; $R_5 = 33.9$; H = 10

5.10 Band Rejection Filters

BRF suppresses a select band of frequencies in a signal but amplifies the rest or allows them to pass with little attenuation. Two possibilities exist: -

⇒ The rejection band is of the order of the centre frequency. Practical situations calling for the use of such filters seem to be rare. However if need arises, the filter is realized by combining an HPF and an LPF of appropriate characteristics. The signal of interest is passed through both filters simultaneously and the respective outputs are added together. This case is not discussed further here.

⇒ The rejection band is narrow compared to the centre frequency of the filter (the signal components at selected narrow band frequencies are suppressed). This filter is in more common use. It is more widely known as the 'Notch Filter'.

Two situations call for the use of notch filters in the signal path. There may be cases where one frequency component of a signal is so dominant, that it makes direct information extraction from the overall signal, difficult. The dominant frequency component may have to be suppressed here. Carrier suppression after AM modulation or demodulation is a typical example. The second case arises when a specific frequency component contaminates the signal quite strongly – the disturbing frequency being within the passband or its periphery. Power supply ripples, line frequency interference *etc.*, are of this category.

5.10.1 Notch Filter

The transfer function of the simplest notch filter has the form,

$$G(s) = \frac{s^2+\omega_n^2}{s^2+2\xi\omega_n s+\omega_n^2} \tag{5.169}$$

Substituting $s = j\omega$

$$G(j\omega) = \frac{\omega_n^2-\omega^2}{\omega_n^2-\omega^2+j2\xi\omega_n\omega} \tag{5.170}$$

For $\omega << \omega_n$ and $\omega >> \omega_n$, $G(j\omega) = 1$; *i.e.*, the filter provides unity gain.
For $\omega = \omega_n$, $G(j\omega) = 0$; *i.e.*, the filter gain is zero. For $\omega = \omega_n + \delta\omega$, where $\delta\omega << \omega_n$

$$G(j\omega) \approx \frac{-\delta\omega/\omega_n}{j2\xi[1+j(1-j2\xi)(\delta\omega/\omega_n)]} \tag{5.171}$$

$$\approx j\frac{1}{2\xi}\frac{\delta\omega}{\omega_n} \tag{5.172}$$

We see that the selection of ξ plays a key role in the filter characteristic. If it is very small (0.1), it affects the notching effect adversely; if large (>>1), it makes the notch wide and blunt attenuating the neighboring frequency components unnecessarily. A value of ξ around unity may be selected.

In some applications the phase characteristics of the notch filter are not important. This allows removal of one constraint on the transfer function; it can be taken in the form

$$G(s) = \frac{s^2+\omega_n^2}{s^2+2\xi\omega_c s+\omega_c^2} \tag{5.173}$$

Here the notch is at ω_n. The filter introduces a phase shift, which varies with frequency. The phase shift changes abruptly around $\omega = \omega_n$ and $\omega = \omega_c$. The filter is not desirable in closed loop schemes and in situations, which call for a good time response.

5.10.2 Notch Filter Configurations and Realizations

The notch filters in vogue, are the simplest ones – the counterparts of first order LPF or HPF. Their realizations are based on classical frequency selective networks or state variable filter configurations.

5.10.2.1 Notch Filters with Twin -T Networks

Two slightly different cases arise.

Case 1: -

The circuit is shown in Figure 5.26. The circuit is of the non-inverting type. The resistance and capacitance values and their ratios have been selected to yield the required gain characteristic directly. The resistances are represented as conductances G and $2G$ to simplify algebraic expressions.

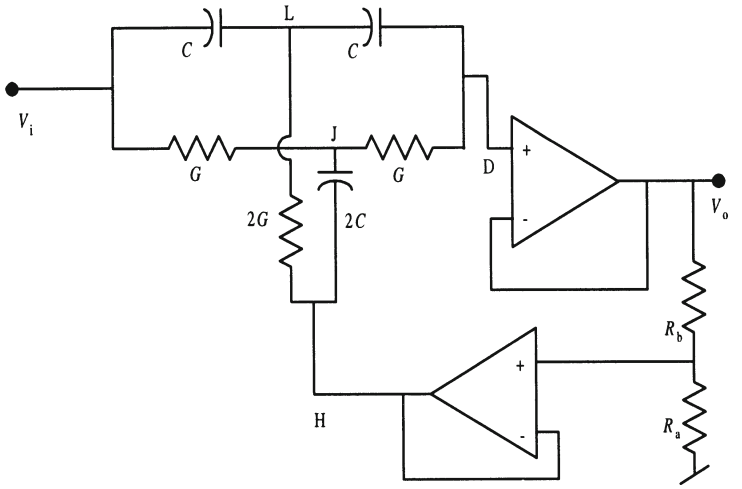


Figure 5.26 Notch filter circuit using twin-T network – case 1

Let

$$k = \frac{R_a}{R_a + R_b} \tag{5.174}$$

Under normal operating conditions

$$V_D = V_o \tag{5.175}$$

$$V_H = kV_o \tag{5.176}$$

Current balance at D gives

$$V_J G + V_L Cs - V_D (G + Cs) = 0 \tag{5.177}$$

Current balance at J gives

$$2(G + Cs)\, V_J - V_o (G + Cs) = V_i G \tag{5.178}$$

Current balance at L gives

$$2(G + Cs)\, V_L - V_o (2kG + Cs) = V_i Cs \tag{5.179}$$

Elimination of intermediate variables, followed by rearrangement of terms and algebraic simplification leads to

$$\frac{V_o}{V_i} = \frac{s^2 + \left(G^2/C^2\right)}{s^2 + 4(1-k)(G/C)s + \left(G^2/C^2\right)} \tag{5.180}$$

Identification of coefficients with Equation 5.169 gives

$$\omega_n = \frac{G}{C} \tag{5.181}$$

$$\xi = 2(1-k) \tag{5.182}$$

Equations 5.174 and 5.182 show that k is positive and has to be less than unity to ensure stable operation. One can realize all values of ξ, from 0 to 2 with $0 < k < 1$. The buffer can be dispensed with and the filter realized by a readjustment of $2G$ connected between L and H in Figure 5.26. But normally the buffer is retained for uniformity and easiness in realization of $2G$. With the use of quality opamps, the resistors representing G and $2G$ can be selected in the 1 MΩ range. This keeps the capacitance sizes small.

Case 2: -

The circuit shown in Figure 5.27 uses only one opamp. Otherwise, it is only slightly different from that of Figure 5.26 above.

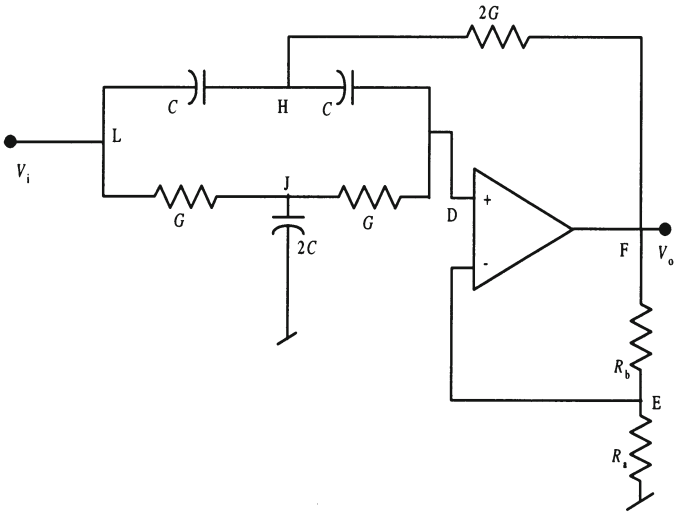


Figure 5.27 Notch filter circuit using twin-T network – case 2

Let

$$k = 1+\frac{R_a}{R_b} \tag{5.183}$$

$$V_D = \frac{V_o}{k} \tag{5.184}$$

Under normal operation, current balance equations at D, H and J are

$$V_H Cs + V_J G - \frac{V_o}{k}(G+Cs) = 0 \tag{5.185}$$

$$2V_H(Cs+G) - V_o\left(2G+\frac{Cs}{R}\right) = V_i Cs \tag{5.186}$$

$$2V_J(G+Cs) - V_o\frac{G}{k} = V_i G \tag{5.187}$$

Eliminating the intermediate variables, rearranging terms and simplifying we get

$$\frac{V_o}{V_i} = \frac{k\left(s^2+\frac{G^2}{C^2}\right)}{s^2+2(2-k)\frac{G}{C}s+\frac{G^2}{C^2}} \tag{5.188}$$

Identification of the coefficients with Equation 5.169gives

$$\omega_n = \frac{G}{C} \tag{5.189}$$

$$\xi = 2-k \tag{5.190}$$

k has to be less than 2, for stable operation. One can realize all ξ in the range 0 to 1, with $1< k < 2$. Here too one can use quality opamps and have the resistances in the MΩ range. This keeps C values too, down to reasonable levels. The passband gain is k here, which lies between 1 and 2. This is in contrast to the last case with unity gain.

5.10.2.2 Notch Filter with State Variable Scheme

The State variable filter of Figure 5.19 has been redrawn here in Figure 5.28. The signals at points A and C have been added through an additional opamp to give the new output V_o'. Expressing V_o in terms of V_i using Equation 5.71

$$\frac{V_o'}{V_i} = \frac{R}{R_1}\frac{s^2+\dfrac{1}{R^2C}}{s^2+\dfrac{k}{C}\left(\dfrac{1}{R}+\dfrac{1}{R_1}\right)s+\dfrac{1}{R^2C^2}} \tag{5.191}$$

Identifying the coefficients

$$\omega_n = \frac{1}{RC} \tag{5.192}$$

$$\xi = \frac{k}{2}\left(1+\frac{R}{R_1}\right) \tag{5.193}$$

The design procedure is similar to that of the LPF. Due to the independence of the variables in the stages of the filter, ω_n and ξ can be realized separately without any constraint. Further, the passband gain can be selected independent of these. The state variable filter of configuration 2 in Figure 5.20 may be modified in an identical manner to form a notch filter.

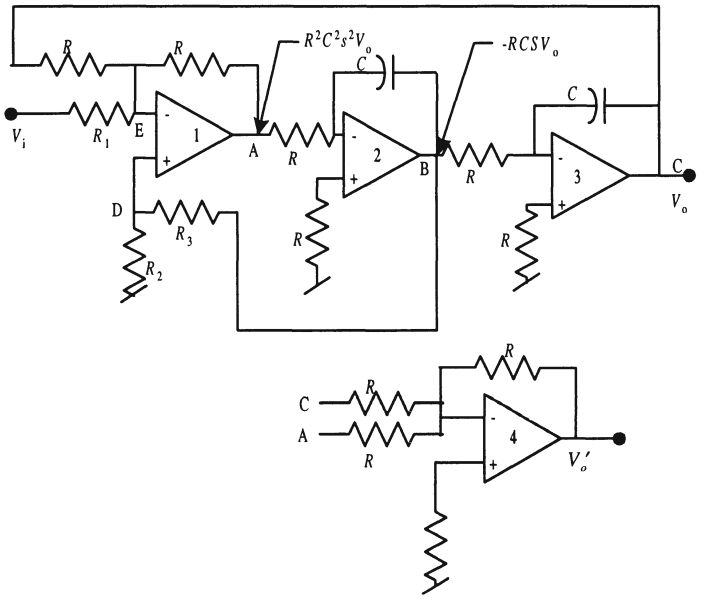


Figure 5.28 Notch filter circuit modifying the state variable scheme shown in Figure 5.20

5.10.2.3 *Notch Filter Circuit Realizations*

The component values for the notch filter configuration, using twin-T network, (case 1) are given in Table 5.7. The notch frequencies selected are the power utility frequencies – 50Hz and 60Hz. The component values for the S-V filter are not reproduced.

Table 5.7 Component values for the Notch filter with the notches being at 50 Hz and 60 Hz. Case 1 of the twin –T filter is selected as the configuration here. In both the cases ξ is taken as 0.1. All the capacitances are in nF and the resistances in kilo-ohms.

f	C	R	R_a	R_b
50Hz	47	67.8	1	20
60Hz	47	56.5	1	20

5.11 Switched Capacitor Filters

The active filters discussed so far are built around resistances, capacitances and opamps. The filters here are for signal processing and do not call for any 'power filtering'. Hence it is possible to replace resistances with their simulated equivalents using capacitors.

Consider a capacitor C switched on to voltages V_1 and V_2 alternately as in Figure 5.29 (a). The switching is done by synchronous non-overlapping clocks ϕ_1 and ϕ_2 as shown in Figure 5.29 (b). The respective on-periods are long enough to allow C to be completely charged and the transients to die down fully. Let f_{cl} be the switching clock frequency.

$$\text{Charge delivered by } V_i \text{ during each clock period} = C(V_1 - V_2) \tag{5.194}$$

$$\text{Average current drawn from } V_i = C(V_1 - V_2) f_{cl} \tag{5.195}$$

$$\text{Equivalent resistance , } R_{eq} = \frac{1}{Cf_{cl}} \tag{5.196}$$

Under the conditions stipulated, the combination of C and the switches acts as a resistance of value $1/Cf_{cl}$. All resistances in an IC can be realized through such 'Switched Capacitors'. The ratios of different resistances realized in an IC in this manner depend only on the ratios of areas for different capacitances. These can be made to track each other with 0.1 % accuracy. Similarly capacitances also can be realized to 0.1 % tracking accuracy. Such switched capacitance type resistances, capacitances themselves and opamps – all these can be integrated in a single IC. One direct application of such ICs is in filters. These are 'Switched Capacitor Filters'. Since the ratios of the areas for the switched capacitances and the capacitances themselves can be adjusted precisely, the filter realization also becomes precise.

Switched capacitor filters are available in IC form from different manufacturers. At one extreme end we have Butterworth filters of 4th, 6th 8th and higher orders where only the filter cut off frequency is decided by the user – done by selecting a suitable clock frequency (f_{cl}). This amounts to frequency scaling of the prototype. The user treats the filter as a pre-designed black box with an adjustable corner frequency. Similar filters of Chebyshev, Bessel types *etc.*, are also available. At the other extreme end switched capacitor type integrators and opamps

in suitably ordered forms and numbers are available. With these, state variable filters of different passband and cut-off characteristics can be realized. Filter design reduces to using a set of look-up tables, nomograms and running a dedicated program to decide f_{cl} and the values of one or two external resistances.

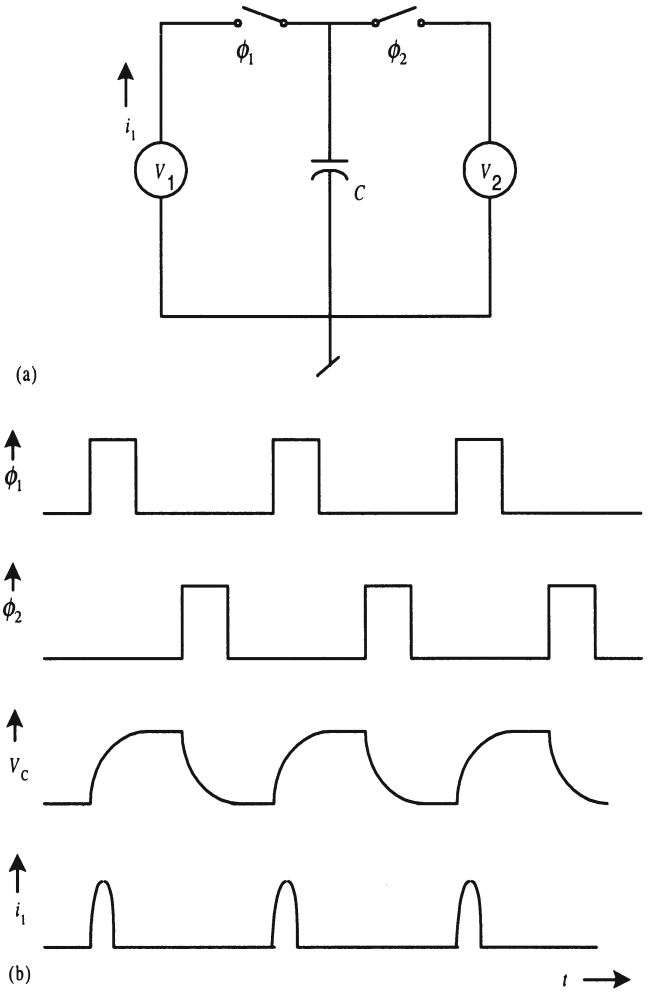


Figure 5.29 Principle of operation of switched capacitor scheme: (a) Basic switched capacitor element (b) Waveforms at different points of the circuit in (a) above

Observations: -

⇒ Switched capacitor filters have clock tunable cut off frequencies. The ratio f_{cl}/f_c – where f_c is the cut-off frequency of the filter – is a fixed parameter of the filter. It may be 50, 100 *etc.* In some versions the ratio may be user selectable. The ratio is set by the ratio of input and feedback capacitors in the integrators inside the filter. The higher the ratio, the closer the approximation is to the expected response.

⇒ Switched capacitor filters often have the facility to operate with external or internal clock. If the filter functions in isolation in an otherwise analog environment, internal clock may be used. If it works along with other switched capacitor filters and/or digital circuits, external clock that synchronizes different blocks is preferable.

⇒ If necessary, multiple switched capacitors may be cascaded to realize necessary cut-off or filtering characteristics.

⇒ Logic propagation delays within the filter and the time required for the capacitor voltages to settle down after each switching, restrict the maximum permissible clock frequency. As of now, it is in the 4 MHz range.

⇒ With 4 MHz clock frequency and f_{cl}/f_c of 50, the maximum signal frequency that can be handled by the switched capacitor filter is 80 kHz.

⇒ Typical input capacitance is of the order of 1pF. With f_c = 80 kHz, the effective filter input resistance is $10^{12}/(80 \times 10^{3})$ = 12.5 MΩ .To realize accuracy of the order of 0.1 %, error due to loading of input signal should be kept still lower. The signal source resistance should be less than 1 or 2 kΩ to achieve this order of accuracy.

⇒ The voltage across the switched capacitor itself drops due to the leakage current of the capacitor itself and the MOS switch in the off- state. The clock frequency should be high enough to replenish this leakage and keep the resulting error sufficiently low. This puts a limit on the lowest value of the clock frequency possible. For example, a leakage of 1 pA across the 1 pF capacitor, causes 4 μV voltage drop per cycle in the switched capacitor voltage. Correspondingly there is an average reduction in the signal of the order of 2 μV; at 1 mV signal level the resulting error is 0.2 %.

⇒ Charges induced due to clocking of the MOS switches, cause 'clock feed through' errors. The transistor dimensions are kept low to reduce this. Clock feed through error is of the order of a few mV.

⇒ The switching noise is proportional to $1/f_{cl}\ C_s$ (= R). Integration capacitors are to be made larger to keep down this noise. The silicon area and power consumption too, increase in turn. Thus there is a trade-off.

⇒ Dynamic range of a switched capacitor filter is the ratio of the maximum signal level that can be accommodated without distortion, to the noise level. With 0 – 5V supplies (typical digital circuit supply level), switched capacitor filters achieve a dynamic range of the order of 80 to 100 dB. As the power supply levels reduce, the signal swing reduces. The MOS switch drive reduces increasing its on-resistance. Both these reduce the dynamic range.

⇒ Signal components at frequencies > $f_{cl}/2$, cause aliasing errors. Hence suitable anti-aliasing filter should precede the switched capacitor filter. With f_{cl}/f_c > 50, these can be realized easily. One of the uncommitted opamps in the switched filter itself may be used for this.

⇒ Typically, switched capacitor filters provide unity gain in the passband. The undisturbed output swing ranges up to ±4V into R_L > 5k Ω, with ± 12 V supply. The cut off frequencies of LPF may range from 0.1 to 40 kHz and the clock frequency can extend up to 4 MHz.

6 Non-linear Signal Processing

6.1 Introduction

Two types of non-linear processing are done on instrumentation signals – band shifting or multiplexing and direct point to point modification.

Often the instrumentation signal is to be kept free of contamination, processed and then extracted. This is carried out by modulating it on a carrier and then processing the modulated carrier in a linear fashion through amplification and filtering. Subsequently it may be demodulated and used for the final purpose. Modulation and demodulation processes are discussed here. The principles are reviewed – the aim being retaining signal-fidelity as best as possible along with optimization of resources. Sampling, multiplexing and demultiplexing too are variants of these. Typical circuit schemes for these processes are discussed subsequently.

Direct modification of the signal on a point to point basis, can take three forms: -

⇒ Obtaining the logarithm of the signal - this is done when the dynamic range of the signal extends over a few decades.

⇒ Amplification of one segment of the signal at the expense of others – when one segment of the signal carries more information compared to others, this is resorted to.

⇒ Attenuation or comparatively low amplification of a selected segment of the signal – this is done when the information content in one segment of the signal, is not of much significance.

Commonly used circuits for signal processing of the above types, are discussed in the latter part of the chapter.

6.2 Modulation and Demodulation

Normally, a well-defined carrier is taken as a base and the signal modulated on it. Modulation amounts to making one characteristic of the carrier – its amplitude, frequency or phase (or other similar characteristics with pulse modulation) – change according to the signal. Once this is done, the signal information is retained in the modulated carrier. The modulated carrier is processed further – this can be in the form of amplification, filtering, frequency shifting *etc.* Subsequently the signal may be retrieved through demodulation.

Modulation (and demodulation) can be of the continuous or the pulsed type. Amongst the pulsed modulation schemes, instrumentation schemes use only the

T. R. Padmanabhan, *Industrial Instrumentation*
© Springer-Verlag London Limited 2000

'sampling' process. Others like the PWM, PPM *etc.*, are not so common now (Some crude though ingenious pulse modulation schemes were in use in some instrumentation schemes in earlier years). Amplitude and frequency modulation schemes are of the continuous type and are in more common use. These will be discussed in detail. Phase modulation schemes – used occasionally – being only variants of frequency modulation schemes, are not discussed separately [Carlson]. Sampling processes are dealt with in Chapter VIII along with ADCs and DACs.

6.2.1 Amplitude Modulation and Demodulation

In an amplitude modulation scheme, a sinusoidally varying voltage at particular frequency forms the 'carrier'; and the signal modulates its amplitude. At a later stage in the scheme, the amplitude alone is retrieved by a demodulation process, to get back the signal proper.

6.2.1.1 Principles of Amplitude Modulation

Let

$$x_s(t) = A_s \sin(\omega_s t + \phi_s) \tag{6.1}$$

be a test signal and let

$$x_c(t) = A_c \cos \omega_c t \tag{6.2}$$

be the carrier. Here A_c is the carrier amplitude in the absence of the signal *i.e.*, for zero signal and ω_c the carrier frequency in rad/s. In the presence of the test signal, the carrier amplitude changes from A_c to one proportional to $x_s(t)$ or having a component proportional to $x_s(t)$.

$$\text{Carrier amplitude after modulation} = A_c + kA_s \sin(\omega_s t + \phi_s) \tag{6.3}$$

$$\text{Modulated signal } y(t) = [A_c + kA_s \sin(\omega_s t + \phi_s)] \cos \omega_c t$$

Expanding,

$$y(t) = A_c \cos\omega_c t + \frac{kA_s}{2}\sin[(\omega_c + \omega_s)t + \phi_s] + \frac{kA_s}{2}\sin[(\omega_c - \omega_s)t - \phi_s] \tag{6.4}$$

Here k is a constant (modulation constant).
Maximum deviation of amplitude from unmodulated level = kA_s

$$\% \text{ modulation} = \frac{kA_s}{A_c} \times 100 \tag{6.5}$$

Observations: -

- ⇒ Equation 6.4 shows that the modulated carrier has three frequency components. One at the carrier frequency ω_c, one at $\omega_c - \omega_s$, and the third at $\omega_c + \omega_s$. The latter two are the 'Lower Side Band (LSB)' and the 'Upper Side Band (USB)' respectively.
- ⇒ After modulation, the amplitude level of the carrier remains unaltered at A_c itself. It does not change with the modulation level, signal frequency *etc.*
- ⇒ Waveforms of the carrier without modulation, with 60 % modulation and 120 % modulation respectively are shown in Figure 6.1. Two things can be seen :-

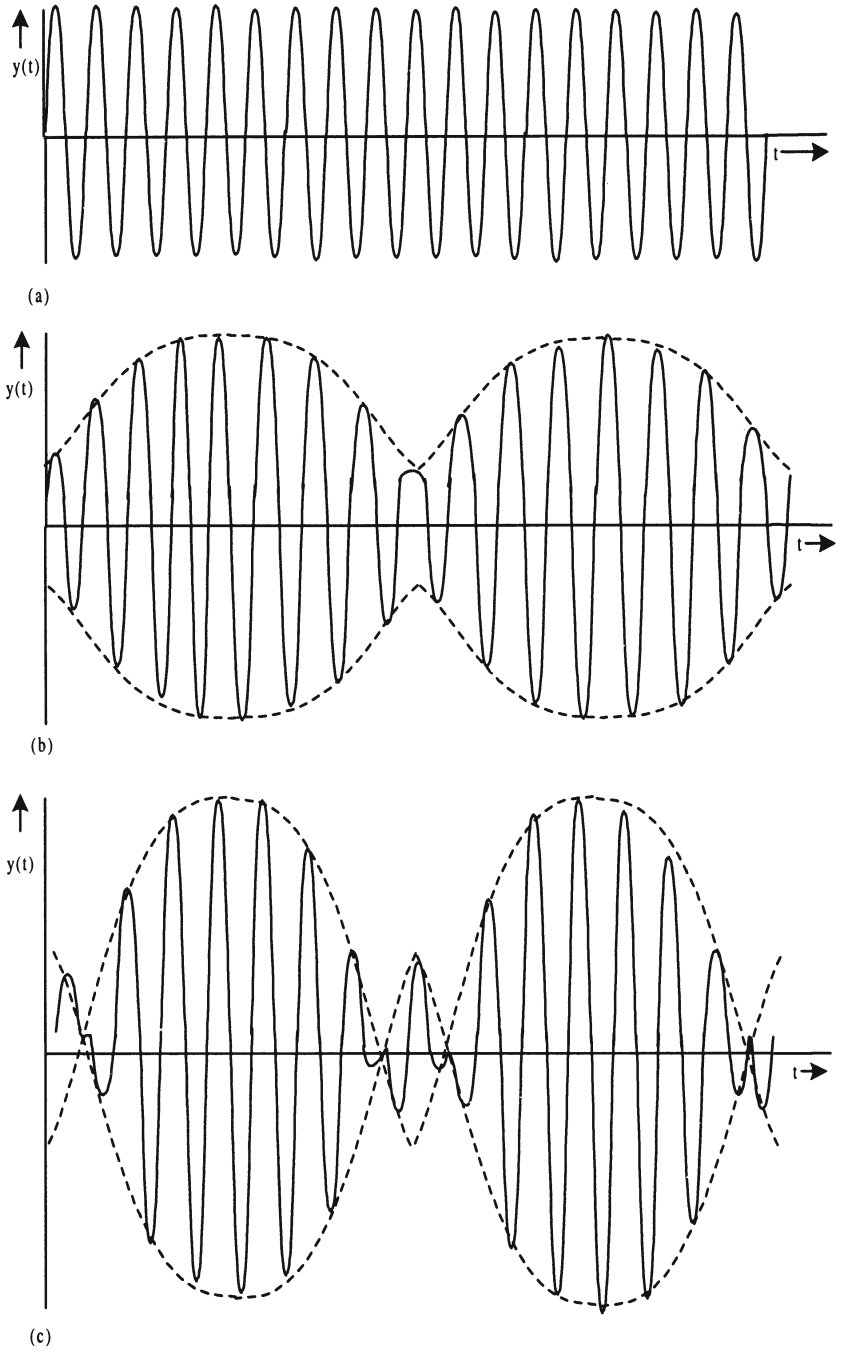


Figure 6.1 Amplitude modulation: Waveforms of (a) Carrier (b) Carrier with 60% modulation and (c) Carrier with 120% modulation

- As long as $kA_s < A_c$, the envelope profile follows the changes in the signal. Sensing the envelope suffices for demodulation.
- If $k A_s > A_c$, the modulated carrier amplitude goes through a zero and the carrier goes through a phase reversal. Under these conditions, the envelope is not representative of the signal. Demodulation has to be done in a more involved manner.

$\Rightarrow$ The signal information is fully available in each side band. As long as $\omega_s \leq (\omega_c/2)$, the modulation process is fully acceptable; but if $\omega_s > (\omega_c/2)$, the scheme functions erroneously. We shall revert to this later.

$\Rightarrow$ The phase lead is carried *in toto* over to the upper side band. But it appears as an equal phase lag ϕ_s in the lower side band.

$\Rightarrow$ The spectral components of the modulating signal, the carrier and the modulated curve are shown in Figure 6.2. The components of the modulating signal are impulses of strength $A_s/2$ at $+j\omega_s$ and at $-j\omega_s$. The modulation process repeats these with gain factor k on either side of $+j\omega_c$ and at $-j\omega_c$.

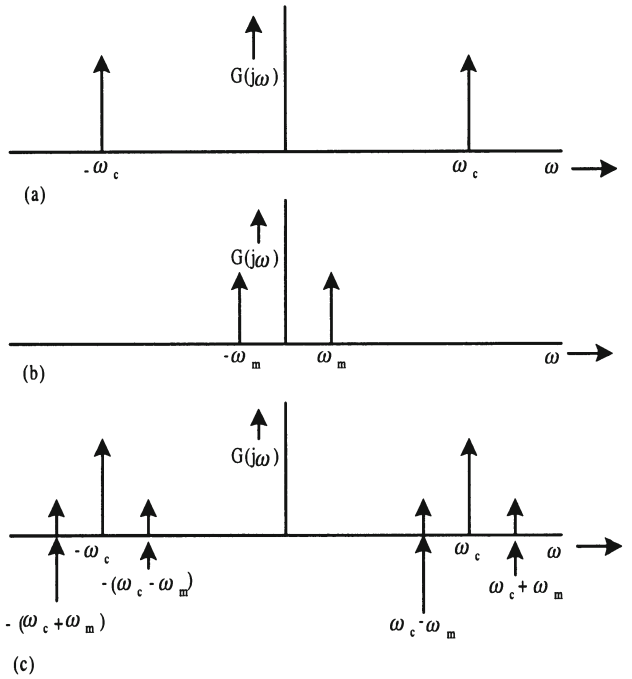


Figure 6.2 Amplitude modulation – Spectral components: (a) Carrier (b) Modulating signal (c) Modulated carrier

Consider a modulating signal composed of two frequency components

$$x_s(t) = A_1 \sin(\omega_1 t + \phi_1) + A_2 \sin(\omega_2 t + \phi_2) \quad (6.6)$$

After modulation (on the same lines as earlier), we get

$$y(t) = [A_c + kx(t)] \cos \omega_c t$$

$$= A_c \cos\omega_c t + \frac{kA_1}{2}\sin[(\omega_c - \omega_1)t - \phi_1] + \frac{kA_2}{2}\sin[(\omega_c - \omega_2)t - \phi_2]$$
$$+ \frac{kA_1}{2}\sin[(\omega_c + \omega_1)t - \phi_1] + \frac{kA_2}{2}\sin[(\omega_c + \omega_2)t - \phi_2] \quad (6.7)$$

Observations: -

⇒ The modulation process treats the two spectral components separately.

⇒ The full information in the modulating signal (amplitude, frequency and phase of individual components) is contained in the LSBs as well as the USBs.

⇒ The percentage modulation is

$$\% \text{ modulation} = \frac{kA_1 + kA_2}{A_c} \times 100 \quad (6.8)$$

⇒ As long as the modulation level is less than 100 %, the signal information can be fully extracted by sensing the envelope of the modulated carrier. If it exceeds100 %, other involved methods are called for.

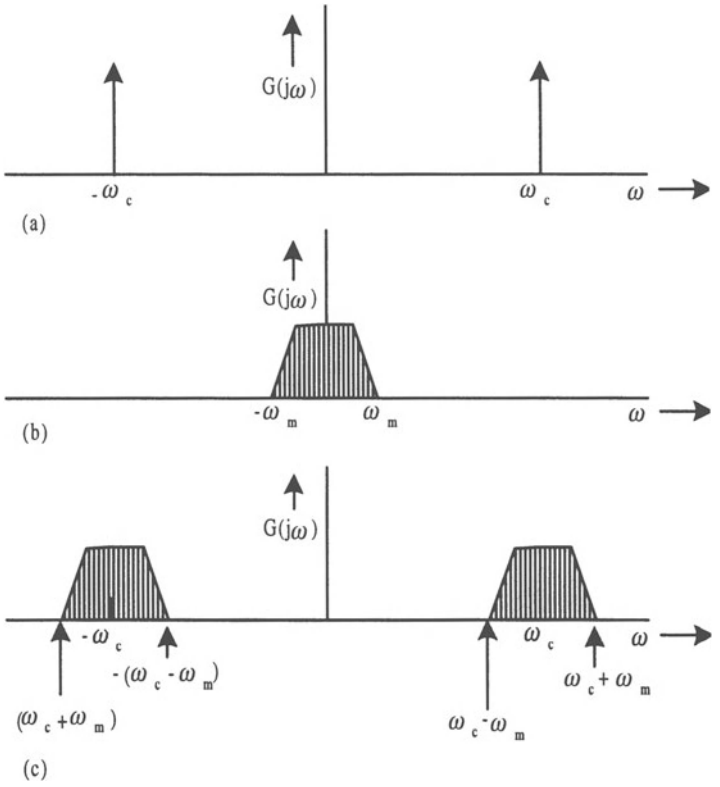


Figure 6.3 AM – Frequency spectrum; (a) Carrier (b) Modulating signal (c) Modulated carrier

⇒ Consider an arbitrary modulating signal with its Fourier spectrum extending up to its bandwidth limit. Figures 6.3 (a) to 6.3 (c) show the spectrum of the carrier, the modulating signal and the modulated signal respectively. The modulation process can be seen to repeat the base band spectrum around $-\omega_c$ and $+\omega_c$.

⇒ As long as ω_m – the largest frequency of interest in the modulating signal – is less than $\omega_c/2$, the base band and the modulated spectra stay clear of each other. But if ω_c is made lower and this condition is not satisfied, part of the two spectra overlap. Referring to Figure 6.3 (c) one can see this happening if

$$\omega_m > (\omega_c - \omega_m) \quad \text{or} \quad \omega_m > \frac{\omega_c}{2} \tag{6.9}$$

⇒ This causes ambiguity and error. Such a situation is to be avoided.

Equation 6.9 shows that the theoretical bandwidth-limit for the modulating signal is $\omega_c/2$ (this conforms to the sampling theorem and the Nyquist frequency). In practice, it may extend up to only $\omega_c/4$ or $\omega_c/6$ depending on the quality level expected of the scheme.

When amplitude modulation is used directly, the carrier level remains constant in the modulated signal; this can be seen from Equations 6.4 and 6.7. In other words, the carrier *per se* does not carry any signal information. However presence of the carrier at its full level here, makes the demodulation process simple – justifying its presence. Alternately one can suppress the carrier at the modulation stage itself by judicious cancelling or filtering. This is done in the 'Double Side Band Suppressed Carrier (DSB-SC)' scheme. Absence of the carrier, makes Demodulation in DSB-SC schemes, more involved. DSB-SC is commonly used in instrumentation schemes [Carr].

We found that the information in the base band is fully available in both the side bands. Hence the upper or the lower side band may be suppressed by proper filtering; the full information in the modulating signal is retained in the remaining side band and only this need be processed further. Such a scheme is called the Single Side Band (SSB) scheme. Demodulation of SSBs is more complex. These are not directly used in instrumentation. When a cluster of processes are transmitted over a few (or more) kms, SSB is an attractive choice. This is not pursued further here. SSB is ideally suited for signals whose active band does not extend below a definite cut off frequency – voice signal is a typical example. This brings a clear separation between the USB and the LSB and facilitates filtering. If the signal bandwidth extends down to zero frequency, filtering out one of the side bands is not effective – since practically realizable filters cannot have a sharp cut off. In such situations, a compromise scheme called the Vestigial Side Band (VSB) is in use. In VSB, the cut off is arranged in a measured manner around the carrier frequency ω_c.

The cut off characteristic is such that

$$G(\omega_c + \omega) + G(\omega_c - \omega) = 2G(\omega_c) \tag{6.10}$$

where $G(\omega_c)$ is the filter gain at the carrier frequency, $G(\omega_c+\omega)$ is the gain at frequency $\omega_c+\omega$ and $G(\omega_c-\omega)$ is the gain at frequency $\omega_c-\omega$. Figure 6.4 shows the cut off characteristic of the filter for a VSB scheme that has the USB retained. During demodulation, when the two USBs are brought back and combined, the tails at the vestiges of the two bands add together to form the original signal. VSB requires more bandwidth than SSB. But the bandwidth required is less than that for DSB or DSB-SC.

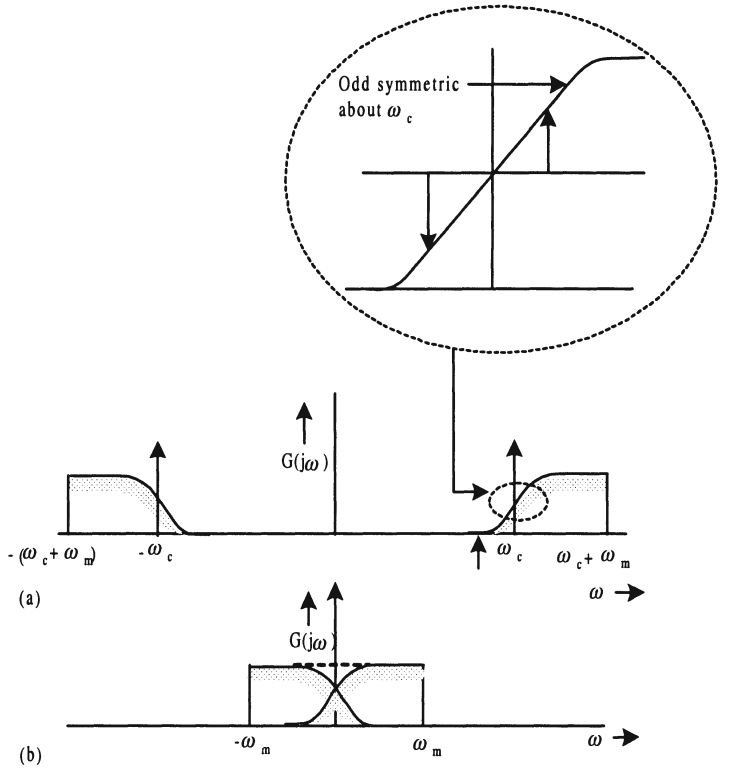


Figure 6.4 Frequency spectrum of VSB: (a) AM modulated spectrum after necessary filtering (b)Spectrum after demodulation. The inset shows the filter characteristic around ω_c

6.2.1.2 *Practical Aspects of Amplitude Modulation*

One approach to AM is to have an oscillator of frequency ω_c and change its amplitude directly by modulating the signal. Alternate approaches use non-linear devices that warrant a more detailed discussion. Consider a device (a resistance, inductance *etc.*,), having a non-linear characteristic of the form

$$y = a_0 + a_1x + a_2x^2 + a_3x^3 + a_4x^4 + ... \tag{6.11}$$

Let

$$x(t) = x_1(t) + x_2(t) \tag{6.12}$$

where

$\Rightarrow$ $x_1(t)$ represents the carrier and

$\Rightarrow$ $x_2(t)$ represents the modulating signal.

For AM schemes $x_1(t)$ can be a sinusoidal carrier at frequency ω_c and $x_2(t)$ the modulating signal. Further for the discussion let the modulating signal be a sinusoidal test signal at frequency ω_2. Substitution from Equation 6.12 into Equation 6.11 gives

$$\begin{aligned} y = {} & a_0 + a_1x_1 + a_1x_2 + a_2x_1^2 + 2a_2x_1x_2 + a_2x_2^2 + a_3x_1^3 + 3a_3x_1^2x_2 \\ & + 3a_3x_1x_2^2 + a_3x_2^3 + a_4x_1^4 + 4a_4x_1^3x_2 + 6a_4x_1^2x_2^2 + 4a_4x_1x_2^3 + a_4x_2^4 + ... \end{aligned} \tag{6.13}$$

where x_1 and x_2 represent $x_1(t)$ and $x_2(t)$ respectively.

Observations: -

⇒ The term a_1x_1 reproduces the carrier that gets added to the modulated signal.

⇒ The term a_1x_2 reproduces the base band signal that has to be filtered out.

⇒ The term $a_2x_1^2$ adds a term at twice the carrier frequency, which has to be filtered out.

⇒ the term $2a_2x_1x_2$ represents the modulated output of interest to be retained.

⇒ The term $a_2x_2^2$ adds a component at $2\omega_2$ – *i.e.*, twice the signal frequency – to the modulated signal. It adds an additional DC term also. In a practical situation, the modulating signal may have spectral components at all frequencies from 0 to ω_m where ω_m is the cut-off frequency. In such a case the term $a_2x_2^2$, spreads the original base band of the modulating signal from 0 to ω_m to 0 to $2\omega_m$. This can be filtered out. However it imposes the constraint on the carrier that $\omega_c - \omega_m > 2\omega_m$ (*i.e.*, $\omega_c > 3\omega_m$) to avoid the spectral component at $2\omega_m$ interfering with that at $\omega_c - \omega_m$.

⇒ The term $a_3x_1^3$ adds a term at $3\omega_c$ (in addition to one at ω_c itself) which has to be filtered out.

⇒ The term $3a_3x_1^2x_2$ adds two types of components. One set adds to the base band and another produces modulated components around $2\omega_c$, all of which are to be filtered out.

⇒ The term $3a_3x_1x_2^2$ adds two types of components. One set increases the carrier amplitude. The increase is proportional to the signal level and will be interpreted as a slow change in the signal level. This causes error at low frequencies. The second set adds spurious modulated components. To minimize these errors the a_3 term in the non-linear characteristic has to be as small as possible.

⇒ The term $a_3x_2^3$ adds a component at three times the signal frequency. In effect, it spreads the base band from 0 to ω_m to 0 to $3\omega_m$. This can be filtered out. It imposes the constraint that $\omega_c > 4\omega_m$ to avoid interference. As mentioned above, if $a_3 << a_1$, the effect of this term may be negligible.

⇒ Considering the term a_4x^4, the only part that can contribute useful output is $a_4x_1^3x_2$. All others have nuisance values or cause errors. It is necessary to have $a_4 << a_2$ to minimize these effects.

From the above, we see that only the a_2x^2 term contributes meaningfully to the modulated output. Higher power terms in Equation 6.11 are to be kept as low as possible to minimize components in the unwanted frequency ranges and errors in the modulated frequency range itself.

Non-linear single valued characteristics like saturation, dead zone *etc.*, can be approximated by polynomials of the type in Equation 6.11. With any non-linearity, it is generally found that the coefficients of higher power terms like a_3, a_4, a_5 *etc.*, steadily decrease in magnitude – the coefficient of x^n will be of the order of $1/n^2$ or even less. This incidentally contributes to the quality of the modulation process. In general, the modulation process is improved in two ways: -

⇒ Keeping a_2 as high as possible as compared to a_3, a_4, a_5 *etc.*

⇒ Keeping signal levels low enough to reduce the contribution of the higher power terms but high enough to have the term $2a_2x_1x_2$, dominant. The modulated signal component can be filtered out and amplified to the required level later.

Quality of the modulation process can be improved in many ways. Two possibilities are suggested below: -

⇒ If we take care to use a non-linearity with only even power terms, *i.e.*, $a_1 = a_3 = a_5 = ... = 0$. From Equation 6.13, we see that the first spurious term in the output is due to $a_4 x_1 x_2^3$. Here a_4 has to be kept small compared to a_2, to keep the distortion due to $a_4 x^4$ low.

⇒ An alternate to the above restriction on the non-linearity is to use a more involved scheme of modulation. Let

$$x_p = x_1 + x_2 \tag{6.14}$$

$$x_n = x_1 - x_2 \tag{6.15}$$

⇒ Substitution in Equation 6.11, and some algebra yields,

$$y_p - y_n = 2a_1 x_2 + 4a_2 x_1 x_2 + 6a_3 x_1^2 x_2 + 2a_3 x_2^3 + 8a_4 x_1^3 x_2 + 8a_4 x_1 x_2^3 + ... \tag{6.16}$$

$(y_p - y_n)$ is characterized by

- Absence of the carrier term (suitable for DSB-SC),
- $4x_1 x_2$ as the modulated output and
- $8a_4 x_1 x_2^3$ as the first spurious term.

Implementation of the latter scheme is more involved. We have to use two identical modulation circuits, generate (x_1+x_2) and (x_1-x_2), process them through the modulator and get their difference.

6.2.1.3 AM Demodulation

The ideal AM output is of the form

$$y(t) = [A_c + kx(t)]\cos\omega_c t \tag{6.17}$$

$A_c + kx(t)$ represents the instantaneous amplitude of the modulated carrier. If we ensure that the modulation index is always less than 100 %, the envelope of $y(t)$ varies as $x(t)$. Hence one can continuously extract the amplitude of $y(t)$ and subtract A_c from it to get back $x(t)$. This technique of signal extraction is called 'Envelope Detection'.

Observations: -

⇒ Envelope detection is used wherever possible – its simplicity is a big plus point.

⇒ Envelope detection requires the presence of a dominant carrier for its operation.

⇒ For satisfactory operation, the circuits used for envelope detection require the modulated signal level to be of the order of a few volts.

⇒ Any amplitude change in the carrier will reflect as a corresponding change in DC level of the modulating signal. Stabilization of the carrier amplitude is not easy. Hence envelope detection is not recommended for signals with DC levels.

Envelope detection can be of use in instrumentation schemes, only if the sensor concerned has no zero-frequency component in its output. Vibration and noise are two of such few signals.

If one does not use envelope detection, A_c – the carrier component in the modulated signal – can be taken as zero. Hence we get

$$y(t) = kx(t)\cos\omega_c t \tag{6.18}$$

This represents the DSB-SC output. The carrier component is absent here. Detection in DSB is done by multiplying $y(t)$ by the carrier itself and filtering the multiplier output. Multiplying $y(t)$ of Equation 6.18 by a carrier reference – $l \cos \omega_c t$ – where l is the amplitude of the reference, we get

$$y(t)\, l\cos\omega_c t = \frac{kl}{2}x(t) - \frac{kl}{2}x(t)\cos 2\omega_c t \qquad (6.19)$$

The band around $2\omega_c$, is filtered out using an appropriate LPF (the band of interest is 0 to ω_m where ω_m is the cut-off frequency of the modulating signal). From Equation 6.19

$$\text{the filtered output} = \frac{kl}{2}x(t) \qquad (6.20)$$

This type of demodulation is referred to as 'Synchronous Demodulation'.

Observations: -

⇒ In an instrumentation scheme the modulation and demodulation are carried out physically close to each other. Hence, it is possible to make the carrier available for the demodulation process, facilitating synchronous demodulation.

⇒ In telemetry the carrier is transmitted through a separate channel and used for demodulation at the receiver.

⇒ Normally the carrier used for modulation and the reference component used for demodulation – both these are derived from the same source. Hence any frequency drift affects both in a similar manner and does not cause any error.

⇒ The drift in the carrier amplitude or in the reference carrier (or its phase) used for demodulation, affects the demodulator output directly and causes error. The errors are cumulative in nature. Thus, there is a need to stabilize the amplitude of the carrier used for modulation and the reference carrier used for demodulation.

⇒ Synchronous demodulation can be carried out directly, even when the modulated signal levels are low.

6.2.1.4 Effects of Harmonics in the Carrier

Ideal sinusoidal carrier has been considered for modulation and demodulation so far. A clear awareness of the implications of a distortion in the carrier wave form is in order. Consider a carrier with a third harmonic present in it: -

$$x_1(t) = A_1 \cos \omega_c t + A_3 \cos 3\omega_c t \qquad (6.21)$$

Consider the modulation process: When processed through the general non-linearity of Equation 6.11, the third harmonic in the carrier gives rise to a number of additional frequency components in the output; these can be considered in two parts: -

⇒ As explained earlier, the $a_2x_1x_2$ term is of primary interest in the modulator output. The third harmonic in the carrier gives rise to a modulated band around $3\omega_c$. This is filtered out in the normal course and hence, is harmless. Similarly, the higher harmonics in the carrier are also harmless.

⇒ The spectral components in the modulator output due to a_3x^3, a_4x^4, *etc.*, are spread over a wide range of frequencies. Some of these are in the base band,

while others are around the frequencies ω_c, $2\omega_c$, $3\omega_c$ *etc*. All these will be filtered out and need not cause any concern. But the base band around zero frequency as well as ω_c spreads out beyond ω_m. As discussed earlier, a_3, a_4 *etc.*, are to be kept small compared to a_2 to minimize errors due to these. Thus we find that to the extent A_3, A_4 *etc.*, are made small, the effect of carrier harmonics is also small.

In short, one need not impose any restrictions on the harmonic content of the modulating signal. Restrictions on the amplitude stability are more important. Similar analysis with the demodulation process leads to the same conclusion. Normally the carrier waveforms used for modulation or synchronous demodulation are rarely sinusoidal.

6.2.1.5 Circuit Schemes for AM Modulation and Demodulation

A typical AM circuit has to carry out the following functions: -

- ⇒ From the modulating signal and the carrier, generate a signal proportional to the product term. This is the 'mixer' stage. With DSB, we have to ensure that the carrier is present at a dominant level in the product while with DSB-SC we have to ensure its absence.
- ⇒ The mixer output is to be suitably filtered. Only the carrier (if present) and the side bands are retained for modulation. The baseband components and all the components around $2\omega_c$, $3\omega_c$, *etc.*, are eliminated here. A BPF or narrowband filter as the case may be, is used for filtering.
- ⇒ With demodulation, only the baseband components are retained. All the frequency components centred on ω_c, $2\omega_c$, $3\omega_c$, *etc.*, are filtered out.
- ⇒ With the DSB scheme with sufficient carrier level, the demodulation is simpler. The received signal around ω_c, is demodulated using an envelope detector. If necessary the detector output is filtered further to remove the components around ω_c, $2\omega_c$, $3\omega_c$, *etc.*

Filters have been discussed in the last chapter. Only the modulation and demodulation circuits are dealt with here. A wide variety of schemes is in vogue for AM [Franco, Schubert, Kennedy and Davis]. Only a select few will be discussed. It is pertinent to point out here that some instrumentation schemes – even though they use the AM modulation and demodulation format – do not require a separate modulator. Some schemes using C or L type sensors are of this category. The sensor is part of a bridge. The bridge is excited at the carrier frequency. As the sensor responds to the variable, the bridge provides an amplitude-modulated output directly. A separate modulator is not called for.

6.2.1.6 Multiplier Based AM Modulator

One direct way of generating an AM signal is to directly multiply the carrier with the modulating signal using the analog multiplier. This generates DSB-SC output directly. The filtering overheads are minimal since other frequency components are not generated at all. If DSB output is required, the carrier may be added subsequently. Quality multiplier ICs have become available in the recent years. These can be used directly for modulation. The analog multiplier is shown in block diagram form in Figure 6.5.

It accepts three differential inputs (x_1-x_2), (y_1-y_2) and (z_1-z_2) and generates an output V_o of the form

$$V_o = A\left[\frac{(x_1 - x_2)(y_1 - y_2)}{SF} - (z_1 - z_2)\right] \tag{6.22}$$

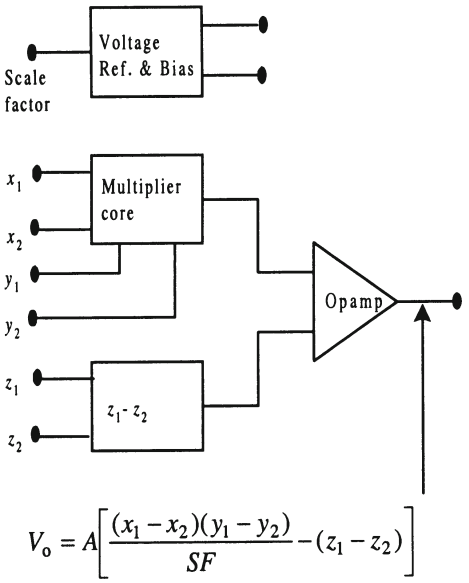


Figure 6.5 Analog multiplier IC in block diagram form

SF is a scale factor here – normally adjusted to 10V. This ensures that when $(x_1–x_2)$ and $(y_1–y_2)$ are 10V each, the multiplier output is also 10V. However, it can be adjusted to other values to match the input signal range. A is the opamp gain. Normally the circuit is arranged in a feedback scheme. The opamp gain being high, under normal operating conditions, the IC brings out an equality between the inputs $[(x_1–x_2)\ (y_1–y_2)/SF]$ and $(z_1–z_2)$. Figure 6.6 shows a commonly used multiplier configuration. The inputs are taken as single ended. x_2 is returned to an adjustable voltage for zero adjustment. It is adjusted to give zero output with zero input at x_1 and y_1.

To ensure balance, from Equation 6.22 we have

$$\frac{x_1 y_1}{SF} = z_1 \tag{6.23}$$

Thus, z_1 is proportional to the product $x_1\ y_1$.

If x_1 is taken as the carrier and y_1 as the modulating signal, we get DSB-SC type output. If z_2 is taken to be the carrier input instead of being grounded, we get DSB output with carrier. Small signal bandwidth of the scheme extends typically to 1 MHz. Full-scale output range is ±10V. The full-scale accuracy with 100 % inputs for x and y, is of the order of 0.3 %.

Only the multiplier based modulator gives a pure AM output. Other circuits to generate AM discussed below produce other unwanted frequency components also (around $2\omega_c$, $3\omega_c$ *etc.*,); as mentioned earlier, these are to be filtered out.

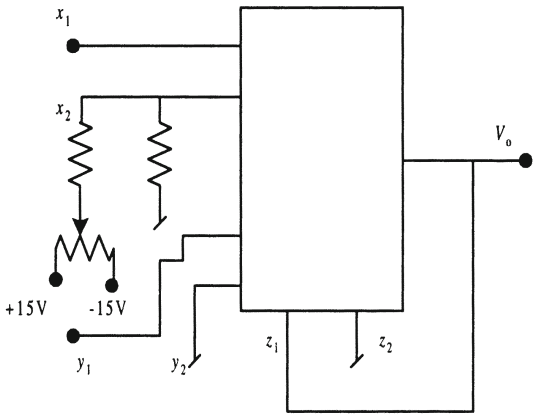


Figure 6.6 Commonly used multiplier configuration with an IC of the type in the Figure 6.5

6.2.1.7 *Simple Modulator with Analog Switch*

A simple modulator is shown in Figure 6.7 (a) in block diagram form. S is an analog switch. x_2 is the modulating signal and x_1 the carrier. The carrier is fed at x_1 as a rectangular pulse train of fixed amplitude [Figure 6.7(c)]. It turns the analog switch on and off alternately. The buffer ensures that the input is not loaded. Since the current drawn from the source – x_2 – is negligible, variation in the on-resistance of the switch does not cause any voltage drop or error [See Section 8.3.1 on analog switches].

The main component of v_o is the signal modulated at the carrier frequency ω_c. It also has other spectral components – the signal modulated at $2\omega_c$, $3\omega_c$ *etc.* The same are removed by a BPF (not shown here). The BPF output is of the DSB-SC type shown in Figure 6.7 (e). If x_2 is biased suitably so that it does not become negative, we get a DSB with the carrier present.

If x_2 is the modulated carrier, the scheme functions as a demodulator. The base band signal is retrieved using a low pass filter on the output side of the buffer. Here one should ensure that the reference carrier used for demodulation is synchronized with the carrier used for modulation and in phase with it.

6.2.1.8 *Chopper Amplifier*

A DSB-SC output is generated directly by the scheme shown in Figure 6.8. The carrier – again in the form of a rectangular pulse train – switches the modulating signal x_2 alternately to the upper and lower sides of the primary of the transformer. The capacitance C on the secondary side is selected so that the secondary tank circuit is tuned to the carrier frequency. The tank circuit acts as a narrow band filter. The signal source has to supply the magnetizing current of the transformer; to that extent it is loaded. The modulated output is directly isolated from the signal which can be a plus point in many situations when common mode signals can cause errors. To keep the magnetizing currents low, special cores of high μ and low loss (μ Metal, Permalloy *etc.*,) are selected for the core. One can use a step-up transformer and enhance the modulating signal level; but this is at the expense of an additional loading of the signal x_2.

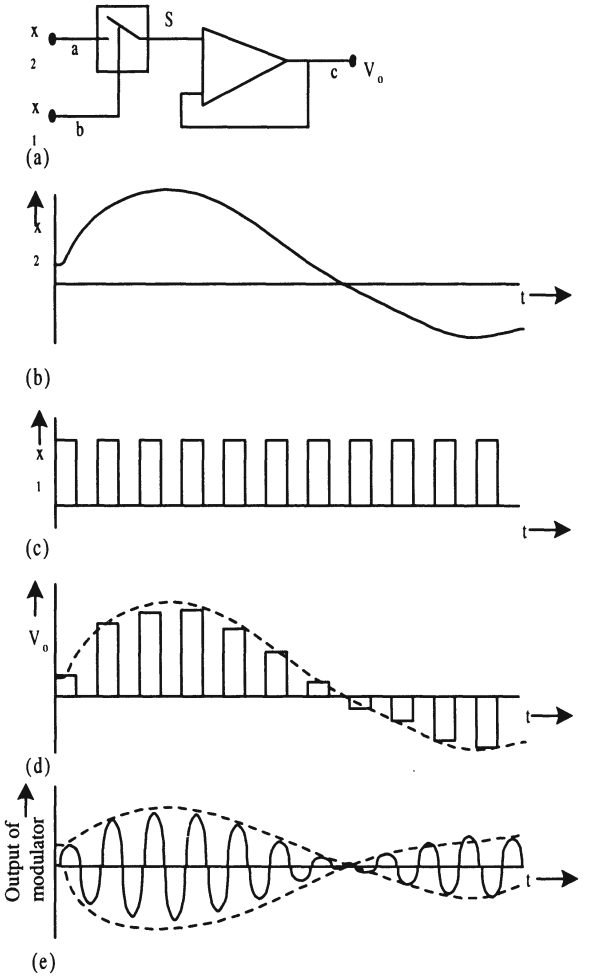


Figure 6.7 A simple modulator using analog switch: (a) Circuit and waveforms of (b) modulating signal, (c) carrier, (d) sampled output and (e) modulated output

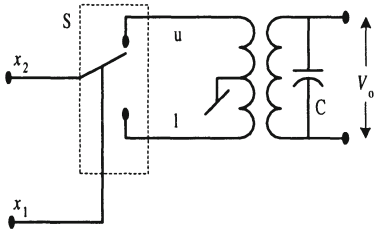


Figure 6.8 Chopper amplifier with centre-tapped transformer

It is possible to use good quality mechanical vibrating switches for S in Figure 6.8. This is what is done in the chopper amplifiers. If quality contact is ensured, drift and voltage drop across the contact can be kept lower than those with electronic analog switches. Such vibrating switches are used at the lowest modulating signal levels. Today, use of vibrating mechanical chopper amplifiers is restricted essentially to this application.

The scheme of Figure 6.8 is not suitable as a demodulator, since the transformer cannot couple low frequencies. The previous scheme or one of its variants is preferred for demodulation.

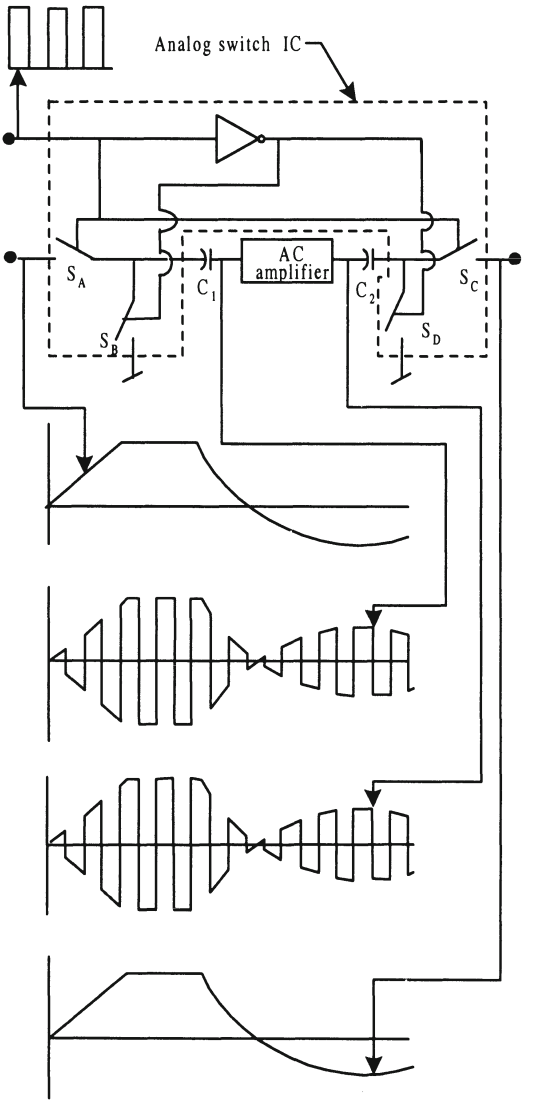


Figure 6.9 Chopper pair using analog switches and associated waveforms

6.2.1.9 Chopper Pair Using Analog Switch

A compact chopper amplifier can be constructed using analog switches. Figure 6.9 shows the scheme along with the waveforms at key points in the scheme [(See Section 8.3.1]. A set of four switches – designated S_a, S_b, S_c and S_d – is used for the purpose. The pair S_a and S_b switched alternately forms the modulator. The amplifier output is alternately connected to the signal and grounded. The coupling capacitor C_1 removes any offset or bias due to the switches. The modulated signal may be amplified and processed further (if necessary) by the AC amplifier. The first stage of the amplifier has to be a buffer of high input impedance. The output stage of the amplifier has to be of a low source-impedance type. Normally, the chopper frequency is kept high compared to the bandwidth of interest of the signal (10 to 100 times). This makes design of the amplifier as well as the tuned filter easy. An identical chopper realized through S_c and S_d does the demodulation. Often the output side of the amplifier may be a transformer secondary, obviating the need for the coupling capacitor C_2. The drive to turn on S_c is in phase with that for S_a. The drive for S_d is the same as for S_c. These ensure that the carrier for demodulation is in phase with that for modulation.

6.2.1.10 Balanced Modulator

A simplified balanced modulator is shown in Figure 6.10. It makes use of the non-linear characteristic of the diodes D_1 and D_2. Normally, matched diodes are selected for D_1 and D_2. The main output v_o is proportional to $(x_1 + x_2)^2 - (x_1 - x_2)^2$ which provides the required modulated output [See Section 6.2.1.2]. Capacitor C is selected so that the tank circuit is tuned to the carrier frequency. If x_2 has DC components in it, transformer T_2 has to be dispensed with and x_2 directly coupled through suitable circuits.

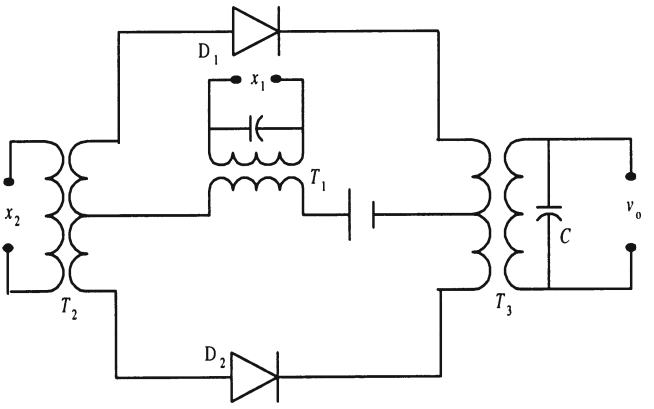


Figure 6.10 A simplified balanced modulator

Due to transformer T_3, the scheme cannot be used directly for demodulation. A more practical scheme is shown in Figure 6.11. The use of FETs in place of diodes as in Figure 6.10, provides power amplification. V_o is available with a low output impedance. Further the transformer T_3 has been dispensed with and two equal resistances R are used instead. Due to this, the scheme is useful as a modulator or as a demodulator. The type of filter used at the following stage changes accordingly.

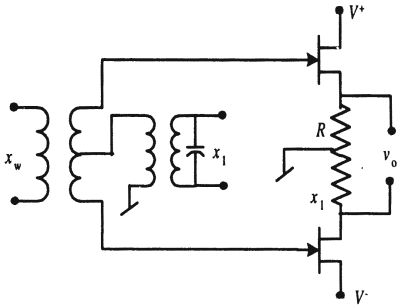


Figure 6.11 A balanced demodulator using FETs

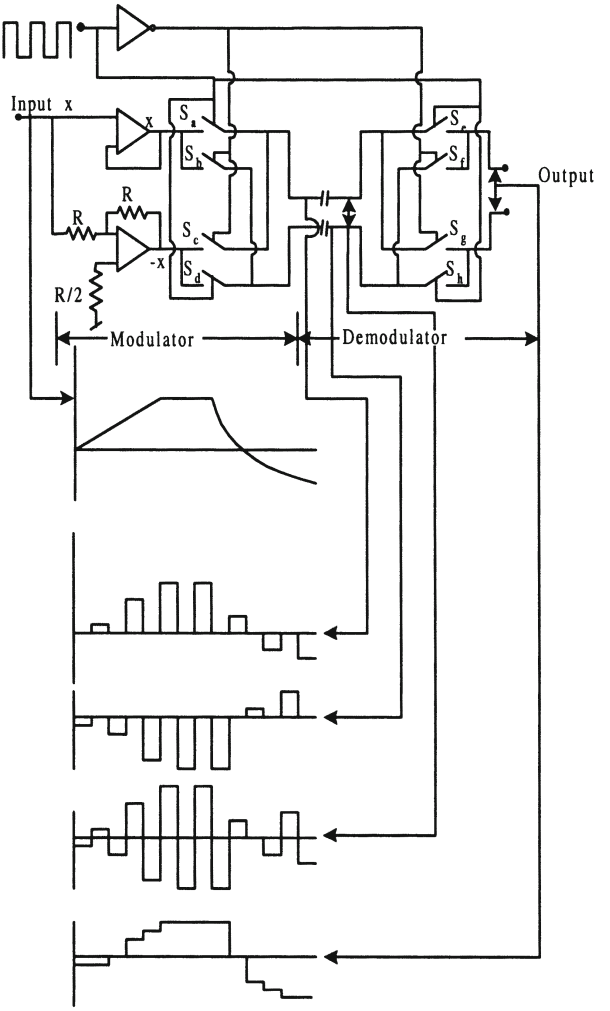


Figure 6.12 Balanced modulator and demodulator pair using analog switches

6.2.1.11 *Balanced Modulator And Demodulator Using Analog Switch*

Analog switches available in IC form can be used effectively for the generation of DSB-SC and its demodulation. A scheme is shown in Figure 6.12. A set of analog switch S_a, S_b, S_c and S_d are used for modulation and another set S_e, S_f, S_g and S_h for demodulation. The same carrier – as a TTL clock input – serves as a reference for both (In an IC this is facilitated by the physical proximity of the modulation and demodulation circuits to each other). The modulated signal and its inverted value are presented to the switch combination. They are alternately switched on to the two output lines. The resulting output is the balanced modulated carrier (When $x = 0$, the output of the modulator is also zero, conforming carrier suppression). The switches S_e, S_f, S_g and S_h convert the modulated wave back into the modulating signal form. This is achieved by identical synchronized switching. The waveforms at different points of the modulation and the demodulation units are also shown in Figure 6.12.

6.2.1.12 *Envelope Detector*

The simplest Envelope detector uses a diode, a resistance and a capacitance as shown in Figure 6.13 a. The modulated carrier is given as v_i to the circuit. v_o forms the demodulated output. Typical v_i and v_o waveforms are shown in Figure 6.13 b.

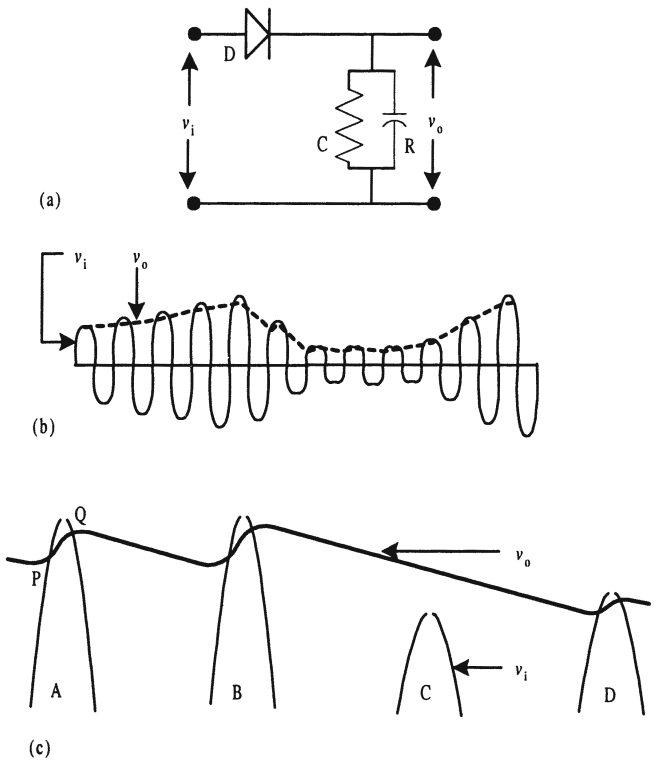


Figure 6.13 Envelope detector and associated waveforms: (a) Detector circuit (b) Input and output waveforms (c) Waveforms in a region where the output rides over the carrier peak

As v_i increases, the diode conducts and the capacitance charges. This continues until the voltage across the capacitance attains the maximum value and the diode current becomes zero. At this instant, the diode becomes reverse biased and stops conduction. Thereafter the capacitance discharges through the parallel resistance and the voltage across it drops steadily. This continues well into the next positive half cycle. At point P (shown in Figure 6.13 c in a magnified form), the capacitance voltage becomes lower than V_i. The diode becomes forward biased, conducts and V_o rises once again. The conduction continues until point Q when the discharge phase starts afresh. If RC is chosen too high, the capacitance discharge may be slow. If the next peak is too low, V_o will ride over and not follow the envelope (as at point C). Too small an RC discharges the capacitance faster causing a conspicuous ripple at $2\omega_c$ in V_o.

The circuit is quite simple – component-wise and function-wise. But the *RC* selection has to be done carefully considering the constraints on its upper and lower limit values.

6.2.2 Frequency Modulation

Consider a sinusoidal carrier of the form

$$x_c(t) = A_c \cos(2\pi f_c t + \phi) \tag{6.24}$$

In amplitude-modulation the amplitude A_c of the carrier was changed by the modulating signal. It is possible to change the phase angle ϕ and do modulation. Two of the common schemes of this type are 'Phase Angle Modulation (PM)' and 'Frequency Modulation (FM)'. If $x_s(t)$ is the modulating signal, we can make ϕ proportional to it.

$$\phi(t) = k_p x_s(t) \tag{6.25}$$

where $k_p x_s(t)$ is the instantaneous phase shift of the carrier. Substitution in Equation 6.22 gives

$$x_c(t) = A_c \cos[2\pi f_c t + k_p x_s(t)] \tag{6.26}$$

As $x_s(t)$ swings between a positive and a negative maximum, the instantaneous phase of $x_c(t)$ changes accordingly. This is 'Phase Modulation' in principle. Alternately we may change frequency proportional to the modulating signal. This is 'Frequency Modulation'.

6.2.2.1 *Principles of Frequency Modulation*

Let $\Psi(t)$ represent the instantaneous phase of the carrier. We have

$$\psi(t) = 2\pi f_c t + \phi t \tag{6.27}$$

The instantaneous frequency – f_i – becomes

$$f_i = \frac{1}{2\pi}\frac{d\psi}{dt} \tag{6.28}$$

$$= f_c + \frac{1}{2\pi}\frac{d\phi}{dt} \tag{6.29}$$

If

$$\frac{1}{2\pi}\frac{d\phi}{dt} = k_p x_s(t) \tag{6.30}$$

with k_f being a constant, the instantaneous frequency change from f_c, is proportional to the modulating signal.

$$\therefore \phi = 2\pi \int_0^t k_f x_s(t)\, dt \tag{6.31}$$

Substitution in Equation 6.24 gives

$$x_c(t) = A_c \cos\left[2\pi f_c t + 2\pi k_f \int_0^t x_s(t)\, dt\right] \tag{6.32}$$

A comparison of Equation 6.26, which gives the phase-modulated output and Equation 6.32, which gives the frequency-modulated output, shows that the carrier, side bands and other characteristics of phase and frequency modulation schemes are similar. Normally, these two are studied and analyzed together. The modulation and demodulation schemes are also similar. Let us take frequency modulation for detailed study. Consider a pure tone test signal

$$x_s(t) = A_s \cos 2\pi f_s t \tag{6.33}$$

The instantaneous frequency – f_i – is

$$f_i = f_c + k_f A_s \cos 2\pi f_s t \tag{6.34}$$

Substituting in Equation 6.31

$$\phi = \frac{k_f A_s}{f_s} \sin 2\pi f_s t \tag{6.35}$$

Substituting in Equation 6.24

$$x_c(t) = A_c \cos\left[2\pi f_c t + \frac{k_f A_s}{f_s} \sin 2\pi f_s t\right] \tag{6.36}$$

The maximum frequency deviation from the mean value = $k_f A_s$.
The test signal and the modulated wave are shown sketched in Figure 6.14. It gives a qualitative feel of the modulation process – the frequency swing between the two limits, and the instantaneous frequency reflecting the corresponding signal level.

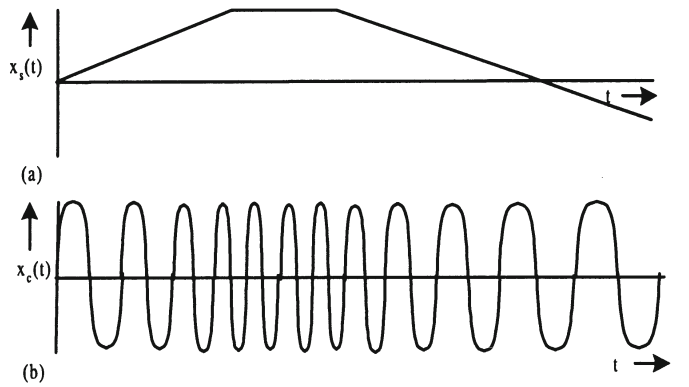


Figure 6.14 Frequency modulation: (a) Waveform of the modulating signal (b) Waveform of the modulated carrier

Here

$$\Delta f = k_f A_s \tag{6.37}$$

is called the 'Frequency Deviation'.

$$\beta = \frac{k_f A_s}{f_s} = \frac{\Delta f}{f_s} \tag{6.38}$$

represents the fractional change in frequency. It is called the modulation index. Using Equations 6.38, Equation 6.36 is rewritten as

$$x_c(t) = A_c \cos\left(2\pi f_c t + \beta \sin 2\pi f_s t\right) \tag{6.39}$$

Fourier series expansion of $x_c(t)$ gives

$$x_c(t) = A_c \,\mathrm{Re}\left[\sum_{n=-\infty}^{+\infty} J_n(\beta) e^{j2\partial(f_c + nf_s)t}\right] \tag{6.39}$$

$$= A_c \sum_{n=-\infty}^{+\infty} \mathrm{Re}\left[J_n(\beta) e^{j2\pi(f_c + nf_s)t}\right] \tag{6.40}$$

where $J_n(\beta)$ is the n^{th} order Bessel function of the first kind.

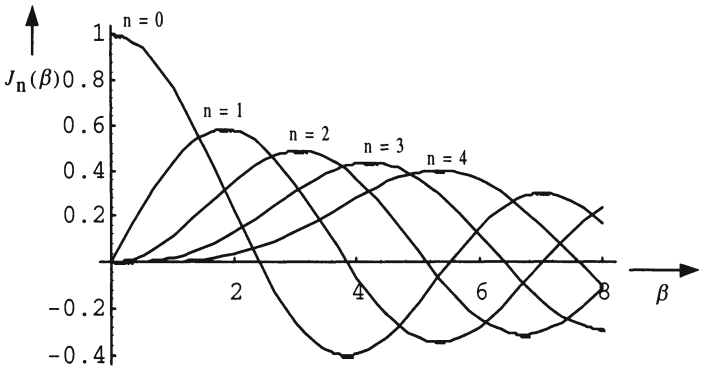


Figure 6.15 Bessel Function of the first kind

Observations :-

⇒ If f_m (the highest frequency of interest in the modulating signal) << f_c, the number of zero crossings per second is a measure of the instantaneous frequency and hence the modulating signal level.

⇒ The amplitude of the carrier is a constant throughout. The total power level in the modulating signal is also a constant.

⇒ The carrier amplitude A_c does not carry any signal information. A variation in it does not contribute to any significant error.

⇒ The modulated signal is composed of a number of frequency components. Their individual magnitudes and relative significance change with β and n.

⇒ J_0, J_1, J_2 *etc.*, are shown plotted against β, in Figure 6.15. In general we have

$$J_n(\beta) = \sum_{m=0}^{\infty} \frac{(-1)^n (\beta/2)^{n+2m}}{m!(n+m)!} \tag{6.41}$$

⇒ J_0 (β) represents the amplitude of the carrier. It is 1 if $\beta = 0$ and reduces as β increases. For small β, Equation 6.41 can be approximated to

$$J_n(\beta) \approx 1-\frac{\beta^2}{2} \tag{6.42}$$

As the modulation index increases, the power in the carrier decrease. We further have

$$\sum_{n=-\infty}^{+\infty} J_n^2 = 1 \tag{6.43}$$

which shows once again that the total power in the modulated signal is constant. It gets redistributed differently amongst the side bands as β increases.

$$J_n(\beta) = (-1)^n J_{-n}(\beta) \tag{6.44}$$

$\Rightarrow$ The side bands are symmetrically distributed on either side of f_c – amplitude-wise and frequency-wise. They are displaced by f_s, $2f_s$, $3f_s$ *etc.*, on either side of f_c. The amplitudes of side bands at $f_c \pm f_s$ are equal; the amplitudes of side bands at $f_c \pm 2f_s$ are equal and so on.

$\Rightarrow$ For small values of β,

$$J_n(\beta) \approx \frac{1}{2^n n!}\beta^n \tag{6.45}$$

Here, only the first set of side bands is significant. As β increases, the second set also becomes significant. In the same manner, others too attain significance as β increases further.

$\Rightarrow$ For $\beta >> 1$,

$$J_n(\beta) \approx \sqrt{\frac{2}{\pi\beta}}\cos\left(\beta-\frac{\pi}{4}-\frac{n\pi}{4}\right) \tag{6.46}$$

i.e., the amplitudes of individual side bands become infinitesimally small and the total power gets redistributed over a large number of sidebands.

6.2.2.2 *Significant Bandwidth of the FM Wave*

In theory, the power in the FM wave is distributed in an infinite number of sidebands. But as we move away from f_c, the amplitude and power levels of the sidebands reduce to insignificant levels. Hence in practice, it is possible to limit the bandwidth of transmission and processing, to definite levels. An estimate of the bandwidth required for these, is in order [Carlson, Haykin, Lathi].

Consider the test signal discussed so far; for any test signal of amplitude and frequency lower than this, the side band amplitudes and their spread on either side, will be lower. Hence one can get an estimate of the bandwidth required, considering a test signal of highest frequency and largest amplitude likely to be encountered.

For small values of β, due to the worst case test signal, the power in the modulated wave is concentrated in the carrier and the first two sidebands at $f_c \pm f_s$. Hence, the significant bandwidth is only $2f_s$. This is also akin to the amplitude modulation case. The same is evident from the spectra for $\beta = 0.5$ shown in Figure 6.16. FM with such low values of β, is referred to as 'Narrow Band FM'. The significant spectral components for a selected set of higher values of β are also shown in Figure 6.16. One can see that as β increases, the significant spectra extend up to Δf on either side. The corresponding active bandwidth is $2\,\Delta f$. In general, one can take the active bandwidth as $2(\Delta f + f_s)$. This is 'Carson's Rule'; it under-

estimates the bandwidth required. Often $2(\Delta f + 2f_s)$ is taken as the bandwidth required, which is a more conservative estimate.

One need not necessarily go by such thumb rules for the final design. From an estimate of signal bandwidth and amplitude levels, FM spectrum can be obtained. From this all spectral components with amplitude > (say) 0.5 % of the unmodulated carrier, may be considered as included. Based on this a precise estimate of the bandwidth required can be made.

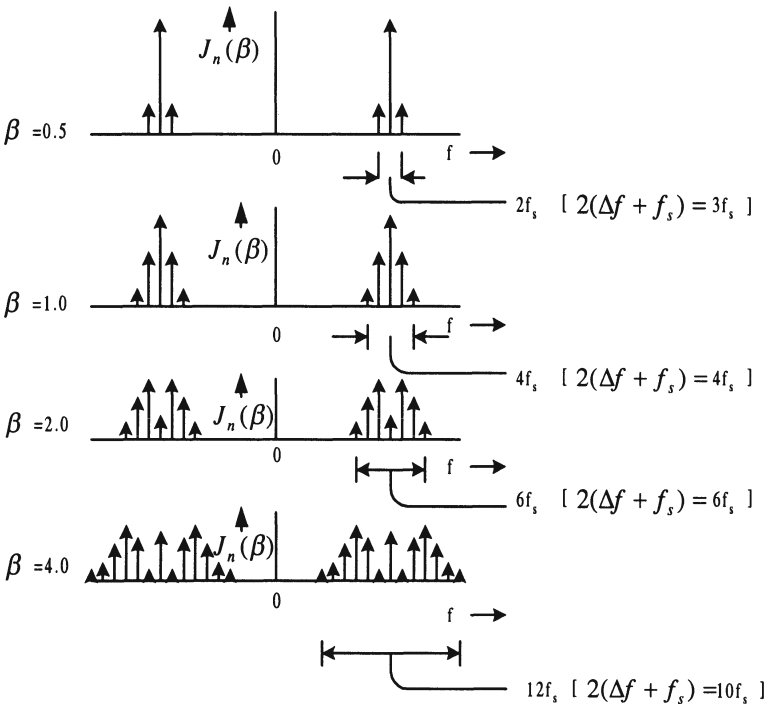


Figure 6.16 Spectral components of an FM wave with a sinusoidal test signal. Four values of the modulation index are considered. Only the significant components and their amplitudes are shown. The spread of significant components and bandwidth according to Carson's rule are also shown.

6.2.2.3 Practical Aspects of Frequency Modulation

Many capacitance and some inductance transducers generate FM output directly. The range of variation of C or L is usually limited to 0.1 to 0.5 %. The frequency deviation is also equally restricted. Once so generated, the modulation level can be enhanced as required, by a frequency multiplication process (discussed below). However, if the modulation level attained is sufficient to ensure overall system accuracy, such enhancement need not be resorted to.

Two methods of generation of FM are in vogue. In the first method, a narrowband FM is generated and processed subsequently to the required level. For $k_p x_s(t) << f_c$, Equation 6.32 can be approximated as

$$x_c(t) = A_c \cos 2\pi f_c t - 2A_c k_f \left[\int_0^t x_s(t)dt \right] \sin 2\pi f_c t \qquad (6.47)$$

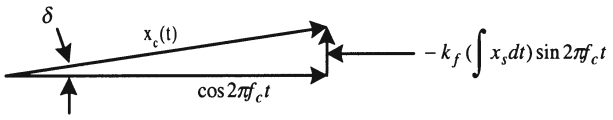


Figure 6.17 Phasor diagram for FM

Formation of $x_c(t)$ from the two sinusoids in quadrature as in Equation 6.47, is shown in Figure 6.17 in phasor diagram form. As long as the frequency deviation is small, FM signal can be generated via AM by adding (or subtracting) the AM signal in quadrature with the carrier. The scheme for this is shown in block diagram form in Figure 6.18. The oscillator generates the sine and cosine waveforms. The signal to be modulated is integrated (with respect to time) and modulated on a carrier – normal AM fashion. Then the two components are added. For the modulation process to be accurate here β has to be very small compared to 1. One advantage of the scheme is the possibility of using crystal oscillator to generate the carrier that ensures good stability of the carrier frequency f_c.

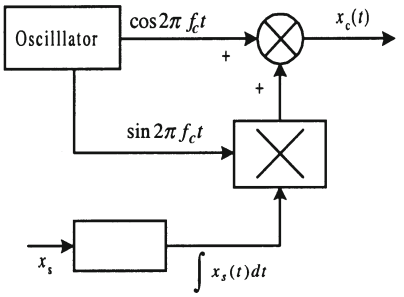


Figure 6.18 FM generation through AM

Consider the signal $x_c^2(t)$. This can be obtained by passing the modulated signal $x_c(t)$ through a non-linear device [See Section 6.2.1.2]. The component at frequency $f_c + k_f x_s(t)$ appears at twice its value *i.e.*, at the frequency $2f_c + 2k_f x_s(t)$. Thus the frequency deviation has doubled. The basic signal remaining the same, the modulation index also doubles. One can use a more severe non-linearity with higher power terms and increase the modulation index further at the same stage. Alternatively, the frequency doubling can be done successively to achieve the same purpose. Once the desired modulation level is attained, the frequency band is shifted to the desired frequency point, by mixing. At every stage necessary narrow band filtering is done to filter out unwanted components. The scheme is shown in block diagram form in Figure 6.19.

The second method of modulation is a direct approach. Modulation is done by directly changing the carrier frequency at the first oscillator stage. This can be by changing a reactive component in the frequency determining side of the oscillator

(similar to the modulation in transducers). Alternately such modulation is done by changing the controlling voltage of a 'Voltage Controlled Oscillator (VCO)'. The modulation index achievable is of a much higher order than with the narrow band FM case. If necessary it can be enhanced and the carrier positioned at any desired frequency using a mixer stage. This scheme is simpler than the previous one. However, the carrier frequency is not stable. Stability has to be brought about by an elaborate feedback scheme.

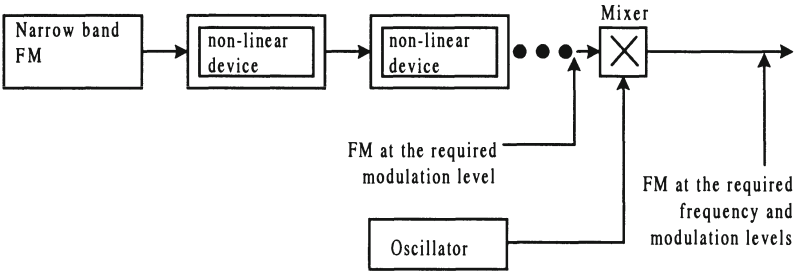


Figure 6.19 Scheme of FM generation through frequency doubling and mixing

Integration of the modulating signal prior to the FM process steadily reduces the weight to the higher frequency components. Thus 100 mV at 10 Hz may appear as it is at the modulator input; but at 1 Hz, it appears as 1 V, while at 100 Hz, it is reduced to 10mV level after the integration. This is inherent in the integration process. Any noise present in the system – taking it as white noise – has a flat spectrum. Hence, at a given noise level, the higher frequency components of the signal proper are more prone to contamination than the lower frequency components. To alleviate this situation, it is normal practice to give a boost to the higher frequency components of the signal prior to the modulation process. This is termed as 'Pre-emphasis'. A first order HPF with a selected corner frequency is used for pre-emphasis. To compensate for this, a 'De-emphasis' is done at the receiver after the demodulation stage. A first order LPF, with the same corner frequency as the HPF earlier, is used for the de-emphasis. The pre-emphasis and the de-emphasis together improve the signal to noise ratio performance of the FM scheme.

6.2.2.4 Circuits for FM Modulation

Generation of FM with L or C type transducers, when they form part of the oscillator tank circuit and FM through the narrowband route are not discussed further here. Direct wideband FM is done today using dedicated standard ICs – this is especially true of instrumentation schemes.

The ICs suitable for FM are more commonly called 'Voltage controlled Oscillators (VCO)'. Broadly, two types of VCOs are in common use: -

⇒ The VCO is an astable multivibrator. The capacitance charging current for either side of the multivibrator, is proportional to the external input voltage. This scheme is less costly, simple in operation and works with lower power supply currents. The output is essentially a square wave. The frequency range is essentially decided by the capacitor in the multivibrator. Some versions have the facility to do current scaling of the multivibrator externally.

⇒ The VCO is essentially built with an integrator, comparator, Schmidt trigger and a switch. A buffer inside the VCO IC charges a timing capacitor over a definite voltage range. The charging current is proportional to the modulating voltage. As soon as a pre-defined threshold voltage level is reached, the charging stops and the capacitor is discharged in a controlled manner. The charging/discharging cycle is continued resulting in a periodic output. The output waveform is not of a square type here. However, this can be achieved by interposing a flip-flop. The scheme is more elaborate and costly, but precise.

Observations: -

⇒ In both the cases, the user can treat the unit as a black box, provided the application related components are chosen conforming to the specifications.

⇒ The VCOs provide a wide linear range – typically 0.01 Hz to 1 MHz. However, the user restricts the range to one or two decades depending on the application.

⇒ Normally the timing capacitor and a scaling resistor are added externally. The lower limit for the capacitor is decided by the stray capacitance levels – *i.e.*, it should be much higher than the strays so that the frequency range is not affected by the strays. 100 pF is typical as the lower limit. This corresponds to the highest frequency range in the region of 1 MHz.

⇒ The upper capacitance limit is used in the lowest frequency range. This may extend down to 0.01 Hz. Offset voltages and error due to drift limit the lowest frequency.

⇒ Upper limits of external scaling resistors are decided by bias and leakage current levels of the IC. These should be $1/100^{th}$ or less than the current levels in the scaling resistors. Lower limits for these resistors are decided by the loading capacity of the switches in series.

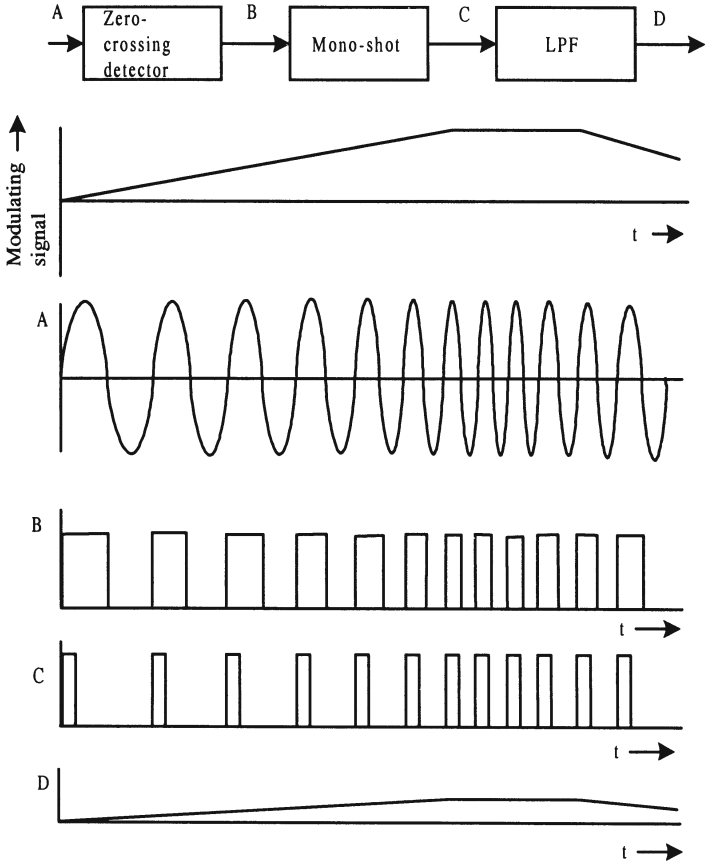
6.2.2.5 Circuits for FM Demodulation

A variety of methods of FM demodulation is possible. Slope detection and its refined version – balanced slope detection – are frequency sensitive linear networks to convert the FM in to an AM and then do envelope detection. Today these are only of academic interest. They facilitate a clearer understanding of the Foster-Seeley Discriminator or the ratio detector. These detectors find wide use in FM radio, TV *etc.*, but are of little relevance in instrumentation schemes. Being out of context they are not being taken up for detailed discussion.

The 'Zero-Crossing Detector' based demodulator finds use in some cases. The scheme is shown in block diagram form in Figure 6.20. The waveforms at different points are also shown. The zero-crossing detector output is zero volts for negative input and +5V when the input is positive. It is a train of pulses; their position and width are decided by the FM signal. Whatever is the input FM amplitude – even if it is varying in nature – the zero-crossing detector output pulse train has the same amplitude. This makes the scheme function independently of any modulation in the amplitude of the carrier.

The zero crossing detector output has a 50 % duty cycle. This forms the input to a monoshot of constant pulse width. The monoshot output is a pulse train – each pulse being of the same height and width. The number of pulses per unit time varies with the signal. One may count the number of pulses for a definite time regularly.

This yields the instantaneous frequency directly (and hence the modulating signal value) in digital form. Alternately it can be passed through an LPF; the LPF output is proportional to the frequency of the FM wave. It has a DC bias corresponding to the FM carrier frequency. Subtraction of the bias from the filter output yields the signal proper. The bias subtraction and low pass filtering can be realized together in one functional block.



Figures 6.20 Block diagram of FM demodulator circuit using zero-crossing detector and associated waveforms

Observations: -

⇒ The propagation delay of digital and logic ICs available today, is of the order of a few ns per stage. With this the overall circuit delay of the scheme can be in the 20-30 ns region. This entails the monoshot pulse width to be 30 μs to limit the indecision in it to 0.1 %. The maximum pulse-repetition rate corresponding to this is 33 kHz. This is the upper frequency limit of the modulated signal, which can be accommodated by the scheme.

⇒ We may take the maximum frequency deviation to be ±5 %. Correspondingly, the monoshot output average has a swing of ±5 % over the

average. Thus, the zero signal frequency of the FM reflects as a bias or a common mode output, which can extend up to twenty times the signal. The bias removal at the output demands an opamp of high CMRR.

⇒ Opamps of 100 dB CMRR are common. Taking a specific illustration, we may have a situation as follows: -

$$\text{Demodulated output with unmodulated carrier} = 1\text{ V} \tag{6.48}$$

$$\text{Rejection ratio with 100 dB CMRR} = 10^5 \tag{6.49}$$

$$\text{Corresponding output error} = 10\ \mu\text{V} \tag{6.50}$$

$$\text{Maximum signal level with 5 \% deviation} = 1 \times 0.05\text{ V} = 50\text{ mV} \tag{6.51}$$

$$\text{Common mode error introduced by the scheme} = \frac{10 \times 100}{50 \times 1000} = 0.02\ \%. \tag{6.52}$$

Equation 6.52 represents the theoretical minimum error attainable. Practical limits will be at least one order higher. The scheme performs well at low frequencies and with maximum frequency deviation possible. The number of building blocks to be used in the scheme, is a deterrent. The advent of good quality PLLs has possibly contributed to the limited use of this scheme of demodulation.

PLLs offer an attractive though indirect method of frequency demodulation [Viterbi]. The potential for the variety of their applications warrants a more detailed treatment.

6.2.2.6 Phase Locked Loops

Figure 6.21 shows the PLL in block diagram form. Three basic building blocks make up the PLL – the analog multiplier, the LPF and the VCO. x_r is the incoming signal; it is multiplied by x_f – the fed-back signal. The product x_e forms the input to the LPF. The LPF output is represented by x_o, which again forms the input to the VCO. The VCO output is x_f whose frequency is proportional to x_o.

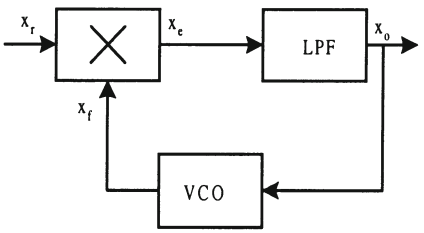


Figure 6.21 PLL in block diagram form

Let

$$x_r(t) = A_r \cos \omega t \tag{6.53}$$

$$x_f(t) = A_f \sin(\omega t + \theta) \tag{6.54}$$

$$x_e(t) = \frac{A_r A_f}{2} \sin\theta + \frac{A_r A_f}{2} \sin(2\omega t + \theta) \tag{6.55}$$

Considering the LPF to be ideal

$$x_o = \frac{A_r A_f}{2} \sin\theta \tag{6.56}$$

Thus the multiplier along with the LPF functions as a phase detector. The output frequency of the VCO changes with x_o. Taking the VCO to have a linear frequency versus voltage characteristic and taking f_0 as the zero signal frequency, we get

$$\text{VCO frequency} = f_0 + \frac{kA_r A_f}{2}\sin\theta \tag{6.57}$$

where k is the constant of proportionality of the VCO. If the frequency of the incoming signal is taken as f_0,

$$\text{Change in VCO frequency} = \frac{kA_r A_f}{2}\sin\theta \tag{6.58}$$

Relating the phase shift θ in Equation 6.54 and the frequency change of Equation 6.58, we have

$$\frac{d\theta}{dt} = \pi k A_r A_f \sin\theta \tag{6.59}$$

Consider steady state operation with input at a constant frequency; the VCO should be working with a steady input. The frequency has to be the same as that of the incoming signal. Any deviation between the two frequencies gets integrated continuously and appears as a continuously varying phase shift between the signals x_r and x_f. Correspondingly, x_o also changes. This in turn causes the VCO output frequency to change. Thus for steady operation, the frequencies of x_r and x_f must be equal. If the frequency of x_r shifts from f_0, a similar and identical frequency shift takes place in x_f too. This comes about by x_0 changing and causing the frequency of the VCO to change correspondingly. Hence, x_0 is proportional to the change in the frequency of x_r from its mean value. It represents the FM demodulated output. Here demodulation is done in an indirect manner through the feedback scheme. Figure 6.22 shows the transfer function model of the PLL. It incorporates the sine non-linearity.

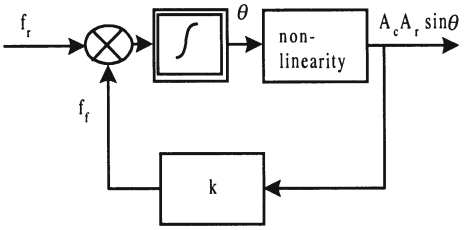


Figure 6.22 PLL – simple mathematical model

For small values of θ, we have

$$\sin\theta \approx \theta \tag{6.60}$$

With this approximation, the system reduces to a linear one. The corresponding loop transfer function P(s) – relating the PLL output to the input frequency – becomes

$$P(s) = \frac{1/k}{s + \left(1/\pi A_r A_f k\right)} \tag{6.61}$$

The simplest PLL with an ideal LPF, functions as a first order closed loop system as can be seen from Figure 6.22.

The cut-off frequency of the system -ω_c - is given by

$$\omega_c = \frac{1}{\pi A_r A_f k} \tag{6.62}$$

Observations: -

⇒ The incoming frequency and the PLL-VCO frequency are exactly equal. The PLL output tracks the input synchronously. This exact frequency matching is due to the type 1 nature of the system.

⇒ x_f and x_r are in exact quadrature at the centre frequency f_0. As the frequency shifts from the centre value, the phase shift too changes from the 90° value.

⇒ Although the PLL loop has been analyzed with the linear approximation of Equation 6.60, the practical operation need not be restricted to such a narrow range.

⇒ As the frequency of the incoming signal deviates from f_0, θ increases continuously. Theoretically θ can increase up to $\pi/2$ in either direction. Correspondingly, the VCO output frequency range is also limited. This represents the maximum theoretical limit of operation on either side.

⇒ In practice, the range is much more restricted. Typically it may extend up to about 50 % of this. Beyond this, the PLL will fall out of synchronism during normal operation. This is the cumulative effect of noise at different points resulting in rapid (though of short duration) shift in θ.

⇒ In general, a large k makes the system respond fast, to changes in input. This widens the frequency range of operation also. But the PLL can be oscillatory or go out of synchronism easily. On the other hand, a small k makes the system slow in response but quite stable. This also limits the frequency range.

⇒ The out of band signals can be rejected more effectively by reducing the loop filter bandwidth. This reduces the capture range and makes the PLL more sluggish.

⇒ Normally, a first or second order filter suffices for the LPF in the PLL. This is due to the wide separation between the signal band and the carrier band. If necessary a higher order LPF may be used. This increases the order of the system loop and affects the margin of stability. Always the lowest order filter, which satisfies the minimum performance specifications, is to be used. Amplitude of the incoming signal changes the output scale factor. To this extent the PLL is sensitive to changes in the modulated carrier amplitude.

The qualitative analysis carried out here, assumes that the PLL is already in synchronism. Based on this, the frequency range of operation has been obtained. However at starting or after any abrupt change in operation, the PLL has to get synchronized before operating in this mode. The input frequency range over which it can get synchronized, is narrower than the frequency range over which the PLL can do frequency tracking [Viterbi].

Practical Aspects of PLL

PLLs are available in IC form from different manufacturers. The phase detector, the LPF and the VCO are built into the IC. A set of resistances and capacitances is to be connected to the LPF to adjust its cut-off frequency. An external capacitor at the VCO selects the active range of frequency of operation and hence the VCO

centre frequency. With such a level of circuit integration, design efforts required are minimal and circuit implementation becomes simple.

The functional blocks and waveforms of IC implementation of the PLL are somewhat different from the hypothetical situation above. Figure 6.23 shows the IC versions in block diagram form. An EXOR gate functions as the phase discriminator. To suit its operation, a limiter or 'Zero Crossing Detector' is interposed between the incoming signal and the gate input. Thus, the signal x_r seen by the EXOR gate is a square wave of the two logic levels. Similarly, the VCO also functions giving a square wave output.

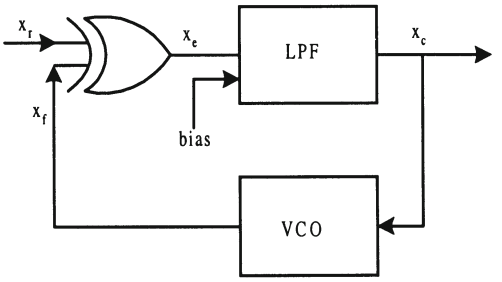


Figure 6.23 IC version of a PLL in block diagram form

Waveforms of x_r, x_f and the average value of the gate output at selected points are shown in the Figure 6.24. The EXOR gate based phase detector is linear through out its active operating range. This characteristic is more acceptable than the sine non-linearity of the multiplier type phase detector. Here the PLL is more stable and easy of analysis.

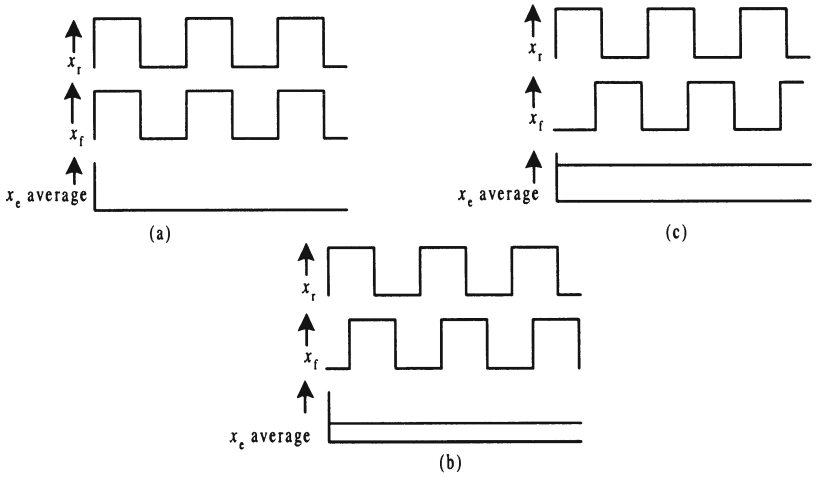


Figure 6.24 Waveforms at different points of the PLL in Figure 6.23 for three different cases: (a) Input at the lowest frequency (b) Input at mid-frequency (c) Input at the highest frequency

Observations: -

⇒ The scheme is much simpler than that of Figure 6.21. The simplicity is mainly due to the use of exclusive-or gate in place of the multiplier.

⇒ The voltage levels of the PLL input x_r and feedback signal x_f are fixed. The same is true of the EX-OR output. This makes the loop sensitivity constant and independent of the input amplitude. Any amplitude modulation present in the incoming signal does not affect the sensitivity or performance of the PLL.

⇒ Some PLL ICs have the provision to divide the incoming signal frequency as well as the feedback signal frequency by definite integers. This allows frequency scaling and makes the PLL more versatile. However, its application in FM demodulation is limited.

PLL applications

The PLL has been discussed above with specific reference to FM demodulation. Availability of low cost monolithic PLL has opened up many new areas of use, which were hitherto considered costly and impracticable. A few such typical applications are considered here.

DSB-SC Demodulation

The demodulation here, requires a carrier to be present [See Section.6.2.1.3]. The modulated signal is multiplied by the carrier and the output passed through an LPF to remove unwanted frequency components. So far, the practice has been to send the carrier through a separate channel or generate it from a master carrier. But a PLL can be employed directly with a received signal to regenerate the carrier. A DSB-SC signal has the form of Equation 6.11. It is a waveform of frequency f_c whose amplitude changes continuously. With this as the input, the PLL directly locks on to the carrier. Its output is at the carrier frequency. The same can be used to multiply the received signal for AM demodulation. As mentioned earlier, the PLL IC is insensitive to amplitude changes in the received signal.

Narrow Band Filter

The PLL can be considered as a narrowband filter – its centre frequency being f_c. It effectively rejects all frequency components outside its capture range. The centre frequency of the VCO can be easily changed or shifted by changing the VCO bias.

Frequency Synthesizer

The scheme of Figure 6.25 is an enhanced version of the PLL. The incoming signal is at a frequency f_r. Through a suitable counter its frequency is divided by an integer n. In the same manner the VCO output frequency f_v is divided by another integer m. The divider output is mixed with another fixed frequency wave at frequency f_d. The mixer output is at frequency $[(f_r/m) - f_d]$ which is synchronized to the incoming PLL.We have

$$\frac{f_r}{n} = \frac{f_v}{m} - f_d \tag{6.63}$$

$$\therefore f_v = \frac{m}{n}(f_r + nf_d) \tag{6.64}$$

By a suitable choice of n and m, one can get a range of frequencies of output. n and m can be made programmable. One can have a stable source for frequency f_r and by selecting f_d , m and n, output at any required frequency can be synthesized. This is the principle of the 'Frequency Synthesizer'.

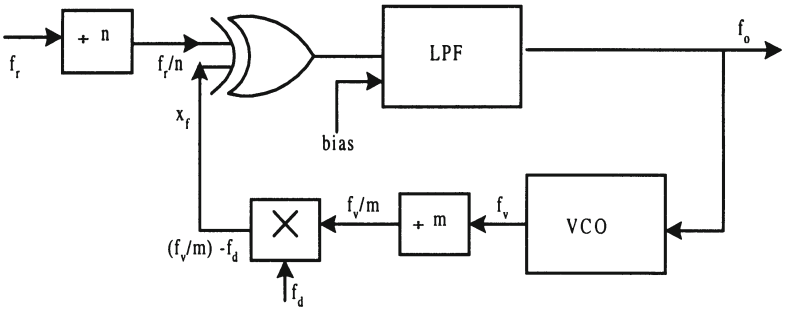


Figure 6.25 Frequency synthesizer in block diagram form

6.3 Non-linear Amplifiers

Use of non-linear resistors like diodes, Zener diodes *etc.*, with opamp based amplifiers gives rise to a variety of non-linear characteristics. One can also realize multi-valued characteristics. All of them use the non-linear element in a feedback scheme. For a given circuit configuration the characteristic can be obtained using the following two aspects of opamp working: -

⇒ The potentials of the inverting and the non-inverting input points are equal.

⇒ The currents drawn by the inverting and non-inverting input leads are zero.

Three types of circuit schemes are of interest to instrumentation schemes; these are discussed here.

6.3.1 Piece-wise Linear Amplifier

Consider the opamp circuit of Figure 6.26 (a). The input-output characteristic is shown sketched in Figure 6.26 (b). Under normal working conditions the potentials of the inverting and the non-inverting input points are zero. As long as the output x_o, is less than V_z, the Zener current is zero and the Zener behaves as an infinite impedance. The circuit is an inverting amplifier of gain $-R_2/R_1$. As x_0 exceeds v_z, the Zener conducts. For all higher values of x_o, the Zener offers zero incremental resistance. The circuit behaves as an inverting amplifier of gain equalling $(R_2 \| R_3)/R_1$. Figure 6.27 (a) shows a modified version, which may be of more likely use. It uses two back-to-back connected Zeners in place of only one in the Figure 6.26 (a). Its input-output characteristic, shown in Figure 6.27 (b), is symmetrical about the origin.

Observations: -

⇒ For stable operation and limiting the noise level, it is customary to put a capacitor of low value across R_2.

⇒ Zener tolerances are normally ± 5 %. Correspondingly, the tolerance of knee points Q and R in the characteristic of Figure 6.27 (b) can change from unit to unit. If the characteristic is to be realized more precisely, the Zeners have to be selected to closer tolerances.

⇒ R_3 times the leakage current of the Zener – when it is in the off state – should be negligible compared to x_i R_2/R_1; *i.e.*, the Zener leakage should be small compared to the current through R_2.

⇒ If R_3 is zero, the slope of the characteristic in the regions PQ and RS is zero. We get a 'Saturating Amplifier'.

⇒ If R_2 is removed ($R_2 = \infty$), the initial slope over region QOR is infinite.

⇒ Amplifiers of this type find application in situations where lower levels of the signal require more amplification compared to the higher levels. V_z may characterize a desired 100 % level. Beyond that, only a trend or an order of signal level, need be known. Typically, acoustic signals are of this category.

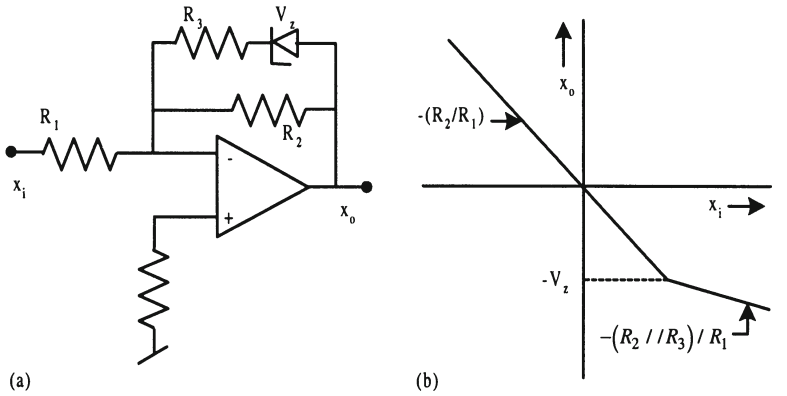


Figure 6.26 A simple piece-wise linear amplifier with two linear segments

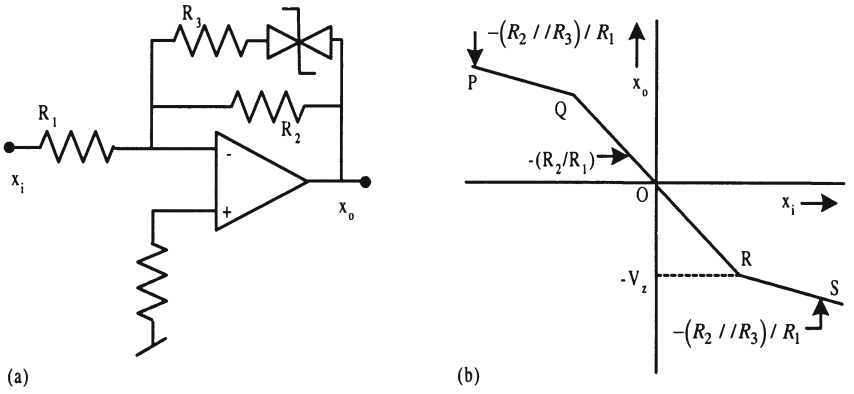


Figure 6.27 A piece-wise linear amplifier with symmetrical characteristic: (a) Circuit (b) Characteristic

The circuit of Figure 6.28 (a) provides a low amplification for low signal levels. The corresponding input-output characteristic is shown in Figure 6.28 (b). As the signal level exceeds a threshold, the amplification increases. The threshold is decided by V_z. Note that the gain changeover points Q and R in the characteristic of Figure 6.28 (b) are decided by input exceeding the V_z value.

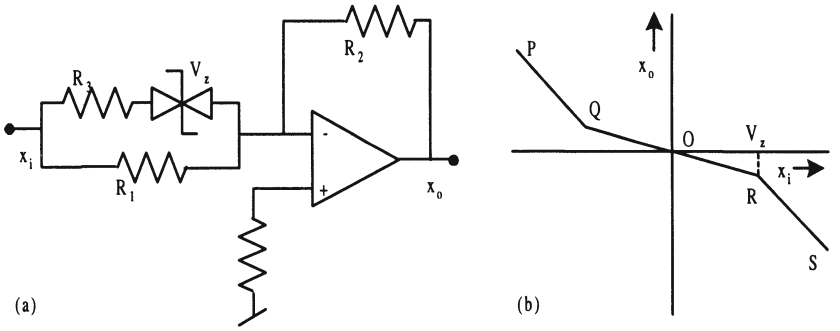


Figure 6.28 A piece-wise linear amplifier with higher gain for larger signal levels: (a) Circuit (b) Characteristic

Both the above circuits can be combined as in Figure 6.29 (a) to give the characteristic of Figure 6.29 (b). This four-segmented characteristic provides high sensitivity amplification over a specific input range (ST and RQ). This type of amplifier is useful when the output of a transducer over a specified range, is of more interest. Outside the range one may be interested only in knowing that the transducer is active or the variable is live or present.

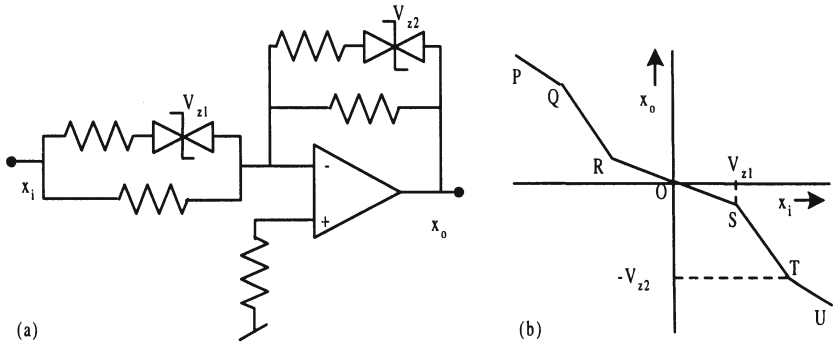


Figure 6.29 A piece-wise linear amplifier with five segments: (a) Circuit (b) Characteristic

6.3.2 Precision Rectifier

Some instrumentation schemes require precision rectification of signals. The widespread use of silicon diodes (almost to the exclusion of others), cause errors due to their high forward voltage drop (about 0.7V). This becomes all the more conspicuous at low signal levels. The circuit of Figure 6.30 (a) uses two identical diodes in the same package (or in close proximity) in an inverting amplifier configuration. It functions as an ideal diode – in the sense that the output is linearly related to the input in one direction but identically zero for input in the opposite direction. When x_i is positive, diode D_1 is forward biased. Throughout the positive swing of x_i, point A is at virtual ground. This voltage is available at output x_0 through R_2. When x_i is negative, D_1 is reverse-biased and D_2 is forward-biased. The opamp functions as an inverting amplifier with the full current drawn by x_i flowing through R_2.

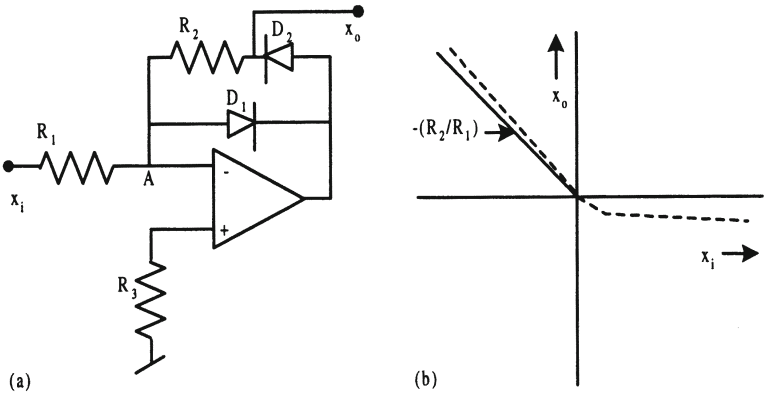


Figure 6.30 Precision half-wave rectifier; (a) Circuit (b) Characteristic

Under these conditions,

$$\therefore x_o = -\frac{R_2}{R_1} x_i \tag{6.65}$$

Combining both the characteristics, we get the characteristic of Figure 6.30 (b).

There are some practical difficulties associated with the direct use of the precision rectifier. When $x_i > 0$, point A is at ground potential. If the output point C is loaded under these conditions, we may get an error depending on the load. Such errors are not caused for negative values of x_i. they can be avoided by using an opamp based buffer at the output of the precision rectifier and connecting the load to the buffer.

A full-wave precision rectifier can be formed using two opamps as in Figure 6.31 (a). The corresponding input-output characteristic is shown in Figure 6.31 (b). The first serves the function of a precision rectifier as above. The second opamp serves as an inverting summer.

For positive v_i, v_E is zero.

$$\therefore v_o = -\frac{R_F}{R} v_E \tag{6.66}$$

For negative v_i,

$$v_E = -v_i \tag{6.67}$$

$$\therefore v_o = -\frac{R_F}{R} v_i - 2v_E \frac{R_F}{R} \tag{6.68}$$

Substituting for v_E from Equation 6.67,

$$v_o = \frac{R_F}{R} v_i \tag{6.69}$$

Combining Equation 6.66 and Equation 6.69

$$v_o = -\frac{R_F}{R} |v_i| \tag{6.70}$$

The 'Full Wave' precision rectifier is actually an absolute value operator. The output is proportional to the absolute value of the input irrespective of its waveform.

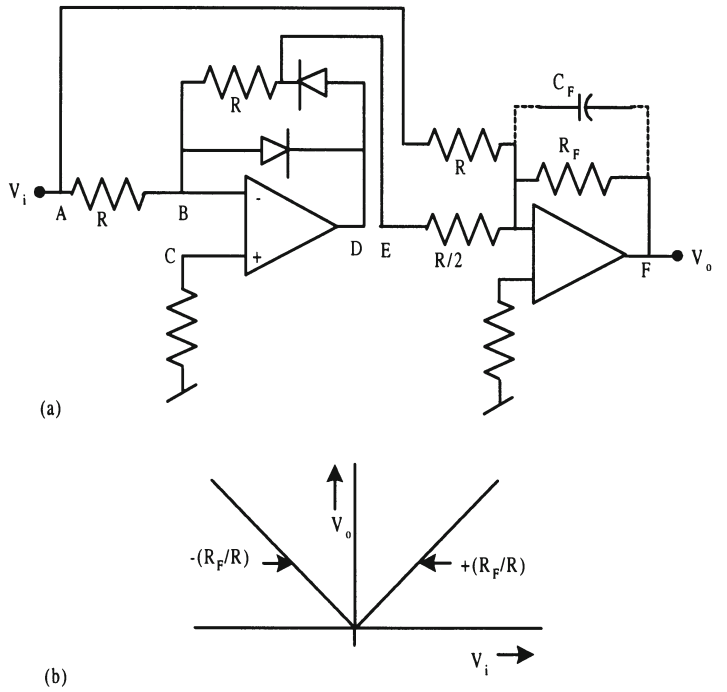


Figure 6.31 Precision full-wave rectifier; (a) Circuit (b) Characteristic

Connecting the capacitor C_f across R_f, filters the harmonics in V_i and makes V_o proportional to the rectified average of $V_{i.}$. This function is useful in many cases. If necessary, one can make a filter configuration of a higher order and get smoother output.

6.3.3 Logarithmic Amplifier

When a BJT is working in the active region, we have [Gray & Meyer]

$$V_{BE} = \frac{kT}{q} \ln \frac{I_C}{I_S} \tag{6.71}$$

where

⇒ V_{BE} is the base-emitter voltage of the transistor
⇒ I_c is the collector current
⇒ I_s is the reverse saturation current
⇒ k is the Boltzmann's constant (= 1.381 $\times 10^{-23}$ J/K)
⇒ T is the absolute temperature of the junction in K and
⇒ q is the charge on the electron (1.602 $\times$ 10^{-19} C).

We get a voltage proportional to the logarithm of the collector current. By a judicious connection of the transistor in a feedback scheme using an opamp, we can get a signal proportional to the logarithm of the input. Figure 6.32 shows one scheme in use to get the ratio of logarithms of two currents I_1 and I_2.

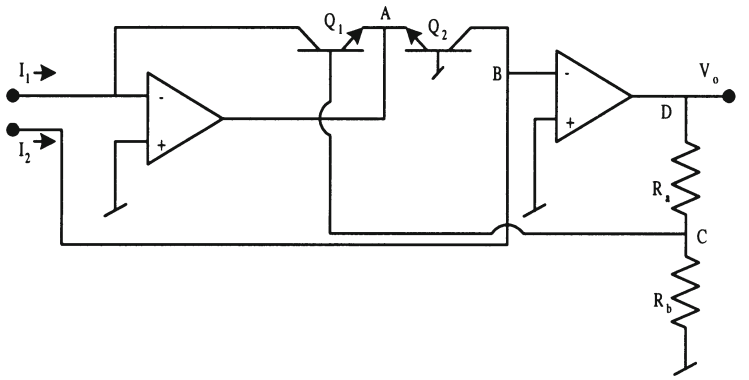


Figure 6.32 Basic circuit to get the logarithm of two currents

Being in the same IC, Both Q_1 and Q_2 are identical; their characteristics are also identical. The Base of Q_2 is at ground potential. Due to its collector current I_2, its emitter potential – the potential of point A – is

$$v_A = \frac{kT}{q}\ln\frac{I_2}{I_S} \tag{6.72}$$

where I_s is the saturation current of Q_2. This is in line with Equation 6.71 above. In the same manner, V_{BE} of Q_1 is proportional to I_1. The two V_{BE}s being subtractive in nature,

$$v_C = v_A - v_{BE} \text{ of } Q_1 \tag{6.73}$$

Substituting for v_A from Equation 6.72 and using the value of v_B obtained in a similar manner

$$v_C = \frac{kT}{q}\left(\ln\frac{I_2}{I_s} - \ln\frac{I_1}{I_s}\right) \tag{6.74}$$

$$= \frac{kT}{q}\ln\frac{I_2}{I_1} \tag{6.75}$$

since the two saturation currents are equal. Using Equation 6.75 we get

$$v_o = \frac{R_a + R_b}{R_b}\frac{kT}{q}\ln\frac{I_2}{I_1} \tag{6.76}$$

(kT/q) is 26 mV at 27 °C. Normally R_b is selected to be sensitive to temperature, with the same temperature coefficient as (kT/q). That makes V_o independent of temperature.

Observations: -

⇒ One form of the log-amp is discussed above. Others are minor variants of this.

⇒ Normal log-amp ICs function over 4 to 6 decades. The corresponding current ranges from 1nA to 1 mA.

⇒ Normally one can operate the log-amp over the full 6-decade range or over a more limited range by suitable gain selection resistances. Limiting the range in this manner improves accuracy.

⇒ The IC manufacturers recommend special capacitors to be connected across the feedback paths (output to the inverting input) of the opamps. These ensure stable operation. The capacitance values range from 5nF at the lowest current range, to 100 pF at the highest current range. The feed back capacitance also extends the active bandwidth.

⇒ At the lowest current range, the bandwidth may extend up to only 100 Hz. The noise level can be comparatively high. Leakage currents too have to be screened off by suitable component layout and provision of guard rings.

⇒ The presence of two deciding currents I_1 and I_2 and their wide range, makes a clear error definition / specification difficult. The log conformity of the circuit is most important. It is best when I_1 and I_2 are in the 1mA range. When used over the full 6 decades, the log conformity error can be 0.5 %. It can improve to 0.1 % when operation is restricted to 3 decades.

⇒ When the log of one current is of interest, the other can be a reference generated through a pre-set current source.

⇒ Log amplifiers have FET input stages with bias currents in the pA range. If good accuracy is desired in the nA range, separate bias current nulling is to be done externally. IC manufacturers give specific application information, in this regard. Similar information is available to null offset voltage also.

⇒ Normally, logamps function best with current inputs. They can be adapted for voltage inputs using suitable series resistances. This limits the dynamic range to 2 to 4 decades.

Conductivity of liquids and gases, leakage currents *etc.*, change over several decades. (Very low gas pressure is measured on-line indirectly by measuring the leakage through specific geometry). Absorbance measurements and optical density measurements also call for the measurement of current over a large number of decades. Log-amps are applicable in all these cases.

7 Noise and System Performance

7.1 Introduction

The level of performance achievable by an instrumentation scheme is limited by various factors. Noise is a primary factor. All round improvement in technology results in better levels of precision and repeatability of components used. To achieve compatible levels of system performance, more attention need to be paid to noise, its effects and ways and means of reducing them. This forms the subject matter of this chapter. In any instrumentation scheme, any voltage or current that contaminates the main signals of interest, can be termed noise. The origin of noise can be due to factors external to the instrumentation scheme as well as those internal to it. The external factors – barring lightning, background radiation *etc.*, – are all of human origin. They are mostly periodic in nature. Their effects can be totally eliminated or substantially reduced by care in design and engineering. Unfortunately, the case with internal noise is different. Firstly, it is random in nature; only its distribution characteristics can be predicted and analysed. Secondly, it can neither be eliminated nor reduced substantially. Only its effects can be reduced by design.

7.2 External Noise

Depending on the type and source of external noise, its power is concentrated in different frequency ranges. Signal contamination can take place in different ways. It can be by direct conduction, by magnetic induction, electric induction or a combination of these [Fish, Ott].

Dirt and imperfections in PCBs can contribute to noise at very low frequencies – up to 1 Hz. Leakage currents, their variation with ambient temperature, or change in humidity *etc.*, can cause such noise. Proper cleaning of PCBs, good soldering practice and coating with humidity sealant, can essentially eliminate these.

Mechanical vibrations and shock when the system is in operation, can cause noise up to a few hundred Hz. Loose connections, terminations *etc.*, cause change in circuit resistance leading to noise. Voltages may be induced by stray fields in leads carrying feeble signals. This can happen in panels, where the signal and power lines run close by.

Susceptibility of instrumentation schemes to power supply frequencies and their first few harmonics is very high. Noise at power frequencies, may be electrically or magnetically induced. Electromagnetic field at the power frequencies is present everywhere in the environment – it is strong enough to cause noisy pick-up in normal circuitry. Even harmonics of power frequencies – mainly second – are produced by rectifiers. They can cause conducted noise, if not properly filtered.

T. R. Padmanabhan, *Industrial Instrumentation*
© Springer-Verlag London Limited 2000

Often the noise is propagated due to poor PSRR [See Section 3.3.10] at low signal level stages. Effective filtering of ripples and selection of opamps with high PSRR at low signal-level stages, is the only remedy here. Saturation in power supply transformers may manifest as noise in the form of odd harmonics of power supply frequency. Here the noise may be conducted through power supplies or magnetically coupled. Effective power supply filtering and use of opamps with good PSRR, minimize conducted noise.

In the 100 Hz to MHz frequency range, the noise may be from a variety of sources: -

⇒ Turning on-off contactors cause disturbances. Conducted noise due to these may be limited to a few kHz only. But radiated and magnetically coupled noise can extend up to much higher frequencies. These are predominant in factory shop floors with different energy conversion devices connected to power mains.

⇒ Modulators, demodulators, choppers, samplers *etc.*, are part of many instrumentation schemes. They generate noise at multiples of carrier frequencies and their side bands. Insufficient filtering of these components or lack of care in their design or circuit layout, can cause noise in conducted or coupled form, in neighboring circuit sections.

⇒ Switched mode power supplies are in wide use in instrumentation schemes and related systems. The ripple at switching frequencies can cause conducted noise. This is especially true of opamps. The opamp selection may be based on an apparently high PSRR. The PSRR may be high enough only at low frequencies but drop down rapidly at hundreds of kHz – the frequencies of working of SMPS. If the power supplies are not effectively screened off, radiation from them, may couple noise into signal circuitry.

⇒ With the advent of IGBTs and POWER MOSFETs, power electronics equipment are in widespread use. High frequency switching at high current levels in these equipment, cause noise to be generated well into the MHz region. Conducted noise can extend up to the kHz frequency range and radiated noise up to the MHz range.

⇒ Radiation by way of broadcasting from various communication systems, extends well into the hundreds of MHz range. By antenna action, circuits can have voltages induced in them. These appear as noise especially when coupled to stages handling weak signals.

7.2.1 Elimination / Minimization of Conducted Noise

Conducted noise can be of three type; these are considered through specific illustrations: -

1. Noise Through Power Supply

A simplified situation is shown in Figure 7.1. C_1 and C_2 are two circuit blocks. Their load currents share a common path with impedances Z_1 and Z_2. Depending on the situation, a variety of measures is adopted to minimize noise coupling: -

⇒ Coupling at low frequencies can be kept in check by increasing the conductor cross-sectional area. Amplifiers with high PSRR are also effective.

⇒ For intermediate frequencies, decoupling capacitors are provided close to the circuit blocks. These absorb noise pulses from supply side as well as the load side.

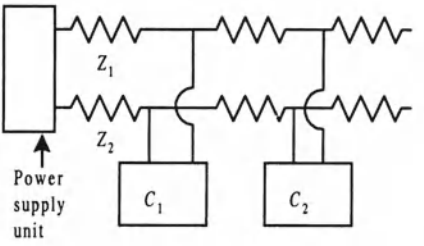


Figure 7.1 Illustration of conducted interference through power supply

⇒ Noise at the highest frequencies encountered in instrumentation schemes, is reduced by keeping the power supply leads as close to each other as possible. Whenever feasible, separate power supply lines are drawn to each load separately. Further for circuits handling weak signals, RC decoupling of power supply lines is provided.

2. Common Mode Noise

Measurement of currents in high voltage lines, is a typical example wherein the common mode noise is conspicuous. Isolation amplifiers are used here to screen off the high level of common mode voltage. Sensor leads running through long lengths can have common mode voltages coupled to them from a variety of sources. The level of common mode signal is low and its bandwidth is also low; instrumentation amplifiers are used here to keep the effect of common mode signals well within check.

3. Common Signal Lines

Figure 7.2 shows a simplified situation. Two circuit blocks – C_1 and C_2 – share a common signal path. Current measurement in power electronics circuits gives rise to such situations. C_1 can be a circuit carrying a few hundred amps of current. The current is to be measured by circuit C_2. Part of the circuit may have to be necessarily common to facilitate measurement. The rest may be unavoidable and cause coupling of unwanted noise. Situations like this, are to be handled on a case by case basis by careful analysis.

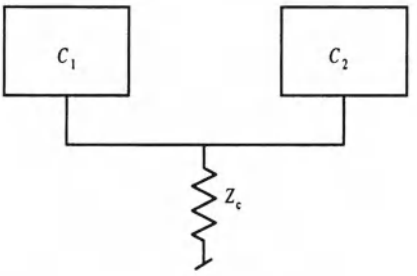


Figure 7.2 Illustration of interference through common circuit path

7.2.2 Elimination / Minimization of Capacitively Coupled Noise

Capacitive coupling can occur due to a variety of reasons. Presence of high voltage lines close to the low voltage signal lines, long signal cables, PCBs with closely lying parallel tracks *etc.*, are examples. Actual physical situations are too complex to be tractable. However, through the analysis of simplified models, one can get a good idea of real situations and leads to remedial measures [Ott]. The assumptions underlying our study are: -

⇒ The physical dimensions of devices and distances we deal with, are small compared to the wavelengths of frequencies of interest. Our assumptions are valid up to about 30 MHz of frequency (The wavelength of electromagnetic waves at 30 MHz, is 10m). Most instrumentation schemes deal with signals of lower frequencies.

⇒ By virtue of the above, effects of electric and magnetic fields can be considered separately. Lumped parameter circuit analysis is valid.

⇒ The target of interference – receptor – does not affect or load the source.

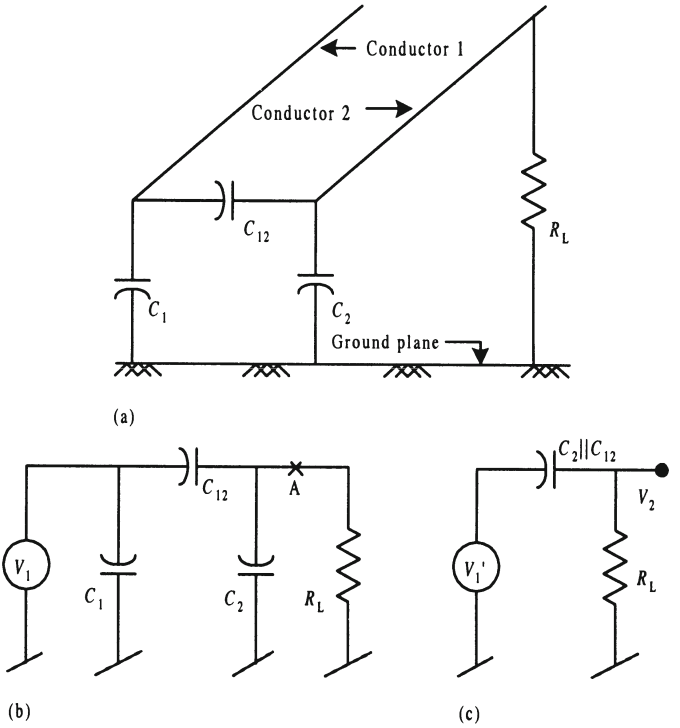


Figure 7.3 Capacitive interference between two conductors

Consider the situation of Figure 7.3 (a). Two conductors 1 and 2 are close to each other. An equivalent ground plane is also shown. The equivalent capacitances to ground are C_1 and C_2. The capacitance between the conductors is C_{12}. The receptor line-conductor 2 has a load R_L connected between itself and the ground. The

conductor C_1 is at a potential V_1 to ground. The equivalent circuit is shown in Figure 7.3 (b). The capacitance C_1 being directly across V_1, does not affect the voltage v_o across the load and hence can be ignored. Replacing V_1 by its Thevenin equivalent looking in at point A, we get

$$V_2 = \frac{C_{12}}{C_{12}+C_2}\frac{jR_L C\omega}{1+jR_L C\omega}V_1 \tag{7.1}$$

where

$$C = C_2 + C_{12} \tag{7.2}$$

and ω is the frequency of V_1. V_2/V_1 is shown plotted against ω in Figure 7.4.

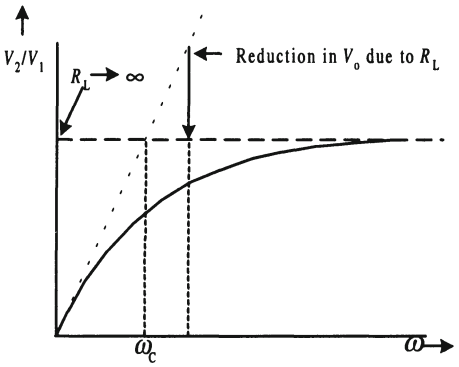


Figure 7.4 Nature of variation of V_o with frequency and R_L

From Equation 7.1, we see that V_o can be reduced by adopting one or more of the following measures: -

⇒ Reduce C_{12}. This is done by increasing the physical separation between conductors 1 and 2. By way of illustration, consider the two conductors to be cylindrical. The capacitance between them is [See Section 10.3.2]

$$C = \frac{\pi\varepsilon L}{\ln\left[\left(D+\sqrt{D^2-4d^2}\right)/2d\right]} \text{ F} \tag{7.3}$$

If $D >> d$, Equation 7.3 can be approximated to

$$C \approx \frac{\pi\varepsilon L}{\ln(D/d)} \text{ F m}^{-1} \tag{7.4}$$

Where ε is the permittivity of the medium.

Here d is the diameter of both the conductors, D the distance between them and L the length of the conductors – all units being in metres. For $D/d > 6$, relative reduction in capacitance is not appreciable.

⇒ Increase C_2. The capacitance to ground, of a cylindrical conductor of diameter d m and length L m, lying parallel to ground at a height of $(D/2)$ m, is

$$C = \frac{2\pi\varepsilon L}{\ln\left[\left(D+\sqrt{D^2-4d^2}\right)/2d\right]} \text{ F} \tag{7.5}$$

If D >> d, Equation 7.5 can be approximated to

$$C \approx \frac{2\pi\varepsilon L}{\ln(D/d)} \text{ F m}^{-1} \tag{7.6}$$

Equations 7.5 and 7.6 show that C_2 can be increased by reducing D *i.e.*, keeping the ground plane close to conductor 2.

⇒ Reduce R_L. This becomes a conspicuous requirement at higher frequencies. As the noise frequency increases, v_o also increases and attains the limiting value of $V_1 C_{12} / (C_2 + C_{12})$. At $\omega = \omega_c$, it is $0.707 v_i$. The presence of load resistance R_L, reduces v_o substantially at higher frequencies. Normally this limit is well beyond the frequencies of interest in instrumentation schemes.

By way of an example, consider a PCB with 3 tracks A, B and G as in Figure 7.5, G being the common ground line for both. Let all the tracks be 0.5mm wide, 25 μ m thick and 100mm long. As a simplifying assumption, we replace them by equivalent cylindrical conductors of same cross-sectional area.



Figure 7.5 PCB track configuration considered in the example in Section 7.2.2

The equivalent conductor diameter is

$$d = \sqrt{\frac{0.5\times10^{-3}\times25\times10^{-6}\times4}{\pi}}$$

$$= 0.126 \text{ mm}$$

Substituting in Equation 7.3, we get

$$C_{AB} = 0.84 \text{ pF.}$$

$$C_{BG} = 1.34 \text{ pF.}$$

Let track A carry a signal at 1 MHz with 1 *V* rms. across it.
Using Equation 7.1, v_o can be evaluated. We get

For $R_L = \infty$

v_o = 285m V

For R_L = 1 MΩ

f_c = 73 kHz

v_o = 284mV

Under these conditions, V_o remains practically unchanged.
If R is reduced to 100 Ω, we get

v_o = 3.9μV

Alternately B and G can be brought closer together and v_o reduced. With this, R_L can be kept at correspondingly higher levels. However, any increase in C_{BG} increases the capacitive loading on the signal line B.

Provision of a ground plane close to the signal lines is possible with PCBs. Especially with multi-layer PCBs, one layer is kept as the ground plane. This can reduce the capacitive coupling of noise especially at lower frequencies. When the signal line is an interconnection, this is not feasible. The best option here is to use a

screened wire to carry the signal and ground the screen as shown in Figure 7.6. C_{12} becomes C_{1G}. Since the screen encloses the conductor fully and is at ground potential, the lead wire is also at ground potential and there is no coupled noise voltage. Provision of the closed screen around the conductor increases C_2 substantially and increases signal loading correspondingly.

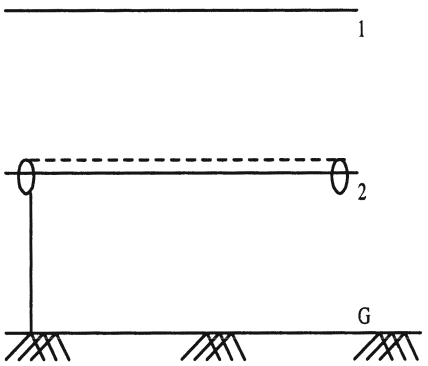


Figure 7.6 Screening of sensitive signal lines

Screening over the entire length of the signal lead is not always possible. In that case, coupling over the unscreened portion remains. As an alternative both the signal-leads can be connected, separately without using the ground return. If both are identically positioned with respect to the source of noise, identical noise voltages are coupled into both. This appears as a common mode noise along with the signal. It can be filtered out with the help of high CMRR opamp at the input stage. Such exact balancing is possible only with respect to one or two definite and known noise sources. In other cases, the balancing will be incomplete.

7.2.3 Elimination / Minimization of Inductively Coupled Noise

Consider two conductors in the vicinity of each other. When one of them carries a current, the flux due to it links with the second. As the current in the former changes, the flux linking the latter also changes and induces an emf in it, which appears as a mutually coupled noise. To get a quantitative idea of this, consider a closed conductor loop kept in a magnetic field. The field flux lines and the loop are as shown in Figure 7.7. The loop is inclined at an angle to the field. For simplicity, the loop is taken to be situated entirely in one plane. The magnetic flux linking the loop is

$$\phi = \int B\cos\theta \, dA \tag{7.7}$$

Here B is the flux density at any location, dA is an infinitesimally small area within which B is constant and θ is the angle between the plane of the loop and magnetic field direction. The voltage induced in the loop due to the field, is $-(d\phi/dt)$. Two conductors carrying a signal affected by an interfering field, is similar to this. The circuit loop of the conductors is represented by the loop of Figure 7.7.

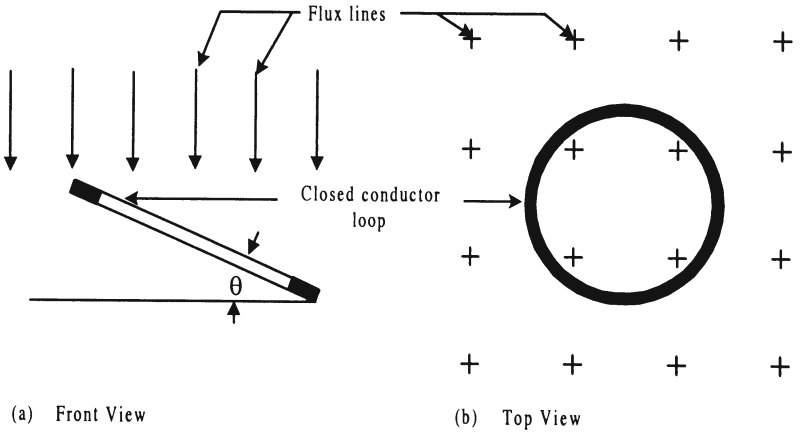


Figure 7.7 A closed conductor path in a magnetic field

Observations: -

The magnetically coupled noise can be minimized by the following measures: -

⇒ Keeping the loop area minimum. The two conductors forming the signal path can be kept close to each other.

⇒ Orienting the signal conductor plane so that cos θ = 0 – *i.e.*, the plane of conductors is parallel to the flux lines. This is not always possible.

⇒ Twisting the two conductors; this reverses the flux linkage and hence the coupled noise at regular intervals. The coupled noise in alternate sections, neutralize each other. The twist pitch has to be low compared to the longest wavelength of interest in the magnetic field.

As the interfering field frequency increases, the coupled noise voltage increases proportionately and its reduction calls for a lot of care in circuit layout and design.

It may not be always possible to keep both the signal conductors close to each other. Shielding of the conductors is effective to a certain extent here. Consider a signal conductor inside an ideal shield as shown in Figure 7.8 (a). Let the shield carry a current I uniformly distributed in it. It produces lines of flux as shown. The magnetic flux density outside the shield is $(\mu_0 I/2\pi r)$T. Here r is the distance of the point of interest from the centre of the shield. Due to the uniform distribution of current in the shield, the field within the shield is zero. Here the flux linking the conductor is equal to the flux linking the shield. Hence the self-inductance of the shield and the mutual inductance between the shield and the conductor within, are equal (The self-inductance of the conductor is different and higher). If the shield covers the conductor throughout and is shorted on itself, the equivalent circuit of the arrangement is as shown in Figure 7.8 (b).

The various quantities shown and the symbols used are as follows: -

⇒ (1) is the main source of magnetic field causing noise.

⇒ (C) is the signal conductor loop.

⇒ (S) is the shield loop.

⇒ (M_{1c}) is the mutual inductance between the source (1) and the signal conductor loop (C). This represents the coupling of the source with the signal loop.

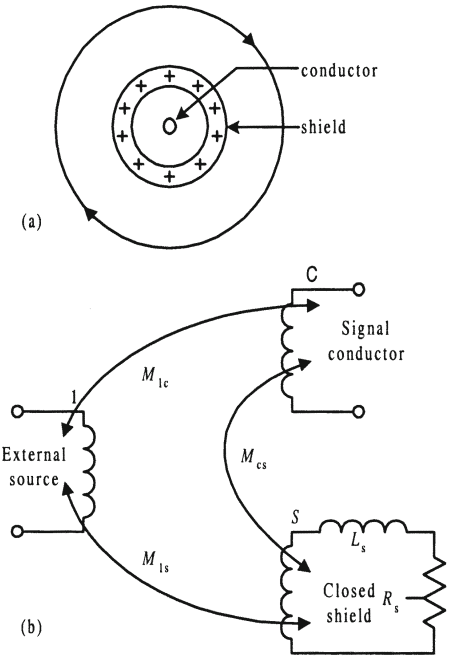


Figure 7.8 (a) A signal conductor inside a closed shield and (b) the equivalent circuit for interference from an external source

⇒ (M_{1s}) is the mutual inductance between the source and the shield loop (S); this represents the coupling of the source with the shield loop. Since all the flux linking the shield, links the conductor also, $M_{1s} = M_{1c} = M$.

⇒ (M_{cs}) is the mutual inductance between the shield loop (S) and the signal conductor loop (C).

⇒ (L_s) is the self-inductance of the signal conductor loop.

⇒ (R_s) is the resistance of the shield loop

If the source (1) carries a current I_1 at frequency ω rad/s, it induces equal emfs – e – in the screen and the signal conductor loop (C). Let E_1 be the rms. value of this emf.

$$E_1 = M_{1c} I_1 s = M_{1s} I_1 s \tag{7.8}$$

let us assume that the signal conductor loop resistance $R_c >> R_s$. Hence the current through it is negligible.

$$\text{Current through the shield loop } I_s = \frac{M_{1s} I_1 s}{R_s + Ls} \tag{7.9}$$

This induces an emf in the signal conductor loop equal to $M_{cs} I_s s$. Using Equations 7.8 and 7.9, net induced emf in the signal conductor loop, v_e becomes

$$v_e = M_{1c} M_1 s - \frac{M_{1s} M_{cs} s^2 I_1}{R_s + Ls}$$

$$= MI_1 s \frac{R_s}{R + Ls} \tag{7.10}$$

since $M_{1c} = M_{1s} = M$ and $L_s = M_{cs}$. From Equations 7.8 and 7.10

$$\frac{\text{Noise emf in signal conductor loop in the absence of screen loop}}{\text{Noise emf in signal conductor loop with screen present}} = \frac{R_s + Ls}{R_s} \qquad (7.11)$$

Observations: -

⇒ At low frequencies, the screen is ineffective. The noise voltage coupled to the signal conductor loop remains undiminished.

⇒ At $\omega_c = R / L$, (the corner frequency), the noise voltage is reduced to 70 % of the value in the absence of the screen.

⇒ At high frequencies, the noise voltage reduces to ω/ω_c times the value in the absence of the screen.

⇒ For the screen to be effective, R_s has to be as small as possible.

⇒ In practical situations, the screen may not cover the signal path fully. The uncovered portion may have flux linkage with the disturbing source. To that extent, a noise voltage is coupled to the signal loop.

Noise due to the magnetic field is coupled into a circuit loop. This involves the forward and the return paths of the loop. Hence grounding one lead by itself does not reduce magnetic coupling. The balancing of emf's on the two leads and cancelling them through good CMR are not possible here (in contrast to the electric field coupling). However, one may do the balancing and cancelling in an indirect manner. The situation (idealized) is shown in Figure 7.9. C_1 and C_2 are the signal conductors and G is the common ground. G is positioned such that the magnetic flux linking loops C_1G and C_2G due to the disturbing field are equal. The signals across C_1G and C_2G are processed in a differential stage. This neutralizes the noise-induced emfs in C_1 and C_2 completely. However, the approach requires a precise knowledge of the disturbing field and its orientation. It cannot neutralize the effect of two or more disturbing sources. Hence, the technique is of limited practical utility.

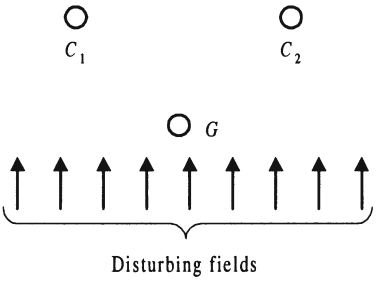


Figure 7.9 Symmetrical positioning of conductors to neutralize the effect of disturbing field

7.2.4 Comparison of Electrically and Magnetically Coupled Noise

The discussions on the two types of noise coupling so far are summarized in Table 7.1. Keeping both the signal lines close to each other and short, are the only

measures to reduce both types of coupled noise. All other measures are specifically targetted at one or the other type of coupled noise only and not both [Paul, Morrison, Walker]. In general, the frequencies of interest in instrumentation schemes are at the low end. The magnetically induced noise as also the measures to reduce them, require closer attention. Effects of electrically induced noise (being at high frequency), may in general be reduced to desired levels by filtering.

Table 7.1 Comparison of electrically and magnetically coupled noise

Electrically coupled noise	Magnetically coupled noise
Noise emf is induced in parallel with the signal	Noise emf is induced in series with the signal
Effect of noise decreases with increase in frequency	Effect of noise increases with increase in frequency
The signal loop impedance is to be kept as low as possible to reduce the effect of noise	The signal loop impedance is to be kept as high as possible to reduce the effect of noise
Keep signal forward and return paths as close to each other as possible	Keep signal forward and return paths as close to each other as possible
In case of signals with ground return, screen with one end grounded, is effective in noise reduction, especially at low frequencies	The measure has no effect on the coupled noise
Screens with both ends grounded, may reduce the main noise coupling; but it may introduce additional noise pick-up	Screens with both ends grounded, is effective in noise reduction especially at high frequencies
Twisting signal conductor pairs is ineffective in noise reduction	Twisting signal conductor pairs is effective in noise reduction. At low frequencies, this is more effective than shielding

7.3 Characterization of Random Signals

Internal noise as well as signals, encountered in instrumentation and other electronics systems, have two specific characteristics: -

⇒ They are functions of time – *i.e.*, their instantaneous values change with time.

⇒ The value at any point of time, cannot be precisely predicted based on the past values. We may guess a value based on some criteria and assign a probability to it; but a precise prediction is not possible (In fact the lack of such an *a priori* knowledge, is the reason for measuring it).

We may loosely term these, as 'Random Variables of time' – such a heuristic description suffices for our purposes. Though random, one can elicit a variety of information regarding their behavior from the observations of successive sample values. These are of use in identifying specific patterns of their behavior and designing signal processing circuitry. We highlight here those characteristics of random variables that are of direct use to us [Davenport and Root, Papoulis].

7.3.1 Amplitude Characteristics

Consider a random variable of time. We can measure it at successively spaced close intervals of time. Using these sample values, an 'Amplitude Density Function', $p(x)$ can be plotted as shown in Figure 7.10. Consider a range of sample values whose amplitudes lie within the band Δx around x_i. $p(x)\,\Delta x$ signifies the relative number of samples whose amplitudes lie within the band of width Δx around x_i.

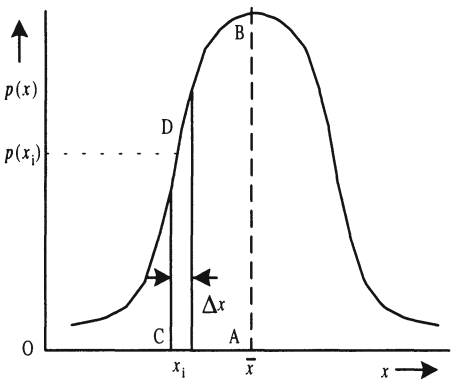


Figure 7.10 Normal distribution

The amplitude density function can take a variety of shapes depending on nature of the variable. With many random variables, it is taken to have a well-known form given by

$$p(x) = \frac{1}{\sqrt{2\pi}\sigma} e^{-\frac{(x-\bar{x})^2}{2\sigma^2}} \tag{7.12}$$

A random variable conforming to this distribution is called a 'Normal' or a 'Gaussian' variable. The following important properties characterize the Gaussian random variable:-

- ⇒ The average value of x is $\bar{x}$. It is represented by OA in Figure 7.10.
- ⇒ The amplitude density function $p(x)$ attains its maximum value at $x = \bar{x}$. *i.e.*, the maximum number of samples crowd around $x = \bar{x}$.
- ⇒ The amplitude density function is symmetrical about $\bar{x}$. $p(\bar{x} + a) = p(\bar{x} - a)$.
- ⇒ The root mean square deviation of x from $\bar{x}$ is σ^2. *i.e.*, the average value of $|x-\bar{x}|^2$ is σ^2. σ is called the 'standard deviation'. σ^2 is called the variance.
- ⇒ Once an $\bar{x}$ and a σ value are known, the distribution function of the variable, is fully known.
- ⇒ If two Gaussian variables x_1 and x_2 with average values $\bar{x}_1$ and $\bar{x}_2$, and standard deviations σ_1 and σ_2 are added, the sum is another Gaussian variable. If the two are independent, the sum has a mean value of $(\bar{x}_1 + \bar{x}_2)$ and standard deviation of $\sqrt{\sigma_1^2 + \sigma_2^2}$. If the two are not independent (*i.e.*, if they are correlated), the sum and standard deviation values are different. This can be extended to any number of Gaussian variables.

⇒ As an extension of the above, it can be shown that when a linear circuit or system is given a Gaussian input signal, its output as well as the signal at every intermediate stage, remains Gaussian.

⇒ $p(x)$ of Equation 7.12 extends from $x = -\infty$ to $x = +\infty$. However in practice, as $|x-\bar{x}|$ increases, $p(x)$ reduces rapidly.

⇒ The fractional time for which $|x-\bar{x}|$ exceeds specified limits, is of importance in many signal processing circuitry.

- For 4.5 % of the time, $|x-\bar{x}| \geq 2\ \sigma$.
- For 0.26 % of the time, $|x-\bar{x}| \geq 3\ \sigma$.
- For 0.006 % of the time, $|x-\bar{x}| \geq 4\ \sigma$.

These are shown in Figure 7.11.

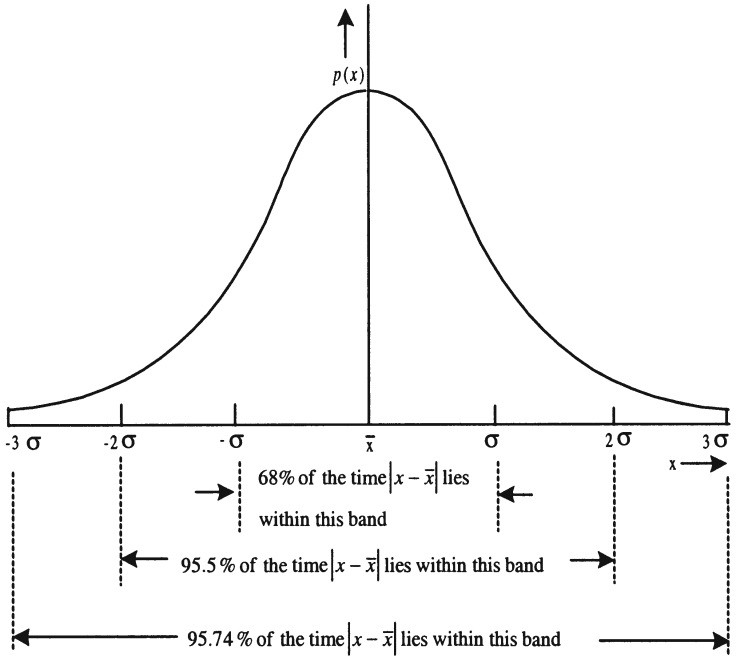


Figure 7.11 Spread of signal information around $\bar{x}$

⇒ As an engineering approximation, it is customary to take the peak of $|x-\bar{x}|$ to lie within the $\pm 3\ \sigma$ band.

⇒ If a number of independent random variables are added, whatever be the nature of their individual distribution functions, the sum function distribution is closer to a Gaussian. The closeness improves, as the number considered increases [Central Limit Theorem].

7.3.2 Frequency Characteristics

Any signal can be considered to be composed of an infinite number of independent sinusoidal signals of different frequencies. If the power level in the signal is taken as definite, those at the individual frequencies will be infinitesimally small – since

the definite power gets divided into an infinite number of components. However one can consider a power density function $q(f)$ with units – watts / Hz. This can be definite at all the frequencies or at least at specific frequency bands. The product $q(f)\ \Delta f$ stands for the total infinitesimal power over the band of frequencies Δf around f. $q(f)$ signifies the relative power level in the signal or noise at frequency f. Depending on the signal or noise source, $q(f)$ can have different nature of variation with frequency. A few representative cases are shown in Figure 7.12. Some of these are discussed in more detail later.

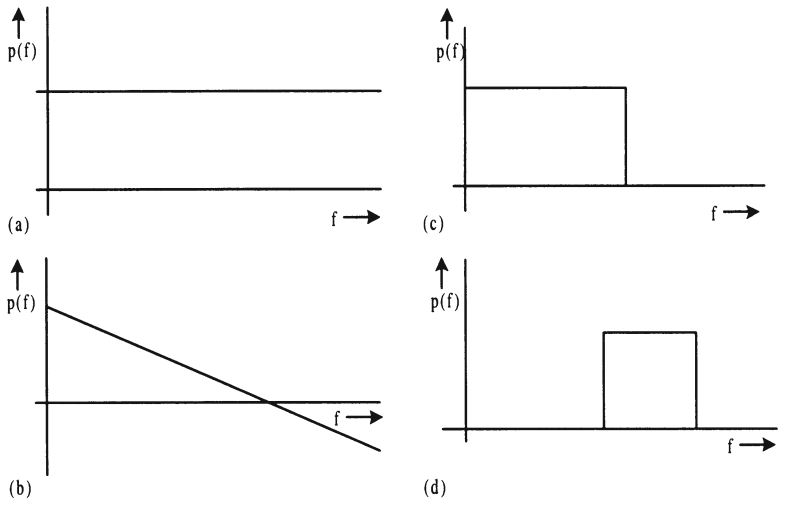


Figure 7.12 Power spectra of noise or signals from typical sources

Figure 7.12 (a) shows a distribution where all frequency components are present – from zero to infinite frequency. All these appear with the same amplitude. Such a random noise source is called a 'White' noise source (White coloured light is composed of all colours in the visible spectrum with equal intensity. The qualifier 'White' is used in an analogous manner with 'White noise'). With white noise, the total power in any specific frequency band remains constant irrespective of the frequency region where the band is selected.

Figure 7.12 (b) shows a power-density distribution function that varies inversely with frequency. The power components at low frequencies are predominant here. This is called as the '1/f' noise or 'pink' noise. Reference to 'pink' is because pink colour is composed of visible spectral bands with power density inversely varying with frequency. A 1/f noise source has equal power in each decade (or octave) of frequency.

Figure 7.12 (c) shows a band limited signal or noise spectra. The band extends from 0 to f_0 Hz. Within this band, the power density remains constant. Beyond f_0, the power content at all the frequencies (and hence the power density), is zero.

Figure 7.12 (d) shows a case where the total power is confined to the frequency band f_1 to f_2. Beyond this, the power content is zero. The power density within this band remains constant. When a signal is modulated on a carrier – in the form of AM or FM [See Section 6.2] – power spectral density function of the modulated signal is akin to this.

7.3.3 Signals from Physical Systems

We use a sensor and an instrumentation scheme around it, to know the quantitative value of a variable on a continuous basis. However, a prior knowledge of the outer bounds on the variable helps in the selection of the sensor and the allied modules. Such bounds can be in terms of the amplitude and frequency spectral distribution characteristics. In most of the cases encountered in practice, this knowledge can be generated by a closer study of the system generating the signal concerned and its environment. One can get an insight into the mechanism of signal generation by studying simplified models.

Typically physical systems are all composed of energy storage and energy dissipation elements characterized by inertia, elasticity, friction, thermal capacity, thermal conductivity and so on. These are akin to L, C and R in electrical circuits. Linking specific elements of this type leads to configurations analogous to electrical filters. By way of illustration, three simplified and idealized first-order systems are shown in Figure 7.13.

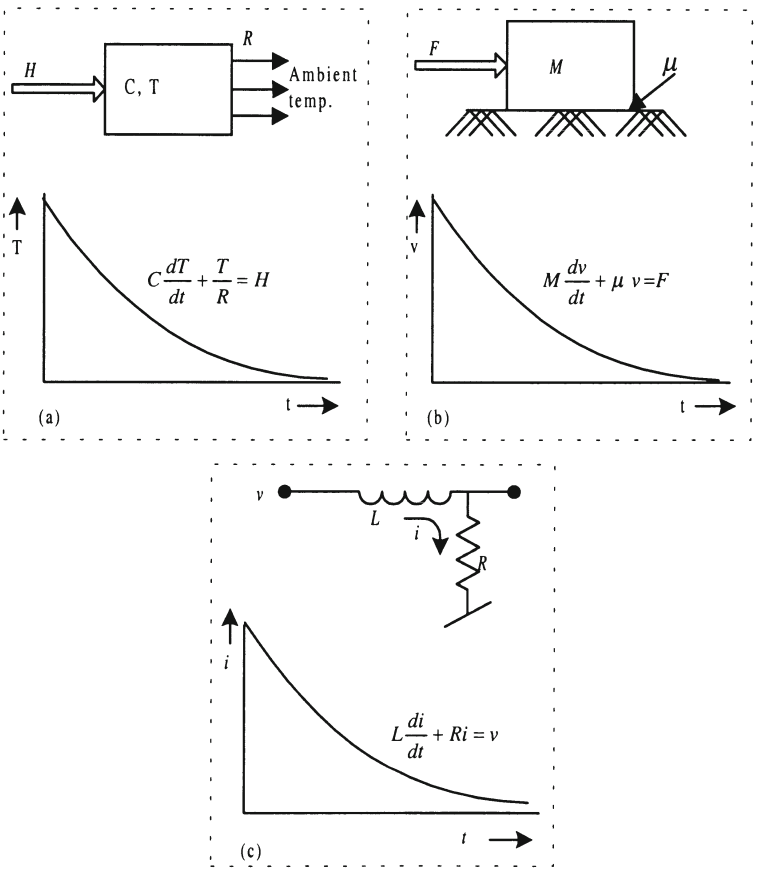


Figure 7.13 Typical idealized first order physical systems and their impulse responses

Figure 7.13 (a) shows a thermal system. A body has a thermal capacity of C joules / °C. It is in contact with ambient air with thermal resistance R °C/W. The body is fed with a heat input of H watts due to which, its temperature changes. This is a highly simplified model of a first order heat transfer system. The temperature rise T and heat input H are related by the differential equation

$$C\frac{dT}{dt}+\frac{1}{R}T = H \tag{7.13}$$

Taking Laplace transform of Equation 7.13 and rearranging terms, we get

$$T(s) = \frac{1/C}{s+(1/RC)}H(s) \tag{7.14}$$

For any type of variation of heat input, the body temperature varies with time and the nature of its variation is governed by the above equation. Considering specifically a unit impulse input, the nature of variation of the temperature becomes

$$T(t) = \frac{1}{C}e^{-(t/RC)} \tag{7.15}$$

The second example is that of a mass M in contact with a body as shown in Figure 7.13 (b). The common contact area is characterized by viscous friction with μ as the coefficient of friction. This again is a simplified model of a practical system. Following the application of a force F, the body moves with a velocity v. We have the differential equation connecting M, v and F as

$$M\frac{dv}{dt}+\mu v = F \tag{7.16}$$

Laplace transformation of Equation 7.16 and simplification yields

$$V(s) = \frac{1/M}{1+(\mu/M)s}F(s) \tag{7.17}$$

A unit impulse force input to the system yields the nature of variation of velocity of the body with time as

$$v(t) = \frac{1}{M}e^{-(\mu/M)t} \tag{7.18}$$

The third example is shown in Figure 7.13 (c). It is an electric circuit with an inductance L and a resistance R in series. The differential equation connecting the current and voltage in the circuit is

$$L\frac{di}{dt}+Ri = v \tag{7.19}$$

Laplace transformation of Equation 7.19 and simplification yields

$$I(s) = \frac{1/\mathrm{R}}{1+(L/R)s}V(s) \tag{7.20}$$

With a unit impulse voltage input, solution of Equation 7.20 gives

$$i(t) = \frac{1}{R}e^{-(R/L)t} \tag{7.21}$$

Consider a more involved (but still hypothetical) case where the resistance R in Figure 7.13 (c) forms the heater of the thermal scheme of Figure 7.13 (a). An impulse input of voltage to the *L-R* circuit, results in the heater current waveform as in Figure 7.13 (c). The heat input to the scheme of Figure 7.13 (a) also changes

accordingly. Therefore, the nature of variation of temperature with time becomes more involved compared to that of Figure 7.13 (a). Practical physical systems and the signals at different points in them are, in general, more complex. They differ from the simplified models of the above types in many respects: -

⇒ The number of energy storage elements and the dissipative elements, can be more than one.

⇒ The elements are closely coupled. The state of one affects the values of physical variables in others very closely.

⇒ Some of the elements may be linked in tandem – the output of one forming the input to another. With others, the link may be mutual or tied to other variables.

⇒ Some of the elements may be distributed in nature giving rise to partial differential equations.

A composite physical system of this type, cannot be represented by a general model. The model in one case can be radically different from that for another. The instantaneous values of different physical variables in the system, are the results of various disturbing inputs at different levels and points. These can be in the form of changes in the ambient conditions, Brownian motion and related effects at different levels and points and so on. Each leads to changes in the values of related physical variables governed by defining differential equations. In turn, these changes affect the following stages. Any physical variable being measured or appearing as noise takes values because of all such composite effects.

Any signal from the source is generated as a result of the composite effect of the changes in the physical variables forming the inputs. As an example, consider one such input – ambient temperature. A change in it can be represented as an impulse input or a series of impulse inputs to the source. It results in corresponding temperature changes in one or more elements inside. These interact with the coupled energy storage and dissipative elements inside changing other physical variables. The cumulative effect of all these, affects the signal from the source. Considering a general case, the signal is the effect of intentional changes in the physical variables as well as changes beyond our control like environmental changes. The signal is characterized by the following: -

⇒ Being the combined and the cumulative effect of different changes, the signal has randomness associated with it. In fact, this is the basic reason for sensing it.

⇒ The output of each first order and second order unit in the model has a specific frequency characteristic. Each has components in a limited frequency range only. For example, each first order unit considered above, has output with low frequency spectral components with a definite cut-off frequency. The cumulative effect of the changes forming the signal, from the source, too has a resultant frequency spectral characteristic. It will be characterized by a frequency distribution, a low frequency cut-off and a high frequency cut-off (The lower cut-off frequency may be zero in many cases).

⇒ All the inputs to the model being tangible physical variables, changes in them will be of limited amplitude. In turn, the signal generated from the source will be of limited amplitude. The amplitude density distribution of the signal can also be predicted from the model to some extent.

Any knowledge of the amplitude and frequency-density distribution functions of the signal is helpful in the selection of the sensors. Often one may be able to predict

these distributions only in terms of orders of magnitudes. For example, we may be able to say that a signal may have

⇒ dominant frequency components up to 20 Hz.,
⇒ beyond 100 Hz, the frequency components are insignificant,
⇒ the signal amplitudes lie mostly in the vicinity of zero,
⇒ the amplitude will rarely exceed +2 units and
⇒ the amplitude will rarely go below -1 unit.

Information of the above type, can be compared with corresponding sensor characteristics and a sensor which is best suited for the application selected. In short, by a close study of the system generating the variable to be sensed, enough information can be generated to facilitate selection of a suitable sensor.

7.3.4 Equivalent Noise Bandwidth

The filtering characteristics of signal processing circuits modify noise power spectra. Thus the filter will retain the noise in the passband *in toto* but attenuate it in the stop band. Since the attenuation is not 100 %, the noise components in this band also contribute to the total noise in the system. Normally an estimate of the total noise is made in terms of the 'Equivalent Noise Bandwidth'. The noise at the output of the filter (or the signal-processing block), is considered as equivalent to an ideally bandwidth-limited noise. In other words, this equivalent noise has a flat spectrum bandwidth extending upto f_e. Beyond f_e the power in the noise is taken as zero (See Figure 7.14).

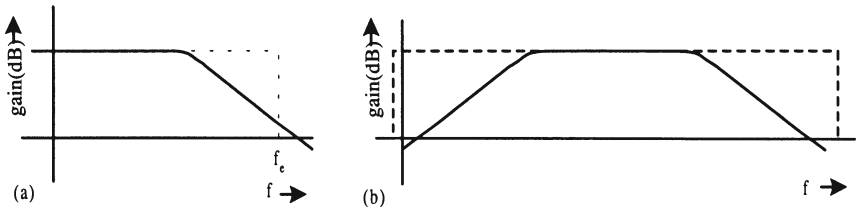


Figure 7.14 Equivalent noise bandwidth: (a) LPF case (b) BPF case

Consider a first order LPF with cut-off frequency f_0 and passband gain of unity. Its gain characteristic has the form

$$|G(f)| = \frac{1}{|1+(jf/f_0)|} = \frac{1}{\sqrt{1+(f/f_0)^2}} \tag{7.22}$$

The equivalent noise bandwidth f_e is

$$f_e = \int_0^\infty \frac{df}{\left(\sqrt{1+(f/f_0)^2}\right)^2} \tag{7.23}$$

Substituting $f = f_0 \tan\theta$ in Equation 7.23 and simplifying we get

$$f_e = f_0 \int_0^{\delta/2} d\grave{e}$$

$$= f_0(\pi/2) = 1.57 f_0 \qquad (7.24)$$

Similar analytical evaluation for higher order filters is cumbersome. In some cases the integral cannot be expressed in a closed form (Graphical methods of evaluating the area, may be resorted to, if necessary). In such cases, the integral may be evaluated numerically to obtain f_e. To get an idea of the representative values, f_e is given in Table 7.2, for the case of cascaded independent first order filters, *i.e.*, when we have the filter characteristic as

$$G(f) = \left[\frac{1}{1+(f/f_0)^2}\right]^{(n/2)} \qquad (7.25)$$

One can see that as n increases beyond 3, f_e does not reduce significantly.

Table 7.2 Equivalent noise bandwidth versus filter order

n - No. of poles of the filter	1	2	3	4	5
f_e / f_0	1.57	1.22	1.15	1.13	1.11

7.3.5 Narrow Band Random Process

The AM and FM outputs considered in the previous chapter, are band limited in nature. Normally they will be filtered through appropriate BPFs to remove the unwanted frequency components; the noise at frequencies lying outside the pass band of the BPF, are also filtered out in the process. Thus the channel that receives the AM or FM modulated signals, also receives noise lying within its restricted pass band. Performance of different modulators *vis-à-vis* such noise is analyzed in Section.7.5. To facilitate this, we consider the 'Narrow Band Random Process' here. The power spectral density of such a band-limited noise is shown in Figure 7.15. A random noise of this nature can be represented in the form [Davenport and Root].

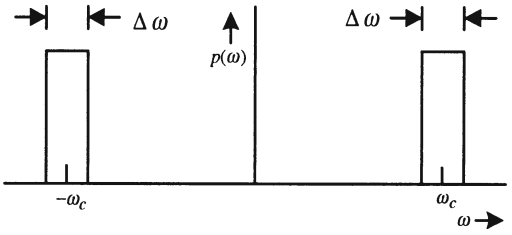


Figure 7.15 Power spectral distribution of a narrow band random process

$$n(t) = n_r(t)\cos\omega_c t + n_i(t)\sin\omega_c t \qquad (7.26)$$

Alternately we have

$$n(t) = R_n(t)\cos[\omega_c t + \phi_n(t)] \qquad (7.27)$$

where $R_n(t)$ is the envelope and $\phi_n(t)$, the phase of $n(t)$.

Here we consider the narrow band noise as a random signal at frequency ω_c. Its in-phase and quadrature amplitudes – $n_r(t)$ and $n_i(t)$ – are slowly varying random quantities. Its amplitude $R_n(t)$ and phase $\phi_n(t)$ are also slowly varying random quantities. By a detailed analysis one can show the following: -

$\Rightarrow$ $n_r(t)$ and $n_i(t)$ – both – are narrow band random processes.

$\Rightarrow$ $n_r(t)$ and $n_i(t)$ have identical power spectral densities.

$\Rightarrow$ $n_r(t)$ and $n_i(t)$ have the same variance as the narrow band random process – $n(t)$.

$\Rightarrow$ $n_r(t)$ and $n_i(t)$ are uncorrelated to each other.

$\Rightarrow$ If $n(t)$ is Gaussian, $n_r(t)$ and $n_i(t)$ are also Gaussian.

$\Rightarrow$ $R_n(t)$ and $\phi_n(t)$ are statistically independent random variables.

$\Rightarrow$ $R_n(t)$ has the probability density function

$$p(r) = \frac{r}{\sigma_n^2} e^{-\left(r^2/2\sigma_n^2\right)} \text{ for } r > 0 \quad \text{and} \quad 0 \text{ for } r \leq 0 \tag{7.28}$$

Here σ_n^2 is the variance of the original narrow-band process considered. The amplitude-density distribution function of Equation 7.28 is plotted in Figure 7.16. It is known as the 'Raleigh distribution'. Its maximum occurs at $r = \sigma_n$ and is equal to 0.607.

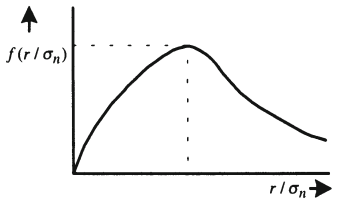


Figure 7.16 Rayleigh distribution

$$\bar{r} = \sigma(\pi/2) \tag{7.29}$$

$\Rightarrow$ $\phi_n(t)$ is uniformly distributed over 0 to 2π.

$$f(\phi_n) = (1/2\pi) \quad \text{for } 0 \leq \phi_n \leq 2\pi \tag{7.30}$$

7.4 Internal Noise

Internal noise is generated by certain random phenomena associated with charges inside conductors. It can be due to the random motion of these due to thermal agitation or due to the random nature of their crossing potential barriers at junctions, contacts and the like. The sources and the nature of each are briefly discussed here.

7.4.1 Shot Noise

Current flow through a potential barrier gives rise to 'Shot Noise' (also called 'Schottky noise'). It is due to the random nature of the electrons constituting the

current, crossing the barrier. Consider a semi-conductor junction diode with a forward bias voltage applied to it. The resulting depletion region near the junction is shown in Figure 7.17 along with the charge concentration levels. There is a potential barrier across the junction and an electric field near its vicinity. The

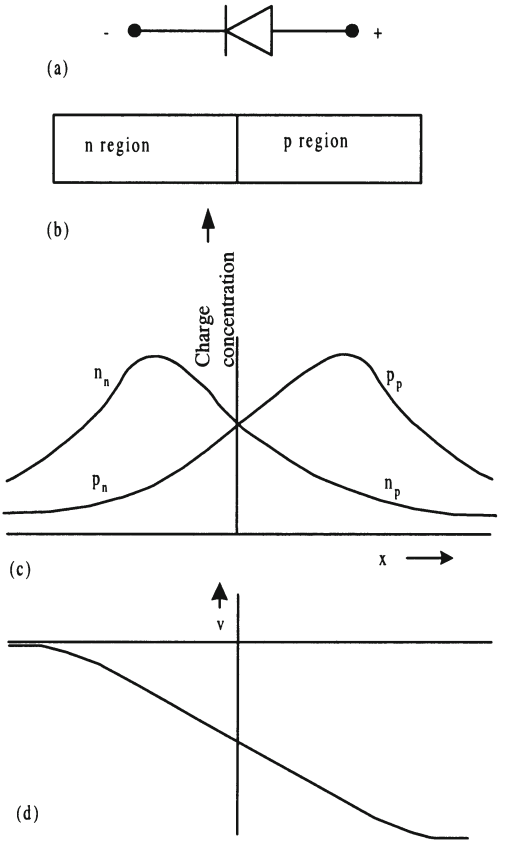


Figure 7.17 Junction diode: (a) Symbol (b) Schematic representation (c) Charge distribution in the vicinity of the junction (d) Potential distribution in the vicinity of the junction

potential change is shown sketched. At any temperature at any given time, the charge carriers are in a continuous state of random motion with a definite energy (velocity) distribution. Near the junction, some of these will acquire enough energy to cross the potential barrier and contribute to a current. This is a statistical phenomenon with the number crossing per unit time being dependent on the junction barrier voltage as well as the junction temperature. If q is the charge on the carrier and τ is the average transit time of charge across the junction, each such barrier crossing constitutes a pulse current of q/τ amp. For an Electron, $q = 1.6 \times 10^{-19}$C and τ may vary from 0.1 to 30 n s (typically). Thus, the junction current is composed of a large number of such spurts of current. The majority carriers being much larger in number, the current spurts in the forward direction far exceed those in the reverse direction. The average current due to all such current

spurts is uni-directional. The pulsed and the random nature of these spurts, gives rise to the term 'Shot Noise'. The spectral density of shot noise remains practically constant until about $1/\tau$ Hz and then it tapers off. We can consider the power spectral density of shot noise as $2qI_D$ A^2 / Hz where I_D is the average forward current of the diode.

In a frequency band of Δf Hz we have

$$\overline{i_s^2} = 2qI_D \Delta f A^2 \tag{7.31}$$

where $\overline{i_s^2}$ is the mean square value of current variation about the average value of current I_D. The amplitude density distribution of current can be considered to be Gaussian in nature with mean value I_D and

$$\sigma = \sqrt{2qI_D \Delta f} \tag{7.32}$$

As an example, consider a diode with a forward current of 2mA in a circuit having bandwidth extending up to 5 MHz. It will generate shot noise with a σ^2 value as

$$\sigma^2 = 2\times1.6\times10^{-19}\times2\times10^{-3}\times5\times10^{6}$$
$$= 3.2\times10^{-15}$$
$$\sigma = 56.5 \text{ nA}$$

The active bandwidth of operation should be kept at the minimum necessary level to keep down the shot noise.

For analysis purposes, shot noise is represented as an equivalent current source in parallel with the device. It generates a randomly varying signal with Gaussian amplitude distribution and a value estimated as above.

7.4.2 Thermal Noise

'Thermal Noise' is also called 'Resistance Noise' or 'Johnson Noise'. It is due to the thermal agitation of electrons within a resistance. Any conductor is characterized by (practically) free electrons inside it. They are in a state of random motion, the average energy associated with each electron being proportional to the absolute temperature of the conductor. Such random motion constitutes a noise source. At absolute zero temperature, the thermal energy associated with each particle within the conductor is zero and they do not execute any random vibration; hence the noise is zero too. In general, we have

$$\overline{v^2} = 4KTR\,\Delta f \tag{7.33}$$

where

- $\Rightarrow$ $\overline{v^2}$ is the rms. value of thermal noise voltage
- $\Rightarrow$ k is Boltzmann's constant
- $\Rightarrow$ R is the value of the resistance
- $\Rightarrow$ Δf is the frequency range of interest

At room temperature,

$$4kT = 1.66 \times 10^{-20} \text{ VC} \tag{7.34}$$

Observations: -

- $\Rightarrow$ Thermal noise represents the absolute minimum noise that a dissipative component can generate. The total noise generated is in general higher.

⇒ The electron drift velocities in a conductor carrying current are of a much lower order compared to the random thermal vibration. Hence, thermal noise is independent of the current through the conductor.

⇒ The thermal noise spectral density is the same at all frequencies up to about 10^{13} Hz. Thus, the noise power density in a 100 Hz band around 1kHz is the same as that in a 100 Hz band around 1MHz.

⇒ Thermal noise is a basic physical phenomenon. It is present in any passive device. This includes resistors and all types of sensors, microphones, loudspeakers *etc.*

⇒ Increase in the ambient temperature does not increase thermal noise significantly. A 30°C rise in the ambient temperature causes only a 5 % increase in the noise.

⇒ In a complex impedance network, the total thermal noise generated is that due to the equivalent resistance component of the impedance.

⇒ The total noise power (due to thermal noise) is

$$\frac{\overline{v_n^2}}{R} = 4KT\Delta f \tag{7.35}$$

This is the total noise power at any temperature T and given bandwidth Δf. It is a constant for all resistances.

⇒ By way of an example, consider a 2 kΩ resistor over a 5 MHz frequency range.

$$\begin{aligned}\overline{v^2} &= 1.66\times10^{-20}\times2\times10^{3}\times5\times10^{6}\\ &= 1.66\times10^{-10}\\ \sigma &= 12.9\ \mu V\end{aligned}$$

Using the Norton equivalent circuit, this is equivalent to a 6.45 nA of noise current source in parallel with a 2 kΩ resistance. This may be compared with the 56.5 nA of shot noise with 2 mA current with the same bandwidth obtained in the last sub-section.

⇒ The amplitude distribution of thermal noise is Gaussian in nature.

⇒ Shot noise and thermal noise – both – have a flat-power density spectrum and both are Gaussian in nature. Once a circuit is made up of diodes, resistors *etc.*, and energized, the total noise generated is due to the shot noise and thermal noise in different components. These are no longer distinguishable.

7.4.3 Flicker Noise

The origins of 'Flicker Noise' are varied. In semiconductor devices, they may be due to the surface leakage, the imperfections in the depletion layers and so on. Flicker noise exhibits a power spectral density different from that of thermal noise or shot noise. The power spectral density is, in general, of the form

$$\overline{i^2} = k\frac{I^a}{f^b}\Delta f \tag{7.36}$$

where

⇒ k is a constant depending on the material or the device concerned

$\Rightarrow$ a is in the 0.5 to 2.0 range

$\Rightarrow$ b is close to unity.

$\Rightarrow$ Δf is a narrow frequency range of interest around f.

The flicker noise is most significant at lower frequencies. Taking $a = b = 1$, we have

$$\overline{i^2} = kI\frac{\Delta f}{f} \tag{7.37}$$

The total noise power in the frequency range f_1 to f_2 is

$$\int_{f_1}^{f_2} \overline{i^2} df = kI \ln\left(\frac{f_2}{f_1}\right) \tag{7.38}$$

The logarithmic nature of this function makes the total contribution over each decade of frequency, constant. Thus, the total noise contribution to noise over the 1s to 1year range is the same as the contribution from 1Hz to 1 MHz. Table 7.3 gives the frequency and the corresponding time-periods at decade intervals.

Table 7.3 Frequency and the corresponding time periods at decade intervals.

Frequency	32 nHz	320 nHz	3.2 μHz	32 μHz	320 μHz	3.2 mHz	32 mHz	320 mHz	3.2 Hz
Time period	1 year	36 days	3.6 days	8.8 hrs	53 mins.	5.3 mins.	32 s	3.2 s	0.32 s

Although the flicker noise power appears to increase rapidly at low frequencies, the total contribution to noise from frequencies below 0.1 Hz, is often too small to be of significance.

Observations: -

$\Rightarrow$ Flicker noise exists only in association with a direct current. It is zero in the absence of a direct current.

$\Rightarrow$ The unknown constant k varies for different types of devices. Within the same type, it varies from unit to unit due to the difference in crystal imperfections and the like.

$\Rightarrow$ The amplitude density distribution of flicker noise is more often non-Gaussian.

$\Rightarrow$ Normally device manufacturers give representative flicker noise figures from a series of sample noise measurements.

7.4.4 Contact Noise

Whenever a current passes through a contact between two dissimilar materials, the current exhibits small random variations about the mean value. These are ascribed to the random fluctuations in conductivity in the region of the contact. Such noise can arise at the contacts of dissimilar conductors, switches, diodes, relays, transistors, ICs, composition resistors *etc*. Contact noise level is proportional to the value of current. Its power density varies as $1/f$. Due to its nature, contact noise is indistinguishable from flicker noise from other sources.

7.4.5 Popcorn Noise

'Popcorn Noise' – also called the 'Burst Noise' – is due to manufacturing defects, metallic impurities in semi-conductor devices, ICs *etc.* It can be reduced substantially by improving the manufacturing processes. It appears as sudden random bursts in amplitudes of currents. The burst amplitude is normally fixed for a device. Being a current related phenomenon, the effect is more pronounced in higher impedance circuit segments – like opamp input circuits.

7.4.6 Total Noise

Thermal (or Johnson) noise is the minimum unavoidable noise produced by a device. The total noise produced in the device – active or passive – will be at a much higher level than the thermal noise. Such excess can be due to the various other noise sources discussed before. In fact, the excess noise over and above the basic thermal noise-level, is a measure of the quality of the device. For a good quality device, the total noise should be as close to the thermal noise level as is possible.

Thermal noise, shot noise, flicker noise, contact noise, popcorn noise are all of independent origin. They are all random and uncorrelated. Hence, total noise power can be obtained by adding the independent noise powers. By the same token, the total noise voltage peak – V_{total} – can be obtained as

$$V_{total} = \sqrt{V_1^2 + V_2^2 + V_3^2 + \ldots} \tag{7.39}$$

where V_1, V_2 *etc.*, are all individual noise peak voltages.

7.4.7 Minimization of Effects of Internal Noise

Some measures of noise reduction are common to all systems: -

- ⇒ Select passive components that contribute low noise. Metal film resistors are the best among resistors. Composite resistors are noisy due to the shot noise at domain interfaces. Carbon resistors too are noisy.
- ⇒ Design the circuit to operate under conditions that reduce noise. Low working currents reduce shot noise as well as noise from other sources. Select passive components with low noise. This is an exercise calling for careful study of their specifications.
- ⇒ Keep the working temperature of the device as low as possible. This reduces thermal noise though only to a marginal extent.
- ⇒ Make a careful estimate of the bandwidth required to handle the signal. Limit the bandwidth of individual signal processing stages to this level. This prevents addition of noise at unwanted frequencies.
- ⇒ When a number of analog signal processing stages function in tandem, the noise in the first stage(s) gets maximum amplification - compared to noise in the subsequent stages. Hence, it is necessary to pay maximum attention to the selection of components for the first stage(s).

7.4.7.1 *Effect of Noise Inside Feedback Loops*

The effect of noise inside feedback loops depends up on the location of the noise source inside the loop as well as the relative gains of individual blocks inside the loop. Consider the general feedback loop arrangement of Figure 7.18. G_1, G_2 and H are the gains of functional blocks in the loop. V_s is the signal voltage, v_n an internal noise voltage and v_o the total output voltage of the scheme.

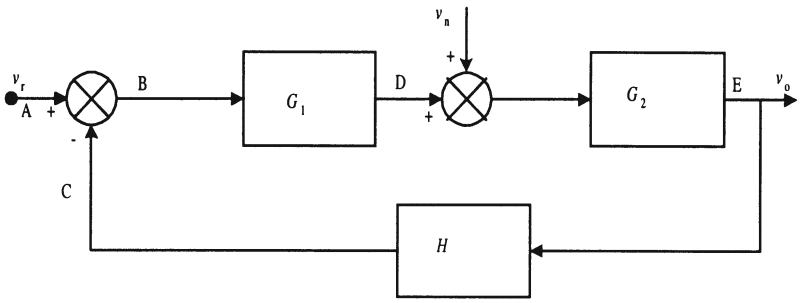


Figure 7.18 closed loop system with additive noise

From Figure 7.18 we get

$$v_o = \frac{G_1G_2}{1+HG_1G_2}v_s + \frac{G_2}{1+HG_1G_2}v_n \tag{7.40}$$

In normal feedback loops, we get $G_1G_2H >> 1$.

$$\therefore v_o \approx \frac{v_s}{H} + \frac{v_n}{G_1H} \tag{7.41}$$

Depending on the relative position of v_n, different cases arise:

⇒ $G_1 = 1$: This represents the case when noise gets added at the input to the loop itself.

$$v_o \approx \frac{v_s}{H} + \frac{v_n}{H} \tag{7.42}$$

⇒ $G_2 = 1$. This represents the case when noise gets added at the output of the loop.

$$v_o \approx \frac{v_s}{H} + \frac{v_n}{G_1H} \tag{7.43}$$

Normally $G_1 > 1$. v_n gets attenuated by G_1 relative to v_s.

⇒ $H = 1$. This represents the unit gain feedback loop.

$$v_o \approx v_s + \frac{v_n}{G_1} \tag{7.44}$$

Here too v_n gets attenuated by G_1 relative to v_s.

Summarizing we find that as the noise source moves away from the point of input, its effect reduces. In other words, noise at and close to the input has to be kept as low as possible.

7.4.7.2 *Amplifier Selection Depending on Signal Source*

As discussed in Chapter 3, opamps with widely differing characteristics are available. When selecting one for amplifying a signal, a proper choice can make a

conspicuous difference to performance *vis-à-vis* noise. Four broadly different cases arise depending on the type of signal. All these four cases are considered here; Subsequently specific examples illustrate design trade-offs. Any signal source may be of the voltage or the current type. In either case, the signal source can be represented by the equivalent Thevenin source – a voltage signal v_s in series with a source impedance R_s. The signal source has been considered only in this form here.

Case 1: v_s is large and R_s small

This is the best case one would like to handle. Any opamp configuration with voltage and current noise levels such that $v_n << v_s$ and $i_n R_s << v_s$ may suffice for signal processing. Such selection is rather easy.

Case 2: v_s is large and R_s is large

An opamp with low noise-current levels is to be selected here; *i.e.*, one has to pay more attention to reduction of i_n as compared to reduction of v_n.

Case 3: v_s is small and R_s is large

The choice of opamp here has to be based on v_n as well as i_n. This may call for a few trials of design with different v_n and i_n combinations.

Case 4: v_s is small and R_s is small

This is the most challenging case. Any choice of opamp affects performance unduly. One can only keep the damage as low as possible (In fact this is the case which continuously motivates development of opamps with better specifications).

Example 7.1 Amplification of Thermocouple Output

The output from Platinum / Platinum 10%-Rhodium thermocouple can be used to measure temperatures up to 1450°C. Its sensitivity varies as shown in Table 7.4. With selected thermocouples, the error is 0.6 °C or 0.1 % whichever is higher (when used to measure temperatures up to 1450°C). The thermocouple output at 1450°C with a cold junction temperature of 30°C, is 14.805 mV. This can be considered to be a source of high v_s and low R_s.

Table 7.4 Sensitivity of Pt/ Pt(10)-Rh thermocouple

Temp(°C)	0	200	400	600	800	1000	1200	1400
Sensitivity(μV/C)	5	8	10	10	11	11	12	12

Consider amplifying the signal to provide 1V full-scale output. An inverting amplifier configuration as in Figure 7.19 is used [Cold junction compensation calls for changes in this circuit (See Section13.7.5)]. The thermocouple resistance is in the range of 100 Ω. The bandwidth is taken as 10 Hz – adequate for most industrial temperature applications.

Error in the output at full scale = 0.1 %

Let us restrict the error due to loading by the amplifier also to 0.1 % at full scale. This puts an lower limit on R_1 as

$$R_1 = \frac{100 \times 100}{0.01}\Omega = 10^5 \Omega$$

$$= 100\ \text{k}\Omega \tag{7.45}$$

$$\text{Required gain} = \frac{1\ \text{V}}{14.805\ \text{mV}}$$

$$= 67.5 \tag{7.46}$$

$$R_2 = 6.75\ \text{M}\Omega^{4} \tag{7.47}$$

$$R_3 = R_1 \| R_2$$

$$= 98.5\ \text{k}\Omega \tag{7.48}$$

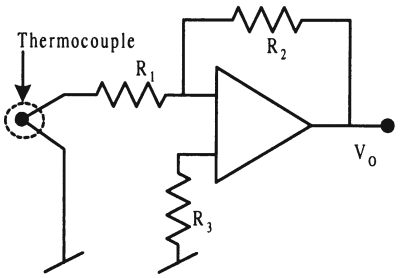


Figure 7.19 Thermocouple with simple amplifier considered in Example 7.1

Table 3.1 lists key characteristics of some common opamps. Offset voltage and Offset drift of FET input type opamps like TL081 or LF356 are high and their use can result in high levels of error. Hence, these opamps are not considered for the present application. OP07 and LM607 are BJT input opamps; between them we opt for OP07 due to its higher input resistance of 20 MΩ (>> 100 kΩ used for R_1).

$$\text{Equivalent resistance for thermal noise} = R_1 \| R_2 + R_3$$

$$\approx 200\ \text{k}\Omega \tag{7.49}$$

Restricting the bandwidth to 10 Hz, the noise equivalent bandwidth is 15.7 Hz. From Equation 7.33, thermal noise is obtained as

$$\overline{v_t^2} = 1.66 \times 10^{-20} \times 200 \times 10^3 \times 15.7\ \text{V}^2 \tag{7.50}$$

$$= 5.21 \times 10^{-14}\ \text{V}^2 \tag{7.51}$$

From the opamp data in Table 3.1,

Input noise voltage of the opamp (up to 10 Hz) = 0.6 μV p-p

This being the 6σ value,

$$\text{equivalent mean square voltage} = 1 \times 10^{-14}\ \text{V}^2 \tag{7.52}$$

Noise current (from Table 3.1) up to 10 Hz = 30 pA p-p

$$\text{Equivalent mean square value} = 25 \times 10^{-24}\ \text{A}^2 \tag{7.53}$$

Passing through 200k, this reflects as a

$$\text{noise voltage} = 25 \times 10^{-24} \times 200^2 \times 10^6\ \text{V}^2$$

$$= 50 \times 10^{-14}\ \text{V}^2 \tag{7.54}$$

Combining the three noise voltages of Eqations.7.51, 7.52 & 7.54,

$$\text{Total noise} = (5.21 + 1 + 50) \times 10^{-14}\ \text{V}^2$$

[4] In practice, one may have to fine-tune the gain. A higher round value of R_2 can be selected and R_1 increased suitably with an additional adjustable resistance in series.

$$= 56.21 \times 10^{-14}\ V^2 \quad (7.55)$$

Equivalent p-p noise voltage $= 4.5\ \mu V$

At full scale of 1450 °C, this is equivalent to a change of $4 \cdot 5/12$ °C.

$$\approx 0.4°C \quad (7.56)$$

This is low compared to 0.1% of reading *i.e.*, 1.4°C and hence may be considered acceptable.

Observations: -

⇒ One may reduce the bandwidth to a lower level (say 1Hz) and reduce noise correspondingly.

⇒ The contribution of noise current to total noise predominates in Equation 7.55. FET input opamps with their much lower noise currents appear an attractive and better alternative. However, the error due to their high offset voltage and offset voltage drift, can be much higher than the error due to noise. These opamps become attractive only if the bandwidth required is two or more orders higher.

⇒ The noise figures given in Table 3.1 being only representative values, calculations that are more precise are not warranted.

Consider the use of the same thermocouple to measure temperature up to a more restricted range of 200°C.

Thermocouple voltage at 200 °C with the cold junction at 30 °C $= 1.268$ mV

This is a case of a source with a low V_s and low R_s.

The gain required to amplify the thermocouple voltage to the 1V level $= (1/1 \cdot 268) \times 10^3$

$$= 788.6 \quad (7.57)$$

This gain can be brought about in two stages. Let the gain of the first stage be equal to 100.

Error in thermocouple output at full scale $= 0.6$ °C

$$\approx 5\ \mu V \quad (7.58)$$

Let us restrict the loading error also to this level.

Loading error allowed $= (5/1268) \times 100$

$$\approx 0.4\% \quad (7.59)$$

With 100 Ω source resistance for the thermocouple, minimum allowable R_1 becomes

$$R_1 = \frac{100 \times 100}{0 \cdot 4}\ \Omega$$

$$= 2.5\ k\Omega \quad (7.60)$$

$R_2 = 250k\ \Omega$

$R_3 = 2.48k\Omega$

Equivalent resistance for thermal noise $= R_1 \,||\, R_2 + R_3$

$$\approx 5\ k\Omega \quad (7.61)$$

thermal noise $\overline{v_t^2} = 1.66 \times 10^{-20} \times 5 \times 10^3 \times 15.7\ V^2$

$$= 13 \times 10^{-16}\ V^2 \quad (7.62)$$

Since R_1 = 2.5 kΩ, LM607 with 2 MΩ input resistance can be an alternative to the use of OP07. For LM607 (from Table 3.1),

input noise voltage (up to 10 Hz) = 0.5 μV p-p

This being the 6σ value,

equivalent mean square voltage = 69.4×10^{-16} V^2 (7.63)

Noise current up to 10 Hz (from Table 3.1) = 14 pA p-p

Equivalent mean square value = 5.44×10^{-24} A^2 (7.64)

Passing through 5 kΩ, this reflects as

a noise voltage = $5.44 \times 10^{-24} \times 25 \times 10^{6}$ V^2

= 1.36×10^{-16} V^2 (7.65)

Combining the three noise voltages of Equations 7.62, 7.63 & 7.65

Total noise = $(13 + 69.4 + 1.36) \times 10^{-16}$ V^2

= 83.76×10^{-16} V^2 (7.66)

Equivalent p-p noise voltage = 0.55 μV p-p (7.67)

At 200°C, this is equivalent to a change of (0.55/8) ≈ 0.07°C. This is low, compared to the full-scale thermocouple output error of 0.6°C and can be considered acceptable.

Observations: -

⇒ The opamp voltage noise is the predominant component here. From Table 3.1, one can see that OP07 also has the same level of voltage noise as LM607. Hence, it could be retained without appreciable loss in accuracy on this count. However, V_{os} drift is higher for OP07.

⇒ The resistance values used in the circuit can be increased somewhat (2 to 3 times) without adversely affecting the total noise levels. In fact the gain due to the reduction in loading may more than offset the increased error due to the noise.

⇒ The second stage is to have an amplification of 7.886. The noise and drift errors due to this are comparatively negligible.

Example 7.2 Amplification of pH Cell Electrode Output

A pH electrode cell gives an output with 200mV range with a resolution of 100 μV. The Cell resistance is 50 MΩ at 30°C and doubles for every 8°C drop in the cell temperature. The signal is to be amplified to 1V level with the cell working down to 15°C.

This is a case of high V_s and high R_s.

$$\text{The signal resolution} = \frac{100 \times 10^{-6}}{200 \times 10^{-3}} \times 100$$

$$= 0.05\% \quad (7.68)$$

To keep the loading error to the same level, amplifier input resistance has to be at least [100 × (50/0.05)] = 10^5 MΩ. Since the source resistance may increase to 200 MΩ at 15 °C, this has to be increased to 4×10^5 MΩ. FET input Opamps like TL081 and LF356 have input resistance of the order of 10^6 M Ω. One of these may be used in the non-inverting configuration.

Gain required = 5

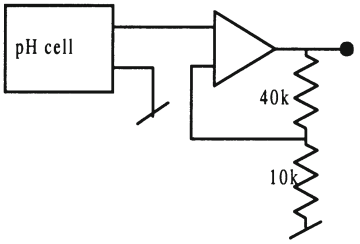


Figure 7.20 pH cell with amplifier considered in Example 7.2

The resistance combination shown in Figure 7.20 suffices for the application. The amplifier bandwidth may be limited to 5 Hz, which is adequate for pH measurements. The resistance values of 10 KΩ and 40 KΩ used in the amplifier are low compared to the cell source resistance in the 50 MΩ to the 200 MΩ range. Hence, the thermal noise of the source alone need be considered.

Thermal noise due to 200 MΩ up to 5Hz with correction for equivalent noise bandwidth $= 1.66\times10^{-20}\times200\times10^{6}\times5\times1.57\ V^2$

$= 26\times10^{-12}\ V^2$ (7.69)

The voltage noise of the opamp at 10 Hz $= 50\ nV/\sqrt{Hz}$

Opamp voltage noise over 4 decades upto 10 Hz $= 2500\times10^{-18}\ln(10^4)$

$= 0.023\times10^{-12}\ V^2$ (7.70)

This is negligible compared to the thermal noise. Hence, there is no need to make calculations that are more precise, by limiting the bandwidth to 5Hz and so on.

The current noise of the opamp is less than 0.01 pA $Hz^{-1/2}$. This figure can be used to estimate the upper limit to the current noise.

The upper limit to the current noise over 4 decades $= 10^{-4}\times10^{-24}\times200^2\times10^{12}\times\ln(10^4)$

$= 36.8\times10^{-12}\ V^2$ (7.71)

From Equations.7.69, 7.70 & 7.71, total noise $= 26\times10^{-12} + 0.023\times10^{-12} + 36.8\times10^{-12}$

$= 62.8\times10^{-12}\ V^2$ (7.72)

Corresponding p-p voltage noise $= 47.5\ \mu V$ (7.73)

This is 25% of the measurement resolution and can be considered acceptable.

⇒ The current noise used is an estimate of the upper limit. Actual noise level may be much lower; in turn, the total noise too will be lower. The p-p noise voltage estimated, based on thermal noise alone, is 30 μV.

⇒ The opamp drift is in the mV range. Zero adjustment of the instrument prior to any reading – is essential. This is to be done with necessary additional circuitry.

⇒ Change in the environmental conditions can affect leakage currents at the input. These are of the same order as the amplifier input currents. Proper guard rings [See Section 4.2.3] and adequate insulation are to be ensured at the input circuit side, to minimize their effects.

⇒ In practice an instrumentation amplifier of very low bias currents, is preferable for this application. Their higher CMRR, lower drift *etc.*, lead to an overall improved performance.

7.5 Performance of Modulation Systems in the Presence of Noise

In instrumentation schemes, modulation is resorted to, out of necessity – since it leads to an overall higher performance level. The basic modulated signal level is low. It is amplified and then demodulated to recover the original signal. The process is shown schematically in Figure 7.21. The modulated signal can get contaminated before amplification and during the amplification process itself. Such contamination cannot be avoided but only minimized. The modulation and demodulation schemes used in instrumentation, differ from those in broadcasting in some respects:-

⇒ In broadcasting, the modulated signal is mixed and taken to a specified frequency spectrum and broadcast. This is done at a high power level. Such frequency shifting through mixing and power-amplification are not present in instrumentation schemes.

⇒ The modulated signal level is low in an instrumentation scheme. The possibility of contamination by noise exists at this stage.

⇒ Before final demodulation, the modulated carrier is band limited. The bandwidth of the BPF used here, is the minimum necessary to retain all the significant frequency components. This operation is common for broadcasting as well as instrumentation schemes.

⇒ In broadcasting systems, the modulated carrier undergoes substantial attenuation before reception. Maximum noise contamination occurs at this stage due to the highly attenuated level of the signal. In instrumentation, the attenuation at this stage is not significant. Hence, the relative noise contamination is at a lower level. The expected accuracy level of signal reproduction in instrumentation is of a higher order than in a broadcasting system.

⇒ In broadcasting systems, it is customary to take the signal power to be uniformly distributed in the bandwidth of interest. However with instrumentation signals, the power is mostly concentrated near the zero frequency-region and the power content at higher frequencies is comparatively lower.

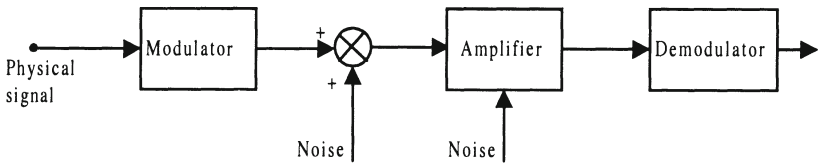


Figure 7.21 Modulation-demodulation scheme with contaminating noise

7.5.1 Noise Performance of AM Systems

The inherent noise discrimination characteristics of modulation – demodulation processes are discussed here. Two cases are of interest in an instrumentation scheme. The DSB-SC and the DSB with envelop detection.

7.5.1.1 DSB-SC:

Let the signal be $x_s(t)$ and the carrier $x_c(t)$ where

$$x_c(t) = A_c \cos \omega_c t \tag{7.74}$$

$$\text{Modulated output} = A_c x_s(t) \cos \omega_c t \tag{7.75}$$

Let ω_m be the bandwidth of the signal. The modulation – demodulation scheme is shown in Figure 7.22. The BPF limits the band of modulated output to $\omega_c \pm \omega_m$. The channel picks up all the noise within this band.

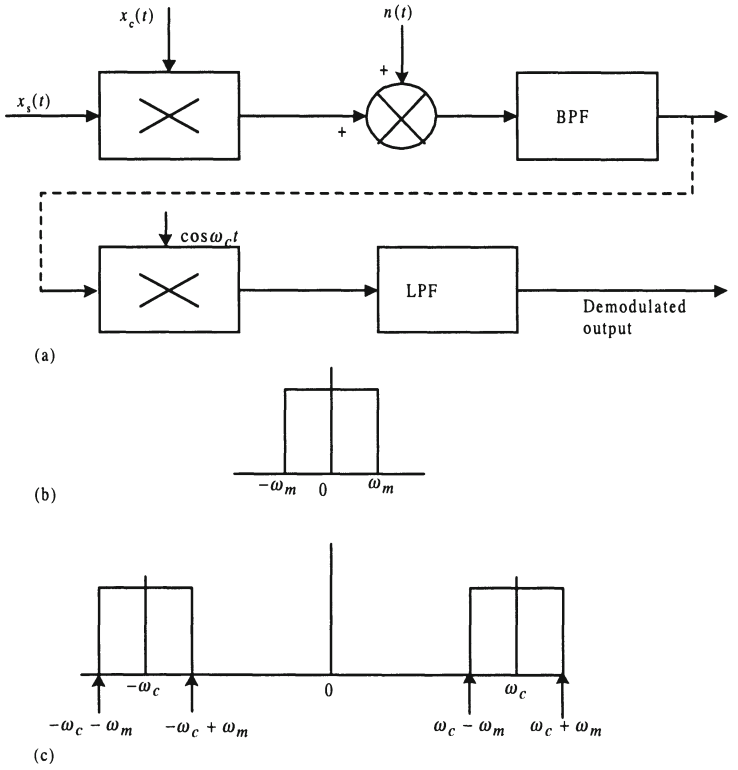


Figure 7.22 Performance of DSB-SC scheme in the presence of noise; (a) Scheme with contaminating noise (b) Baseband spectrum (c) Modulated spectrum

$$\text{Signal at the modulator output} = A_c x_s(t) \cos \omega_c t + n(t) \tag{7.76}$$

where $n(t)$ can be represented as in Equation 7.26.

$$n(t) = n_r(t) \cos \omega_c t + n_i(t) \sin \omega_c (t)$$

$$\text{Power content in noise} = N_i = \overline{n^2(t)} \tag{7.77}$$

$$\text{Power content in signal after modulation} = S_i = \frac{A_c^2}{2}\overline{x_s^2(t)} \tag{7.78}$$

Multiplying the right hand side of Equation 7.76 by cos $\omega_c t$ and substituting for $n(t)$ from Equation 7.26, we get $y(t)$ – the input to the LPF of the demodulator.

$$\begin{aligned} y(t) &= \cos\omega_c t\, x_s(t) A_c \cos\omega_c t + \cos\omega_c t\, n(t) \\ &= A_c x_s(t)\cos^2\omega_c t + n_r(t)\cos^2\omega_c t + n_i(t)\sin\omega_c t\ \cos\omega_c t \\ &= \frac{A_c}{2}x_s(t) + \frac{1}{2}n_r(t) + \left[\frac{A_c}{2}x_s(t) + \frac{1}{2}n_r(t)\right]\cos 2\omega_c t + \frac{1}{2}n_i(t)\sin 2\omega_c t \end{aligned} \tag{7.79}$$

The LPF filters out the bands centred around $2\omega_c$.

$$\therefore \text{LPF output} = \frac{A_c}{2}x_s(t) + \frac{1}{2}n_r(t) \tag{7.80}$$

$$\text{Signal power content in the output } S_o = \frac{A_c^2}{4}\overline{x_s^2(t)} \tag{7.81}$$

From Equation 7.78 and 7.81,

$$S_o/S_i = 1/2 \tag{7.82}$$

From Equation 7.80,

$$\text{the power content in noise output } N_o = \frac{1}{4}\overline{n_r^2(t)} \tag{7.83}$$

$$= \frac{1}{4}\overline{n^2(t)} \tag{7.84}$$

From Equation 7.77 and 7.84,

$$N_o/N_i = 1/4 \tag{7.85}$$

From Equation 7.52 and 7.55,

$$\frac{S_o/S_i}{N_o/N_i} = 2 \tag{7.86}$$

This is on par with what we obtain when the signal is directly transmitted without any modulation.

7.5.1.2 *Envelope Detection*

For the envelope detector to be effective, a dominant carrier is to be present in the demodulator output. With this *proviso*

$$\text{Modulated carrier output} = A_c[1 + mx_s(t)]\cos\omega_c t \tag{7.87}$$

where m is the modulation index.

$$\text{Power used in signal } S_i = \frac{1}{2}A_c^2\left[1 + m^2\overline{x_s^2(t)}\right] \tag{7.88}$$

$$\begin{aligned} \text{Added noise [Equation 7.26]} &= n(t) \\ &= n_r(t)\cos\omega_c t + n_i(t)\sin\omega_c t \end{aligned}$$

$$\text{Power content in noise} = N_i = \overline{n^2(t)} \tag{7.77}$$

$$\text{Input to demodulator} = A_c[1 + mx_s(t)]\cos\omega_c t + n_r(t)\cos\omega_c t + n_i(t)\sin\omega_c t \tag{7.89}$$

The envelope detector extracts the amplitude of the carrier at ω_c.

$$\text{Envelope detector output} = \left\{[A_c + mA_c x_s(t) + n_r(t)]^2 + [n_i(t)]^2\right\}^{1/2} \quad (7.90)$$

First, consider the case when the carrier amplitude is large compared to the noise levels.

$$i.e., A_c >> n_r(t) \quad (7.91)$$

$$\text{and } A_c >> n_i(t) \quad (7.92)$$

These justify the approximation of Equation 7.90 to

$$\text{Envelope detector output} = A_c + m A_c x_s(t) + n_r(t) \quad (7.93)$$

Power content in noise output

$$N_o = \overline{n_r^2(t)} = \overline{n^2(t)} \quad (7.94)$$

From Equation 7.77 and Equation 7.94[5]

$$N_o/N_i = 1 \quad (7.95)$$

From Equation 7.73, the power content in the received signal,

$$S_o = m^2 A_c^2 \overline{x_s^2(t)} \quad (7.96)$$

Note that the power content in the carrier proper *i.e.*, A_C is not useful. From Equation 7.88 and Equation 7.96

$$\frac{S_o}{S_i} = \frac{2m^2 \overline{x_s^2(t)}}{1 + m^2 \overline{x_s^2(t)}} \quad (7.97)$$

From Equations 7.95 and 7.97

$$\frac{S_o/S_i}{N_o/N_i} = \frac{2m^2 \overline{x_s^2(t)}}{1 + m^2 \overline{x_s^2(t)}} \quad (7.98)$$

For the Envelope detector to be useful, $|mx_s(t)| \leq 1$ always. For the extreme case when $|mx_s(t)| = 1$, Equation 7.68 becomes

$$\frac{S_o/S_i}{N_o/N_i} = 1 \quad (7.99)$$

Comparison with the corresponding figure in Equation 7.86 for DSB-SC shows that the envelope detector is inherently inferior in performance. In practical situations, the modulation levels used are much lower with further deterioration in performance.

The above analysis is valid only when the carrier level is large compared to the signal and noise levels. When this condition is not satisfied, the analysis is cumbersome. However, we may consider the other extreme case where noise dominates. Being an envelope detector, the envelope of the noise will be available as output. To obtain this, consider noise in the polar form

$$n(t) = R_n(t) \cos[\omega_c t + \phi_n(t)] \quad (7.100)$$

The received signal is

$$x_s(t) = A_c[1 + mx_s(t)]\cos \omega_c t \quad (7.101)$$

Since noise dominates

---

[5] N_o/N_i for the envelope detector is apparently different from that for DSB-SC. But this and similar differences in S_o/S_i are due to the different scales used for the demodulator outputs. The $[(S_o/S_i)/(N_o/N_i)]$ ratio normalizes these.

$$A_c[1 + m(t)] \quad << \quad R_n(t) \tag{7.102}$$

Hence, only the component of the received signal, in phase with the noise, contributes to the envelope.

$$\begin{aligned} \text{Envelope } E(t) &\approx R_n(t) + A_c[1 + mx_s(t)]\cos \phi_n(t) \\ &= R_n(t) + A_c \cos \phi_n(t) + A_c\, mx_s(t) \cos \phi_n(t) \end{aligned} \tag{7.103}$$

$\phi_n(t)$ is a random variable uncorrelated with the signal $x_s(t)$. Hence, $E(t)$ does not contain any component directly decipherable as the signal.

The foregoing analysis shows that one can detect the signal only if the carrier level exceeds a 'threshold' relative to the noise. If the carrier level is lower than the threshold level, the carrier and signal are not decipherable at the output. In contrast, the threshold effect is absent in synchronous detection (as with the DSB-SC case). Thus for relatively low signal levels, DSB-SC is superior in performance. At higher signal levels, envelope detector performs better but is inferior to the synchronous detector.

AM based instrumentation schemes mostly use synchronous detection. Envelope detection is used only when cost and simplicity are the governing criteria and high levels of performance are not expected.

7.5.2 Noise Performance of FM Systems

As with AM, the channel noise gets added to the modulator output. Considering the demodulator output

$$\text{Received signal} = A_c \cos\left[\omega_c t + k\int x_s(t)dt\right] + n_r(t)\cos\omega_c t + n_i(t)\sin\omega_c t \tag{7.104}$$

Consider the case $n_i << A_c$ and $n_r << A_c$; *i.e.*, when the received signal power is high compared to the noise power. The received signal phasor diagram is shown in Figure 7.23. Since n_i is small, its effect is only to shift the phase of the received signal by $[n_i/(A_c+n_r)]$. The amplitude remains practically unaffected at $(A_c + n_r)$. The detector can be taken as insensitive to the received amplitude changes.

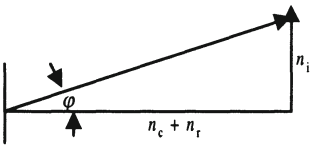


Figure 7.23 Phasor diagram of FM received signal when $n_i << A_c$

$$\begin{aligned} \text{Received phase angle} &= \frac{n_i}{A_c + n_r} + k\int x_s(t)dt \\ &\approx \frac{n_i}{A_c} + k\int x_s(t)dt \end{aligned} \tag{7.105}$$

since $n_r << A_c$.

Differentiating the right hand side of Equation 7.105 with respect to t, we get

$$\text{Instantaneous frequency deviation} = \frac{1}{A_c}\frac{dn_i}{dt} + kx_s(t) \tag{7.106}$$

$$S_o = k^2 \overline{x_s^2(t)} \tag{7.107}$$

$$S_I = \frac{A_c^2}{2} \tag{7.108}$$

$$\therefore \frac{S_o}{S_i} = \frac{2k^2 \overline{x_s^2}}{A_c^2} \tag{7.109}$$

Equation 7.106 shows that the demodulator modifies the noise component of output due to the term dn_i/dt. This is equivalent to multiplying the noise power density at any frequency ω by ω^2. Let the signal cut-off frequency be ω_0 and noise power-density η – as a flat white noise spectrum.

$$\text{Output noise spectral density} = \frac{\eta\omega^2}{A_c^2} \tag{7.110}$$

$$\text{Total noise output power } N_0 = \frac{\eta}{A_c^2}\int_{-\omega_0}^{+\omega_0} \omega^2 d\omega$$

$$= \frac{2\eta\,\omega_0^3}{3A_c^2} \tag{7.111}$$

Total noise input power in the $-\omega_0$ to $+\omega_0$ band

$$N_i = 2\omega_0\eta \tag{7.112}$$

From Equations.7.111 & 7.112

$$\frac{\text{Output noise power}}{\text{Input noise power}} = \frac{2\eta\,\omega_0^3}{3A_c^2} \times \frac{1}{2\omega_0\eta}$$

$$= \frac{\omega_0^2}{3A_c^2} \tag{7.113}$$

$$\therefore \frac{S_o/S_i}{N_o/N_i} = \frac{2k^2 \overline{x_s^2(t)}}{A_c^2} \times \frac{3A_c^2}{\omega_0^2}$$

$$= \frac{6k^2 \overline{x_s^2(t)}}{\omega_0^2} \tag{7.114}$$

k represents the deviation ratio – frequency deviation / signal bandwidth. Signal to noise performance of the FM scheme is directly related to it. For a given band-limited signal, an increase in the modulated bandwidth improves the signal to noise ratio as the square of the bandwidth used. This is valid as long as the carrier power level is high compared to the noise power. In effect, this implies that we can improve system performance with FM as much as desired. A bandwidth versus signal to noise trade-off is possible with FM which is not possible with the AM schemes.

Analysis of the case where the signal power is not high compared to noise power is much more involved. However, we can have a qualitative look at the other extreme case of high noise level.

$$\text{Received signal + noise} = A_c \cos[\omega_c t + k\int x_s(t)dt] + n_r \cos\omega_c t + n_i \sin\omega_c t \tag{7.115}$$

Using the polar form of representation of noise, we get

$$\text{Received signal + noise} = A_c \cos[\omega_c t + k\int x_s(t)dt] + R_n(t)\cos[\omega_c t + \phi_n(t)] \quad (7.116)$$

If $R_n(t) >> A_c$, from the Phasor diagram of Figure 7.24 we have

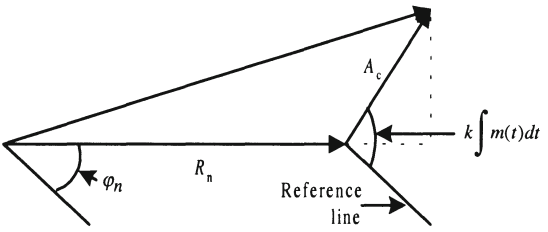


Figure 7.24 Phasor diagram of FM received signal when $R_n >> A_c$

$$\text{Received signal + noise} = R_n \cos\left[\omega_c t + \phi_n(t) - \frac{A_c \sin[k\int x_s(t)dt - \phi_n(t)]}{R_n(t)}\right] \quad (7.117)$$

$$\text{Received instantaneous phase angle} = \phi_n(t) - \frac{A_c \sin[k\int x_s(t)dt - \phi_n(t)]}{R_n(t)} \quad (7.118)$$

Differentiation of the right hand side of Equation 7.118 yields the received signal. The received signal does not have any explicit component that can be identified with the original modulating signal. We can see a threshold effect with FM also. If the received signal to noise ratio is below a threshold level, the signal is absent in the output. However, for signal power well above the threshold, the performance of the system can be superior to the AM case.

Observations: -

- ⇒ With FM, every doubling of the bandwidth used improves system performance by a factor of four. This is true of wideband FM.
- ⇒ With narrowband FM, the bandwidth used is of the same order as that with AM. The performance is also on par. The changeover to wideband FM occurs at a modulation index of around 0.6.
- ⇒ The modulation process alters the noise power-density spectrum. Components farthest from the zero frequency are given maximum weight. Most instrumentation signals are characterized by a spectrum centred around zero frequency. The components at higher frequency levels (noise and vibration can be exceptions) are much lower in amplitude. One can fruitfully do pre-emphasis before modulation and de-emphasis after demodulation. With this, the feeble higher frequency components are given a boost and more faithfully reproduced. This improves system performance by a definite extent.
- ⇒ With signals of the type encountered in instrumentation schemes – where the power is more concentrated near the zero frequency than at the bandwidth edge – phase modulation performs better than FM. This is because with phase modulation, the noise power-density is not given the weight by ω^2

[Equation 7.110]. Despite this, phase modulation is not in wide use in instrumentation schemes.

8 Analog-Digital Interface

8.1 Introduction

Process variables, with few exceptions, are continuous by nature. Instrumentation schemes convert them into equivalent signals and provide corresponding continuous outputs. Many simple instrumentation schemes still conform to this structure – an analog sensor, analog signal processing, analog output and an analog display. Here 'Signal Processing' essentially implies amplification and filtering (and of course, the other analog processing activities like linearization, non-linearization, multiplication and normalizing which are not so common). The developments in the digital arena in the recent years, have ushered in a radical shift in the approach to the design of instrumentation schemes. The signal is converted into a digital form; it is stored, processed, retrieved and displayed in digital form in a variety of ways. The major factors contributing to this and the benefits perceived are: -

- ⇒ 8 and 16 bit microprocessors and microcontrollers have become widely available at low prices
- ⇒ Standardized hardware blocks and software modules, aid design and development work.
- ⇒ A variety of configurations that are easily changeable and upgradable, is possible.
- ⇒ 12 bit ADCs and DACs offering up to almost 0.01 % resolution, have become industrial standard.
- ⇒ A variety of digital processing is possible. Some of them like linearizing and filtering may improve the performance of instrumentation schemes by one order. Others like FFT and pattern recognition add new dimensions to the use of instrumentation schemes.
- ⇒ Different display systems and formats have become common place. Many instrumentation schemes use these beneficially.
- ⇒ Intelligence, logging and their judicious use make instrumentation schemes powerful tools.
- ⇒ User friendliness is often touted as a benefit or a plus feature.

Incorporation of digital functions into the essentially analog domain of instrumentation schemes, call for proper interfaces. Analog to Digital Converters (ADCs) and Digital to Analog Converters (DACs) play these pivotal roles. Their requirements, characteristics, specifications and circuit schemes form the main subject matter of this chapter.

T. R. Padmanabhan, *Industrial Instrumentation*
© Springer-Verlag London Limited 2000

8.2 Signal Conversion – Basics

Conversion of the analog signal into its equivalent digital form, is a two-step process – 'Sampling' and 'Quantization'. Sampling is the process of preparing a time sequence of analog voltages representing the continuous signal. Quantization is the conversion of each such sample into a corresponding number. In the analog-to-digital interface, the continuous signal is sampled and the sampled sequence quantized and converted into equivalent digital form. In the digital-to-analog interface, a sequence of numbers is converted into equivalent analog samples. From the sample sequence, the original signal or one of its variants can be reconstructed.

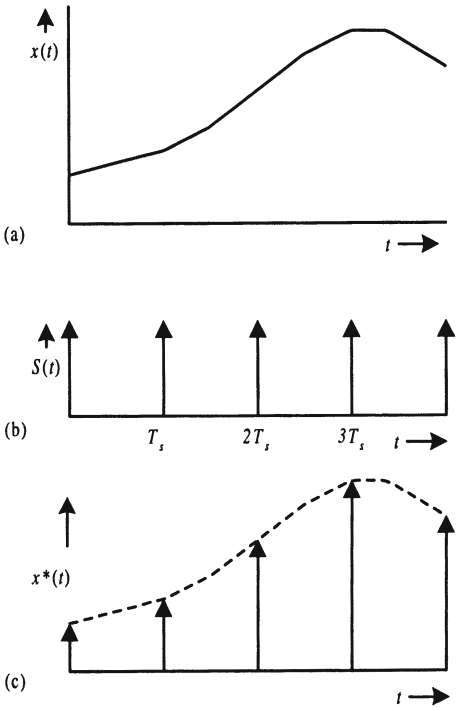


Figure 8.1 Sampling process; (a) Signal waveform (b) Waveform of the sampling signal (c) Waveform of the sampled signal

8.2.1 Ideal Sampling

Consider a signal $x(t)$ varying with time. If it is multiplied by the unit impulse function $\delta(t-\alpha)$ as in Figure 8.1, we get the value of $x(\alpha)$. Theoretically, this represents the process of sampling. For our purposes, the signal is to be sampled at regular intervals. Such a regularly sampled sequence has to retain all the information in the signal. Consider the periodic unit impulse train

$$S(t) = \sum_{-\infty}^{+\infty} \delta(t - nT_s) \tag{8.1}$$

If the signal is multiplied by this periodic unit impulse train, we get the ideal sampled output of the signal shown in Figure 8.1c.

If $F_s(\omega)$ represents the Fourier series of the unit impulse train, we have

$$F(\omega) = \sum_{n=-\infty}^{+\infty} C_n e^{[+j2n\pi/T_s]} \tag{8.2}$$

where

$$C_n = \frac{1}{T_s}\int_{-T_s/2}^{+T_s/2} S(t)e^{[-j2k\pi/T_s]}dt \tag{8.3}$$

Thus, the unit impulse train is equivalent to a Fourier series function with all the harmonics of equal amplitude. Consider $x(t)$ to be a band limited signal of bandwidth ω_m. Multiplication by a sinusoidal periodic signal of frequency ω_c is equivalent to amplitude modulation by a carrier at frequency ω_c [See Section 6.2]. Multiplication of $x(t)$ by the unit impulse train, is equivalent to modulating it simultaneously by a sinusoidal carrier at frequency ω_c, another at frequency $2\omega_c$, yet another at frequency $3\omega_c$ and so on and then adding all the modulated outputs. The frequency spectrum of such a modulated output is a periodic repetition of the base band spectrum. In short, in the sampled output, the baseband spectra extending from frequency 0 to ω_m, is repeated to the same scale at regular frequency intervals of ω_c. Figure 8.2 shows the spectra.

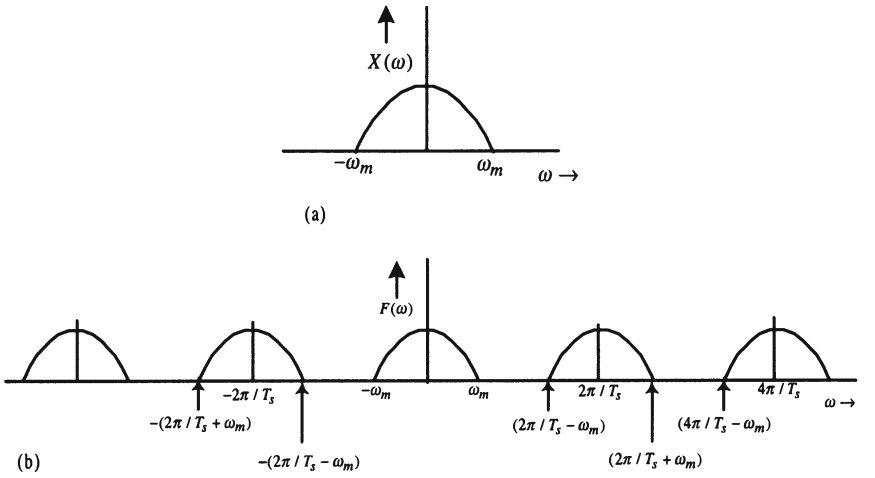


Figure 8.2 Spectral change brought about by sampling: (a) Signal spectrum (b) Spectrum of the sampling signal

Observations: -

⇒ The base band signal is repeated around every harmonic of the sampling frequency. These modulated bands appear with the same power levels at every harmonic. Thus, the bandwidth of the sampled signal is infinite.

⇒ The base band spectrum extends up to ω_m (in the positive direction). The band around the sampling frequency ω_c extends down to $\omega_c - \omega_m$. To avoid signal corruption, it is essential to ensure that $(\omega_c - \omega_m) > \omega_m$ or

$$\omega_c > 2\,\omega_m \tag{8.4}$$

This is the well-known 'Sampling Theorem' – *i.e.*, the sampling frequency has to be at least twice the maximum frequency of interest in the signal [Carlson].

In case the signal contains spectral components at frequencies above $\omega_c/2$, the error caused by these, is called the 'aliasing error'. Before sampling, the base band signal has to be band limited using an 'Anti-aliasing Filter'. Consider the base band spectrum and the spectrum around ω_c. In Figure 8.3, ABCD represents the signal spectrum. The useful signal components extend up to B. Due to the presence of the Anti-aliasing filter, the signal components are attenuated and the spectral amplitudes fall off as BCD. Due to the sampling process the spectra is repeated around ω_c (It appears as EFCG. At the frequency $\omega_c/2$, the two are equal). At frequency ω_m, the aliasing error component due to the spectra around ω_c, is GH.

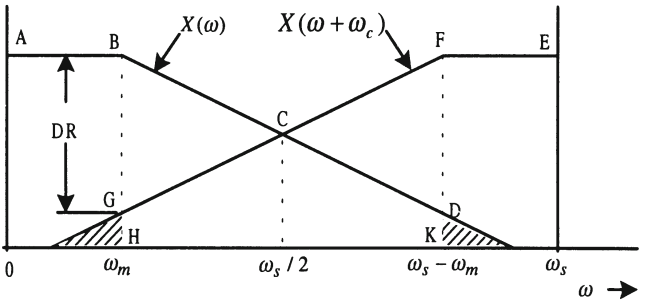


Figure 8.3 Aliasing error due to sampling and the dynamic range

This has to be below the permissible error limit. With 12 bit resolution, this is 0.012 %. The range BG is the 'Dynamic Range'. The dynamic range is such that the attenuation of the anti-aliasing filter from ω_m to $(\omega_c - \omega_m)$, has to be 0.012 % or 20 log 2^{13} = 78 dB minimum. The ω_c/ω_m ratio and the minimum order of filter required in each case to maintain accuracy, are related as

$$n \geq \frac{\log[(\omega_c/\omega_m)-1]}{0.301(k+1)} \tag{8.5}$$

where k is the number of bits in the ADC. The smallest integer satisfying the inequality 8.5, is the value of n. For the example considered, the values of n for representative values of ω_c/ω_m are shown in Table 8.1

Table 8.1 Number of stages required for the anti-aliasing filter for a 12-bit system for different values of ω_c/ω_m

ω_c/ω_m	3	4	6	10
n	13	9	6	5

Observations: -

⇒ Although the ideal sampling frequency is only twice the signal bandwidth, in practice it has to be much larger.

⇒ Figure 8.4 shows the relation between the minimum ω_c/ω_m and the number of filter stages required to be used for the anti-aliasing filter for different dynamic ranges. In general, for a given dynamic range, as ω_c/ω_m is reduced, n increases rapidly.

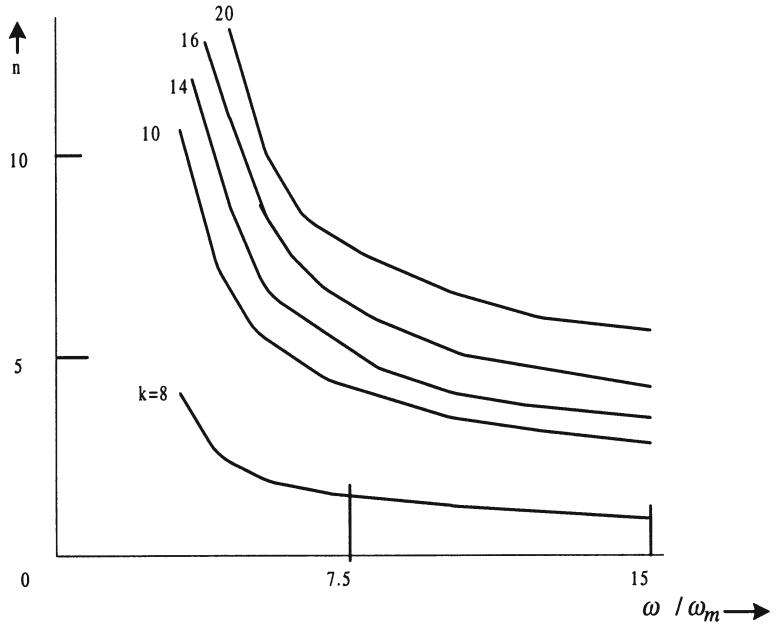


Figure 8.4 Number of minimum stages of the filter required for different sampling frequencies to realize the required dynamic range for the signal. Normalized signal frequency is the x-co-ordinate. k—where 2k is the dynamic range—is the running parameter.

⇒ Most practical instrumentation signals are characterized by lower spectral component levels close to the band limit of ω_m as well as reduced accuracy requirements for such components. These make the anti-aliasing filter requirements less severe.

⇒ Communication systems require the amplitudes of the spectral components to be reproduced faithfully but not the phase characteristics. Elliptic filters with their sharp cut-off characteristics (though with poor phase response), are well suited here and are in wide use. In contrast, instrumentation schemes require the amplitude and the phase characteristics of the signal to be reproduced faithfully. The Bessel filter is better suited here. Due to its comparatively lower cut-off rate (See Sections 5.4 & 5.5), a higher order filter than that with a communication system, has to be used.

⇒ From the above, we see that we have a clear trade off between conserving bandwidth and anti-aliasing filter complexity. Instrumentation schemes are characterized by only (mostly) one signal being processed in a 'channel'. As such, the bandwidth conservation does not appear to be a direct need. However, any increase in the sampling frequency ω_c, entails the use of a correspondingly faster ADC and faster digital system. As discussed subsequently, these are sufficiently challenging design-wise and cost-wise.

8.2.2 Practical Sampling

The ideal sampler senses the signal at the sampling instant. Any spike noise that corrupts the signal at the sampling instant, can distort the sample value (Of course the anti-aliasing filter is expected to filter out such noise). The fact that $\omega_c > 2\omega_m$, ensures that the signal remains sensibly constant between two successive sampling instants. However, the noise spike can appear between the filter output and the sampler itself. Different measures can be adopted to avoid such errors. One common and simple method is to use a rectangular sampling pulse (in place of the ideal sampler). The rectangular periodic pulse train for sampling as in Figure 8.5 (a) has the same Fourier series as in Equation 8.2.

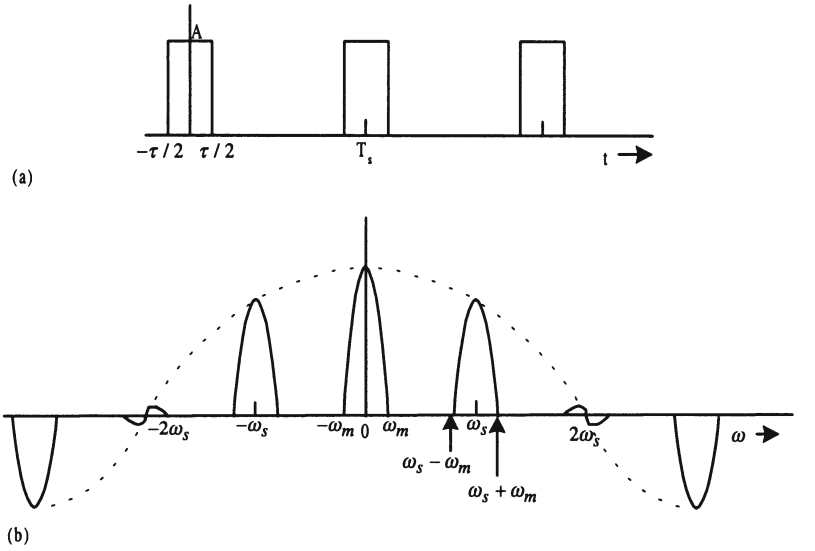


Figure 8.5 Modulation with a rectangular pulse train (a) Waveform of the pulse train (b) Frequency spectrum of the pulse train

For C_n we have the relation

$$C_n = \frac{A\omega_c}{2\pi}\int_{-\tau/2}^{+\tau/2}\exp(-jn\omega_c t)dt$$

$$= \frac{A}{n\pi}\sin\frac{n\omega_c\tau}{2} \tag{8.6}$$

where

$$\omega_c = \frac{2\pi}{T_s} \tag{8.7}$$

Sampling with the periodic pulse train is equivalent to simultaneous modulation with a series of sinusoidal carriers – one with a fundamental frequency of ω_c and the others as its harmonics. Amplitudes of the modulated spectra around the harmonics reduce with the order of the harmonic. The envelope of the harmonics as well as that of the spectra, is a sinc function (of the form $\sin/x$). When the signal is

sampled with the rectangular pulse train, its spectrum appears as in Figure 8.5 (b). Bandwidth requirements of the signal processing stages following the sampler are decided by the bandspread of the sampled signal; hence, it is desirable to conserve this bandspread by a proper choice of the sampling function. Window functions like the 'Triangular window', 'Gaussian window', 'Hanning window', *etc.*, are used as sampling functions [See Section 9.3] to bring about such bandwidth conservation. However, such 'shaped sampling' is not warranted *vis-à-vis* instrumentation schemes, on two counts: -

⇒ Using a carefully shaped sampling pulse is too much involved to be cost-effective.

⇒ Whenever a sampler is used in an instrumentation scheme, it is followed by an ADC, physically very close to it. Often the two are realized in the same IC. Since no signal processing is involved in between, no serious bandwidth constraint comes into picture,

Another measure commonly employed to reduce 'spike error' is to smooth out the sample. The sampled pulse is integrated over the sampling period and the integrated average used as the sample value. This reduces the spike errors substantially. The integrator provides another level of first order filtering of the spectra. This reduces the higher frequency spectral components further.

8.2.3 Quantization

Quantization is the process of converting an analog sample into an equivalent digit. For the present, the 'quantizer' is treated as a black box receiving the analog sample as input and giving out a corresponding number as output. Figure 8.6 shows a simple case by way of illustration. The input to the quantizer can take any value from –1.5 V to + 1.5 V. The output has three states namely –1, 0, and +1. For input in the range OA (*i.e.*, 0 to 0.5 V), the output is at zero level. For input in the range C to E (*i.e.*, 0.5 V to 1.5 V), the output is at 1 level. Similar relationship holds good for the negative side as well.

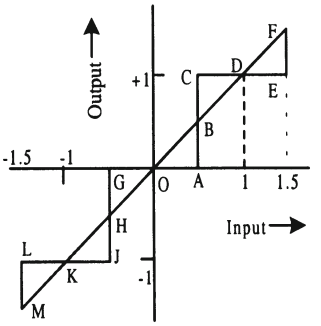


Figure 8.6 Illustration of quantization

Observations: -

⇒ Only at three points namely K, O and D do the input and output match; the conversion error is zero at these points.

⇒ At points F, B, H and M, the conversion error is a maximum and equal to 0.5 V.

⇒ The step size for conversion is one here. The maximum quantization error is 0.5.

⇒ Alternately we could have arranged the output to be 0 for all inputs from zero to one; 1 for inputs from one to two and so on. Here the quantization error is 1.

The arrangement shown in Figure 8.6 has the minimum quantization error. In the general case, if q is the quantum step size, the maximum quantization error is $q/2$. With a total of N steps and quantization level of q, the analog input range covered is Nq. Since the quantized output is used in binary form, it is customary to have N as a power of two.

$$2^k = N \tag{8.8}$$

$$\text{Quantizer range} = Nq \tag{8.9}$$

$$\text{Maximum quantization error} = q/2 \tag{8.10}$$

$$= (100q/2Nq)\%$$

$$= (50/N)\%$$

$$= 50\times 2^{-k}\ \% \tag{8.11}$$

k versus the maximum quantization error is shown in Table 8.2. Low-end instrumentation schemes use k = 8. Most use k = 10 or 12. Only very precise schemes use higher values of k.

Table 8.2 k versus maximum quantization error

k	6	8	10	12	16	18	20	22
Maximum quantization error	0.78 %	0.2 %	0.05 %	0.012 %	7.6 ppm	2 ppm	0.5 ppm	0.12 ppm

A pure sinusoidal test waveform, the corresponding quantized output and quantization waveforms are shown in Figure 8.7. The quantization error is a serrated wave; It is distributed over the range $-q/2$ to $+q/2$. For normal signals (which are not necessarily as orderly as a pure sine wave) and a large number of quantized steps, the quantization error is taken as uniformly distributed in the range $-q/2$ to $+q/2$. It is random and uncorrelated to the input and hence appears as noise. The amplitude density distribution of the quantization error is as shown in Figure 8.8. The mean square value of the quantization noise n_q is given by

$$\overline{n_q^2(t)} = \int_{-q/2}^{+q/2} \frac{x^2}{q}\,dx \tag{8.12}$$

$$= \frac{q^2}{12} \tag{8.13}$$

$$\text{rms. value of quantization error} = \frac{q}{\sqrt{12}} \tag{8.14}$$

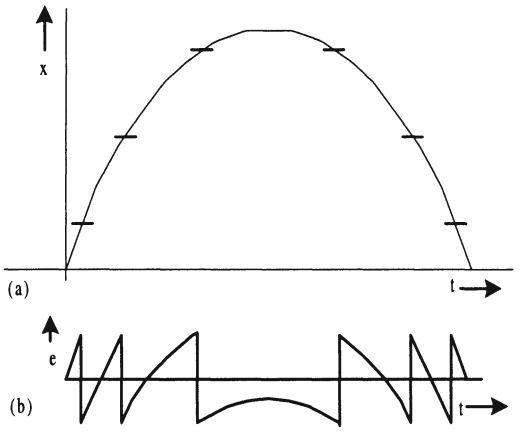


Figure 8.7 (a) Sinusoidal signal and (b) corresponding quantization error waveform

The power in the quantization error is distributed over a wide frequency range. For sinusoidal test signals and comparatively smaller number of quantum levels, the spectrum tends to crowd around the harmonics of the test signal. Otherwise the spectra are evenly distributed over a wide frequency range and appear as uncorrelated white noise. Being uncorrelated, its mean square value can be directly added to the mean square value of other noise to get total effective noise.

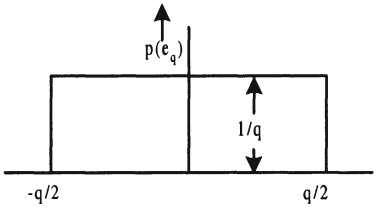


Figure 8.8 Amplitude density distribution of quantization error

8.2.4 Signal Reconstruction

We have seen that the sampled sequence retains the full signal information in the base band. The same is also repeated around the sampling frequency and each one of its harmonics. Two approaches of signal recovery are possible: -

⇒ The sampled sequence is passed through a low pass filter with cut-off frequency ω_m. This passes all the baseband frequency components but filters out the rest. The cut-off rate has to be high enough to ensure that the neighbouring band spectra around the frequency ω_c are filtered out. ω_c - ω_m being the lowest frequency of this interfering spectrum, it is enough to ensure sufficient attenuation at this frequency.

⇒ The spectra centred around ω_c, may be used for signal extraction. For this, the sample sequence may be multiplied by a carrier at frequency ω_c itself; *i.e.*, the sampled sequence may be sampled again at ω_c. As we have seen in Section 6.2.1, this reproduces the baseband signal itself. Again, it can be

extracted by a low pass filter. This procedure is adopted with chopper amplifiers [See Section 6.2.1] but not so common with sampling schemes.

Direct sampling of samples yields low signal levels. The signal output level is improved by using a hold circuit. A 'Zero-Order Hold' is the most common. It 'captures' the sample and holds its value until the next sample. Figure 8.9 shows the zero-order hold circuit in block diagram form. Its impulse response as well as the input and output waveforms for a typical signal, are also shown in the figure.

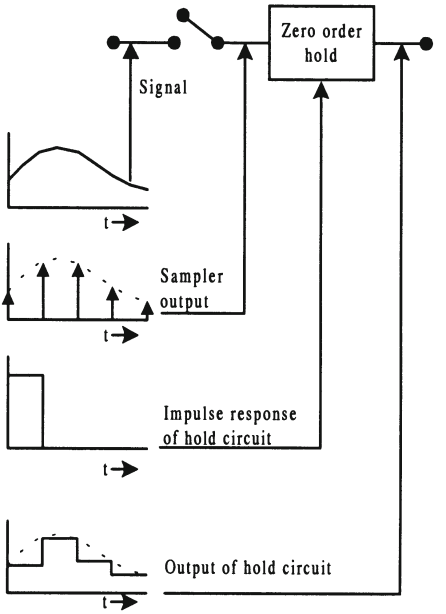


Figure 8.9 Sampler with zero—order hold

The transfer function of a zero-order hold – $H(s)$ – is obtained by taking the Laplace transform of the impulse response. We get

$$H(s) = \int_0^{T_s} \exp[-st]\,dt$$

$$= \frac{1-e^{[-sT_s]}}{s} \tag{8.15}$$

Where T_s is the sampling period. Substituting $s = j\omega$ in Equation 8.15 and simplifying we get

$$H(j\omega) = T_s \exp\left(-\frac{j\omega T_s}{2}\right)\text{sinc}\left(\frac{\omega T_s}{2}\right) \tag{8.16}$$

Observations: -

⇒ The gain of a zero order hold reduces from unity at zero frequency to zero at the sampling frequency *i.e.*, at ω_c.

⇒ Successive frequency bands of the sampled signal are passed through with successively decreasing amplitudes. However, the cut-off is slow.

⇒ The gain is not constant in the pass band from 0 to ω_m. To this extent, the signal is distorted. But as long as $\omega_m << \omega_c$, the reduction in gain is negligible.

⇒ The phase shift varies linearly with frequency. This is a desirable characteristic.

⇒ Use of higher order holds improves performance but at the expense of circuit complexity.

The scheme to convert the quantized data available in digital form into equivalent analog signal, is shown in block diagram form in Figure 8.10. The quantized data will be available as a time sequence at a digital port. The port provides the digital output through a set of logic lines - each line representing a bit. At one end we have the LSB b_0 and at the other end the MSB b_n. At any time, the port will hold these bits of data in a set of dedicated registers. These will remain valid until the next

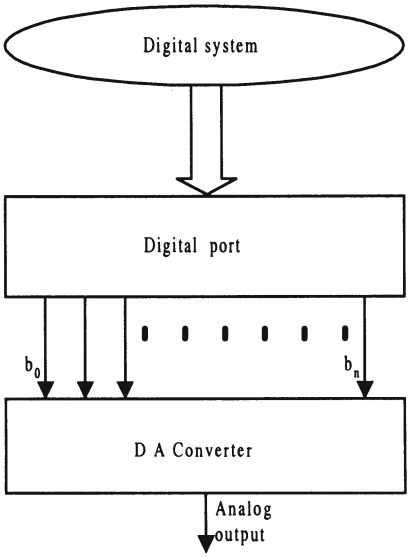


Figure 8.10 Scheme to convert the output of a digital system into equivalent analog form

digital data is written into the port by the digital system. Normally the DAC converts the digit into equivalent analog form directly. Once a digital data is loaded into the port, it is available in converted analog form at the DAC output (with a delay, the propagation delay time of the DAC). This output remains until the next digital data is loaded into the port and converted. Thus, the zero-order hold function is inherent in the conversion scheme. Figure 8.11 shows the relevant waveform. The possible step changes at regular loading instants, cause an output jitter at the sampling frequency. It can be eliminated by introducing a filter at the DAC output. Normally a first order filter suffices for this.

The filtered output from the DAC – though smooth enough – departs from the expected continuous analog signal. The difference is essentially due to filtering out the signal components beyond the frequency ω_m in various stages. This difference can be made negligible by proper design.

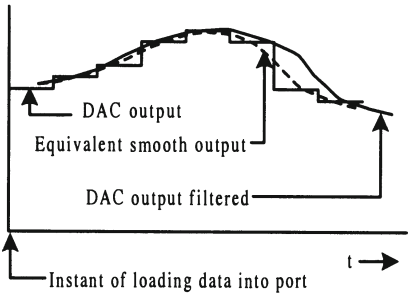


Figure 8.11 Actual and filtered outputs from the digital system

8.3 Sampling Hardware

Analog to digital conversion is mostly preceded by sampling and holding. Often the ADCs handle more than one analog signal simultaneously. This is achieved through multiplexing. The analog switch is central to the operation of all these. Similarly, DACs may employ demultiplexers to sift out signals to individual channels. These too are configured around analog switches.

8.3.1 Analog Switch

An ideal analog switch (See Figure 8.12) provides a zero impedance path between its input A and output B when in the on-state. The impedance is infinite when the switch is in the off-state. The changeover from one to the other state is by the control input given at C. Normally a TTL or CMOS input decides this. If the analog switch is BJT based, its on-state saturation voltage – V_{sat} – gets added in series with the signal. By a judicious use of multiple transistors in series, this may be compensated. The R_{on}/R_{off} ratio of BJT based analog switches, is of the order of 10^8. In general, BJT based analog switches use comparatively involved circuitry. These are suited for very high speed applications but not commonly used in instrumentation schemes.

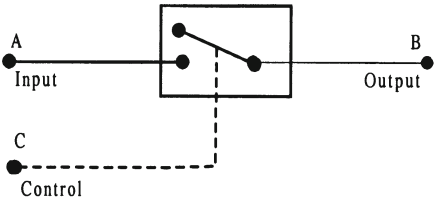


Figure 8.12 Ideal analog switch

FET based analog switches perform better than BJT based analog switches in many respects. The FET switch needs a level shifter and does not provide any isolation between the analog signal and the control signal (Neither does a BJT based switch provide such an isolation). A MOSFET switch scores on both counts.

A p and an n channel MOSFET pair connected in 'anti-parallel' fashion as shown in Figure 8.13 (a), has become the widely used analog switch. Its control is done through a complementary CMOS gate. This configuration is easy of fabrication and is universally adopted.

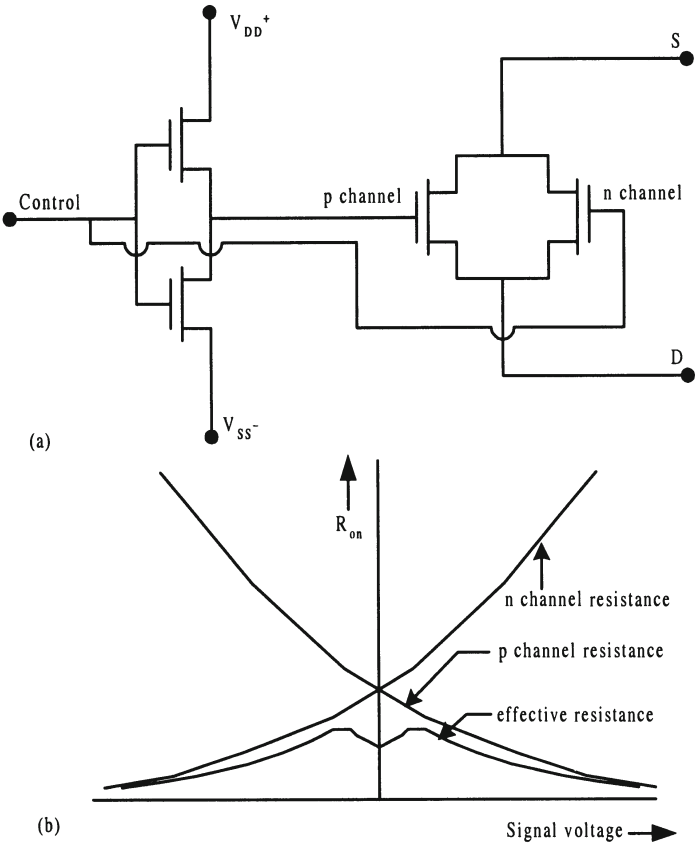


Figure 8.13 (a) Complementary MOSFET-based analog switch and (b) its on-resistance characteristic

A logic-high input turns on the n and p channel MOSFETs simultaneously. The MOSFETs function as controlled resistances in both directions. The on-resistance of the MOSFETs change with the signal level as shown in Figure 8.13 (b). The n channel resistance is low for negative signals and increases for positive signals. The p channel resistance is high for negative signals but decreases for positive signals. The effective parallel resistance of the two varies much less. The R_{off} of the individual MOSFETs, is in the 10^{10} Ω to 10^{12} Ω range. The off-resistance of the parallel combination, though less, remains in the same range.

The effective on-resistance is a function of the control voltage – the higher the voltage level, the lower the resistance. Whenever possible, the analog switch is operated at the highest possible control voltage. Being channel resistances, the R_{on}s increase with temperature. The effective resistance of the parallel combination also increases with temperature. Throughout the operating temperature range as well as

the signal range, R_{ON} remains in the 20 Ω to 100 Ω range. The basic analog switch is prone to latch-up under abnormal operating conditions; by care in design and use, these are avoided.

8.3.1.1 Specifications of Analog Switches

Normally, a number of analog switches are housed in the same package. The simplified functional equivalent circuit of one is shown in Figure 8.14. An adjacent one is also shown to bring out the coupling between the two.

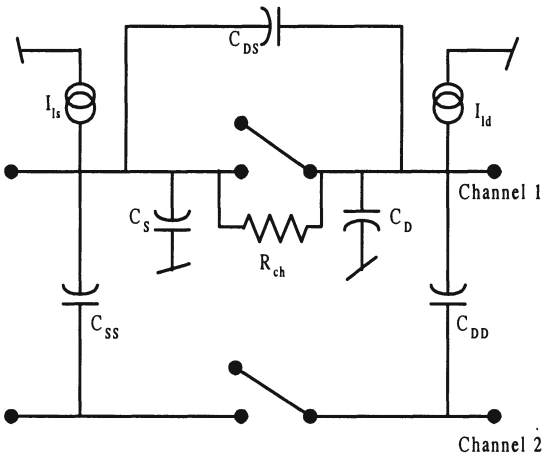


Figure 8.14 Equivalent circuit of analog switch

The various parameters of the equivalent circuit shown, are as follows: -

- ⇒ R_{ch} is the channel series resistance. It is in the 20 Ω to 100 Ω range for the whole operating range of the switch.
- ⇒ C_{DC} is the input to output coupling capacitance – typically 1pF.
- ⇒ C_s is the input to ground capacitance – typically 10 pF.
- ⇒ C_D is the output to ground capacitance – typically 10 pF.
- ⇒ C_{SS} is the coupling capacitance between the two inputs – typically 0.5pF.
- ⇒ C_{DD} is the coupling capacitance between the two outputs – typically 0.5 pF.
- ⇒ I_{ls} is the equivalent leakage current at the input.
- ⇒ I_{ID} is the equivalent leakage current at the output.
- ⇒ I_l is the total leakage current associated with each analog switch.

Observations: -

- ⇒ When the analog switch is in the on-state, only the effective R_{on} and I_l are in the picture. The effect of I_l can be reduced by operating the channel at a low signal level. The effect of R_{on} can be reduced by keeping the load resistance high compared to it. If the error due to R_{on} is to be kept < 0.02 %, $R_L > 5000\ R_{on}$; *i.e.*, R_L has to be greater than 500 kΩ.
- ⇒ The off-channel coupling of input to output, cross-talk, bandwidth, rise and fall times, propagation delays *etc.*, depend on the application concerned. These are dealt with later.

⇒ Apart from sampling and multiplexing, analog switches find application in programmable gain amplifiers, active filters with adjustable cut-off frequency *etc.*

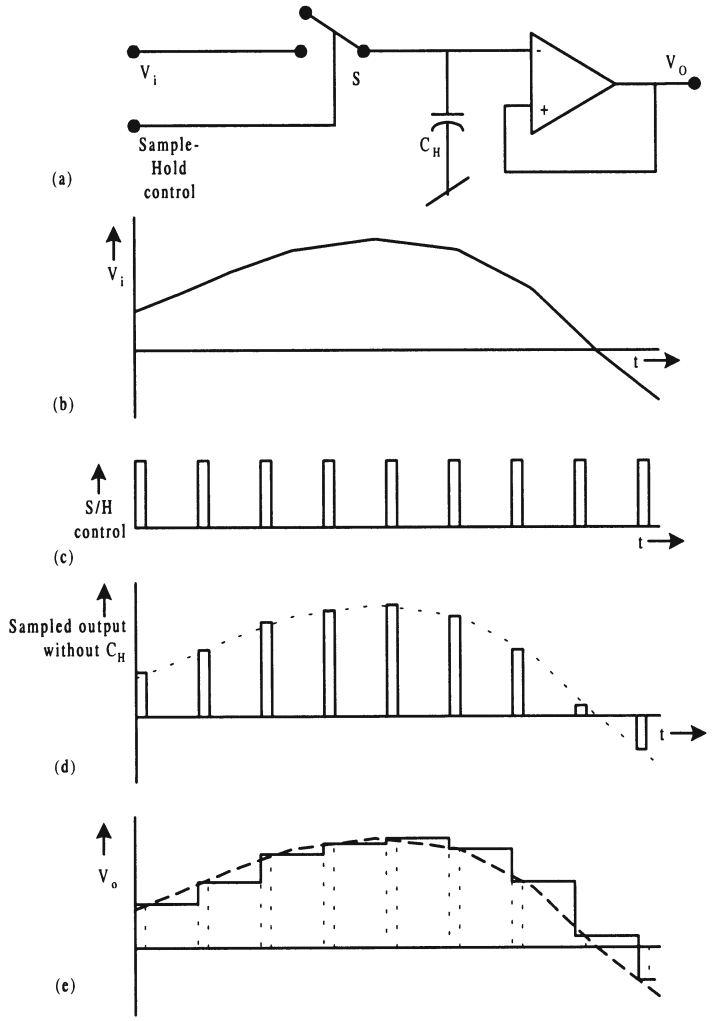


Figure 8.15 Sample-hold operation: (a) Circuit (b) Input signal (c) Sample-hold control signal (d) Sampled output in the absence of the Hold-capacitor (e) Output

8.3.2 Sample and Hold Operation

In an ADC the input is to be held steady during (or at least the in the final part of) the conversion. This ensures accuracy. The sample and hold circuit serves this function. It also ensures that the sampling is carried out at a specific and desired instant of time. The sampler samples the analog input and transmits it to the output

side. Here it is held at the same level throughout the following ADC operation or (if necessary) until the next sample is taken. Figure 8.15 shows an ideal sample-and-hold circuit along with the signal and control waveforms. V_i and V_o are the analog input and the sample-and-hold output respectively. S is the analog switch and C_H the hold capacitor. When S is on, V_i appears across C_H and also as V_o after buffering. When S turns off, C_H retains the charge and hence is at the signal level at the end of sampling. This is retained until S turns on, for the next sampling. V_o is a replica of the voltage across C_H. A number of errors arise in the operation of the sample and hold circuit due to the departures from the ideal conditions described here. Such errors occur for the four states of the circuit – namely: -

⇒ Hold to sample transition
⇒ Sample interval
⇒ Sample to hold transition and
⇒ Hold interval.

8.3.2.1 Hold to Sample Transition Errors

Following a sample command, the sampled and held value changes from the previously held V_o, to the new input value. A typical transient waveform associated with this transition is shown in Figure 8.16. This is for the case when V_i has increased conspicuously from the previously held value. The initial rate of rise of V_o is limited by the charging time constant of C_H and the series combination of the source resistance and the R_{ON} of the analog switch. The slew rate of the buffer also contributes to this. The voltage may overshoot the final value and settle after some amount of ringing. The final value may differ from the desired V_i level. The sample-hold output may be considered as settled when V_o enters the allowable error band finally (Point P). The allowable error band is decided by the resolution of the ADC. For a 12 bit ADC, it is 0.025 % (1 in 2^{12}). Normally the sample-hold settling is specified in terms of the 'Acquisition Time'. It is the time taken for V_o to settle to the final value following a change in input from minimum to maximum specified value. Thus, if the ADC range is 0 to 5V, the acquisition time is the time to settle within the allowable error band following an input change from 0 to 5V. The circuit output can be taken as valid only after the delay of acquisition time. Acquisition time is the major sample-hold error. It is strongly dependent on the value of C_H.

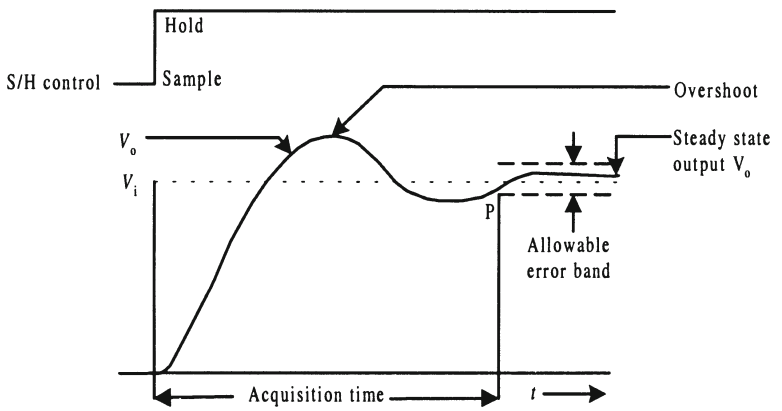


Figure 8.16 Sample-hold output following a 'Sample-command'

Even if Vi has not changed, V_o may experience a transient following a sample command – mainly due to the charge injection from the analog switch during turn-on. But these transients die down much faster and their duration is negligible compared to the acquisition Time.

8.3.2.2 Sample Errors

During the sampling interval, V_o follows V_i, thanks to the buffer. In practice, one may use the buffer or one of the amplifier configurations. All possible errors associated with them manifest as sample errors [See Sections 3.4 & 4.8]: -

- ⇒ *Gain Error*: This may be due to the difference in gain deciding resistances due to their tolerance. Gain error is typically 0.001 %. If necessary it may be adjusted or trimmed by a calibration procedure prior to sampling.
- ⇒ *Linearity Error*: This is due to the output not-following the input in a linear fashion. Common mode errors of buffers and non-inverting amplifiers are typical causes.
- ⇒ *Offset Error*: The offset in V_o with V_i grounded. The offset may be mainly due to the opamp and its amplifier configuration used. Normally the offset error may be neutralized by a (automatic) calibration procedure.
- ⇒ *Offset drift Error*: Drift in V_{os} due to ambient temperature changes, is the main cause of this. Offset may be compensated during calibration; but such compensation requires sufficiently frequent and cyclic calibration.
- ⇒ *Settling Time Error*: The sample-hold circuit has to remain in sample mode long enough to allow the sampling transients to settle (Acquisition Time). Too short a sampling time (small window width) may cause an error.

8.3.2.3 Sample to Hold Transition Errors

When the command changes from 'Sample' to 'Hold', sample-hold circuit is expected to hold the value of the signal at the immediately preceding level. In practice, there is a delay between the command and the compliance. This is the 'Aperture Delay Time'. Any change in the signal during this time interval causes an error (See Figure 8.17). If the aperture time is a constant, the hold command may be

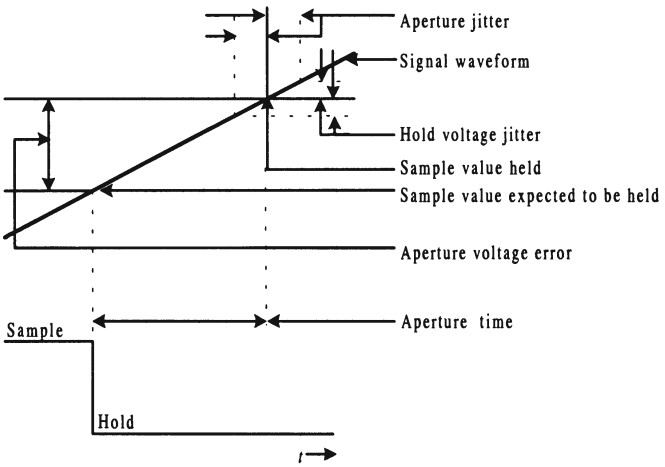


Figure 8.17 Sample-hold transition errors

advanced by this time interval and the error nullified. However, a fraction of the aperture time is indecisive. It is called the 'Aperture jitter', since it appears as a random jitter in the aperture time.

Change in the input during this time, causes an error – called the 'Jitter error'. If $(dv/dt)_m$ is the maximum time rate of change of the signal and ε the maximum aperture Jitter error, we have

$$\text{Maximum Jitter Error } \Delta v = \varepsilon \left(\frac{dv}{dt}\right)_m \tag{8.17}$$

For ADCs, Δv should be less than (LSB/2). For a sinusoidal signal

$x(t) = v_m \sin 2\pi ft$,

$$\left(\frac{dv}{dt}\right)_m = 2\pi f v_m \tag{8.18}$$

$$\Delta v = 2\pi f v_m \varepsilon \tag{8.19}$$

For a 12 bit ADC,

$$\frac{\Delta v}{v_m} = 2^{-13} \tag{8.20}$$

Substitution in Equation 8.19 and rearrangement yields

$$\varepsilon = \frac{2^{-14}}{\pi f} \tag{8.21}$$

For ε = 100 ns (typical), Equation 8.21 gives

$$f_{max} = 194\,\text{Hz} \tag{8.22}$$

Proceeding on the same lines, for the general case of the n-bit ADC, we have

$$\pi f \varepsilon = 2^{-(n+2)} \tag{8.23}$$

For a given aperture time as n – the number of bits of the ADC – increases, f reduces. For every additional bit of resolution, the maximum signal frequency that can be handled, halves.

Sample-Hold Offset:

When the analog switch turns off, an additional transient charge is 'dumped' into the hold capacitor. The stray and the wiring capacitances of the sample-hold switches transfer these on to the C_H when the control signal changes. Such change in the output can be minimized by

⇒ increasing C_H (which slows down the analog switch),

⇒ providing a guard ring around C_H to reduce coupling and

⇒ reducing the peak-to-peak voltage change of the control signal.

If C_H is external to the sample-hold circuit, the offset voltage is not known and not specified directly. Normally a charge in pC is specified. One can calculate the change in the held voltage due to this. A 1 pC charge on a 0.5 nF value of C_H causes a 0.5 mV of offset.

8.3.2.4 Hold Interval Errors

Once in hold mode, a sample-hold circuit is expected to hold charge faithfully *ad infinitum*. However, this seldom happens. The leakage current of the analog switch in the off-state, the bias current of the opamp on the output side and the self-leakage of the capacitor itself – all these add together to cause a current through C_H. The

current may charge the hold-capacitance or discharge it depending on its direction as shown in Figure 8.18 (the capacitor leakage discharges it. But with good quality capacitors of today, leakage may be ignored). FET input opamp reduces bias current. Specific amplifier configurations keep the leakage from the analog switch low. In addition to these, we may increase C_H directly to reduce effective droop. As discussed earlier, any increase of C_H reduces the speed of operation of the sample-hold circuit and hence its bandwidth.

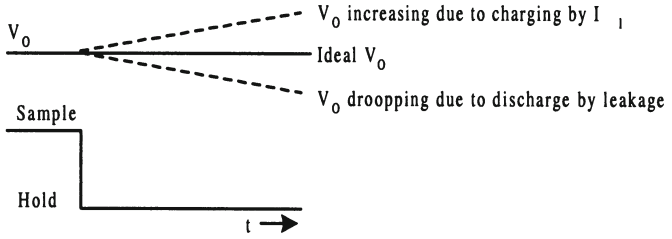


Figure 8.18 Hold interval errors

Droop rate of 1μV / 1μs is typical at normal operating temperature. For a 12 bit ADC— with (say)10 μs conversion time and 5Vrange —this is negligible.

8.3.2.5 Feedthrough Error

From the equivalent circuit of the analog switch in Figure 8.14, we see that when the analog switch is in the off state, V_i is coupled to output side through C_{DS}. As a result, V_o changes in sympathy with V_i in the hold mode as shown in Figure 8.19. With multiple samplers (as in multiplexers), adjacent channels too can get coupled in this manner. With C_{DS} = 0.5 pF and C_H = 500 pF, the feedthrough error is ~0.1%. Usually it is specified in terms of a specified high frequency input (10k Hz) signal.

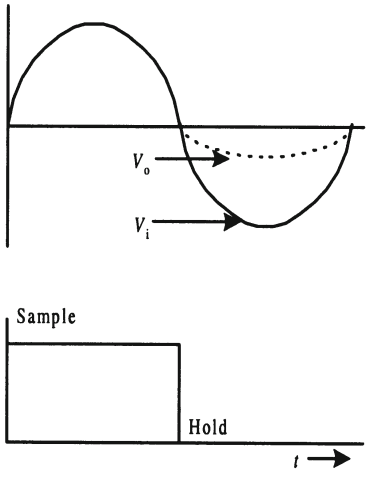


Figure 8.19 Feedthrough error introduced by an analog switch

8.3.2.6 Other Errors

Dielectric Absorption:

All plastic film capacitors exhibit the 'Dielectric Absorption' phenomenon. When a voltage is applied to a capacitor, the molecular dipoles in it get aligned over a period of time. As the capacitor is discharged, the alignment disappears but only over a period of time. If a charged capacitor is shorted for a brief period, and the short removed, the voltage slowly reappears due to the residual aligned dipoles. This is the basic 'Dielectric Absorption' phenomenon. Consider a hold capacitor holding a sample. When connected to the next sample, V_0 will build up to the next sample value and will be held there after sampling. However, due to the dielectric absorption, the voltage across C_H will, creep back towards the previously held value (See Figure 8.20). Creep is a comparatively slow phenomenon – being of the order of 1 % in 1 Hour. As such the error due to dielectric absorption is often negligible in sample-hold circuits. It matters only in high end ADCs of 20 bits and above due to their higher resolution and longer time of conversion. Amongst the plastic film capacitors, Teflon offers the lowest dielectric absorption.

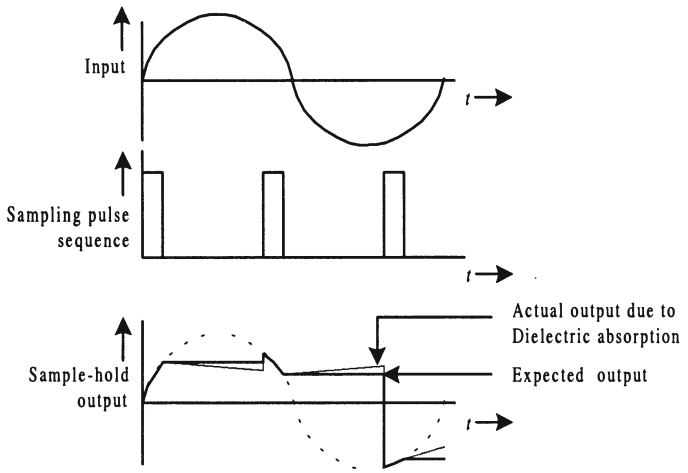


Figure 8.20 Sample-hold error due to dielectric absorption

Noise Errors:

The inherent noise in the opamp and the components of the amplifier around it, get added to the held voltage of the sample-hold circuit. It has to be low enough and carefully band limited to avoid errors. Use of MOSFET input opamps, reduces bias current and related errors. But the noise level increases. Currents with FET input opamps, are comparatively higher but still low enough, not to cause errors with common ADCs. Their noise levels are also lower.

Drift Errors

Thermal drift of offset quantities of opamps are comparatively slow phenomena. They do not cause errors at the sampling frequencies normally used with sampling systems in instrumentation.

8.3.3 Sample-Hold Topologies

Most sample-hold circuits fall into a few well-defined topologies. A brief discussion of each with specific characteristics and limitations, follows. The specific application dictates the selection in each case.

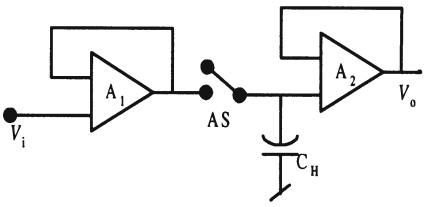


Figure 8.21 A simple sample-hold topology

Figure 8.21 shows a simple topology. Both opamps are connected as buffers. Opamp A_1 offers infinite input impedance for V_i and a hard drive for C_H. Opamp A_2 keeps the load on C_H low but provides low output impedance. The analog switch AS is interposed in between. The overall response time is decided by the time constant – $R_{on}\,C_H$ where R_{on} is the on-resistance of the analog switch – and the slew rate of opamp A_2. A_2 is normally a FET input opamp with negligible loading error. The main sources of error of the configuration are: -

- ⇒ The common mode error at opamp A_2. This also affects linearity at high signal levels.
- ⇒ The leakage error at A_2 and the droop due to it. A FET input opamp is used for A_2 to minimize this.
- ⇒ Comparatively higher feedthrough through the analog switch when it is in the off-state. The low output impedance of A_1 driving C_{ds} is the cause of this.
- ⇒ The charge dumping error at the analog switch. The voltage across C_H at any time depends upon the input signal. Hence, the charge dumping error too changes with signal level.

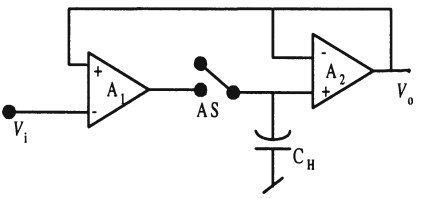


Figure 8.22 Sample-hold topology with overall feedback

The configuration in Figure 8.22 differs from that of Figure 8.21 due to the change in feedback to A_1. The output error due to the offset of opamp A_2, is reduced due to the overall feedback. The feedthrough in the hold mode is also reduced. This is valid only during sampling. The fact that there are 2 opamps in the loop, increases overall settling time. Since the opamp A_1 is working in open loop fashion during the hold-mode, its output drives to saturation. Hence during every sampling, it has to come to the active region and track V_i. This increases acquisition

time. The common mode error, the leakage and the droop-error at A_2 and the charge dumping error, are all as in the configuration in Figure 8.21.

Some of the feedthrough problems associated with the above two topologies can be overcome with some additional analog switches. In the scheme of Figure 8.23, analog switch S_2 is introduced so that switches S_1 and S_2 together function like a single-pole double-throw switch. When in sample-mode, S_2 is off and the scheme is similar to that of Figure 8.22. When S_1 is turned off and S_2 turned on, the output of opamp A_1 is grounded through resistance R_g. This reduces the feedthrough error substantially. Introduction of R_g increases the effective series resistance in sample-mode. This increases the charging time of C_H as well as the acquisition time.

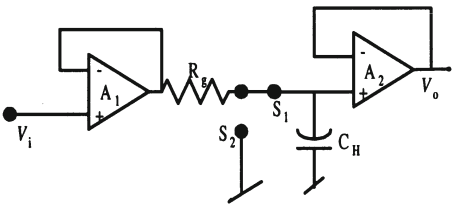


Figure 8.23 Sample-hold circuit with reduced feedthrough error

The scheme of Figure 8.24 uses feedback through two opamps. C_H is connected in the feedback path of opamp A_2. Hence, opamp A_2 functions as an integrator. Since point P is at virtual ground, the leakage current is low and the droop due to it in the hold mode, is also low. The charge dumping by the analog switch during switching, remains constant and appears as an output offset. It can be nullified by regular 'auto-zeroing'. The integration action brings about better loop stability but increases acquisition time.

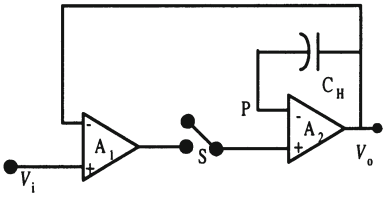


Figure 8.24 Sample-hold scheme with C_H in the feedback path

The scheme of Figure 8.25 is a modification of that in Figure 8.24. Use of four analog switches adds to the complexity but improves the performance conspicuously. Its specific features and benefits are as follows: -

⇒ Analog switches S_1 and S_2 operate simultaneously in an identical fashion. For any charge dumping into C_{H1} by S_1 switching, an equal charge is dumped into C_{H2} by S_2 switching. These two operate in a differential mode reducing the charge dumping error substantially.

⇒ Opamp A_1 is always in a feedback mode. Hence, its output does not saturate during hold mode. This reduces the acquisition time.

⇒ The additional pair of switches at the input S_3 and S_4, operate as a single pole double throw switch. S_3 is on during sampling and S_4 is on during hold. Since the input is grounded during hold, the feedthrough error is reduced substantially.

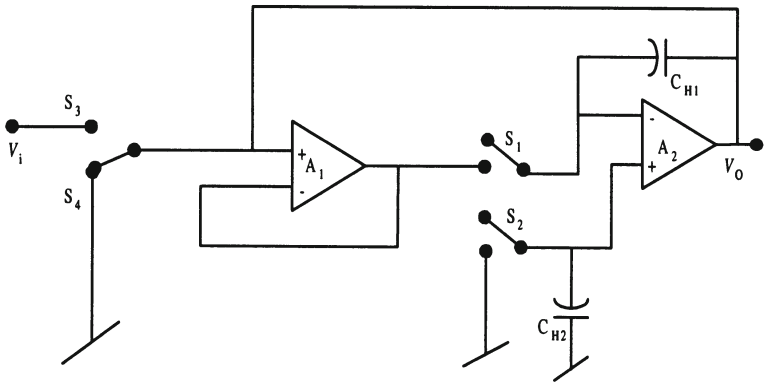


Figure 8.25 Sample-hold scheme with improved performance

8.3.4 Multiplexing

The bandwidth of signals to be handled by instrumentation schemes, and data acquisition systems is relatively limited by today's standards. The ADCs and microprocessors which handle digital signals are relatively much faster. This disparity opens up the possibility of multiplexing analog signals and processing

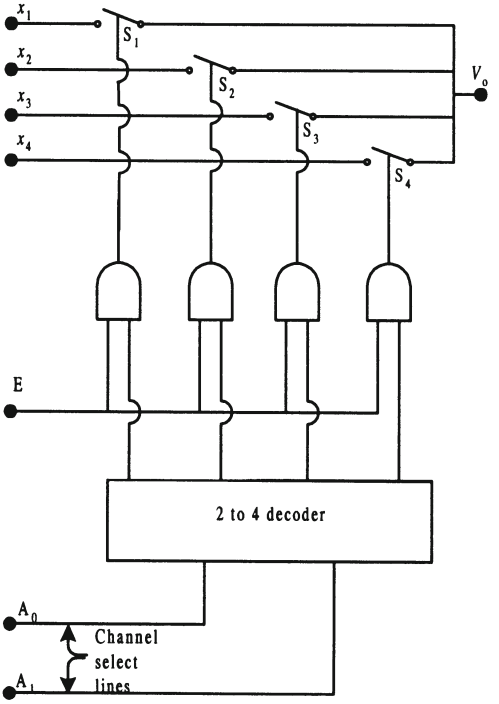


Figure 8.26 Analog multiplexer scheme

them. The practice – conventionally termed 'Time Division Multiplexing (TDM)' – has become quite common. It makes the overall digital system compact and economic. Functionally a multiplexer is a number of analog switches with their outputs connected together. Figure 8.26 shows a 4-input single-output multiplexer (termed as 'Mux' in short form) in functional form. Two address lines A_0 and A_1 select the individual channels to be turned on and steered to the output V_o. The selection is done through the decoder. Normally a separate enable input (E) is provided to enable or disable the overall chip. When E = 0, none of the channels is selected. When E =1, the selected channel is turned on. S_1 to S_4 are the analog switches which function as the connecting or disconnecting links.

Normally a sample-hold circuit or an ADC is connected as the load on the output side of the mux. The static and dynamic performance of the mux is discussed here with respect to the single and multiple channel behaviour.

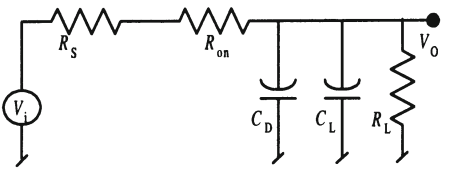


Figure 8.27 Equivalent circuit of one channel of a mux

Single Channel Behaviour

The equivalent circuit of the single channel under on-conditions is shown in Figure 8.27. Here V_i is the input signal and V_o the output. R_S is the source resistance. C_D is the net capacitance at the drain (output) side of the mux plus the wiring capacitance. C_L is the load capacitance and R_L the load resistance. The parameters R_S, C_L and R_L are external to the mux. From the equivalent circuit, under steady state conditions, we have

$$\frac{V_o}{V_i} = \frac{R_L}{R_L + R_S + R_{ON}} \tag{8.24}$$

$$\text{Error in } V_o = \frac{R_S + R_{ON}}{R_L + R_S + R_{ON}} \times 100\% \tag{8.25}$$

where R_{on} is the on-state resistance of the analog switch. The condition

$$R_S + R_{on} \ll R_L \tag{8.26}$$

reduces the error. Normally R_{on} is of the order of 200 Ω in a Mux. For 12 bit accuracy R_L has to be greater than 1.6 MΩ with this level of R_{on} even with $R_S = 0$. With practical R_S values, R_L has to be in the 10 MΩ to 100 MΩ range. Under dynamic conditions, the 3 dB bandwidth of the switch is decided by the corner frequency of $[(R_S + R_{on})|\,|R_L]$ and $[C_D|\,|C_L]$. Since $R_L >> R_S + R_{on}$, we have the corner frequency f_c as

$$f_c = \frac{1}{2\pi} \times \frac{1}{(R_S + R_{ON})(C_D + C_L)} \tag{8.27}$$

To increase the corner frequency R_S and C_L have to be reduced as much as possible. R_S is decided by the signal source but may be reduced to the extent possible. However, reduction of C_L affects the switch performance adversely. It increases the

'pedestal error' and the charge dumping error unduly. As discussed earlier these are kept down by increasing C_L. The trade off is decided by the system requirements.

Apart from the definite load resistance, the load bias current also introduces an error. It flows through $R_s + R_{on}$ and causes a voltage offset. Normally FET input opamps with low bias currents are used at the load end to minimize this error.

Multiple Channel Behaviour

The presence of the additional channels – though all of them are in the off-state – affects the performance of the on-channel. The effect is referred to as 'Cross-talk'. Each channel has a leakage current at the output side under Off-conditions. (Normally it doubles with every 10 °C rise in temperature). All these leakages add in parallel and contribute to the drift. Typically, the output leakage current of each channel – I_L– is 1 nA. To keep its effects within allowable limits, the drop – $(R_S + R_{on})(n\text{-}1)I_L$, where n is the number of channels of the Mux – has to be kept lower than (LSB/2). This puts an upper limit on R_S.

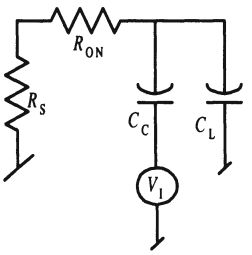


Figure 8.28 Equivalent circuit to analyze cross-talk in an analog mux

The dynamic cross-talk has two dimensions to it. First, consider one off-channel and its effect on the on-channel. The equivalent circuit is as shown in Figure 8.28. Here R_L is neglected since it is high compared to $(R_S + R_{on})$. Similarly the capacitances C_D, C_S, C_{DS} *etc.*, are small compared to C_L and therefore neglected. Since normally $C_C << C_L$, the dynamic cross-talk corner frequency f_{dc} is

$$f_{dc} = \frac{1}{2\pi} \times \frac{1}{C_L(R_s + R_{ON})} \tag{8.28}$$

Spectral components of V_i below this frequency can be ignored *vis-à-vis* cross-talk. Only the higher frequency components get coupled. The coupling effect is reduced by keeping $R_S + R_{on}$ low and making C_L large compared to C_C. Of course, any increase in C_L reduces response bandwidth directly. The discussion so far, is equally valid for all the effect of all the off-channels. In practice, any mux operates on the 'break-before-make' principle. When switching over from one channel to another one, the mux remains in the off-state for a minimum time in-between. This is to prevent the shorting of two analog channels through the mux. This increases the equivalent resistance seen by the interfering channel. f_{dc} in Equation 8.28, reduces correspondingly.

The second type of dynamic cross-talk is the adjacent channel 'Cross-talk'. Consider the mux switching over from (say) channel1 to channel 2. The relevant equivalent circuit is shown in Figure 8.29 along with its waveforms. The source resistances for the two channels are assumed to be the same for simplicity. The on-resistances R_{on} are also the same. The series switches S_1 and S_2 are turned on by

select commands Sel_1 and Sel_2. Sel_1 goes low turning off-switch S_1. With a delay T_{br}, Sel_2 goes high turning on switch S_2. A signal voltage V_1 is present as input to channel 1. The input at channel 2 is V_2. When S_1 is on, V_o is connected to channel1 and settles to input V_1. When S_1 turns off, V_o across C_L discharges through R_L with a time constant

$$\tau_1 = R_L C_L \tag{8.29}$$

Since R_L is in the 100 MΩ range, and C_L is in the 1nF range, τ_1 is in the 100 ms range. Hence the discharge of C_L is very slow. This situation continues throughout the T_{br} period. At that instant, S_2 is turned on, shunting R_L by $R_S + R_{on}$ which is of the order of 200Ω only. The discharge time constant is

$$\tau_2 = (R_S + R_{on})\, C_L \tag{8.30}$$

τ_2 is of the order of 200 ns. The discharge is completed in about 5 time constants (1μs). Only after this, the data on the output side, can be taken as settled. Thus the adjacent channel cross-talk, essentially puts an upper limit on the speed of operation of the mux.

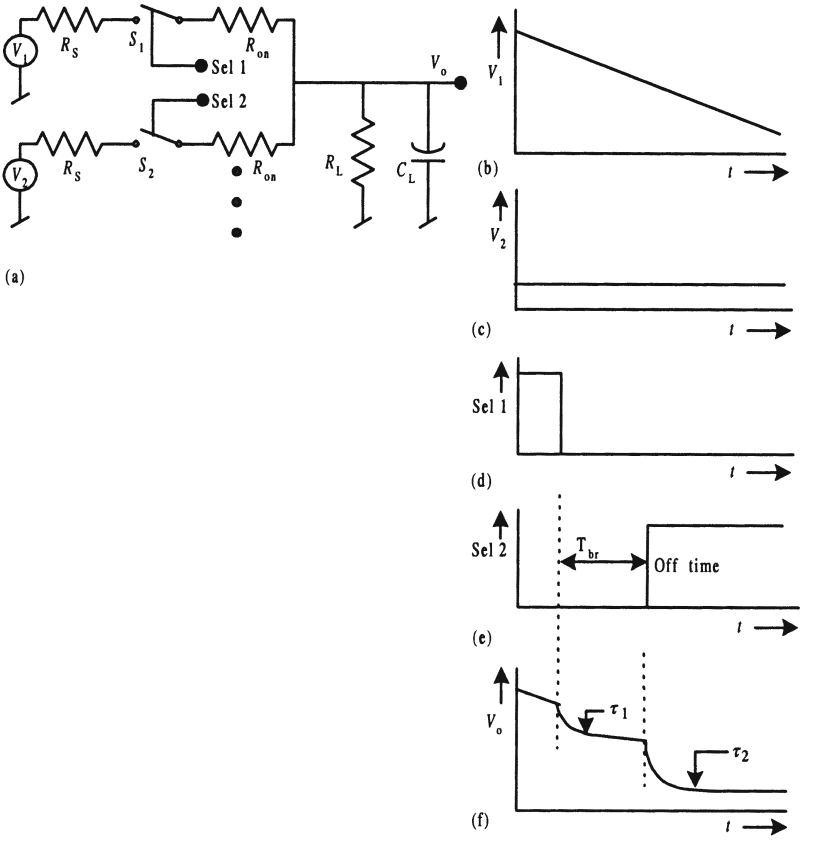


Figure 8.29 Adjacent channel cross-talk in an analog mux: (a) Equivalent circuit for analysis (b) Channel 1 input signal (c) Channel 2 input signal (d) Sel 1 command (e) Sel 2 Command (f) Output signal

The term 'adjacent channel' is used here in the sense of time sequence and not being physically adjacent. The cross-talk is not of the mutual type. Thus if the channels switch in the sequence 1-2-3-4-1...

⇒ Channel 1 causes adjacent channel cross-talk in Channel 2
⇒ Channel 2 causes adjacent channel cross-talk in Channel 3
⇒ Channel 3 causes adjacent channel cross-talk in Channel 4
⇒ Channel 4 causes adjacent channel cross-talk in Channel 1
and so on.

Observations: -

⇒ Use mux with low R_{on}. R_{on} can be reduced by increasing the control voltage to (say) 15V. This increases feedthrough.
⇒ Switching both the signal lines - differential sampling - reduces feedthrough; but it calls for extra hardware.
⇒ Keep R_S low for all the channels.
⇒ Keep stray wiring capacitances low.
⇒ Use as low a clock frequency for multiplexing as can meet system bandwidth requirements.
⇒ Keep T_{br} as low as possible.
⇒ Use of twisted pair signal lines everywhere ensures common-mode capacitance balance and reduces stray signal pick-up. If possible a shield may be used with a common mode guard drive [See Section 4.12].
⇒ Use of high R_L is mandatory. Leakage from the load is to be kept as low as possible. FET input opamp is considered well suited for this.

8.4 Voltage References

All AD and DA conversions are carried out with reference to a reference voltage. In ADCs, the reference may represent 50 % of the full-scale value and the converted digital output is decided by comparing the two. In a DAC, the reference represents the scaling. Accuracy of the reference voltage used has a direct bearing on the accuracy of the conversion process. Let V_R be the reference of an ADC and let it represent the full-scale value. For an error δV_R in V_R, the MSB representing 50% of the scale, is in error by $\delta V_R/2$. This represents the maximum error in the conversion process due to δV_R. If the ADC is n bits wide, the LSB represents ($V_R \times 2^{-n}$) Volts. For satisfactory operation, the error in MSB due to δV_R must be less than LSB/2. Equating the two and simplifying

$$\frac{\delta V_R}{V_R} = 2^{-n} \tag{8.31}$$

Equation 8.31 gives the maximum acceptable error in V_R over the full temperature range of interest. Table 8.3 gives the worst case acceptable errors in V_R for different representative values of n. Since other factors also contribute to the error, the acceptable level of ($\delta V_R/V_R$) must be much less than that in the table (say 1/10 times). Thus a 12 bit ADC may tolerate an error due to δV_R of only 24 ppm and a 14 bit ADC only 16 ppm. All these are equally true of DACs as well. Incidentally, the conventional standard cell has a temperature tolerance of ±30 ppm/°C. Hence

even over a very limited temperature range, it cannot serve as a voltage reference for ADC or DAC. IC based voltage references meeting the tolerance requirements of ADCs and DACs have become available in the recent years. Often they are directly built into the ADC or DAC concerned. Broadly, two types of voltage references are available – 'Zener' based and 'band-gap reference' based [Grey and Meyer].

Table 8.3 Acceptable limits of error for Voltage References for ADCs and DACs of different resolutions

n	10	12	14	16	18	20	22
$\delta V_R/V_R$(ppm)	997	244	61	15	4	1	0.24

8.4.1 Zener Based Reference

Reverse breakdown of diodes is of two types. Below about 6V, the breakdown mechanism is dominated by quantum mechanical tunnelling through the depletion layer [Gray and Meyer] – this is the 'Zener Breakdown'. Here the temperature coefficient of the breakdown voltage is negative. At larger voltages, the avalanche multiplication at the depletion layer dominates – this is the 'Avalanche Breakdown'. The temperature coefficient of the breakdown voltage is positive here. At around 6V, the net temperature coefficient of the breakdown-voltage is close to zero. Hence, Zener diodes of about 6V are normally used for references.

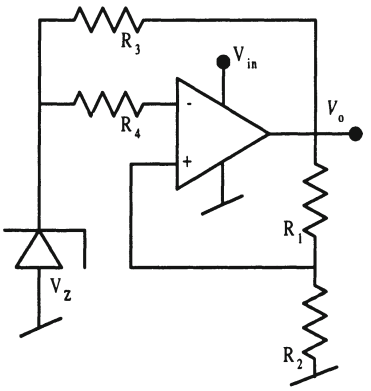


Figure 8.30 Voltage reference built around a Zener diode

Figure 8.30 shows the circuit commonly used for generating 10.000V reference. V_Z is a Zener of zero temperature coefficient as described above. Its output is amplified through a non-inverting amplifier so that,

$$V_o = V_z\left(1+\frac{R_1}{R_2}\right) \tag{8.32}$$

V_o supplies the Zener bias current. Since V_o is stabilized, the Zener bias current is also fixed. Hence, the voltage drop in the incremental series resistance of the Zener

remains unchanged. Further the current drawn by the non-inverting input of the opamp is negligible keeping the load on the Zener zero. R_1 and R_2 being on the same IC, track each other with close tolerance. Voltage references of this type are available with 10.000V or 10.240 V as output. The latter gives the round figure of 10 mV/LSB for a 10-bit converter. Some of them have the provision to trim V_0 to finer values. Typical specifications of a good quality Zener-based reference are: -

Voltage	:	10.000 mV ± 2 mV (can be trimmed externally).
Drift	:	1 ppm/ °C over 25 °C to 70 °C
Input voltage range	:	13.5 V to 16.5 V
Line regulation	:	100 μV/V
Noise (0.1 Hz to 10Hz) p-p	:	20 μ Vp-p
Long term stability	:	50 ppm/1000hrs
Load current	:	< 5 mA

8.4.2 Band Gap Based Reference

Zener diode based voltage references require supplies in excess of 6V. ADCs and DACs of lower voltage ranges require references of lower values. The band-gap based reference is commonly used at such voltages [Grey and Meyer; see also Baracchino]. The band-gap voltage of Si is 1.205 V. It has a positive temperature coefficient. The forward voltage drop of a Si diode is about 0.7 V and it has a negative temperature coefficient. By judicious proportioning and adding the two, one can get a voltage reference with a low enough temperature coefficient. Well-adjusted band-gap references have output voltage of 2.6 V at room temperature (25°C). Specifications of a good-quality band-gap reference are:

Voltage	:	2.600 V ± 20 mV
Drift	:	20 ppm/ °C over 0°C to 70°C
Input voltage range	:	4 V to 25 V
Line Regulation	:	100 μV/V
Noise (0.1 Hz - 10 Hz)	:	60 μV p-p
Long term stability	:	100 ppm/1000Hr

Observations: -

⇒ Performance-wise Zener-based references are superior to band-gap based references.

⇒ Band-gap based references are suitable for only converters of lower resolution.

⇒ Zener-based references are superior to standard cells – in respect of drift, noise and tolerance. Standard cell can be loaded only to a very limited extent without hampering its repeatability. Semiconductor based references do not have this handicap.

8.5 Specifications of ADCs and DACs

When an ADC or DAC is used in a scheme, errors introduced by it are carried forward without any possibility of correction. This calls for a need to identify

different possibilities of errors and quantify each type as a corresponding specification. Other specifications relate to the resolution and speed of conversion. Most specifications are same or similar for ADCs and DACs and are dealt with together here.

8.5.1 Quantization Error

Quantization error is inherent to the conversion process. It has been dealt with in Section 8.2.3. The quantization error is normally LSB/2.

8.5.2 Conversion Rate

The minimum number of conversions that can be carried out by the ADC/DAC in unit time, represents the conversion rate. This is an indirect measure of the maximum bandwidth of the signal that can be handled by the converter (See Section 8.2.1).

8.5.3 Accuracy

Accuracy represents the maximum deviation of the stepped digital/analog relationship from the ideal straight line (Figure 8.31). It represents the sum total of all the deviations due to all possible reasons and imperfections of the converter. In the ideal case, it should not exceed the quantization error – LSB/2. Thus for a 12-bit converter, the best accuracy we may expect is 1 in 2^{13} – *i.e.*, 0.0122 %. Normally data sheets list individual errors separately. One has to consider the cumulative effect of all these to elicit the overall accuracy.

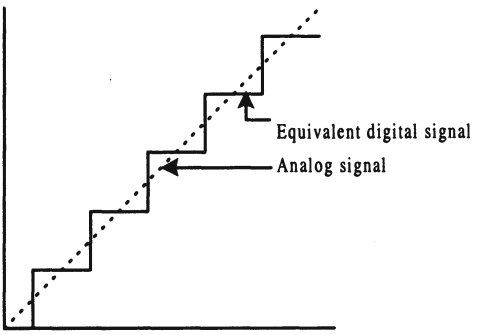


Figure 8.31 Analog and equivalent stepped digital signals

8.5.4 Offset Error

In a DAC, one expects the output for zero-input conditions, to be the analog equivalent of (LSB/2). It may deviate from this value due to the offset in the output side opamp and other reasons. This offset will appear as a constant (Figure 8.32)

throughout the characteristic. Its effect is most severe at low signal levels. In an ADC, the offset is mainly due to the inherent quantization and the comparater threshold. Offset changes with the operating temperature (See Section 3.4).

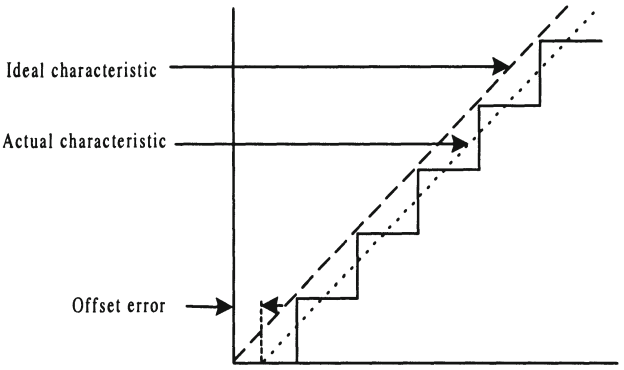


Figure 8.32 Offset error in converters

8.5.5 Gain Error

The analog output of the DAC for any code can be larger or smaller than what is expected ideally. The former case is shown in Figure 8.33. The deviation increases proportional to the signal level. The gain error expressed as a percentage is a constant throughout the operating range. It affects all the codes by the same percentage. In an ADC, the gain error manifests as a proportionate change in the analog input for all coded output numbers. In a DAC, the gain error reflects as a proportionate change in the analog output for all the coded input number values. A change in the voltage reference value (due to drift, aging, change in power supply *etc.*), is a common cause. Changes and tolerance of gain determining resistances, is another cause of DAC gain errors.

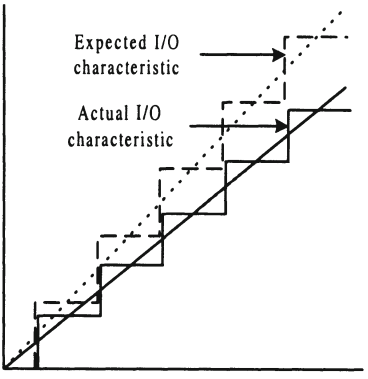


Figure 8.33 Gain error in converters

8.5.6 Linearity Error

The ideal linear transfer curve of the ADC or DAC is the straight line joining the ends representing the zero and the full-scale input-output points. The extent of deviation of the stepped transfer curve from the ideal represents the linearity error. Figure 8.34 shows a highly simplified case. The departure from linearity can be of different types. Normally two types are defined.

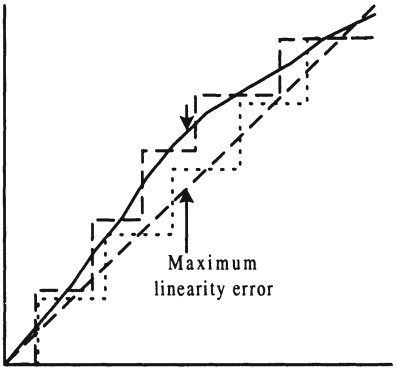


Figure 8.34 Linearity error in converters

8.5.6.1 Integral Non-linearity

Often this is referred to as the 'Non-linearity or Relative accuracy'. Consider the actual input-output stepped curve of the converter. Maximum deviation of this from the ideal straight line through the end-points, represents the 'Integral non-linearity'. This may occur anywhere in the defined range of the converter. Normally it is specified in terms of the LSB – (LSB/4), (LSB/2) and so on. Figure 8.35 shows a case.

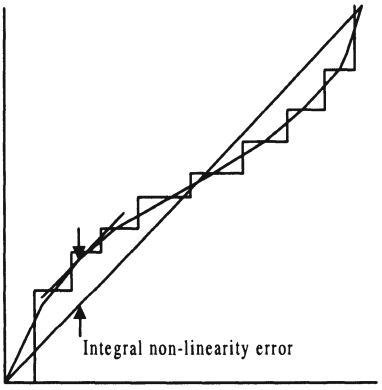


Figure 8.35 Integral non-linearity error in converters

8.5.6.2 *Differential Non-linearity*

In a DAC, a change of one bit in the input, is followed by a corresponding change in the analog output. Wherever be the input change, the output change must be the same. Any disparity leads to 'Differential non-linearity'. As an example, consider a 12-bit ADC with a 5 V reference. One LSB represents $(5/2^{12})$ V = 1.2207 mV. If at any one point in the scale, change of one bit in the input, changes the output by 1.5 mV, the differential non-linearity is (1.5 – 1.2207) = 0.2793 mV (≈LSB /4).

A gradual shift in the differential non-linearity value, over a large number of consecutive bits, reflects itself as an integral non-linearity or relative error as explained above. Abrupt changes in consecutive bits appear as conspicuous differential non-linearity. Low differential non-linearity and integral non-linearity, are important for instrumentation schemes.

8.5.7 Monotonicity

Consider a DA converter. If a bit increase in the digital input is always followed by an increase in the analog output, the input-output characteristic is 'Monotonic' in nature. However, this may not always happen, especially if the differential non-linearity is excessive. Consider an extended case of the above example. Table 8.4 shows a hypothetical case of digital inputs and outputs from mid-scale onwards, for a set of consecutive bit changes in input. It is seen that the output continuously increases until the input is 1000 0000 0110 and then for the increase in the next bit, it decreases. The transfer characteristic is not monotonic in this region. The same is illustrated in Figure 8.36. A non-monotonic characteristic can lead to oscillations or even instability problems in a feedback loop.

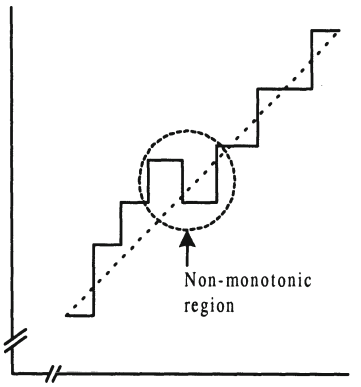


Figure 8.36 Monotonicity error of a converter

8.5.8 Dynamic Range

The 'dynamic range' of an ADC, is the ratio of maximum to minimum signal magnitude that can be converted. The minimum is the threshold on par with noise level. For an n bit ADC, the resolution is 2^{n+1} and the dynamic range achievable, is 2^{n+1}. In practice, the effective range is less than this. The 'Spurious-Free Dynamic

Range (SFDR)', represents the ratio of the rms. signal amplitude to the rms. value of the peak spurious spectral content measured over DC to $f_s/2$. It is normally expressed as dB at full scale. Improving the resolution does not necessarily improve SFDR of the ADC. The dynamic range and the SFDR are important specifications of ADCs.

Table 8.4 Input / Output characteristic of a DAC which is not monotonic in nature

Digital input	Actual analog output (mV)	Ideal analog output (mV)	Actual increase in output (mV)
0000 0000 0000	0.6104	0.6104	
0000 0000 0001	1.831	1.831	1.2207
...	...	...	...
...	...	...	...
0111 1111 1111	2499.3897	2499.3897	1.2207
1000 0000 0000	2500.6104	2500.6104	1.2207
1000 0000 0001	2502.1104	2501.8311	1.5
1000 0000 0010	2503.6104	2503.0518	1.5
1000 0000 0011	2505.1104	2504.2725	1.5
1000 0000 0100	2506.6104	2505.4932	1.5
1000 0000 0101	2508.1104	2506.7139	1.5
1000 0000 0110	2509.6104	2507.9346	1.5
1000 0000 0111	2509.1553	2509.1553	– 0.4551

8.5.9 Sensitivity to Power Supply Variations

The conversion process may be affected by variations in the power supply. The error due to this, is expressed as a percentage change in analog value for a percentage change in power supply. The error here may be due to the change in reference or the common mode error of the opamp within the converter IC. In DACs, the maximum effect of power supply changes is due to the current sources driving the ladder rungs.

8.5.10 Temperature Coefficient

The number of bits and resolution are basic characteristics of the converter. All other performance specifications may change with change in the operating temperature. Temperature coefficients are normally specified for these.

Observations: -

⇒ The specifications of ADCs and DACs do not follow a common or widely accepted format. (e.g., different manufacturers specify non-linearity in different ways). This has to be kept in mind when comparing products of different manufacturers.

⇒ The best accuracy possible from a converter is (LSB/2). If an error is 1 LSB or more, one can settle for a converter of lower resolution (and lower cost). Hence, each of the errors specified, has to be much less than (LSB/2). This

may not be the case with the converters of 14 or more bits of resolution. Thus in a DAC, differences in the voltage-drops across analog switches, offset voltages and their effects on the two sides of the summing amplifier, changes in the feedback resistances due to the changes in signal level – all these add to the cumulative error at any time.

⇒ For instrumentation schemes, good linearity and high stability are essential. One should also aim at good differential and integral non-linearity over the temperature range, low offset, low gain-drift, low PSRR and low noise. In contrast, for video applications, speed and bandwidth are more important.

⇒ Differential non-linearity and drift, specified separately, may look harmless and acceptable. But their combined effect can upset monotonicity. This can happen if the total drift over the specified range and differential non-linearity together exceed 1 LSB. Note that for instrumentation schemes, monotonicity of the characteristic at the expense of resolution, is more acceptable than *vice versa*.

8.6 Digital to Analog Converters (DAC)

A DAC accepts a digital quantity in binary form. Each bit is converted into a proportionate signal. All such proportionate signals are added with appropriate weight to obtain the final analog equivalent output. Two principles of conversion are in vogue (others do exist but are much less common). In one method, currents proportional to the individual bits are generated and all these currents added together, to form the analog output. In the second case, voltages proportional to the individual bit values are generated and all the voltages are added together.

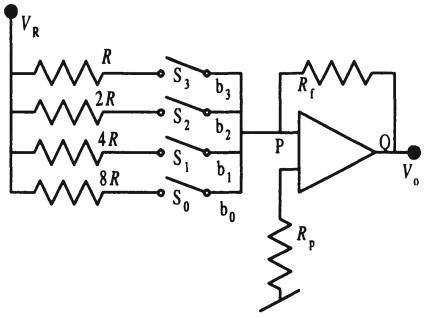


Figure 8.37 DA converter with weighted resistors

8.6.1 Current Based Conversion

Figure 8.37 shows a scheme for a four-bit converter. The reference voltage V_R is connected to a set of resistors R, $2R$, $4R$ and $8R$. These are switched on to the summing junction P of an inverting amplifier, through analog switches S_0 to S_3. The 4-bit number to be converted is represented as its binary equivalent $b_3b_2b_1b_0$. Thus if $b_0 = 1$, S_0 is closed feeding a current of V_R /$4R$ to the summing junction.

Similarly, S_1, S_2 and S_3 turn on or off the V_R to the resistors $4R$, $2R$ and R respectively.
Thus the total current I flowing into the junction is

$$I = \frac{V_R}{R}\left(\frac{b_0}{8}+\frac{b_1}{4}+\frac{b_2}{2}+b_3\right) \tag{8.33}$$

Using this, for the output voltage V_o we get

$$V_o = -V_R\frac{R_f}{R}\left(\frac{b_0}{8}+\frac{b_1}{4}+\frac{b_2}{2}+b_3\right) \tag{8.34}$$

We get an output voltage, which is proportional to the digital quantity.

Observations: -

- ⇒ V_R, R_f and R have a say in the accuracy attainable. V_R is of a type discussed in Section 8.4 and of high enough quality. All the resistors track each other closely. This is possible with thin film resistors.
- ⇒ All analog switches operate close to the ground. Hence, the effects of their errors are minimum.
- ⇒ If R_f is built into the IC, it provides tracking and gain stability. External R_f can change gain.
- ⇒ The currents through the different analog switches are different. To this extent, the respective voltage drops are different. To minimize this effect, the resistances are chosen much larger in value than the on- resistances of the analog switch. The chip areas of individual analog switches may be made proportional to the respective currents to reduce this error.
- ⇒ The equivalent resistance seen by the opamp at its inverting input, changes with the values of the individual bits. Hence the resistances seen by the opamp at its inverting and the non-inverting inputs are not matched. This can cause offset error.
- ⇒ The stray capacitance to ground at P can reduce slew rate and affect stability. A suitable capacitance across R_f alleviates the problem (See Section 4.3.1).
- ⇒ In the scheme of Figure 8.37, the load on V_R changes as the individual bit values change. The resultant change in V_R – however small it may be – can cause a conversion error. The scheme can be modified such that each analog switch switches the current on to the summing junction P or ground depending on the status of the corresponding controlling bit. This keeps the load on V_R constant irrespective of the digital value converted. The step avoids variation of V_R and consequent errors.
- ⇒ In IC fabrication, obtaining R values with close tolerances extending over ratios of 1:20, is not feasible. Hence, this approach of DAC conversion is practical only up to 4 bits. Beyond this, the bits are handled in groups of 4 by quad analog switches. Subsequently, outputs of individual quad switches are summed with proper weight. With this modification, the use of current based conversion is extended to 12-bit to 16-bit DACs.

8.6.2 Voltage Based Conversion

One attractive type of realization of a DAC is shown in Figure 8.38. It is centred around 'an R-$2R$ Ladder Network'. Each bit switches an assigned pole of the

network to ground or V_R, depending on whether the bit is zero or one respectively. The net voltage at point P is proportional to the number being converted.

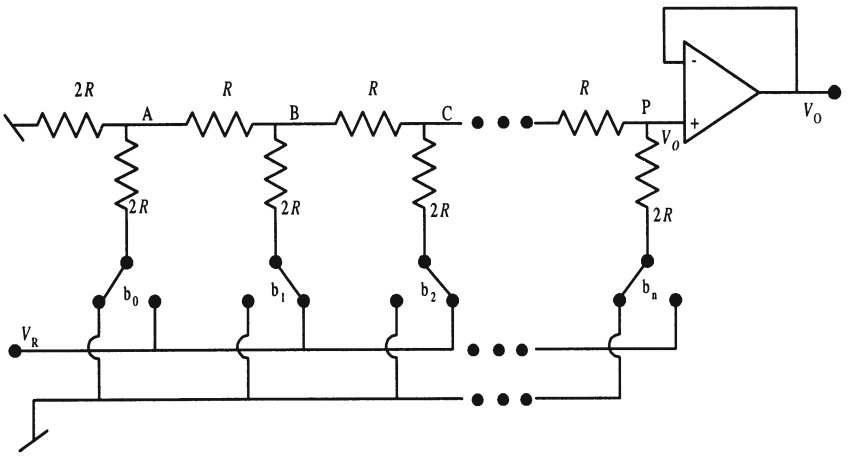


Figure 8.38 R-2R ladder type DA convertor

Let us assume that $b_0 = 1$ and all the other bits are zero. If we break open the network at point A, the portion to the left can be replaced by its Thevenin equivalent.

$$\text{Thevenin source voltage} = V_R/2 \tag{8.35}$$

$$\text{Source resistance (} 2R \text{ and } 2R \text{ in parallel)} = R \tag{8.36}$$

If we restore the connection at point A and break open the network at point B, the portion to the left can be replaced by its Thevenin source voltage of $V_R/4$ and resistance R. Continuing this process, we get for the potential V_P at point P

$$V_p = 2^{-(n+1)} V_R \tag{8.37}$$

One may repeat this procedure for each of the bits, which are in the 1 state. By superposing all the individual V_p's obtained in this manner, we get

$$V_p = V_R [\, b_0 2^{-(n+1)} + b_1 2^{-n} + b_2 2^{-(n-1)} + \ldots \ldots + b_n 2^{-1}] \tag{8.38}$$

$$\therefore \text{Effective } V_p = V_o \text{ (the desired output)} \tag{8.39}$$

Observations: -

⇒ In the scheme shown, consider the case when all the bits are set to one. The loading on the analog switch connected to b_n is maximum and that on the analog switch connected to b_0 is minimum. A total equality can be brought about by connecting $2R$ to ground at P. This makes the loading on the entire set of analog switches equal and brings about total symmetry in the circuit. This reduces the gain to 2/3 of the previous value. However, the equality of loading does not hold good for other values of the bits.

⇒ Compared to the previous scheme, circuit realization is easier and tracking better - only two values of resistances are involved. However, the number of resistances used is twice of that with the current based summing.

⇒ All resistances and the analog switches are identical. The accuracy attainable is also better. The scheme is more widely used than the previous one.

⇒ The *R*-2*R* ladder can be easily modified to provide an inverting configuration as shown in Figure 8.39. Here point P is at virtual ground. The resistances in the two input legs of the opamps are equal. Offset errors due to the respective i_bs are neutralized.

⇒ The arrangement can be modified as in Figure 8.40. The net output current I_o is proportional to the digital quantity to be converted. Compared to the previous cases, the operation of the analog switches is better on two counts. They see equal currents. They operate close to the ground potential avoiding associated errors (See Section 8.3). I_o can be converted to the necessary voltage through an opamp.

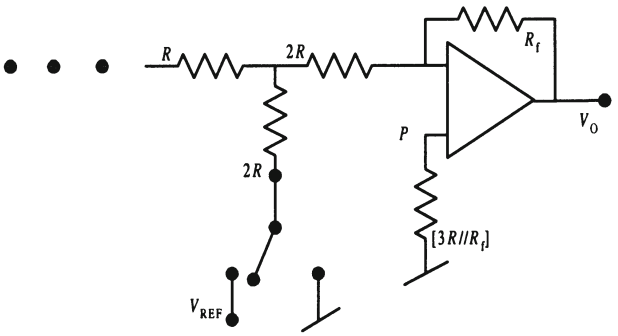


Figure 8.39 Modification of *R*- 2*R* ladder network to provide inverted output

⇒ Using diffusion techniques, resistance ladder networks with linearity of 500 ppm and differential non-linearity of 120 ppm are achievable. This is suitable up to 10-bit DACs. Thin film technologies (Silicon-Chromium) are suitable for ladder networks of higher resolutions – up to 16 bits with linearities of 120 ppm and differential non-linearities of 10 ppm (and hence DAC s).

⇒ CMOS ICs and hence DACs are realized using MOS transistors and thin film resistors. With analog switch operation at virtual ground, R_{on} is independent of signal level. The whole DAC linearity is maintained at low signal levels also. In contrast with the bipolar process, linearity degrades at low signal levels.

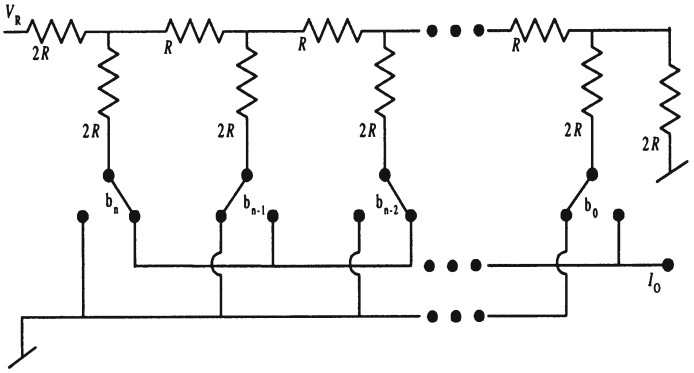


Figure 8.40 R-2R ladder network modified to give current type output

⇒ Consider a 16 bit DAC; the LSB is 15 ppm. An MSB error of this level suffices to upset monotonicity. Hence, a blanket use of the *R*-2*R* Ladder is not always resorted to. The low-end bits are converted through an *R*-2*R* ladder. The high-end bits (two to four numbers) are converted separately and added to the above. Alternately the MS bits and the LS bits are converted through separate *R*-2*R* ladder segments and the respective output currents are added subsequently with proper weights.

8.6.3 Microcomputer Interface

Many DACs have μC-interface built in them. Building-in additional functionality being easy, a variety of facilities is being built-in. Minimal additional interface is shown in Figure 8.41. The interface shown can accommodate a variety of control bus formats. The DAC is fed digital data to be converted by the data register. It is as wide as the number of bits of the DAC. As long as it holds the data, the DAC gives out the converted output. The data input to the IC is loaded into the input register – as wide as the data register. The loading of the input register is done under μC command by activating $\overline{WR}$ and $\overline{LB}$. During such loading, the data register content and the DAC output remain unchanged. Subsequently the input data can be transferred to the data address register under μC control by activating $\overline{WR}$ and $\overline{LDAC}$. Thus, the DAC operation and the input data loading are independent of each other. The D/A register can be cleared by a separate clear command at $\overline{CL}$ line.

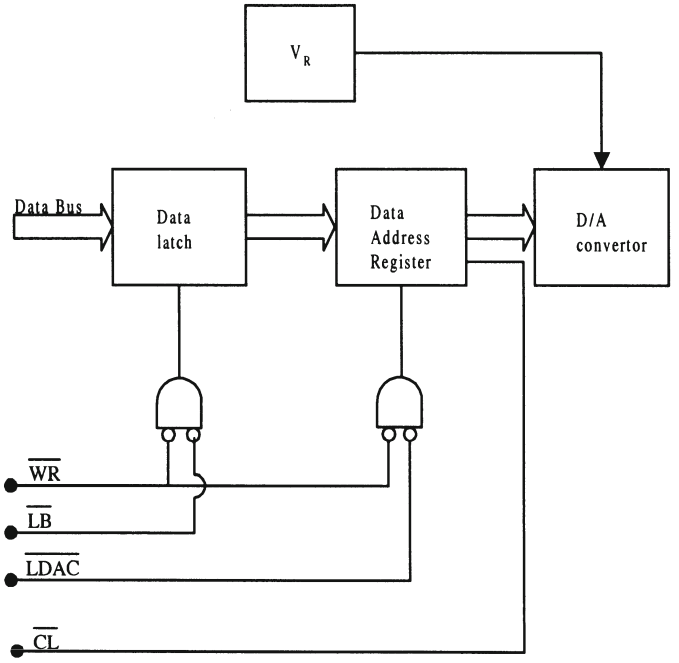


Figure 8.41 DAC with microprocessor interface

Observations: -

⇒ $\overline{LB}$ and $\overline{LDAC}$ can be combined together and both registers treated as one. This makes the DAC reflect the input digital data as equivalent analog output immediately on loading.

⇒ For DACs 10-bit or more wide, different data loading facilities may be available. Data may be loaded as bytes sequentially from an 8-bit bus or all data lines may be loaded simultaneously from a wider bus.

⇒ Some DACs have the provision for serial data loading. This reduces the pin-outs of the DAC.

⇒ The *R*-2 *R* ladder network may be realized through switched capacitors [See Section 5.11]. This reduces the active chip area and hence cost. The clocking can be internal or external (synchronized to the main system clock).

8.7 Analog to Digital Convertors

Different types of ADCs are available to suit the needs of resolution, speed, application and cost. The major types available are:

⇒ Dual Slope ADC
⇒ Successive Approximation ADC
⇒ Flash ADC
⇒ Sub-ranging ADC
⇒ Serial or Ripple ADC
⇒ Sigma-Delta Converter type ADC
⇒ Combinations of Flash and Successive Approximation type ADCs
⇒ Voltage to frequency conversion type ADC

Features of all the above types are discussed here. In each case, the application area is also highlighted.

8.7.1 Dual Slope ADC

The dual slope ADC is shown in block diagram form in Figure 8.42 (a). This is a simplified form of the commercial versions in common use. Opamp-1 has an integrator built around it. Opamp-2 functions as a comparator. Before the start of conversion, switch S_2 is kept on, so that the integrator output remains clamped to zero. At start of conversion, S_2 is turned off, enabling the integrator. Simultaneously the switch S_1 is turned on to the signal to be converted V_s. The integrator output starts increasing from zero onwards – Figure 8.42 (b). The integration continues for a definite time-period T_r. This is decided by the clock and the control logic. At the end of the time-period T_r, the integrator output reaches the value B. Since the *RC* value of the integrator is fixed and the integration is done for a definite time, output V_x of the integrator at the end of the integration period [identified by point D in Figure 8.42 (b)] is given by

$$V_x \text{ at time } D = \frac{1}{RC}\int_0^{T_r} V_i\,dt \tag{8.40}$$

i.e., V_x at time D, is the time average of V_i to a definite scale. At time D, the control logic switches S_1 over to the reference voltage V_R. Normally the polarity V_R is opposite to that of V_i. The integrator output starts reducing from its peak value at B. It drops continuously and crosses zero at time C. The zero-crossing is detected by the comparator. Time interval DC – denoted by T_s – is related to the time interval T_r by the equation

$$\frac{1}{RC}\int_0^{T_r} V_i dt = \frac{1}{RC}\int_{T_r}^{T_r+T_s} V_R dt = \frac{V_R T_s}{RC} \tag{8.41}$$

$$\therefore T_s = \frac{1}{V_R}\int_0^{T_r} V_i dt \tag{8.42}$$

Equation 8.42 shows that the time interval T_s is a measure of the average value of V_i. V_R provides the 100 % reference level. The control logic routes the clock pulses to the counter during the time interval T_s. Thus the number of clock pulses allowed through, is a measure of the voltage V_i. The count remaining in the counter at time C, is a measure of the input signal V_i and forms the required digital output.

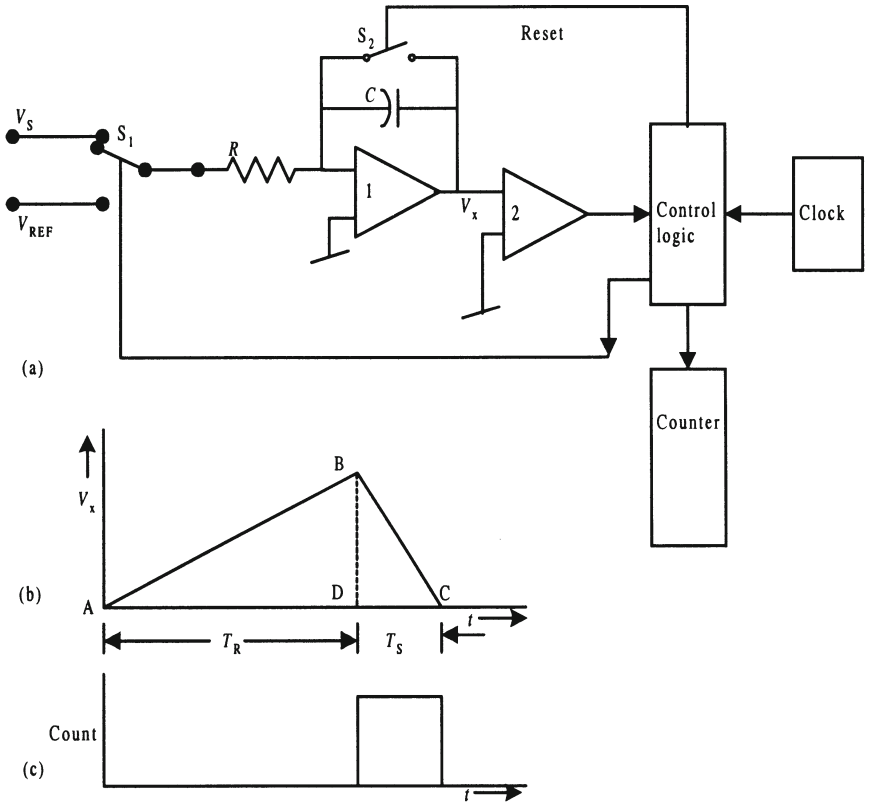


Figure 8.42 Operation of the dual slope ADC: (a) Circuit in block diagram form (b) Waveform of integrator output (c) Count command signal

Practical realizations of the dual slope ADC use a compensation technique to nullify errors due to offset voltage and temperature drift. With the input grounded, one can go through the dual-slope integration process. The counter content at the end of this cycle is a measure of the drift in the integrator and the comparator. Such a compensatory conversion cycle precedes the main conversion cycle above. The count remaining at the end of the compensating cycle is automatically subtracted from the main count during the conversion. Thus, the 4 modes of operation together, ensure a conversion free of drift-errors.

Normally the count output is loaded into a register with tri-state output, at the end of the conversion cycle. The register output may be read under μC control. Control signals normally available are as follows: -

⇒ *Start Conversion*: Enabling this input, initiates a new conversion cycle.
⇒ *End of Conversion* (*Busy*): This goes active as soon as a conversion cycle is completed and the converted data loaded into the output register.
⇒ *Read / Strobe*: Read the output data.
⇒ *Chip Select*: Selects the chip for initiating conversion. Reads the chip after the completion of conversion.

Observations: -

⇒ Some ADCs have the facility to provide BCD coded outputs. Others provide direct drive to 7 segment display drivers. These are useful for direct measurement and display.
⇒ The conversion process is independent of R, C and their tolerance. RC should be selected such that $T_s < T_r$ (but T_s should not be less than 20 % of T_r for good accuracy). Conversion is also independent of clock frequency.
⇒ Conversion accuracy is solely decided by V_R. Hence, tolerance and drift of V_R are very important.
⇒ For long conversion periods, dielectric absorption (See Section 8.3.2.6) of the integrator capacitor C, may cause an error. Polypropylene capacitors have relatively low dielectric absorption.
⇒ The average value of V_s during the signal integration phase is converted. This is equivalent to a first order low pass filter and provides filtering of 6 dB per octave.
⇒ Normally T_r is chosen as a multiple of power supply period. (For 50 Hz, T_r = 60 ms is typical.). This ensures that the pick-up at the power supply frequency and its harmonics are attenuated substantially (Filter attenuation at these frequencies is infinite).
⇒ Due to the very process of integration based conversion, all codes exist, resulting in excellent differential non-linearity.
⇒ The converter is capable of very high accuracy. 20-bit conversion has become common. At 200 kHz clock frequency, a single conversion takes 5s. The conversion bandwidth is of the order of only 0.01 Hz. Data acquisition systems use these with comparatively slowly varying signals (chemical processes). These also find application in laboratory calibration systems.
⇒ Sigma-delta converters discussed in Section 8.7.6 have come into vogue in the recent years with the advent of sub-micron technology. They offer an attractive alternative to dual slope integrating analog-to-digital convertors.

8.7.2 Successive Approximation Type of ADCs

Successive approximation ADCs work on a feedback principle and achieve full conversion through an iterative process of successively better approximations and corrections. The basic scheme is shown in block diagram form in Figure 8.43. It has five functional blocks. For an n bit converter, the 'Successive Approximation Register (SAR)' is n-bit wide. At the end of conversion, its content represents the converted output. The DAC converts the SAR output to equivalent analog form.

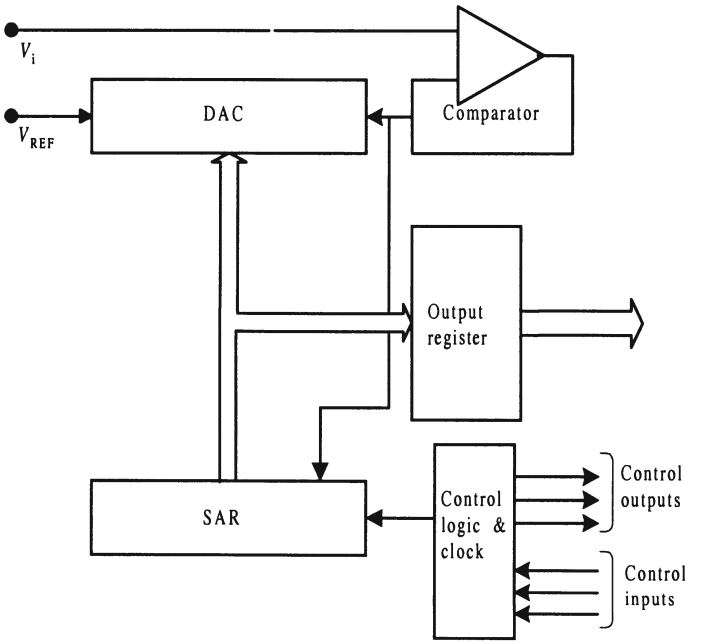


Figure 8.43 Successive approximation ADC – circuit in block diagram form

The analog output is compared to the analog input to be converted, by the comparator. The comparator output decides whether the SAR content is to be increased or decreased. The step by step procedure for conversion is as described below: -

⇒ The SAR is cleared on receipt of a 'Start Conversion' command. All the bits of the DAC input are zero. The converted output of the DAC is also zero. The comparator output is high. All these together represent the initialization process.

⇒ During the first clock cycle, MSB of the SAR is set. The comparator output is high or low depending on whether V_i, the analog voltage to be converted, is greater than the analog equivalent of the MSB or *vice versa*.

⇒ If the comparater output is low, the MSB is reset. If not, it remains high. This is done in the second half cycle. At this instant, the MSB is decided and the difference (V_i – the DAC output), is less than half of the full-scale output.

⇒ In the next clock cycle, the bit next to MSB is decided in the same manner.

⇒ The process is continued until all the bits of the SAR are decided. The basic conversion is completed in n clock cycles (one clock cycle / per bit).
⇒ The 'End of Conversion (EOC)' bit is activated signalling that the conversion is completed. The microcontrollers (or other devices requesting services) can read the output by activating the tri-state output register.

Observations: -

⇒ All the blocks shown in the Figure 8.43 and the voltage reference are realized in a single IC. Now-a-days sample and hold unit as well as the multiplexer are also, integrated into the analog-to-digital convertor.
⇒ Often additional features as serial data output and gain adjustment for scaling of the analog signal, are built-in.
⇒ CMOS versions of 12-bit ADCs take 15 μs for conversion. High speed versions using bipolar technology for the analog side do 12 bit conversion in less than 1 μs.
⇒ A 12 bit ADC with *R*-2*R* ladder network based DAC, consumes about 400 mw. Some versions, which use switched capacitor based ladder network for DAC, consume about 100 mw. These may be 20 to 30 % slower.
⇒ The resolution available with successive approximation type ADCs has increased over the years. Today they are available with widths up to 16 bits.
⇒ Successive approximation type ADCs offer cost effectiveness with good accuracy and bandwidth. They are the most widely used ADCs. Barring high-accuracy laboratory instrumentation, most other instrumentation schemes use successive approximation type ADCs for conversion.

8.7.3 Flash ADCs

The Flash ADC is shown in Figure 8.44 in block diagram form. The reference voltage V_R is applied to a resistance based potential divider chain, which generates references at $q/2$. $3q/2$, $5q/2$, and so on where q is the quantization level. An n bit convertor has 2^n such references. V_i is compared with all these references through n comparators. If $\{(q/2) + kq\} < V_i < \{(q/2) + (k + 1)q\}$, all comparators from the lowest to the k^{th} have 1 as output. All the rest have zero output. This coding is often referred to as 'Thermometer Code'. These outputs are subsequently decoded to provide binary (or other decided) outputs.

Observations: -

⇒ Flash converter is the fastest of all ADCs. Conversion time is the total propagation delay plus the time to encode the thermometer code output to binary form.
⇒ An 8-bit conversion has 256 references and 256 comparators. The following encoder has 256 inputs and 8 outputs. A 9-bit converter has 512 references, comparators and encoder inputs. The ADC circuit is complex and the complexity increases rapidly with increase in the desired resolution.
⇒ For fast operation, all the comparators have to run at high power. This increases power dissipation to the order of 500 mw.
⇒ For the above reason the reference current chain has to work at a high current level – 10 mA is common. This causes a heavy load on the reference.

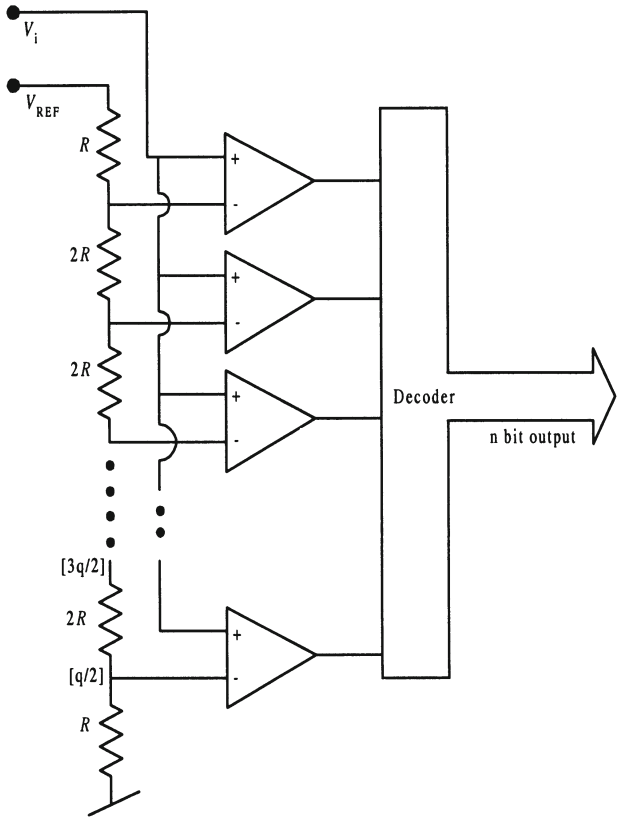


Figure 8.44 Flash type ADC circuit in block diagram form

⇒ The input is applied directly to all comparators simultaneously. Thus, the ADC is a sampling converter. No separate sample and hold amplifier is used. With fast changing signals, the aperture error can be significant.

⇒ 8-bit flash ADC is common. Conversion rate is to the tune of 500 M samples/s. A 10-bit flash ADC (not so common), can convert up to 300 k samples/s.

8.7.4 Sub-Ranging ADC

The limited resolution of flash ADCs can be overcome by modifying it with the help of the successive-approximation approach. Such an ADC – called the 'Sub-Ranging' ADC, is shown in Figure 8.45 in block diagram form [Analog Devices]. The sample-hold amplifier samples the signal and holds. This is converted into digital form by a Flash ADC. Its output forms the 6 MS bits of the converted output. This is converted back into analog form by a 6 bit DAC. Its output is subtracted from the sample. The difference - for a 12 bit converter - is lower than V_R /64. It is amplified (normally by 64 to bring it up to the full-scale level) and once again converted to 6 bit digital form. The latter 6 bits represent the 6 LS bits of converted output. They are combined with the 6 MS bits to form the 12 bit output.

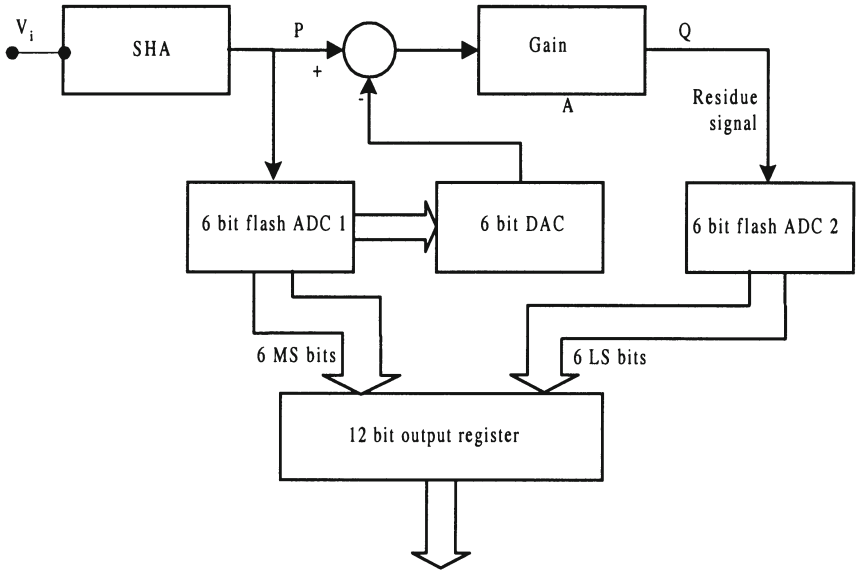


Figure 8.45 Sub-ranging in block diagram form

Observations: -

⇒ The accuracy of the 6-bit DAC has to be better than 2^{12}, since the errors introduced by it, are not corrected.

⇒ ADCs using one switch per level, (63 for 6 bit ADC), are common. They ensure good linearity and low transients.

⇒ An additional sample-hold amplifier (SHA2) can be introduced at point Q in Figure 8.45. This makes the operation of the MS and LS sections staggered and sequential. While the LS half of the first sample is being converted by the second half of the unit, the corresponding analog value is held by SHA2. During this time, SHA1 can hold the next sample and MS bits of the same are decided. The original sampling rate of one flash ADC is maintained. The full output becomes available with a delay of one clock cycle (Latency of one clock cycle).

⇒ The fast conversion process can lead to non-linearity errors and missing codes. The LS half of the unit can be made one more bit wide. Its MS bit overlaps with the LS bit of the MS side. The two are combined and error-correction implemented. This modification eliminates one major source of non-linearity error.

⇒ The resolution can be improved by additional stages of cascading. In each case, the sample rate remains the same. Only the latency increases. Thus with three stages, the full converted output of the n^{th} sample becomes available only when the $(n + 2)^{th}$ sample is being input. (Normally the number of cascaded stages is limited to two or three).

⇒ High-speed data acquisition systems and imaging systems use this fast high resolution ADCs. Instrumentation schemes which require on-line information extraction through DSP, also use these ADCs

⇒ A typical 2 stage sub-ranging ADC of 12-bit resolution, can sample at 20 MHz. It consumes 600 mw and has an input impedance of 200 Ω.

8.7.5 Serial or Ripple ADC

The basic building block of the serial ADC is shown in Figure 8.46 (a) [Analog Devices]. The input is given to a Zero Crossing Detector [ZCD]. The zero crossing detector output is 1 or 0 depending on whether the input is positive or negative. The input is also fed to an amplifier of gain 2. The ZCD operates a single pole double throw switch and switches $+V_R$ or $-V_R$ to a difference amplifier. If $V_i > 0$, V_o the residue R becomes

$$R = (2V_i - V_R)$$

If $V_i < 0$,

$$R = (2V_i + V_R)$$

Always the residue lies within the $\pm V_R$ range as long as V_i lies within the $\pm 2 V_R$ range [Figures 8.46 (b)]. The stage converts the analog input into a one bit digital output –available at the ZCD output and amplifies the residue by a factor of two – *i.e.*, scales it up to the full-scale level. By repeated sequential use of the basic building block, we can get an ADC of the required precision. The scheme of Figure 8.47 and the related characteristics, pertain to a 3-bit convertor using the basic building block of Figure 8.46 (a). The output is available in binary form directly. The transitions in the converter are marked by abrupt changes. At mid-range when the MSB changes from 0 to1, all bits change simultaneously. This can cause maximum propagation delay, oscillations *etc*. These also occur at some other transitions though not at such severe levels.

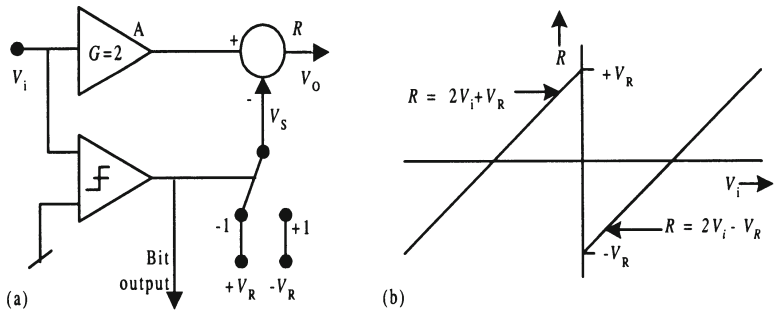


Figure 8.46 Ripple ADC (a) Basic building block (b) R versus V_i characteristic

The basic building block of Figure 8.46 (a) has been modified in Figure 8.48 (a) to provide Gray code type output. Here V_R is retained and $+2V_i$ or $-2V_i$ is switched on to the difference amplifier. The residue can be seen to go through a smooth transition throughout. Further, the output has the Gray code format as can be from the waveforms in Figure 8.48 (b). A 3-bit converter using this building block and the corresponding output levels, are shown in Figures 8.49 (a) & 8.49 (b). The Gray code output can be converted into binary form through suitable decoders.

The serial ADC is somewhat slower than the flash ADC. Barring this, the performance is on par.

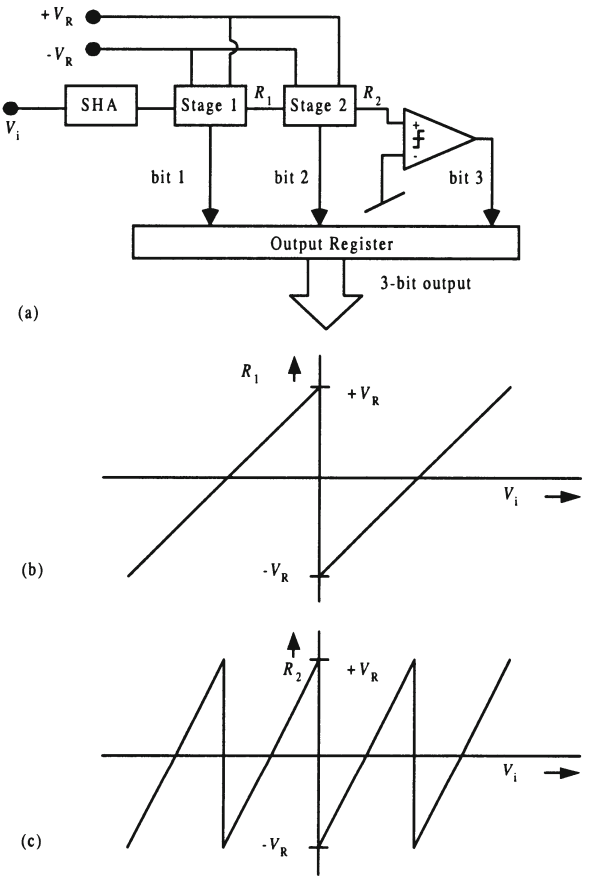


Figure 8.47 Ripple ADC with binary output (a) Circuit in block-diagram form (b) R_1 versus V_i characteristic (c) R_2 versus V_i characteristic

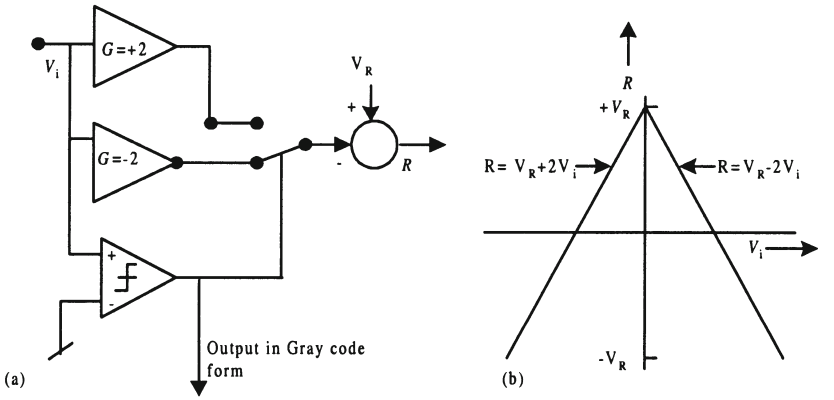


Figure 8.48 Modification to the basic building block of the ripple ADC to give output in Gray code form: (a) ADC in block diagram form (b) Nature of variation of Residue *R* with input

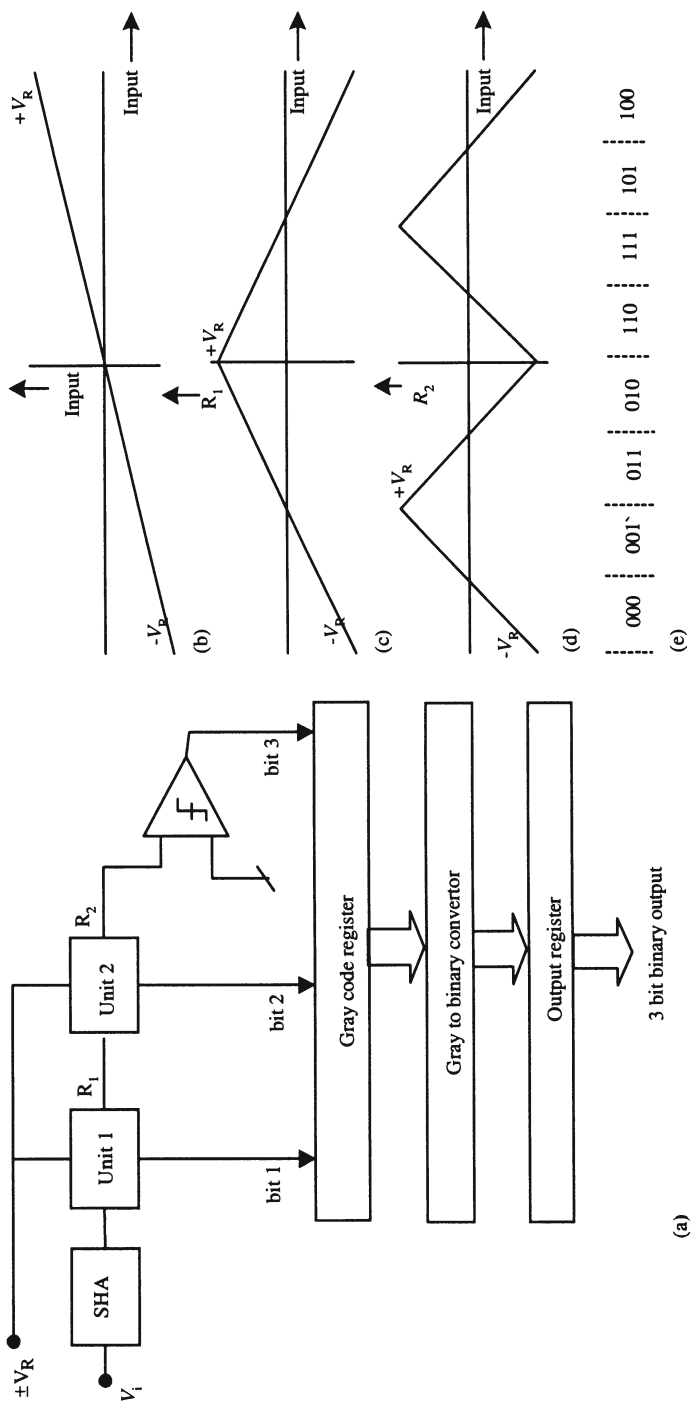


Figure 8.49 Modified form of 3-bit ripple ADC; (a) Circuit in block diagram form (b) Input (c) Nature of variation of R_1 with input (d) Nature of variation of R_2 with input (d) Gray code outputs for different input ranges

8.7.6 Sigma Delta Converter

Conventional ADCs sample the signal directly and quantize the same. Any increase in the resolution required, results in a reduction in the sampling frequency and hence the allowable signal bandwidth directly. Thus increase in the resolution of conversion and increase in the bandwidth of the signal converted, are conflicting requirements. These two issues can be segregated using 'Differential Quantization' [Proakis and Manolakis]. Here the changes in the signal from the last sample value – the converted value of the last sample to be more precise – is quantized. The quantizer provides only a single bit output (See Figure 8.50). In a subsequent stage, this bit is suitably augmented with the previous bits, to obtain the ADC output. For a satisfactory operation of the scheme, the change in the signal, between two successive sampling instants, has to be less than q. This requires the sampling frequency to be high compared to the signal bandwidth.

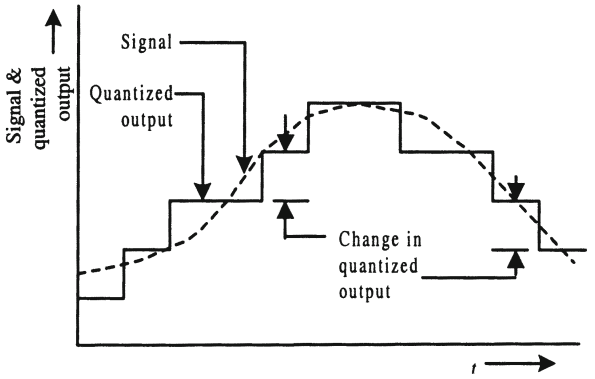


Figure 8.50 One bit quanization

The 'Sigma Delta Modulator (SDM)' uses the differential quantization principle in an ingenious manner. It is a feedback scheme as shown in Figure 8.51 in block diagram form. It generates the difference between the analog signal to be converted and a two-state output ($+V_R$ and $-V_R$). This difference (error) is integrated and fed to

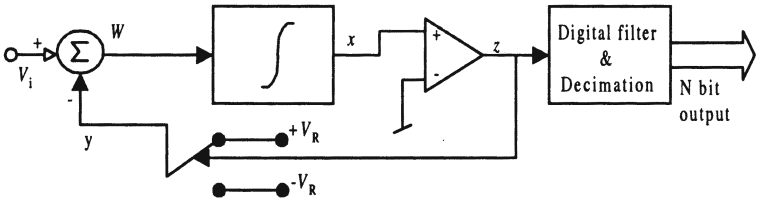


Figure 8.51 Sigma-delta convertor in block diagram form

a ZCD. The ZCD output is at state 1 or 0. When in one state it switches $+V_R$ to the error-detector and when in zero state, $-V_R$ to the same. The converter output is a stream of 1s and 0s. Under stable operating conditions, the average value of the integrator input is zero; else its output will increase continuously leading to instability. In turn, $\bar{y}$ – the average value of y – must be equal to v_i. Since the

switching of y to $+V_R$ and $-V_R$ is done at a fast rate compared to the cut-off frequency ω_m of the signal v_i, we have

$$\bar{y} = v_i \tag{8.43}$$

$\bar{y}$ = (Number of 1s - number of 0s over the period of averaging) V_R.

Or

$$\text{Number of 1s - number of 0s of the ZCD output} = \frac{\bar{y}}{V_R} \tag{8.44}$$

Hence the difference evaluated as in Equation 8.44 represents the signal v_i. The steady state operation of the scheme is illustrated here through three specific examples (See Figure 8.52). The associated numerical values are given in Table 8.5. In every case the average output is seen to be the input itself.

Table 8.5 v_i and the corresponding output values of the SDM for the waveform in figure 8.52

Characteristic	Case 1	Case 2	Case 3
v_i (ε is a small value)	$V_R/2$	$V_R(1-\varepsilon)$	ε
Slope of segment AB	$-V_R/2$	$-\varepsilon V_R$	$V_R(1-\varepsilon)$
Slope of segment BC	$+3.V_R/2$	$(2-\varepsilon)V_R$	$V_R(1+\varepsilon)$
No. of clock cycles required for averaging	4	$(2/\varepsilon)$	$(1/\varepsilon)$
No. of 1s - No. of 0s over the averaging period	2	$(2/\varepsilon)-1$	1
Average output [V_R(No. of 1s - No. of 0s over the averaging period)]	$V_R/2$	$V_R(1-\varepsilon)$	$V_R\varepsilon$

The discrete time model of the SDM is shown in Figure 8.53. G(z) represents the sampled transfer function equivalent of the integrator {See Appendix A]. n_q stands for the quantization noise (See Section 8.2.3).

From Figure 8.53, we get

$$Y(z) = \frac{G(z)}{1+G(z)}X(z) + \frac{1}{1+G(z)}N_q(z) \tag{8.45}$$

where

$$G(z) = \frac{z^{-1}}{1-z^{-1}} \tag{8.46}$$

Substitution in Equation 8.45 and simplification yields

$$Y(z) = z^{-1}X(z) + (1-z^{-1})\,N_q(z) \tag{8.47}$$

$$= Y_s(z) + Y_n(z) \tag{8.48}$$

where

$$Y_s(z) = z^{-1}X(z) \tag{8.49}$$

and

$$Y_n(z) = (1 - z^{-1})N_q(z) \tag{8.50}$$

$Y_s(z)$ represents the signal component of $Y(z)$ and $Y_n(z)$ represents the quantization noise component in it. Equation 8.49 shows that $X(z)$ appears at the output side without any distortion – but only with a fixed time delay. The quantization noise undergoes a spectral modification.

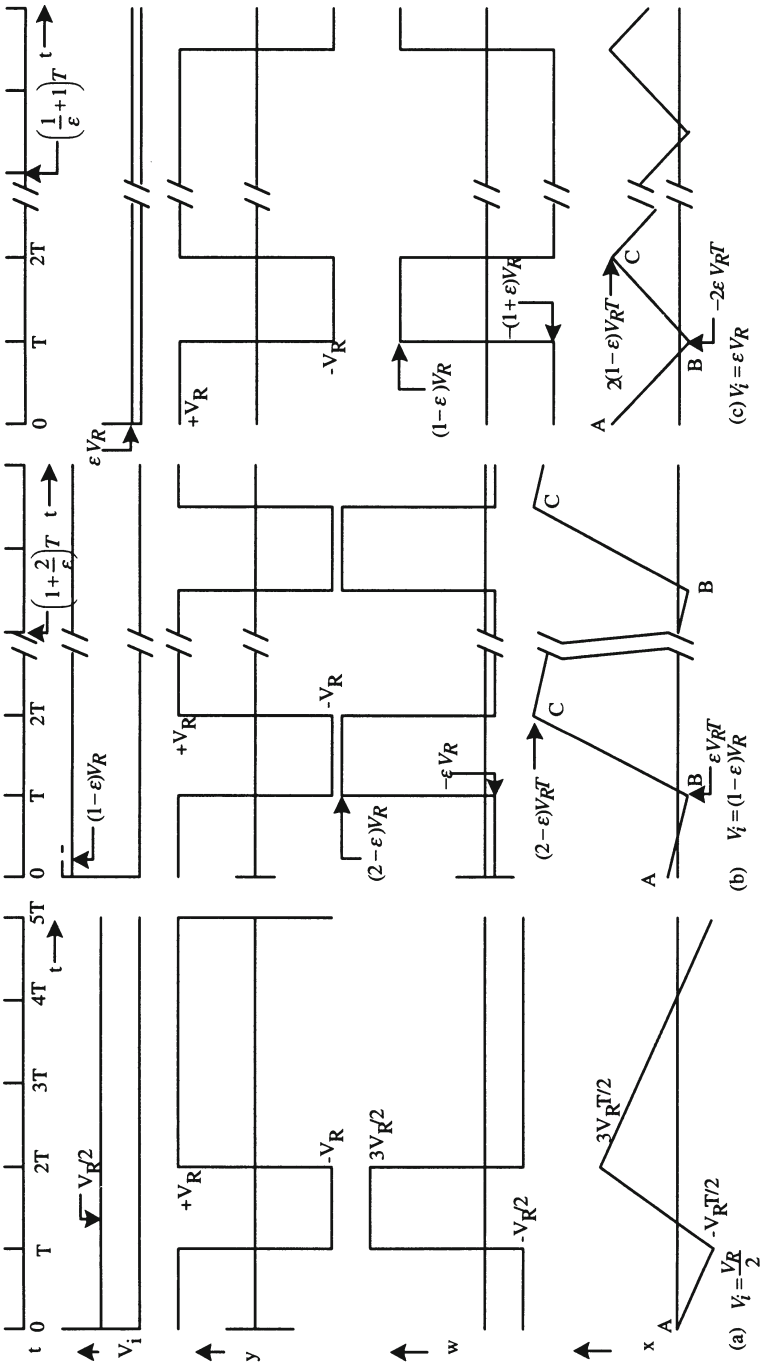


Figure 8.52 Waveforms of signals at different points of the sigma-delta convertor of Figure 8.51 for three different cases

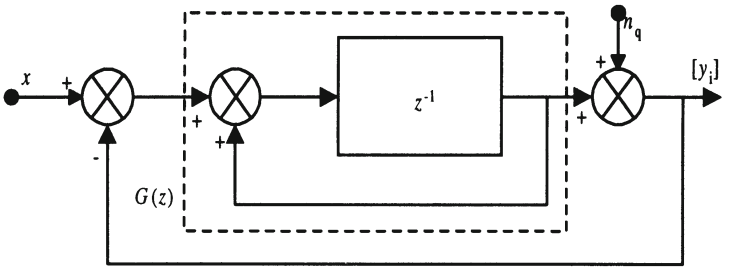


Figure 8.53 Discrete-time model of the sigma-delta convertor

From Equation 8.13

$$\overline{n_q^2} = \frac{q^2}{12}$$

Taking this to be uniformly distributed over the whole range of frequencies – $(-f_s/2)$ to $(+f_s/2)$ –

$$\text{Power spectral density of } n_q = \frac{q^2}{12\omega_s} \tag{8.51}$$

where

$$\omega_s = \frac{1}{2\pi T_s} = 2\pi f_s \tag{8.52}$$

Substituting $z^{-1} = \exp[-j\omega T]$ in Equation 8.50 and using Equation 8.51, the power spectral density $|Y_n(j\omega)|^2$ of $Y_n(z)$ is obtained as

$$|Y_n(j\omega)|^2 = \frac{q^2}{3\omega_s}\sin^2\frac{\omega T}{2} \tag{8.53}$$

Equation 8.53 shows that the quantization noise undergoes a spectral modification. The low frequency components are attenuated [Note that at $\omega = 0$, $|Y_n(j\omega)|^2 = 0$). Since the signal spectrum extends up to only ω_m, the components beyond ω_m may be filtered out. This is done by the digital filter at the output side of the SDM loop. With this *proviso*, noise in the output is obtained by integrating $|Y_n(j\omega)|^2$ over $-\omega_m$ to $+\omega_m$. This gives the net quantization noise at the output side as

$$\overline{y_n^2} = \int_{-\omega_m}^{+\omega_m} \frac{q^2}{3\omega_s}\sin^2\frac{\omega T}{2}\,d\omega$$

$$= \frac{q^2}{3\omega_s}\left(\omega_m - \frac{\sin\omega_m T}{T}\right) \tag{8.54}$$

With $\omega_s >> \omega_m$, Equation 8.54 can be approximated to

$$\overline{y_n^2} = \frac{\pi^2}{3}\left(\frac{2f_m}{f_s}\right)^3\overline{n_q^2} \tag{8.55}$$

From Equations 8.13 and 8.55 we have

$$10\log\left(\frac{\overline{y_n^2}}{n_q^2}\right) = 5.2 + 30\log\left(\frac{2f_m}{f_s}\right)dB \qquad (8.56)$$

Equation 8.56 shows that doubling of f_s reduces the quantization noise component on the output side by 9dB.

In effect $[y_i]$ in Figure 8.51, is a serial stream of 1s and 0s. Their sum taken over long segments of the stream represents the converted output. The quantization noise component in this can be reduced by filtering with a corner frequency of ω_m. This twin function of summing samples in non-overlapping intervals and filtering with corner frequency ω_m, is achieved through decimation and digital filtering [See Section 9.3]. The filtering is done with a digital filter of 4 to 8 poles to provide effective attenuation of off-band noise. The salient features of the scheme and its advantages are as follows: -

- ⇒ The SDM always converts the last bit. Hence, its effective sampling rate is high. It is a one bit high speed converter.
- ⇒ For an analog signal of bandwidth 0 to f_m, sampling frequency $f_s = 2nf_m$, where n is decided by the resolution desired. n is called the 'Over-Sampling Ratio'. It can be in the 64 to 1000 range.
- ⇒ The stop band frequency of the anti-aliasing filter can be as high as $f_s/2$ (equal to nf_m). Due to the large value of n, even a first order filter suffices for this
- ⇒ The quantization at $2nf_m$, spreads the quantization noise spectrum uniformly over the 0 to nf_m range. Contrast this with the conventional sampling, where it is spread over a restricted frequency range, and hence appears with a correspondingly larger power spectral density.
- ⇒ The digital filtering and decimation done on the output bit stream [See Section 9.3], filters out components of frequencies greater than f_m. Very sharp cut-off digital filters are used. With this, the quantization noise in the band f_m to nf_m is substantially eliminated. Thus, there is a two-stage reduction in the quantization noise (See Figure 8.54).
- ⇒ The SDM loop described here, is a simple first order one. The dynamic range can be improved by going in for higher order loops. Third, fourth and fifth order loops are common. Derivations similar to that with Equation8.56 show that with every increase in the order of the SDM loop, the quantization noise in the output reduces by 6dB. However with such high order loops, loop stability has to be analyzed through careful loop analysis, and design before implementation.
- ⇒ Due to the 1 bit quantization, SDC offers excellent differential and integral non-linearity performance.
- ⇒ Over-sampling ratio, loop order and digital filter complexity can be traded off in different combinations to suit needs. Increase in clock frequency improves overall performance.

The conspicuous gain of the SDM based ADC, is the substantial reduction in the effective noise in the converted output, due to quantization [See Yamada and Watanabe for a novel application]. With this, it has been possible to improve resolution substantially without sacrificing accuracy. Key specifications of two representative SDM type of ADCs are given in Table 8.6.

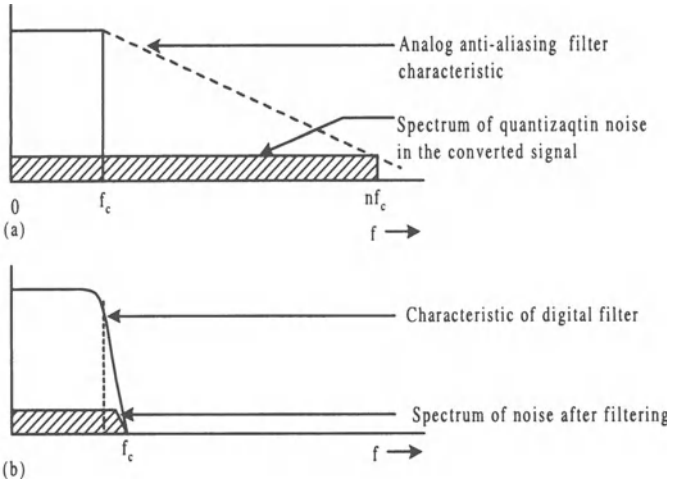


Figure 8.54 Noise-reduction in sigma-delta convertor: (a) Characteristic of the analog filter preceding ADC along with the spectral characteristics of quantization noise (b) Characteristic of the digital filter at the output side and that of the noise spectrum passed through

Table 8.6 Key specifications of two ADCs of SDM type.

Property	AD 1849	AD 7701
Signal frequency range	0 to 20 Hz	0 to 10 Hz
Number of bits	18	16
Over-sampling ratio	64	800
Stop band attenuation	118 dB at 26kHz	55 dB at 60 kHz
Digital filter	4096 taps FIR type	6 pole
SDM loop order	5	2
Power consumption	900 mW(Dual channel ADC)	40 mW
Suggested application	Digital audio	Process Instrumentation

8.7.7 Microcomputer Interface

All ADCs provide minimal interface to μCs. The interface is in terms of the output buffer, the start conversion command, the end of conversion flag and an output enable command. All these have been discussed as part of the different types of ADCs considered so far. The minimal set of control lines, is as follows: -

⇒ *Start Conversion* (*SC*): This logic input initiates the conversion operation

⇒ *End of Conversion* (*EOC*): This logic output signifies that the conversion is complete and the output data may be read. Often this is used as an interrupt input to the μC. As part of the interrupt service routine, the μC may read the converted digital output.

⇒ *Read* (*RD*): This is a logic-input command. It reads the output register and makes the data available on the data bus of the μC.

⇒ *Chip Select* (*CS*): Activation of this logic selects the ADC. It is activated to start conversion as well as to read the converted output on to the μC. Through this, the ADC is given a specific address assignment in the μC.

Observations: -

⇒ In multi-channel ADCs, the analog mux may be part of the converter IC. The address lines for channel selection will be additional inputs here. Some ADCs may have a separate address register. With this, channel selection and starting of conversion can be separate events.

⇒ Some high resolution ADCs have the provision to reduce resolution optionally. They have a separate mode select input. e.g., a 12 bit ADC may be worked in a 10 bit mode at an increased speed.

⇒ Some ADCs have the provision for serial data output. The output is available as a bit sequence synchronized to the ADC clock. These may have the provision to function with external clock input.

⇒ 8-bit ADCs are interfaced to microcontrollers with the 8-bit output lines directly connected to the data bus. With ADCs of more bandwidth, the output may be read byte-wise. Different types of interfaces are available. Some provide all bits as parallel outputs simultaneously. Through suitable external multiplexing, these may be read byte-wise sequentially. In others, such multiplexing and sequencing facility is built-in. Such ADCs may be interfaced to microcontrollers more easily.

9 Digital Signal Processing for Instrumentation

9.1 Introduction

When a sensor signal is converted into a digital form through an ADC, the digital output is normally in binary form; it is further processed by a microcomputer. In many cases, the processing may involve some rudimentary checks and display. Checks to see whether signals remain within safe limits or not and logical decisions based on the same are of this category. Others like handling keyboards and displays, binary to BCD and other number conversions, are common to microcomputer routines also. Corrections for extraneous factors like cold junction compensation of thermocouples, normalization, simple algebra (obtaining power from current and voltage, obtaining square root to determine flow rate from head drop), are somewhat more involved. Though quite varied in nature, these are accommodated easily in ordinary microprocessor based design. Activities like calibration, which call for execution of carefully planned sequences and minimal computation are also of this category. These are all specific to instrumentation schemes and allied areas. At the other extreme, we have the front-end software applications and those of a specialized nature as used with data acquisition systems, or image processing applications. These are too specialized or exhaustive to find place here. There are some common routines that find repeated and skilful use in instrumentation. These form our object of discussion here. The topics dealt with are: -

⇒ Linearization and non-linearization through Look-up-tables (LUT).
⇒ Interpolation and extrapolation (Prediction).
⇒ Differentiation
⇒ Integration
⇒ Filtering
⇒ Fast Fourier Transform (FFT).

Commonly used algorithms for the above, are discussed and salient features brought out in each case. Wherever relevant, a C / C++ program is also included. The discussion is essentially from an utilitarian view; derivations, proofs and rigour have been left out; text books on digital signal processing may be consulted for the same [Oppenheim and Schafer, Proakis and Manolakis, Rabiner and Gold].

9.2 Handling LUTs

A number of situations arise in instrumentation schemes, which call for the use of LUTs. In some cases the sensor output is inherently non-linear and requires linearization (e.g., base metal thermocouples). A slightly different situation arises when the magnitude of a physical variable is to be ascertained from the sensor

T. R. Padmanabhan, *Industrial Instrumentation*
© Springer-Verlag London Limited 2000

output – the two being related through a monotonic function (e.g., orifice type flow meters). In other cases, the sensor output is to be corrected depending on the changes in the ambient conditions (gas flow meters and corrections for temperature and pressure variations). In all such cases, the necessary information or data is available in the form of LUTs. The microcomputer has to use these in the required manner.

9.2.1 Direct Reading

The output of a sensor and a physical variable may be related through a sequence of entries in tabular form. The sensor output is represented by n discrete equally spaced values. Each of these has a corresponding value stored in a LUT. Let it be stored in n successive locations starting with the address M_1. Specifically

⇒ Location M_1 has the first entry
⇒ Location M_2 has the second entry
⇒ Location M_3 has the third entry
and so on.

Let the number M_0 (representing the address of M_0 in above sequence) be stored as an address, in a register R_1 in the microcomputer and let R_2 be a destination register to store the corresponding value of the variable. Consider a sensor output 'k'. Execution of the program sequence

⇒ Add k to the content of R_1 [R_1 contains the address of memory location M_k]
⇒ Fetch the data stored in location pointed by R_1 [M_k contains the required value of the physical variable].
⇒ Store the fetched data in R_2 [results in R_2 containing the corresponding value of the physical variable].

This three-line program suffices for all single byte entries. To obtain enough precision, sometimes, the output quantity may be two or three bytes wide. The bytes representing each value of the variable, may be stored in successive locations. In such cases, k in the first line of the above routine is replaced by $(2\ k - 1)$ or $(3\ k - 2)$ as the case may be.

As a specific example, consider a thermocouple LUT. For a 0°C to 400°C range with 0.1°C resolution, we have 4000 discrete states and as many entries in the table. The LUT occupies 4k, 8k or 12k bytes for 8,16 and 24 bit resolutions respectively. With today's microcontrollers, this is not a significant overhead. But if the precision required or the range required (or both) increases, a brute force LUT of this type, may not be the best solution. A better alternative is to decide the output of required precision in two stages with two separate LUTs. The first LUT can be of 400 words with entries at 1°C intervals; the second may store the respective mean differences. For a well-behaved function the mean difference does not change abruptly (those we encounter in practice are mostly of this category); hence the second table will be of relatively smaller size. The desired value for any specific sensor output can be obtained using both the tables, by interpolation.

Let $x_1, x_2, x_3, \ldots$ be the equally spaced sensor output values.

Let $y_1, y_2, y_3, \ldots$ be the corresponding main outputs sequentially stored.

Let $\Delta y_1, \Delta y_2, \Delta y_3, \ldots$ be the respective mean differences stored in an auxiliary table of mean difference. The value of y for an x lying between x_n and x_{n+1}, is obtained as

$$y = y_n + \Delta y_n \frac{x - x_n}{x_{n+1} - x_n} \quad (9.1)$$

$$= y_n + y_n(x - x_n) \quad (9.2)$$

since

$$x_{n+1} - x_n = 1 \quad (9.3)$$

Example 9.1

Consider the case of an Iron-Constantan thermocouple. A portion of the table of thermo-emfs at 1°C intervals is shown in Table 9.1. The cold junction is taken to be at 0°C. The C language routine to obtain these, using the power series for thermo-emfs [See (NBS)] is given as Program 9.1 at the end of the chapter. The table of mean differences in thermo-emfs at 5°C intervals is in Table 9.2. For a temperature of 78.3 °C, the thermo-emf is obtained from these two tables in the following manner: -

Table 9.1 EMF of Iron-Constantan Thermocouple

(Cold junction temperature = 0°C)					
Hot junction temperature	Thermo-emf (mV)	Hot junction temperature	Thermo-emf (mV)	Hot junction temperature	Thermo-emf (mV)
70.000000	3.648734	77.000000	4.024254	84.000000	4.401216
71.000000	3.702287	78.000000	4.078020	85.000000	4.455179
72.000000	3.755872	79.000000	4.131815	86.000000	4.509169
73.000000	3.809488	80.000000	4.185639	87.000000	4.563186
74.000000	3.863134	81.000000	4.239491	88.000000	4.617229
75.000000	3.916811	82.000000	4.293372	89.000000	4.671298
76.000000	3.970518	83.000000	4.347281	90.000000	4.725393

Table 9.2 Mean differences at 5°C intervals (μV/0.1°C)

Temperature range(°C)	70-75	75-80	80-85	85-90
Thermo-emf(μV/0.1°C)	5.36	5.37	5.39	5.40

From Table 9.1,

$$\text{Thermo-emf at } 78°C = 4.07800\text{mV}$$

$$\text{Mean difference in the } 75°C \text{ to the } 80°C \text{ range} = 5.37\mu\text{V}/°C$$

$$\therefore \text{Thermo-emf at } 78.3°C = 4.07800 + 5.37 \times 0.3 \times 10^{-3}\text{mV}$$

$$= 4.09411\text{mV}$$

A more precise calculation using the polynomial form gives the figure of 4.094156mV for this temperature. The error here is 11ppm.

The precision for main and auxiliary tables has to be decided by some trial and error. The options to be considered are: -

⇒ For a selected interval, the accuracy in the main table can be traded off for that in the auxiliary table. Thus in the above case, the thermo-emf may be

entered with 4-digit accuracy and the mean differences with 2-digit accuracy; or the thermo-emf with 5-digit accuracy and the mean differences with 1-digit accuracy and so on. There are two factors to be considered:

- In today's microcontrollers, the shortest entry is one byte wide. Correspondingly, one need not reduce mean difference width below two digits.
- The maximum deviation of the interpolated output value from the actual value, over the full range of interest, has to be minimum.

Both these are common to all the options considered below.

⇒ The interval for the main entries can be reduced (increased) marginally. This increases (decreases) the size of the main LUT but decreases (increases) the width of the mean difference table. The LUT access time may increase (decrease) marginally but the computation of interpolated values takes less (more) time due to the reduced (increased) width of mean differences.

⇒ A main LUT, an auxiliary LUT of mean differences and another auxiliary LUT of second order mean differences may be stored. With these three tables, a second order interpolation may be carried out (See Section 9.5.2). This can be used to reduce memory-size, improve resolution or achieve a combination of both. An increase (decrease) in the size of the main interval may reduce (increase) access time marginally but increases the interpolation overhead. One can go a step further and use tables of higher order differences. However, this is not normally warranted or practiced.

⇒ One can have only a main table with a coarse interval. A well-selected prediction algorithm (See Section 9.5.2) can be used to obtain the interpolated values. This minimizes memory size and access overheads but increases computational overheads to the maximum.

9.2.2 Indirect Reading

Thermocouple LUTs are more easily available as emfs at equally spaced temperature intervals. When using a thermocouple for temperature measurement, one gets an emf from which the temperature is to be decided. This calls for an indirect reading of the LUT. Similar situations arise with other sensors too. Different approaches are possible.

One can use the Seebeck coefficient (in μV/°C) in the temperature range of interest, estimate the temperature by linear extrapolation and 'check back'. The checking back can be brute force sequential scanning of the table on either side of the extrapolated value until the desired temperature is obtained.

Example 9.2

Seebek coefficient for Iron-Constantan thermocouple = 54 μV/°C. We have to estimate the hot junction temperature corresponding to a thermo-emf of 4.094156mV with the cold junction being at 0°C.

$$\text{Approximate (first approximation) temperature using the Seebek coefficient} = \frac{4.094156}{54 \times 10^{-3}}$$

$$= 75.8°C$$

$$\text{From table 9.1, thermo-emf at } 75° = 3.916811 \text{ mV}$$

$$\begin{aligned}
\text{From Table 9.2, mean difference} \\
\text{[in the interval 75°C to 80°C]} &= 5.37\mu\text{V for } 0.1°\text{C} \\
\text{Refined temperature value} \\
\text{(second approximation)} &= 75 + \frac{4.094156 - 3.916811}{5.37 \times 10^{-3}} \\
&= 78.3025°\text{C}
\end{aligned}$$

The actual temperature is 78.3°C.

An iterative procedure is an attractive alternative. Let (x_1, y_1) and (x_n, y_n) be the first and the last entries in the table. Knowing the value y_k, we have to identify the corresponding x_k; an algorithmic procedure for this is as follows: -

Let $x_c = (x_1 + x_n)/2$

If $x_c - x_1 = 1$, terminate the loop.

Get y_c from the LUT.

If $y_c > y_k$, replace y_n by y_c. Proceed to step (1).

If $y_c < y_k$, replace y_1 by y_c. Proceed to step (1).

If $y_c = y_k$, terminate the loop.

n can be chosen as a power of 2. Then x_c in step (1) – taking it to be in binary form – can be formed by right shifting $(x_1 + x_n)$. For a table of m entries, $\log_2 m$ iterations are required.

One can refine the above procedure and improve the accuracy by linear interpolation between adjacent samples. The C language routine of program 9.2, given at the end of the chapter, combines the above type of iteration with a final stage of interpolation.

Example 9.3

For a thermo-emf of 4.094156 mV, the hot junction temperature is obtained using the routine of program 9.2. Data of Table 9.1 is generated as part 1 of the program; subsequently in part 2, the required temperature is computed. The estimated temperature as obtained from the program, is 78.29995°C; compare this with the actual value of 78.3°C.

The precision of interpolation can be improved upon, using the Lagrange formula for unequal intervals. The formula for four consecutive samples, is

$$\begin{aligned}
x = &\frac{(y-y_2)(y-y_3)(y-y_4)x_1}{(y_1-y_2)(y_1-y_3)(y_1-y_4)} + \frac{(y-y_1)(y-y_3)(y-y_4)x_2}{(y_2-y_1)(y_2-y_3)(y_2-y_4)} + \\
&\frac{(y-y_1)(y-y_2)(y-y_4)x_3}{(y_3-y_1)(y_3-y_2)(y_3-y_4)} + \frac{(y-y_1)(y-y_2)(y-y_3)x_4}{(y_4-y_1)(y_4-y_2)(y_4-y_3)}
\end{aligned} \tag{9.4}$$

Here x_1, x_2, x_3 and x_4 are the successive address locations in the LUT and y_1, y_2, y_3 and y_4 the respective entries. The algebra is cumbersome here and time consuming. This is due to the inherently non-uniform spacing of values of the independent variable. Alternately one can prepare a LUT with a limited number of entries spanning the full range of x and y. This along with the Lagrange interpolation formula can be used to compute the desired value of the variable. Reduction in LUT size is achieved here at the expense computational simplicity.

Example 9.4

Let us compute the hot junction temperature x using 4 sets of values x and y. The selected values of temperatures and respective emf's are given in Table 9.3.

For

$$y = 4.094156\text{mV}$$

Substitution in the Lagrange interpolation formula of Equation 9.4 gives

$$x = \frac{0.177345\times(-0.091483)\times(-0.361023)\times 70}{(-0.268077)\times(-0.536905)\times(-0.806445)} + \frac{0.445422\times(-0.091483)\times(-0.361023)\times 75}{0.268077\times(-0.268828)\div(-0.538368)} + \frac{0.445422\times 0.177345\times(-0.361023)\times 80}{0.536905\times 0.268828\times(-0.270179)} + \frac{0.445422\times 0.177345\times(-0.091483)\times 85}{0.806445\times 0.538368\times 0.270179}$$

$$= 78.1737°\text{C}$$

Note that the actual temperature for this thermo-emf is again 78.3°C. Considering the fact that (x_1, y_1), (x_2, y_2), (x_3, y_3) and (x_4, y_4) have been taken at widely spread out intervals, the result is quite accurate (accuracy of 0.16%). This is essentially due to the smoothness of the temperature versus thermo-emf characteristic.

Table 9.3 x (°C) and y(mV) co-ordinates for Example 9.4. The values are from Table 9.1

$x_1 = 70$	$x_2 = 75$	$x_3 = 80$	$x_4 = 85$
$y_1 = 3.648734$	$y_2 = 3.916811$	$y_3 = 4.185639$	$y_4 = 4.455179$

9.2.3 Corrections for Parametric Changes

For convenience, consider an illustrative example. Gas flowmeters are provided with calibration curves. These can be translated into LUTs and used in the manner discussed above. Normally the readings require corrections for changes in the ambient temperature and the pressure in the gas line. The calibration curves are provided as a family with temperature and pressure as running parameters. Each curve of the family, can be realized as a LUT – each LUT being treated as a page of memory. Reading is a two step process here – selecting the page and selecting the entry in the page concerned. The value sought does not necessarily lie in the given page. This calls for a two-dimensional or multi-dimensional interpolation. Different procedures and trade-offs are possible. These are similar to the interpolation in one-dimension (See Section 9.5.2).

9.3 Digital Filters

Filter characteristics and analog filters have been discussed in Chapter 5. Such filters can be realized in digital form also. Other types of filters are also possible to be realized in digital form. In general, all such digital filters fall into two categories: -

⇒ The digital filter is realized as the exact counterpart of a selected analog filter. For this a recursive relation, which is the difference-equation counterpart of the differential equation representing the analog filter, is used. Such filters are called 'Infinite Impulse Response (IIR)' filters.

⇒ Alternately, the filtered output can be obtained as a weighted-sum of a definite number of samples of the input. These are called 'Finite Impulse Response (FIR)' filters.

IIR and FIR filters have some difference in characteristics. Each type has its own sphere of application.

9.3.1 Finite Impulse Response Filter

For the same level of performance, an FIR filter is more complex than the IIR filter – the complexity is in terms of representation and realization. Despite this, FIR filters have two definite advantages: -

⇒ However long the filter chain may be, the filter does not have a stability problem. This is in sharp contrast to an IIR filter, where stability can be a problem as the filter order increases (say beyond two).

⇒ FIR filters can be designed to have the linear phase characteristic. The same is not possible with IIR filters. Where the nature of time variation of the signals is to be faithfully retained, – as is the case with instrumentation signals – linear phase characteristic is important. This makes the FIR filter the preferred choice for instrumentation applications, notwithstanding its complexity.

The n^{th} sample output of an FIR filter, is expressed as a weighted-sum of a definite number of samples of the input. The weight is evolved from a pre-defined unit impulse response of the filter. The z-transform of the impulse response has the form

$$G(z) = g_0 z^{-0} + g_1 z^{-1} + g_2 z^{-2} + \ldots + g_{k-1} z^{-(k-1)} \quad (9.5)$$

Here g_n represents the filter output at the n^{th} sampling instant following a unit impulse input to the filter at the zeroth sampling instant. It is assumed that the filter response is limited to only a definite number of samples and the response is zero at all the subsequent sampling instants. With this, the difference equation connecting the input sample sequence $[x_i]$ to the output sample sequence $[y_i]$, can be expressed as Equation A.9 [See Appendix A].

$$y_n = \sum_{i=0}^{k} g_i x^{-(n-i)} \quad (9.6)$$

Any desired filter characteristic can be realized using the FIR filter. The general approach to the design is as follows: -

⇒ Define the desired impulse response of the filter in terms of the independent variable *i*. The desired impulse response can be arrived at, in various ways. The inverse Fourier transform of a desired frequency response function, is a commonly used base – especially when the variables *x* and *y* are functions of time. When the independent variable is other than time, – say distance (and $[x_i]$ and $[y_i]$ represent the values of *x* and *y* respectively at regular intervals of the distance) – the impulse response can be defined from local physical considerations. Here *i* represents the discrete value of the independent variable (distance in the example considered).

⇒ Approximate the impulse response by a function $g(i)$ which extends only over a definite interval of x.; *i.e.*,

$$g(x) = 0 \begin{cases} x > x_2 \\ x < x_1 \end{cases} \tag{9.7}$$

where

$$x_2 > x_1 \tag{9.8}$$

⇒ From the approximated impulse response function, form the discrete impulse response sequence $[g_i]$, represented in Equation 9.5. x_1 was taken as zero in Equation 9.5; this was to conform to the fact that a physically realizable system responds only after the input is given to it. No such constraint exists, if the independent variable is other than time. In such cases, the z-transform of the impulse response of an FIR filter takes the more general form

$$G(z) = g_{-j}z^{-j} + g_{-(j-1)}z^{-(j-1)} + g_{-(j-2)}z^{-(j-2)} + \ldots\ldots + g_0 z^{-0} + g_1 z^{-1} + g_2 z^{-2} + \ldots\ldots + g_{k-1}z^{-(k-1)} \tag{9.9}$$

With this, the response to a general input-sequence $[x_i]$ takes the form

$$y_n = \sum_{i=-j}^{k} g_i x^{-(n-i)} \tag{9.10}$$

This is the general relation defining the n^{th} sample of the FIR filter output, in terms of its input sequence $[x_i]$.

9.3.1.1 *Linear Phase Filters*

An ideal lowpass filter has two characteristics: -

⇒ The gain is a constant in the pass band but zero in the stopband.

⇒ The filter should not cause any phase distortion in the passband range of frequencies. This being impractical, an acceptable alternative is a fixed time delay introduced by the filter.

Thus if $x(t)$ is the filter input, its output $y(t)$ can be

$$y(t) = x(t - \tau) \tag{9.11}$$

where τ is a constant quantity. Taking Laplace transform of both the sides,

$$Y(s) = \exp[-s\tau]\, X(s) \tag{9.12}$$

The substitution

$$s = j\omega \tag{9.13}$$

leads to

$$Y(j\omega) = \exp[-j\omega\tau]\, X(j\omega) \tag{9.14}$$

Equation 9.14 shows that the output will be delayed by a fixed time interval, if the phase shift introduced by the filter varies linearly with frequency.

The linear phase characteristic can be realized in two ways. Both are discussed here.

Method 1

Make

$$g_n = g_{k-1-n} \tag{9.15}$$

substituting in Equation 9.5 and rearranging, we get

$$G(z) = z^{-m}[g_0(z^m + z^{-m}) + g_1\{z^{(m-1)} + z^{-(m-1)}\} + g_2\{z^{m-2} + z^{-(m-2)}\} \ldots + g_m] \quad (9.16)$$

for odd values of k and

$$G(z) = z^{-m}[g_0(z^m + z^{-m}) + g_1\{z^{m-1} + z^{-(m-1)}\} + g_2\{z^{m-2} + z^{-(m-2)}\} \ldots.] \quad (9.17)$$

for even values of k.
In Equations 9.16 and 9.17

$$m = \frac{k-1}{2} \quad (9.18)$$

The Fourier transform of the filter $G(j\omega)$ is obtained by the substitution

$$z = \exp[j\omega T]$$

in Equations 9.16 and 9.17. Simplification following this substitution gives

$$G(j\omega) = \exp[-jm\omega T]\,[2g_0\cos m\omega T + 2g_1\cos(m\text{-}1)\,\omega T + \ldots.g_m] \quad (9.19)$$

for odd values of k and

$$G(j\omega) = \exp[-jm\omega T]\,[2g_0\cos m\omega T + 2g_1\cos(m\text{-}1)\,\omega T + \ldots.] \quad (9.20)$$

for even values of k.

Equations 9.19 and 9.20 show that the linear phase characteristic is satisfied by $G(j\omega)$ due to the term $\exp[-jm\omega T]$. Any digital filter satisfying the symmetric response characteristic of Equation 9.15, will have a linear phase relationship.

Method 2

The substitution

$$g_n = -g_{k-1-n} \quad (9.21)$$

and subsequent simplification leads to

$$G(j\omega) = -j\exp[-jm\omega T]\,[2g_0\sin m\omega T + 2g_1\sin(m\text{-}1)\,\omega T + \ldots.g_m] \quad (9.22)$$

for odd values of k and

$$G(j\omega) = -j\exp[-jm\omega T]\,[2g_0\sin m\omega T + 2g_1\sin(m\text{-}1)\,\omega T + \ldots.] \quad (9.23)$$

for even values of k.

Here again the linear phase characteristic is satisfied. Any filter with the odd symmetric characteristic of Equation 9.21, will satisfy the linear phase relationship. Combining both we find that any sample sequence $\{g_i\}$ representing the FIR impulse response, that has an odd or even symmetry about a sample point, satisfies the linear phase constraint [Parks *et al.*]. The filter coefficients can be determined by minimizing selected indices [Remez, Shpak and Antoniou].

9.3.2 FIR Filter Design

The theory of FIR Filter Design – being out of place – is not discussed here in depth. Only the procedures are outlined. Two lines of approach are in vogue. Here these are discussed with reference to LPF, since LPFs are the most common with instrumentation schemes. But the approach remains similar for other filters as well.

9.3.2.1 Approach 1

The gain characteristic of an ideal continuous LPF may be defined as

$$G(j\omega) = \begin{cases} 1 & \text{for } 0 < \omega < \omega_c \\ 0 & \text{for } 0 > \omega > \omega_c \end{cases} \quad (9.24)$$

where $G(j\omega)$ is the gain of the filter at frequency ω and ω_c is the cut-off frequency. The impulse response $g(t)$ of the filter satisfying Equation 9.24 has the form

$$g(t) = \frac{2\sin \omega_c t}{\pi t}$$

$$= \frac{2\omega_c}{\pi} \text{sinc } \omega_c t \qquad (9.25)$$

$G(j\omega)$ and $g(t)$ are shown sketched in Figure 9.1. The type of $G(j\omega)$ used is often referred to as the 'Window Function' – it defines a 'window' which allows only a selected set of frequency components to pass through. $\{g_i\}$ is formed from $g(t)$ by sampling it at the desired regular intervals; as such $g(t)$ forms the envelope of the sequence $\{g_i\}$. $\{g_i\}$formed in this manner has two limitations:-

⇒ $\{g_i\}$ is spread over i extending from - ∞ to + ∞ .

⇒ $\{g_i\}$does die down on ether side of g_0; but the decay is too slow and calls for the use of a large number of terms in $\{g_i\}$ to obtain a reasonable accuracy of performance.

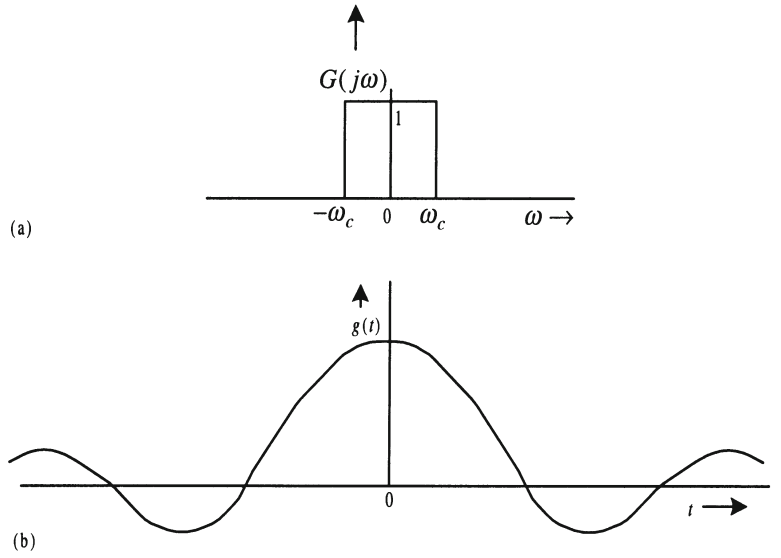


Figure 9.1 Frequency and time response characteristics of an ideal LPF

For the filter to be of use in practice, all terms of $\{g_i\}$ for $|i| > k$, are assumed to be negligible and ignored. The resulting truncated $\{g_i\}$ is subsequently delayed so that g_0 coincides with the latest sample [*i.e.*, delayed by k sample periods] and convolution carried out (See Figure 9.2). With this, the filter output y_n becomes

$$y_n = x_{n-2k}h_{2k} + x_{n-(2k-1)}h_{2k-1} + x_{n-(2k-2)}h_{2k-2} + \ldots + x_{n-1}h_1 + x_n h_0 \qquad (9.26)$$

where

$$h_i = g_{-k+i} \qquad (9.27)$$

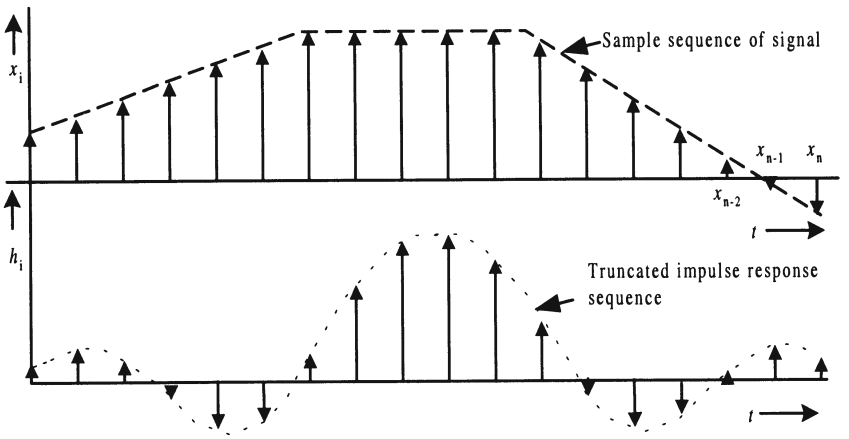


Figure 9.2 Adaptation of ideal LPF for digital realization

Observation: s-

⇒ $\{h_i\}$has been formed by truncating $\{g_i\}$and delaying it to conform it to realizability conditions.

⇒ The $\{h_i\}$ used as an approximation, does not represent the ideal value required – that we started with. To this extent, the filter is imperfect.

⇒ The convergence of $\{h_i\}$ is very slow; to obtain accuracy, a large number of terms are to be considered.

⇒ The abrupt truncation carried out with $\{g_i\}$ to form $\{h_i\}$, modifies $G(j\omega)$ from the ideal, causing prominent side lobes in it. This appears too severe a price to be paid.

The ringing in $\{h_i\}$ and undue side lobes in the frequency response as shown in Figure 9.1, are due to the abrupt changes in the frequency cut-off characteristics that we imposed in Figure 9.1 (a). Smoother window-functions yield better results though with some amount of accommodation in the frequency characteristics. They are smoother and better in the sense that

⇒ the range of i in $\{h_i\}$ is limited and

⇒ simultaneously the corresponding frequency response range is restricted.

Different windows have been suggested and have been in use in communication systems. Commonly used window functions and their key spectral-characteristics are given in Table 9.4. These can be used and $\{h_i\}$ for FIR obtained from them.

Observations: -

⇒ The design procedure involves the selection of a window function and selection of number of taps representing the FIR.

⇒ The larger the number of taps used to realize a function, the better the approximation to the concerned window. Minimum attenuation for the filters realized with 31 taps in each case, are also shown in the Table.

⇒ With the Kaiser window, one has some flexibility. One can have a trade-off between the side-lobe minimum-attenuation and the width of the main lobe and decide the window accordingly.

Table 9.4 Commonly used window functions

Name	Window function	Peak first side-lobe amplitude (dB)	Main lobe bandwidth	Minimum stopband attenuation (dB)	Minimum stopband attenuation of 31 tap filter (dB)
Rectangular	$\omega(n) = 1,$ $0 \le n \le (N-1)$	-13	$4\pi/N$	21	23
Barlett	$\omega(n) = \frac{2}{N},$ $0 \le n \le \frac{(N-1)}{2}$ $\omega(n) = \frac{22n}{N},$ $\frac{(N-1)}{2} \le n \le (N-1)$	-25	$8\pi/N$	25	smooth characteristic
Hanning	$\omega(n) = \left(\frac{1}{2}\right)\left[1-\cos\left(\frac{2\pi n}{N}\right)\right]$ $0 \le n \le (N-1)$	-31	$8\pi/N$	44	44
Hamming	$\omega(n) = 0.54-0.46\cos\frac{2\pi n}{N}$ $0 \le n \le (N-1)$	-43	$8\pi/N$	53	51
Backman	$\omega(n) = 0.42-0.5\cos\frac{2\pi n}{N} +$ $0.08\cos\frac{4\pi n}{N},$ $0 \le n \le (N-1)$	57	$12\pi/N$	74	74
Kaiser	$\omega(n) = \frac{I_0\left(2\beta\sqrt{\frac{n}{N-1}-\left(\frac{n}{N-1}\right)^2}\right)}{I_0(\beta)}$ $0 \le n \le (N\text{-}1)$ where I_0 is the modified zeroth order Bessel function of the first kind		*	*	*

* The attenuation levels depend on the value of β used.

9.3.2.2 *Approach 2*

The windowing approach discussed above yields workable filters in most of the cases. The design procedure is also straightforward. However, the fact remains that for a given number of taps, one can design a better filter – a best fit filter in the sense of it satisfying an optimization criterion. Or a given set of performance criteria can be realized with a minimum number of taps using such optimization criteria.

Consider an FIR filter of impulse response sequence $\{g_i\}$. As discussed in Appendix A, we obtain its Fourier transform $G(j\omega)$ which is its frequency response. Let the ideally desired filter have the response characteristic $H(j\omega)$. For a low pass filter we can have

$$H(j\omega) = \begin{cases} 1 & \text{for } 0 < \omega \leq \omega_c \\ 0 & \text{for } \omega > \omega_c \end{cases} \quad (9.28)$$

The error in the frequency response, between the yet-to-be realized FIR filter and the ideal E(jω) is

$$E(j\omega) = H(j\omega) - G(j\omega) \quad (9.29)$$

One can give different weights to error over frequency and evolve minimization criteria. Based on this, the coefficient of $\{g_i\}$ can be obtained. The Chebyshev approximation allows $G(j\omega)$ to swing on either side of $H(j\omega)$ throughout the frequency range with Equi-ripple characteristic [Figure 9.3]. The number of maxima and minima exceeds the number of coefficients in $G(j\omega)$ by two. With this criterion, for a specified $H(j\omega)$, one can arrive at a set of non-linear equations connecting the coefficients $\{g_i\}$. The solution to these, leads to the unique and desired $\{g_i\}$ combination. Several iterative procedures are available for a solution of these equations. The Remez exchange algorithm and its refinements, are in wide use. A number of design software packages for these iterative approaches to the solution, are also available.

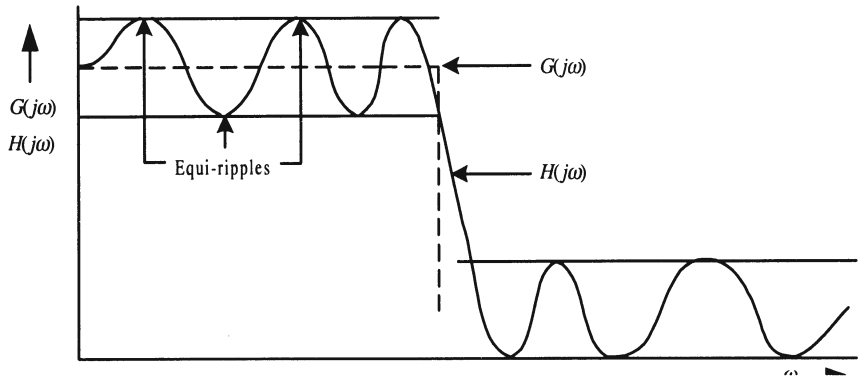


Figure 9.3 Chebyshev approximation to LPF

9.3.3 Other Applications

FIR filters can be useful in many other situations also. One class of common applications is depicted in Figure 9.4. The problem is to find $\{x_i\}$ from known $\{y_i\}$ and $\{g_i\}$. Here $\{x_i\}$ forms the input sequence to a system. The output sequence of the system is $\{y_i\}$. $\{g_i\}$ represents the equivalent of 'unit impulse response'. If $\{x_i\}$, $\{y_i\}$ and $\{g_i\}$ are time sequences, $\{g_i\}$ has to satisfy the physical realizability condition – *i.e.*,

$$g_i = 0 \text{ for } i < 0 \quad (9.30)$$

Nevertheless, g_i may extend for all positive time. In practice $\{g_i\}$ is approximated to a definite number of samples. All subsequent sample values are taken as insignificant (zero). When the independent variable is other than time (say distance), the constraint of Equation 9.30 does not exist. However, $\{g_i\}$ will extend in either direction of zero. Through three specific applications, both the situations are considered.

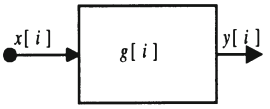


Figure 9.4 Block diagram representation of digital filter function

9.3.3.1 Determination of Centroid

Consider the determination of the position of an object by a CCD array [See Section 15.6.3]. The essential functional elements relevant to the present discussion are shown in Figure 9.5. The object has a CCD array in front. It generates outputs on the array-pixels in its vicinity. The precise position of the object is not apparent here. One way of ascertaining the object position, is to obtain the centroid of the samples. For this, locate a convenient origin in the line of CCD pixels; let the pixels be numbered sequentially 1,2,3, ... *etc.*, from the chosen origin. Let s_1, s_2, s_3, ...*etc.*, be the signals at the respective pixels. By taking moments with respect to the origin O, we get the estimated position of the object as the k^{th} pixel where

$$k = \frac{s_1 + 2s_2 + 3s_3 + ...}{s_1 + s_2 + s_3 + ...} \tag{9.31}$$

The same procedure may be adopted in other cases also.

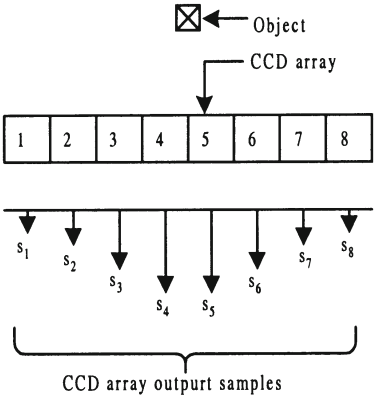


Figure 9.5 Use of CCD array to determine position

9.3.3.2 Edge Detection

Figure 9.6 shows an object kept in front of a dark background. The CCD pixels give outputs as shown in the figure. The lateral extent (diameter) of the object can be determined, if the object edges can be identified from the pixel outputs. Different edge-detection algorithms are available. One simple algorithm of estimating the edge uses the samples in the vicinity of one edge as in Figure 9.7. We ensure that the origin is taken well away from the edge so that

$$s_1 = s_2 = s_3 \ldots$$

representing the constant illumination signal received away from the edge. Edge detection is equivalent to replacing the above set of samples by k number of samples each of height s_1 (Here we have used the 'equating the areas approach').

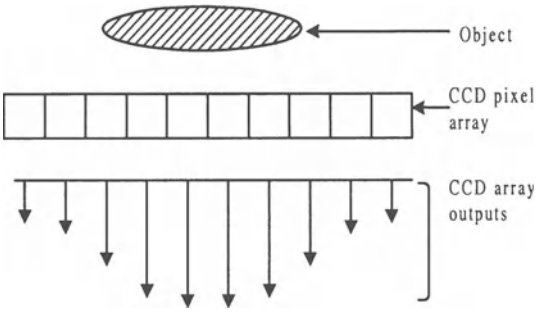


Figure 9.6 Object size detection using CCD array

This is equivalent to assuming that the same amount of radiation is received by an equivalent idealized source-detector combination in the form shown in Figure 9.7 (b) k is obtained as

$$k = \frac{\sum_{i=1}^{n} s_1}{s_1} \tag{9.32}$$

k decides the edge. An identical procedure can be used to detect the second edge. The procedure can be modified and extended to detect similar dimensions of multiple objects in front of the CCD array.

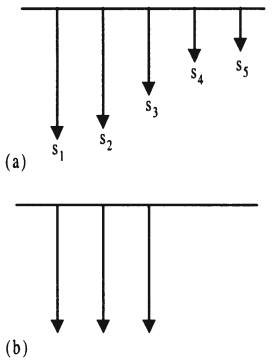


Figure 9.7 CCD array outputs near one edge of the case in Figure 9.6: (a) Actual outputs (b) Replacement of the actual output sequence with an equivalent ideal one

9.3.3.3 Profile Detection

There are situations where certain static characteristics of objects are to be estimated when the object is in motion. 'In-motion-weighing' is an example [See also Norden]. The object is distributed and is in motion. It can be considered as a collection of infinitesimally small elements kept sequentially. The weight of each such element can be approximated by an equivalent impulse-weight. With this approximation, the sensor output is a weighted-sum of individual impulse-weights. The sequence of these weights can be considered as analogous to the impulse response of a hypothetical linear discrete system. The series of impulse-weights and

the sensor output sequence are analogous to the input and output sequences of the system respectively. Let $\{g_i\}$ – i ranging from $-k$ to $+M$ – represent the impulse response sequence of such a system. Outside this range $g_i = 0$. Let $\{x_i\}$ be the input sequence. The output sequence is $\{y_i\}$. The n^{th} output sample is obtained as

$$y_n = \sum_{i=-k}^{+M} g_i x_{n-i} \tag{9.33}$$

The problem of determining the weight distribution is one of estimating $\{x_i\}$ from the output sequence $\{y_i\}$. This is sometimes referred to as the 'Deconvolution' problem. For the case of limited size of $\{x_i\}$, $\{y_i\}$ and $\{g_i\}$, deconvolution is direct though laborious; the same is dealt with here in principle.

Let

⇒ $\{x_i\}$ $0 < i < n$ be the desired input sequence: Outside this range of i, $x_i = 0$,

⇒ $\{y_i\}$ $-k < i < (n + M)$ be the output sequence: Outside this range of i, $y_i = 0$ and

⇒ $\{g_i\}$ $-k < i < +M$ be the impulse response sequence: Outside this range of i, $g_i = 0$

By repeatedly using Equation 9.33 we get

$$y_{-k} = g_{-k}x_0 \tag{9.34}$$

$$y_{-k+1} = g_{-k}x_1 + g_{-k+1}x_0 \tag{9.35}$$

$$y_{-k+2} = g_{-k}x_2 + g_{-k+1}x_1 + g_{-k+2}x_0 \tag{9.36}$$

and so on. x_0 can be obtained from Equation 9.34. Substituting the value of x_0 in Equation 9.35, x_1 can be obtained. By repeated computation in the above manner, all x_i can be computed. The computation can be carried out in a succinct manner using a recursive relationship. If the impulse response extends beyond a few samples, the computation becomes laborious and time consuming.

9.4 IIR filters

Any desired IIR filter characteristic may be obtained by realizing the filter in a closed loop form; the generalized scheme is shown in Figure 9.8. In the figure,

⇒ $G_1(z)$ and $G_2(z)$ are multiple-input-multiple-output discrete transfer functions and

⇒ $G_3(z)$ is a multiple-input-single-output discrete transfer function.

In general, an IIR filter accomplishes the same level of performance as an FIR filter but with a relatively smaller number of taps. This makes it compact and fast in response. But compared to the FIR filter, it has a few shortcomings: -

⇒ While an FIR filter is inherently stable, the IIR filter can become unstable. The problem exists even with second order IIR. The filter has to be designed for stability.

⇒ Closed loop specifications in terms of the amplitude response can be met effectively. However, the phase response is a casualty. The problem is the same as with the analog filters.

⇒ Any disturbance or undue transients in the input can cause prolonged ringing. This is essentially one manifestation of the stability issue.

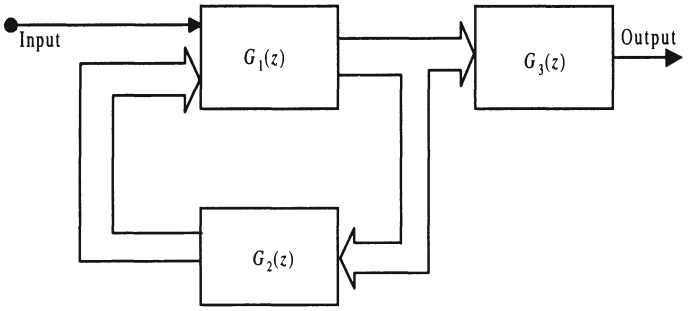


Figure 9.8 Generalized IIR filter scheme

Whenever the application concerned does not demand specific phase response, an IIR can be used. Many instrumentation signals demand a linear phase response in the passband; an FIR filter is preferable here.

9.4.1 Design of IIR Filters

Different analog filter configurations and their design procedure can be directly adapted for IIR. Normally the design is fully carried out in analog form and the same is subsequently converted into an IIR filter. Although a variety of approaches is possible, only two methods are discussed here.

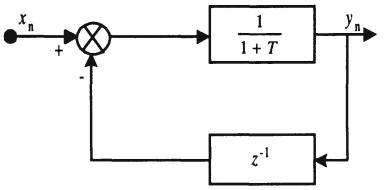


Figure 9.9 Realization of first order IIR filter

9.4.1.1 Approximation of Derivatives

The first order approximation for the derivative is

$$\left.\frac{dy}{dt}\right|_{t=nT} = \frac{y_n - y_{n-1}}{T} \tag{9.37}$$

This approximation uses the backward difference formula. Correspondingly, the Laplace operator s may be approximated in discrete form as

$$s = \frac{1-z^{-1}}{T} \tag{9.38}$$

One can substitute this in the analog transfer function of any desired filter and realize it in closed loop form. For example, the normalized first order filter

$$G(s) = \frac{1}{1+s} \tag{9.39}$$

takes the discrete form

$$G(z) = \frac{1}{1+\left[\left(1-z^{-1}\right)/T\right]} = \frac{T}{1+T+z^{-1}} \tag{9.40}$$

Figure 9.9 shows the realization of the corresponding IIR filter.

Observations: -

⇒ Higher order filters also can be realized in a similar manner.

⇒ As the filter loop order increases, it is preferable to realize the filter as a set of second order sections [See Section 5.7] in tandem. With this, the filter stability is more easily ensured. However, the filter complexity increases slightly.

⇒ With the first-order approximation for s as done here, the order of the IIR filter remains the same as that of its analog counterpart.

⇒ The IIR filter response is close to that of its analog counterpart, if the sampling frequency is high compared to the filter bandwidth.

⇒ The forward difference formula can be used in place of the backward difference formula. This makes the filter less stable.

⇒ One can use a more refined approximation for the derivative. This replaces s by a second or third degree polynomial in z. It increases the filter order correspondingly. This amounts to using a lower-order analog filter model and approximating it to a higher order. Using a higher order analog-filter model may yield better results.

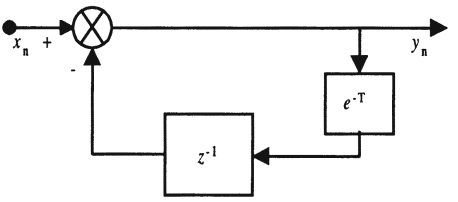


Figure 9.10 Realization of first order digital filter through impulse invariance method

9.4.1.2 *Impulse Invariance*

An IIR can be considered to be on par with its analog-counterpart, if its response sequence coincides with that of the analog filter at its sampling instants. This is ensured if we make sure that the respective impulse responses match – *i.e.*, the impulse response sequence of the IIR coincides with the response values of the analog filter at the corresponding sampling instants. Consider the first order analog filter of Equation 9.39. Its impulse response is

$$g(t) = e^{-t} \tag{9.41}$$

The corresponding sampled transfer function is

$$G(z) = \sum_{i=0}^{\infty} e^{-iT_s - i}$$

$$= \frac{1}{1-e^{-T_z}z^{-1}} \tag{9.42}$$

The realized filter is shown in Figure 9.10.

Observations: -

⇒ The filter order remains the same as that of the analog filter

⇒ The model analog filter is to be split down to a series of second order filters and (if necessary) a first order filter. Each is realized separately and all of them put in tandem.

⇒ The filter structure remains the same as that obtained with the difference formulae of Section 9.4.1.1. However, the gain constants associated with the individual delays are different.

⇒ If the sampling frequency is sufficiently high compared to the signal bandwidth, the frequency response of the filter coincides with that of its analog counterpart.

9.4.1.3 Other Methods

Other methods of IIR design are of two categories: -

⇒ Methods of approximating an analog filter model

⇒ Methods that realize the IIR directly without comparing it with the analog filter model.

⇒ In general, the response conforms to the analog counterpart if the signal bandwidth is low compared to the sampling frequency. In other words, once this condition is satisfied, more involved methods do not seem to be warranted.

9.4.2 IIR Filter Realizations

An IIR filter designed by any of the methods above has the form of a ratio of two polynomials [See Appendix A].

$$G(z) = \frac{Q(z)}{P(z)} \tag{A.10}$$

Cross multiplication and rearrangement yields

$$y_n = -\sum_{i=1}^{L} p_i y_{n-1} z^{-1} + \sum_{j=0}^{M} q_j x_{n-j} z^{-j} \tag{A.14}$$

The filter can be directly realized through a program to compute y_n from the set of x and y samples as in Equation A.14. The same is represented in Figure 9.11, in block diagram form. The filter realization here, is in two parts. The first part realizes the numerator polynomial (the zeroes) and the second, the denominator polynomial (the poles). The block that realizes the poles requires careful analysis before implementation. This is due to the tendency of sampled systems to oscillate and become unstable as the system order increases beyond 2. The problem can be alleviated by splitting the filter as a sequence of first and second order systems. Thus, by factorizing the numerator and the denominator polynomials, $G(z)$ can be expressed as

$$G(z) = \frac{(1+c_{00}z^{-1})(1+c_{11}z^{-1}+c_{12}z^{-2})(1+c_{21}z^{-1}+c_{22}z^{-2})\ldots}{(1+d_{00}z^{-1})(1+d_{11}z^{-1}+d_{12}z^{-2})(1+d_{21}z^{-1}+d_{22}z^{-2})..} \quad (9.43)$$

c_{00} and d_{00} may be zero or not depending on whether M and L in Equation A.11 and A.12 are odd or even respectively. The above form of $G(z)$ shows that it can be composed of five types of factors as below:

$$F_1(z) = \frac{1}{1+p_0z^{-1}} \quad (9.44)$$

$$F_2(z) = \frac{1}{1+p_0z^{-1}+p_1z^{-2}} \quad (9.45)$$

$$F_3(z) = \frac{1+q_0z^{-1}}{1+p_0z^{-1}} \quad (9.46)$$

$$F_4(z) = \frac{1+q_0z^{-1}}{1+p_0z^{-1}+p_1z^{-2}} \quad (9.47)$$

$$F_5(z) = \frac{1+q_0z^{-1}+q_1z^{-2}}{1+p_0z^{-1}+p_1z^{-2}} \quad (9.48)$$

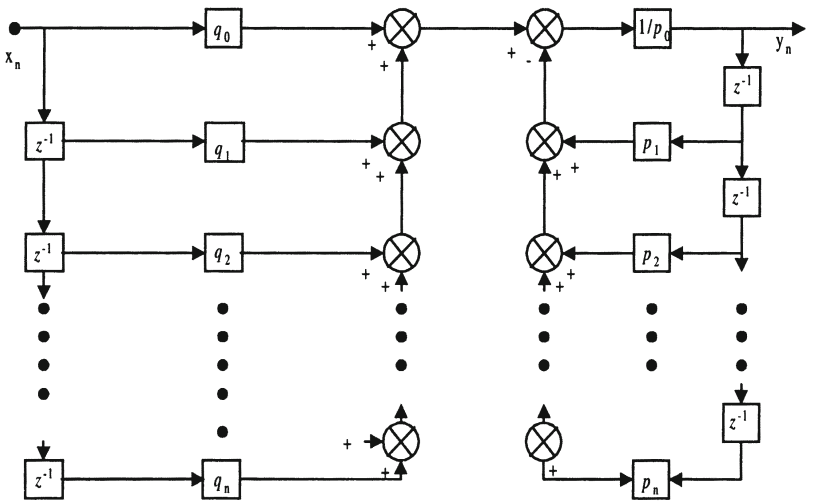


Figure 9.11 Block diagram representation of direct IIR filter realization

$F_1(z)$ and $F_2(z)$ can be realized directly as in Figures 9.12 (a) and 9.12 (b) respectively. Figure 9.13 (a), shows one form of realizing $F_3(z)$ directly. By rearranging the blocks, the same can be realized in the form shown in Figure 9.13 (b) also. The latter is referred to as the 'Canonical Form'. Similarly, $F_5(z)$ can be realized directly as shown in Figure 9.14 (a). The corresponding canonical form – shown in Figure 9.14 (b) – is obtained by rearranging the blocks. $F_4(z)$ can be seen to be a special case of $F_5(z)$ – *i.e.*, with $q_1 = 0$.

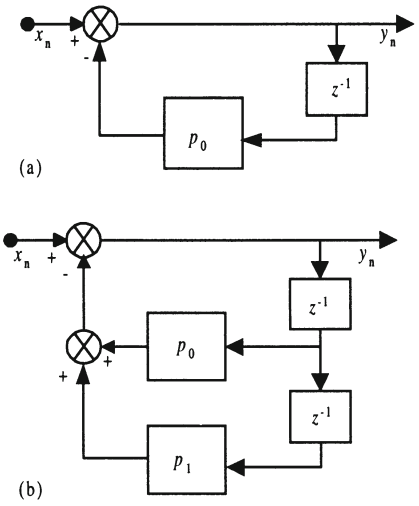


Figure 9.12 Block diagram representation of direct realization of (a) first and (b) second order terms of an IIR filter

The canonical form of realization involves only two time delay blocks; *i.e.*, only two previously computed, intermediate sample variable values need be stored and used. This makes the program shorter and faster in execution. However, the round-off error propagation is more pronounced with the canonical form. Normally the canonical form of the filter is preferred for implementation.

All the individually realized first and second order blocks as in Figures 9.12 to 9.14 can be connected in tandem to realize the overall filter.

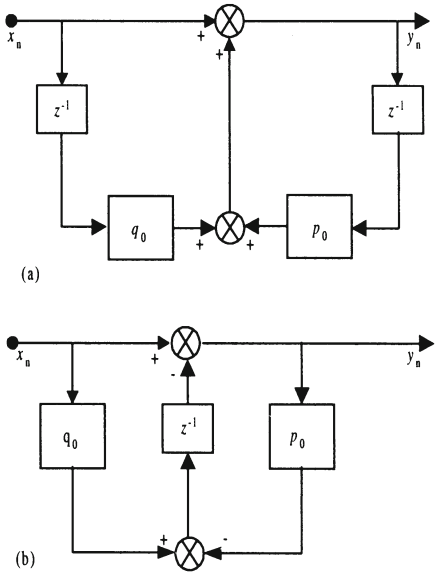


Figure 9.13 Block diagram representation of realization of $F_3(z)$ of Equation 9.46: (a) Direct form (b) Canonical form

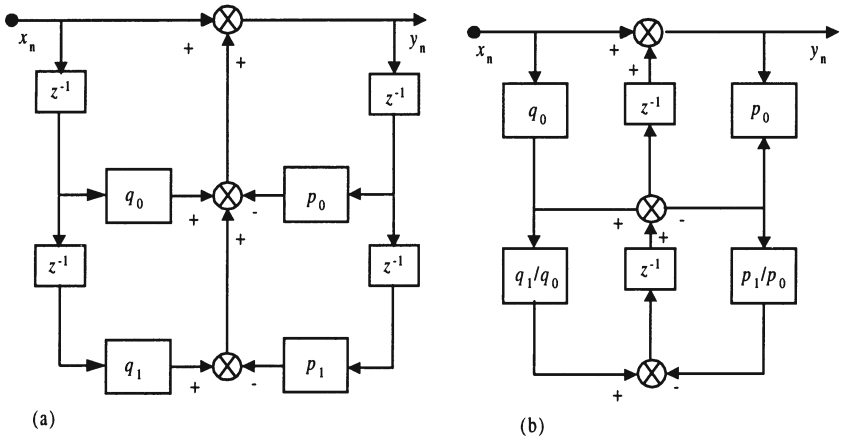


Figure 9.14 Realization of $F_5(z)$ of Equation 9.48: (a) Direct form (b) Canonical form

9.5 Other Linear Operations

Derivatives, integrals, interpolation and extrapolation are the other linear operations often required to be performed on signals. Numerical methods in literature make use of differences of various orders for these [Cheney]. These can be directly adapted by us for direct substitution of sample values in the respective expressions. DSP literature also provides a variety of methods (Antonio, Oppenheim and Schafer). We deal with a few which provide working relationships. Some general observations are in order here: -

⇒ As the over-sampling ratio increases, accuracy of the result improves.

⇒ Generally the indecision in computation is of the order of $(f_s / 2 f_m)^{-n}$.
Where
- n is the number of samples used
- f_s is the sampling frequency and
- f_m is the signal bandwidth.

For example, with $f_s / f_m = 4$, and 5 samples being used for computation, the indecision is of the order of 1 in 1000. This is on par with the accuracy of a 10 bit ADC. With 6 samples, it is 1 in 4000 – on par with 12 bit ADC and so on. This is only a guideline and not to be taken quantitatively.

⇒ As the number of samples used increases beyond a limit, the accuracy does not improve. Due to the round-off errors, it may even decrease.

⇒ Different formulae are available for each of the functions to be realized. In general, if the over-sampling ratio is sufficiently high, all formulae involving the same number of samples, yield results of the same order of accuracy.

⇒ For each function, three approaches are possible depending on the location of the function to be realized.
- When the sample sequence is spread on either side of the of instant of interest, we may use the 'Central Differences'.
- When the sample sequence is ahead of the instant of interest, we may use the 'Forward Differences'.

- When the sample sequence is behind the instant of interest, we may use the 'Backward Differences'.

9.5.1 Derivatives and Integrals

The forward and backward difference formulae for different approximations are given in Appendix B. These can be used to calculate the respective derivatives and integrals.

9.5.2 Interpolation and Extrapolation

The same set of formulae is used for interpolation as well as extrapolation. Two approaches are possible. The first uses the forward and backward difference formulae to provide the interpolated and extrapolated functional values. The second approach uses linear filtering algorithms judiciously to carry out interpolation and extrapolation. Apart from these, one can use specific error criteria and minimize the same to evolve necessary filters [Remez]. The last approach is not pursued further here.

Approach 1:
The forward and backward difference formulae for different approximations are given in Appendix B. These can be used to carry out interpolation as well as extrapolation. Depending on the type of on-line computation and the accuracy required, an approximate formula is selected; subsequently the same is realized as an IIR filter [See Section 9.4.2 above].

Observations: -

⇒ For $0 \leq x \leq 1$, Equations B.8 to B.11 provide interpolated values of the function between successive sampling instants, with forward differences. For $x = 0$ and $x = 1$, the interpolated values coincide with the respective sample values.

⇒ For $-1 < x \leq 0$, Equations.B.19 to B.22, provide interpolated values of the function between successive sampling instants, with backward differences. For $x = 0$ and $x = -1$, the interpolated values coincide with the respective sample values.

⇒ For $-1 < x \leq 0$, Equations B.8 to B.11 provide extrapolated values of the function outside the available sample range. This is the case with forward differences. For $x = 0$, the extrapolated value coincides with the sample value.

⇒ For $0 < x \leq 1$, Equations B.19 to B.22 provide extrapolated values of the function outside the available sample range. This is the case with backward differences. For $x = 0$, the extrapolated value coincides with the sample value.

⇒ For non-integral values of x, interpolation and extrapolation become cumbersome even when a low order approximation is used. Evaluation of the coefficients calls for substantial computational effort.

Approach 2:

Consider a continuous signal $x(t)$ input to a low pass filter $G(s)$, the output being $y(t)$ as shown in Figure 9.15 (a).

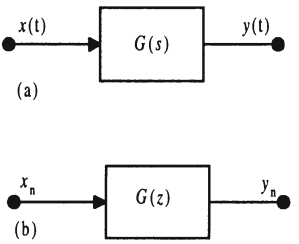


Figure 9.15 Linear system with (a) continuous input and output and (b) discrete input and output sequences

Laplace transform of $y(t)$ is

$$X_o(s) = G(s)\, X_i(s) \tag{9.49}$$

The time variation of $y(t)$ is given by the convolution integral,

$$y(t) = \int x(t-\tau)g(\tau)d\tau \tag{9.50}$$

where $g(t)$ stands for the impulse response of the system. Knowing the nature of time variation of $x(t)$ and the impulse response $g(t)$, we can evaluate $y(t)$ at any time [See Appendix A]. Figure 9.15 (b) shows the corresponding discrete case. $\{x_i\}$ and $\{y_i\}$ are the input and output pulse trains respectively. We can get the sample sequence $\{g_i\}$ representing the impulse response of the filter and express $\{y_i\}$ as

$$y_n = \sum_{i=0}^{n} g_i x^{-(n-i)} \tag{A.8}$$

Equation A.8 can be used judiciously for interpolation and extrapolation under various conditions. The filter can be selected so that $g(t)$ is one of the window functions of Table 9.4. Two cases are illustrated in Figure 9.16.

To estimate the value of y_n in terms of a set of previous samples, convolution can be done in the manner indicated earlier. The same is shown in Figure 9.16 (a). This can be used for interpolation and extrapolation in terms of a set of preceding samples. The instant of estimation need not necessarily coincide with the sampling instant. g_0 being zero, x_n g_0 is zero; Thus y_n is evaluated only in terms of the samples preceding the n^{th} instant. This is similar to using the backward differences in the Approach 1 above.

When interpolation and extrapolation are to be done in terms of samples succeeding the instant of interest, one may proceed as in Figure 9.16 (b). This formulation is useful for interpolation and extrapolation at the sampling instants as well as intervening instants. g_0 being equal to zero, y_0 is expressed here only in terms of the succeeding sample values. This corresponds to the forward differences of approach 1 above.

The procedure can be used in a more generalized manner to estimate the value of y at any desired instant in terms of sample values spread on either side of it. The case is illustrated in Figure 9.16 (c). Here y_n can be expressed as

$$y_n = \sum_{-a}^{+b} x_{k-i} g_i \tag{9.51}$$

Here $\{g_i\}$ is taken to extend from g_{-a} to g_{+b}. Depending on the availability of sample values on either side of the instant of interest, g_0 may be positioned. The above two cases are the two extremes of this. Equation 9.51 can be adapted to give values of y at non-sampling instants as well.

Observations: -

⇒ If the instant of interest of estimation always coincides with the sampling instant, the computation is faster. All sampled values of $g(t)$ can be pre-calculated and stored in a LUT. These can be used to do the algebra.

⇒ If the instant of estimation does not coincide with the sampling instants, the adapted form of Equation 9.51 has to be used. The computation is more cumbersome here. This is the price paid for the generality of the method.

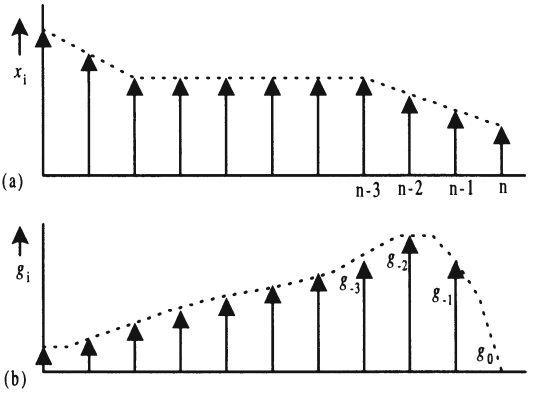


Figure 9.16 Interpolation and extrapolation near the end of a sequence; (a) Input sequence (b) Equivalent impulse response sequence

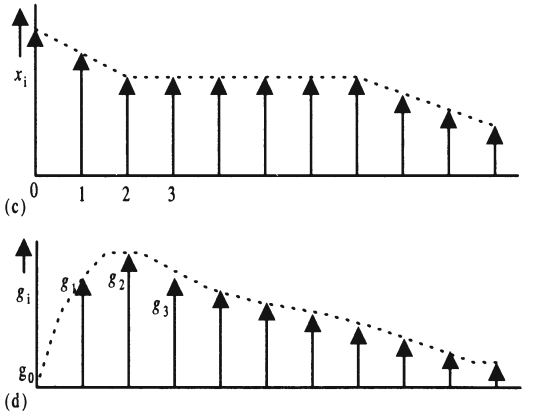


Figure 9.16 (Cont'd): Interpolation and extrapolation near the beginning of a sequence; (c) Input sequence (d) Equivalent impulse response sequence

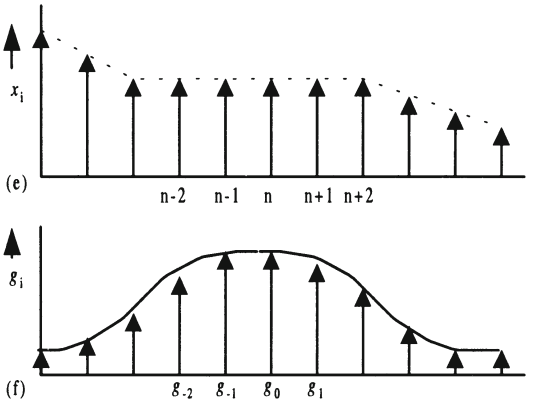


Figure 9.16 (Cont'd). Interpolation and extrapolation near the middle of a sequence; (e) Input sequence (f) Equivalent impulse-response sequence

9.6 DFT and FFT

There are many instances where an information derived from an instrumentation scheme is used for display, transmission, decision-making or control. Effective and intensive extraction of information, from sample sequences has become possible with DSP techniques. DFTs represent one commonly used set of computations for these. A few instances of its application are cited here to highlight its importance.

⇒ Ball mills powder lumpy hard material to required grain size. These are further used in processes. The noise pattern of the ball mill (signature), changes as the powdering operation progresses. One can maintain a signature template representing the desired state (*i.e.*, level of powdering), compare the signature of the mill at work and decide on stopping or continuing with powdering. The signature here is maintained in terms of its Fourier components.

⇒ The vibration profile of rotating machinery changes depending upon the health of the machinery. Different defects and faults cause different types of spectral changes in the vibration. With a spectral analysis of vibration, faults and types of faults can be identified.

⇒ Consider M successive equally spaced samples of a signal. The number M should be chosen to be large compared to their period of the lowest frequency of interest. Ten to twenty full periods of the lowest frequency may be enough. Further, the sampling rate has to be large enough to accommodate the full signal bandwidth. Under these conditions, one can obtain the DFT of the signal as

$$X_k = \frac{1}{M}\sum_{n=0}^{M-1} x_n e^{-j\left(\frac{2\pi kn}{N}\right)} \tag{9.52}$$

X_k here represents the amplitude of the k^{th} harmonic component. One can plot k versus X_k that represents the amplitude distribution of the spectral components. The DFT becomes simpler to compute and easy of execution, when $M = 2^N$, where N is

an integer. With this constraint, the possible values that M can take are 2, 4, 8, 16, 32, 64, 128, 256, 512, 1024, 2048, 4096 and so on. A few elegant algorithms are available and are in wide use.

Program 9.1

```
#include <stdio.h>
/* program to calculate the emfs of Iron-Constantan Thermocouple in the */
/* range 70°C to 90°C; the emfs are in millivolts */
main()
{
  float temp, emf, eemf;
  printf("EMF of Iron-Constantan Thermocouple\n");
  eemf=3.5;
  for(temp=70.0;temp<=90.0;temp++)
  {
    emf=(-9.6391844859e-17*temp+1.9416091001e-13)*temp-1.7022405966e-10;
    emf=((emf*temp+1.3348825735e-7)*temp-8.5669750464e-5)*temp+3.0425491284e-2;
    emf=(emf*temp+5.0372753027e+1)*temp/1000.0 ;
    printf("%f\t%f\t%f\n",temp,emf,(emf-eemf));
    eemf=emf;
  }
 }
```

Program 9.2

```
#include <stdio.h>
/* This program has two parts */
/* Part 1 calculates the emfs of Iron-Constantan Thermocouple in the */
/* range 70°C to 90°C; the emfs are in millivolts */
/* Part 2 uses an x-y relationship in tabular form; For any given y */
/* it computes the corresponding x value; */
/* Successive iterations and a final interpolation is used here*/
main()
/* part 1*/
{
  float temp=70.0, emf, t[25],y,tt,n2m1;
  int n1=70,n2=90,k;
  n2m1=n2-n1;
  for(k=0;k<=(n2m1);k++)
  {
    emf=(-9.6391844859e-17*temp+1.9416091001e-13)*temp-1.7022405966e-10;
    emf=((emf*temp+1.3348825735e-7)*temp-8.5669750464e-5)*temp+3.0425491284e-2;
    emf=(emf*temp+5.0372753027e+1)*temp/1000.0 ;
    t[k]=emf; /*t[k] are the Thermo-emfs in the 70 to 90 degree Celsius range*/
    temp++;
  }
/* Part 2 */
  printf("Thermo-emf?");
  scanf("%f",&y);
  n1=0; /* t[0] is the first entry in the table */
  n2=n2m1; /* t[n2m1] is the last entry in the table */
  while((n2-n1)>1)
  /* Iterate in the given range until the solution converges */
  {
    k=(n1+n2)/2;
  if(t[k]>y)
    n2=k;
  else
    n1=k;
  }
  tt= 70.0+n1+(y-t[n1])/(t[n2]-t[n1]);/*Interpolate to get precise value of x*/
  printf("\n Temperature for Thermo-emf of %f mV is %fdegree Celsius",y,tt);
 }
```

10 Generic Structures of Instrumentation Schemes

10.1 Introduction

There is a wide variety in the variables sensed and the sensors used with them. Despite this variety, a sizeable number of them fall into three broad categories: -

⇒ Resistance-sensors
⇒ Capacitance-sensors and
⇒ Inductance-sensors

Taking the specific case of resistance-sensors, the whole instrumentation scheme built with the basic resistance-sensor, follows specific structures notwithstanding the difference in the nature of physical variable sensed. We can elicit a 'generic structure' of the instrumentation scheme that retains features common to many of them. Similar generic structures can be elicited for capacitance and inductance type instrumentation schemes also. Such generic schemes and their features are discussed in this chapter. The feedback instrumentation scheme is another such common form of generic scheme of instrumentation, which is also discussed. The idea may possibly be extended to identify other generic forms of instrumentation too; but these are not pursued here due to the limited variety in each case.

10.2 Instrumentation Schemes Based on Resistance Sensors

The resistance of a conductor R, is given by

$$R = \frac{\rho l}{A} \Omega \tag{10.1}$$

where

⇒ ρ is the resistivity
⇒ l is the length of the conductor and
⇒ A is the area of cross section of the wire of the conductor.

If the geometry is not regular where A and l cannot be identified in such a simple manner, the resistance is obtained by integration. Any physical variable, which affects any of the above three parameters, can be sensed using a resistance-sensor. The change in R is used as a measure of the change in the physical variable. Possibly, resistance-sensor is the most widely used of the sensors. Most of the physical variables sensed affect ρ directly. Some affect the dimensions as well as the ρ value.

T. R. Padmanabhan, *Industrial Instrumentation*
© Springer-Verlag London Limited 2000

10.2.1 Resistance as a Circuit Element

Some features are common to all resistance-sensors.

⇒ Resistance-sensors function with a current passing through. This causes a power loss and a corresponding self-heating. The self-heating affects the resistance of the sensor and causes an error. This has to be kept lower than the expected threshold value. The equivalent thermal resistance is normally in the 0.05 mW/°C to 0.50 mW/°C range. As an example, consider a resistance strain gauge of 600 Ω with $1V$ across it. The power dissipation in it is

$$P = V^2/R \tag{10.2}$$

$$= 1.67 \text{ mW} \tag{10.3}$$

With 1 mW / °C thermal resistance
Temperature rise = 1.67 °C.
Temperature-coefficients of resistance of metals are in the 4 % range.
Resulting change in resistance = 0.67 % / °C.

⇒ Often the applied voltage, power loss and the error are more than the values above. Circuits used with resistance-sensors compensate for such self-heating errors.

⇒ The self-heating may be reduced by spreading the resistance. But the sensing point gets blurred and leads to a 'weighted average' sensing. This also increases the effective time constant of the sensor. For the majority of applications, this is not a shortcoming. If the sensing location is to be more sharply defined, the sensor is kept more concentrated. The increased thermal resistance due to this calls for suitable compensation for self-heating effects.

⇒ Self-heating can be reduced by increasing the base resistance of the sensor. Any such increase calls for a corresponding increase in the input impedance of the following circuitry. It also increases the thermal noise level [See Section 7.4.2]. Susceptibility to pick-up also increases. Normally the application environment puts an upper limit to the value of resistance for the sensor.

⇒ The resistance of the sensor introduces thermal noise in the circuit. The same has to be kept low compared to the detection threshold. Reduction of the sensor resistance to reduce the thermal noise may increase the power loss and self-heating. A suitable balance has to be struck in each case.

⇒ Carbon based resistance-sensors, sintered resistance-sensors *etc.*, may introduce substantial shot noise [See Section 7.4.1]. These are used only if inevitable.

⇒ Resistance-sensors are quite fragile and require appropriate support. If supported through mandrels or dedicated structures, the resistance has to be made stress-free (by annealing) to ensure consistency of the characteristic. Alternately it is deposited on a ceramic or similar base or embedded. The thermal expansion characteristic of the sensor and base is to be matched to minimize stress-related errors.

⇒ The simplest exciting arrangements for resistance-sensors (shown in Figure 10.1) apply a constant voltage to the sensor and pass a current through it or pass a constant current through the sensor and measure the voltage drop

across it. In both cases self-heating can cause errors. In addition environmental factors also affect the sensor working and cause errors.

⇒ The necessity to compensate for these has led to the widespread use of bridge form of detectors with resistance-sensors. These can be Wheatstone bridges analyzed in Section 2.2 or their modifications using opamps. Of course, there are schemes, which are non-bridge configurations. They are characterized by two factors :-

- *Pulsed excitation of the sensor resistor*: Here short time periodic pulses of current or voltage are used for the sensing resistor. These ensure that self-heating and the errors thereto, are negligible. The pulses are shaped to avoid sharp edges and resultant thermal shocks to the sensor.
- *On-line calibration*: Regular on-line calibration is carried out with the help of a reference. By comparing the sensor output in the calibration phase with that in the measuring phase, many of the errors are eliminated.

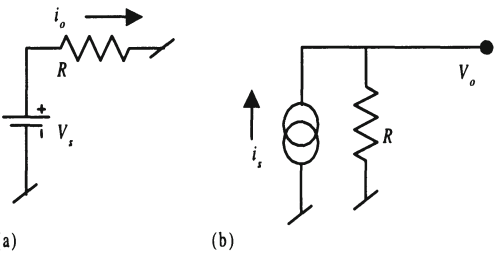


Figure 10.1 Two simple methods of getting electrical outputs from resistance-sensors: (a) Applying constant voltage and sensing the current through the sensor (b) Passing a constant current through the sensor resistor and sensing the voltage drop across it

10.2.2 Circuit Configurations for Resistance Sensors

In the light of the discussions above, three types of circuit configurations are possible with resistance-sensors:-

⇒ Wheatstone bridge type sensor
⇒ Modification of the Wheatstone bridge using an opamp and
⇒ Cyclically self-calibrating scheme.

10.2.2.1 Wheatstone Bridge Type Sensor

Wheatstone bridge behaviour under slightly unbalanced conditions has been analyzed in Section 2.2. The following can be deduced in the light of that: -

⇒ The bridge built around the resistance-sensor is operated with unity ratio with all arms being of equal resistance at balance. This provides maximum sensitivity and minimum output impedance.
⇒ The bridge is normally excited with DC. The whole signal processing is with DC circuits. This is due to the comparatively high signal to noise ratio available with resistance-sensors.
⇒ The bridge may be set up in various ways (See Figure 10.2):-

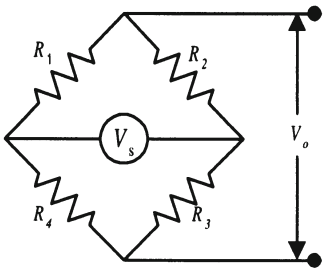


Figure 10.2 Wheatstone bridge

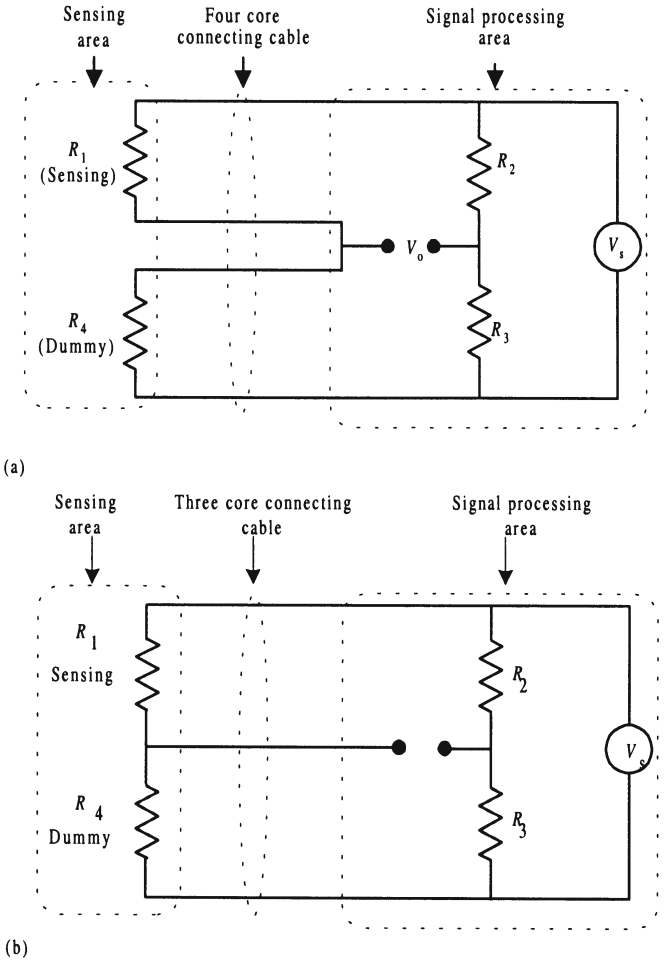


Figure 10.3 Resistance-sensor connections to reduce errors: (a) Four-wire scheme (b) Three-wire scheme

- R_2 and R_3 may be fixed resistors. R_1 is a sensor and R_4 a dummy resistor placed close to R_1. Extraneous factors like ambient temperature changes, affect R_1 and R_4 identically and hence do not cause any error. The leads of R_1 and R_4 (2 each), are kept close by as shown in Figure10.3 (a). This eliminates any error due to changes in the lead resistances – again due to environmental changes. This requires a cable with four wires to be used to connect the sensor. An alternate scheme that uses a three-core cable is shown in Figure 10.3 (b). The third core is in series with the detector. Though not as effective as the last scheme, this is in wide use. Use of opamps with high input impedance, makes it effectively as good as the four wire scheme (This type of compensation scheme is common with RTDs). More elaborate schemes based on the Kelvin double bridge, are also possible [Harris]. Nevertheless, they are used only for precision laboratory calibration.
- $R_1$and R_3 are sensors and R_2 and R_4 are dummies (if necessary). This offers twice the sensitivity of the bridge with one sensor as above.
- R_1 and R_4 are sensors. Here R_2 and R_3 remain fixed at the base value. R_1 and R_4 are sensors of opposite direction. For example, R_1 may be a resistance strain gauge sensing tensile strain while R_4 may be another resistance strain gauge sensing compressive strain – both from the same source. Their use in adjacent arms ensures that effects of extraneous factors are nullified. The sensitivity may often be double that of the bridge with one sensor.
- All the four resistors are sensors. This is also commonly used with strain gauges. R_1 and R_3 sense one type of strain (say tension) while R_2 and R_4 sense the opposite type (compression). All the extraneous changes are compensated for. The bridge sensitivity can be four times that of the single sensor-bridge.

Depending on the power supply available, different types of processing circuits can be used. Figure 10.4 shows a few possibilities. The features of different amplifier schemes were discussed in Sections 4.3 and 4.4. The configuration in Figure 10.4 (a) is possibly the simplest non-inverting one. The supply is required to be floating. The bridge is not loaded. The common mode signal seen by the inputs is limited to the level of the bridge unbalance.

When a centre-tapped supply is used to excite the bridge, neither output point of the bridge can be grounded calling for the use of an instrumentation amplifier (See Section 4.12) as shown in Figure 10.4 (b). The instrumentation amplifier does not load the bridge. The common mode signal seen by the scheme is limited to the extent of bridge unbalance. When the bridge supply is single-ended as in Figure 10.4 (c), the same instrumentation amplifier configuration is used. The common mode signal seen by the scheme is $V_s/2$.

One opamp based inverting configuration is shown in Figure 10.4 (d). When close to balance, the gain of the scheme is $2R_f/R$. The bridge is loaded in the scheme, reducing sensitivity to that extent. If necessary, a buffer can be interposed to eliminate loading and simultaneously provide an independent gain stage.

10.2.2.2 Modifications of the Wheatstone Bridge

In the schemes considered earlier, the unbalanced Wheatstone bridge serves the function of sensor plus compensation arrangement. The opamp that follows is

configured to provide the necessary gain. Many circuit configurations have been suggested and used in practice, where the two functions are judiciously integrated [Anderson, Chirlian, Franco, Giacoletto, National Semiconductor, Wait *et al.*]. These reduce component count, increase linear range or provide some other decided benefits. A few configurations are considered here.

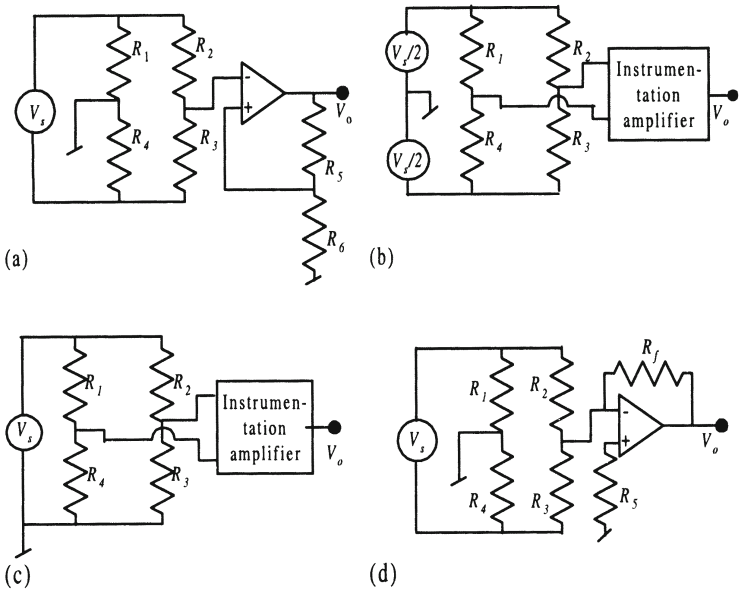


Figure 10.4 Amplifier schemes with Wheatstone bridge type sensors: (a) Non-inverting amplifier scheme (b) Instrumentation amplifier with zero common mode input (c) Instrumentation amplifier with a common mode input (d) Inverting amplifier with zero common mode input

Scheme 1

The scheme of Figure 10.5 (a) uses a 2.5 *V* reference to supply the sensor bridge (See Section 8.4). The 2.5 *V* reference is inverted using an inverting amplifier with IC_2 having unity gain. Bridge supply is symmetrical around ground. Thus

$V_A = +2.5$ V

$V_C = -2.5$ V

The bridge output across B and D is close to the ground potential. IC_1 requires a positive supply while IC_2 requires a set of positive and negative supplies. Their values need not be well stabilized. Here any combination of the bridge arms can be used for sensing as well as for compensation for ambient variations. A slight variant of the above is shown in Figure 10.5 (b). V_A is a stabilized 2.5 V supply. Normally the bridge is used with unit ratio; R_2, R_3 form the sensing and compensating arms; and $R_1 = R_4 = R$ remain fixed. IC_2 ensures that $V_D = 0$. Since the current through R_1 and R_4 are equal, $V_{AD} = V_{DC} = 2.5$ *V*. This scheme is more compact than the previous one. However, it has the restriction that only R_2 and R_3 are available for sensing and for compensation.

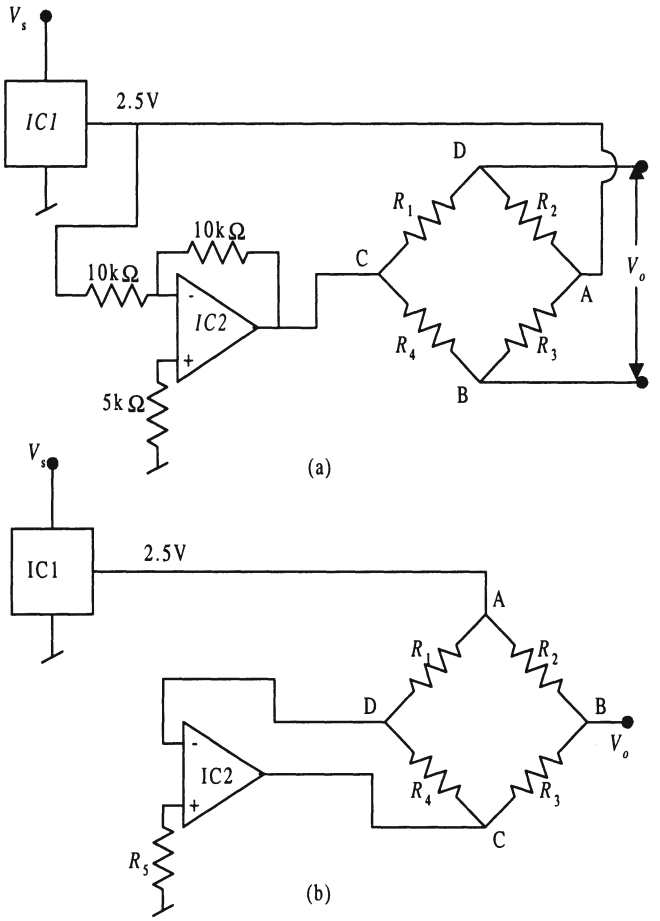


Figure 10.5 Adaptations of the Wheatstone bridge for sensors: (a) Scheme with ±2.5V supplies to the bridge (b) Scheme with –2.5V generation by making the sensor bridge part of the opamp feedback scheme

Scheme 2

In the scheme of Figure 10.6 (a) with unity ratio, we have

$$R_1 = R_2 = R_4 = \frac{R_3 R_5}{R_3 + R_5} \tag{10.4}$$

R_1, R_2 and R_4 can be sensors - singly or in combinations. Under balanced conditions

$$V_A = V_B = \frac{V_S}{2} \tag{10.5}$$

Let R_2 and R_4 be used as sensors (as in a strain gauge). Let $R_2 = R_4 = R + \varepsilon$ with slight unbalance. The equivalent circuit for incremental signals is shown in Figure 10.6 (b). V_A increases slightly above ground as shown. V_B also increases by an equal amount to restore balance.

$$V_A = \frac{1}{2}\frac{V_S \varepsilon}{2R} = V_B \tag{10.6}$$

This requires $V_o(R_3/R_3 + R_5)$ to be $V_S\varepsilon/R$ in magnitude and in the direction shown.

$$\therefore \frac{V_o R_3}{R_3 + R_5} = \frac{V_S \varepsilon}{R} \tag{10.7}$$

Linearity is maintained only for small signal levels. For large signals, the current through R_2 and R_4 differ causing an error. This is normally avoided. The scheme is quite useful where the bridge arm resistances cannot be reduced below tens of kilo-ohms.

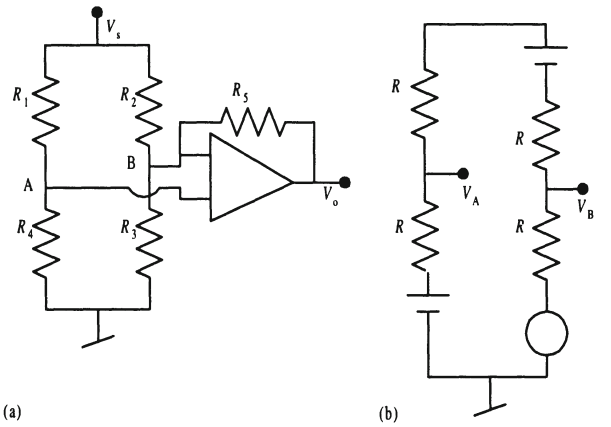


Figure 10.6 Adaptation of Wheatstone bridge for sensors: (a) Scheme (b) Incremental equivalent circuit

As an example, with

$$\begin{aligned} R &= 10\,\text{K}\Omega \\ \text{Gain} &= 100 \\ R_5 &= 1\,\text{M}\Omega \\ R_3 &= \frac{100}{99} \times 10k\Omega \\ &= 10.101\,\text{k}\Omega \end{aligned}$$

The source impedance seen by the opamp at the two inputs is R each. Here it is only 10 kΩ. One can afford to increase it to the level permitted by the opamp. Every time one has to ensure that R_5 (in the MΩ range) can be realized with the expected level of accuracy.

Scheme 3

The scheme shown in Figure 10.7 integrates the Wheatstone bridge with a difference amplifier. Under active operating conditions, we have

$$V_A = V_B = V_S \frac{R_4}{R_1 + R_4} \tag{10.8}$$

$$\therefore \text{ Current through } R_2 = \text{Current through } R_3$$

$$= \left[V_S - V_S \frac{R_4}{R_1 + R_4}\right] \frac{1}{R_2} \tag{10.9}$$

$$= V_S \frac{R_1}{R_1 + R_4} \frac{1}{R_2} \tag{10.10}$$

From Equation 10.10

$$\text{Voltage drop in } R_3 = V_s \frac{R_3}{R_4} \frac{R_1}{R_1 + R_4} \tag{10.11}$$

From the figure we get

$$V_o = V_B - \text{voltage drop in } R_3 \tag{10.12}$$

Substituting from Equations 10.8 and 10.10 in Equation 10.11 and simplifying we get

$$V_o = \frac{V_s}{R_1 + R_4}\left(\frac{R_2R_4 - R_1R_3}{R_2}\right) \tag{10.13}$$

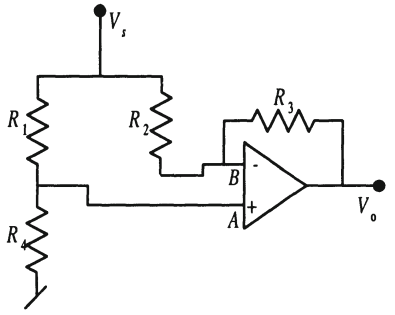


Figure 10.7 Adoption of Wheatstone bridge for sensor with single opamp based difference amplifier

Consider the general case where all the resistances change from balance by incremental amounts only. Substituting,

$$R_1 = R + \varepsilon_1$$
$$R_2 = R + \varepsilon_2$$
$$R_3 = R + \varepsilon_3$$
$$R_4 = R + \varepsilon_4$$

and assuming

$$\varepsilon_1, \varepsilon_2, \varepsilon_3, \varepsilon_4 \ll R \tag{10.14}$$

we get

$$V_o = \frac{V_s}{2}(\varepsilon_2 + \varepsilon_4 - \varepsilon_1 - \varepsilon_3) \tag{10.15}$$

This is the same as we get with the Wheatstone bridge alone. However, the output is buffered, single-ended and available with reference to ground potential. The gain of the bridge is unity.

The most attractive form of the bridge occurs when $R_1 = R_2 = R_4 = R$ and R_3 is the sensor. If $R_3 = R + \varepsilon$, from Equation 10.13 we get

$$V_o = \frac{V_S}{2}\frac{\varepsilon}{R} \tag{10.16}$$

Equation 10.16 shows that the output voltage is linear throughout the operating range. Further the current through all the resistances remains constant at $[V_s/2R]$ throughout the operating range. The disadvantage of the scheme is that neither terminal of the sensor is at ground potential.

10.2.2.3 Self-Calibrating Schemes

These are for resistance-sensors for which the unit to unit tolerance is high. Correspondingly, the sensitivities too can differ substantially. Ambient changes can affect them widely. Due to the apparent indecision levels, they are not directly useful in sensing bridge configurations. Light Dependent Resistors (LDR) and Infrared (IR) detectors are typical examples. With the availability of cost-effective electronic processing circuits, these devices are used to form sensors. Such sensors function with an on-line calibration facility and sense the variable concerned in normalized form. This compensates for the variations due to extraneous factors. The involved processing has led to many variations of implementation. A commonality in the schemes adopted is not easily discernible. One possible approach is described here with reference to Figure 10.8. It is intended to sense the total amount of radiation received by LDR_1. The radiation to be sensed is received

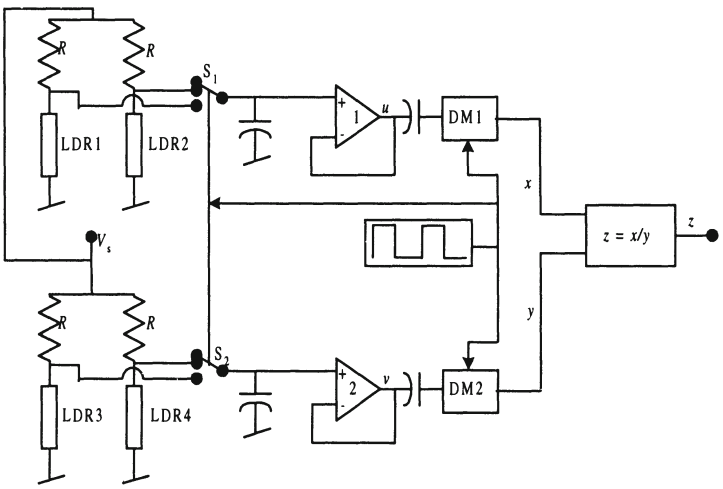


Figure 10.8 A typical self-calibrating instrumentation scheme with resistance-sensors

by LDR_1 while LDR_2 – kept in the same environment as LDR_1 – receives only the background radiation. These two are switched alternately through switch S_1 on to buffer 1. u – the output of buffer 1 – has two levels; one represents the signal to be sensed and the other the background. It is AC-coupled and given as input to a synchronous demodulator DM1. The AC swing is proportional to the radiation to be sensed and the effect of background radiation is removed. Another pair of LDRs – LDR_3 and LDR_4 – is similarly switched to buffer 2 whose output is represented as

v. LDR_3 is subjected to a reference radiation and LDR_4 to background radiation. *y* – output of the synchronous demodulator DM2 – is proportional to the reference radiation. The ratio x / y provides the normalized output. The scheme compensates for variations and error due to changes in ambient conditions. Changes in sensitivity are also compensated for. As mentioned earlier, many variations of the scheme are in vogue [Morris, Nachtigal].

10.3 Capacitance Transducers

Ideally, the capacitance of an electrode pair is $\varepsilon_0\ \varepsilon_r$ F for every m^2 of overlapping area and 1m of spacing between the electrodes. Capacitance-sensors can be used to measure ε_r of a medium and changes in effective ε_r. They can be used to measure change in area or distance between the electrodes. Physical variables or changes in physical variables, which can be directly related to one of the above parameters affecting capacitance, can be sensed using capacitance-sensors. Capacitance-sensors by themselves are easy to fabricate and conform to application requirements. However, the relatively low values of capacitances associated with capacitance-sensors make the associated impedances high. Susceptibility to leakage, stray effects and noise are correspondingly high. Identifying the sources, removing them and compensating for them in each case leads to substantial improvement in performance and consistency [Heerens, Jones and Richards, Kosel].

10.3.1 Capacitance as a Circuit Element

When using a capacitance-sensor, the changes in capacitance can be converted into equivalent voltage or current [Yang, Ramsden]. With a constant applied voltage, the change in capacitance is converted into an equivalent current [Figure 10.9 (a)]. Referring to the figure,

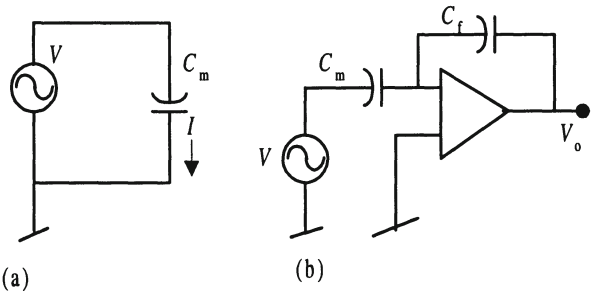


Figure 10.9 Conversion of changes in capacitance value of a capacitance-sensor into an equivalent output (a) Scheme with current output (b) Scheme with voltage output

$$I = j\,C\,V\omega \tag{10.17}$$

Here *V* is the rms. voltage and ω the excitation frequency. The excitation frequency is taken as quite high compared to the signal bandwidth (See Section 6.2.1). *V* and ω are to be constant so that changes in current will be direct measures of corresponding changes in *C* value. The current through the capacitance is measured

through an inverting amplifier configuration. The same is shown in Figure 10.9 (b). C_m is the sensing capacitance and C_f the feedback capacitance.

$$V_o = \frac{C_m V\omega}{C_f \omega} \tag{10.18}$$

$$= V\frac{C_m}{C_f} \tag{10.19}$$

$$\Delta V_o = V\frac{\Delta C_m}{C_f} \tag{10.20}$$

With this addition, the input-output relation is independent of the excitation frequency.

As an alternative to the above, the capacitance-sensor may be driven at a constant current at a fixed excitation frequency. The voltage developed across the capacitor may be used as a measure of the capacitance. The low capacitance values of capacitance-sensors reflect as relatively high impedances at practical operating frequencies; driving them with constant current sources, constrain the source impedance to be of a higher order. Since this is not practical, constant current drive is not used with capacitance-sensors.

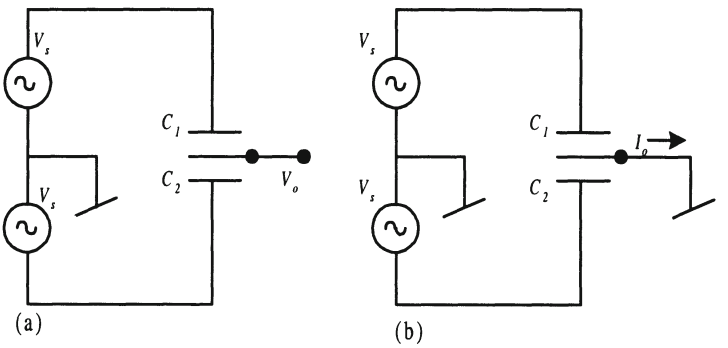


Figure 10.10 Differential capacitance schemes: Under zero input conditions C1 = C2: (a) Scheme with voltage output (b) Scheme with current output

Whenever possible, the differential-capacitance-sensor scheme is used. As explained in Section 2.3, this removes the need to separately sense the change in capacitance. Typically, the schemes have the form shown in Figure 10.10. In Figure 10.10 (a), under zero signal conditions, $C_1 = C_2 = C$ and $V_o = 0$. The current through the capacitor is

$$I = j V_s C\omega \tag{10.21}$$

When the capacitors work in differential mode, as one capacitance increases, the other one decreases by the same amount (This holds for all capacitance-sensors where the change in capacitance is small compared to the steady state capacitance). Taking the impedances of C_1 and C_2 as Z_1 and Z_2, we get for the current through the combination

$$I = \frac{2V}{Z_1 + Z_2} \tag{10.22}$$

$$\therefore V_o = V - IZ_1 \tag{10.23}$$

$$= V\frac{Z_2 - Z_1}{Z_2 + Z_1} \tag{10.24}$$

$$= V\frac{\frac{1}{C-\delta C} - \frac{1}{C+\delta C}}{\frac{1}{C-\delta C} + \frac{1}{C+\delta C}} \tag{10.25}$$

Simplifying this we get

$$\frac{V_o}{V_s} = \frac{\delta C}{C} \tag{10.26}$$

The fractional change in the output voltage is twice the fractional change in the individual capacitances. The output is independent of frequency. Since only the ratio $\delta C/C$ decides the output, the value of ε_r does not affect the measurement. The output impedance remains high at $1/j2\omega C$.

Instead of the output voltage, one can use the current when the middle electrode is grounded or kept at ground potential as shown in Figure 10.10 (b). The current can be seen to be the open circuit voltage of the scheme of Figure 10.10 (a) applied to the equivalent source-impedance of $[Z/2]$. This gives

$$I_o = 2\,j\omega V\delta C \tag{10.27}$$

Here the output leads the supply voltage by 90°. It is a function of ω, and supply voltage. However, the middle electrode remains at ground potential, simplifying the problems of shielding and leakage substantially.

10.3.2 Electrode Geometries and Capacitances.

A few electrode geometries are common with capacitance-sensors [Baxter]. Capacitances of simple geometries and their variations with the sensed parameters are discussed here. For other geometries, the derivations and expressions are too involved to yield easy relationships [Cheng, Haus, Plonus]. For these cases, simplified models are used and the discussions and results are useful in a qualitative sense.

10.3.2.1 Parallel Plate Capacitance

The capacitance shown in Figure 10.11 is formed with two plates of dimensions $b \times w$, kept parallel to each other at a distance d. If the intervening medium has permittivity ε_r, the capacitance of the combination is

$$C = \frac{\varepsilon_0\varepsilon_r A}{d} \tag{10.28}$$

$$= \frac{\varepsilon_0\varepsilon_r bw}{d} \tag{10.29}$$

Here it is assumed that $d << b$ and $d << w$. Changes in any of the parameters in the expression for the capacitance of Equation 10.29, affect the capacitance directly – opening up the possibility of sensing any of these using capacitance-sensors.

Equation 10.29 is derived assuming the electric flux lines to be normal to the plate. This condition is not satisfied at the plate edges. The resulting fringing

increases the capacitance. The fringing effect is equivalent to increasing b and w by 3.5 d on either side (approximately). With this correction, we get

$$C_c = \varepsilon_0 \varepsilon_r \frac{(b+7d)(w+7d)}{d} \quad (10.30)$$

where C_c is the corrected value of the capacitance. For $b = w = 25$ mm and $d = 1.25$ mm

$$C = 2.5\varepsilon_0 \varepsilon_r \text{ F} \quad (10.31)$$

and

$$C_c = 2.86\varepsilon_0 \varepsilon_r \text{ F} \quad (10.32)$$

The parametric changes, which reflect as changes in the value of sensor C, do not affect fringing; *i.e.*, the increase in capacitance value due to fringing remains sensibly constant. Hence one need not apply any correction factor for the same (When d is of the same order as b or w, the situation is different).

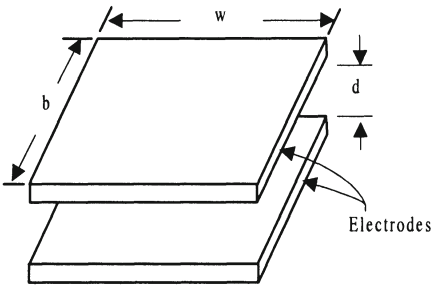


Figure 10.11 Parallel plate capacitor

Change in b or w, reflects as proportionate change in capacitance. Normally this is brought about using one as a fixed plate (electrode) and the other as a moving plate (electrode). Thus if b is changing, d and w are to remain constant to ensure that the change in capacitance is solely due to change in b. To avoid error due to any undesired lateral movement, one plate is made wider; this provides an overlap on either side as in Figure 10.12 (a). Note that for movements in y direction the common area and hence the capacitance value, remains unchanged. Movement in x direction affects b and hence the area A directly; the capacitance changes proportionately.

In Figure 10.12 (b), the capacitance change is brought about by the movement of the dielectric, with both the electrodes remaining fixed (sensing of fluid level, bin level detection *etc.*, are typical applications). Here the overall capacitance is the parallel combination of the two parts – one with the dielectric and the other air.

$$C = \frac{\varepsilon_0 w}{d}(\varepsilon_r x + b - x) \quad (10.33)$$

$$= \frac{\varepsilon_0 wb}{d} + \frac{\varepsilon_0 wx}{d}(\varepsilon_r - 1) \quad (10.34)$$

Here again the capacitance change is proportional to the displacement x. The dielectric can be made to extend on either side to avoid errors due to lateral movements. Normally d is of the order of 100 μm. Variations of a few μm in d affect the capacitance. This scheme is useful for sensing deviations of the order of a

few μm. However, the mechanical fixture has to take care that during regular operation, any change in d due to vibration during regular operation is much lower than the 1 μm. level.

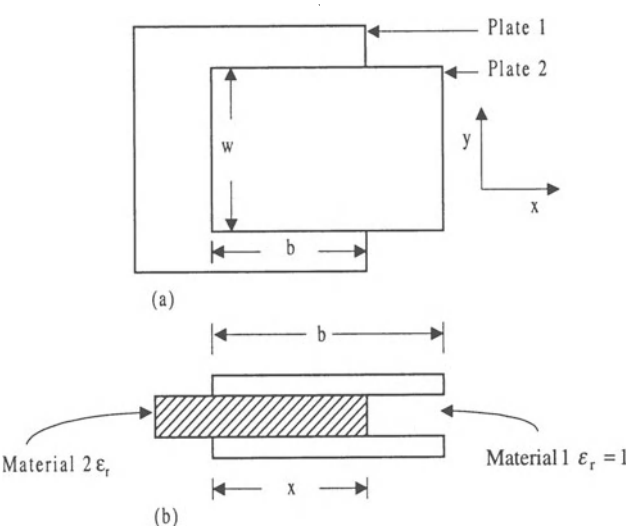


Figure 10.12 Parallel plate capacitor modified as a capacitance-sensor: (a) Modification to avoid error due to lateral movement (in y direction) (b) Modification to detect displacement or change in a property of a dielectric

10.3.2.2 Concentric Cylinders

The capacitance of two concentric cylinders [Figure 10.13 (a)] is

$$C = \frac{2\pi\varepsilon_0\varepsilon_r}{\ln(b/a)}L \tag{10.35}$$

where

⇒ L is the length of the two cylinders
⇒ a is the outer diameter of the inner cylinder and
⇒ b is the inner diameter of the outer cylinder.

The configuration has the advantage that the active capacitance region is confined to the annular zone. If the outer annular cylinder is kept at the same potential as the surroundings (Ground), the sensor performance becomes substantially independent of the position, geometry, *etc.* In turn, the smallest capacitance change that can be sensed increases.

10.3.2.3 Parallel cylinders

The capacitance between two parallel cylinders [See Figure 10.13 (b)] is

$$C = \frac{\pi\varepsilon_0\varepsilon_r}{\ln\left[\left(b+\sqrt{b^2-4a^2}\right)/2a\right]}L \tag{10.36}$$

where

⇒ L is the length of the cylinders
⇒ b is the distance between the cylinders and
⇒ a is the radius of the cylinders (both radii are taken as equal).

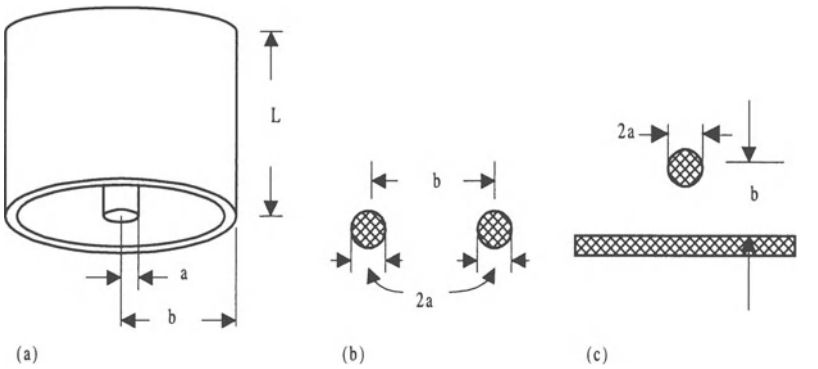


Figure 10.13 Differential capacitor configurations for sensors: (a) Concentric cylinders (b) Parallel plate cylinders (c) Cylinder and parallel plate

This configuration is also in use for level sensors. But the capacitance is sensitive to the position of the cylinder pair with respect to the environment. However, capacitor geometry, construction and maintenance are simpler. This is suitable as a sensor for less demanding applications.
If $b >> a$ we get,

$$C = \frac{\pi\varepsilon_0\varepsilon_r}{\ln\left(b/a\right)} \tag{10.37}$$

The case $b >> a$ is more of pathological interest due to the very low values of associated capacitance. The scheme can be of use for displacement sensing (and sensing of other parameters which result in a displacement) where the displacement manifests as a corresponding change in b. However, the sensitivity expressions are involved and not easily tractable.

10.3.2.4 Cylinder and Plane

The capacitance C is given by [See Figure 10.13 (c)]

$$C = \frac{2\pi\varepsilon_0\varepsilon_r}{\ln\left[\left(b+\sqrt{b^2-a^2}\right)/a\right]} \tag{10.38}$$

where

⇒ b is the height of the cylinder above the plane and
⇒ a is the radius of the cylinder. The capacitance is insensitive to any lateral movement of the cylinder. When used as a displacement sensor, the plate (electrode) moves in the direction of b. The scheme can be used for the measurement of level also. Here the plate can be the side of the vessel and the cylinder the other electrode.

10.3.3 Circuit Configurations

Barring some customized solutions, choice of circuit configurations available with capacitance-sensors is limited. Three possible types are discussed here.

10.3.3.1 DC Circuits

Figure 10.14 (a) shows one circuit configuration.

$$V_o = V\frac{C_1}{C_2} \tag{10.39}$$

When change in area or ε_r is measured, C_1 can be the sensing capacitance. When displacement is sensed C_2 can be the sensing capacitance. This choice provides a linear input-output relationship.

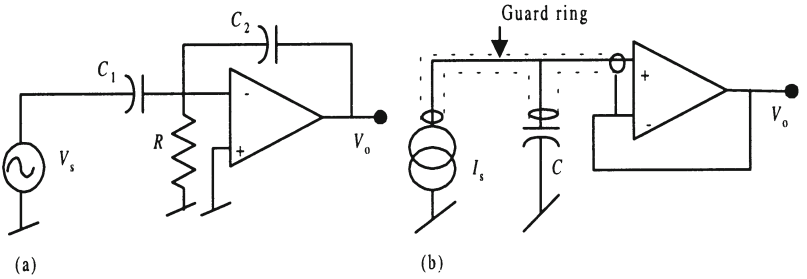


Figure 10.14 Circuit configurations with capacitance-sensors: (a) Sensor with constant voltage supply (b) Sensor with constant current supply. A guard ring is also shown in the latter

Observations: -

- ⇒ V has to be well stabilized and should have enough drive capability.
- ⇒ Charging of the parallel combination of C_1 and C_2 and saturating the opamp output is to be avoided; for this, the opamp chosen should have FET or MOSFET type input with femtoamp level of input current. Electrometer type amplifier is to be used here.
- ⇒ A separate bias resistor may be provided as shown. This limits the lower cut-off frequency of the sensor to $1/R$ $(C_1 \| C_2)$. Only comparatively faster changes in the value of the capacitance will be sensed.
- ⇒ The opamp has to be of the self-compensated well-stabilized type.
- ⇒ The current noise at low frequencies can cause substantial error. Opamps with low i_n are to be selected for the application.
- ⇒ At signal-zero, the circuit gives a steady V_o. If necessary, this has to be nulled at a following amplifier stage.
- ⇒ One end of the measuring capacitance is at virtual ground. The capacitor electrode for this can be suitably chosen to minimize stray effects *etc.* For example, with a concentric cylinder-type capacitance-sensor, the outer cylinder may be connected to the inverting input of the opamp. A further improvement may be brought about using a guard ring.

⇒ Due to the large values of the resistances at the input side, thermal noise is likely to be high. To keep its effect low, as high a value of V as permissible is to be used. The bandwidth is also to be kept at the minimum.

⇒ In specific cases, the capacitance ratio reduces to the ratio of geometric dimensions. This makes the sensor response independent of extraneous factors.

A high input impedance on the opamp-side is ensured with the alternate scheme in Figure 10.14 (b). Referring to the figure

$$V_o = \frac{I_S}{C\omega} \tag{10.40}$$

At constant AC current, the output voltage is proportional to the sensor impedance.

Observations: -

⇒ Sensors that sense the distance between the electrodes provide linear output.

⇒ Although input impedance of the configuration is high, opamps with ultra-low bias currents (with FET or MOSFET input stage), are to be used.

⇒ Leakage and stray effects can adversely affect performance and cause errors. This is due to the potential at the sensing electrode. A guard ring connected to the inverting lead bypasses these and reduces error substantially.

⇒ The voltage level of the signal is low here and its source impedance is high. The performance level with such signals, is rather limited (See Section 7.4.7.2). Both v_n and i_n can contribute to reduction of accuracy.

⇒ With constant AC current input, the output represents the signal in amplitude modulated form.

Whenever possible, instrumentation with capacitance-sensor and DC amplifier is avoided. Laboratory measurements, which are highly specialized in nature and the ones that use low capacitances, resort to this method. The user has to be well aware of the sources of leakage and stray capacitances and systematically eliminate their causes and effects.

10.3.3.2 Oscillators

The capacitance of the capacitance-sensor can be made part of an oscillator circuit. LC oscillator is the most common. It can be Colpitt's, Hartley's or one of the tuned oscillators [Schubert and Kim, Terman]. The oscillator frequency is given by

$$f = \frac{1}{2\pi\sqrt{LC}} \tag{10.41}$$

The oscillator output is FM modulated. The square-root term makes the sensor characteristic highly non-linear. Normally the useful range is limited to 1% to 2% of the capacitance range (See also Section 2.4). Within such limited ranges, change in oscillator frequency can be considered as proportional to the change in capacitance.

Observations: -

⇒ Due to the low capacitance levels of the sensors, the oscillator frequency is in the 0.1 MHz to the 10 MHz range.

⇒ To avoid stray effects in this high frequency range, the sensor and oscillator dimensions are kept small.

⇒ Normally one electrode of the sensor capacitance is grounded. A guard ring is provided around the other; A guard ring is provided around the Inductor as well as any other frequency determining elements of the circuit. This makes all the capacitance and inductance values definite and reduces drift. However it increases the standing capacitance conspicuously and affects sensitivity.

⇒ Range of frequency shift achievable is limited to 1% to 3%. To get (say) 0.2% accuracy, the zero signal oscillator frequency has to be stabilized to better than 0.03 × 0.002 = 60 PPM. Compare this with the frequency stability of crystal oscillators (in the range of 20 PPM).

⇒ Normally only air core inductors are used for the frequency determining inductance element of the oscillator. This is to ensure stability of the inductance. The inductor is well shielded. This avoids inadvertent feedback and spurious oscillations due to them.

⇒ Once well designed and engineered, the sensor performance is highly repeatable.

⇒ Only FM demodulation schemes can be used to retrieve the signal. PLL is proving to be increasingly attractive [Viterbi].

10.3.3.3 Amplitude Modulated Schemes

Amplitude modulated schemes are probably the most commonly used with capacitance-sensors. Two types of configurations are possible depending on whether the capacitance is single-ended or differential. The circuits of Figure 10.14 (a) & (b) discussed earlier provide the necessary output for the single-ended case. However even with zero signal level, they give a steady output. Normally this is difficult to be neutralized at the carrier frequency stage itself. The output is demodulated and the offset removed at the demodulation output. Due to all these, the scheme is cumbersome and not suitable for high accuracy applications. It is used only when other approaches are not possible.

With the differential capacitance sensing, the capacitance-pair form two adjacent arms of a bridge (see Figure 10.15). The two voltages are equal (=V). They may be outputs of a centre-tapped secondary of a transformer. The capacitances are equal under zero signal conditions and the bridge is balanced. As the capacitances change, V_o appears in the modulated form at the excitation frequency, its magnitude being proportional to $(C_1 - C_2)$ and phase depending on the sign of $(C_1 - C_2)$. The demodulated output represents the true change in capacitance.

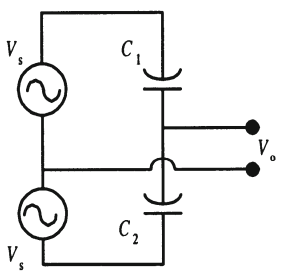


Figure 10.15 Skeletal bridge circuit with differential capacitance-sensor

Observations: -

⇒ Whenever possible, the capacitance-sensor is used in this mode.

⇒ Due to the differential nature of the capacitances, linear range is good and the sensitivity high.

⇒ Often low value trimmers are connected across C_1 and C_2. These are for the adjustment of the signal value to zero at signal-zero conditions.

⇒ As far as possible, geometric symmetry of the capacitance pair and its leads is maintained. This compensates for the stray effects *etc.*

⇒ The oscillator amplitude and frequency are to be well stabilized. This is to ensure that the sensor sensitivity remains unchanged.

⇒ Due to the low levels of C_1 and C_2, capacitance due to the leads and stray capacitances are not negligible. Hence, V_0 may not have the expected phase relationship with the exciting signal. Normally a small phase shift for the reference signal for the demodulator does not cause any error. It reduces the overall sensitivity by a small but definite amount. If necessary one can compensate for this, by phase-shifting the reference.

⇒ The excitation frequency can be chosen high enough to have the capacitive reactance within manageable limits. This also reduces the constraints on the input impedance levels of subsequent demodulation stage.

⇒ Due to the differential capacitance and geometrical symmetry, shielding and guarding are easier than with the oscillator type transducer.

10.3.3.4 Signal Threshold with Capacitance Sensors

The signal-threshold *vis-à-vis* noise can be determined in comparatively simple configurations. Figure 10.16 shows the scheme considered earlier with C being the sensor capacitor. C_f is the feedback capacitance. V_n and i_n are the equivalent noise voltage and current of the opamp and the resistances connected. The threshold – *i.e.*, the minimum change in capacitance that can be detected – is that value which produces an output voltage equal to the noise voltage. This represents the minimum detectable signal. Depending upon the operating conditions and the opamp used, different possibilities arise. Two cases are considered here.

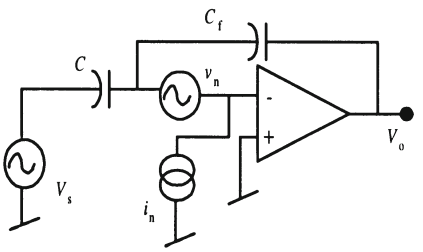


Figure 10.16 Typical capacitance-sensor circuit shown along with equivalent noise source

Case 1: v_n dominates

This corresponds to a case where the total noise current over the bandwidth of interest, is negligible compared to the noise voltage v_n. This is the case with opamps having FETS or MOSFETs at the input. For example, TL081 has negligible i_n. From Table 3.2 one can estimate the noise voltage as

$$v_n = \left[50^2\times10^{-18}\times10+28^2\times10^{-18}(100-10)+25^2(1000-100)\right]^{\frac{1}{2}} \quad (10.42)$$

$$= 811\ \mu V \quad (10.43)$$

Here the bandwidth is taken as 1 kHz. With V = 10 V rms. (at 1 MHz), and C = 2 pF, an output voltage of this magnitude represents a capacitance change of δC, where

$$\delta C = 2\times\frac{811\times10^{-6}}{10}\text{pF} \quad (10.44)$$

$$= 0.16\times10^{-15}\text{ pF} \quad (10.45)$$

$$= 0.008\ \%\text{ of C} \quad (10.46)$$

Full-scale range of a capacitance-sensor is of the order of 2 %.

$$\text{Hence the minimum detectable signal change} = \frac{0.008}{2}\times100\% \quad (10.47)$$

$$= 0.4\ \% \quad (10.48)$$

Case 2: i_n dominates

With the use of bipolar opamps, voltage noise level can be one order lower. Consider the use of OP07. From Table 3.2 the noise current can be estimated as

$$i_n = \left[0.8^2\times10+0.23^2\times(100-10)+0.17^2(1000-100)\right]^{\frac{1}{2}}\text{ pA} \quad (10.49)$$

$$= 6.09\text{ pA} \quad (10.50)$$

Here again, 1 kHz is taken as the bandwidth of operation of the opamp for the signal. At 1 MHz, the current through the capacitance is

$$i_c = 2\pi\times10^6\times10\times2\times10^{-12}\text{ A} \quad (10.51)$$

$$= 126\ \mu\text{ A} \quad (10.52)$$

$$\text{Change in current for a 2 \% change in capacitance} = 2.4\ \mu\text{ A} \quad (10.53)$$

Typically, this represents the full scale.
From Eqations10.38 and 10.41,

$$\text{Minimum detectable signal} = \frac{6\times10^{-12}}{2.4\times10^{-6}}\times100\% \quad (10.54)$$

$$= 250\times10^{-6}\ \% \quad (10.55)$$

$$= 2.5\text{ ppm} \quad (10.56)$$

Similar estimates can be made with other configurations and circuits used. However in practice, the threshold will be at least one order higher than the levels estimated here.

10.3.4 Guard Ring and Shielding

The capacitances associated with capacitance-sensors are of the same order as the stray capacitances (often referred to as 'strays'). Blind use of a capacitance-sensor results in a considerable reduction in sensitivity due to strays. Further, the change in strays due to change in physical orientation of the sensor, changes in the

environment *etc.*, – all these – change stray effects and cause a considerable level of indecision in sensitivity. All capacitance transducers use proper shielding to bypass the stray effects. A few cases are dealt with here. Figure 10.17 shows a single-ended capacitance-sensor considered earlier. C_s represents the capacitance-sensor. The lead from the sensor to the buffer is fully shielded and connected to the inverting lead of the buffer. Since the shield and the sensing lead are at close potentials, the bypass current between them is negligible. The current from the shield to the ground and supply lead AB to the ground, increases loading on the buffer and loading on the sensor supply respectively. The resulting change in sensitivity is negligible. This type of shielding is useful especially when the buffer (or signal processing circuitry) is at a distance from the sensor proper. The connecting cable capacitance is typically of the order of 50 pF/m while the sensor capacitance is only in the 1pF range. Sensor working without shielding is not practical here. However, a coaxial cable and a separate supply lead are necessary to connect the sensor to the buffer.

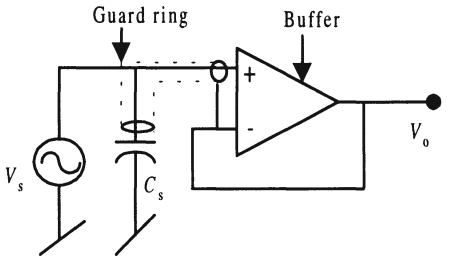


Figure 10.17 Single-ended capacitive sensor along with shield

In all cases involving weak signals, the principle used is the same – a separate point whose potential is the same as the sensing point is identified. This has to be in the signal processing circuit. The full signal path is screened and the screen connected to this point. In some cases, such shield current can cause error due to the common path with signal or associated circuitry. In such cases, a separate drive is provided through a buffer. Specific schemes are discussed in the sequel.

Figures 10.18 (a) & (b) show a differential capacitance type sensor with displacement being sensed by the motion of electrode 3. The electric field near region R is uniform. However, at the edges P and Q, it is not uniform. For low values of displacement, *i.e.*, as long as P and Q are away from R, the field uniformity is not disturbed and the sensor output changes linearly with input. As the end P of the electrode Figure 10.18 (b) approaches the gap *R*, field lines in the sensing area are no longer uniform. This causes the response to be non-linear adding to the indecision due to strays. A guard ring 4 is provided in Fig 10.18 (c) and grounded (since electrode 3 is close to ground potential). This rectifies the field profile at the edges of 3 and makes it definite too. The guard ring 4 and the sensing electrode 3 are mechanically coupled and move together. The transfer characteristic of the sensor retains its linearity even as the edge P or Q of the electrode 3 approaches the gap R thus extending the linear range. Further, the error due to strays is reduced substantially. However as pointed out earlier, the sensor sensitivity reduces due to this.

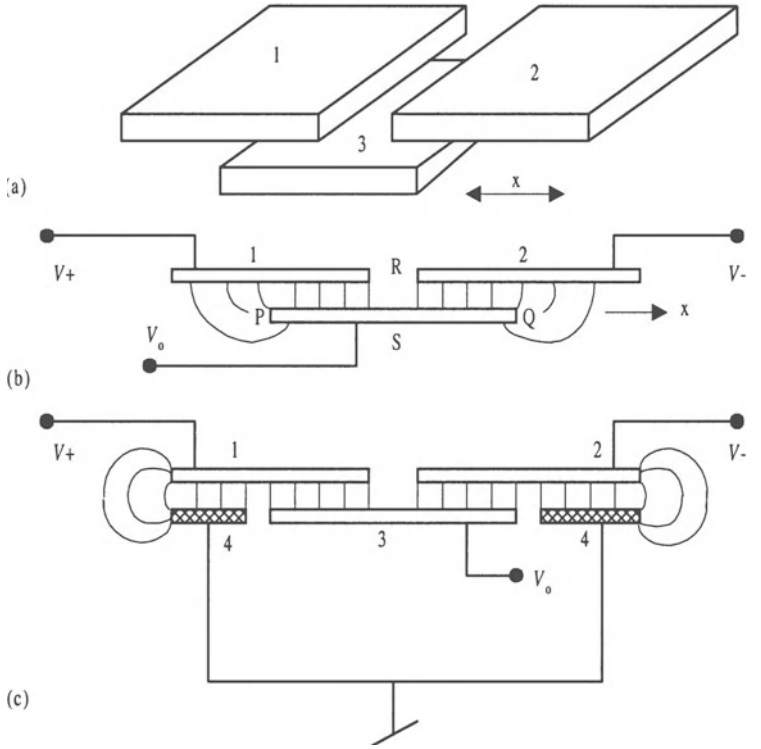


Figure 10.18 Differential capacitance-sensor shown for displacement sensing: (a) Basic arrangement for electrodes (b) Sensor with field profile when excited (c) Effect of ground ring on the field profile

Figure 10.19 (a) shows a non-inverting amplifier using the differential capacitance-sensor of Figure 10.18 (c). Over the active range of the sensor, the potential difference between electrodes 3 and 4 is limited to only a few percent of the supply voltage. The corresponding signal bypass is also negligible. This scheme is modified in the non-inverting configuration of Figure 10.19 (b); this provides a drive to the guard ring in the feedback mode, so that it tracks the potential of electrode 3. The error due to signal bypass is substantially less here compared to the last case. Figure 10.19 (c) uses a feedback scheme and keeps the sensing electrode and the guard-ring at ground potential. Due to the feedback and the high gain of the opamp

$$V_A = 0 \tag{10.57}$$

$$\therefore \frac{V+V_o}{V-V_o} = \frac{C_2}{C_1} \tag{10.58}$$

Simplification yields

$$\frac{V_o}{V} = \frac{C_2-C_1}{C_2+C_1} \tag{10.59}$$

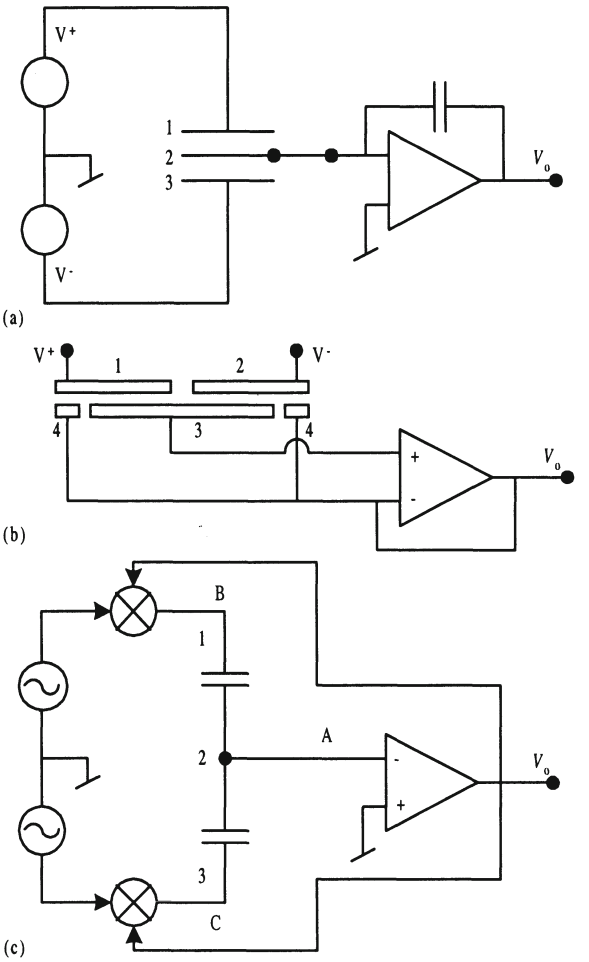


Figure 10.19 Circuits with differential capacitance-sensor: (a) Simple inverting amplifier (b) Scheme with guard ring drive (c) Feedback balancing scheme

Observations: -

⇒ Stray capacitances from the terminal of electrode 3 to the to the inverting input lead A of the opamp, see only ground potential throughout. Hence their current is zero.

⇒ Stray capacitances at points B and C increase the loading on the oscillator source and the opamp and hence do not directly affect the sensor operation.

⇒ Stray capacitance between the inverting input lead and the feedback lead (to the supply side summing junctions), function as an equivalent feedback capacitor for the opamp. This causes only a high frequency roll-off of gain and limits the bandwidth of the sensor.

The substantial improvement in performance achieved here is at the expense of a more elaborate circuit. Note that the two summing junctions shown require additional opamps to be used – not shown explicitly here.

10.4 Inductance Transducers

The self- inductance of a coil is governed by the reluctance of the flux path. Mutual inductance between two coils is governed by the coupling between them. The reluctance in the former and the coupling in the latter cases, are governed by the geometry and the change in the magnetic characteristics of the material of the flux path. Displacements – linear as well as angular – and the changes in the (magnetic) properties of the magnetic medium, can be sensed by inductance-sensors. Apart from these two primary areas, inductance-sensors are used in a variety of secondary transducers. All of them transform the variable to be sensed into an equivalent linear displacement that is sensed by the inductance-sensor. A discussion of aspects common to inductance-sensors, is in order here: -

- ⇒ Inductance-sensors are built around magnetic materials. Their relative permeability – μ_r – is much higher than that of vacuum or air. Hence, the inductance levels are also much higher than the stray inductance levels. Hence, stray effects do not haunt them as severely as they do with capacitance-sensors. The need for guarding and shielding are also much less (With inductance-sensors, shielding is more often to prevent their affecting other components).
- ⇒ Coils, stack of stampings or ferrite cores are common to all inductance-sensors. The relatively poor consistency associated with them, reflects as poor repeatability and poor accuracy. We use the term 'poor' here only in relation to capacitance-sensors.
- ⇒ The output signal levels of inductance-sensors are one or two orders higher than those of capacitance-sensors. They are more easily processed. Their source impedance levels are lower and contamination possibility is less. Both these contribute to a larger dynamic range for inductance-sensors.
- ⇒ Permeability of iron and its alloys are functions of temperature, frequency of operation and the applied voltage. Respective variations are not of negligible order.
- ⇒ The inevitable use of iron-based or other magnetic materials with inductance-sensors, makes the inductance far from perfect (Contrast with the near perfect nature of the capacitance-sensor). This also contributes to lower accuracy levels of inductance-sensors.
- ⇒ Normally the inductance-sensors work in the 2 kHz to 20 kHz frequency range (in extreme cases, this may extend up to 1 MHz). The comparatively lower frequencies here make signal processing easy. Often circuits built around 'run-of-the-mill' opamps suffice.

10.4.1 Inductance as a Circuit Element

The relationship connecting the voltage and current of an ideal inductance is

$$V = j I\omega L \tag{10.60}$$

where

- ⇒ V is the rms. voltage across the inductance in volts.
- ⇒ I is the rms. current through the inductance in amps.
- ⇒ ω is the supply frequency in rad /s and

$\Rightarrow$ L is the inductance in henries.

Normally the resistance of the coil forming the inductance is not negligible at low frequencies. Accounting for the resistance, we have

$$V = I\sqrt{R^2 + L^2\omega^2}\angle -\varphi \tag{10.61}$$

$$\varphi = \tan^{-1}\frac{L\omega}{R} \tag{10.62}$$

where

$\Rightarrow$ V is the rms. voltage across the inductance

$\Rightarrow$ I is the rms. current through the inductance

$\Rightarrow$ L is the inductance

$\Rightarrow$ R is the resistance of the coil of wire forming the inductance and

$\Rightarrow$ φ is the phase shift between the current and voltage.

If L changes by δL – as long as such changes are small – we get from Equations 10.61 and 10.62

$$\delta V = \frac{IL\omega^2}{\sqrt{R^2 + L^2\omega^2}}\delta L \tag{10.63}$$

$$\delta\varphi = \frac{R\omega}{R^2 + L^2\omega^2}\delta L \tag{10.64}$$

Here the current through the inductance is taken as constant.

Similarly, if the voltage across the inductance is kept constant, we get

$$\delta I = -\frac{I\omega^2 L}{R^2 + L^2\omega^2} \tag{10.65}$$

$$\delta\varphi = \frac{R\omega}{R^2 + L^2\omega^2}\delta L \tag{10.66}$$

Observations :-

$\Rightarrow$ δL due to the change in the variable being sensed (displacement, iron content *etc.*), is relatively large. This makes the sensitivity high and the detectable threshold low.

$\Rightarrow$ The change in the output current or voltage with respect to δL, is linear only over a restricted range. Non-linearity and asymmetry of the characteristic affect performance even at moderate signal levels. The definite coil resistance is the main contributing factor for this.

$\Rightarrow$ The effective inductance and resistance are functions of applied frequency and the induction level. These are not brought out by the above equations.

The effect of coil resistance can be reduced by increasing the frequency. But the inter-turn capacitance of the coil wire comes into play beyond 100 kHz. to 1 MHz. To get a quantitative picture of this, consider an air core inductance with closely spaced turns forming an inductance as in Figure 10.20. Each wire is of 0.2 mm diameter with a 0.1 mm thick insulation over it.

$$\text{Total length of wire} = 2\pi d \tag{10.67}$$

$$= 62.83\text{mm} \tag{10.68}$$

$$\text{Resistance of copper wire } (\rho \text{ of copper} = 1.73 \times 10^{-8}\ \Omega) = \frac{1.78\times10^{-8}\times62.83\times10^{-3}}{\pi\times25\times10^{-6}}\Omega \tag{10.69}$$

i.e. Resistance of the wire = 13.8 μΩ (10.70)

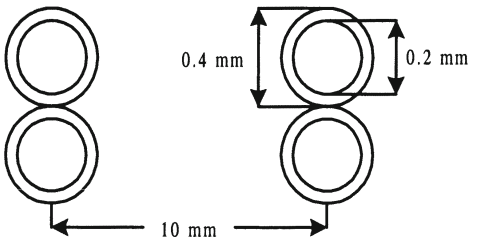


Figure 10.20 Example to calculate the inter-turn capacitance of an inductance coil

The inductance of the two-turn coil can be calculated from the formula

$$L = \frac{\mu_0}{2a}\pi a^2 N^2 \tag{10.71}$$

where N is the number of turns in the inductance coil. Substitution of numerical values for the different quantities and simplification yields

$$L = 78.96 \text{ nH} \tag{10.72}$$

The inter-turn capacitance of the coil is obtained in a similar manner as

$$C = \frac{\pi \varepsilon_0 \varepsilon_r \times 4\pi \times 10^{-2}}{\ln(0.4/0.2)} \text{F} \tag{10.73}$$

$$= 5.04 \text{ pF} \tag{10.74}$$

Using the inductance from Equation 10.71 and capacitance from Equation 10.73, the respective reactances have been computed at a selected set of frequencies and given in Table 10.1

Table 10.1 Inductive and capacitive reactances of a two turn coil

f	1 kHz	10 kHz	100 kHz	1 MHz	10 MHz
Lω (Ω)	0.496×10^{-3}	4.96×10^{-3}	49.6×10^{-3}	0.496	4.96
1 / Cω(Ω)	31.58×10^{6}	3.158×10^{6}	315.8×10^{3}	31.58×10^{3}	3.158×10^{3}

Observations: -

⇒ At 1 kHz, $L\,\omega/R$ = 35.9. Even at this low frequency, the resistance is not negligible.

⇒ At 10 MHz, the reactance due to the inter-turn capacitance is of the order of 1/1000th of the inductive reactance; its effect is definitely not negligible at higher frequencies.

⇒ With the use of magnetic core, L increases by 10 to 100 times. Correspondingly, L/R and LC too will improve. This apparently widens the frequency range of operation. However, the magnetic core loss and heating, limit the high frequency use. Usually in the kHz and MHz ranges, ferrite cores are used. Table 10.2 shows that with increase in the frequency of operation, μ_i decreases. $f\mu_i$ product represents Lω. Around 10 kHz, the Lω

product increases rapidly. As the frequency increases, the increase in the value of f μI, is not appreciable. This explains (partially) the use of frequencies of around 10 kHz with inductive sensors.

Table 10.2 Key characteristics of ferrite cores

f	100 MHz	10 MHz	1 MHz	100 kHz	10 kHz	1 kHz
Ferrite type	Ni Zn	Ni Zn	Ni Zn	Ni Zn/Mn Zn	Mn Zn	Mn Zn
μ_i (Initial permeability)	10	30	250	2000	2500	3000
$f\mu_i$	1000	300	250	200	25	3

⇒ The fact that so many factors affect the operation, limits the viability of the sensor. Hence, a single inductor based sensor is not common (There are exceptions like the copper purity or σ test set. This measures the σ of standard and test specimens in quick succession and compares them.).

⇒ The energy stored in an inductance is

$$E = \frac{1}{2} I^2 L \tag{10.75}$$

Due to any displacement (during sensing) L changes, causing a force

$$F = \frac{dE}{dx} \tag{10.76}$$

$$= \frac{1}{2} I^2 \frac{dL}{dx} \tag{10.77}$$

to be experienced by the moving member. The sensor sensitivity is proportional to dL/dx. Hence as the sensitivity increases, the force experienced also increases. This is to be suitably restrained (Such a force exists in the case of capacitance-sensors also; but it is negligibly small).

Inductive sensors discussed here find two types of applications. In one, the amount of iron content in a powder or a sintered product or the compaction level is measured. Here the value of the parameter of interest is judged by the effective relative permeability of the core of the inductor. The second type is the eddy current based sensor. A metallic object brought near an inductor excited at a frequency has eddy currents induced in it. These oppose the main flux and reduce the same. Hence, the effective inductance also reduces. The amount of change in L can be used as a measure of closeness (or proximity) of the metallic object, as a measure of its thickness or as a measure of its conductivity.

Apart from the scheme above, inductive sensors are mostly used in differential mode. Two schemes are in common use [Figures 10.21 (a) & (b)]. The scheme of Figure 10.21 (a), is excited at terminals 'A' and 'C'. At zero signal conditions, the net inductive drops in sections AB and BC are equal. The presence of a signal causes the inductance of one half to increase and that of the other half to decrease. The relative imbalance is sensed and used as a measure of the value of the physical variable (e.g., displacement). Factors like change in frequency, ambient temperature, supply voltage *etc.*, affect both halves equally and compensate themselves.

The scheme of Figure 10.21 (b), is a differential transformer. The primary winding P is excited at a fixed frequency and voltage. The two seconderies S_1 and

S_2 are identical. At zero signal condition, the induced emfs in both are equal. In the presence of a signal, the balance is upset. The difference between the two emfs represents the signal to be sensed. The scheme offers isolation amongst the three windings. This is a decided advantage compared to that of Figure 10.21 (a). The additional winding is the price paid for the Isolation achieved.

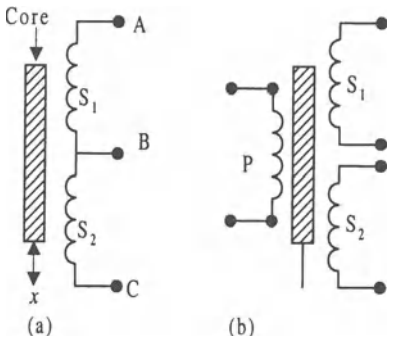


Figure 10.21 Two basic schemes of differential inductance-sensor: (a) Closely coupled inductor (b) Differential transformer

10.4.2 Sensor Geometries and Inductances

Even simple geometries defy an easy analysis and derivations of respective inductance values [Cheng, Haus, Instrument Society of America, Plonus]. Expressions for self-inductance values of a few configurations are given in Table 10.3. Even these are sufficiently involved. However approximations of the geometries by simplified idealizations, yield results with 5 % accuracy or better; all these cases replace the actual geometry by an equivalent solenoid of infinite length and uniform current distribution.

Table 10.3 Inductance values for different geometries of coils

Configuration		Inductance value
Parallel strips	a - distance between the strips b - width of the strips	$\frac{\mu_0 a}{b}$ H/m
Parallel wires	a - radius of the wires d - distance between the wires	$\frac{\mu_0}{\pi}\left(\frac{1}{4}+\ln\frac{d}{a}\right)$ H/m
Co-axial conductors	a - radius of the inner conductor b - inner radius of the outer conductor	$\frac{\mu_0}{2\pi}\left(\frac{1}{4}+\ln\frac{b}{a}\right)$ H/m
Flat coil	a - radius N - no. of turns	$\frac{\mu_0 a N^2}{2}$ H
Long solenoid / toroid	N - no. of turns l - length A - area of section	$\frac{\mu_0 N^2 A}{l}$ H

Configuration		Inductance value
Short solenoid	N - no. of turns l - length a - radius	$\frac{\mu_0 N^2 A}{\sqrt{l^2+4a^2}}$ H
Ring with circular cross-section	r - radius of the wire R - radius of the ring	$\mu R\left[\ln\left(\frac{8R}{r}-2\right)+\frac{1}{4}\right]$ H

10.4.3 Circuit Configurations

Three types of inductance configurations were considered in Section 10.4.1 above. A specific type of signal processing is used for each. These are discussed here.

10.4.3.1 Oscillator Scheme

When the sensor is a single inductor whose inductance changes with the physical variable, the inductor is made part of an oscillator circuit. Any LC oscillator configuration is suitable. The oscillator frequency f is given by

$$f = \frac{1}{2\pi\sqrt{LC}} \tag{10.78}$$

where C is a fixed capacitance. The variation in frequency is a measure of the change in L.

Observations: -

- ⇒ The change in L can be due to the change associated with the magnetic material. Alternately, it may be the effective inductance felt by the oscillator as in a proximity sensor or in a conductivity meter.
- ⇒ C is selected so that the oscillator frequency is in the 5 kHz to 20 kHz range. A good quality low-loss C is selected. Use of PPF capacitor is common.
- ⇒ Change in L and changes in f are limited to 2 % to 4 % only.
- ⇒ Closeness of metallic objects affects the oscillator frequency. Hence, the whole sensor and oscillator are enclosed inside a conducting enclosure. The enclosure thickness should be 2 to 4 times the depth of penetration of magnetic flux. Only the sensing area is kept exposed.
- ⇒ The sensor output is in FM form. Any FM demodulator may be used to demodulate it and retrieve the signal (See Section 6.2.2). With the present state of technology, PLL (See Section 6.2.2.6) appears to be the preferred scheme.

10.4.3.2 Bridge Schemes

The scheme of Figure 10.22 (a) has two tightly coupled inductive arms. Any deviation from balance causes an output voltage. This inductance pair is normally connected in a unit-ratio-bridge configuration as shown in Figure 10.22 (b). If a centre-tapped supply is available, the scheme of Figure 10.22 (a) suffices. Otherwise, the scheme of Figure 10.22 (b) is used. Two equal capacitances can be used in place of the resistances. The output V_o is zero under zero input conditions and changes according to changes in input. The availability of V_o around ground potential ensures that the error due to strays is minimized. The bridge output is in

the form of a DSB-SC AM. It can be demodulated using a multiplying type balanced modulator / demodulator IC (See Section 6.2.1). The reference carrier for

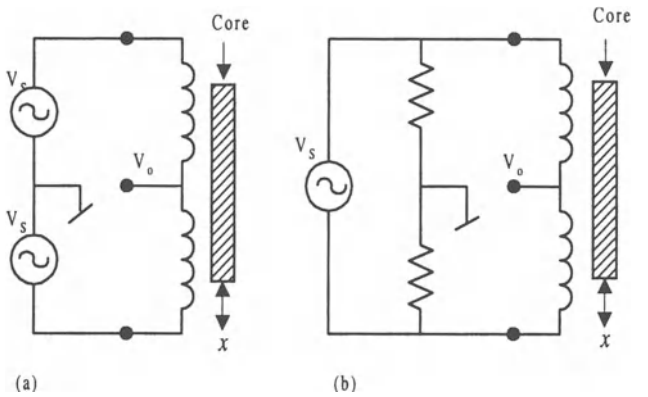


Figure 10.22 Ratio arm bridge connection with differential inductance-sensor: (a) Scheme with centre-tapped supply (b) Scheme with floating supply

the demodulation is obtained from the source itself. Figure 10.23 shows a scheme in block-diagram form. The balanced demodulator output is filtered to remove components beyond the bandwidth of interest. The demodulator incorporates a minimal amount of amplification. Subsequent amplification is provided after filtering. With 5 kHz operation, 800 Hz bandwidth for dynamic operation, is normal. Small signal response may extend up to 1 kHz.

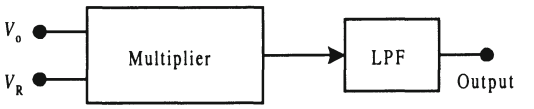


Figure 10.23 Balanced demodulator in simplified block diagram form: V_0 is the output of the bridge in Figure 10.22. V_R is derived from the V_s of figure 10.22 through attenuation and phase shift (if necessary)

Observations: -

⇒ Normally V_0 need not be in phase with V_s. This is mainly due to the coil resistance being definite. Lack of identity between the two halves, also contributes to this.

⇒ Normally under zero-input conditions, V_0 will be at a low definite level. This is due to the imperfections in manufacture and asymmetry due to it. The low level of harmonics generated by the core, also contribute to this.

⇒ With synchronous demodulation, the effects of harmonics are normally neutralized – since the products of these with the reference carrier, fall outside the output filter. The effects of residuals cannot be neutralized in this manner. A proper DC voltage is added at the output side to neutralize these unwanted components.

⇒ Due to the phase shift between V_o and V_s, the carrier component used for demodulation can be correspondingly phase-shifted – may be by a few electrical degrees. This improves sensitivity.

10.4.3.3 Differential Transformer Scheme

The differential transformer of Figure 10.21 (b), due to its very nature, offers more flexibility. The two outputs may be connected in series opposition and the net output demodulated as shown in Figure 10.24. The output is floating in nature and not single-ended. A symmetric demodulator can be used with a corresponding slight

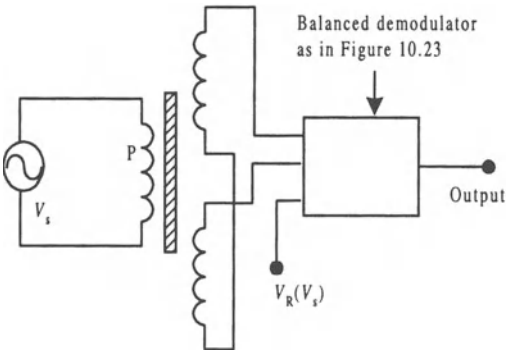


Figure 10.24 Simplified block-diagram form of differential transformer type inductor sensor

improvement in accuracy. Alternately a crude demodulator as in Figure 10.25 may be used. Here the individual secondary outputs are rectified and filtered as in an envelope detector. The DC voltages are subtracted from each other. Under ideal conditions, the output is zero for signal-zero conditions. The output changes in magnitude and sign depending on the change in input.

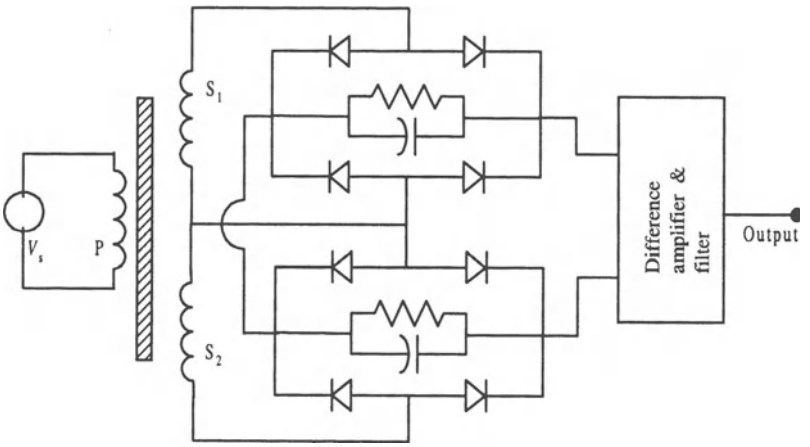


Figure 10.25 Simpler scheme of processing differential transformer output

The scheme exhibits the following drawbacks (See also Section 6.2.1.3): -

⇒ Contributions due to harmonics and residual effects are carried over to the output side of the bridge rectifier. Subtraction of the average values provides some neutralization. However, it is not as good as the phase sensitive detector. This affects accuracy adversely.

⇒ Schottky diodes with their low forward drops are best suited for the bridge rectifier here. Their presence is equivalent to subtracting a fixed voltage from both the output-halves. At low signal levels, this is acceptable but not as it approaches the full-scale level. For example, if the output at S_1 increases and that at S_2 decreases, the corresponding rectified difference should represent the change in the input. But on the S_2-side, the rectifier drop dominates; this causes non-linearity in the characteristic to set in, earlier than with the synchronous demodulator. Hence, the useful range of the detector is more restricted.

⇒ The asymmetry and the tolerances in the diode characteristics, introduce an additional source of error.

⇒ The circuit scheme is apparently simpler than a synchronous demodulator. However, the availability of the synchronous demodulator in IC form, has neutralized this apparent advantage. Hence, the scheme is no longer as attractive as it used to be. The absence of any need for detailed design, perhaps, makes it still attractive for comparatively low performance schemes.

10.5 Feedback Transducers

The feedback transducer scheme is employed in a variety of fields in different ways. It uses the 'Inverse Transducer' in a feedback path and balances the forward transducer effect. The input to the inverse transducer is used as a measure of the variable to be sensed. Figure 10.26 shows the scheme in a generalized block diagram form. The variable to be sensed is converted to another form by a forward transducer. The forward transducer output is the reference to the feedback scheme. The feedback signal is derived from an inverse transducer shown here as $H(s)$. The error is fed to the forward loop comprising of $G(s)$. The forward loop invariably has an integrator as part of it. The forward loop output forms the transducer output. The same is converted back to a signal by the inverse transfer function $H(s)$. Two factors contribute to the effective functioning of the scheme: -

$$\text{The closed loop transfer function is} = \frac{G(s)/s}{1+G(s)H(s)/s} \tag{10.79}$$

⇒ For $G(s)/s >> 1$, this reduces to $1/H(s)$. The presence of the integrator ensures that this condition is satisfied at the frequencies of interest. Under these conditions the error $e(t) = 0$. This forces $c(t)$ to follow changes in $r(t)$ faithfully.

⇒ $H(s)$ and $K(s)$ are similar transfer functions working under the same environmental conditions. Hence, extraneous factors affecting one affect the other too in a similar fashion. This ensures that $z(t) = x(t)$. Often a constant scale factor may be involved in addition to this, making $x(t)$ a scaled (manageable) version of $z(t)$.

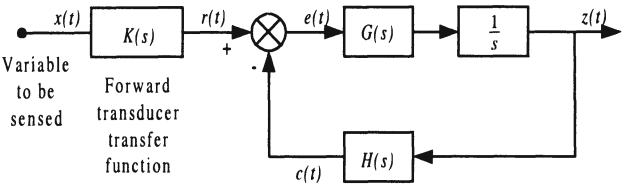


Figure 10.26 Generalized block-diagram form of feedback transducer scheme

Observations: -

⇒ Two types of situations make a feedback transducer attractive.

- The transducer used is easily affected by extraneous factors and its sensitivity cannot be made constant and consistent easily (e.g., Hall-effect based current and voltage transducers).
- The active or useful range of the transducer is highly restricted (Force balance schemes).

⇒ $K(s)$ and $H(s)$ may not exist separately in some situations. Both may function around one transducer to bring about balance (Hall effect based current and voltage sensor).

⇒ Presence of the term $G(s)$ may restrict the bandwidth and speed of response of the overall scheme to a much narrower range compared to the forward transducer. Nevertheless, the accuracy of the scheme within the restricted bandwidth, is the benefit for which the bandwidth is traded off (e.g., Self-balancing potentiometer).

⇒ In some cases, a separate integrator may not be present in the system forward loop. This causes a steady state loop error. But the forward loop gain is made large enough to keep the error small (e.g., Force balancing scheme using bellows).

Part II

Schemes

11 Displacement Instrumentation

11.1 Introduction

Displacement is one of the basic and most widely measured quantities in the industry. The displacement sensed may be linear or angular. Different methods are in vogue – overlapping in nature *vis-à-vis* range and characteristics [Beckwith Buck and Marangoni, Donati Falzoni and Merlo, Neubert]. With each potential application, we have a choice and trade-offs. Applications, which require the displacement to be sensed directly, are as common as those, which use displacement sensing indirectly. In the latter case, the displacement is used as a measure of another physical variable. Strain and related quantities are often sensed in this manner. These are dealt with in subsequent chapters; here we restrict ourselves to sensing of displacement and quantities directly related to displacement.

Four types of displacement transducers are in use: -

⇒ Potentiometer
⇒ Variable differential transformer
⇒ Capacitance
⇒ Encoder

All are used to sense linear as well as angular displacement. The first three provide analog or continuous output. The fourth provides direct encoded digital output. Hybrid versions where the encoder is integrated with the sensor (in the former types of cases), also give direct digital output.

11.2 Potentiometers

Potentiometers (referred to as 'pot' in short form) constitute one of the simplest forms of displacement sensing. A resistance R_p (Figure 11.1) is uniformly distributed over the range of displacement of interest and a fixed voltage applied across it. If x represents the displacement (relative to the full-scale value), the output is

$$V_o = V_R x \tag{11.1}$$

R_p the potentiometer resistance and its fractional values do not directly enter the expression for x here. Hence, changes in R_p due to changes in the ambient temperature and the like do not affect the sensitivity. However, the source resistance R_s presented to the load changes.

$$R_s = R_p x(1-x) \tag{11.2}$$

R_s is zero at both ends and increases to a maximum at the mid-point. In case the source resistance becomes a potential problem in subsequent signal processing, a

T. R. Padmanabhan, *Industrial Instrumentation*
© Springer-Verlag London Limited 2000

buffer is introduced between the potentiometer and the load. The sensitivity of the potentiometer is

$$S = \frac{dV}{dx} \Rightarrow \tag{11.3}$$

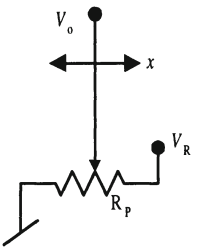


Figure 11.1 Potentiometer as a position sensor

For a given displacement span, S is maximized by maximizing the applied voltage. The power dissipated in the potentiometer is V_s^2 / R_p. The total surface area of the sensor restricts the upper limit to this – say to P_L. Hence, the maximum permissible applied voltage becomes $\sqrt{P_L R_P}$. Although the sensitivity can be increased by increasing R_p, three factors restrain this: -

- ⇒ Maximum source resistance that the following signal processing circuitry can tolerate.
- ⇒ Noise generated by the resistance – its upper limit being the detection threshold
- ⇒ Mechanical strength of R_p: As the value of R_p increases, the section forming it becomes smaller affecting its strength and physical stability adversely.

Potentiometers in use are mostly of three types; these are discussed here.

11.2.1 Wire Wound Potentiometers

Potentiometer can be in the form of a single slide wire or a helical toroid wound on a mandrel (see Figure 11.2). Angular potentiometers take the form of multi-turn pots also. The latter provides an extended span. By suitable gearing, linear displacement can be sensed using a rotary pot. Use of the multi-turn pot increases the sensitivity in this case. Wipers having low contact resistance and voltage drop with respect to the potentiometer material and good mechanical characteristics, are

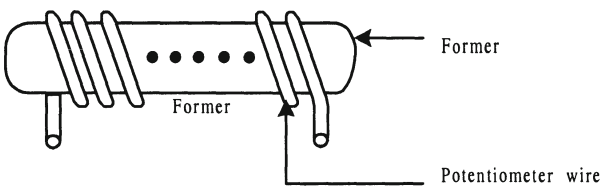


Figure 11.2 Wire wound potentiometer for sensing of displacement

used for moving / rubbing contact. With the contact wire as a toroid, the moving contact traverses over it turn by turn. This causes a quantization effect and step changes in output. Further, the moving contact rubbing against the wire may cause a low vibration ('stick-slip' phenomenon) and a corresponding ripple in the output. Both these are smoothed out with a capacitor at the potentiometer output [Neubert, Norton].

11.2.2 Conductive Plastic Potentiometer

Graphite particles finely dispersed in a polymer medium or one of the conducting polymers itself can be used as the potentiometer resistor. It is moulded into a uniform strip of requisite length and suitable width. Due to the continuity of the resistance element, it provides infinite resolution. However, the lack of uniformity in the distribution of resistance along the strip length, reduces precision and hence resolution substantially. Resolution attainable is of the order of 1 % compared to 0.25 % with wire wound pots. The contact resistance and tolerance in the potentiometer resistance are higher. The permissible contact current is lower.

11.2.3 Magneto-resistance Potentiometers

Resistance of certain materials changes conspicuously in the presence of a magnetic field. These are referred to as 'Magneto-Resistors (MR)'. If a portion of the resistance is under the influence of a magnetic field, its resistance increases. This phenomenon is used judiciously in the scheme of Figure 11.3. Two identical MRs are connected in series and their junction forms the output point. With a fixed voltage applied to the series combination, potential of the output point varies depending on the extent to which the two sides are influenced by the magnetic field. A permanent magnet is attached to the sensing point of the pot. It remains close to the two MRs and moves over them in a plane parallel to them. At one extreme position, one MR is fully under the influence of the magnet and its resistance is a maximum. As the magnet moves, resistance of this MR decreases and that of the alternate one increases. When the magnet is positioned symmetrically with respect to both the MRs, both are influenced equally and the output is zero. As the magnet continues to move and is finally fully over the second MR, its resistance is maximum while the resistance of the first MR reduces to a minimum. The input-output characteristic of the MR based pot is shown in Figure11.3 (b). The characteristic is single-valued over the ± 90° range but the linear range is restricted to ±50° (approximately) only. The main advantage of the MR based potentiometer, is its contactless operation. Friction, wear and tear are absent. The main disadvantages are two-fold: -

⇒ The range of variation of the resistance value of the MR is quite restricted. The displacement sensitivity is correspondingly restricted.

⇒ The resistance values of MRs are quite sensitive to ambient temperature variations. The sensitivity also changes with ambient temperature. Suitable temperature compensation circuits are to be used with the sensor.

⇒ The resolution possible with MR based sensor is 1 % to 1.5 % of the full scale signal level. Despite the attractive feature of contactless operation, MR based pot type sensors have not yet been widely adopted.

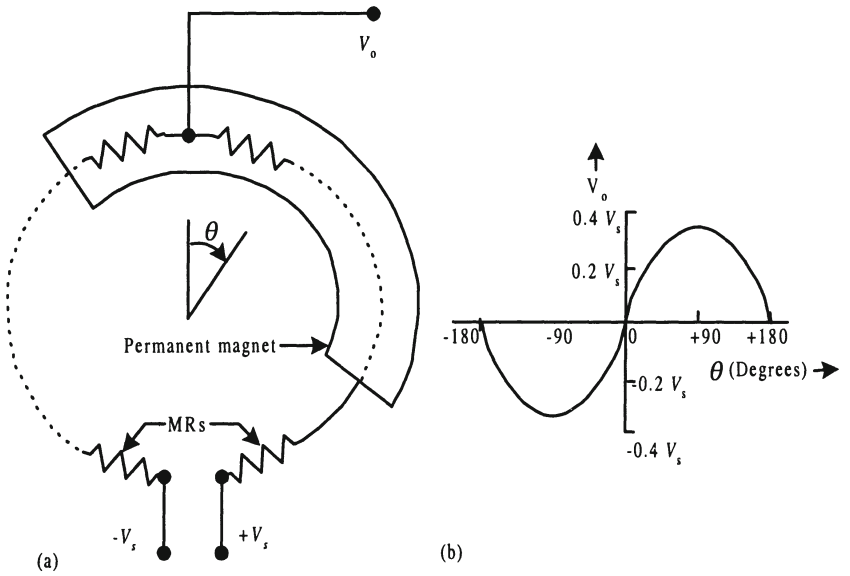


Figure 11.3 Displacement sensor using two identical MRs: (a) Circuit arrangement (b) Input-output characteristic

11.2.4 Comparison

Figure 11.4 gives a brief comparison of the three types of pots. A few observations are in order here: -

⇒ Conducting polymer and MR type pots appear better *vis-à-vis* resolution. However, the wire wound pot is better in practice due to its better resolution.

⇒ As far as speed, torque or force required for operation and life (number of operations) go, MR based pot is much better.

⇒ Wire wound pot can operate (normally) at a maximum speed of a few rpm. This limits the sensor bandwidth considerably. MR based pots are better by two orders.

⇒ The wire wound pots have the widest range possible – a few mm to 300 mm. MR pots have a range of a few mm only. Conducting polymer pots have range extending from a few mm to 20 mm.

⇒ All the three types are suitable and available for rotary as well as transitional sensing.

11.2.5 Signal Processing with Pot Based Position Sensors

Normally DC voltages are used to excite the pots. The excitation voltage may extend up to 15 V. With wire wound pots and conducting polymer pots, a buffer (See Section 4.8) suffices to provide impedance isolation. Since the input signal range is high, no separate amplification is called for (Self-balancing potentiometer

is an exception). If the pot is remotely located (as with process industries), the output may be buffered with minimal gain; an instrumentation amplifier may be used for this (See Section 4.12).

MR based pots have a more restricted range of output voltage. Further, the output is available riding on a common mode voltage of $V_s/2$ with a single ended supply of V_s Volts. Hence, these signals are best amplified using difference amplifiers or preferably instrumentation amplifiers. In either case suitable gain is built into the amplifier stage itself.

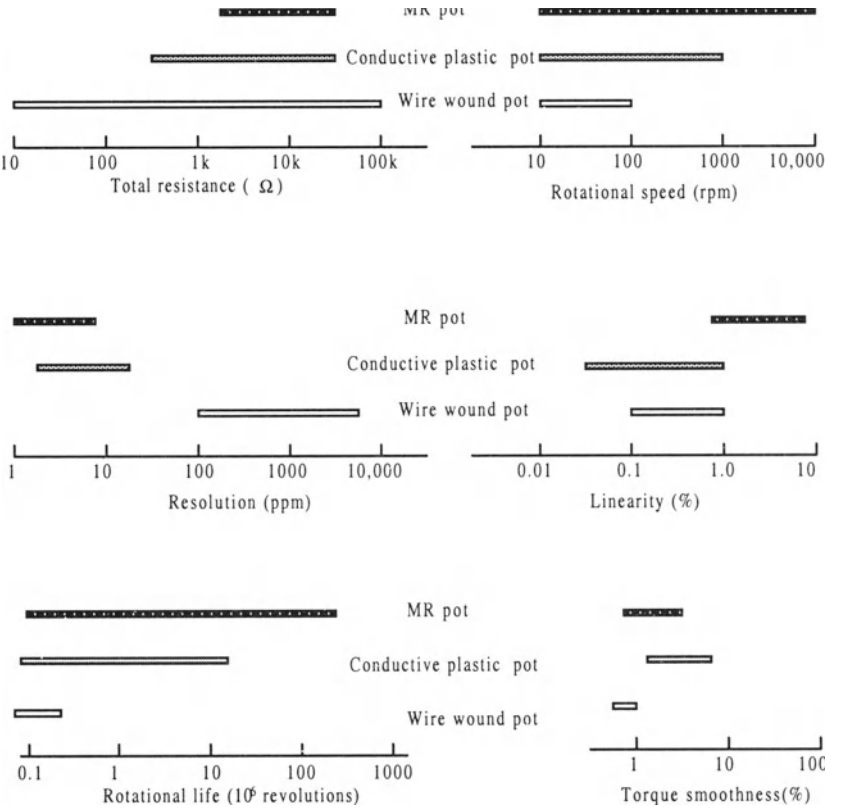


Figure 11.4 A rough quantitative comparison of the three types of pots

11.3 Differential Transformers

A variable differential transformer suitable for sensing translational motion is shown in Figure 11.5 (a). It is known as the 'Linear Variable Differential Transformer (LVDT)'. The electrical functional circuit of the LVDT is shown in

Figure 11.5 (b). The windings are normally shielded by providing an annular magnetic cylinder over them. This provides a return path for magnetic flux and helps in flux concentration (In some cases, the annular outer cylinder may be absent). The central magnetic core too is of a magnetic material. A ferrite material, which has low loss but the highest possible permeability at the operating frequency, is used for these. The armature is rigidly connected to the member whose displacement is to be sensed. The mechanical connection is through a non-magnetic push rod. The primary exciting winding (P) is in the middle and the two secondaries (S_1 and S_2) are symmetrically positioned on either side. The number of turns on individual secondaries, their spread, length and profiles are adjusted to suit the range and ensure linearity over the full range. Normally, these are proprietary information and vary from manufacturer to manufacturer.

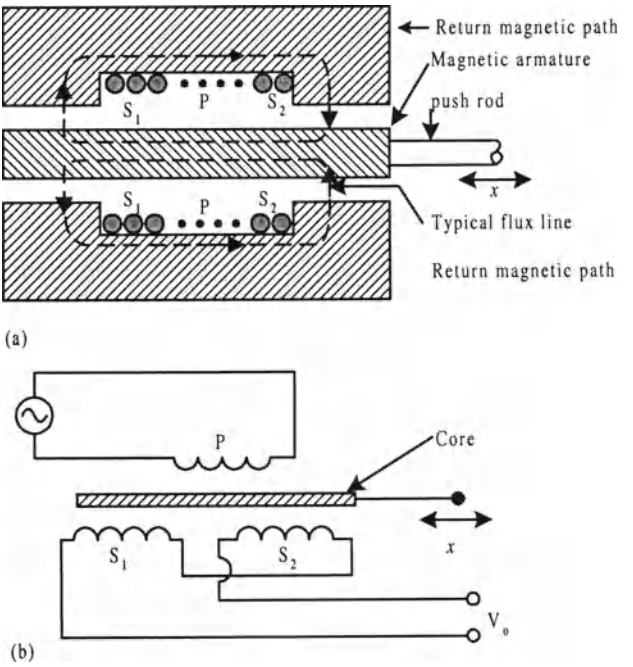


Figure 11.5 Schematic arrangement of LVDT: (a) Functional arrangement (b) Connection diagram. P is the exciting primary winding. S1 and S2 are the two secondary windings symmetrically placed with respect to P.

With 5 kHz 5 V excitation, the full displacement range may vary from 1 mm to 1 m. As the range increases, the full-scale output increases up to a certain extent. Thus a 1 m-range unit may have 10 V rms output at full scale; but a 5 mm full-scale output unit may have only 200 mV as full-scale output. Normally, the sensitivity reduces as the range increases. Hence, the unit with the shortest length that meets the operational needs is to be used. With 5 kHz excitation frequency the signal bandwidth can extend up to 500 Hz.

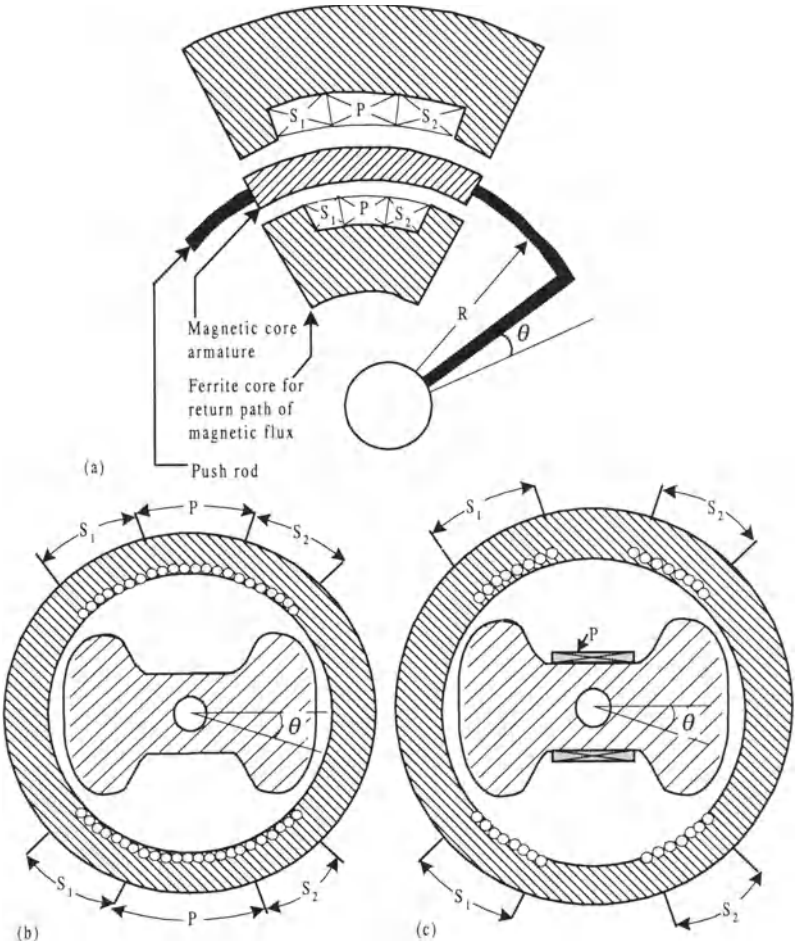


Figure 11.6 Variants of RVDTs: (a) Direct re-engineered version of LVDT (b) RVDT with stationary coils (c) RVDT with exciting coil on the moving member

The rotational counterpart of the LVDT is identical in principle to that of the LVDT. It is called the 'Rotational Variable Differential Transformer (RVDT)'. The RVDT may take various constructional forms. Three versions of the RVDT are shown in Figure 11.6. Figure 11.6 (a) shows a version, which is essentially an LVDT re-engineered to suit rotary motion. Due to the curved nature of the core, it is not practical to be assembled from stampings. The core has to be of ferrite. Due to the limited curvature possible, two cases arise: -

⇒ An RVDT of limited size with rotational motion restricted to a few degrees on either side with low sensitivity. This one has a small value of R.

⇒ An RVDT of comparatively larger size with large R. This one can have rotational motion of ±20° and better sensitivity. More often than not, the unit turns out to be too unwieldy to be cost effective.

The versions of RVDT in Figures 11.6 (b) & (c) are similar. The flux path and the windings are similar to those of rotating machines. The version of Figure 11.6 (b) has the exciting winding and the sensing coils on the stator while that of Figure 11.6 (c) has the exciting winding on the rotor and the two sensing windings on the stator itself. The former is more robust but has lower sensitivity compared to the latter. In both the cases, the core can be assembled of stampings. The sensitivity is one order better than that for the version of Figure 11.6 (a). Reduction of the air gap between the stationary member and the rotating member increases sensitivity at the expense of linear range. Normally the inner surface of the stator will be that of a right circular cylinder. The rotor surface will be carefully profiled to maximize linear range for a given sensitivity.

In general, the active range of displacement of RVDTs is limited to ±20° or so. The RVDT can be constructed with a minimal air gap. This increases the sensitivity and resolution. The torque required for motion (source loading), will also increase correspondingly. Applications with signal bandwidth requirement up to 60 Hz, do with RVDTs assembled with fine special sheet stampings. Ferrite based armature and core are used for sensors of larger bandwidth requirements. Their size is reduced to keep inertia to the minimum. Adaptations of the RVDT for high-performance displacement-transducers are discussed in the sequel.

11.3.1 Signal Processing with Differential Transformers

The preferred arrangement for the LVDT/RVDT is for the two secondaries to be connected in series opposition internally; only the differential output is available. Normally, this is characterized by a threshold output of the order of 1 mV rms. at the excitation frequency and a phase lag of the output voltage with respect the input. Manufacturers guarantee the phase shift to be less than a prescribed limit (~10°). The low threshold level requires a synchronous (balanced) demodulator to be used (See Section 6.2.1.3). This improves the overall accuracy of the instrumentation scheme. The reference used for demodulation may be suitably phase-shifted with respect to the applied excitation voltage to improve resolution.

Observations: -

- ⇒ Comparatively low cost schemes may rectify the two output voltages independently and use the difference as output voltage as shown in Figure 11.7 (See Section 6.3.1.3). Threshold level and the accuracy attainable here are comparatively lower.
- ⇒ Although the excitation frequency can extend up to 5kHz, many applications can do with a few Hz of signal bandwidth. In such cases, use of a tuned filter at the output side of the LVDT/RVDT, may improve the signal to noise performance and accuracy (may be only marginally). As filter Q is increased, the signal bandwidth reduces. The excitation frequency also requires to be stabilized correspondingly.
- ⇒ Normally, variations in the excitation frequency do not affect the performance of the scheme, directly (If a high-Q filter is used at the output side of the LVDT/ RVDT, any variation in the excitation frequency reflects as a change in sensitivity).

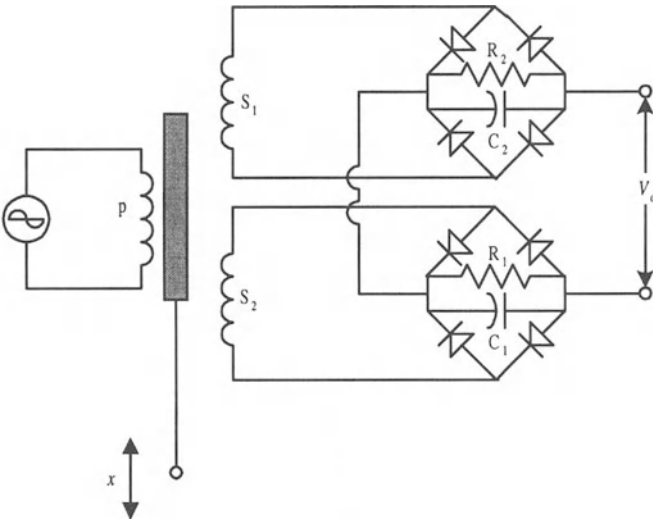


Figure 11.7 Low-cost instrumentation scheme with LVDT: The bridge rectifiers, R_1 & R_2 as well as C_1 & C_2 are identical

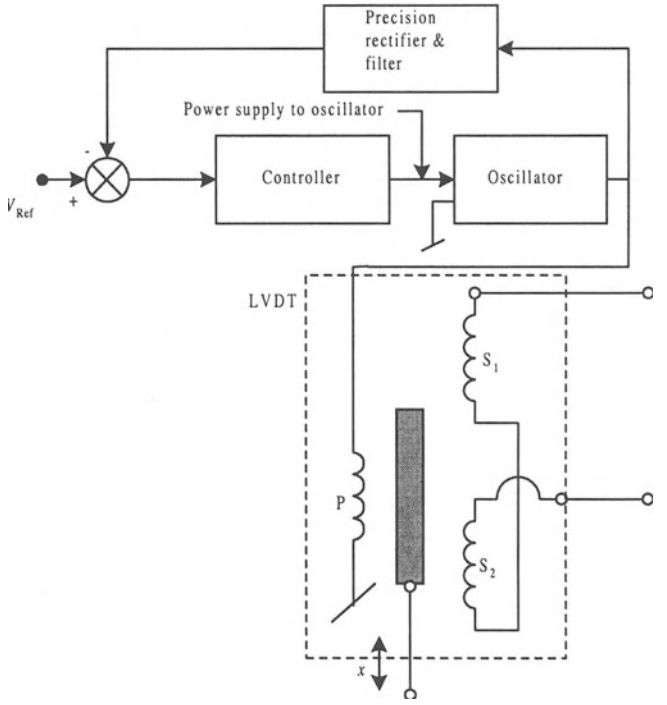


Figure 11.8 LVDT with amplitude stabilized excitation

⇒ High performance systems have a separate oscillator-amplitude stabilization-loop as shown in Figure 11.8. A stabilized Zener is used as a reference here (See Section 8.4.1). To ensure stable working of the overall system, it is necessary that

- The cut-off frequency for amplitude stabilization-loop is about $1/10^{th}$ of the excitation-frequency or less and
- the displacement-signal bandwidth does not exceed $1/10^{th}$ the cut-off frequency of the amplitude-stabilization loop.

The above are essentially guidelines and not rigid figures.

Some miniaturized versions of LVDTs have the whole instrumentation scheme integrated within. The oscillator at the input side and the synchronous demodulator, filter and amplifier on the output side, are all built-in. These require their DC supply to be within a specified range; they give a DC output proportional to the displacement being sensed. Being standardized products, neither the zeroing facility nor the facility to use external components with tight tolerances is available with them. These make the attainable accuracy levels slightly poorer.

11.3.2 Variants of the Differential Transformer

Many variants of the differential transformer are in vogue. The basic principle remains the same – motion of a magnetic armature from the position of symmetry causes a differential voltage to appear at the output; it is modulated at the carrier frequency. The demodulation schemes remain unaltered.

11.3.2.1 Resolvers

Resolvers are rotating transformers. They provide excellent repeatability and high sensitivity. They are useful for precision angular position sensing as in radar, antennae, telescopes *etc.* The magnetics and winding schemes used with resolvers are similar to those of two-phase alternators. The two-phase windings are distributed on the stator, in quadrature with each other. A third winding is on the rotor – wound in the form of a coil around a well-shaped rotor. The magnetic path is formed by stacked stampings of special material. Figure 11.9 shows a schematic diagram and an equivalent circuit. The resolver can be operated in two modes.

Mode 1

The rotor is excited at a fixed voltage at the carrier frequency. The current through the rotor winding produces a corresponding alternating flux. This flux links both the stator windings causing an induced emf in each. For a specific rotor position θ, the two stator emfs can be expressed as follows: -

$$\text{Induced emf in winding } S_1 = E_m \sin\theta \cos\omega t \quad (11.4)$$

$$\text{Induced emf in winding } S_2 = E_m \cos\theta \cos\omega t \quad (11.5)$$

Where ω is the excitation frequency in rad / s.

Stator windings being identical, both peak values of both the emfs are equal - each is equal to E_m. For any rotor position θ, the two emfs are proportional to sin θ and cos θ respectively. Both the emfs are at the carrier frequency and in phase. One can get the amplitudes of the emfs and comparing their relative values, the rotor angle θ can be obtained.

A_1 – the amplitude of emf in winding S_1 = $E_m \sin\theta$ (11.6)

A_2– the amplitude of emf in winding S_2 = $E_m \cos\theta$ (11.7)

From the above two equations,

$$\theta = \sin^{-1} \frac{A_1}{\sqrt{A_1^2 + A_2^2}} \quad (11.8)$$

With the help of suitable computations or look-up tables, θ can be computed. The maximum possible active span for θ is 180°.

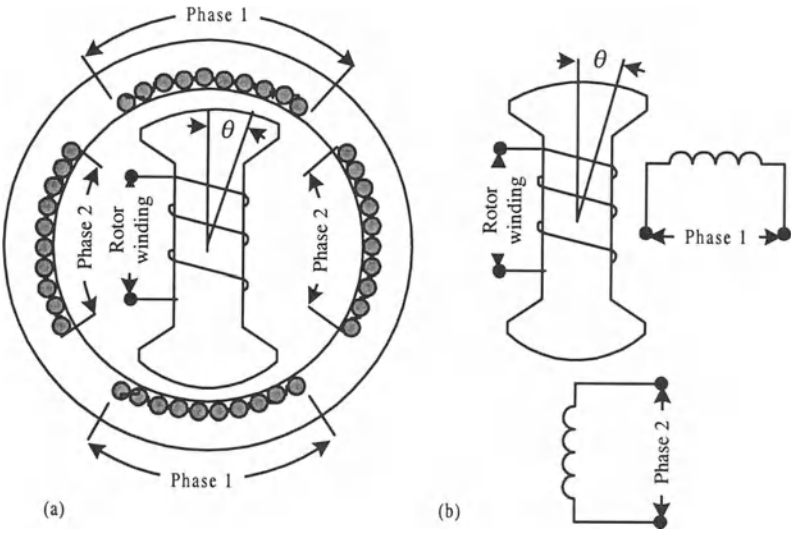


Figure 11.9 Resolver: (a) Schematic arrangement (b) Circuit representation

Mode 2

In this mode, the two stator-windings are excited by a balanced set of two-phase voltages. In turn, a rotating magnetic field is produced in the air gap. The field magnitude and speed remain invariant whatever be the rotor position. For any position of the rotor, the rotor winding has an emf induced in it given by

$$e_r = E_m \cos(\omega t + \theta) \quad (11.9)$$

where

⇒ e_r is the instantaneous emf induced in the winding

⇒ E_m is the peak value of the emf induced and

⇒ θ is the relative phase angle of the emf.

Here E_m and ω remain constant. As the rotor position changes, θ changes correspondingly. Multiplying e_r in Equation 11.9 by $\sin \omega t$, we get

$$e_r \sin\omega t = E_m \sin\omega t \cos(\omega t + \theta)$$

$$= \frac{1}{2}E_m \sin\theta + \frac{1}{2}E_m \sin(2\omega t + \theta) \qquad (11.10)$$

If the component around the frequency 2ω is filtered out, we get $E_m \sin \theta$ as the output. With fixed excitation amplitude, E_m remains fixed. Hence, the output is proportional to sin θ. From sin θ, one can get θ with the help of LUTs. The multiplication and filtering together constitute synchronous detection (See Section 6.2.1.3).

Observations: -

⇒ Resolvers are robust and can withstand adverse environmental conditions.

⇒ Output signal isolation and high CMR are inherent in the system.

⇒ The high sensitivity and the inherently modulated nature of the output, allow remote position sensing and signal processing at a panel. This is especially true of mode 2, due to its amplitude remaining constant for all rotor positions.

⇒ Mode 2 is normally preferred for the reasons cited above. The output(s) can be processed by analog signal processing circuitry to give voltage or current proportional to the angular displacement. Accuracy attainable, is of the order of 0.1 % of full scale. Alternately one can use suitable ADCs followed by computations and LUTs to yield output of 16-bit accuracy. This is more compatible with the precision level available with resolvers.

⇒ Use of 'Two-speed Resolvers' improves resolution by one order. One resolver is connected directly on the shaft whose angular position is to be detected. A second resolver is connected to another shaft geared to the first with a step-up ratio (of 24 or 32). These form a pair of coarse and fine resolvers. The two together is used to decide angular position. This scheme is referred to as a 'two speed' scheme.

⇒ The excitation frequencies normally used are 400 Hz, 1000 Hz and 1600 Hz. The respective signal cut-off frequencies are in the range of 40 Hz, 100 Hz or 160 Hz.

⇒ Due to the precision called for in the stampings, dimensions and windings, resolvers are costly and justify use only when the accuracy demanded is of the order of 0.1 % or better and the signal environment calls for its robustness.

11.3.2.2 Microsyn

One version of RVDT called 'Microsyn' is shown schematically in Figure 11.10. For the connection of exciting windings in the figure, instantaneous pole positions for the current directions are as shown. When the rotor is symmetrically positioned with respect to the poles, the flux linking all the windings is equal. Net output voltage is zero. If it moves in the anti-clockwise direction slightly, the flux linking the poles marked, 'S' is more. Emfs induced in the corresponding sections of the output windings, are more than the other two, causing a net output voltage. If the armature moves in the opposite direction by the same amount, the output voltage is the same in magnitude but has opposite phase. One can use an exciting winding of a large number of ampere-turns to improve sensitivity. Careful design of the magnetics, enhances the sensitivity. An armature without any windings on it makes the unit quite robust. Gyros, which require precise sensing of deviations in position, form an application area for the microsyn.

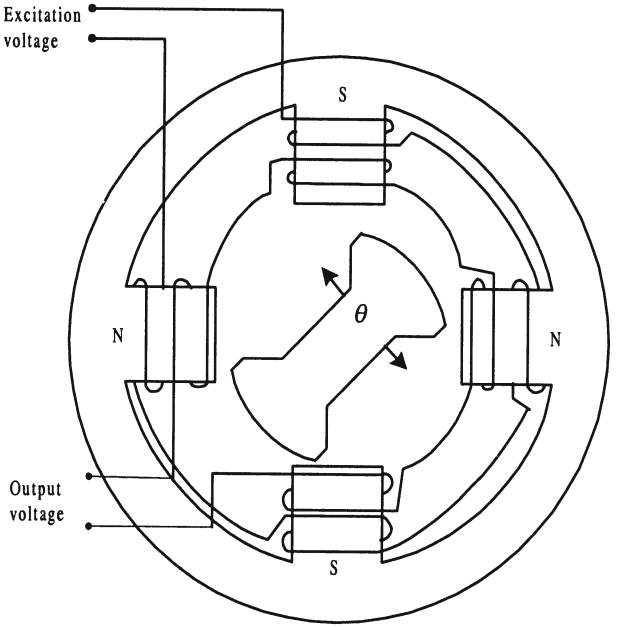


Figure 11.10 Schematic arrangement of Microsyn: 'N' and 'S' signify only instantaneous directions of magnetization due to the excitation

11.3.2.3 Variable Reluctance Transformer

Figure 11.11 (a) shows one variant of the LVDT. The exciting winding is wound over the moving member A kept in the middle. The two halves as seconderies are on the two side 'C' limbs – B and D. When the moving member is exactly in the middle, the emfs in the two halves are exactly equal and the net output voltage is zero. If 'A' moves closer to the limb 'B', emf e_1 > emf e_2, giving rise to a net output

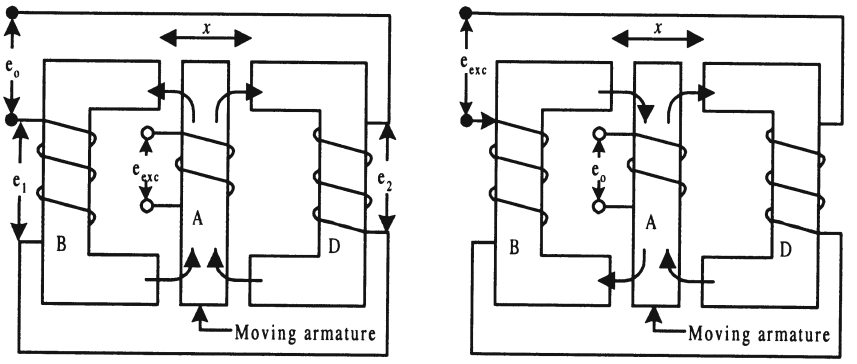


Figure 11.11 Variable reluctance transformer – two schemes: (a) Rotor excited type (b) Stator excited type. In both the cases, the armature A is connected to the tie rod

emf. If 'A' moves closer to 'D', emf e_1 < emf e_2 and the net emf is of opposite phase. The linear range is restricted to 10 % to 20 % of the gap. The total range is of the order of a few hundred microns. However, the sensitivity is one order better than that the LVDT of Figure 11.5 (a) due to the increased flux levels.

The scheme of Figure 11.11 (b) is a slightly altered version of the above one; normally the windings on the limbs B and D are connected in series and excited. The windings are such that the moving limb A sees only the differential flux. The output winding is on limb A. At zero displacement condition, net flux linking the output winding is zero and the induced emf is zero. Motion in either direction upsets balance and results in an output. The differential action here is at the flux level itself. The range, sensitivity and accuracy are all on par with those of the scheme of Figure 11.11 (a).

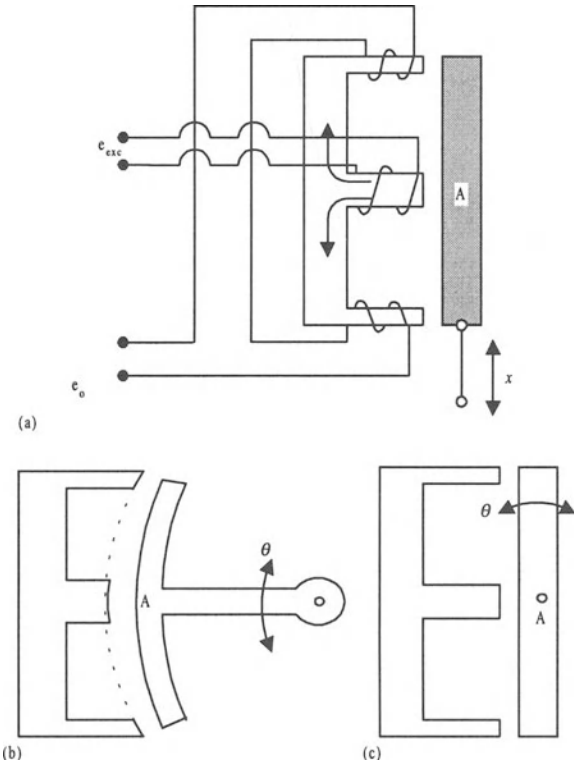


Figure 11.12 Variants of the variable reluctance transducers: (a) Linear displacement type (b) Angular displacement type with wide range (c) Angular displacement type with narrow range

The scheme of Figure 11.12 (a) is electrically similar to that of Figure 11.11 (a). It is intended to sense linear displacement along the axis of member 'A' [In Figure 11.11 (a), it is normal to the axis of 'A'.]. The range of motion and sensitivity attainable are intermediate between that of Figure 11.11 (a) and the LVDT of Figure 11.5 (a). If the magnetics is confined to one side as shown, the pull

on A will be much larger than that of Figure 11.11 (a). The unit is sensitive to angular and lateral spurious displacements (but not so in the case of the units of Figure 11.11 – at least to a first order). The unit of Figure 11.12 (a) is re-engineered as in Figures 11.12 (b) & (c) for angular displacement sensing. Here also, the roles of the exciting and the output windings can be interchanged. The scheme of Figure 11.13 has only one exciting winding. It is intended to sense angular displacement over a restricted range. At zero position, the flux in both halves is equal. The differential flux is zero. Any angular movement causes a corresponding differential flux which links the output coil and causes an emf to be induced in it. A similar scheme can be used for linear displacement along the axis of A also.

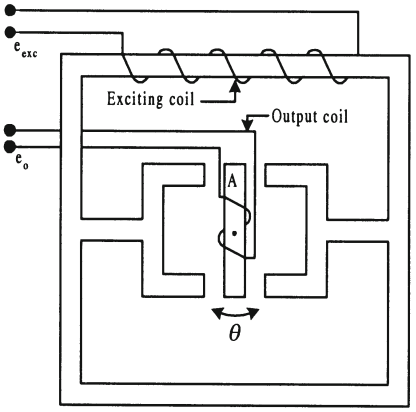


Figure 11.13 A variant of the variable reluctance transducer with a single exciting winding: The arrangement can be used for linear as well as angular displacements

11.3.3 Differential Inductance Transducers

Consider an inductor in the form of a solenoid with its midpoint brought out; it has an armature within. This is similar to the LVDT without the exciting or the primary winding. When excited as shown in Figure 11.14, the applied voltage is shared

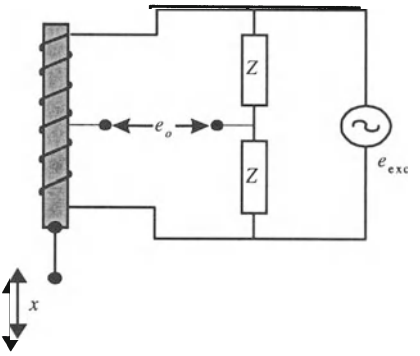


Figure 11.14 Differential inductance transducer

equally between the two halves. Two equal impedances Z may be connected in series across the same supply. The combination forms an 'Inductively Coupled Ratio Arm Bridge' (See Section 2.3.5). As the armature moves in either direction, V_o changes correspondingly in magnitude and phase. It is demodulated through a synchronized demodulator (See Section 6.2.1.3). The bridge output need not be in phase with the supply voltage. The reference used for demodulation has to be suitably phase-shifted to account for this.

Each of the differential transformer schemes considered earlier can be realized as its two winding counterpart. These are referred to in literature by various names – some generic, others proprietary. The basic principle remains the same for all. These are not discussed any further here.

11.4 Capacitance Transducers

Capacitance transducers by their very nature, require working in the MHz range. This calls for specialized skills in circuit design, layout and engineering. However, once done, they are robust, reliable and precise. Three types of capacitance sensors are possible [Other capacitance transducer schemes are discussed in Baxter, Heerens, Hordeski, Jones and Richards, Norton and Neubert].

⇒ Parallel plate type with the distance d between the plates representing. The distance between the plates is of the order of 0.5 mm. For meaningful sensing, the displacement range should be limited to ±10 % of this *i.e.*, 50 μm. The detection threshold is of the order of 0.5 μm. A simple scheme and one with improved sensitivity, are shown in Figure 11.15 (a) & (b).

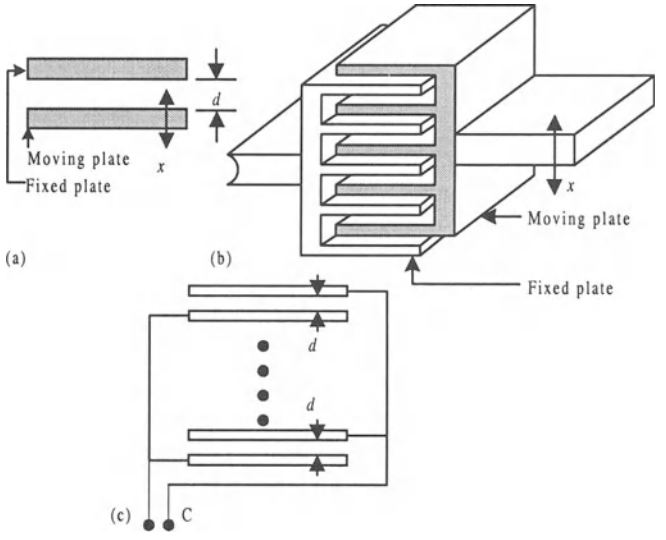


Figure 11.15 Capacitive type linear displacement transducers: (a) A simple scheme (b) Modification of (a) with enhanced sensitivity (c) Equivalent circuit for the scheme in (b)

⇒ Parallel plate type with the change in the overlapping area representing the displacement to be sensed. The area is typically 30 mm X 30 mm. The capacitance changes linearly with area as long as d is small compared to the linear dimensions of the area. This allows an overall range of 10 mm of displacement. The detection threshold is of the order of 100 μm. A simple scheme and three other schemes with enhanced sensitivity are shown in Figure 11.16. One of them is for linear motion and the other two for rotary motion.

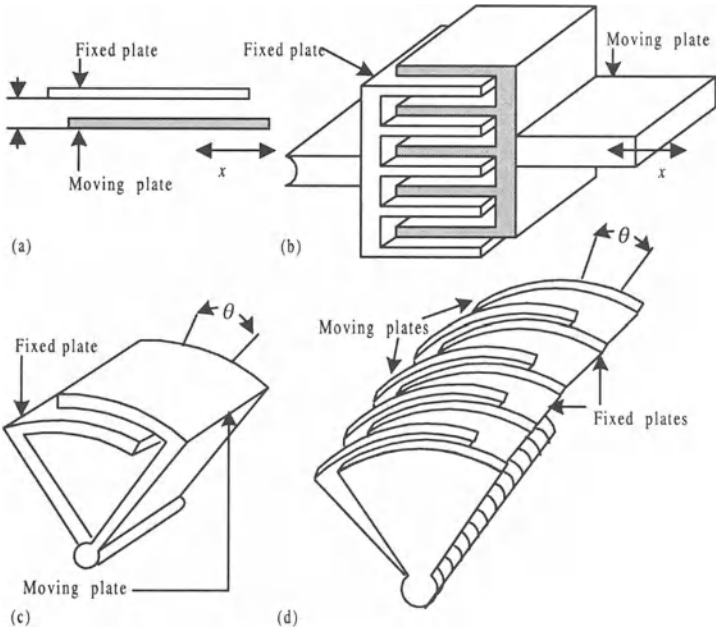


Figure 11.16 Parallel-plate capacitor type of displacement sensor: (a) & (b) are for linear displacement while (c) & (d) are for angular displacement.

⇒ The differential capacitance type sensor can be adapted to sense displacement. Either the distance '*d*' or the area 'A' can be made to change differentially depending on the displacement. The ranges and the measurement threshold remain unaltered; but linearity improves and sensitivity doubles. Four schemes are shown in Figure 11.17; two are for linear displacement and the other two for angular displacement. The last two offer enhanced sensitivity with angular displacement.

11.4.1 Comparison of Inductance and Capacitance Type Sensors

Processing circuits to be used, measures to minimize stray effects and reduce errors due to lateral motion, have been discussed already. A few points by way of comparison of inductance and capacitance sensors are in order here: -

⇒ Inductance sensors work typically at a few kHz while capacitance sensors work at a few MHz.
⇒ Capacitance sensors are smaller and can be fitted in locations that are more intricate.
⇒ The source loading of capacitance sensor is negligible compared to that of inductance sensor.
⇒ The detection threshold and the range of capacitance sensors are one or two orders lower than those of inductance sensors.
⇒ Ambient temperature variations affect inductance sensors more than capacitance sensors. Changes in ambient pressure and humidity do not affect either directly.

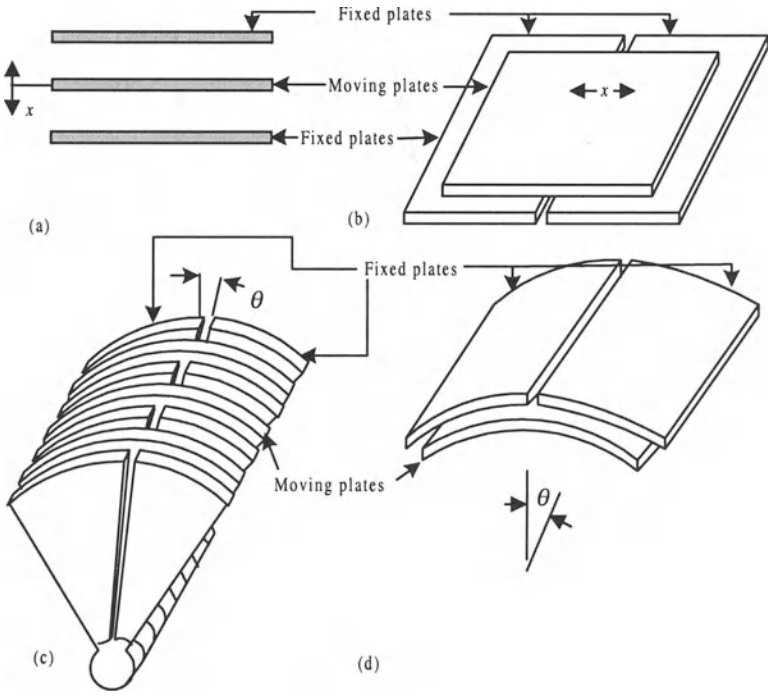


Figure 11.17 Differential-capacitor type of displacement sensor: (a) & (b) are for linear displacement and (c) & (d) for angular displacement

11.5 Encoders

Encoders provide direct digital output representing displacement. When digital output is desired, they are preferred and analog sensing followed by ADC is avoided. They find use in a variety of applications. Volume-wise, machine tools, robotics and gauging represent major applications.

A variety of conversion schemes was prevalent so far – those using magnetized strips and conducting strips with brushes being more common [Considine, Orlosky and Avolio]. But now all encoders use the electro-optics route. Relative simplicity of construction, long life, robustness and high resolution attainable with the electro-optic encoders, are responsible for their universal popularity to the exclusion of other methods. LEDs and photo-detectors are used to detect displacement. Only these are discussed here. One category – absolute encoders – directly provides digital output representing the absolute displacement. The second category – incremental encoders – provide an output representing the incremental displacement only. Both are used with angular as well as linear displacements.

11.5.1 Principle of Electro-optic Encoder

Consider a strip of material with alternate transparent and opaque stripes on it as shown in Figure 11.18. It is kept in the line of sight of an LED and a phototransistor. The radiation from the LED source falls on the phototransistor when a transparent strip is in front. The phototransistor conducts and gives a '0' (low) output. When an opaque strip is in front, the radiation path is obstructed. The photo-transistor is off giving a '1' (high) output. If the strip moves in one or the other direction, the output changes from 0 to 1 or 1 to 0 as the case may be. The arrangement essentially achieves quantization – each pulse of 1 representing a quantum change in the displacement. All the electro-optic encoders are built around this basic unit.

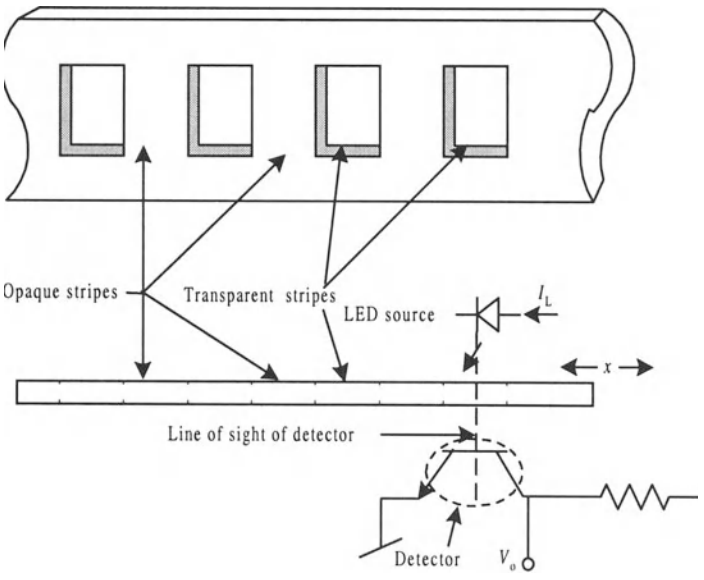


Figure 11.18 Basic optic-encoder arrangement

Observations: -

⇒ The strip and the phototransistor combine – the displacement detector module – is to be enclosed and kept away from ambient light. This is to avoid the ambient light falling on the phototransistor causing any error.

⇒ Often an Infrared (IR) source and detector are preferred. The detector can be selected to have a response with restricted spectral width. This is done to minimize the effect of visible spectral radiation in the ambient area. Note that 'opaque' and 'transparent' refer to the concerned IR band.

⇒ The strip or the LED- phototransistor assembly may be made to move with the member whose displacement is to be sensed.

⇒ The scheme is equally useful for linear as well as angular displacement sensing.

11.5.2 Incremental Encoders

The incremental encoder uses a strip of alternate stripes with an LED and phototransistor pair as described above. Any increment in the displacement in either direction gives one output pulse. The encoder is not complete in two respects. There is no way of knowing the direction of displacement and the absolute displacement.

To detect the direction of motion, another LED – phototransistor – set is used along with the strip. The second sensor is displaced a quarter cycle from the first one. It yields another 0 - 1 output sequence ¼ cycle phase-shifted from the first one. Figure 11.19 shows the arrangement (For clarity L_B and Q_B are shown away. In practice, they are at the same level as L_A and Q_A. The two pairs can be displaced with respect to each other without any loss of accuracy. The distance can be 5/4, 9/4 *etc.*, cycles away). The case shown corresponds to the bright stripe. Dark stripe ratio of (1/3) : (2/3). Normally a ratio in this range is used. For the direction of motion of the strip, outputs at points A and B are as shown. Output of point A lags that of point B by a quarter cycle. A and B are given as the D input and the clock input to a D flip-flop. The flip-flop output is 1 for the direction of motion shown. It is zero for the opposite direction of motion. Thus Q gives the direction of motion and A or B the quantum change. A and B can be decoded using a 2 to 4 decoder. This improves the resolution of the encoder four fold.

The pulse train available from the encoder (A, B or the 2 to 4 decoded outputs), is counted using an up/down counter. The D flip-flop output Q decides whether to count up or count down. With this modification, we get cumulative displacement at any time as the up/down counter output. To fix an absolute reference point (zero of the scale), the strip is provided with a separate dark spot with a dedicated LED-phototransistor pair for it. When this pair has the dark spot across, the position is taken as zero. The up/down counter is cleared and counting started afresh. With these two changes, sensing of absolute position and direction of motion are effected.

11.5.3 Design of Incremental Encoders

Precise assemblies of LED-phototransistor pairs are available. These are tailored to the encoder applications. Depending on the precision desired, two approaches are in vogue for encoder design; both are illustrated here through specific examples.

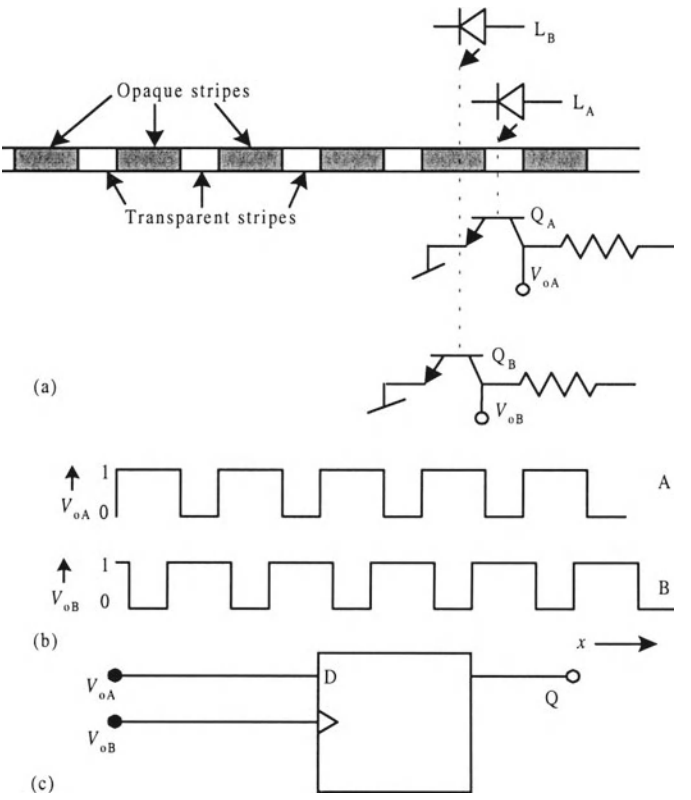


Figure 11.19 Optical incremental encoder scheme: (a) schematic arrangement of strip and sensors (b) Waveforms of detector outputs: V_A lags for the direction shown. (c) D flip-flop to sense direction: Q = 1 for the direction shown

11.5.3.1 Approach 1

Figure 11.20 shows the arrangement of a typical optical switch pair. The LED sources as well as the phototransistor detectors have rectangular apertures in front [See Figure 11.20 (a)]. A strip with alternate rectangular transparent and opaque stripes is rigidly attached to the body whose position is to be sensed and encoded. The strip moves in the slot of the sensor as can be seen in Figure 11.20 (b). Each transparent stripe is to be wide enough to allow radiation from the LED to fully cover the aperture. With the aperture size 0.25 mm X 2 mm, the transparent slot may be 0.3 mm X 2 mm. With 1 : 2 ratio for the transparent stripe : opaque stripe, the opaque stripe can be about 0.6 mm wide. The corresponding stripe pitch is 0.9 mm. This represents the best resolution attainable with one sensor. The aperture distance and stripe pitch are related by the equation

(n + ¼) 0.9 mm = 5.4 mm.

Where n is the maximum number of stripe pitches spanning the two apertures. ¼ represents the quarter cycle shift between A and B sensors. 0.9 mm is the minimum

stripe pitch obtained above; 5.4 mm is the distance between two consecutive apertures.

N = 6 – 0.25
= 5.75

Assigning the next lower integral value for n, we have
the maximum possible value for n = 5
Corresponding minimum stripe pitch = 5.4 / 5.25
= 1.00 mm (rounded off)
Quarter pitch = 0.25 mm
Transparent stripe width selected = 0.33 mm

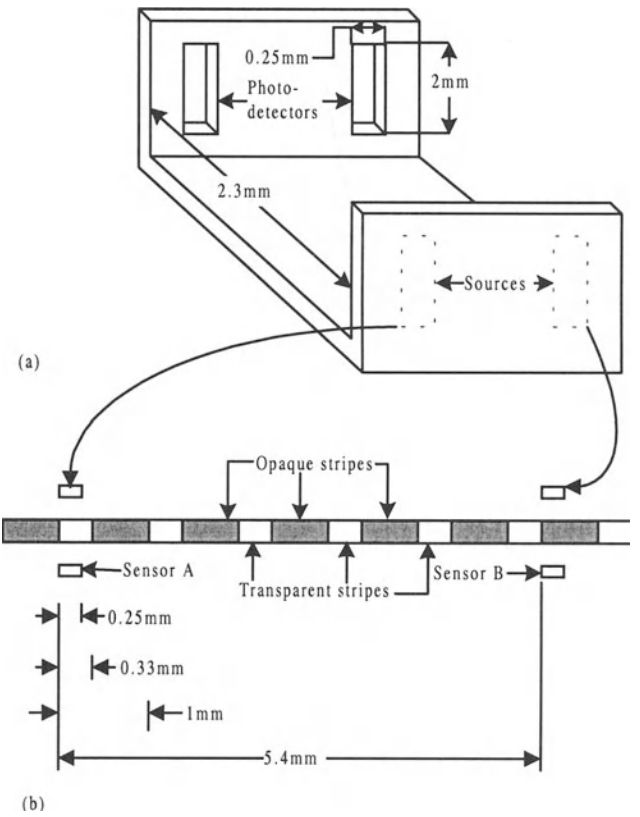


Figure 11.20 Displacement sensing with optical encoder

The rounding-off causes a slight shift in the relative phases of the waveforms. But this does not affect resolution. The stripes and the apertures A and B are shown for a typical condition in Figure 11.20 (b). If A and B outputs are decoded to yield the four outputs, the least count becomes 0.25 mm. This is the best attainable from the scheme.

The above represents the best that can be obtained directly from the optical switch. Any substantial improvement calls for reduction of aperture width by (say)

half. However, with ordinary LEDs and phototransistors, the illumination level received at the phototransistor will be too feeble to be effective.

With transparent and opaque stripes provided on a circular disc, the above scheme becomes angular encoder as in Figure 11.21. To get 0.25° least count, the stripe pitch has to be 1°. This corresponds to the 1mm linear stripe pitch above. The corresponding disc radius is 57.3 mm. One can increase the disc diameter and improve angular resolution correspondingly.

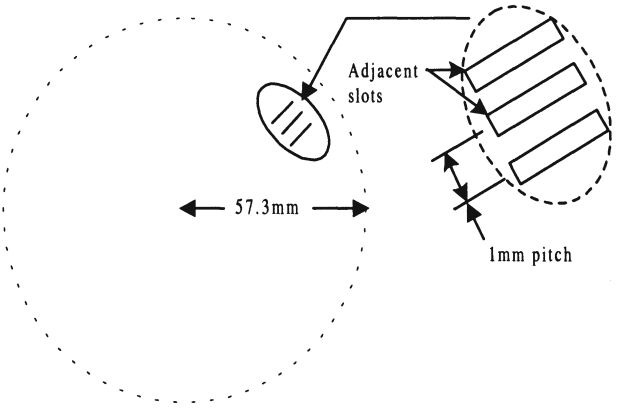


Figure 11.21 Wheel for incremental angular encoder

11.5.3.2 Approach 2

It is possible to have the strips representing displacement with 10 μm stripe pitch. However, such resolution is not feasible with optical switches as explained above. A way out is to use 'reticles' in front of the detector apertures as shown in Figure 11.22. The active length of the reticle used here is 250 μm – the same as the aperture in Figure 11.20 (a). It has alternate rectangular opaque and transparent stripes with 10 μm pitch. The moving strip also has identical stripes throughout its active length. When the transparent stripes of the reticle and those of the strip are in front of each other, the detector receives maximum illumination. As the strip moves by half-a-pitch *i.e.*, 5 μm, the opaque stripes of the strip come in front of the transparent stripes of the reticle reducing the illumination received at the detector to zero. As the strip moves a further 5 μm, the received illumination becomes maximum. Two adjacent maxima of the received illumination, are one stripe pitch away (The practical limit for the width of the transparent stripe is ~ 30% of the pitch. With this limit, the maximum illumination received by the photo-detector is 30% of that of the previous case). Any further increase in the width of the transparent stripe causes light bleeding when the opaque stripes of the reticle are in front of the transparent stripes of the strip. This affects contrast adversely.

Let us consider a specific example.

Stripe pitch (best attainable)	=	10 μm
Minimum reticle length to cover aperture fully	=	0.25 mm.
Number of stripes per aperture	=	250/10
	=	25

With A and B sensors and 2 to 4 decoder,

least count = 2.5 μm.

The reticles in front of the two apertures are to be displaced by ¼ of a cycle (equal to 2.5 μm).

Use of the reticle has improved resolution 40 times compared to the direct approach above. This represents the best resolution attainable here.

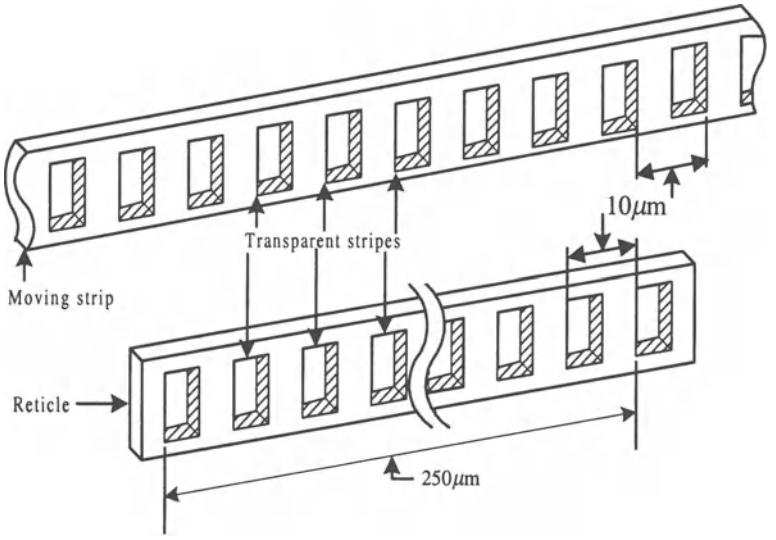


Figure 11.22 Reticle and corresponding strip for precision displacement sensing: The dimensions shown are for a typical scheme considered in Section 11.5.3

11.5.4 Encoder Disc / Strip

The material and performance of the encoder disc / strip has to be compatible with the expected performance levels. The coefficient of thermal expansion of metals, is in the range of 10 to 20 ppm / °C. Special alloys like Invar have the coefficient at 1.0 ppm / °C. With precision encoders as above, the temperature range over which the measurement is done, will be restricted.

Moulded plastic disc/strip is economic and durable. However, it is not rigid. Thermal stability is limited. These are usable for resolutions up to 2 stripes / mm. Thin etched metal discs are reasonable in cost and thermally more stable. They are more rigid and robust. They are useable up to 6 stripes / mm. Mylar film can have resolution of 40 stripes / mm; but it is quite fragile. Thermal stability is on par with other plastics. It is sensitive to humidity. Chrome deposited on glass provides very good resolution - 100 stripes / mm. It offers excellent optical quality and thermal stability and mechanical stability. It is not affected by humidity. The refined processing and precision involved, makes it the costliest. It is used for encoders calling for the best resolution.

11.5.5 Absolute Encoders

With incremental encoders, cumulative or relative position is decided by reading the up/down counter. A separate zero position detector decides the absolute zero value for displacement. Whenever the unit is turned on, reset or the power supply is interrupted and restored, the unit has to be zeroed (Normally encoders come with battery backed-up RAM eliminating the need for re-zeroing). Absolute encoder provides the digital output corresponding to the position directly. Each bit position is separately encoded through a dedicated LED-photo-detector pair. Figure 11.23 illustrates the principle for a 4-bit case. The strip representing position has alternate transparent and opaque stripes on it - one set for each bit. Bit transition error is minimized by using 'Gray' code. Bit values in Gray code are given in Table 11.1 for a 4-bit case; it can be easily extended for larger number of bits [Doebelin (1990). The specific characteristic of interest to us here, is the fact that only one bit undergoes change at any time resulting in minimum transition error. Before further digital processing, the position information in Gray code is converted into equivalent binary number.

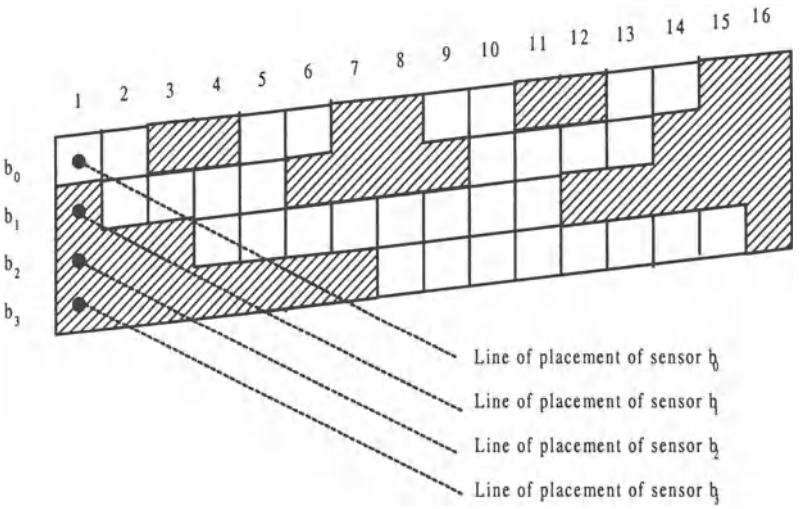


Figure 11.23 Absolute encoder with Gray code: Only a 4-bit case is illustrated

With 10 to 16-bit type converted output, as many optic switches with coded strips are used. When angular position is detected, the LSB is in the outermost circular strip. To avoid crowding of the optic switches at any one place, the LSB is kept at the place where displacement is to be sensed. More significant bits are shifted successively by a definite angle and the coded strips are also shifted accordingly. This staggering is purely an engineering convenience or constructional convenience. As mentioned earlier, the incremental encoder has come to be universally adopted. The absolute encoders of the type discussed are not so common with newer systems.

Table 11.1 Four bit Gray code and binary representation of equivalent decimal numbers

Decimal number	Equivalent Gray code $b_3b_2b_1b_0$	Equivalent binary $b_3b_2b_1b_0$
00	0 0 0 0	0 0 0 0
01	0 0 0 1	0 0 0 1
02	0 0 1 1	0 0 1 0
03	0 0 1 0	0 0 1 1
04	0 1 1 0	0 1 0 0
05	0 1 1 1	0 1 0 1
06	0 1 0 1	0 1 1 0
07	0 1 0 0	0 1 1 1
08	1 1 0 0	1 0 0 0
09	1 1 0 1	1 0 0 1
10	1 1 1 1	1 0 1 0
11	1 1 1 0	1 0 1 1
12	1 0 1 0	1 1 0 0
13	1 0 1 1	1 1 0 1
14	1 0 0 1	1 1 1 0
15	1 0 0 0	1 1 1 1

11.5.6 Information from Encoder Output

A variety of useful information can be extracted from encoder outputs [Beckwith Buck and Marangoni, Broch]. Appropriate DSP techniques can be used in each case. A few specific illustrative examples are discussed here.

11.5.6.1 Velocity

The content of the up / down counter associated with the incremental encoder in Section 11.4.2, represents the relative displacement. It can be read by an associated μC at regular intervals. These represent samples of the displacement obtained at equal intervals of time. Using a differentiation algorithm (See Section 9.5.1), the differential coefficient of displacement with respect to time representing its velocity, can be obtained. This procedure holds good for both linear velocity (with linear encoders) and angular velocity (with angular encoders).

Observations: -

⇒ By extending the above approach, one can obtain the second derivative of displacement with respect to time. This represents the linear / angular acceleration. However such successive differentiation is of limited accuracy and not commonly used.

⇒ The sample values above can be used and an FFT carried out. This gives the spectral distribution of displacement. Multiplying it by ω (the angular velocity in rad/s) and ω^2, one can get the spectral distribution of the velocity and acceleration also. Such derived information remains to be exploited.

11.5.6.2 Surface Roughness

Surface characteristics of machined parts require to be precisely quantified in a macroscopic scale. They are significant in deciding various contact characteristics like heat conduction, friction, leakage, surface cleanliness *etc*. Two activities are involved here – measuring the surface undulations with respect to a reference datum level and deriving surface roughness information in terms of specific indices. To carry out the measurement, a stylus is moved on the surface laterally at a steady speed. Displacement of the stylus in a direction normal to the plane of the surface is the characteristic of interest here. Typically, an LVDT attached to the stylus through its push-rod measures the displacement. Normally, the term 'roughness' signifies the short-term variations of the surface about its mean level (See Figure 11.24). The term 'waviness' signifies longer-term variations. Two commonly used indices of surface finish are: -

⇒ R_a – represents the average of the absolute excursions of the profile from the mean value.

$$R_a = \frac{1}{L}\int_0^L |z - \bar{z}|dx \tag{11.11}$$

$$\bar{z} = \frac{1}{L}\int_0^L z dx \tag{11.12}$$

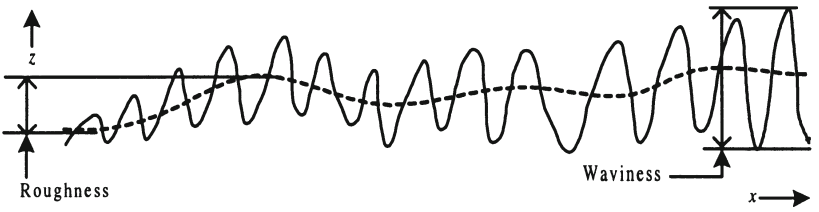


Figure 11.24 Typical surface finish showing roughness and waviness (one dimensional)

where, referring to Figure 11.24,

- x is the lateral distance from the origin.
- z is the normal displacement measured.
- L is the assessment length and
- $\bar{z}$ is the mean surface level.

⇒ R_q – represents the root mean square of the deviations around the mean value.

$$R_q = \sqrt{\frac{1}{L}\int |z - \bar{z}|^2 dx} \tag{11.13}$$

By the very nature of the definitions, R_q gives more weight to the larger excursions from the mean. One can use many other definitions of roughness.

11.5.6.3 The Bearing Ratio Curve

This represents the cumulative integral of the amplitude-density distribution function around the mean (Figure 11.25). At any height, the amplitude-density signifies the extent of wear required to ensure a desired level of contact surface area

for the bearing. All such information as well as other similarly defined indices can be computed using appropriate DSP algorithms. By quantifying the surface profile at regular intervals, one can define it fully in a two-dimensional plane – this characterizes the profile excursions z with respect to the x and y coordinates. A two-dimensional FFT of this, can yield a variety of information regarding the surface-quality of machining, health of machining source, possible causes for wear, tracking of wear source and the like. As of now, these tools remain more in exploratory realms than in established practice.

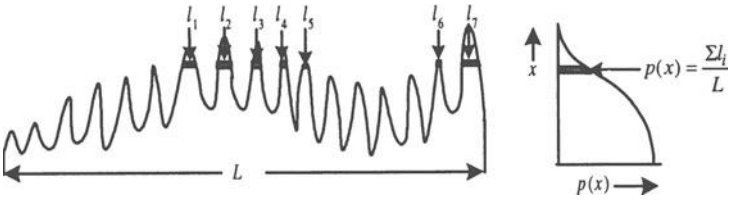


Figure 11.25 Illlustration of computation of bearing ratio curve for a one-dimensional surface profile

11.6 Rotational Speed Transducers

Speed sensing is mainly for direct indication and control. Speed control systems often demand precise speed sensing. Majority of the speed sensors use the principle of electromagnetic induction.

11.6.1 Homopolar Generator

Figure 11.26 shows the active parts of a 'Homopolar' generator. The shaft, whose speed is to be sensed, is connected to the shaft S of the homopolar generator. This has a cylindrical magnet over it, with the outer surface of the cylinder forming one pole (north). An annular magnetic material core B, surrounds this. A south pole is

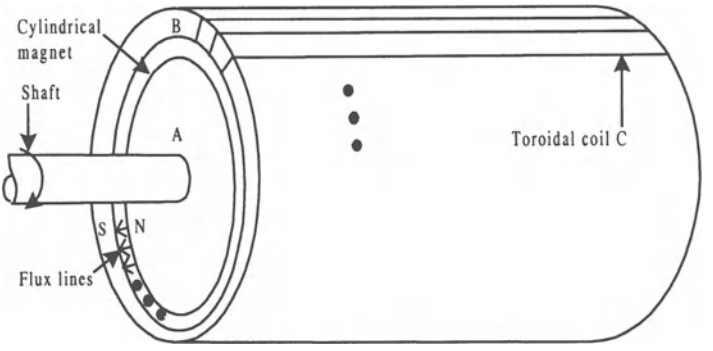


Figure 11.26 Homopolar generator – schematic form

induced on its inner surface. The lines of magnetic flux cross the air gap radially between these two cylindrical surfaces. A toroidal coil C is uniformly wound on the annular core B. With the permanent magnet and a uniform air gap, the gap flux remains uniformly constant. As the Homopolar generator rotates, a DC emf is induced in the coil C. The emf is proportional to the speed. It changes direction when the direction of rotation of the shaft reverses.

The homopolar generator is robust, linear throughout its working range and provides a smooth (ripple-free) output. With the use of permanent magnets of good quality, the sensitivity remains constant over time. It can work over a wide speed range. The main disadvantage of the homopolar generator is its low sensitivity.

11.6.2 DC Tachogenerator

A DC tachogenerator is a miniature DC generator [Clayton and Hancock]. The DC generator with ring winding is shown in Figure 11.27 (a). Functionally, the DC generator of today is very close to it, though constructionally quite different. The ring wound generator shown here, is easy to understand. R is a soft iron ring with a set of coils of wire C_1, C_2, ... *etc.*, wound and uniformly spaced over it. The figure shows only 8 such coils. These coils are all of copper wire. The ends of the adjacent coils are connected to a set of circular segments of copper called 'Commutator Segments (CS)'. Thus, one end of coil C_1 is connected to the commutator segment CS_1 along with one end of coil C_2. The other end of coil C_2 is connected to the commutator segment CS_2 along with one end of coil C_3 and so on. Continued in this fashion, all the coils together form a closed winding. The iron ring along with the closed ring winding is kept in the field of a magnet with poles N and S. If the ring is rotated around its axis, each of the coils experiences an induced emf. It is a maximum in coils C_4 and C_8 and zero in coils C_2 and C_6 for the position of the ring shown. Since the coils are all in series, these emf's add up in series in the form shown in Figure 11.27 (b) where e_1, e_2, e_3, ... *etc.*, represent emf's in coils C_1, C_2, C_3, ... *etc.*, respectively. A little reflection on the scheme brings out the following: -

- ⇒ The net emf around the closed winding loop is zero.
- ⇒ The emf measured between points P and Q is a maximum. Here points P and Q are points fixed in space along the 'Neutral Axis (NA)' of the scheme. Here neutral axis means the location on the ring where a coil experiences zero induced emf.
- ⇒ As the ring rotates, each coil takes different positions and the emf induced in it changes. However, the total emf between P and Q – sum of emf's in all the coils on one side (or the other side) – remains the same.
- ⇒ The emf between P and Q is of DC type. It increases proportional to the speed of rotation.
- ⇒ The emf can be tapped by two brushes – one at P and the other at Q – in physical contact with the commutator segment in front. As the machine rotates, the commutator segments also move in a circle. The commutator segments are kept insulated from each other at the joints. The brushes remaining fixed in space, always make contact with the commutator segment in front. Thus, there is a regular switching action of the brushes, which ensures that the contact is always made at the point at the NA.

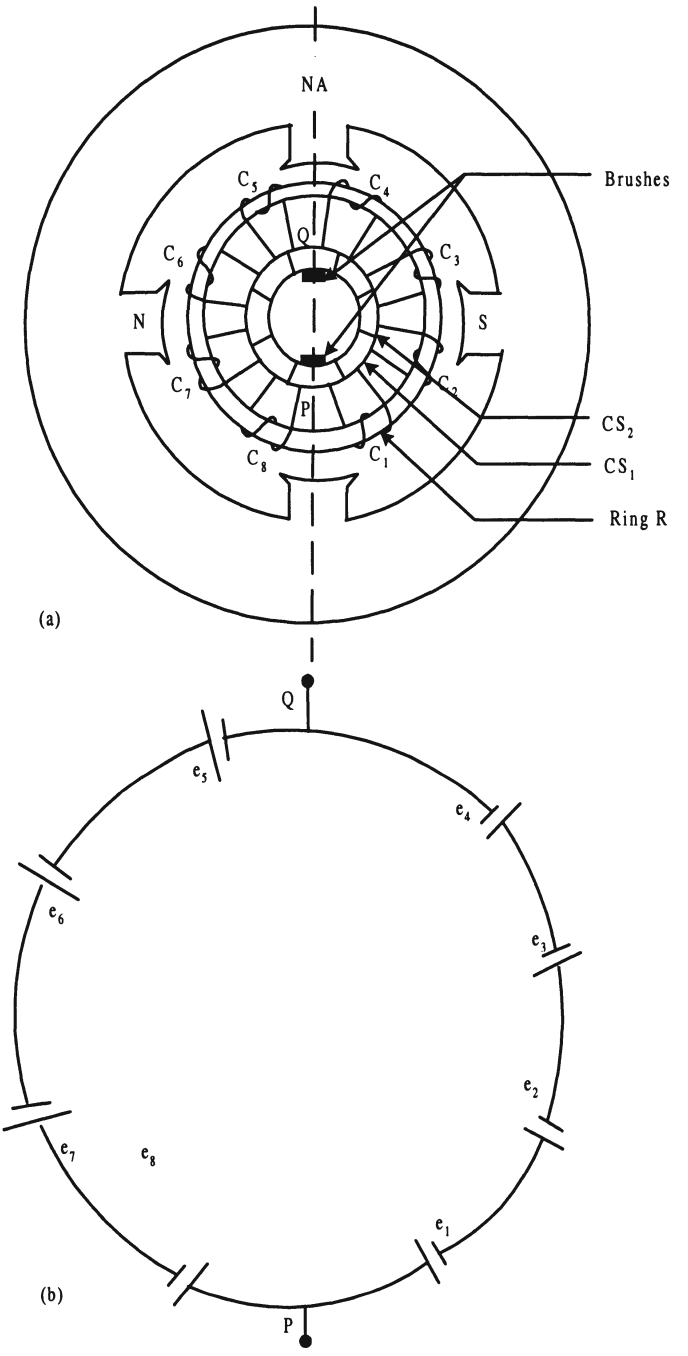


Figure 11.27 Simplified form of ring wound DC generator: (a) Skeletal generator diagram (b) Circuit of equivalent emfs

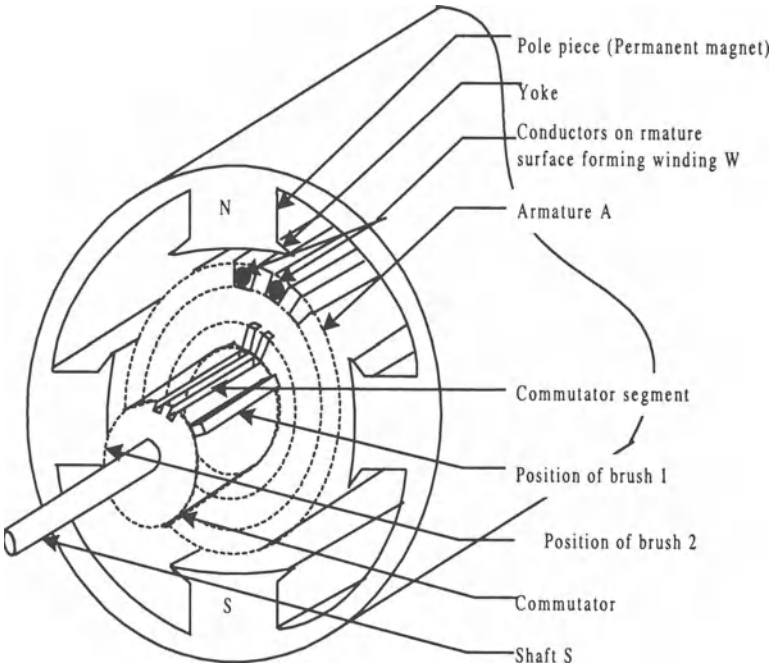


Figure 11.28 DC generator in schematic form

In principle, a practical DC generator of today remains the same as the ring wound generator above. The magnetic path, the uniformly wound coils forming a closed winding, the set of commutator segments arranged uniformly around a circle each being connected to the junction point of adjacent coils on the winding and brushes in the NA – all of them are similar to the ring wound machine. However, the structural construction is radically different – mainly due to the ring being replaced by a magnetic drum with attendant mechanical and performance benefits. Figure 11.28 shows the permanent magnet DC generator of today in simplified form. Only the electrically significant components are shown. The magnetic ring is replaced by a magnetic-drum assembled of stampings; the coils are wound over it in a manner somewhat close to the above scheme. On one side of the drum, an extension is provided to each turn of the winding through a copper strip. All such copper strips are again arranged around a cylinder and rigidly attached to it. These are the commutator segments; all such commutator segments together form the commutator. The brushes make contact with the commutator segments and tap the voltage. The Yoke Y is of a magnetic material with embedded permanent magnets. A two-pole configuration is shown in the figure. The drum is called the 'Armature (A)'; it is also of magnetic material but assembled with thin laminations. The winding (W) comprising the coils is uniformly laid on the armature surface housed inside slots suited for them. Specifically selected points on the winding are connected to the commutator segments C. Two graphite-brushes namely B_1 and B_2, make contact with the commutator segments. Two conductors connected to the brushes serve as leads for the output.

The shaft, whose speed is to be sensed, is connected to the shaft S at the centre of the armature. As the armature rotates, an alternating emf is induced in the winding W. Through the commutator and the brushes, it is rectified into DC. The DC voltage at the brushes is directly proportional to the speed. Use of quality permanent magnet, ensures that the air gap flux level remains constant over time. With this, the tachogenerator sensitivity remains constant.

Observations: -

⇒ The speed versus output voltage characteristic of the DC generator remains linear over the full speed range.

⇒ The DC tachogenerator has a wide speed range; but it is lower than that of the homopolar generator.

⇒ The ripple content in the output changes with speed. At low speeds, it may be high enough to have nuisance value.

⇒ The brushes require occasional cleaning and (infrequent) replacement.

⇒ An alternate configuration instead of the full-fledged DC generator is feasible. The rotor can carry the permanent magnet and the winding can be on the stator. With this change, the unit produces an alternating voltage whose magnitude and frequency are proportional to the speed (FM and AM modulated). This can be rectified using a precision rectifier to provide a DC voltage proportional to the speed. The commutator and the brushes are totally eliminated here.

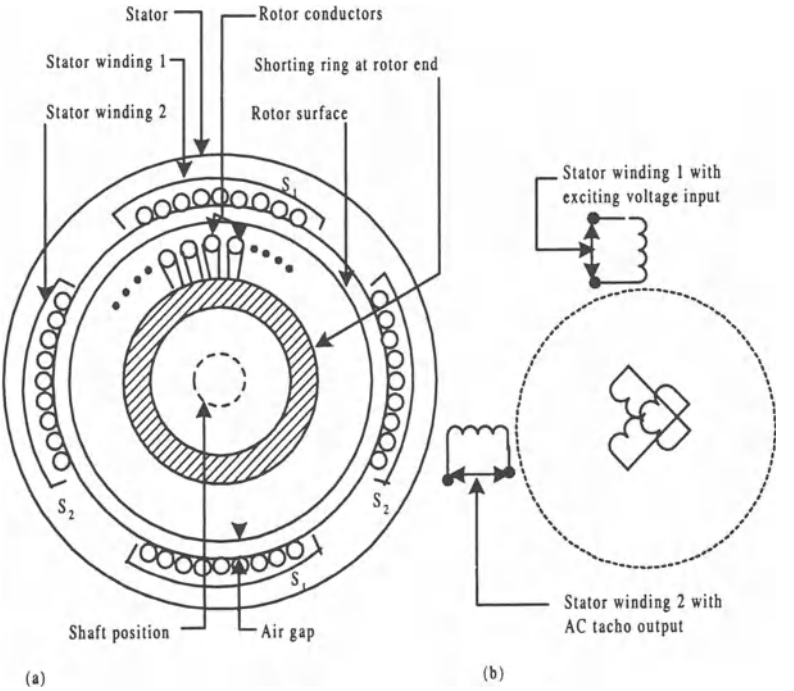


Figure 11.29 AC tachogenerator: (a) Skeletal diagram of the generator (b) Equivalent circuit

11.6.3 AC Tachogenerator

An AC tachogenerator is a modified version of an induction motor (Figure 11.29). The rotor surface is cylindrical. The stator inner surface is also cylindrical. The air gap is minimal – of the order of 0.2 mm. Both – stator as well as rotor – are assembled using special (Silicon) steel-stampings. In addition, the rotor carries a winding shorted on itself – called a 'squirrel cage'. The squirrel cage winding is arranged in slots around the rotor periphery. The stator has two uniformly distributed windings. Normally they are spread out at 90° (electrical) to each other. One winding is excited at the carrier frequency. As the rotor rotates, the emfs induced in the bars of the rotor-cage force currents through them. The combined effect of these currents and the current in the exciting winding on the stator, is to set up a rotating magnetic field in the air gap. The flux due to this field links the second (quadrature) winding on the stator and induces an emf in it. The magnetic field in the air gap always rotates at synchronous speed corresponding to the carrier frequency. The emf induced in the second stator winding is thus always at the fixed synchronous frequency or carrier frequency. Its amplitude is proportional to the speed.

Observations: -

- ⇒ AC tachogenerator requires a carrier supply for excitation. If its amplitude changes, the sensitivity is affected correspondingly.
- ⇒ The AC tachogenerator provides high sensitivity. It can go up to 0.1 V / rpm (or even more).
- ⇒ The tachogenerator output is modulated on the carrier. It can be used directly in a carrier based control system or demodulated (synchronously) and used as a corresponding DC output. The linear speed range is limited to 20 % to 30 % of the carrier frequency. With a two-pole scheme, which is commonly used, with a carrier frequency of f_c, the useful speed range extends up to 0.2 f_c to 0.3 f_c.
- ⇒ Carrier frequencies of 50 Hz, 60 Hz, and 400 Hz are common.
- ⇒ The AC tachogenerator above has a heavy rotor and a corresponding high inertia. This affects the speed of response considerably. Where the speed of response is critical or when the inertia of the tachogenerator is not negligible compared to that of the main shaft with its load, the construction is modified and a drag cup type unit used. Here a copper or aluminium cup forms the rotor. The rest of the iron / magnetic path is also made stationary. This reduces the inertia and the response time correspondingly.

12 Force and Allied Instrumentation

12.1 Introduction

Force, stress, strain, torque and acceleration are all closely related to each other. With few exceptions, instrumentation of all these quantities is carried out through strain measurement. Further, such strain instrumentation is almost universally done using resistance Strain Gauges (SG). Resistance SG and allied instrumentation is the main topic of this chapter [Doebelin, Hix and Alley]. Instrumentation of force and allied variables, are also discussed. Strictly speaking, pressure too comes within our purview here. However, pressure instrumentation along with that of flow – due to their importance in industry – is dealt with separately in a later chapter.

12.2 Principle of the Resistance Strain Gauge

The resistance R of a conductor of any homogeneous material is

$$R = \frac{\rho l}{A}\Omega \tag{12.1}$$

where

$\Rightarrow$ R is the resistance of the conductor,
$\Rightarrow$ ρ is the resistivity of the material of the conductor,
$\Rightarrow$ l is the length of the conductor and
$\Rightarrow$ A is the area of cross-section of the conductor.

When the conductor is subjected to a stress, its resistance changes. This change is the sum total of changes due to changes in ρ, l and A [Dally and Riley]. Let the conductor be rectangular in cross-section with p and q being the two sides.

$$\therefore A = pq \tag{12.2}$$

$$R = \frac{\rho l}{pq} \tag{12.3}$$

Considering first order changes we have

$$dR = \frac{l}{pq}d\rho + \frac{\rho}{pq}dl - \frac{\rho l}{p^2 q}dp - \frac{\rho l}{pq^2}dq \tag{12.4}$$

$$\therefore \frac{dR}{R} = \frac{d\rho}{\rho} + \frac{dl}{l} - \frac{dp}{p} - \frac{dq}{q} \tag{12.5}$$

Let – dl/l – the linear strain causing the above changes, be represented as

T. R. Padmanabhan, *Industrial Instrumentation*
© Springer-Verlag London Limited 2000

$$S = \frac{dl}{l} \tag{12.6}$$

Substituting in Equation 12.5,

$$\frac{dR/R}{dl/l} = 1+\frac{d\rho/\rho}{dl/l}-\frac{dp/p}{dl/l}-\frac{dq/q}{dl/l} \tag{12.7}$$

dp/p and dq/q represent the lateral strains due to the strain dl/l. The non-dimensional ratio [(dR/R)/(dl/l)] is called the 'Gauge Factor (GF)'. The ratio

$$\sigma = -\frac{dp/p}{dl/l} = -\frac{dq/q}{dl/l} \tag{12.8}$$

is the 'Poisson's ratio'. Substitution in Equation12.7 gives

$$\begin{aligned} \text{GF} &= \frac{dR/R}{S} \\ &= \frac{d\rho/\rho}{S}+1+2\sigma \end{aligned} \tag{12.9}$$

The quantity [$(d\rho/\rho)/S$] represents the fractional change in resistance due to the change in the resistivity of the material. This is known as the 'piezo-electric' effect. For normal metals and alloys, σ is in the range of 0.3 to 0.4 and [(dρ/ρ)/S] is in the 0.2 to 0.6 range. With these we have

$$1.8 < \text{GF} < 2.4 \tag{12.10}$$

For metals and alloys, the GF is normally slightly greater than two. It is customary to take the nominal value of GF as two. Manufacturers of SGs specify the GF for the material used.

12.3 Practical Considerations

Conventional SGs are mostly made of alloys like Constantan and Karma. Constantan is most widely used for SGs. High GF, high elongation-capability and high fatigue-resistance are its plus points. Due to its higher resistivity, small grids with high R, can be easily formed. However, its continuous drift when operating at temperatures above 65°C, makes it unsuitable for operation at elevated temperatures. Karma is a Nickel-Chromium alloy. High fatigue-resistance and stability, are its plus points. Variation of its resistance with temperature being linear over a wider temperature range, temperature compensation done with SG of Karma is accurate over a wider temperature range than that with Constantan. Four methods of forming SGs are in vogue.

12.3.1 Unbonded Metal Wire Gauge

The metal or alloy wire forming the gauge, is stretched between fixed supports in a zigzag fashion. If subjected to tension, the SG wire is stretched further. If subjected to compression, the stretch decreases. The SG wire is not allowed to go slack. This arrangement is carried out separately for each application. It is not amenable for mass production. The SG offers high sensitivity. Due to its fragile nature, the scheme is essentially restricted to laboratory applications.

12.3.2 Bonded Foil Gauge

The gauge formation is akin to that of the printed circuit board. The gauge material, in the form of a foil, is rolled and bonded to the base called 'Carrier Matrix'. Polyimide is a commonly used carrier. By suitable masking and etching, the required pattern of the SG is retained and the rest etched out. The gauge is subsequently sealed to make it weather proof. The formed SG is subsequently heat-treated to impart specific mechanical and thermal properties to it. The bonded foil type of SG is the most widely used one.

12.3.3 Vacuum Deposited Foil Gauge

The gauge is directly deposited on the base. This type of gauge is used with sensors – typically, diaphragms to sense pressure. A thin film of insulating carrier is directly deposited on the diaphragm in a vacuum chamber. The gauge material is vacuum-deposited on it by an evaporation and condensation process. The required pattern is obtained by masking off the undesired areas with the help of suitable templates. Characteristics and precision attained with direct formation of SG in this manner, are one order better than those of the schemes using bonded gauges.

12.3.4 Sputter-Deposited Foil Gauge

After forming the insulating carrier base, the gauge material is sputter-deposited on it uniformly in a vacuum chamber. Subsequently, the desired pattern of the gauge is retained and the rest removed by photo etching. Sputter-deposition is done for sensor gauges as an alternative to vacuum deposition.

12.3.5 Semiconductor SGs

As seen from Equation 12.10, the GFs of metals and alloys are of the order of 2. Dimensional changes are the primary contributory factors for this. The resistivity changes little with strain. With semiconductors – mostly doped Si or Ge – the change in ρ with strain is substantial – this is the 'piezo-resistance' effect. The gauge factor with these materials may extend up to 200. These SGs are formed on a silicon-oxide substrate by etching, masking, doping and so on – a procedure akin to the IC formation. Due to the high GF and the relatively high values of ρ of these materials, SGs and SG bridges using semiconductors, can be fabricated in relatively small sizes. In turn, the point of strain measurement can be more precisely defined. The small size makes them faster in response. Semiconductor gauges are more rugged and better at fatigue life. Their elastic range can extend up to 20 % – one order higher than that of metal or alloy SGs. The Semiconductor GF is highly sensitive to temperature. This can be alleviated to some extent by using highly doped Si for the gauge material. Unit-to-unit repeatability is also poor. However, the possibility of building the primary signal processing circuitry and compensating for lack of repeatability, temperature dependence and the like with it, – all these in one IC itself – make them attractive for many future applications. As of now, the

application of semiconductor SGs is limited to situations calling for high sensitivity and fast dynamic strain measurement.

12.3.6 Backing Material

The SG is bonded and formed on the backing material. The backing material has three roles: -

⇒ A base for the foil pattern, for easy handling during installation.

⇒ A uniform base which can be bonded to the test surface through an adhesive.

⇒ Effective electrical insulation between the gauge and the test object.

Polyimide is the most widely used backing material. Toughness, flexibility, wide temperature range of operation (–195°C to +175°C) and long elongation capability (> 20 %) are its characteristic features.

Glass-film-reinforced epoxy phenolic is used as a backing material for precision work. It is better suited for static and dynamic strain measurements. It can operate over a wider temperature range (–269°C to +290°C). However, maximum elongation that it can withstand is limited to 1% to 2 % only.

12.3.7 Adhesive

Resin based adhesives are recommended for all commercial and industrial applications. Normally the SG manufacturers supply the adhesive as part of a user-kit. The curing time for the adhesive may extend from a few minutes to days in some extreme cases.

12.3.8 Quantitative details

The nominal resistance values for resistance SGs are 120 Ω, 350 Ω, 600 Ω, and 700 Ω. The excitation voltage per gauge is normally in the 1V to 5V range. The active strain may extend up to 2% to 3%. The most common gauge lengths are in the 3mm to 6mm ranges. However gauges with lengths as low as 0.2mm and as high as 100mm are available – Gauges with such extreme dimensions are used for specialized applications. Normal operating temperature range is –100°C to +200°C. The full-scale strain is in the range of 1200 με to 3000 με[6]. Manufacturers guarantee operation for 10^5 to 10^8 cycles.

Often for obvious reasons, the strain is measured at the point of maximum stress. The strain gradient can be high here and the gauge measures the average strain over its active length (See Figure 12.1). This is less than the peak value. To avoid such peak masking, the gauge length has to be small (~ 10%) compared to the dimensions causing the peak – like a fillet, diameter of a hole or notch and the like. If this dimension itself is less than 12mm, the gauge length is too small to ensure reliable reading. Larger gauges are easier to handle and more effective in power

[6] It is customary to express strain *S* in 'microstrains'. It is represented by the combination symbol 'με'.

dissipation - this is more important when the test object is plastic, concrete and the like.

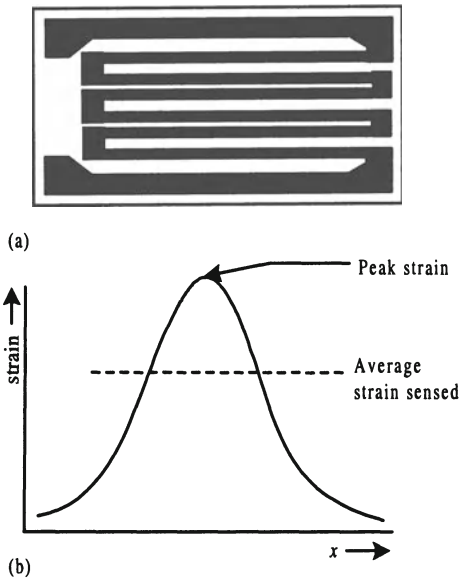


Figure 12.1 Measurement error with SG: (a) Typical SG pattern (b) Actual and sensed strains

12.4 SG Patterns

The basic pattern used for strain gauges, is decided by two considerations: -

Size: - As we move away from the point of measurement, the strain may change rapidly. This calls for restricting the SG size as much as possible to ensure measurement of the true value of strain. Within such an available space, the gauge is formed as a fine wire. On the other hand, if one can increase the size of the SG, the gauge wire length and hence its resistance too can be increased correspondingly. In turn, the SG sensitivity increases. Hence, these two are conflicting requirements calling for a trade-off.

Directional Response: - The gauge foil is rigidly attached to the member undergoing strain in one plane. It responds to strains in the longitudinal direction as desired as well as the transverse direction, which is not desired. The foil geometry has to be such that the response to transverse strain is minimal without sacrificing longitudinal response. The pattern of a typical single element SG is as shown in Figure 12.2.

Observations: -

⇒ The SG is laid out to sense strain in the x-direction. The total active length is the sum of all independent 'gauge lengths l' in the x direction.

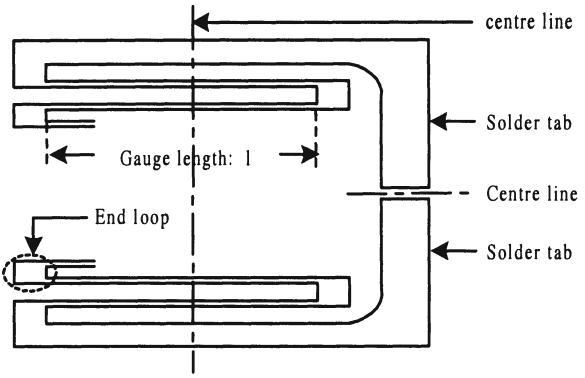


Figure 12.2 Typical SG pattern

⇒ The end-loops and solder tabs constitute the gauge lengths in the *y* direction. These are made much wider than the active lengths l (10 times or more). Thus, the contribution of the end-loops and the solder tabs to the total gauge resistance, is made as small as desired. In turn, the transverse sensitivity is reduced.

⇒ When measuring point strains, SGs with the shortest possible gauge lengths are to be used; this is to make the gauge output more representative of the point strain. However, as the length reduces the relative contribution of the end-loops and solder tabs to the overall resistance, increases. This increases lateral sensitivity and affects the SG adversely. The more miniaturized an SG is, the more its relative lateral sensitivity. Hence, one should use as long an SG as the application permits.

⇒ The centre-lines in the *x* and the *y* directions are separately marked to identify the equivalent point of measurement.

SGs are mostly connected in Wheatstone bridge form and operated close to balance (See Section 2.2.2). When strain sensing is done with a single sensing element, the gauge has the form shown in Figure 12.2. Multiple elements are used in different bridge arms to increase sensitivity and to provide compensation. In all such cases, the gauge layout is 'tuned' to suit the application. A single gauge is used only when the stress is uni-axial at the point and the directions of the principal axes are known. Two gauges are laid out normal to each other when measuring strains in two known normal directions – *i.e.*, when the principal axes are known beforehand as these two (Figure 12.3). The two gauge elements form adjacent arms

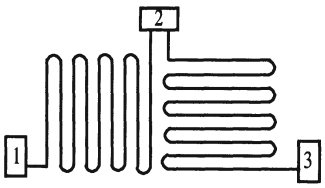


Figure 12.3 A two-gauge set to measure strains in two normal directions

of a strain gauge bridge. The two elements in this manner measure respective strains at two points slightly away from each other; it is assumed that the stress conditions at these points are the same. In case such measurable change in strain is possible, the two gauges are kept one above the other and mounted on the same carrier with insulation in between. When measuring strain in one direction alone and compensation for leads, temperature variations and the like are required, one gauge is rigidly mounted on the member and the other kept as a dummy above that. The dummy sees the same environmental conditions as the active gauge and facilitates compensation through Wheatstone bridge.

The SG layout of Figure 12.4 is to have all the four arms of the bridge for sensing. Two diagonally opposite gauges sense strain in one direction while the other two, sense strain in a direction normal to it. The scheme offers high sensitivity and facilitates compensation for lead length, temperature change *etc.* As in the previous case, the equivalent points at which the strains are measured by the four elements are slightly displaced with respect to each other. The measurement is meaningful only if the strain values in the material, at these distances, remain the same.

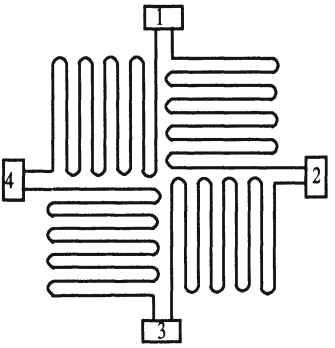


Figure 12.4 A four-gauge set arranged to measure strains in two normal directions

Torque causes maximum stresses to occur in two normal directions. These are inclined to the axis of the torque at 45°. Similarly, force applied on a cantilever, causes maximum stresses along the two directions normal to each other. These are inclined at 45°, to the length of the cantilever. The two gauges laid out as shown in Figure 12.5 (b), facilitate this type of measurement (Note that the two gauge configuration of Figure 12.5 (a), cannot be directly used here. It causes the respective measuring points to be in different planes).

When the principal axes are not known, strain in three axes can be measured using Rosettes shown in Figure 12.5 (c) or 12.5 (d). Rosettes at 0 - 45° - 90° and 0 - 120° - 240° are more common. Based on the three strains measured by a rosette, orientation of the principal axes, principal stresses, as well as stresses in any other direction can be determined. Rosettes with 3 SGs in a single plane as well as 3 stacked SGs are available. Single plane rosettes have SGs closer to the object. Hence, they are more accurate. Their heat conduction is superior; hence, their accuracy and stability are better. Stacked version is better and preferred only if the strain gradient in the region of measurement is large.

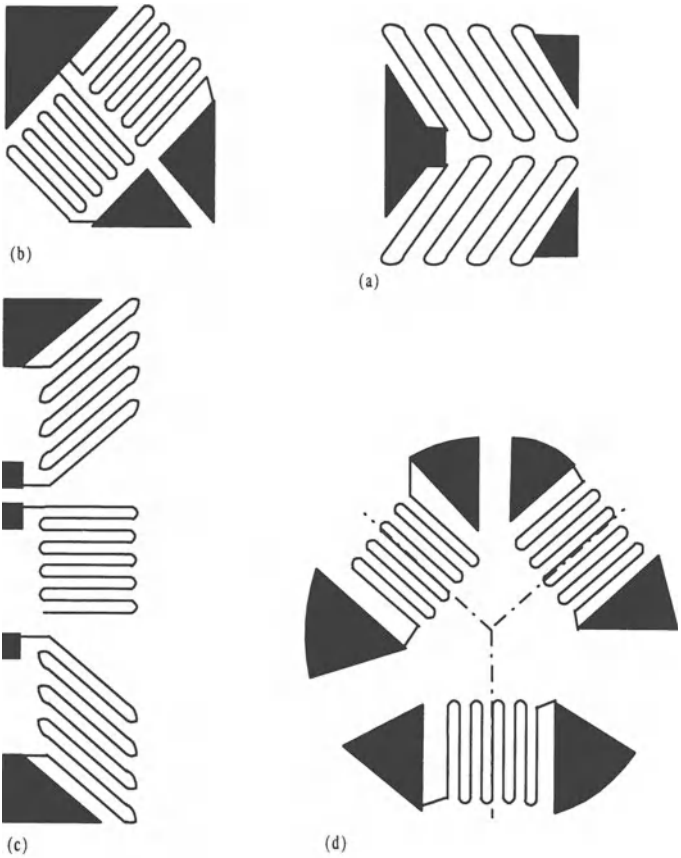


Figure 12.5 Different strain gauge rosettes

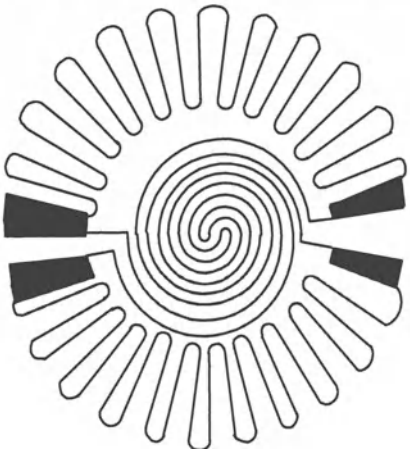


Figure 12.6 A set of four gauges arranged to sense strains in radial and circumferential directions

Absolute pressures and pressure differentials can be measured using diaphragms (See Section 14.2.4). When subjected to such pressure differential on either side, the diaphragm undergoes compressive (tensile) strain radially and tensile (compressive) strain circumferentially. Four SG elements can be arranged in bridge form to sense these and provide maximum sensitivity, as shown in Figure 12.6. The direct-deposition method of forming the SG is in wide use for this. With a bonded SG, aligning and positioning it precisely will be difficult. Indecision on this count is practically absent with the direct deposited-gauge.

12.5 Error Compensation with SG Bridges

The SGs are kept on the member whose strain is to be sensed while the rest of the circuit is kept along with the signal processing circuitry. The external leads to the SG can cause error on two counts: -

⇒ The length of the lead wire adds a resistance in series with the SG. This changes with the length and can cause an error.

⇒ The lead wire resistance changes with temperature causing a corresponding error. To compensate for this, equal and identical leads are connected in adjacent arms. Their effects are cancelling in nature (See Section 10.2.2).

When a single SG is used for sensing, the leads are connected as shown in Figure 12.7. R_2 is the SG for sensing; lead L_1 is in series with R_2. An identical lead L_3 is connected in series with bridge arm R_3. The lead L_2 is in series with the bridge output. Effects of changes in the resistances of L_1 and L_3 cancel each other. Changes in the resistance of L_2, do not affect bridge operation since L_2 is in series with the bridge output.

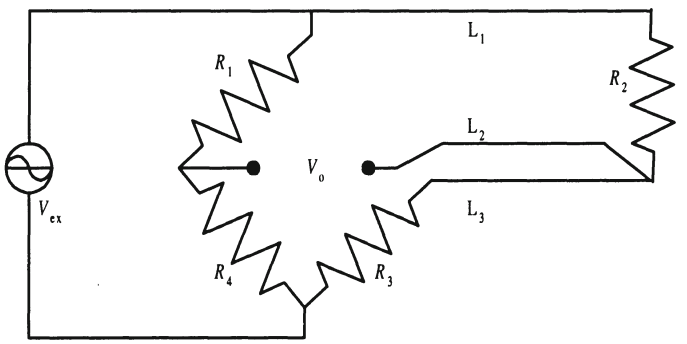


Figure 12.7 A single strain gauge in a Wheatstone bridge with the three-lead scheme for error compensation

When two SGs are used, they form adjacent arms of the bridge as in Figure 12.8, with L_1, L_2 and L_3 connected as shown. L_1 and L_3 are to be identical in length and resistance values. L_2 being in series with the output, its resistance value and variations in the same do not affect the unloaded bridge output. The same scheme is used when one SG is a sensor and the other a dummy for compensation.

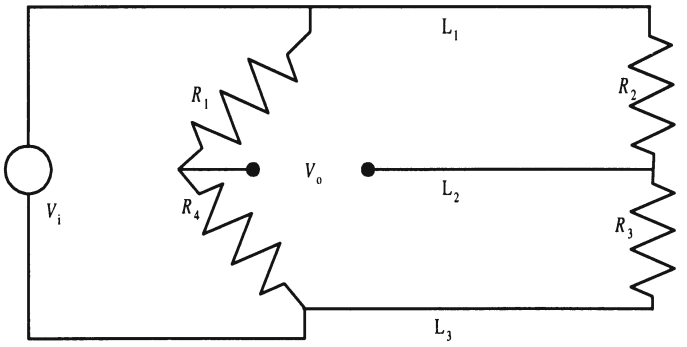


Figure 12.8 Strain gauge bridge with 2 gauges and error compensating leads

When all the four arms of the bridge are SGs as in Figure 12.9, there are no lead resistances to affect the bridge balance. Hence, changes in their values do not affect bridge performance directly. However a four core cable is to be used here, (two being supply leads and the other two being bridge output leads) in contrast to the three core cable in the earlier cases.

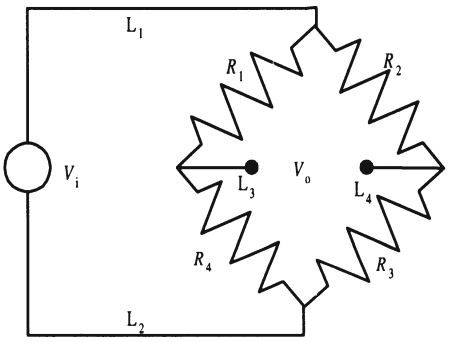


Figure 12.9 Strain sensing bridge with four gauges and corresponding leads

Apart from the possible errors due to lead resistances discussed above, the SG bridge can have erroneous output due to various departures from idealizations. These may be due to:

⇒ differences in the GFs of individual gauges. Such differences may be induced due to the differences in the mounting, local surface differences and the like.

⇒ differences in the thermal expansion coefficients of SG and the test specimen.

⇒ differences in the individual resistance values and the like.

Apart from the above, the overall bridge sensitivity may differ from the desired value and change with temperature. These are corrected for in three steps: -

⇒ *Step 1*: Consider the unit-ratio bridge. Let δ_1, δ_2, δ_3 and δ_4 be the fractional changes in the resistances of the four arms from the balance values. Generalizing the approach followed in Section 2.2.4, we get

$$\frac{V_o}{V_i} = \frac{1}{4}(\delta_1 - \delta_2 + \delta_3 - \delta_4) \qquad (12.11)$$

With a fixed applied voltage V_i, we get V_o at two temperatures T_1 and T_2. Let their difference be ΔV_o. We have,

$$\text{Fractional change in output/° C} = \frac{\Delta V_o}{V_i}\frac{1}{T_2 - T_1} \qquad (12.12)$$

⇒ *Step 2*: If the fractional change in the output /°C in Equation 12.12 is positive, it can be compensated for, by adding a resistance in series with R_2 such that its value changes by the same amount /°C. If we select copper resistance for this with 0.39% /°C as temperature coefficient, the resistance R_c to be added in series becomes, [See Equation 2.16]

$$R_c = \frac{\Delta V_o}{V_i} \times \frac{1}{T_2 - T_1} \times \frac{R}{0.0039} \times 4 \qquad (12.13)$$

where R is the resistance of each arm.

If the output is negative, R_c is calculated as above and added in series with R_1.

⇒ *Step 3*: After the above correction, get V_o / V_i at room temperature. This is composed of any residual output due to bridge imbalance plus that due to R_c introduced above. If it is positive, it is nulled by increasing R_2 by ΔR_2 where

$$\Delta R_2 = \frac{V_o}{V_i} \times 4R \qquad (12.14)$$

If it is negative, R_1 may be increased correspondingly. This resistance has to be of a material with negligible temperature coefficient (since the error due to the temperature variations, has been corrected already in step 1). Manganin or Eureka wire may be used for the purpose.

Example 1

A SG bridge is set up with each SG of 600 Ω nominal value. The bridge is excited at 2.4V. In the absence of any strain (zero signal condition) its output values are obtained as follows:

$$\text{Output at 20 °C} = 200\ \mu V$$
$$\text{Output at 40 °C} = 212\ \mu V$$

Substituting in Equation 12.12,

$$\text{Fractional change in output/ °C} = -\frac{212 - 200}{2.4} \times \frac{1}{20 - 40}$$
$$= 0.25 \times 10^{-6}$$

Using Equation 12.13,

$$\text{Copper resistance to be added in series with } R_2 \text{ (}i.e.\text{, } R_c\text{)} = \frac{0.25 \times 10^{-6} \times 600 \times 4}{0.0039}$$
$$= \mathbf{0.154\ \Omega}$$

Bridge output voltage after adding R_c in series with R_2 at 20 °C and zero signal conditions (measured value) = 50 μV

Additional resistance to be added in series with R_2 = $\dfrac{50\times10^{-6}\times600\times4}{2.4}\ \Omega$

= **50 mΩ**

This resistance of 50 mΩ has to be of Eureka or Manganin.

12.6 Strain Gauge Signal Processing

The bandwidth of the SG based instrumentation scheme can extend up to 50 kHz. In most of the applications, the measurement is from DC signal onwards. As such the difference amplifier, the single-ended inverting and non-inverting amplifier or their modifications are in use. Instrumentation amplifiers are also in wide use due to their specific characteristics; often they are the preferred ones.

Observations: -

⇒ Wherever possible, the SG bridge is excited with a balanced supply voltage; $+V_s$ and $-V_s$. This makes the common mode voltage in the bridge output zero (See Section 10.2.2.2).

⇒ The amplifier bandwidth is kept at the minimum required level. This reduces the noise level and improves the minimum detectable threshold. Thus with very large bodies and structures, the bandwidth may be of the order of 10 Hz. When process related variables are measured (weighing of silos and bins), the bandwidth may be only a fraction of a Hz. With small bodies or when sensing shock, it may extend up to 100 Hz. When sensing vibration it may extend up to 10 kHz depending on the application.

⇒ With the availability of low cost instrumentation amplifiers, they are preferred for strain gauges, wherever possible.

⇒ Size, accuracy and power dissipation are the criteria for the selection of the SG for any application. The resistance value and the bandwidth required are to be matched with the following amplifier stage. At this stage, one can compute the threshold voltage that can be detected and confirm it to be low enough. If not, the design cycle may have to be repeated with an SG set of lower resistance values.

⇒ Excitation voltage of the SG bridge should be normally as high as possible – to give maximum sensitivity. The power dissipation in the gauge is V^2 / R where V is the rms. value of the applied voltage and R the equivalent bridge resistance. The power dissipation can be 0.3 to 1.5 W/cm^2 when the gauge is directly mounted on metal surfaces (which have very large heat capacity and good thermal capacity). However, when mounted on non-conducting surfaces like concrete, plastic and the like, the gauge power is not carried away by the base body. The gauge power dissipation has to be limited to 1.5 mW/cm^2 to 7.5 mW/cm^2.

⇒ When the gauge power dissipation has to be limited to very low levels, DC excitation has to be limited to very low levels. In such cases, the excitation can be in the form of periodic pulses of 10 V or so with a low duty cycle (10 %). With the active bandwidth of the SG extending up to 50 kHz, we can use 200μs pulses width repeated at 500 Hz. The corresponding system bandwidth may extend up to 100Hz.

⇒ Nowadays AC excitation of SG bridges is essentially limited to strain measurement with rotating shafts (See Section 12.13 on torque sensing). The bridge is excited at a constant frequency and fixed amplitude. The output is of the SC-DSB modulated type. Demodulation is done through a synchronous demodulator.

12.7 Direct Measurement of Strain

The major considerations in the layout of SG bridges used for the direct measurement of strain are the following: -

⇒ Locate the SGs in places that are strained to the maximum extent. This ensures maximum bridge sensitivity.

⇒ Ensure that the centre-lines of the SGs are properly aligned. This is to avoid error due to extraneous strains.

⇒ Use an SG of the maximum size that the context permits. As the size reduces, the transverse sensitivity factor (k_t = GF $_{transverse}$ / GF $_{longitudinal}$) increases contributing to undue error. If the SG size increases unduly, the strain sensed will be a weighted average and less representative of a 'Point Strain'.

⇒ Use SGs in orientations and combinations that lead to maximum bridge sensitivity. This also provides compensation for ambient temperature variations.

The commonly used configurations (with appropriate illustrations on the following pages) are discussed below.

When the strain on a member due to direct axial loading is to be sensed, SGs are used in all the four arms of the bridge. Two G1 and G3 - sense the direct strain and the other two – G2 and G4 – sense the lateral strain, which is of opposite nature. Figure 12.10 shows different possibilities. The overall bridge sensitivity is $2(1 + \sigma)$ times the sensitivity of the bridge with one gauge. The bridge leads and ambient temperature variations do not cause error.

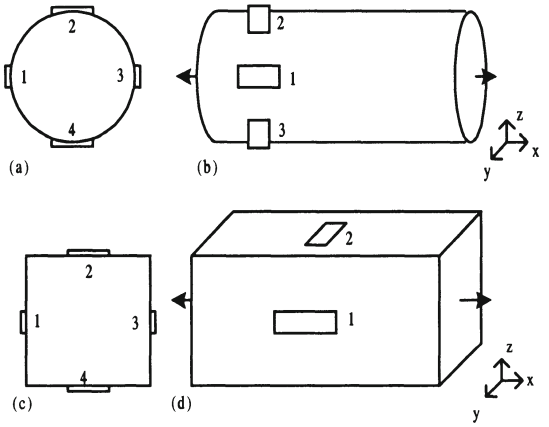


Figure 12.10 Commonly used SG configurations for axial loading: In all the cases, the arrows show the direction of force or stress concerned. (a) & (b) Horizontal circular cylinder; (c) & (d) Horizontal rectangular prism

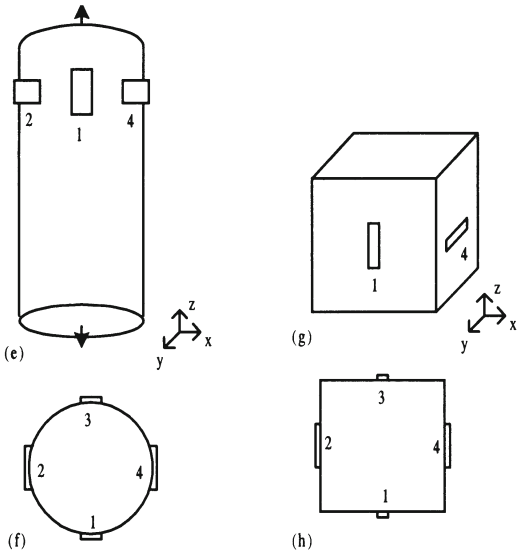


Figure 12.10 (continued): (e) & (f) Vertical circular cylinder; (g) & (h) Vertical rectangular prism

Beams and cantilevers undergoing bending have compressive stress at the bottom and tensile stress at the top or *vice versa*. The directions depend on the nature of the load. The presence of both types of strains allows all 4 arms to be of SGs. Diagonally opposite arms are on top and bottom of the member undergoing strain. Figure 12.11 shows different possibilities.

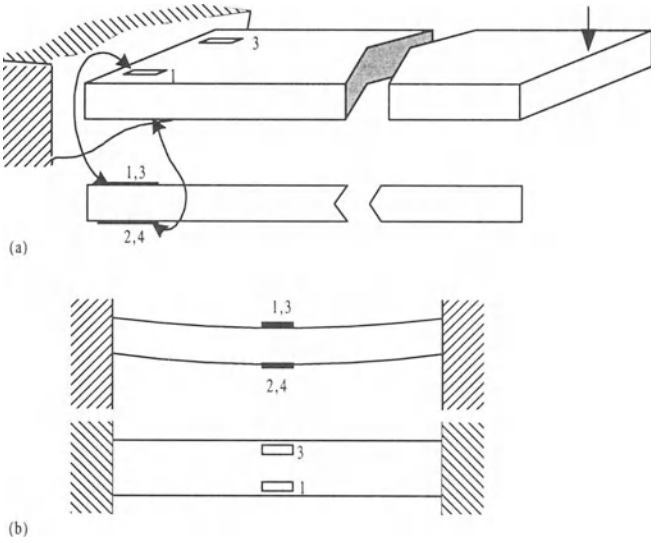


Figure 12.11 Sensing of strain in beams and cantilevers: Arrows show the direction of force applied. (a) Cantilever (b) Beam. Numbers 1,2,3 and 4 represent respective SG positions

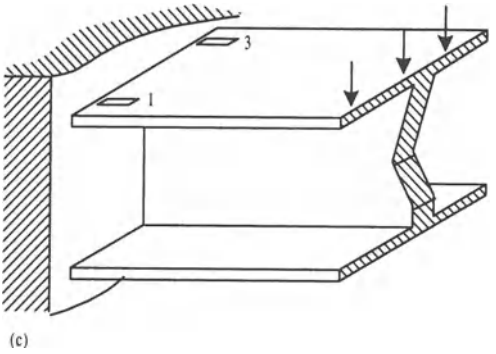


Figure 12.11 (continued) (c) Beam with I-section

The shear strain due to bending is a maximum along the neutral axis. Further, it is a maximum in a direction at 45° to the beam length. The two axes at 45° to the longitudinal axis experience strains of opposite directions. Hence all the four arms can be gauges with G_1 & G_3 oriented in one direction and G_2 & G_4 oriented in a normal direction as shown in Figure 12.12. Note that the line of maximum shear stress is the same as that of zero compressive or tensile stress. This explains the difference in the position of strain gauges. Gauges of the type in Figure 12.5 (a) are tailored to this application.

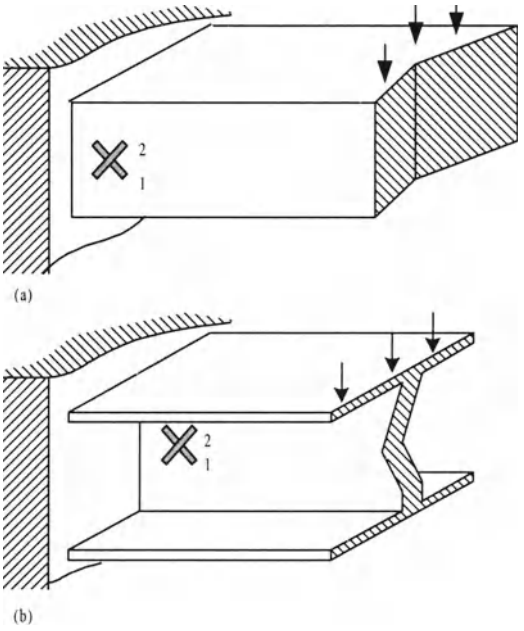


Figure 12.12 Sensing strain in a cantilever with SGs located at the point of maximum shear stress: Stressed member is of rectangular cross-section in (a) and I-section in (b)

12.8 Load Cells

When mechanical quantities – acceleration, force, weight and torque – are to be sensed, first they are converted into equivalent strain. Then the strain is sensed using an SG [Holman and Gajda, Norden, Norton, Smith]. The primary sensor that converts the variable into equivalent strain is of phosphor-bronze or aluminium or stainless steel [See Table in Appendix]. It comes in well-defined shapes. This along with the SG mounted or formed on it, is called a 'Load Cell'. The load on the load cell causes a strain on it, which is measured by the SG. Load cells are available with full-scale force values ranging from 0.1 N to 10^6 N or more. The shape of the material and the location of SGs on it are chosen such that both compressive and tensile strains are present. This allows all the four arms of a strain gauge bridge to be of SGs - maximizing sensitivity and obviating the need for compensation due to changes in ambient conditions. The desired strain can be produced by axial loading, bending of the load member or in shear. Bending beam type load cell is more common. It is simpler in construction and hence lower in cost. The shear-beam based load cell offers certain conspicuous performance advantages. It offers higher side-load rejection, lower creep and faster return to zero after load removal. However, for the same geometry and size, it has lower sensitivity.

The load cell SG bridge excitation voltage is of the order of 10 V DC. Full-scale output is typically 20 mV and accuracy 1 %. By additional temperature compensation and the like, the accuracy can be improved to 0.2 %. The commonly used load cells and their application areas are discussed here.

12.8.1 Column Type Load Cells

The column type load cell is normally cylindrical in shape (See Figure 12.13). Two of the SGs sense normal (tensile or compressive) strains in the direction of the applied force, while the other two sense the lateral (compressive or tensile) strain.

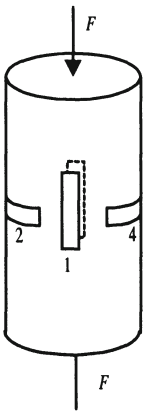


Figure 12.13 Column-type load cell: 1,2,3 and 4 are the positions of the SGs

The overall sensitivity is $2(1 + \sigma)$ times that of a single SG. The arrangement is insensitive to eccentric loading as long as the eccentricity is small. Column type

load cells are available with full-scale outputs ranging from 50gm to 25 metric Tons. A variety of engineered versions is available: -

⇒ Columns with both ends free for compressive loading.
⇒ Columns with threaded extensions or tapped holes on either side for both compressive and tensile loading.
⇒ Columns with end rings for connecting hooks on either side for tensile loading
⇒ Columns with one end supported for weighing bins, silos *etc.*, in process industries.

The column type load cell has to be long enough (compared to its cross-section) to ensure that the strain in the region of SG is uniform.

Figure 12.14 shows a column type load cell where the strain is sensed in shear. The shear strains are sensed by positioning SGs in tension and compression at 45° to the axis of the load. These are housed in holes in the shear webs.

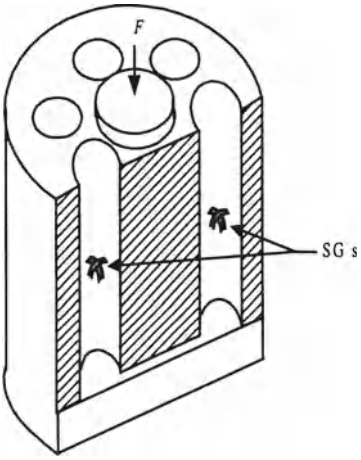


Figure 12.14 Column-type load cell with the SGs sensing shear strain: The SGs are concealed and protected making the load cell robust

12.8.2 Cantilever Type Load Cells

The cantilever-type load cell of the bending beam type is shown in Figure 12.15 (a). This offers better sensitivity compared to that of the column-type load cell; it is used for sensing smaller values of forces. In the case of the bending beam type load cell [Figure 12.15 (a)], SGs 1 and 3 are on top and SGs 2 and 4 are at the corresponding positions at the bottom.

For the shear-beam load cell [Figure 12.15 (b)], the SGs are kept on the neutral axis where the shear stress is a maximum. The two SGs are at 45° to the axis of the load cell, so that maximum strain is sensed. As mentioned earlier, lateral load rejection is better with the shear beam.

The 'Proving Ring' load cell shown in Figure 12.15 (c) is an alternative to the cantilever for measuring small forces. It is of the bending beam type. The position of the SGs and the applied forces are as shown in the figure.

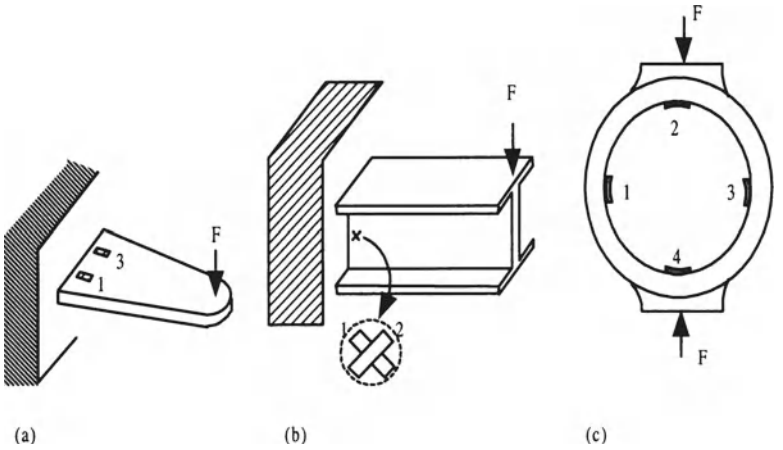


Figure 12.15 Different types of load cells: (a) Cantilever (b) Cantilever with sensing of shear strain and (c) Proving-ring

12.8.3 S Beam Type Load Cell

The S beam type load cell shown in Figure 12.16, is available for a wide range of loads. Different types of mounting arrangements make it suitable for a variety of applications. The load cell can be of the bending beam or the shear beam type. The shear beam type provides better side or lateral load rejection.

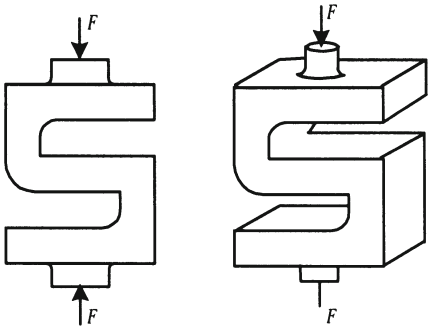


Figure 12.16 S-Beam type load cell: The direction of applied force is shown

12.8.4 Thin Beam Load Cell

The thin beam load cell is shown in Figure 12.17. Both ends are rigidly attached to the load-carrying member. The applied load is always of the moment type. The two types of applied moments and the resultant displacement are shown in Figures 12.17 (b) & 12.17 (c). Two SGs are mounted – both on one side. One of them is under tension and the other under compression. The other two SGs of the remaining two bridge arms too can be mounted similarly. With the type of loading mentioned,

the strains in the two SGs are always opposite in sense. The basic load cell can be adapted easily for a variety of load conditions. Two possibilities are shown in Figure 12.17 (d) & 12.17 (e). The beam sensor material can be of phosphor bronze, aluminium or stainless steel. The full-scale force values range from 1 N to 200 N.

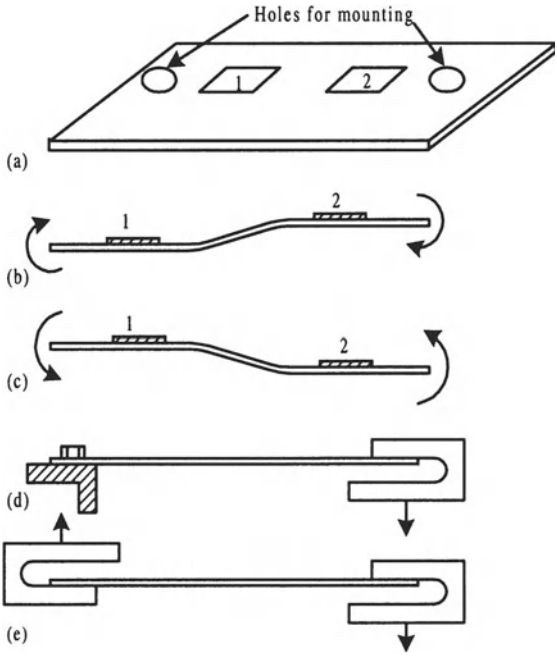


Figure 12.17 Thin beam load cell: (a) Load cell (b) & (c) Deflection of the load cell for the two types of applied moments (d) & (e) Adaptation of the load cell for two types of loads. The arrows show the direction of applied moment / force.

Principle of the thin beam load cell – application of applied load as moment in the load cell *per se* and positioning the SGs with the same orientation – is used with a variety of configurations. Two of these are shown in Figures 12.18 (a) and 12.18 (b). Positions of the SGs are also shown. Both have good lateral-load rejection. The parallelogram type in Figure 12.18 (b) is popular and available for a wide range of loads. It can be easily adapted for a variety of loading conditions. A few possibilities are shown in Figure 12.19.

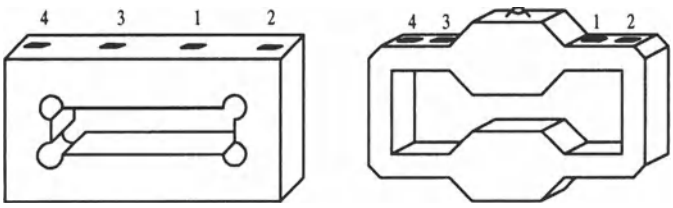


Figure 12.18 Two load cell configurations that use the principle of the thin beam load cell: Numbers 1,2,3 and 4 are the respective SGs

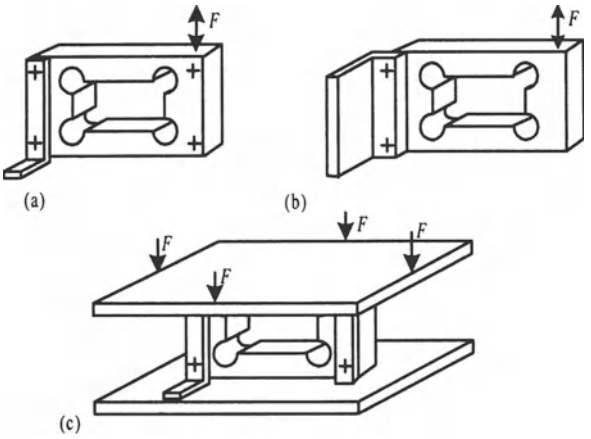


Figure 12.19 A few adaptations of the parallelogram type load cell: In the case of (c) the load is to be (preferably) symmetrically positioned so that all the F values are equal.

General Observations: -

- ⇒ The equations relating strains and applied load are used as design guidelines only.
- ⇒ The loading of the load cell has to be in the specified direction only. Load has to be properly aligned and eccentricity avoided.
- ⇒ Normally the load cells are calibrated along with the SG bridge mounted in the final form.
- ⇒ The support structure for the system has to be carefully designed to avoid 'load shunt'. The possibility exists very much when mounting bins, silos and reaction vessels on load cells for on-line weighing. Structural members may be introduced inadvertently for lateral support. They may share part of the load and the same may go undetected. Often their presence will be reflected as a lack of repeatability of load cell performance.
- ⇒ A series of load cells, which use a spring as the primary sensing element, has been introduced recently. These span a wide load range. Insensitivity to off-axis loading and high overload-capability, are the plus points [Bruns].

12.9 Piezo-Electric Sensors

Certain crystalline objects have a voltage or charge induced across two opposite faces, when subjected to a stress across another set of faces. This is the basic phenomenon of 'piezo-electricity' [Neubert, Norton, Ramsay, Stein]. Such crystals are compounds with a crystalline structure, such that due to crystal symmetry, there is no net charge accumulation on any face, under normal conditions. However, when subjected to a stress in a specific direction, the crystal gets deformed and the symmetry is upset. The positive and negative radicals of the individual molecules, in the crystal lattice take positions, which result in a net charge across two of the faces. The charge accumulation is proportional to the applied stress. Such materials can be used for strain and related sensing. Quartz and some other natural materials

exhibit the piezo-electric effect. Some synthetic piezo-electric materials are also available and in common use. Table 12.1 lists some of these along with some of the common properties. By the very nature of the phenomenon, the piezo-electric effect is present only for specific directions of applied stress and in specific directions of the output. It is maximum and in use only in specific combinations of these directions. From a knowledge of these, normally the crystal is cut into slices in specific directions and used as sensor. Conventions of identifying the axes and directions of cut are well established [Terman]. (Piezo-electric materials also exhibit the complementary phenomenon of undergoing deformation along one axis on application of a voltage across another. This is used in ultrasonic exciters, crystal oscillators *etc.* See Section 14.4.8 for a typical application). After manufacture, the piezo-element is subjected to a polarizing electric field in the selected direction. (This is analogous to polarizing a permanent magnet). It is plated on two sides with copper and other materials to form the electrodes. These offer rigid low-resistance electric contacts for use as sensor.

Observations: -

- ⇒ Piezo-electric materials have a low capacitance and a high source resistance. The induced charges across the electrode faces will not leak through internally. However even with careful construction, external leakage is enough to affect sensitivity substantially.
- ⇒ Due to the low internal capacitance and high source resistance, DC amplification is difficult. Hence, piezo-electric sensors are not normally suited to measure steady force or strain. Normally MOSFET based ultra-high input impedance type amplifiers are used with the piezo-electric sensors.
- ⇒ Now-a-days piezo-sensor manufacturers use amplifiers with high input impedance, close to the sensor as an impedance buffer. This comes as a built-in amplifier.
- ⇒ Any change in the applied stress changes the induced electric charge Q. dQ/dt can be more easily sensed than Q itself; *i.e.*, the sensor is suited to measure the rate of change of the applied force.
- ⇒ Due to the low capacitance of the piezo-electric sensor, the connector cable has a part to play in the sensor performance. The cable has a capacitance between its leads and a charge builds across it. If the cable is flexed, the induced charge here changes. This may be large enough to interfere with the sensor (called the 'Turbo-electric effect'). This is true of frequencies up to 20Hz to 30Hz.
- ⇒ Small size, high sensitivity, high linearity, wide measurement range and high frequency range are characteristic of piezo-electric sensors. Sensitivity can be as high as 1 V/με. (Contrast with the μV/με range of resistance type strain gauges). Load cells with 0.01 N full-sale reading are possible with piezo-electric sensors. (Contrast with the minimum range of 0.1 N with resistance SGs.).
- ⇒ Unit to unit repeatability is only of the order of 20 %. Hence, piezo-electric sensors are more attractive for use for relative measurements, comparison *etc.*
- ⇒ The same piezo-electric element can function as a mechanical exciter or as a strain sensor. Often both these functions are time multiplexed in

applications. Ultrasonic detectors of metal faults, level detectors *etc.*, are typical applications of this category.

Table 12.1 Properties of piezo-electric materials

Material	Crystal cut and mode	ε_r	*d*-coefficient $(C/N)\times10^{12}$	Density (kg/m^3)	Young's modulus (N/m^2) $Y\times10^{-6}$	Temp. range
Quartz	0°x-TE 0°x-LE	4.5 4.5	2.3 2.3	2.65	80	550°C
Tourmaline	0°z-TE 0°z-VE	6.6 6.6	1.9 2.4	3.10	160	1000°C
Rochelle salt	0°x-FS 45°x-LE 0°y-FS 45°y-LE	350 350 9.4 9.4	550 275 54 27	1.77	– 19.3 – 10.7	45°C
ADP (Ammonium dihydrogen phoshate)	0°z-FS 45°z-LE	15.3 15.3	48 24	1.80	– 19.3	125°C
Lithium sulphate	0°y-TE 0°y-VE	10.3 10.3	16 13.5	2.06	46 –	75°C

Note: The resistivity of ADP is in the 10^8 Ω m range; for all others it exceeds 10^{10} Ω m

12.10 Force Transducers

A variety of techniques of force sensing is possible, the most common ones being load cells using strain gauges.

12.10.1 SG Based Force Sensors

Load cells using SGs are intended to measure force by converting them into equivalent strain. The cantilever and the column type are used for force measurement. The cantilever type load cell offers high sensitivity and is suitable for forces of low levels. Due to the high stiffness and low mass, their natural frequency is inherently low. This limits the bandwidth of operation. In contrast, the column stiffness is high and its natural frequency can be one or two orders higher than that of the cantilever. The bandwidth is also correspondingly higher. These two types of load cells together can cater to a wide range of forces to be measured.

12.10.2 LVDT Based Force Sensing

The force to be sensed can be transformed into an equivalent displacement using a helical spring (or any other elastic member). The displacement can be sensed using a displacement sensor like LVDT. An insight into the limitations of the scheme can

be obtained by a simplified analysis. The equation governing performance of the scheme is

$$m\frac{d^2x}{dt^2} + d\frac{dx}{dt} + kx = F(t) \tag{12.15}$$

where

⇒ $F(t)$ is the force to be measured,
⇒ k is the stiffness of the spring,
⇒ d is the damping constant of the mass-spring system and
⇒ m is the mass of the tie-rod and armature of the LVDT.

Mass of the spring is assumed to be negligible here. For the sensing to be reliable, the term kx has to be large compared to the other two. Normally the damping will be quite small and negligible. But the term representing the acceleration of the mass m is dominant and affects performance at low-mass levels. If the spring constant k is made large, the (md^2x/dt^2) term becomes relatively small; the natural frequency ω_0, given by

$$\omega_0 = \sqrt{k/m} \tag{12.16}$$

increases; in turn the bandwidth also increases. However, the sensitivity decreases. If k is increased 4 times from a base value, sensitivity reduces to $1/4^{th}$ of its initial value; but bandwidth increases only by a factor of two. Thus at low force levels, bandwidth becomes impracticably small. The scheme finds use only for high levels of force where the LVDT size is small compared to the size of the spring and the like. In such cases, the term (Md^2x/dt^2) becomes automatically negligible.

12.10.3 Force Balance System

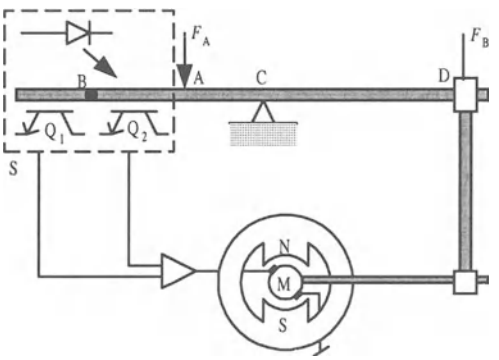


Figure 12.20 Feedback type force-balance scheme

The force balance system is a feedback transducer system (See Section 10.5) of sensing force. The system gives a current output proportional to the applied force. The operation can be understood from the schematic diagram of Figure 12.20. A balancing lever BACD has fulcrum at point C. Force to be measured F_A, is applied at point A of the lever and tends to upset the lever balance. This is sensed optically by the phototransistors Q_1 and Q_2 on either side of the beam. Light source S provides a line beam of sight falling on Q_1 and Q_2 kept on either side of the lever at

B. If the beam moves from the rest position, output of the Q_1-Q_2 pair gets unbalanced. The same is amplified and used to drive the coil of the moving coil torque motor M. It provides a torque, which balances the applied force. At balance $F_A = F_D$ (assuming that they are equidistant from the fulcrum C) and the current driving the torque motor coil, is a measure of the applied force.

Observations: -

⇒ Under steady state conditions, the lever is at the same position for all values of F_A. This reduces the loading of the source considerably. It also improves measurement accuracy.

⇒ Normally the gain of the feedback scheme is very large. Hence, the overall accuracy of the scheme is decided by the accuracy of the torque motor. Accuracy attainable (0.2 %), is one order better than that based on SGs.

⇒ The feedback loop is normally fast-acting. The small signal bandwidth almost approaches that of the SG based schemes. However, the high inductance of the torque motor limits the slew rate and hence the large signal bandwidth. By a proper design and selection of the torque motor, the system damping can be finely tuned. The temperature sensitivity of damping can be made minimal.

⇒ The force range measured and converted is low compared to the SG type transducer. The fact that the force is converted and available directly, as an equivalent current, is an advantage in process control applications.

⇒ The basic scheme shown is realized with minor variations by different manufacturers. In one common variant, the deviation of the balancing lever from the null position is sensed using an LVDT.

12.11 Tension Sensing

Many continuous processes require a moving filament, wire and the like to be maintained at a specified tension level. With a steel sheet or paper, lack of enough tension can cause slackening and coiling around rolls. If the tension is too high, the sheet may become thinner affecting product quality. A conventional approach has been to sense the level of the sheet and maintain it within two-set limits. Alternately a spring-loaded idler roller is interposed in the sheet path; its position is used as a measure of tension of the sheet or web. With the advent of SGs, more precise and faster sensing of tension is possible. One scheme is shown in Figure 12.21. A pair of cylindrical cantilevers C_1 and C_2, support an idler roller [See Section 12.8.2]. The moving sheet or web passes over this. The idler is free to rotate as the web or sheet moves. If the web or sheet tension is T, the net downward force on the two cantilevers is

$$F_T = 2\,T\cos\theta + w_I \tag{12.17}$$

where

⇒ $2\,\theta$ is the angle between the incoming and outgoing halves of the sheet or web.

⇒ w_I is the free weight of the roller.

Here the resultant force F_T is taken to be vertically downwards. Due to this, both the cantilevers are subjected to bending stresses. We can position the four SGs –

two in tension and the other two in compression – on the cantilever and form an SG bridge. The bridge output is directly proportional to F_T. Depending on the application and the positioning of the rollers, F_T can be in different directions. In each installation, the cantilever has to be precisely positioned such that SG_1 & SG_2 as well as SG_3 & SG_4, are in line with the line of action of F_T. This is to ensure SG loading in the proper direction.

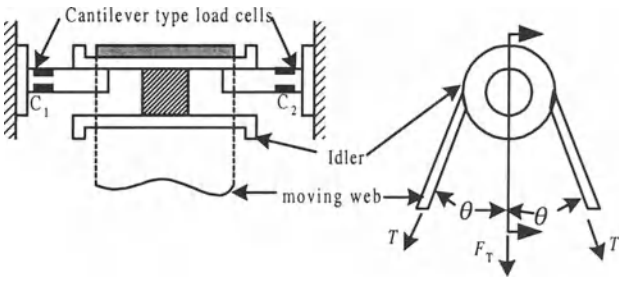


Figure 12.21 Sensing web tension using load cell

12.12 Acceleration Transducers

Acceleration-sensing has two areas of application – vibration and related measurements and acceleration of vehicles such as aircraft, submarines, space vehicles and the like [Norton, Trietley, Stein]. One inherent limitation with the sensing is the absence of an absolute frame of reference for the displacement concerned. The measurement is invariably carried out in an indirect manner. The principle can be understood from Figure 12.22. x_i represents the displacement; the corresponding acceleration $\ddot{x}$ is to be sensed. m is a proof mass connected to the body of x_i through a spring of proportionality constant k. Viscous damping is provided with damping constant d. x_o represents the relative displacement of the proof mass.

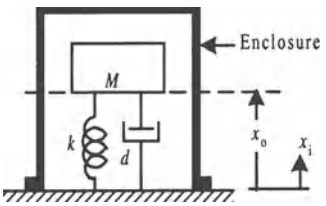


Figure 12.22 Principle of the accelerometer

The relation connecting x_i and x_o is

$$m\ddot{x}_o + d\dot{x}_o + kx_o = m\ddot{x}_i - ma_i \tag{12.18}$$

Taking Laplace transform and rearranging we get

$$\frac{x_o}{a_i} = \frac{1}{s^2 + 2\xi\omega_0 s + \omega_0^2} \tag{12.19}$$

Where

$$2\xi\omega_0 = \frac{d}{m} \tag{12.20}$$

$$\omega_0^2 = \frac{k}{m} \tag{12.21}$$

and a_i is the acceleration to be sensed.
Equation 12.19 shows that if the damping is chosen close to unity, x_o can be seen to be proportional to the input acceleration for $\omega < \omega_0$.

Accelerometers are mostly of the deflection type or of the null balancing type. The accelerometers for vibration are universally of the deflection type while those used for sensing vehicular acceleration, can be of either type. As mentioned earlier, the null balance scheme has a comparatively higher level of accuracy [Broch, Dally, Rangan *et al.*].

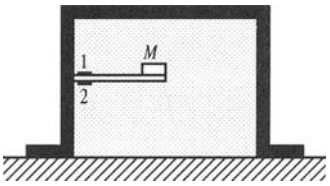


Figure 12.23 Accelerometer using flexure beam and SGs; 1 & 2 are the SGs.

The deflection type uses a proof mass supported on a thin flexure beam. Necessary damping is provided by enclosing this and filling it with silicone oil (See Figure 12.23). Bending of the beam is sensed using SGs on either side. The beam essentially acts as a cantilever-type load cell. Semiconductor SGs with their large GF and small size are ideally suited for accelerometers. The high sensitivity allows low proof mass to be used. The natural frequency and bandwidth also increases. An accelerometer with ± 10g full-scale level, can have 500 Hz bandwidth with 10 mV/g sensitivity. Use of stiffer beams, increases the acceleration range and bandwidth. The output signal swing reduces. A 500 g unit can have 3kHz bandwidth and give 0.2 mV/g sensitivity. With such reduced swing, fluid damping is not effective. Only the inherent damping of the sensor is present. This being low, the signal bandwidth is limited to about 20 % of ω_0 (may extend up to 50 kHz). Such tri-axial Accelerometers are available as single units – they provide three outputs representing acceleration along the three independent axes simultaneously [Khalsa and Ramsay(1996)].

Observations: -

- ⇒ SG based accelerometers of wider bandwidths are available. But the piezo-electric type is more commonly used in this range.
- ⇒ The SG type accelerometer senses the strain of the flexure member. Alternatively the displacement of the flexure member (at the proof mass – the displacement being maximum here), can be measured to sense acceleration. The displacement can be sensed using resistance potentiometer, LVDT or a differential capacitance transducer. Potentiometer sensing offers lowest cost and lowest bandwidth. LVDT and capacitance transducers offer higher bandwidth at higher cost – both increasing in that order. The LVDT

sensing is provided as an extension. In contrast, with differential capacitance sensing, the outer electrodes can be along the housing and the middle one made integral with the proof mass. This makes the sensor compact and robust. Signal processing circuits used with R, C and L type accelerometers are all similar to those discussed in respective sections.

⇒ The null balance type accelerometer is similar in principle and construction to the null balance type force transducer (See Section 12.10.3). The proof mass and flexure are added to translate the acceleration to an equivalent force.

12.12.1 Piezo-Electric Accelerometers and Vibration Sensing

High sensitivity, wide bandwidth and relatively small size are characteristic of the piezo-electric sensors. These make them ideally suited for vibration sensing – the small-size vibration meter has become the exclusive domain of piezo-electric sensors. A typical construction is shown in Figure 12.24. The principle of operation has been explained already. Normally, the proof mass has a steady applied compression. This ensures the sensor to be always in compression throughout its active range (It prevents the sensor going 'slack' during operation). The steady output voltage developed due to the initial stress, leaks off and does not affect the operation. Vibration sensors intended to operate for ambient temperature < 120 °C, have a built-in pre-amplifier stage. It consists of a MOSFET with a suitable gate resistor (R_g). Only the drain and the source of the sensor are connected through a coaxial cable. Typical recommended first amplifier stage is as shown in Figure 12.25. V_s is the supply voltage from which a constant current (typical recommended value – 2mA) is derived and forms the drain load. The output at the drain is capacitively coupled. At point A, the output impedance of the sensor is typically 1 kΩ. This makes the output practically independent of the cable length. Capacitance of the sensor C_p in series with the gate resistor R_g, decides the lower cut-off frequency of the sensor (10Hz typical). The higher cut-off frequency is decided by the sensor resonant frequency. The sensor damping being low ($\xi = 0.01$), the higher cut-off frequency is of the order of ($\omega_0/5$) where ω_0 is given by Equation 12.21.

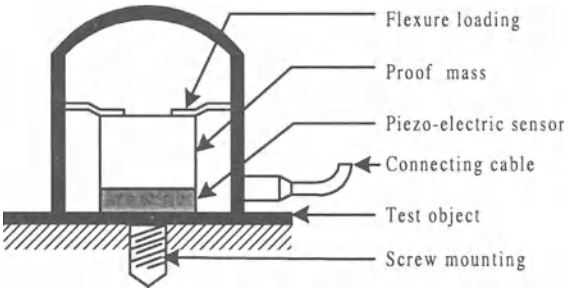


Figure 12.24 Piezo-electric accelerometer

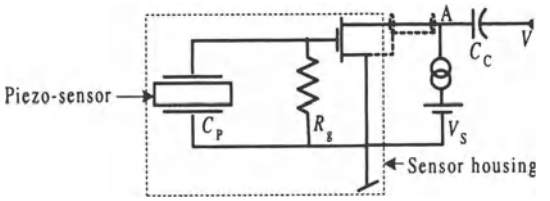


Figure 12.25 Piezo-electric accelerometer sensor and circuit

With a source resistance of 10^9 Ω for the sensor, R_G is of the order of 10^{11} Ω. The corresponding Johnson noise decides the 'floor noise' voltage level of the sensor. The typical threshold can be taken as 2 to 3 times this. With V_s as the supply voltage, the bias voltage of the drain can be taken as $V_s/2$. The maximum signal swing is typically

$$0.8 \times (V_s/2) = 0.4\ V_s$$

Example 2

Floor noise level = 30 μ V rms [Calculated from R_g and the operating temperature]

Minimum threshold sensed = 3×30 μV

= 90 μV

Supply voltage = 24 V

Bias voltage of point A = 12 V

Maximum output swing = 12× 0.8 = 9.6 V

With sinusoidal test input = maximum output

= 0.707× 9.6 = 6.8 V rms

Maximum dynamic range = $\frac{6.8}{90\times10^{-6}}$

= 76×10^3

= 78 dB

Let the sensitivity of the sensor = 10 mV /g

Minimum acceleration sensed = $\frac{90\times10^{-3}}{10}$

= 0.009g rms.

Maximum acceleration sensed without distortion = 680 g rms.

Provision of the MOSFET pre-amplifier stage, limits the maximum ambient temperature to 120 °C. However, the piezo-electric sensor *per se*, can safely function up to a temperature of 300 °C ambient. When designed to sense vibration at such a high temperature, the sensor output is brought out directly through a suitable cable. At a close enough distance, the signal is amplified using a charge amplifier designed around a high input-impedance MOSFET input type opamp (See Section 4.7). The resistor R_g provides bias-current and avoids amplifier saturation; it also restricts the cut-off frequency. The screen of the cable is grounded and a full

guard ring provided around the input stage to minimize the effect of leakage and stray capacitances (Figure 12.26).

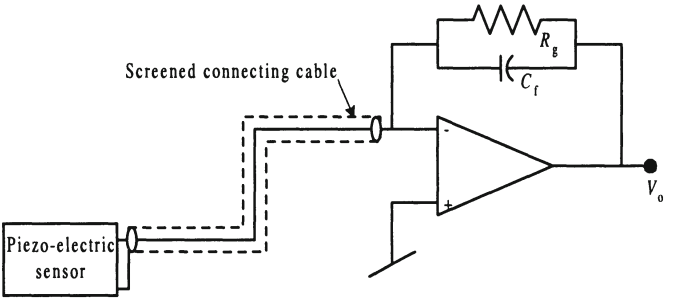


Figure 12.26 Piezo-electric acceleration sensor with charge amplifier

Observations: -

⇒ With piezo-electric vibration sensors, there is a trade-off between sensitivity and bandwidth. Increase in the size increases the sensitivity and reduces the resonant frequency (and hence the bandwidth). A sensor intended for vibration sensing can give 1000 pC/g sensitivity with 7 kHz as upper cut-off frequency. Another with 250 kHz as cut-off frequency has a sensitivity of only 0.04 pC/g. This is suited for shock sensing.

⇒ The cross-axis sensitivity of piezo-electric sensors is higher than that of other strain sensors; the disparity is typically 2 % to 4 %.

⇒ The low mass of the sensor, adds minimum dead weight to the test object. Corresponding reduction in the resonant frequency of the test object is minimal.

⇒ Sensitivity of piezo-electric sensors reduces with increase in the operating temperature. The reduction is typically 1 % for every 10 °C rise in temperature.

⇒ Sudden change in the ambient temperature (thermal shock), results in a spurious output of the sensor. This can be due to two reasons: Differential mechanical stress in the vicinity of the sensor due to the sudden temperature changes and electrical output due to any thermal gradient in the piezo-electric crystal (pyro-electric effect). Normally the output due to thermal shocks has a very low bandwidth. It lies below the lower cut-off frequency of the sensor and its effect is often negligible.

12.13 Torque Transducers

Static torque or turning moment can be directly converted into equivalent force through simple linkage mechanisms and sensed as such. Torque transmitted by rotating shaft, requires schemes that are more involved. Two approaches are in vogue. Measurement of the reaction force on a stationary support and direct measurement of torque by interposing a torque transducer directly on the transmission shaft.

12.13.1 Reaction Force Sensing

Torque is transmitted through a rotating shaft from a prime mover like a generator, engine *etc.*, to a load. The source as well as the load exerts a reaction force on the respective supports. This can be measured and multiplied by the radius of action of the reaction force to compute the torque transmitted. The measurement can be carried out at the prime mover end or the load end. Figure 12.27 shows one scheme of sensing. The prime mover is hinged on one side at fulcrum L and on the other side, an extended arm rests on a load cell. The weight of the system is supported at the bearings. When balanced, in the absence of torque transmission, the force on the fulcrum as well as the force exerted on the load cell are zero. As the shaft rotates and transfers a torque, the reaction force F exerted on the load cell is sensed by it. With the compression-type load cell, the sensing is effective only for the direction shown.

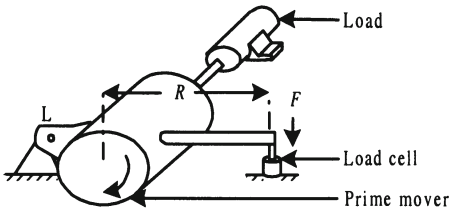


Figure 12.27 Torque transducer using load cell to sense the reaction force

Observations: -

⇒ The load cell can be changed to the compression and tension sensing type and the unit made bi-directional in operation.

⇒ The sensing can be done at the load end or the prime mover end. The respective torque values differ only by the bearing friction torque.

⇒ Dynamic imbalance, vibration *etc.*, reflect as corresponding changes in the reaction forces. They can have enough nuisance value *vis-à-vis* the desired measurement. Often, a good LPF is to be made part of the signal processing circuitry to suppress them (In fact, by a proper analysis of the fluctuations in the reaction forces, meaningful information regarding imbalance, vibration and the like can be obtained.).

⇒ The scheme as shown here can be used only with low power transmission. As the torque level increases, more elaborate schemes of support and sensing, are called for. Any symmetrical structure can be used to support the prime mover stator. Reaction-forces on all the direct-load-carrying members, are to be measured.

One simple scheme is shown in Figure 12.28. The SG positions are marked 1,2,3 and 4. These four together can form the SG bridge. The scheme can sense torque for either direction of rotation. In arrangements of this type, three things are to be ensured: -

⇒ The radial distance of all the SGs from the shaft axis must be equal.

⇒ The supports (four in number here) should be such that their longitudinal axes meet on the shaft axis.

⇒ No load-shunt is present.

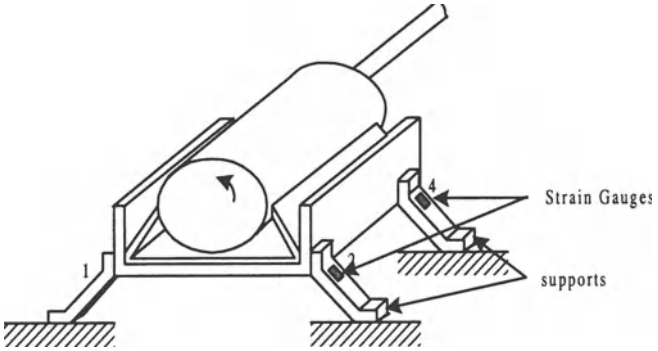


Figure 12.28 Torque transducer, which senses reaction force at the supports

12.13.2 Direct Torque Sensing

When a shaft transmits a torque along its axis, it undergoes deflection (See Appendix D). The corresponding principal axes are inclined at 45° to the shaft axis on either side. The stress along one is compressive while that along the other is tensile. These two can be sensed by respective SGs (Figure 12.29). SG rosettes suitable for this measurement are available. Normally two SGs are fixed on one side while the other two are kept at the respective diametrically opposite points.

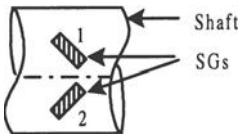


Figure 12.29 Torque sensing with SGs mounted directly on the shaft

Some manufacturers prefer square shaft sections to circular. With the square section, the SGs can be positioned precisely more easily. The level base is also easier for bondage. Further, the far edges of the rectangular edges are ideally stress-free and are convenient locations for soldering, termination *etc.* Regarding bridge excitation, three possibilities exist: -

⇒ The bridge is supplied power through a pair of slip rings. Another pair is used as leads for the bridge output. With such four insulated slip rings, the SG bridge can be excited and used in the same manner as the bridges in load cells so far. With the use of best brush and slip ring combination, the maximum possible speed of shaft, is 8000 rpm. Bridge accuracy and sensitivity are practically on par with other types of load cells.

⇒ The power is transferred to the load cell through a transformer. The core is specially built and it remains stationary. The primary and secondary windings are concentrated coils – one below the other {See Figure 12.30). The core has enough air gap to allow structural support to the secondary from the shaft side. The secondary output is used to excite the bridge. Such AC excitation of the bridge is in the 3kHz to the 4kHz range. The output side of the bridge is an identical transformer. The primary side is excited by the

bridge output on the rotor side; the secondary winding is stationary. The emf induced in it, is a measure of the torque transmitted. The electrical performance of the scheme is on par with that of all the stationary load cells: It is somewhat better than the previous scheme with rotating contacts. Due to the absence of moving or rubbing contacts, the unit is capable of operation up to 30,000 rpm. that is More involved nature of the construction and the fact that it is an AC instrumentation scheme, make it costlier than the previous one.

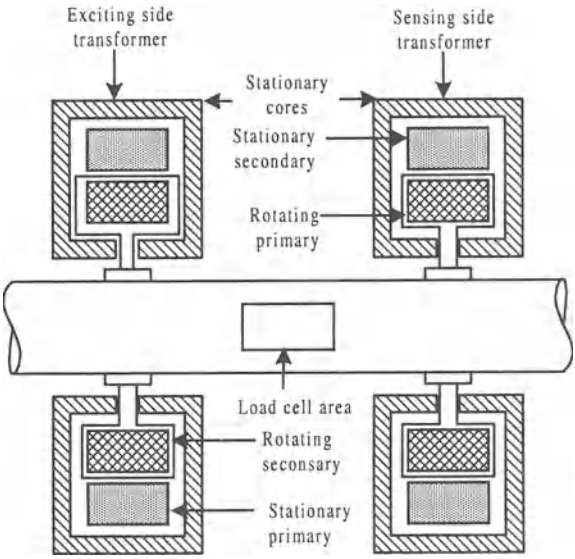


Figure 12.30 Non-contact type torque transducer

⇒ A third alternative is to use a battery power supply housed in the rotor itself. The battery powers the bridge. The bridge output can be modulated on a carrier (preferably FM) and 'broadcast' from the rotor. A separate FM demodulator on the stator recovers the base band signal. Such isolated schemes are often prohibitively costly. When a number of variables are to be sensed on the rotor side and the relevant information made available at the stator, a full fledged telemetry scheme may be implemented. This may prove to be an economic solution.

13 Process Instrumentation I

Temperature

13.1 Introduction

Temperature is the most widely measured quantity in process industry. Its wide range of application and varied environment of operation, call for a variety of engineering adaptations of the temperature transducer [Magison, McGee, Quinn]. Nevertheless, the basic methods of sensing which have proved to be popular, are only a few. As with other physical variables, exotic and novel methods of sensing have been suggested. They are either restricted to highly specialized *niche* areas or of limited utility. Bimetallic strips and thermistors have been in wide use for local indication, compensation and protection applications. They are used to sense temperature and temperature-changes and effect a local action. These uses are characterized by simplicity and low cost at the expense of accuracy and flexibility. Barring these, thermocouple remains the main temperature sensor accounting for about half of all applications. Resistance Thermometer Detectors (RTD) form about half of the rest (*i.e.*, about 25% of all the applications). Thermistors account for about 10% to 15% of all applications. Semiconductor sensors and different types of radiation pyrometers span most of the rest.

13.2 Temperature Scale

Units for the fundamental physical quantities – length, mass, time (and current) – have been defined and refined by different International committees. All other quantities have units derived from these. Further in every case, one can multiply and divide the basic specified unit to measure the different quantities to different scales. Temperature remains the odd one out here. One cannot use a defined unit in multiples or sub-multiples for scaling. A full 'temperature scale' has to be defined. The Kelvin scale affords an elegant way of doing this without having recourse to arbitrarily defined unit intervals. This has been adopted for the basic temperature scale.

The classical Carnot cycle forms the basis of the Kelvin scale. Consider two infinite reservoirs of heat at temperatures T_1 and T_2, with $T_1 > T_2$. Let the first reservoir transfer some heat energy of Q_1 to the second and the second return an amount of energy Q_2 to the first reservoir, the two transfers conforming to the Carnot cycle. Then the two temperatures are related by

$$\frac{T_1}{T_2} = \frac{Q_1}{Q_2} \tag{13.1}$$

T. R. Padmanabhan, *Industrial Instrumentation*
© Springer-Verlag London Limited 2000

This is valid for any unit of temperature and energy. A series of International committees from 1927 onwards, have been defining and refining the temperature scale., the last one being in 1990. The International temperature scale – ITS-90 – as adopted in 1990, is characterized by the following: -

⇒ Kelvin scale forms the basis for the definition.

⇒ The 'triple point of water' is the temperature reference point. It is assigned the value 273.16 K. As of now, the same is reproducible with an accuracy of 0.0005 K.

⇒ The triple point of water has a temperature value of 0.01 °C in the Celsius scale.

⇒ The interval from the 'Ice point' to the 'Boiling point' of water is divided into 100 equal parts in the Kelvin scale. With this we have
The ice point temp = 273.15K (0 °C)
Boiling point of water = 373.15 K (100 °C)
Note that these two temperatures are not reference points. They are used to define the unit temperature interval in conformity with the Celsius scale. With this
- One degree interval in Kelvin scale = One degree interval in Celsius scale
- The two scales are related such that
$T = t + 273.15$
where
- T is the temperature in K and
- t is the same temperature in °C.

⇒ Practical realization of the temperature scale is done to conform to the Kelvin scale as closely as possible. It is done in the following manner:-
- A set of 17 temperature reference points have been defined (See Table 13.1 at the end of the chapter)
- The range 0.65 K to 5.0 K is defined in terms of the vapour pressure-temperature relations of 3He and 4He.
- The range 5.0 K to 24.5561 K is defined in terms of Helium gas thermometers.
- The range 13.8033 K to 1234.931 K is defined in terms of platinum resistance thermometers.
- Beyond 1234.93 K, Plank's radiation law is used for definition.
- In the intervening intervals, the thermometers specified are used after calibration within the neighbouring reference points from the 17 mentioned above.

For details, refer ITS90 [Preston-Thomas].

13.3 Conventional Methods of Temperature Sensing

Bimetallic strips, gas thermometers (of constant volume and constant pressure types), and liquid filled thermometers have been in wide use for decades. They provide accuracy down to 0.5%. They are mostly for indication purposes.

Construction is highly standardized and cost-effective. Size, limited ranges and lack of flexibility have restricted their utility. Now, all of them are used essentially for simple localized indications only. They are no longer considered as sensors for instrumentation.

13.4 Resistance Thermometer Detectors (RTD)

Resistance of all pure metals changes with temperature, in a highly predictable and repeatable manner. RTD makes use of this change in resistance, to measure temperature. For any resistance wire of a metal, over a restricted temperature range we have

$$R_1 = R_0 [\, 1 + \alpha (T_1 - T_0)] \qquad (13.2)$$

where

⇒ T_1 and T_0 are two temperatures. T_0 is normally taken as 0°C (Reference temperature).

⇒ α is the temperature coefficient of resistance

⇒ R_0 is the resistance at temperature T_0 and

⇒ R_1 is the resistance at temperature T_1.

For all metals α lies in the 0.35 % /°C to 0.60 %/° C range. It reduces with increase in the impurity level of the material (In fact the ratio R_{100}/ R_0 is often taken as a yardstick of the purity of the metal). If the ambient temperature T_0 is taken as reference, from Equation 13.2, we get

$$\Delta R = R_0 \alpha \Delta t \qquad (13.3)$$

Where

⇒ Δt is the rise of temperature of the resistance material above ambient and

⇒ ΔR is the increase in R from R_0.

The linear relationship between Δt and ΔR exists only over a restricted temperature range. For larger values of Δt, a polynomial relationship is used.

$$R_1 = R_0 [\, 1 + \alpha_1 (\Delta t) + \alpha_2 (\Delta t)^2 + \alpha_3 (\Delta t)^3 + ...] \qquad (13.4)$$

Normally R_0 is taken at 0°C and Δt is considered as temperature change above 0°C. Coefficients α_1, α_2, α_3, ... *etc.*, are specified for each material separately. Second to fourth degree polynomials are used over wider temperature ranges. ΔR of Equation 13.4 is converted into an equivalent voltage in two ways: -

13.4.1 Unbalanced Wheatstone Bridge

The unbalanced Wheatstone bridge of the single sensor type, converts ΔR into an equivalent output voltage (See Section 2.2). This is to be amplified – using an instrumentation amplifier. The configuration retains linearity with respect to ΔR, only over a small range. Either the use has to be restricted or the output suitably linearised. Unlike many other types of Wheatstone bridge sensors, with RTDs, R varies over a wide range. For example, over 100 °C range, ΔR is about 40 % of R. The corresponding non-linearity in the input-output characteristic is not negligible.

13.4.2 Direct Conversion

Different configurations all formed around opamps, are possible for the direct conversion of ΔR into a corresponding voltage. One common configuration is shown in Figure 13.1. R_T is the RTD here and all other resistors are fixed resistors. The current through R_T is kept fixed at $V^+/2R$. When $R_T = R$, $V_o = 0$. For other values of R_T

$$V_o = -\frac{V^+}{2R}(R_T - R) \tag{13.5}$$

Thus, we have a linear relation between V_o and change in the RTD resistance value. The non-linearity in the characteristic is separately linearized when necessary. Typically, an approach based on the LUT is common (See Section 9.2). Resistance values of RTDs follow a certain standard – 100 Ω is the most common. 50 Ω, 200 Ω, 500 Ω, 1000 Ω and 2000 Ω are also in use, though they are less common.

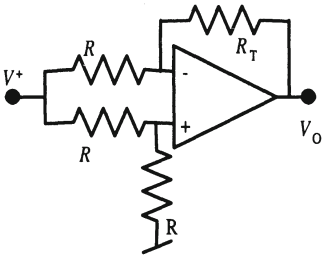


Figure 13.1 A commonly used configuration to convert resistance changes into equivalent voltage

Observations: -

⇒ The current through the RTD causes power dissipation and corresponding 'Self-heating' leading to errors. The self-heating error is of the order of 0.5 °C/ mW in free air (most common). When airflow around is at 1m/s, the temperature error reduces to 0.05 °C/mW.

⇒ The RTD wire has to be pure and stress-free to get good repeatability of measurement. For stress release, after formation of the sensor *in situ*, it is annealed at a pre-determined higher temperature.

⇒ The RTD wire in bifilar form may be loosely hung in place as a coil in a former. This minimizes stress and increases the exposed area. The self-heating error reduces in turn. The bifilar form of winding reduces the coil inductance. The increased size and the delicate nature of construction make it inflexible. Response time also increases. Such RTDs are mostly used in laboratory or in investigative work, which call for precision. More often, the RTD is formed as a film resistance deposited on an insulation base and laser trimmed. Then it is hermetically sealed. Such sealed outfits are formed on glass, alumina, quartz etc. They have small size and rigidity. The sealed construction increases RTD life. However, the confined nature of the RTD, causes a small self-heating error.

⇒ The RTD lead wires are subjected to different temperatures, depending on the application environment. Resistance of the wire and change in resistance due to such temperature variations can lead to errors. Such errors are minimized using 3-wire (or sometimes 4-wire) configurations (See Section 10.2.2).

Different RTD materials and their characteristics are briefly discussed in the Sub-sections that follow.

13.4.3 Platinum

Platinum (referred to as Pt in short form) can be purified and used with comparative ease. The wide temperature range, high corrosion resistance, high stability and repeatability of the characteristic have made platinum, the most commonly used RTD material. For pure platinum, α is taken as 0.385%. α for Chemically pure platinum, can attain a value of 0.392 %. These values are in the 0 °C to the 100 °C range; the departure from linearity is 0.2 % in the 0 °C to 100 °C range. It increases with the range of use and in the 0 °C to 800 °C range, it is 1.2 %. A more precise relationship connecting the resistance and temperature is

$$R_t = R_0 + R_0\alpha\left[t - \delta\left(\frac{t}{100} - 1\right)\frac{t}{100}\right] \tag{13.6}$$

where

⇒ $\alpha = 0.00392$ and

⇒ $\delta = 1.49$

This relation, known as Calendar relation, is valid for t > 0 °C. ITS90 lays down clear-cut procedures to obtain the coefficients of higher degree polynomials of the above type. These are obtained using interpolation formulae and measured resistance values at reference points. Use of such polynomials, is restricted essentially to calibration work.

Pt RTD wire supported on mica arbour can work up to 600°C. Beyond that mica swells, embrittles and gives off the water of crystallization. Above 600 °C, quartz is more common as a base for Pt wire support – its stability and mechanical strength favour its use. Such RTDs can be used up to 1300 °C. Embedding the Pt wire in pure alumina, makes it robust and extends its higher temperature limit to 1600 °C. At the lower side, Pt RTDs can be used down to –260 °C. Since the RTD resistance drops down to very low values at these temperatures, separate low resistance measuring circuits have to be used for signal processing.

13.4.4 Copper

Copper can be used as an RTD from –200 °C to +120 °C. Enameled copper wire may be used directly for this. The substantially lower resistivity of copper, which is 16 % of that of Pt makes the RTD size large. With Silicone or PVC insulation, its use can be extended up to 180 °C. The temperature coefficient of resistance of copper, is 0.426 % in the 0 °C to the 100 °C range and remains reasonably constant over the full measuring range. Earlier copper RTDs were commonly used up to 120 °C. However, the present tendency is to use Pt over this range as well.

13.4.5 Nickel

Nickel can be used as an RTD up to 200 °C. Its resistivity is 61 % of that of platinum and size-wise, it compares well with Pt. Nickel has the highest α value (0.67 %) amongst all the metals and hence offers maximum sensitivity. The resistance versus temperature characteristic is non-linear. The temperature coefficient is very sensitive to impurities. The repeatability is poor. Nickel is easily oxidized and it is no longer in common use as an RTD material.

13.4.6 Other RTDs

Balco (an iron-nickel alloy), with a temperature coefficient of 0.52 %, tungsten (temperature coefficient of 0.45 %), iridium and molybdenum can also be used as RTDs. Molybdenum and tungsten are suited for temperatures up to 1200 °C. However, as mentioned earlier, Pt has become the essential and the sole RTD element in wide use

13.5 Thermistors

Thermistors are sintered ceramics. Oxides of manganese, cobalt, nickel and other metals, are mixed in well-defined proportions and sintered. Close control of the mix proportion and sintering process, is necessary to ensure repeatability of the characteristics. Repeatability attainable in manufacture is only ~10 %. Closer tolerance is obtained more often by measuring and sorting. Thermistors in bead form hermetically sealed with glass offer stable and reliable performance. These also have good mechanical strength and heat resistivity. Epoxy coated versions in polyimide tubes, are suited for operation at lower temperatures. Thermistors are also available as discs and chips – their stability and reliability is not as good as the hermetically sealed beads. Thermistors of this type have a negative temperature coefficient (NTC). Barium titanate based positive temperature coefficient (PTC) thermistors are also available but are not so common for sensor applications.

NTC thermistors have a large temperature coefficient – typically, ten times that of RTDs. The resistance decreases tenfold as the temperature increases by 70 °C (With RTDs the corresponding change in resistance is ~40 %). This high temperature sensitivity can be put to advantage in many respects. Further, they can be made with much higher resistance values compared to RTDs – typically, resistance values at 25 °C, are in the 2 kΩ to the 1.5 MΩ range. This makes the relative lead-resistance values small. The error due to the leads becomes negligible. These are two conspicuous advantages of NTCs. On the flip side, two disadvantages make them unsuitable for more general use: -

⇒ First the self-heating effect and the resistance due to the self-heating is large. This is mainly due to the large value of NTC. Typically the power dissipation constant is 2mW/°C in still air. When submerged in a liquid, the power dissipation can increase 5 to 6 times.

⇒ Second, unit to unit repeatability is not good - despite tight control in the production process.

Two expressions are in common use to characterize the resistance versus temperature characteristic of thermistors.

$$R_2 = R_1 \exp\left[\beta\left(\frac{1}{T_2} - \frac{1}{T_1}\right)\right] \tag{13.7}$$

Where

⇒ T_1 and T_2 are temperature values in Kelvin

⇒ R_1 and R_2 are the resistance values at the temperatures T_1 and T_2 respectively and

⇒ β is a constant depending on the thermistor. β lies in the 3000 K to 5500 K range.

The Steinhart-Hart equation – an empirical relation – describes the R-T characteristic quite closely over the working range. It has the form

$$\frac{1}{T} = a + b\ln R + c(\ln R)^3 \tag{13.8}$$

Here a, b and c are constants dependent on the thermistor. Both the relations relate $\ln R$ to $1/T$. The first one requires one parameter to be defined in terms of two resistance measurements. The Steinhart-Hart equation, requires three such measurements (preferably at equal intervals of $1/T$) to be done to define the a, b and c constants. NTC thermistors are used over the –50 °C to +500 °C range. Some versions cover the –50 °C to the 200 °C range while the others cover the other extremes of –20 °C to +500 °C range. Direct use of NTC thermistors for temperature sensing, is limited to low-cost applications which do not call for high accuracy. Typically one NTC may be employed for temperature sensing over 0 °C to 100 °C range with an accuracy of ±0.5 %. The sensor is re-calibrated whenever the thermistor is changed.

NTC thermistors are in wide use for temperature compensation and in a variety of sensors and other applications which use the NTC characteristic in an indirect manner.

13.5.1 Temperature Sensing Using Thermistors

Two approaches of using thermistors for temperature sensing are common; the first is direct and simple. A thermistor forms the temperature sensor. The sensor output is available as a voltage from an unbalanced Wheatstone bridge or a difference amplifier configuration using a constant current supply. In either case, the output voltage is related to temperature change in a non-linear manner. Through an ADC it is converted into an equivalent digital number and the temperature read from a ROM-based LUT (See Section 9.2). Here the range is typically limited to 100°C. The thermistor used as sensor is usually not interchangeable. If a change is inevitable, the manufacturer recommends the thermistor type to be used and specifies selection of a piece with a specified numerical value of resistance.

The second approach is to have a much more elaborate transducer with on-line calibration. The scheme is shown in block diagram form in Figure 13.2. The functioning is broadly as follows: -

⇒ The thermistor is connected in place.

⇒ The reference temperature source (as a bath / thermo-well) is actuated, with the RTD and thermistor sensing the same temperature.

⇒ Temperature values as measured by the RTD and the connected bridge, are used to measure the thermistor resistance at specific temperature values.
⇒ A program resident in the PC calculates the β of Equation 13.7, or the a, b and c coefficients of Equation 13.8. This completes the calibration.
⇒ Whenever the thermistor is used for temperature measurement, the measured resistance value is used and the temperature calculated using the relevant equation and the constants decided during calibration.

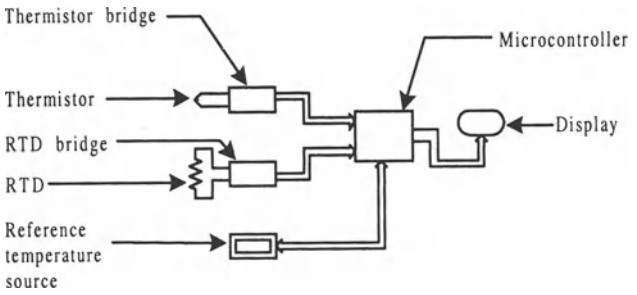


Figure 13.2 Scheme of automatic calibration and display of temperature with thermistor sensor

The large NTC value of the thermistor allows resolution of 10^{-4} °C to be obtained. However, the accuracy is limited by the accuracy of the RTD used as well as that of the on-line calibration. With the use of RTDs calibrated in Standards Laboratories, manufacturers claim an accuracy of 0.005 °C with this approach.

13.6 Semiconductor Temperature Sensors

Consider two identical transistors with collector currents I_1 and I_2. The difference between the respective base-emitter voltages is [See Section 6.3.3]

$$\Delta V_{BE} = \frac{kT}{q} \ln \frac{I_1}{I_2} \tag{13.9}$$

The difference voltage is directly proportional to the absolute temperature of the transistors. Such a voltage difference is converted into an equivalent current in an IC. The IC draws a current from the supply, which is proportional to the absolute temperature of the IC.

AD590 and AD592 are typical of such devices - they are two terminal devices. Over a specified range of applied voltages, the current drawn by the device is dependent on the absolute temperature only. Typical characteristics are shown in Figure 13.3. As long as the voltage across the device is greater than 5 V, the current is independent of the voltage. Further, as the device temperature rises, the current rises proportionately. Manufacturers trim the characteristic such that at 25 °C (298.2 K), the nominal current is 298.2 μA. Further the nominal temperature coefficient of current is 1 μA/K. This forms a compact and cost-effective sensor, over the –50 °C to +150 °C temperature range. Due to the trimming, unit-to-unit repeatability is ±0.1 °C at 25 °C. However, the μA/K slope may change from unit-

to-unit. The corresponding calibration error may extend to ± 5°C. This has to be trimmed by suitable circuitry.

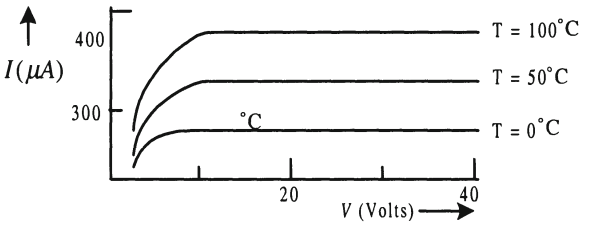


Figure 13.3 V-I characteristic of a typical semiconductor temperature sensor

Semiconductor temperature sensors find wide application up to 150 °C. They are suitable for low-cost temperature sensing with limited accuracy. A typical application circuit is shown in Figure 13.4. A sensor IC_1 is connected in series with resistance R_1. R_1 is selected to provide a convenient range for V_s over the operating range of interest. V_{Ref} is a constant voltage reference source supplying potential divider comprising resistance R_2 in series with potentiometer P_1. V_R – the output of P_1 – is adjusted such that V_o is zero at the desired low end of the scale. Thus V_R nullifies the effect of the standing current through IC1 and provides a convenient zero. R_G is the gain adjustment resistance of the instrumentation amplifier. It ensures a desirable gain for the unit. Further, by an adjustment, one can compensate for the tolerance on the sensor gain in μA/K. With these measures, overall accuracy of 0.2 °C can be achieved for the scheme. However, this requires calibration on a unit to unit basis.

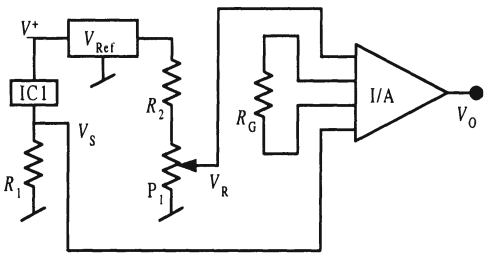


Figure 13.4 Typical application of a semiconductor type temperature sensor

Observations: -

⇒ A 1V change in the supply results in a 0.5μA change (typically) in the device current. This is equivalent to 0.5°C of error. Hence, it is necessary to stabilize the supply voltage.

⇒ It is desirable to keep the sensing resistor R_1 as low as possible. With R_1 = 1 kΩ,

drop across R_1 at 25°C = $298.2\times10^{-6} \times 10^3$ V
= 0.2982 V.

A 1°C change in the device temperature, causes 1 mV change across R_1. Correspondingly, the device voltage changes by 1 mV. This causes a

temperature error of ±0.005 °C, which is negligible. However, if R_1 is increased to 100 kΩ, the corresponding error increases to ±0.5 °C – the same order as the device accuracy.

⇒ To a first order, the operation is independent of the lead-resistance values of the device. This is a direct extension of the above argument.

⇒ The device characteristic is linear throughout the operating range.

⇒ The device is in wide use for cost-effective temperature indicators, for thermal protection (of electrical and other equipment) and for cold junction compensation for thermocouples.

ICs that have the additional biasing and amplifier that are built-in, are also available. LM35 series of National Semiconductors, is a typical example. It has a sensitivity of 10 mV / °C of change in temperature. These provide a voltage type output, a convenient value of sensitivity and output referred to the Celsius scale rather than the Kelvin scale. These are more convenient to use in certain applications.

13.7 Thermocouple Based Temperature Sensing

Thermocouples are the most widely used temperature sensing devices in the industry. Their capacity to sense without any external source of power, excellent repeatability at reasonable cost and easiness of manufacture may be primarily responsible for this.

13.7.1 Basics of Thermocouples

Any metal or alloy has a number of electrons in the conduction band. The number available, changes with temperature. Consider a junction of two such dissimilar materials at any temperature. The difference in the concentration of electrons at the junction causes a diffusion of electrons across the junction. Due to this, a potential difference is built across the junction. This forms the contact potential. Consider the wires of two such materials P and Q joined to form junctions at A and B (Figure 13.5). With both the junctions at the same temperature, the potential differences across them are equal in magnitude but opposite in direction. There is

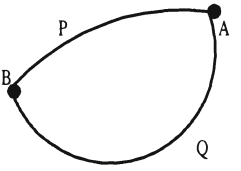


Figure 13.5 Thermocouple loop with two dissimilar materials

no net emf acting in the loop. If the junction A is heated, due to the difference in the nature of the change of the characteristics of the two materials with temperature, the potential difference across junction A, changes. This causes a net emf in the loop. This is the 'Thermo-emf'. The pair of wires P and Q joined at A is the thermocouple with A as the thermocouple junction. Junction A is called the 'Hot

Junction' and B the 'Cold Junction' of the thermocouple. One specific characteristic of all metals and alloys, is the excellent repeatability of the thermo-emf versus temperature characteristic. Further, it is mostly a monotonic function of the temperature difference. These two together make any thermocouple a good temperature sensor.

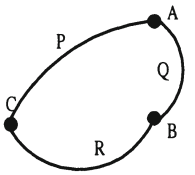


Figure 13.6 Thermocouple loop with three dissimilar materials

Consider wires of three different materials – P, Q and R – joined end to end at junctions A, B and C to form a loop as shown in Figure 13.6. If all the three junctions A, B and C are at the same temperature, electrodynamic equilibrium dictates that there be no energy transfer and hence no current in the loop. Hence, the net emf acting in the loop is zero; *i.e.*, the sum of the three thermo-emfs at junctions A, B and C is zero.

$$e_{PQ} + e_{QR} + e_{RP} = 0$$

or

$$e_{PQ} = -(e_{QR} + e_{RP})$$

Here e_{PQ} *etc.*, are the thermo-emfs between concerned materials. Thus, if a metal or alloy R is connected between two others P and Q, the thermo-emf developed and available at the free ends of P and Q, is the same as that obtained if the wire R is absent. This is true provided the junctions formed at the two ends of R are at the same temperature as the junction of P and Q taken alone.

Based on the above discussion, the laws of thermocouples may be stated as follows: -

⇒ In any closed loop of a homogeneous material, differences in the temperatures at different points, do not cause any thermo-emf or loop current.

⇒ In any loop of wires of two or more materials, net thermo-emf is zero if all the junctions are kept at the same temperature. This implies three things of significance:-

- When a thermocouple junction is formed by welding, bracing, soldering *etc.*, the materials used for such jointing, do not affect the thermocouple output as long as the whole junction is at the same temperature.
- Consider a thermocouple hot junction at B formed with materials Q and R. A third material P connects the free ends of Q and R at junctions A and C as shown in Figure 13.7. If the junctions A and C are at the same temperature, the two together with material P function as one cold junction. Use of extension wires, isothermal blocks for cold-junction compensation *etc.*, make use of this fact.
- If the thermo-emfs of two materials P and Q are known with respect to a third material R as e_{PR} and e_{QR}, the thermo-emf of material P with respect to material Q is e_{PR}~e_{QR}.

⇒ The thermo-emf is independent of changes in the wire cross-sections.

⇒ A thermocouple of two materials has the cold and hot junctions kept at temperatures T_1 and T_2; the thermo-emf e_1 is a function of T_1 and T_2. When this thermocouple is worked with temperatures T_2 and T_3 at the junctions, the corresponding emf developed is e_2, which is a function of T_2 and T_3. Now if the thermocouple is worked with temperatures T_1 and T_3 respectively, the thermo-emf developed is $e_1 + e_2$. This is true of all temperatures and all materials and alloys.

⇒ The thermo-emfs are not affected by temperatures anywhere else.

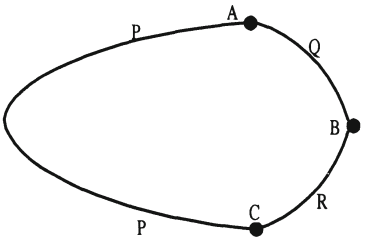


Figure 13.7 Thermocouple loop with three dissimilar materials with 'R' being extension-wires

General Observations: -

⇒ When a thermocouple is used to measure the temperature of a hot junction, the cold junction is to be kept at a fixed temperature called the reference temperature. Then the output voltage is proportional to the hot junction temperature. Alternately the cold junction temperature is measured by other means and a voltage equal to the cold junction voltage added to the thermocouple output. This is termed as the 'cold junction compensation'. Methods adopted for cold junction compensation are treated in Section 13.7.5.

⇒ If either of the wires forming the thermocouple junction, is non-homogeneous and has a temperature gradient along its length, the same generates a thermocouple voltage which gets added to (subtracted from) the main thermocouple voltage of interest to us. This causes an error. To avoid such errors the thermocouple wires have to be homogeneous along their lengths.

⇒ When working over wide temperature ranges, the thermocouple voltage becomes a non-linear function of the temperature difference between the junctions. The non-linearity has to be accounted for, in the calibration. Further with some thermocouples in some ranges, the characteristic is not monotonic, *i.e.*, the thermocouple has the same voltage at two different hot junction temperatures; in such cases, the application is to be restricted to a narrower monotonic range.

13.7.2 Thermocouple Types

With a variety in the availability of metals and alloys, infinite possibilities of forming the thermocouples exist. However only a few combinations are preferred and used in practice. These have specific and well-known type designations. Their

voltage versus temperature characteristics have been well studied and documented. Each one is recommended for a specific temperature range. US NBS gives specific polynomials relating temperature to thermocouple voltage for the popular thermocouples. In each case, NBS specifies maximum range of allowable errors over the active range of use. Common thermocouples, their useful range of application and other characteristics specific to each, are given in Table 13.2 at the end of this chapter. Detailed tables, relating the thermo-emf to temperature, are available in literature. The relationships are also available in polynomial forms [NBS].

13.7.3 Junction

Reliability and long service are the prime criteria in the formation of the measuring junction of the thermocouple. The most commonly used approach is to join the two wires through a twist and weld the tip - gas or electric welding is used. The welded tip forms a fine bulb. Thermocouples for lower temperature service may have soldered junctions. If the welded or soldered joints are found too big for precise working, fine joints or junctions are made by capacitance discharge welding. A sufficiently large capacitor is charged to a suitable voltage and shorted through the junction. The shorting surge current causes intense localized heating of the junction (Heat energy input = current × thermal emf × Δt) for a short time. This results in the welding of the joint. However, such junctions are delicate and not suited for the rough industrial service.

13.7.4 Thermocouple Outfit

The thermocouple probe is used bare *i.e.*, without any enclosure or protective shield around when the measured object is small in size (mass-wise or volume-wise) and is electrically non-conducting. This reduces the loading due to the thermocouple. The bare wire probe also has lowest response times. It may be only 2ms for fine wires. The signal processing circuitry or at least the part directly handling the voltage should be as close to the target as possible. This is to minimize pick up *etc.* An extreme case of application is where the thermocouple junction is directly welded at the point of interest – e.g., thermocouple wattmeter.

Next in complexity is the probe with the exposed junction. The leads are fully protected but the junction *per se* is exposed. This allows the sensing junction to be in contact with the hot object and measure its temperature directly (typical use – measurement of temperature of hot gas). Since the rest of the thermocouple leads are protected, the probe is more rugged and reliable than the bare wire type. Response time can be one order more than the bare probe. The response time is of the order of 1s; it reduces to 0.1s at 20 m/s of air velocity and 0.05 s in still water. The junction – being exposed – can get corroded as easily as the bare wire type. Typical application is to measure the temperature of a gas flowing in a pipe or liquid in motion. (Bare wire thermocouples and probes with exposed junctions will not withstand the full temperature range of the thermocouple.). Absence of protective covering for the junction necessitates careful handling to avoid physical damage to the junction.

Thermocouples housed in sheaths and thermo-wells are widely used in industries. The thermocouple is physically protected and isolated from high-pressure fluids, and corrosive and other adverse influences of the medium. The space around the thermocouple inside the sheath or well is often filled with an electrical insulator with reasonable thermal conductivity. Different refractory cements are available as fillers up to the highest temperatures. MgO with its reasonable thermal conductivity and good electrical insulation characteristic, is such a good filler. The filler also adds mechanical rigidity and strength to the thermocouple. It also reduces the response time of the thermocouple; it is of the order of 1s to 100s. In a sizable number of process applications, response time of this order is not a deterrent. When sheathed, the thermocouple is normally connected to the sheath (*i.e.*, grounded). However, when it is used in a noisy environment or runs long lengths through conduits *etc.*, to avoid ground loops, the thermocouple is normally kept electrically isolated from the sheath. Such insulated thermocouples are also useful, when measuring temperatures of conducting liquids. This measure of course, increases the response time further. The sheaths are normally of stainless steel (SS304) or 'Inconel' (79 % nickel, 13 % chromium and 6 % iron). They are suitable for vacuum, oxidizing or inert atmospheres. Stainless steel is suitable up to 900 °C and Inconel up to 1150 °C. When used in corrosive environments, Teflon coated sheaths are ideal. They can be used in processes up to 150 °C. Teflon coating increases response time. The insulation filling in the sheath is of Magnesia (MgO) or Alumina (Al_2O_3). Magnesia is a reasonably good thermal conductor and compacts well but is hygroscopic. Hence, it requires filling and hermetic sealing. It can withstand temperature up to 1650 °C. Al_2O_3 is to be compacted well under pressure and is not a good thermal conductor. Hence, sheaths with Al_2O_3 filling have longer response times (Often thermocouple response time is not a constraint in processes. Hence, this is more of academic interest). Alumina can withstand temperatures up to 1550 °C. Berylia (BeO) is good filler. Its thermal conductivity is very good and it compacts well. It can be used up to 2300 °C. However, its highly toxic nature, and the fact that its use requires clearance from Govt. Atomic Energy Agencies, deters its use in practice.

13.7.5 Cold Junction Compensation

The thermocouple voltage is a function of the difference between the hot junction temperature T_A and the cold junction temperature T_B (Figure 13.5). If the cold junction temperature is kept fixed or constant, the thermocouple output is a measure of the hot junction temperature T_A. In laboratory work, the cold junction B can be kept continuously dipped in melting ice or at the triple point of water. Junction B being at a fixed and known temperature, sensing is done with reference to this. In an industrial environment, this is not practical. The cold junction temperature will change with the ambient temperature and cause corresponding errors. Cold junction compensation is the process of compensating for this error. Three approaches of doing this are in vogue.

13.7.5.1 Approach 1

Here a voltage proportional to the cold junction temperature is generated; its sensitivity in mV/°C is adjusted to be identical to that of the cold junction of the

thermocouple. This voltage is subtracted from the net thermocouple voltage. As the ambient temperature changes, the compensating voltage also changes automatically. Usually such a compensating voltage is generated, using a copper RTD or a thermistor.

By way of an example, consider an 'S' type thermocouple. It generates 5.5 μV/ °C around 0°C. The compensating device should be at the ambient temperature and subtract 5.5 μV/°C, for every 1 °C rise in the ambient temperature. Consider a copper RTD with 1mA steady current through it.

Temperature coefficient of resistance of copper = 0.41 %/ °C
Consider one ohm of copper resistance carrying the 1mA current here.
Voltage drop in the copper resistance = 1mV
Change (increase) in voltage drop for every 1°C
temperature rise = $(0.41/100)\times10^{-3}$ V
= 4.1μ V
Copper resistance required to provide 5.5μV/°C = 5.5/4.1
= 1.34 Ω

The cold junction compensating circuit can be realized in different ways. Figure 13.8 shows one simple scheme. 2.5 V source is a fixed reference voltage.

With R_2 = 2.5kΩ (2.49866kΩ to be more precise),
Current through R_3 = 1ma

R_1, R_2, and R_4 are Manganin resistances (with temperature coefficient ≈ 0).

$R_1 = R_2 = 2.49866k\Omega$
$R_4 = 1.34\Omega$

R_3 is a copper resistance of value 1.34 Ω at 0°C. With these values, the compensating voltage V_c changes at the desired rate with temperature (–5.5μV/°C). Further V_c is zero at the designated temperature *i.e.*, the temperature at which R_3 = 1.34 Ω (0 °C here). V_c can be subtracted from the thermocouple voltage. Instead of the 2.5V reference, one can use any other convenient reference voltage and change R_1 and R_2 accordingly. Similar calculations can be made for other thermocouples as well. The cold junction and the compensating RTD can be kept enclosed without being subjected to any extremes of environment. One can also use an NTC thermistor instead of the copper wire. Numerical values of the resistances in the compensating circuit can be calculated to suit the NTC characteristics of the thermistor. As long as the current through the copper RTD or the thermistor is kept small enough, the self-heating error is small and negligible.

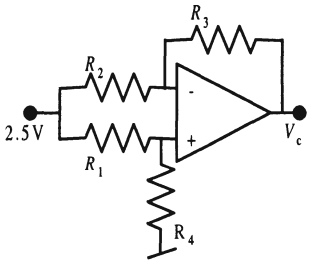


Figure 13.8 Circuit for cold junction compensation using Wheatstone bridge. R_3 is of copper and all other resistances are of manganin or nichrome.

13.7.5.2 Approach 2

Cold junction compensation can be effected in an elegant manner with the help of the temperature sensing ICs like AD590/AD592 etc. From Section 13.6, it is seen that the IC has a sensitivity of 1 μA /K and a standing current of 298.2 μA at 25 °C. It can be used to provide a measured drop across a resistance. Thus to provide a compensating voltage of 5.5 μV/°C, the IC current is passed through 5.5 Ω. The steady voltage of $5.5 \times 298.2 \times 10^{-3} = 1.640$ mV, can be offset at the amplifier stage. The 5.5 Ω resistance has to be of Manganin or Nichrome, to ensure zero temperature coefficient of resistance. A typical circuit is shown in Figure 13.9. V_o provides the compensating voltage. The 5.5 Ω Manganin or Nichrome resistance and the 1 Ω potentiometer can be changed suitably for other thermocouples. Similar compensation can be brought about using LM35 also.

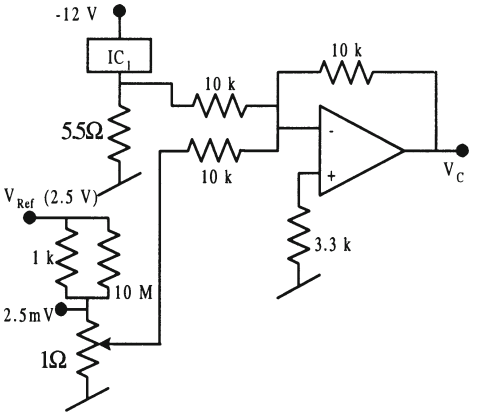


Figure 13.9 Cold junction compensation using a semiconductor type (IC_1) temperature sensor

13.7.5.3 Approach 3

The above two approaches provide cold junction compensation whereby a voltage equal to that generated at the cold junction, is added to the voltage of the thermocouple. Alternately one can adopt a direct approach. The cold junction temperature may be measured separately (using an RTD). An equivalent voltage may be generated and added to the thermocouple voltage. This approach is attractive in data acquisition systems (DAS) where a single cold-junction unit may cater to a number of thermocouples.

The normal procedure is to have an 'isothermal block' (a block of metal with a good thermal capacity). Cold junctions of all the thermocouples in the system are in physical contact with the block with the result that all of them are at the same temperature as the block. The block temperature is measured by a separate RTD. The DAS generates separate cold junction compensating voltages, for each type of thermocouple in digital form. This is done through appropriate LUTs in ROMs. As and when a thermocouple output is sensed and converted into digital form, the DAS corrects it for the temperature variations of the cold junction. The cold junction compensation is updated once every scan cycle of the DAS – typically this may last from a few seconds to a few minutes. Since the ambient temperature changes are relatively slow in nature, a low sampling frequency suffices for the compensating mechanism.

13.7.6 Extension Wires

In processes, temperatures are often measured at points and locations, which may not be accessible for safety reasons. Such situations call for long leads to be connected to the thermocouple and the processing circuitry kept away from the hot junction. Often the thermocouples are of noble metal wires and wires of thin section. It is preferable to limit the lengths of costly and fragile thermocouple wires and use thicker (robust) wires of lower cost over the running length to connect the thermocouple to the signal processing circuitry. Such connecting wires are called 'Extension Wires' (or 'Compensating Cables'). They are selected such that their junction emf characteristic matches that of the measuring thermocouple over the range of cold junction temperatures. This requires the two extension wires to be matched to the respective thermocouple wires in thermo-emf characteristics.

Observations: -

⇒ The Extension wires have to run through long lengths in adverse conditions. Hence, they are thick multi-strand wires - insulated and well sheathed.

⇒ For some of the base metal thermocouples, extension wires are the same as the respective thermocouple wires. For chromel/alumel thermocouple, the extension wires are usually of copper and constantan respectively. For Pt/Pt-Rh thermocouple, they are of copper and an alloy of copper with nickel.

⇒ For the base metal thermocouples, the extension wires are normally rated to withstand temperature up to 100°C. For noble metal thermocouples, they are designed to withstand temperature up to 200°C.

⇒ Specific colour code schemes are used for thermocouple wire insulation as well as for extension wire insulation. There is no universally accepted convention; some commonality exists: -

- USA—Red colour for the negative wire of the thermocouple as well as extension
- IEC—White colour for the negative wire of the thermocouple as well as the extension wire
- UK—Blue colour for the negative wire of the thermocouple as well as the extension wire
- DIN & JISC—Red colour for the positive wire of the thermocouple as well as the extension wire
- French (NFE)—Yellow colour for the positive wire of the thermocouple as well as the extension wire

Further in every case, the thermocouple wires as well as the extension wires, are of the same colour; *i.e.*, the positive wire of the thermocouple and the positive wire of the extension wire are of the same colour and the negative wire of the thermocouple and the negative wire of the extension wire are of the same colour.

13.7.7 Processing of Thermocouple Signals

The thermocouple output is characterized by: -

⇒ Sensitivity in the 10 μV/ °C range; For 0.1 °C resolution, the noise threshold has to be 1 μV or less.

⇒ Normal thermocouples have total resistance in the 100 Ω range – *i.e.*, the source resistance can be considered to be small.

⇒ The output signal, in general, has a non-linear relationship with temperature. However, it can be considered linear in segmented linear ranges. Depending on the resolution desired, the individual segments can be divided. Figure 13.10 shows a typical thermocouple characteristic. The same has been shown approximated by a piece-wise characteristic ABCD. The segment positions and slopes are so chosen that the maximum deviation from the actual is kept at a specified limit – it is δ°C in Figure 13.10.

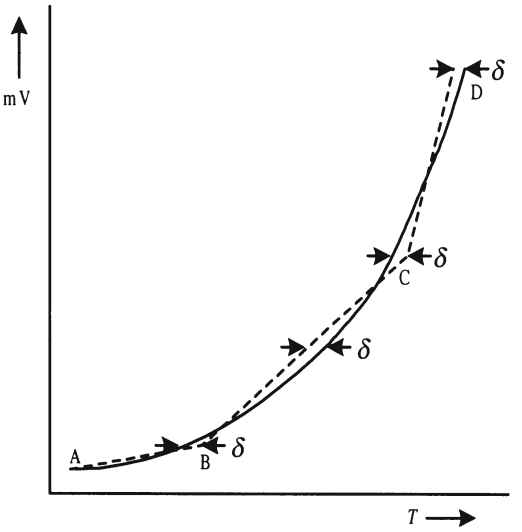


Figure 13.10 Thermocouple output and its approximation by piece-wise linear segments

⇒ In many applications, the thermocouple leads run over tens of metres before being processed. Despite care, the signal can get contaminated with common mode voltages and high frequency differential signals (often at power frequencies).

⇒ Every application requires cold junction compensation to be provided.

Use of a microcomputer for the processing of thermocouple output has become universal practice. A typical scheme maybe as shown in Figure 13.11 in block-diagram form. The low voltage low impedance nature of the signal, calls for an amplifier with low noise voltage (noise current level can be relatively higher). Further, the bandwidth of the signal is of the order of a few Hz. Amplifiers with low noise in this frequency range are preferred. Whenever the signal leads are long or common mode contamination is possible from other sources, use of instrumentation amplifiers is common.

The functions of the microcomputer and other aspects of the system working are as follows: -

⇒ Due to the limited bandwidth of the signal, an LPF is incorporated into the signal amplifier itself.

⇒ In dedicated schemes, cold junction compensation is done in hardware. The compensating voltage is added directly at the amplifier stage itself.

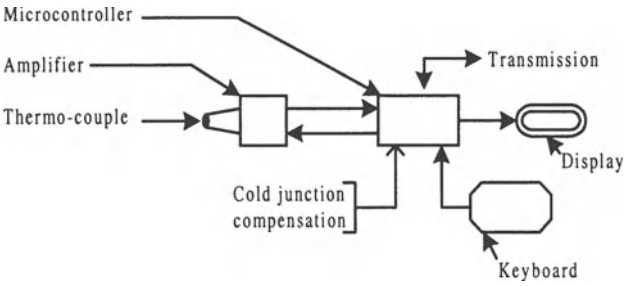


Figure 13.11 Thermocouple instrumentation scheme in block diagram form

⇒ The thermocouple is treated as a delicate sensor with the possibility of its opening out (called 'Burnout' when it occurs at the junction due to prolonged use and the like). Such burnouts lead to hazardous situations (When a controller is present, low signal at the thermocouple end due to the burn-out, is followed by an 'increase heating' command. The process temperature may increase, but the same is not sensed by the thermocouple due to the burnout. The 'increase heating' command is sustained, eventually leading to a hazard.). The microcomputer regularly checks the continuity by injecting a voltage and sensing the current. The resistance is confirmed to be below a threshold level. Thus, during normal operation, the scheme alternates between an 'operate' and a 'burnout check' mode.

⇒ Due to the limited bandwidth of the thermocouple signal, whenever multiple thermocouple outputs are handled, one microcomputer can do it in a multiplexed fashion. In such situations, the cold junction is arranged as a separate isothermal block and its temperature sensed through an RTD (See Section 13.4). The microcomputer computes the cold-junction compensation voltage separately for each thermocouple (depending on the type of thermocouple) and adds it to the respective thermocouple voltages in software. Since the range of cold junction temperatures is limited, sensitivity can be taken as constant (as at 25 °C) and the compensating voltage V_c computed as

$$V_c = K_c (T_c - 25) \tag{13.10}$$

where

V_c is the compensating voltage

K_c is the sensitivity of the thermocouple at 25°C and

T_c is the temperature of the cold junction

⇒ Depending on the type of thermocouple, the temperature range and the resolution desired, the inherent non-linearity of the thermocouple characteristic is accounted for in various ways. At the lowest end where the temperature range is limited, and expected resolution is not very high, the thermocouple characteristic is approximated by one straightline segment and the thermocouple voltage suitably offset and amplified. Specific dedicated ICs are available for this. (AD594 and AD595 of Analog Devices). Hand-held thermocouple temperature indicators are of this type.

⇒ As the desired range widens, or resolution reduces, or non-linearity is too severe to allow such single line segment approximation, the thermocouple characteristic is approximated by 2 or 3 linear segments. Depending on the

thermocouple output, the microcomputer computes the measured temperature using the appropriate segment.

⇒ At the other extreme end where the temperature range is widest, the resolution is highest and / or the non-linearity is too severe, the actual non-linear characteristic is stored in a LUT in ROM, PROM or EPROM. The microcomputer computes the temperature with the help of this LUT. Elaborate data acquisition systems, laboratory calibration-standards *etc.*, adopt this approach [See examples in Section 9.2].

⇒ With the provision of microcomputer and the availability of ample memory with it, characteristics of different thermocouples can be stored in different LUTs in the same microcomputer. With this, it is possible to use a single thermocouple instrument and select the thermocouple to be serviced by it through a keyboard. Such programmability has become standard with many thermocouple instruments.

⇒ Thermocouple instruments often have the facility to transmit the measured temperature over a serial link in specified standard formats. Often the programming and the configuration too can be done through the serial link.

⇒ Dual-slope type ADCs (See Section 8.7.1) are preferred with thermocouples. With this, the signal threshold can be reduced taking advantage of the low bandwidth of thermocouple signals. Sigma-delta converter type ADCs (Section 8.7.6) with their superior characteristics, are likely to replace these.

General Observations: -

⇒ Molybdenum/tungsten/rhenium thermocouples are used to sense temperatures up to 2000 °C (and beyond that on a short time basis). The measurement accuracy claimed is 1 % subject to a minimum of 5 °C. Beyond this range, only non-contact temperature sensing (radiation pyrometry) is feasible. Type designation and output versus temperature relationships are not yet standardized for these.

⇒ In demanding applications, the thermocouples are housed in sheaths. The following are the more common ones amongst these: -

- Tantalum sheath can withstand temperatures up to 2300 °C. It can be used in vacuum, acidic and alkaline environments. It can be used in oxidizing atmospheres up to 300 °C.
- Sheaths of platinum and rhodium alloys can be used in inert and oxidizing atmospheres. These are resistant to corrosion by SO_2 up to 1100 °C. They are not for use in silica lined furnaces or in halogen atmospheres.
- Inconel 600 can be used up to 1150 °C in inert, vacuum or oxidizing atmospheres. It is not suitable in atmospheres containing sulphur (causes corrosion) or hydrogen (embrittles).

⇒ Wires of good homogeneity are to be used for the thermocouple. Lack of homogeneity can cause errors due to the high temperature gradient near the hot junction. This may affect accuracy to the tune of 10 °C to 20 °C. The noble metal thermocouples, thermocouples of tungsten, molybdenum and rhenium are more vulnerable in this respect.

⇒ Selection of sheath for the thermocouple has to be done with care. Ceramics, which appear to be robust and inert at lower temperatures, are more vulnerable at higher temperatures. Some of these become conducting

causing leakage across the thermocouple wires. With some other ceramics the impurities and chemicals present, may migrate into the thermocouple wires affecting their homogeneity and cause undue errors.

⇒ The fact that different colours are specified for thermocouple wires requires specific dyes to be used in the insulation. Some of them may cause electrolytic action in the presence of water leading to gross errors.

⇒ Type B thermocouple – Platinum-30% Rhodium/Platinum-6% Rhodium – has a double valued characteristic from 0°C to 40°C (See Figure 13.12). Hence, it cannot be used over this temperature range.

⇒ Table 13.3 gives its sensitivity at selected temperatures.

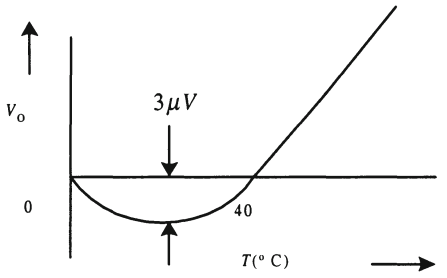


Figure 13.12 Characteristic of type B thermocouple near 0°C

Table 13.3 Sensitivity of type B thermocouple at selected temperatures

Hot Junction Temp (° C)	100	500	1000	1500
Sensitivity (μV/° C)	1	5	9	11

Normally Type B thermocouple is recommended for use beyond 800 °C; it has an error of 0.5°C. So long as the cold junction is kept in the 0 °C to the 40 °C range, error due to variations in the cold junction temperature, is less than 1.5 μV. The corresponding temperature error is less than 0.2 °C and negligible. Hence, this thermocouple does not require any cold junction compensation.

⇒ Mineral insulation of the thermocouple wires ('Minerally Insulated' thermocouples) provides substantial protection for them. The thermocouple wire is covered with insulation like MgO. It is brought down to a uniform desired size by compaction and rolling, drawing, swaging etc. The mineral insulation may form 80 % (by volume) of the thermocouple. The mineral coat provides electrical insulation, mechanical strength and protection against many chemicals.

- Gas and water vapour may still intrude through the mineral insulation and corrode the wire.
- Manganese (if present in the environment), may enter through the mineral (in the vapour phase) in a similar manner and get deposited on the wire surface. This affects the homogeneity of the wire and causes errors as explained earlier.

- Differential expansion of the thermocouple wires and the sheath, causes undue stresses in the fragile thermocouple wire. This also causes fatigue due to repeated thermal cycles of use and affects thermocouple life.
- MgO is hygroscopic. Moist environment (even prolonged storage under humid conditions) can affect the thermocouple life substantially.
- Stainless steel has 1% to 10 % of manganese content. The manganese can get vapour-deposited in the thermocouple wires at high temperatures. This affects wire homogeneity and causes error. Roughly, each additional 1% manganese causes about 10 °C offset due to 1000 hrs of use at 1100 °C.

13.8 Infra-Red Thermometry

Non-contact sensing is a novel characteristic of 'Infra-Red Pyrometry (IRP)'. Moving targets, targets in vacuum, targets in hostile or hazardous environments, or those with geometry limitations, intermittently appearing targets, target scanning- all come under its purview. The principle is well established and used in a limited manner over decades - especially for the measurement of temperature, which cannot be done otherwise. The variety of factors that affect measurement as well as the need for skill on the part of the user, have deterred users so far. Often IRP has been pre-judged as 'inaccurate'. However, the flexibility of electronic circuits and the sophistication in signal processing which has become possible in recent years, have reduced the indecision and imponderables to a level where IRP can be more fruitfully utilized.

13.8.1 Basics of Radiation

Consider a body at a temperature TK. It receives a certain amount of radiation from the environment. It gives out a certain amount of radiation too. As far as the energy received or given out is concerned, in general we can say that

$$E(\lambda) + r(\lambda) + t(\lambda) = 1 \qquad (13.11)$$

where

$\Rightarrow$ $E(\lambda)$ is the fractional energy radiated by the body at wavelength λ,

$\Rightarrow$ $r(\lambda)$ is the fractional energy reflected by the body at wavelength λ and

$\Rightarrow$ $t(\lambda)$ is the fractional energy transmitted by the body at wavelength λ .

The above relation is valid for every wavelength from 0 to ∞ as well as the total energy at all wavelengths put together. From equilibrium considerations, it is known that the energy absorbed by the body at any wavelength, must be equal to that given out by it at the same wavelength. This gives

$$E(\lambda) = a(\lambda) \qquad (10.12)$$

Here $E(\lambda)$ is called the 'Emittance, and $a(\lambda)$ the 'Absorbance' of the body. In the case of bodies of interest to us here, we take

$$t(\lambda) = 0 \qquad (13.13)$$

For those bodies, which do not have this as identically equal to zero, we will be interested in those frequencies at which this is identically equal to zero. We select λ

values where the body is opaque. Glass, plastics etc., are such examples: They are opaque in selected IR bands. With this, Equation 13.11 becomes

$$E(\lambda) + r(\lambda) = 1 \qquad (13.14)$$

A body which has $r(\lambda) = 0$, absorbs all the incident radiation energy. Such an ideal body is referred to as a 'Black Body'. A cavity in a hollow body (the size of the cavity being small, compared to the internal dimensions of the body) with all parts of the body being at the same temperature, is close enough to such an idealization. It will absorb all received radiation without reflection and give out radiated energy at all wavelengths. The radiation from a black body is given by (Plank's equation)

$$W_{\lambda} = \frac{C_1}{\lambda^5 [\exp(C_2 / \lambda T) - 1]} \qquad (13.15)$$

where

⇒ λ is the wavelength in m

⇒ W_λ is the hemispherical spectral radiant intensity in w/cm^2 μm

⇒ C_1= 37143 w μm^4/cm^2

⇒ C_2= 14388 μmk and

⇒ T is the absolute temperature of the black body in Kelvin.

W_λ is the amount of radiation emitted from a unit flat surface into the hemisphere per unit wavelength at the wavelength λ. For all practical purposes of interest to us, the Plank's equation can be approximated by the Wein's equation

$$W_{\lambda} = C_1 \lambda^{-5} \exp(-C_2 / \lambda.T) \qquad (13.16)$$

Figure 13.13 shows a few typical plots of W_λ versus λ.

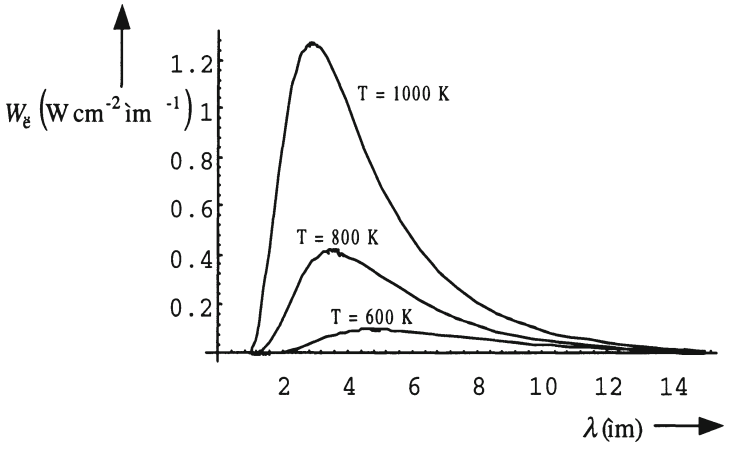


Figure 13.13 Nature of variation of radiation from a black body: The radiation characteristics are shown plotted for three different temperatures of the body. As the body temperature rises, the wavelength λ for peak radiation shifts steadily to lower wavelengths

Observations: -

⇒ At every temperature of the black body, there is a definite amount of radiation at every frequency.

⇒ Consider a plane surface of target area ΔA_t with hemispherical spectral radiation intensity W_λ w $^{cm-2}$ μm^{-1} (Figure 13.14). A detector of plane surface area ΔA_d is kept at a distance r from the source. PQ is the line joining the centres of the source and the detector. PQ makes an angle θ_1 to the normal at the target and angle θ_2 at the detector.

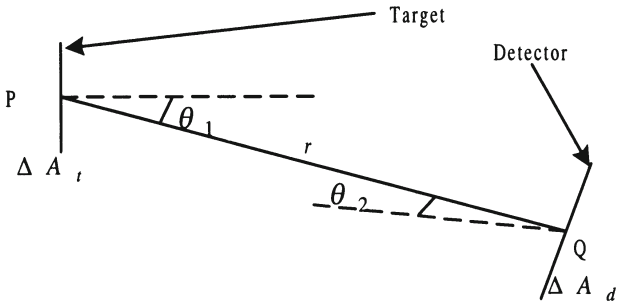


Figure 13.14 Basic radiation target and detector scheme

$$\text{The solid angle subtended by the detector at the source} = \frac{\Delta A_d}{r^2}\cos\theta_2 \text{ steradian} \quad (13.17)$$

$$\text{Total radiation emitted into the hemisphere} = W_\lambda \Delta A_t \text{ into } \pi \text{ steradians} \quad (13.18)$$

$$\text{Total radiation received at Q} = W_\lambda \Delta A_t \cos\theta_1 \cos\theta_2 \frac{\Delta A_d}{\pi r^2} \quad (13.19)$$

Normally radiation detectors are aligned such that

$$\theta_1 = \theta_2 = 0$$

Substituting in Equation 13.19 we get

$$\text{Total radiation received at Q} = W_\lambda \Delta A_t \frac{\Delta A_d}{\pi r^2} \quad (13.20)$$

For a given sensor, ΔA_d is constant. $(\Delta A_t / r^2)$ represents the solid angle subtended by the source at the detector. Hence, the total radiation received by the sensor is proportional to the solid angle subtended by it at the detector and the total radiation output by the source.

⇒ The radiation is zero for $\lambda = 0$ and $\lambda = \infty$. At any black body temperature, the radiation increases with λ, reaches a peak and drops back to zero as $\lambda \rightarrow \infty$.

⇒ The λ value, for which W_λ is a maximum, reduces steadily as the black body temperature raises. In turn, the body temperature changes from dull red to white as the black body temperature rises. In fact, the wavelength λ_p where the W_λ attains the maximum, is

$$\lambda_p = \frac{2891}{T} \mu m \quad (13.21)$$

Integrating Equation 13.15 over 0 to ∞ of λ, we get

$$W_t = 5.67 \times 10^{-12} T^4 \text{ w/cm}^2 \quad (13.22)$$

where W_t is the total radiation from 1cm^2 of the body surface at temperature TK. This is called the 'Wein's Equation'.

⇒ The relative amount of radiation from a body at any wavelength λ, is called its emittance- represented by the symbol ε_λ. In general, the emittance is a function of λ and the body temperature.

⇒ Bodies, which have a constant emittance at all wavelengths, are called 'Gray bodies'. The Plank's equation for gray bodies, is

$$W_{\ddot{e}} = \frac{\varepsilon_r C_1}{\lambda^5 [\exp(C_2 / \lambda T) - 1]} \quad (13.23)$$

where ε_r is the emittivity of the body. The other quantities are as in Equation 13.15. The Wein's equation for gray bodies, is

$$w_t = 5.67 \times 10^{-12} \varepsilon_r T^4 \text{ w/cm}^2 \quad (13.24)$$

w_t and T are as in Equation 13.22. Exhaustive tables of emittivities of bodies are available in literature [Benedect, Dewitt and Nutter].

⇒ For any body at any temperature, one can identify a significant band of wavelengths that contribute to substantial part of the total radiation from the body. Substantial here can mean 90 %, 95 % or any other defined percentage of the total radiation. Thus, at 25 °C, 90 % of the total radiation is in the 3 μm to the 20 μm band. As the body temperature rises, both the limits reduce. In practice, one can take any body as gray , if its emittance is sensibly constant over the significant band of wavelengths referred to as above. Table 13.4 gives the emittivities of a few such bodies.

⇒ The very nature of the change in significant bands with temperature dictates measurement to extend to longer wavelengths at lower temperatures. The range becomes smaller at higher temperatures. Hence, infrared pyrometry is easier and more accurate at higher temperatures.

Table 13.4 Some common materials and their emissivities at 300K

Material	Emissivity
Aluminum-polished and degreased	0.027
Aluminum-sandblasted	0.210
Aluminum-anodised	0.750
Gold-plated on stainless steel and polished	0.028
Magnesium-polished	0.070
Paint-aluminum	0.045
Paint-TiO_2-gray	0.87
Paint-TiO_2-white	0.77
Stainless steel-type 18-8 sandblasted	0.44

13.8.2 Emissivity

Emissivity characteristics of the target and the absorption in the intervening media, are central to the use of infrared pyrometry. An opening of a hollow sphere, with a

uniform temperature in its inside surface, is close to an ideal black body. It has an ε_r of 0.998. With practical materials, ε_r is decided by the molecular structure and the surface smoothness characteristics. In general, polished surfaces have a low ε_r. It becomes higher and comes closer to unity at smaller values of λ. For most opaque bodies, it is in the 0.85 to 0.90 range. Most unoxidised metals have ε_r in the 0.2 to 0.5 range. (For gold, silver and aluminium, it is very low and in the 0.02 to 0.04 range; IR pyrometry is difficult to use with them). It increases with increase in the temperature of the unit.

When a target is viewed to sense the IR radiation from it, the absorption and the transmission characteristics of the medium between the target and the IR pyrometer affect the results. Some schemes sense the radiation at two frequencies for which the absorption and the transmission are the same and obtain temperature from their ratio. Others sense the radiation in a select band of wavelengths over which the transmittance is sufficiently high. Thus if there is an intervening air column, the 8 μm to the 14 μm band of wavelengths, is used. The absorption in this band, is relatively low (and hence the transmittance is high).

Elaborate published data is available on emittance and emissivity and their variation with wavelength and temperature. These can be stored as detailed LUTs and used judiciously. For example, steel has a low emissivity (~0.1) at low temperatures. When heated in an induction furnace, as the temperature increases, the oxide thickness on the surface increases depending on the time-temperature profile. Correspondingly, the emissivity also changes. The temperature – time information can be used with a LUT and correction applied. This improves the accuracy of the IR pyrometer substantially.

13.8.3 Methods of Sensing

A variety of techniques has been used to measure temperatures of objects by detecting the radiation from them. The optics is essentially common to all of them. The subsequent part of the scheme can be of two categories, namely indirect detection and direct detection.

13.8.3.1 Indirect Detection

The radiation from the body is made to fall on an isolated thermal mass of very low reflectivity (and transmittance). All the received radiation is absorbed by the thermal mass and its temperature rises. The rise is used as a measure of the source temperature. This mode of operation functions according to the Wein's law. The non-linear nature of the relation between the energy received and source temperature limits the active range of operation.

13.8.3.2 Direct Detection

Radiation is sufficiently filtered and made to fall on dedicated photo-detectors. The detector response is directly correlated to the source temperature. A variety of schemes is possible depending on the type of detector used, the way the wavelength band or bands are selected and the method of relating the output to the source temperature.

Both indirect and direct methods of radiation detection are discussed in detail in later sections.

13.8.4 Optics

The simplest schemes have a single lens and the detector at the focus of the lens as in Figure 13.15. The target – normally at a large distance compared to the focal length of the lens – forms its image at the focal plane; hence, the detector is kept there. The size of the detector decides the size of the image and hence the target. The angle subtended by the image at the centre, of the lens – 2θ – is the 'Field-of-View (FOV)'. The target also subtends the same angle 2θ at the lens. Hence, 2θ – the FOV – is a measure of the size of the object that can be accommodated. The FOV may vary from 5° down to 0.25°. Often FOV is specified as the ratio of target size to its distance from the lens (This is the radian equivalent of the FOV in degrees). Due to diffraction, all the incident radiation within the FOV is not fully confined to the geometric image area. The spill over at the periphery depends on the relative ratio of λ/f. Considering this, the FOV is defined as the angle, which confines 90 % of the incident energy on to the detector area.

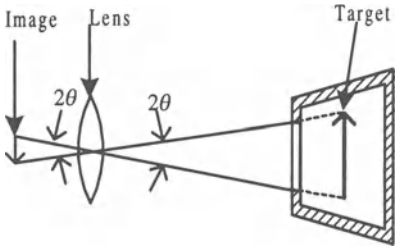


Figure 13.15 Simplest optics scheme for radiation detection

Whenever indirect detection is used, the total IR energy in the FOV is captured and made use of for sensing. Hence, the distance of the target from the IR pyrometer is a factor deciding calibration. The distance is to be known to get exact temperature values. When only the relative temperature values are significant, the quantitative value of the distance need not be known accurately, as long as it is kept the same. In case of IR pyrometer schemes, which compare the radiation at two distinct wavelengths, the distance is not important as long as it is within specified limits.

13.8.5 Indirect Methods - Thermal Detection

All the radiation from the target – within the FOV – is collected and focused on to a well defined small area with a thermal sink in the focal plane of the lens. The sink is coated with a black material and absorption kept as high as possible. Due to the heat received, the sink material gets heated. The final temperature attained and the time to attain the same are decided by the thermal mass (mass × specific heat) and its heat insulation level. If the thermal mass is kept low, the temperature rise and hence the sensitivity increase. However, the response time also increases. The temperature range required of the instrument decides the trade-off. Temperature of the thermal sink can be sensed by any conventional method. The practice followed is one of the following: -

⇒ A thermistor can be used as the temperature sensor (called the 'Bolometer'). Due to its high temperature coefficient of resistance, the bolometer has high sensitivity but limited range. It is used for IR thermometers of comparatively lower temperature ranges.

⇒ Semiconductor temperature sensor with 1 μA /°C sensitivity which has come into vogue in recent years, can be used as the sensor. It provides reasonable sensitivity over a wide range. Its characteristic is linear throughout the range.

⇒ A thermopile – composed of a number of thermocouples in series – can be used for sensing. All the hot junctions are on the thermal sink that receives the radiation from the target; the cold junctions are on a separate heat sink. The use of the thermocouples in series as a thermopile increases the sensitivity of sensing. In general, a thermopile sensor is used for IR thermometers up to the highest temperatures. J and K type thermocouples are commonly used.

⇒ Pyroelectric detectors can be used to sense a temperature change. These are electro-ceramics. Some of these get polarized when heated (See Table 13.5) – the extent of polarization is a measure of the temperature change. The pyroelectric material forms the dielectric of a sensor capacitor. The increase in the polarization gets reflected as an increase in the capacitance value. This is converted into an equivalent electrical signal using capacitance transduction techniques.

Table 13.5 Characteristics of Pyroelectric detectors

Material	Curie temperature (°C)	Pyroelectric coefficient ($nC\ cm^{-2}K^{-1}$)	Dielectric constant
TGS	49	30	30
$LiTaO_3$	618	6	58
$BaTiO_3$	126	20	160
$LiNbO_3$	1190	4	30
SBN	115	60	380
PVF_2	200	3	10
PZT	200	35	250

The received radiation energy at the thermal sink raises its temperature. The above sensors respond to the absolute temperature of the thermal sink. Changes in the ambient temperature reflect as drift in the sink characteristics. To compensate for this, the instrument has to measure the ambient temperature regularly and compensate for its variations. Two approaches are in vogue. In one case, the radiation from the target and the ambient are directed through the lens system to the sink alternately. This is done with the help of a rotating disc with alternating slots and mirrors. The alteration is done typically at 25 Hz – about 10 times the worst-case-drift-bandwidth. In many applications, the target appears on the scene only intermittently; so this is taken advantage of, in the second method where the ambient temperature sensing and the corrections for it, are done automatically. Whenever the target is absent (detected by a steep change in the received radiation), the received radiation is taken as that from the ambient. In both the cases, the detector output alternates between two levels – one corresponding to the exposure to the target and the other corresponding to the exposure to the ambient. The

difference between the two represents the radiation from the target. Hence, the output is normally AC coupled, amplified and synchronously demodulated.

IR thermometers are universally built around microcontrollers. The microcontroller tasks include the following: -

⇒ Do zero correction for the instrument.

⇒ Normally the ε_r value can be set by the user in steps of 0.01. Use set value to compute the received energy as

$$E = \varepsilon_r \times 5.67 \times 10^{-12} T_t^4 A_t \quad (13.25)$$

where

- E is the received energy
- ε_r is the emissivity
- T_t is the target temperature (to be computed) and
- A_t is the area of the target viewed

⇒ Based on the energy received when sighting the ambient area, compute the ambient temperature. This can be done by extracting the fourth root, using a LUT or through piece-wise linear approach; the last is the most common.

⇒ Using the rise in the sensor temperature, compute the energy received by it from the target. From this and the ambient temperature computed above, compute actual target temperature. This is also done by one of the methods above; again the piece-wise linear method is the most common.

⇒ The thermal sink radiates energy due to its elevated temperature. The lens system forms its image on the target causing a slight change in its temperature. This is enough to cause an error. This error can be computed by the microcontroller and compensated for. This reduces the overall error correspondingly.

⇒ Emissivities of materials depend on temperature. This information can be stored in a LUT and used to refine the estimated temperature values.

Observations: -

⇒ The thermal detector type IR pyrometer normally captures energy over a wide IR band. Normally it may extend up to 40 μm. If atmospheric air intervenes between the target and the sensor, use of 8 μm to 14 μm window, is common up to 550 °C. It avoids error due to radiation absorption by moisture.

⇒ As the emissivity comes closer to unity, the accuracy of reading improves.
e.g., Change in ε_r from 0.90 to 0.91 increases the reading by 0.28 %.
Change in ε_r from 0.20 to 0.21 increases the reading by 1.2 %.
Hence for targets at higher emissivities, even a roughly estimated- setting, suffices. Incidentally, opaque non-metallic materials have emissivity in the 0.80 to 0.90 range.

⇒ The alternating time-period between the target and the ambient temperature has to be better than $1/10^{th}$ of the time constant of the ambient temperature changes. In turn, the sensor response time has to be lower than $1/10^{th}$ of this value. Typically the sensor response time is a few ms.

⇒ The thermal IR pyrometer senses the average temperature of the target area. Hence, the target has to fill the full target area for correct operation. For the same reason, presence of any object other than the target behind it, can cause error.

⇒ As the target temperature increases, the significant wavelength bandwidth shrinks. Up to 550 °C, 8 μm to 14 μm band is common. The bands used for higher temperatures are progressively smaller.

⇒ Majority of the IR pyrometry applications does not seek a precise knowledge of the target temperature. One is more interested in relative changes, sensed with enough repeatability and low drift. A precise emissivity setting is not important in such cases.

Normally manufacturers guarantee a resolution of 1 % and accuracy of 2 % over a restricted temperature range. 5 % accuracy over a wider range is also guaranteed. With this, the actual emissivity is immaterial as long as it lies within a reasonable (though wide) band. (All opaque non-metals have emissivity in the 0.80 to 0.90 range. This reflects as a range of $\sqrt[4]{0.80} = 0.95$ to $\sqrt[4]{0.90} = 0.97$ in the coefficient determining the target temperature using Equation 13.25)

13.8.6 Direct Methods - Radiation Detection

In the direct methods, the intensity of radiation from the target is measured at one or two (or sometimes even three) wavelengths. There are specific radiation detectors for this. The radiation from such narrow slots used here, is one order lower than the corresponding total radiation (in the thermal methods discussed above). The sensors used here have to be more sensitive or we have to compromise on resolution. A more sensitive sensor is noisier. Many such sensors, which can sense low thresholds of radiation, have to be worked at cryogenic temperatures to keep the noise level low. These are not suitable for industrial use and hence not dealt with here.

In general, the radiation sensor has a crystal lattice structure with a low energy gap between the valence and the conduction bands. Part of the radiation incident on it causes charge carriers to be liberated. Due to this, an electrical parameter *i.e.*, resistance, current or voltage associated with the sensor and its circuit, changes. This change is related to the total radiation received (See also Section 15.6). For radiation at wavelength λ we have

$$E = \frac{hc}{\lambda q} \tag{13.26}$$

where

⇒ λ is the wavelength of radiation

⇒ c is the velocity of light

⇒ h is the Plank's constant

⇒ E is the energy in electron volt and

⇒ q is the charge on the carrier.

For a material whose energy gap is E_g eV, incident photons of wavelength $< \lambda_c$, are absorbed and cause charge carriers to be released. Here

$$\lambda_c = \frac{hc}{qE_g} \tag{13.27}$$

$$= \frac{1.238}{E_g} \tag{13.28}$$

where

⇒ E_g is in electron volts and

$\Rightarrow$ λ_c is in μm.

Part of the incident radiation is reflected and the rest enters the material. With increasing depth, more of it is absorbed and converted into charge carriers. The electron-hole generation rate is [Sze]

$$g(x) = (1-r)E_q a e^{-ax} \tag{13.29}$$

where

$\Rightarrow$ $g(x)$ is the electron-hole generation rate

$\Rightarrow$ r is the Fresnel reflectance

$\Rightarrow$ E_q is the photon irradiance and

$\Rightarrow$ a is the absorption coefficient.

Total charge carriers N generated down to a depth of d is

$$N = \int_0^d g(x)\,dx \tag{13.30}$$

Substitution of g(x) from Equation 13.29 and integration over the 0 to d range gives

$$N = (1-r)E_q[1-e^{-ad}] \tag{13.31}$$

The ratio (N/Eq) represents the number of independent electrons produced per photon of irradiant energy. This is referred to as the 'Quantum Efficiency' of the detector material – represented by the symbol η. From Equation 13.31, we get the expression for η as

$$\eta = (1-r)[1-e^{-ad}] \tag{13.32}$$

The absorption coefficient a is a function of incident wavelength.(among other things). It is low for $\lambda > \lambda_c$ and increases steeply for $\lambda < \lambda_c$. Depending on a, the depth d and the reflectance r, the quantum efficiency η changes for different detectors. It is about 30 % for extrinsic photo-conductors and 10 % for photo-emissive sensors. In contrast, η is of the order of 1 % for photographic films.

13.8.6.1 Photoconductors

Lead sulfide and lead selenide are two photo-conductors, which can function at room temperature. Both are of the intrinsic type and have η ~ 60%. Their characteristics are given in Table 13.6. Extrinsic photoconductors are available where photoconductivity is brought about by introducing low band gap energies by doping. Due to the sparse presence of dopants, their η is low (~30%). Their inherent noise level is high. They are to be operated at cryogenic temperatures and hence are of no interest in most industrial applications.

Table 13.6 Characteristics of ordinary photo-conductors

Material	Typical η	λ(μm)	Resistance (MΩ/square)	Time constant (μs)	Nominal temp (K)
PbS	50	3	18	200	300
PbSe	50	5	25	1.5	300

Equivalent circuit of a photoconductor is shown in Figure 13.16. The photo-conductor absorbs part of the incident radiation – essentially of $\lambda < \lambda_c$ and generates charge carriers inside. Due to this, its resistance R_D reduces. Change in the

resistance value is used as a measure of the incident radiation, which constitutes sensing.

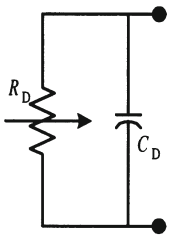


Figure 10.16 Equivalent circuit of a photoconductor

PbS has an energy gap of 0.37 eV at room temperature. The corresponding λ_c = 3.3 μm. It can be used as a radiation detector up to this wavelength. The operating temperature can be up to 80 °C. Above this temperature, an oxidation process renders it ineffective as a sensor. Typically, PbS is deposited on glass or quartz substrate over gold electrodes. Leads are soldered to the electrodes for external connection. The whole device is hermetically sealed within a metal can and enclosed with a glass window over the active material. PbSe detector is also formed and offered in a similar manner. Its room temperature spectral response extends from 1.5 μm to 5.8 μm. Both PbS and PbSe, offer linear response over almost 13 decades of incident radiation at room temperature.

13.8.6.2 Photo-voltaic Sensor

Photo-voltaic sensors are p-n junctions exposed to radiation. They form the most common and widely used radiation detectors. When a p-n junction is formed, some electrons from the n region migrate to the p region and holes from the p region migrate to the n region. This causes a potential barrier across the junction and either side of the junction is depleted of charge carriers over a restricted zone (depletion zone). Subsequently there is no net charge transfer across the junction or current through it. Under these conditions, any radiation incident at or near the junction, in the depletion zone, may be absorbed (See Section 15.5) and result in electron-hole pair generation. They migrate across the junction and cause a voltage to be developed across the junction or a current through it depending on the circuit conditions. Note that radiation incident on the material away from the junction (beyond the depletion zone) also may cause electron-hole pair generation. However, they recombine within a short time and distance and do not contribute to any net output current or voltage. The current and voltage of a diode are related as

$$i = i_0\left[\exp\left(\frac{qv}{bkT}\right)-1\right] \tag{13.33}$$

where

⇒ i_0 is the reverse saturation current
⇒ v is the applied voltage
⇒ q is the charge on the electron
⇒ b is the non-ideality factor
⇒ k is the Boltzmann constant and
⇒ T is the temperature in K.

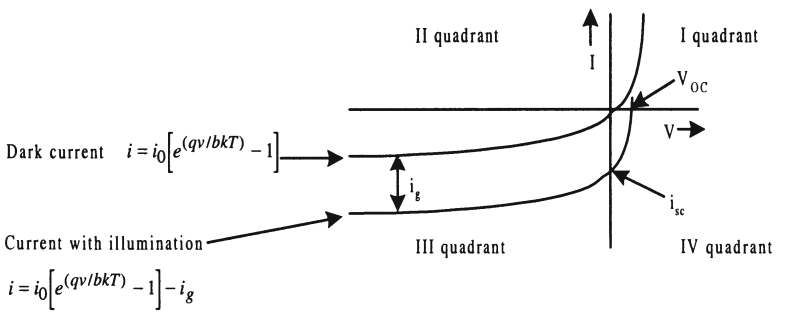


Figure 13.17 Photodiode characteristics

When the applied voltage $v = 0$, the current $i = 0$. When radiation is incident on the diode, it causes an additional current i_g to flow [Streetman].

$$i_g = \eta\phi_d q \tag{13.34}$$

$$\phi_d = Ae_q \tag{13.35}$$

Where

$\Rightarrow$ ϕ_d is the total incident photon flux

$\Rightarrow$ A is the total active detector area and

$\Rightarrow$ E_q is the irradiance.

With this, Equation 13.33 and Equation 13.34 together give the total diode current as

$$i = i_0\left[\exp\left(\frac{qv}{bkT}\right) - 1\right] - \eta\phi_d q \tag{13.36}$$

Typical v-i relations for the photodiode are shown sketched in Figure 13.17. In radiation detector applications, the photo-sensor is operated in the 2nd or 3rd quadrant. When the diode is operated in an open circuited condition, v_{oc} – the voltage across its terminals can be obtained from Equation 13.33. It becomes

$$v_{oc} = \frac{bkT}{q}\ln\left(\frac{i_g}{i_0} + 1\right) \tag{13.37}$$

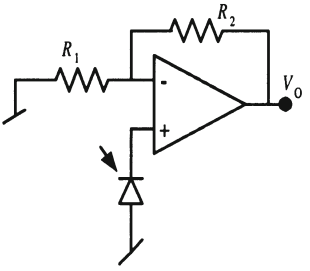


Figure 13.18 Circuit with photodiode in the open circuit mode

When $i_g >> i_0$, the output voltage v_{oc} is a function of the incident radiation, as can be seen from Equation 13.34. This mode is used in the non-inverting configuration as shown in Figure 10.18. The comparatively larger value of the diode equivalent resistance causes the thermal noise level of the diode to be high. However, shot noise is zero. Effect of opamp current noise is low as long as $R_1 \| R_2$ is high enough.

Voltage noise effect being significant, an opamp with low noise voltage is to be selected. When operated under short circuit conditions, as in the trans-impedance amplifier shown in Figure 10.19, the voltage across the diode is essentially zero and all the current flowing through the junction is the photo-generated current ($I = i_g$).

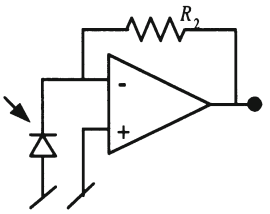


Figure 13.19 Circuit with the photo-diode in the short circuit mode

The low equivalent circuit resistance across the diode, ensures that the junction noise is low; the effect of the opamp noise (current as well as voltage) is low. This configuration is better in performance compared to the open circuited operation as above. When the photo-diode is operated with a reverse bias as in Figure 10.20 (3rd quadrant), the current under zero radiation conditions, is essentially the reverse saturation current. In the presence of radiation, it increases by giving rise to a corresponding change in the output. The zero signal output has to be nullified, using a subsequent differential amplifier. The low equivalent-circuit resistance makes thermal noise to be low but shot noise increases from zero. However, the net noise effect from the diode alone is low, when it is operated with a slight negative bias.

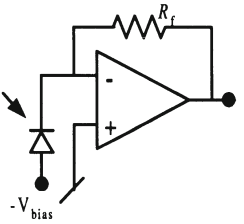


Figure 13.20 Circuit with a reverse-biased photo-diode

The junction capacitance of the reverse biased diode is low. This reduces response time and increases the effective bandwidth. The zero-voltage biased operation is termed the photo-voltaic (PV) mode. The negative biased operation is termed the photo-conductive (PC) mode. The PC mode is preferable for high-speed operation. (>100 kHz). The overall noise performance (considering the device and opamp together) is better for the photo-voltaic mode when the bandwidth is limited. Its noise performance is conspicuously superior if the bandwidth is limited to (say) 1 kHz. This is often the preferred mode for IR pyrometry.

Silicon photo-diode is the most common photo-diode. Its spectral response range is 0.2 μm to 1.15 μm the peak being at 0.9 μm. The visible and the near IR region are its forte. Germanium photo-diodes have spectral response range of 0.6 μm to 1.8 μm covering a wider IR range. They offer good sensitivity at a low cost. InGaAs has a spectral response close to that of germanium but has a lower dark current and higher sensitivity. Its spectral response extends from 0.7 μm to 1.7 μm.

13.8.6.3 Photo-emissive Sensors

Photo-emissive sensors have a photo-cathode and an anode; the anode is kept at a suitable positive potential with respect to the cathode. The potential gradient in the inter-electrode region, is enough to attract all the freed electrons to the anode resulting in an anode current. The cathode is coated with an optically transparent substrate -which is a suitable photo-emissive material. The materials used should have a high absorption, long free path for any electron freed and a low work function to allow the freed electrons to escape even with a low energy. Normally known photo-emissive materials and their relevant properties are listed in Table 13.7. These are useful in the near IR and the visible regions only. Their quantum efficiency is low.

Table 13.7 Properties of commonly used Photo-emissive materials

Material	λ_c (μm)	η %
Ag-O-Cs	1.1	1
Cs-Nag-K-Sb	0.9	20
Ga-As-P	0.9	30

13.8.7 Direct Method-Execution

Two approaches are in vogue. The basic detector and the initial processing of the detected signal are similar in both cases.

13.8.7.1 Two-colour Method

The 'Two-Colour method' compares the intensity of radiation received at two distinct wavelengths – λ_1 and λ_2 (hence the name). Using Equation 13.16 we get the ratio of intensities of radiation at the two wavelengths as

$$\frac{W_{ë1}}{W_{ë2}} = \left(\frac{\lambda_1}{\lambda_2}\right)^{-5} \exp\left\{-\frac{c_2}{T}\left[\frac{1}{\lambda_1}-\frac{1}{\lambda_2}\right]\right\} \qquad (13.38)$$

Once the wavelengths are known, T is directly related to the ratio of the respective intensities. In practice, the total radiation over a narrow window of $\Delta\lambda$ is received in each case and compared. Emissivity of the material does not affect the reading. Since only the relative intensities at the two wavelengths are compared, the object need not fill the FOV. Intervening gases, moisture, glass window, *etc.*, do not affect the reading provided λ_1 and λ_2 are selected such that their emissivities are the same at these wavelengths.

Detectors are available which are specifically tailored for two-colour detection. They use a sandwich structure with a Si photo-diode of the transmitting type on top and a photo-diode (Ge) or a photo-conductor (PbS or PbSe) type detector underneath. The Si photo-diode senses the radiation at 0.94 μm (typical). The second wavelength is chosen depending on the material used – it may be 2.2 μm with PbS, 3.8 μm with PbSe or 1.55 μm with Ge or InGaAs. Normally, λ_1 and λ_2 are selected such that both are lower than λ_p – the wavelength at which the radiation is a maximum [See Figure 13.21]. This puts an upper limit to the temperature that can be sensed. Ideally, it occurs at the temperature for which $\lambda_2 = \lambda_p$. The practical

limit is somewhat lower. With this constraint, PbSe and Si sensors can be used up to about 450 °C, PbS and Si up to about 1000 °C and Ge and Si as well as InGaAs and Si up to about 1500 °C.

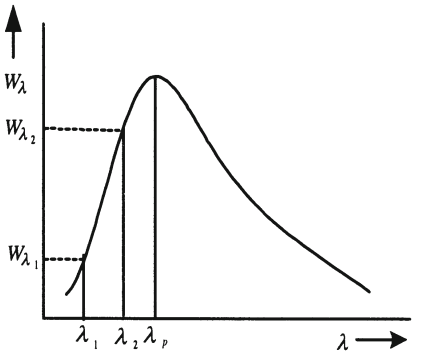


Figure 13.21 Selection of wavelengths for the two-colour pyrometer

All the IR pyrometers of today are microcontroller-based versions. They sample the signals from the two colours alternately. They are converted to digital form and only then, the ratio is computed. Dual sensors in the same housing one behind the other, enables one common optical path for both (The earlier practice was to have two optical paths with individual sensors. These used mechanical choppers and synchronous switching).

A typical arrangement is shown in Figure 13.22. The two detectors are D_1 – a photo-voltaic diode and D_2 where D_2 can be a photo-voltaic diode or a photo-conductor. The voltages v_1 and v_2 are proportional to the respective received radiation. $R_f \| C_f$ is selected to provide a cut-off compatible with sensor response-time requirements. Limiting the bandwidth reduces the noise at the opamp level. Amplifiers A_1 and A_2 amplify and bandlimit these signals. The gains are adjusted such that the full-scale output levels correspond to the full-scale input levels of the ADCs. The μC samples these two signals alternately at a high enough frequency – usually a few kHz. The sampled signals are converted into digital form by the ADC and input to the μC. The μC computes the ratio of the received radiations and computes the source temperature according to Equation 13.38. The non-linear ratio between the intensity ratio and the temperature is handled using a piece-wise linear segment of the characteristic or a LUT or a combination of the two.

Observations: -

⇒ The two-colour method avoids inaccuracies due to absorption in the intervening medium. The numerical value of ε_r of the target need not be known. The only constraint is that ε_r at both the wavelengths should be the same. Thus, temperatures of different targets can be measured using the same instrument without the need for recalibration or readjustment.

⇒ Unlike the total-radiation detection method, the target need not fill the viewing area.

⇒ If the intervening medium has particles of the same sizes as the wavelengths used, the results may be erroneous. However, note that the other methods are no better in such cases.

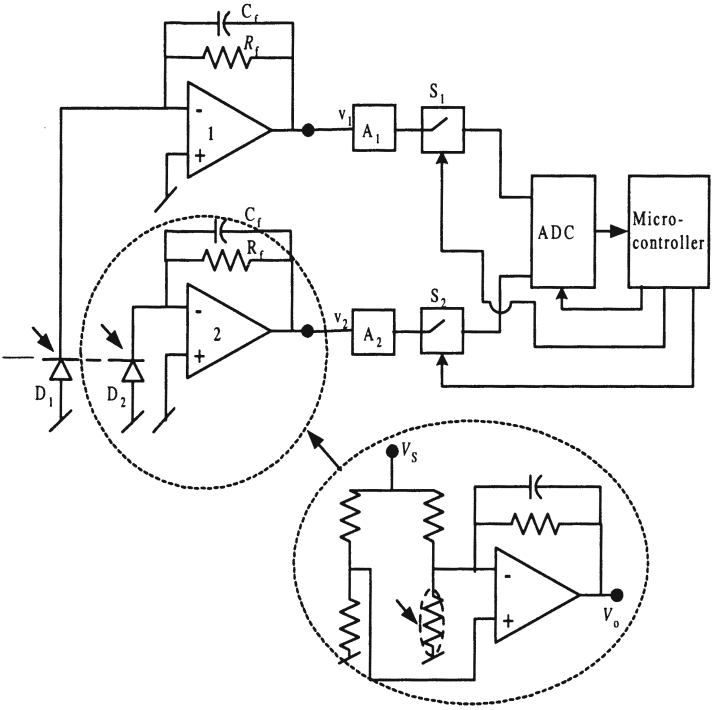


Figure 13.22 Block diagram of two-colour pyrometer using two photo-diodes. If a photo-conductor is used in place of one of these, the corresponding circuit block is replaced as shown aside

⇒ Two colour instruments tailored to individual applications are available. They sense radiation at specific wavelengths in the bands suitable for the target concerned. 7.9 μm is suitable for plastics up to 600 °C. 4.8 to 5.2 μm is suitable for glass, ceramic surfaces *etc.* The corresponding temperature range may be 300 °C to 1500 °C. Flame monitoring is with 3.86 μm in the 500 °C to 1500 °C range. 1.1 μm to 1.65 μm is used for metal viewing through glass with a wide temperature range of 250 °C to 2500 °C. All these applications have bands of wavelengths not conforming to the dual sensor modules discussed above. These instruments use two separate sensors with the received radiation directed to either, through optical filters. The radiation is directed to them, through mechanical choppers. Subsequent part of the instrument remains similar.

⇒ Accuracy of the thermocouple pyrometer is typically 1 %. The FOV is in the 0.5° to 2.5° range, making room for a focusing range of 50m to infinity. Response time is of the order of 300ms. The sophistication in sensing and circuitry make these instruments costly. They are 5 to 20 times costlier than the thermal-detector type pyrometers.

⇒ More sophisticated versions of the pyrometers are also available. They use three colours and account for the change in ε_r with wavelength. These are not widely used.

13.8.7.2 *Single Colour Pyrometer*

The 'Disappearing Filament' type optical pyrometer was the only type available to do non-contact measurement of temperature. This was used in the days prior to electronics circuits becoming versatile and economic. This uses a heated filament in the FOV. The filament current is adjusted such that the filament disappears in the background (The FOV has a red filter). The filament current is calibrated in °C. The method essentially matches the intensity of radiation from the filament to that in the source in the FOV, at a selected narrow bandwidth. The single colour type pyrometers use the same principle. Manufacturers use different and often patented realizations. Typically, the radiation from the target is focused and filtered in the instrument's optics. The instrument has an internal radiation reference source. This can be in the form of an LED – aged and stable. The LED current can be adjusted until the two radiations match. The comparison is done by directing the radiation from either source alternately on to a sensitive detector (photo-multiplier tubes). The LED current is adjusted until the two currents match. The LED current now, is a measure of the target temperature.

The schematic is simpler in principle and execution, compared to the two-colour scheme. It is less costly. However, it requires the ε_T of the target to be known. Normally short wavelengths (Red — 0.64 μm) are used so that the sensitivity to changes in ε_T is low.

13.8.8 Temperatures of Inaccessible Locations

Fibre optic bundles can be used to sense the radiation from inaccessible locations. The individual fibres are of glass of 5 μm to 25 μm diameter. The bunch is bundled and held together by high temperature epoxy. A sheath holds the bundle together and offers mechanical protection. The front-exposed-face of the fibres is levelled and polished to ensure that the reflectivity is low and the face is well defined. A separate lens may be provided at the front to focus the radiation and provide a clearly defined field of view. The cable is normally ½ m to 4m long. The end of the cable is terminated on the detectors; as such the radiation sensing and the instrumentation remain identical to the schemes discussed in the previous section.

Table 13.1 The fixed temperature points of ITS-90

No.	Temp. (K)	Substance	State	No.	Temp. (K)	Substance	State
1	Defined through vapour-pressure temperature relations of He in the 3K – 5 K range			9	273.16	H_2O	T
				10	302.9146	Ga	M
2	13.8033	e-H_2	T	11	429.7485	In	F
3	≈ 17	e-H_2	V	12	505.078	Sn	F
4	≈ 20.3	e-H_2	V	13	692.677	Zn	F
5	24.5561	Ne	T	14	933.473	Al	F
6	54.3584	O_2	T	15	1234.93	Ag	F
7	83.8058	Ar	T	16	1337.33	Au	F
8	234.3156	Hg	T	17	1357.77	Cu	F

Meanings of symbols in the last column: T—Triple point; V—Vapour pressure point; M—Melting point; F—Freezing point

Table 13.2 Thermocouples, their characteristics and areas of application

Thermocouple type with percentages of components	ANSI std. type designation	Recommended range in °C	Maximum accuracy	Maximum sensitivity μV/	Application environment	Remarks
Iron/ Constantan (Cu 54,Ni 44 & Mn, Fe 0.5)	J	0 t0 500	2.2 °C or 0.75%	51	Useful in oxidizing and reducing atmospheres. Upper limit can extend up to 700 - 800 °C	Most widely used due to low cost and high sensitivity ◊ Even small levels of impurities in iron, can affect accuracy adversely ◊ Abrupt magnetic transformation in crystalline structure, at high temperatures, causes non-recoverable decalibration. Hence even transient over-temperatures are to be avoided
Chromel/ Alumel (Ni 90,Cr 10) (Ni 94, Mn 3, Al 2, Si 1)	K	–200 to 1300	2.2 °C or 0.75%	40	Non-reducing atmosphere up to 1300 °C	Best among base metal thermocouples for free air atmosphere; Resists oxidation over full range ◊ Fairly linear characteristic ◊ Chromel gets oxidized above 500 °C; even when sheathed, the low oxygen content beneath suffices to oxidize Chromium; hence the life of the thermocouple is limited when used at high temperatures
Copper/ Constantan (Cu 57,Ni 43)	T	–200 to +350	1 °C or 0.75%	40	Essentially for laboratory application	Oxidation of copper at higher temperatures, limits upper operating temperature ◊ Highly stable characteristic ◊ One wire being of copper, no need of separate compensating cable

Table 13.2 (continued)

Thermocouple type with percentages of components	ANSI std. type design.	Recommended range in °C	Maximum accuracy	Maximum sensitivity μV/°C	Application environment	Remarks
Chromel/ Constantan (Ni 90, Cr 9.5, Si 0.4) (Cu 57,Ni 43)	E	–200 to +900	1.7 °C or 0.5%	60	Good for low temperature applications	High sensitivity & low thermal conductivity ◊ Low corrosion resistance (See the observations on Chromel under K type thermocouple)
Pt Rh 13/Pt	R	0 to 1400	0.25% or 1.5 °C	7	Oxidizing atmospheres	Noble metal thermocouple ◊ Chemically inert, stable in oxidizing atmospheres at high temperatures ◊ Rapid deterioration in reducing atmospheres ◊ In vacuum even at 500 °C, Platinum sublimes, rapidly weakening the thermocouple ◊ Most stable amongst all hermocouples ◊ At high temperature metal vapour can diffuse into Platinum causing error; use sheath of Alumna or so to avoid the same ◊ Type B requires negative cold junction compensation in the 0 to 40 °C range
Pt Rh10/Pt	S					
Pt Rh30 /Pt Rh 6	B	to1700	0.5%			
Tungsten / Tungsten 26, Re	G	400 to 2300			In vacuum, hydrogen or inert atmospheres ◊ For the highest Temperatures that can be measured with a Thermocouple	Oxidizing atmospheres to be avoided even at lower temperatures These are not ANSI standard
Tungsten 5, Re /tungsten26, Re	C					

14 Process Instrumentation II

Pressure, Flow & Level

14.1 Introduction

Temperature is the most widely sensed process variable in industry. The same has been discussed in detail in the last chapter. Pressure, flow and (to some extent) level – perhaps in that order – are the next most-widely sensed process variables. These three relate to fluids. Often same or similar techniques are used to sense and process them. These justify their being clubbed together for discussion here.

14.2 Pressure Instrumentation

Pressure measuring devices are second only to temperature measuring devices in terms of numbers used in Industry. Technology-wise, pressure sensing does not have variety. Broadly, only two main types of sensing are in vogue [Benedict, Cerni and Foster]: -

⇒ Pressure sensing using an elastic member like Bourden gauge or bellows.

⇒ Pressure sensing using a diaphragm and measuring the strain on the diaphragm using strain gauges.

Techniques, apart from the above two, are essentially limited to specialized applications [Ajluni, Considine].

14.2.1 Types of Pressure Measurement

Pressure sensing is normally carried out with different references (See Figure 14.1).

⇒ 'Absolute Pressure' is the absolute pressure exerted by the fluid. Absolute pressure sensors sense them directly. Often a sealed vacuum chamber is used as zero reference pressure for this.

⇒ Sealed pressure sensors use a fixed reference pressure; the pressure measurement is done with respect to this. The fixed reference pressure is often 14.7 psi – the atmospheric pressure at STP conditions. Air or an inert gas is filled and sealed in an enclosure at 14.7 psi for this purpose. Altimeter is one popular area of application for this.

⇒ 'Gauge pressure' sensors measure the pressure of the fluid relative to the atmospheric pressure of the environment. At STP conditions, this is 14.7 psi. At other temperatures and altitudes, it changes from this value.

T. R. Padmanabhan, *Industrial Instrumentation*
© Springer-Verlag London Limited 2000

⇒ 'Differential pressure' sensors measure the difference between two pressures. They find application in flowmeters, viscosity measurement, density measurement, level gauge *etc*. Often the other types of pressure sensing mentioned above are carried out using differential pressure sensors. One of the two pressures is fixed, the other being the pressure to be measured.

⇒ 'Vacuum gauges' measure pressure below the atmospheric. They can be of the relative type when pressure relative to the atmosphere is measured. They can be of the absolute type also when they measure the pressure directly above the absolute zero value.

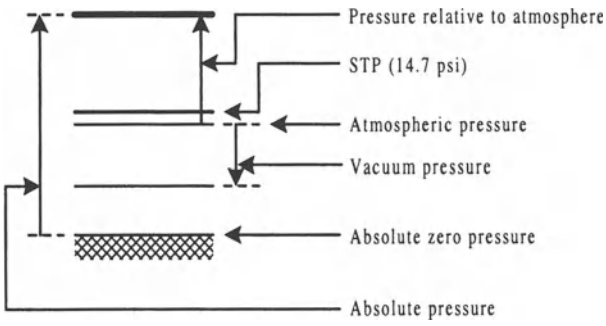


Figure 14.1 Illustration of different ways of expressing pressure

14.2.2 Units of Pressure

Pressures encountered in practice span a wide range. Moreover, for historical reasons, different units are used to express pressure. A conversion table amongst the units is given in Appendix E. Often the pressure is expressed in psi or multiples of atmospheres. When referred to water circuits, it is expressed in inches of water column. Low pressures are expressed in terms of mbar, mm of Hg or microns.

14.2.3 Bourdon Tube and Bellows

The Bourdon tube is well established; it forms one of the oldest methods of pressure measurement. The tube has an elliptical or a flattened cross-section. It is normally formed as a circular arc, a spiral, a helix or in a twisted tube form. It is made of phosphor bronze, beryllium-copper or stainless steel. One end of the tube is closed and the pressure to be sensed, applied at the other end. As the pressure is applied, the tube tries to take a circular cross-sectional shape. In the process, it undergoes deflection – essentially straightening (See Figure 14.2). The resultant displacement of the free end is a measure of the fluid pressure. Through levers, the displacement is converted into equivalent angular displacement of a pointer in front of a dial gauge. This is the widely used and popular pressure gauge. Bourdon tube measures the differential pressure. If the pressure inside and outside are equal, the tube does not experience any deformation of this type.

The displacement, which is proportional to the pressure measured, can be sensed using any of the displacement sensors and converted into equivalent electrical form. LVDTs, differential capacitance sensors and force balance systems can be used for this.

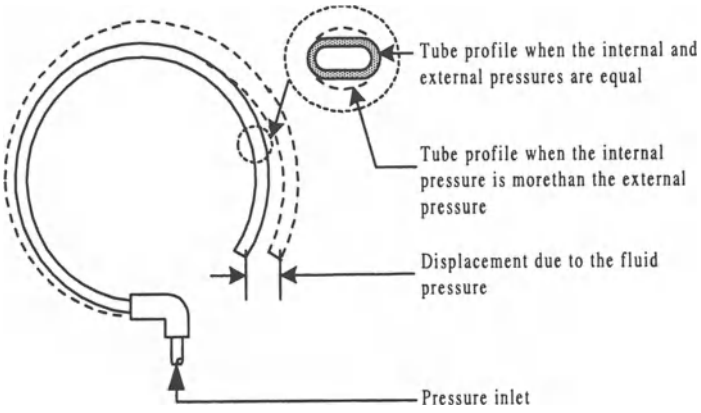


Figure 14.2 Bourden gauge

Bellows provide only linear displacement (See Figure 14.3) proportional to the pressure to be sensed. They measure relative pressure. For differential pressure measurement, the two pressures are applied to either side of the bellows or two separate bellows can be used in the differential mode. Since Bourdon gauges are not sensitive below ~15 psi, bellows are used in this range. Bellows can be used for absolute pressure measurement also. By linking the bellows to the tie rod of displacement sensors like LVDTs, the measured pressure can be converted into an equivalent electrical form.

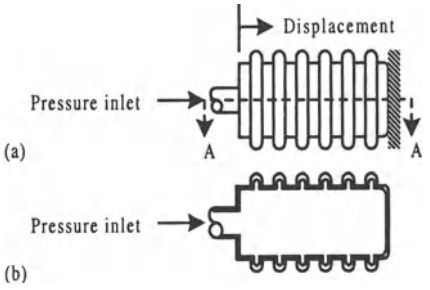


Figure 14.3 (a) Bellows for pressure sensing (b) Section through 'AA'

Bourdon tubes and bellows provide accuracy of 2 to 3 %. Their performance is affected by temperature. Some gauges have built-in temperature compensation. With this, the accuracy improves to 1 %. Accuracy is comparatively lower in the ranges below 100 psi. When using a displacement sensor to convert a displacement to electrical form, their high sensitivity can be taken advantage of, and the active range of operation of the sensor restricted. With this, the repeatability and accuracy improve. Accuracy possible is in the 0.25 % range.

Capsules are more sensitive than bellows (See Figure 14.4) and are used when the pressure to be sensed is low. Capsules also offer better repeatability and accuracy. Bourdon tubes and bellows are widely used as direct reading pressure gauge elements. But at present their use for transducer type application, is rather limited.

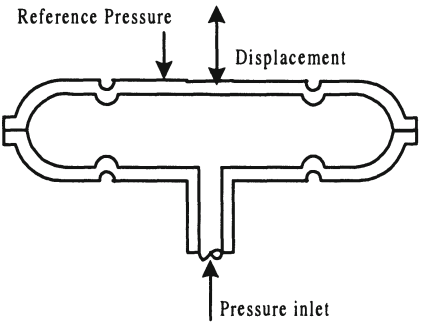


Figure 14.4 Capsule for pressure sensing

14.2.4 SG Based Pressure Sensors

Many pressure sensors of today use diaphragms as the primary sensors. The resultant strain in the diaphragm is sensed using SGs. Consider such a diaphragm subjected to pressures P_1 and P_2 on either side with $P_1 < P_2$. The diaphragm undergoes deflection. Figure 14.5 shows the diaphragm in the original form (dotted line) and after deflection. Near the centre of the diaphragm D, the radial and circumferential stresses are tensile and close to the periphery where it is clamped, these are again tensile. Assuming uniform clamping all round, we get the following relationships:

The radial stress at a radius r from the centre of the diaphragm D, is

$$s_s = \frac{3pR^2\eta}{8t^2}\left[\frac{1}{\eta}+1-\left(\frac{3}{\eta}+1\right)\left(\frac{r}{R}\right)^2\right] \tag{14.1}$$

The corresponding tangential stress is

$$s_t = \frac{3pR^2\eta}{8t^2}\left[\frac{1}{\eta}+1-\left(\frac{1}{\eta}+3\right)\left(\frac{r}{R}\right)^2\right] \tag{14.2}$$

The respective strains are given by

$$\varepsilon_r = \frac{s_r - \eta s_t}{E} \tag{14.3}$$

$$\varepsilon_t = \frac{s_t - \eta s_r}{E} \tag{14.4}$$

where

⇒ R is the radius of the diaphragm
⇒ p is the difference in the pressures
⇒ t is the thickness of the diaphragm

$\Rightarrow \eta$ is Poisson's ratio
$\Rightarrow r$ is the radial distance of the point of interest from the centre of the diaphragm
$\Rightarrow s_r$ is the radial stress
$\Rightarrow s_t$ is the tangential stress
$\Rightarrow \varepsilon_r$ is the radial strain and
$\Rightarrow \varepsilon_t$ is the tangential strain and
$\Rightarrow E$ is the modulus of elasticity of the material of the diaphragm.

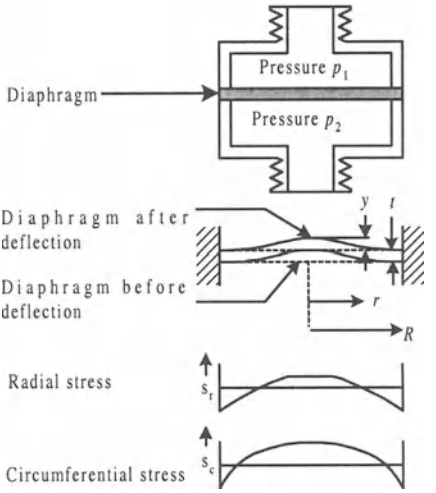


Figure 14.5 Diaphragm for pressure sensing. The nature of radial and circumferential stresses due to the pressure differential on the two sides is also shown

The circumferential strain near the centre is tensile and that near the periphery (on the same side) is compressive. SG rosettes [See Section 12.4] specifically intended to sense these two strains are available. Using this, the four-arm bridge can be formed for sensing. From the measured strains, one can obtain the pressure. The above equations give the relationships necessary to compute the pressure value from the measurement at a point. Since the SGs are spread out to increase sensitivity, these relationships cannot be used directly. The output of each SG is a weighted-sum of the strains along its length. Still the output can be directly related to pressure. In practice, the SGs are fixed on the diaphragm and the combined transducer calibrated as a whole.

14.2.4.1 Diaphragm with Bonded SG

Stainless steels are normally used as the diaphragm material. The SG rosette is sputtered and formed on it. Sensitivity, excitation to be used *etc.*, have been dealt with in Section 12.3. Use of stainless steel makes the diaphragm quite robust. Any liquid or gas that does not corrode the stainless steel used, can be the medium whose pressure is to be sensed. This covers a wide range. The GF of around 2, necessitates a comparatively wider area for the gauge rosette. Pressure sensors normally give 1 % accuracy at full scale. Some offer 0.1 % accuracy.

14.2.4.2 *Diaphragm with Semiconductor SG*

Silicon SGs are formed directly on crystalline silicon wafers. On a circular crystal wafer of Si, a circular cavity is etched (Figure 14.6). This defines the sensing diaphragm. The unetched portion forms the rigid (relatively inelastic) support. It also serves as the base for bonding leads. The gauge resistances are formed directly on Si, by a process akin to IC formation. The gauge and the leads are all on one side – the non-etched side. The fact that the gauge and the diaphragm are of the same material ensures that there is no relative thermal expansion between the gauge and the diaphragm. Absence of a bonding – due to the direct gauge formation – increases the reliability and the life of the gauge and sensor substantially. The high GF extending up to 200 increases basic sensitivity and reduces size. Normally Si SGs are fabricated with bridge arm resistances in the 1000Ω range.

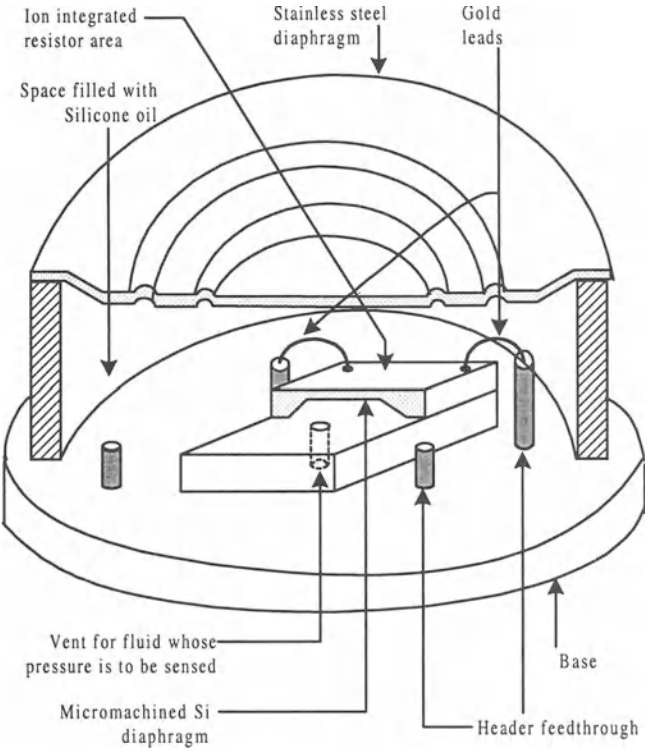


Figure 14.6 Si etched type diaphragm gauge

Lack of repeatability, limits the accuracy substantially. With judicious addition of external resistances, thermal coefficient and allied error, gain error and offset are adjusted. These impair the sensitivity but improve the overall performance specifications. With these corrections, 1% full scale accuracy is normally guaranteed by manufacturers. Since the diaphragm is of Si in crystalline form, it is an ideal elastic material. Hysteresis error is negligible. It is very close to an ideal primary sensing diaphragm that one can have.

14.2.4.3 *Application Considerations*

⇒ Normally the maximum pressure to be sensed in an application is estimated; based on this, the full-scale value of the pressure transducer is selected. Manufacturers specify the continuous overload that the pressure transducer can withstand. It is 200 % to 250 % with some, while others specify 500 % overload.

⇒ The fluid, whose pressure is to be measured, should not react with the diaphragm or corrode it. In this sense, stainless steel diaphragm can withstand a variety of liquids and gases. In contrast, Si diaphragm gauges are essentially limited to dry gases.

⇒ Both types of diaphragm transducers are available over a wide pressure range extending up to 100,000 psi. However, for pressures less than 100 psi, semiconductor gauges are preferred due to their better accuracy.

⇒ For mediums in vessels or enclosures, up to 150 °C, the pressure transducer can be directly mounted on it. However at higher temperatures, the pressure transducer is connected through a short length of tubing. Typically, a 6" long and 0.25" dia. piping will protect the pressure transducer from an enclosure up to 600 °C. Manufacturers provide recommended pipe lengths for various high temperature environments.

⇒ With high-pressure lines, flow lines *etc.*, water hammer can cause sudden pressure transients. Pressure 'Snubbers' are provided to damp out these surges and protect pressure transducers used. Snubbers are generally porous stainless steel obstructions between the pressure transducer and media supply. They reduce the response bandwidth considerably.

⇒ Basic bandwidth of the pressure transducer extends up to ~1 kHz; With semiconductor gauges, it can be much higher. Direct flush mounting of the transducer on the medium housing, does not affect bandwidth. However, the tubing, the connection chamber *etc.*, reduce the effective bandwidth. In process applications, bandwidth of pressure transducer is rarely a limiting factor.

⇒ Pressure transducers provide typically 30 mV output at full scale. This can be used up to 60 m length directly. If the signal processing station is farther away, the transducer output is amplified to the voltage levels before transmission. Typically, 300m is the limit of transmission here. 4-20 mA format extends the length. However for longer transmission lengths, a digital link is to be used.

⇒ Pressure sensor can be filled with Silicone oil or other patented fluids and sealed. With these, the pressure to be measured is applied to a diaphragm, which separates the sensor from the medium. Thus insulated, the sensor can be adapted to sense pressure of a variety of liquids and gases.

14.2.5 Capacitance Type Pressure Transducers

The differential capacitance type sensor (See Section10.3), is ideally suited to measure differential pressure of fluids using a diaphragm gauge. The differential gauge and capacitor are integrated here as shown in Figure 14.7. The stainless steel diaphragm in the middle forms the common electrode. The two cups of ceramic (glass) on either side form the chambers where the fluid is allowed in. Both the cups

are metallized inside (with gold). The metallized surfaces form the two outer electrodes of the differential capacitance. The whole scheme can be precisely defined and assembled with minimum effective clearance for the dielectric. This increases the effective capacitance. Movement of the diaphragm in either direction reflects as corresponding changes in the two capacitances. Only dielectric fluids (non-conducting) can be used as the medium. Often the two side chambers are filled with silicone oil and sealed. The pressures are applied to the outer sides of the respective isolating membranes. The whole transducer assembly becomes rugged and gets insulated from the vagaries of the application.

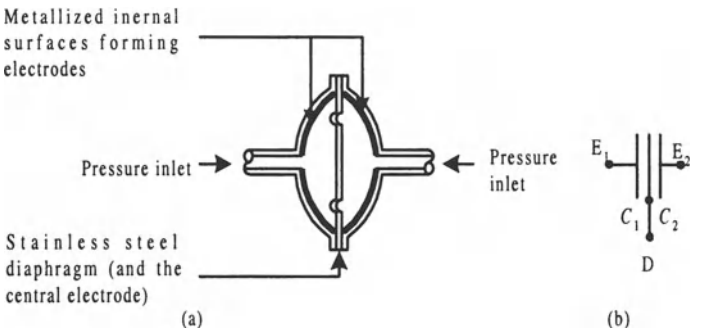


Figure 14.7 Capacitance type differential pressure gauge with diaphragm (a) Schematic diagram (b) Equivalent circuit

14.2.6 Low Pressure Instrumentation

Bourdon tubes are useful for pressures down to 10 Torr. and bellows down to 0.1 Torr. With diaphragm and semiconductor gauges one may sense pressures down to 10^{-3} Torr (1 micron). For lower pressures, other unconventional and indirect methods are used. For industrial applications, transducers of three types cover three overlapping ranges. In all these cases, the measurement gives an order of the pressure concerned rather than a precisely measured value.

14.2.6.1 Pirani Gauge

Thermal conductivity of a gas varies linearly with pressure for pressures lower than 10^{-2} Torr. For higher pressures also, a one-to-one functional relationship exists though not linear. The Pirani gauge exploits this to measure pressure indirectly. The common form of the Pirani gauge uses a pair of tungsten wire resistances supported inside glass tubes. One forms a reference. It is evacuated to a low definite pressure and sealed. The other tube is used to measure the pressure of the medium. These two along with two other equal resistances, form a Wheatstone bridge (Figure 14.8).

When a current is passed through the sensing resistor, its temperature rises due to the power loss in it. It attains a steady temperature depending on the thermal conductivity of the gas medium. The heat is transferred to the environment through conduction and radiation through the gas. The enclosure tube is kept cool enough to keep the radiation loss low. Thus most of the heat energy is carried away by

convection, which is decided by the thermal conductivity of the medium and hence the pressure of the medium. The reference element is kept in the same environment as the measuring element – both are at the same temperature. This compensates for errors due to temperature changes.

The filament resistance changes by about 10 % over a dynamic range of $1:10^3$. Pirani gauges can be used over the 0.01 to 100 Torr. range. The gauge has to be calibrated separately for each gas. Normal accuracy is of the order of 15 %. When calibrated and restricted to a narrower range, it may be better (~5 %). Due to the low thermal conductivity of the gas, the thermal time constant of the scheme is of the order of a few seconds. Hence, the response time is of the order of a minute.

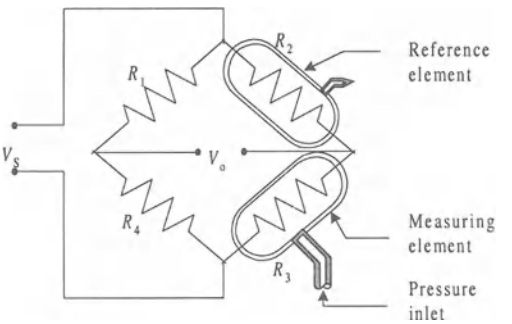


Figure 14.8 Pirani gauge for measuring low pressures

14.2.6.2 Thermocouple Gauge

Thermal conductivity of a medium can be measured indirectly, using a thermocouple gauge. A definite current is passed through a metal strip of resistance element kept in a tube with the medium whose pressure is to be measured, inside. The metal strip has a thermocouple welded to it. Voltage developed by the thermocouple is used as a measure of the temperature of the strip and hence that of the pressure in the medium. Here again the enclosure tube is to be kept cold to minimize heat transfer through radiation. A separate isolated supply is used to heat the metal strip. This facilitates direct processing of the thermocouple voltage. The heating can be carried out from an isolated secondary of a transformer. Some manufacturers use two metal strips in an enclosure and connect the thermocouple output in series to improve sensitivity. An identical unit kept in an evacuated sealed tube, can be used in series opposition to the above. This provides compensation for ambient temperature variations.

Thermocouple gauges have active ranges somewhat lower than the Pirani gauge. They are used in the 10 to 10^{-3} Torr. range with an accuracy of 25 %. This improves to 5 % with temperature compensation and range restriction.

14.2.6.3 Ionization Gauges

A variety of ionization gauges is available. No specific configuration can be said to be dominant or common. All of them ionize the gas at a definite rate, measure the ionic current and use it as a measure of the gas pressure. The simplest works on the conventional cold-cathode principle. For pressures less than 10^{-3} Torr., the electrical discharge through the gas increases with pressure. Roughly, it is proportional to the

logarithm of the pressure. A cold cathode tube is to be used for the purpose (See Figure 14.9). The two-electrode tube has the medium whose pressure is to be sensed. A high voltage (2 kV to 5 kV) is applied to the anode with a current limiting resistor R_a in series. The current is sensed at the cathode end using a log amplifier. Its output is directly proportional to the pressure of the medium. The unit requires a highly stabilized voltage and all necessary protection for the low voltage circuitry. It can be used to measure pressure in the 10^{-6} Torr. to 10^{-3} Torr. range.

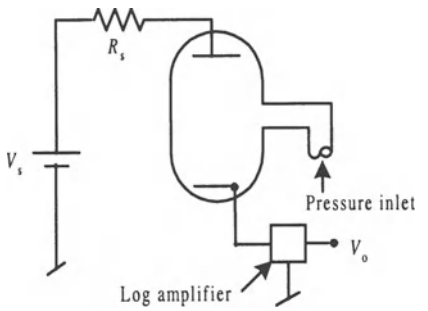


Figure 14.9 Ionization gauge

One modification of the cold-cathode tube arrangement uses a steady transverse magnetic field. Due its presence, the charged particles traverse a longer path causing more collisions and increasing the ionic current. This allows the anode voltage to be reduced without sacrificing sensitivity. These are used down to 10^{-6} Torr. of pressure. Accuracy is normally limited to 25 %.

A compact version of the ionization gauge makes use of the hot cathode for electron emission. Structure-wise it is similar to the conventional triode (See Figure 14.10). It has a hot cathode surrounded by a wire mesh type grid and an anode. The grid is kept at a positive potential with respect to the cathode – typically 100 V. The anode is kept at a negative potential. The electrons emitted by the cathode are accelerated thanks to the grid potential. As they move, they collide with

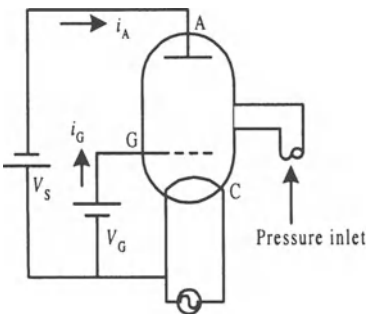


Figure 14.10 Hot-cathode type ionization gauge

the neutral atoms in the medium and ionize them. The electrons are attracted and collected by the grid and form the grid current. The positively charged ions are accelerated towards the anode and are collected by it as anode current. As the gas

pressure increases, the number of neutral molecules ionized per unit time, increases and the anode current increases. Due to the lower voltages employed, the gauge is comparatively compact. The voltages applied and the point of measurement of anode current, make the electronics more cumbersome compared to the cold-cathode tube.

The hot cathode type sensor can be used to measure pressures down to 10^{-10} Torr. Again, the accuracy attainable is limited to 20 %.

14.3 Basics of Fluid Flow

The factors that have a bearing on the flow and influence the relation between the flowmeter reading and the quantity flowing, will be discussed here. The bulk-modulus of liquids, is so high that for the pressures encountered in practice, the change in the volume of the liquid, is insignificant – in fact its effect on flow measurement error, is small enough to justify it being neglected. In flow instrumentation, all liquids are considered incompressible; in contrast, all gases are compressible and the compressibility is to be accounted for, in gas flow instrumentation.

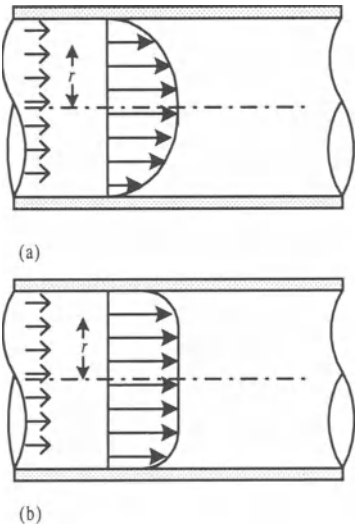


Figure 14.11 Flow of a liquid through a pipe: Velocity profile at any cross section for (a) laminar flow and (b) turbulent flow

14.3.1 Flow of Fluids

At low velocities, the fluid flows through the medium in distinct streamlines or layers; viscous forces have a say in the behavior of the fluid – liquid as well as gas. If we consider a pipe through which a fluid is flowing, the velocity profile through

it has (almost) a radial symmetry and will appear as in Figure 14.11 (a). The layer at the periphery in contact with the inner surface of the pipe – the boundary layer – is stationary. The fluid velocity at the boundary layer, is zero. As we move inside through successive layers, the fluid velocity increases steadily reaching a maximum along the central line of the pipe. The velocity distribution is parabolic in nature. The total quantity of fluid flowing is

$$Q = \bar{v}A \tag{14.5}$$

where

⇒ A is the area of section of the pipe through which the fluid is flowing
⇒ $\bar{v}$ is the average velocity of the fluid in the pipe and
⇒ Q is the volume flow rate.

As the flow rate increases, the streamlined flow gives way to turbulent flow. The velocity profile may be more flattened and may be as shown in the Figure 14.11 (b). In this region, the inertial forces dominate over the viscous forces. Reynolds's number for the fluid in motion distinguishes between the two motions. The Reynolds's number is a non-dimensional quantity. It is given by

$$N_R = \frac{\rho v D}{\mu} \tag{14.6}$$

where

⇒ N_R is the Reynolds's number
⇒ ρ is the density of the fluid
⇒ v is the velocity of the fluid.
⇒ D is the diameter of the pipe (For non-circular pipe sections, an equivalent diameter is considered) and
⇒ μ is the coefficient of absolute viscosity

When all the quantities are considered in consistent units, N_R is a non-dimensional number. More often N_R is expressed in engineering units as follows: -

$$N_R = \frac{3160 Q_{gpm} S_p}{\mu_{cp} D} \text{ (Liquid)} \tag{14.7}$$

$$= \frac{379 Q_{cfm} \rho}{\mu_{cp} D} \text{ (Gas)} \tag{14.8}$$

where

⇒ Q_{gpm} is the volume flow rate in gallons /min.
⇒ Q_{cfm} is the volume flow rate in cubic feet /min.
⇒ S_p is the specific gravity of the fluid
⇒ μ_{cp} is the coefficient of viscosity in Centi-poise
⇒ D is the diameter of the pipe in inches.

The transition from laminar to turbulent flow is far from abrupt. Generally flow conditions with $N_R < 2000$, represent laminar flow and those with $N_R > 10{,}000$, represent turbulent flow. The region in between, is the transition region.

Liquids being incompressible, only viscosity (and of course flow rate) decides R_N. Viscosity of liquids changes with temperature. Figure 14.12 shows the general nature of variation. A flow rate, which is laminar at one temperature, can become turbulent at a higher temperature – due to a reduced viscosity.

Observations: -

⇒ The velocity profile of a liquid across a cross-section varies with flow conditions.

⇒ Often a flowmeter reading requires a correction to account for this variation.

⇒ Knowing the fluid temperature, one can get its viscosity. From this and the approximate flow rate, N_R can be calculated.

⇒ When $N_R < 2000$, the flow is laminar and the peak velocity and flow rate can be related using the parabolic distribution of Figure 14.11 (a).

⇒ When $N_R > 4000$, the flow can be taken as turbulent. The velocity can be taken as constant across the whole cross-section.

⇒ For $2000 < N_R < 4000$, the profile is more involved and not tractable analytically. Empirical relations are more common in this range.

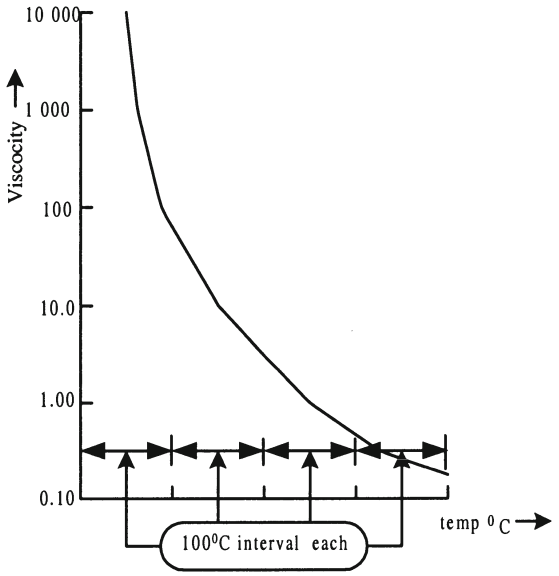


Figure 14.12 Nature of variation of viscocity of a liquid with temperature

14.3.1.1 Flow of Gases

The demarcation between laminar and turbulent flows, holds good for gases also; *i.e.*, for $N_R < 2000$, the flow is laminar. For $N_R > 4000$, it is turbulent; for N_R values in between, the flow is in the transition region. However, for the majority of the cases encountered in practice, the flow is in the turbulent region.

14.3.1.2 Viscosity of Gases

Viscosity of gases is much less dependent on the temperature. It is in the 8 to 40 millipoise range and varies over this range as the gas temperature varies from 0°C to 400°C. Figure 14.13 shows the nature of variation of viscosity of gases with temperature. Normally the viscosity of a gas can be taken as constant over the range of interest of flow.

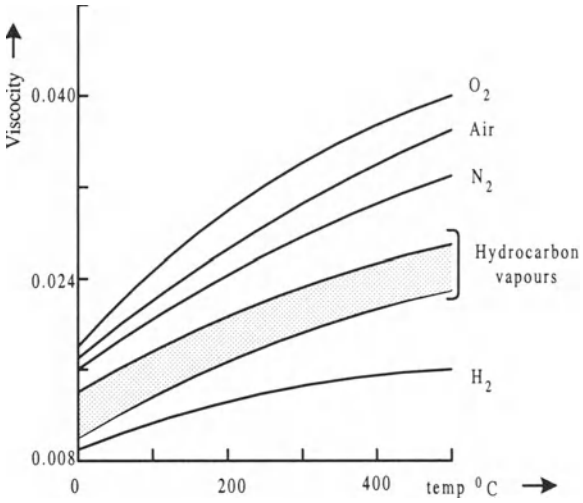


Figure 14.13 Nature of variation of viscocity of gases with temperature

14.3.2 Density of Gases

The density of a gas varies with temperature and pressure. The nature of variation is involved and changes from gas to gas. Under idealized conditions, it is governed by the well-known gas law

$$\frac{PV}{T} = nR \tag{14.9}$$

where

⇒ P is the pressure of the gas
⇒ V is the volume of the gas
⇒ T is the absolute temperature of the gas
⇒ n is the number of mols of the gas considered and
⇒ R is the universal gas constant.

If any of the two quantities, P, V or T is known, the third can be computed using Equation 14.9. A gas obeys the gas law in the above form only under low pressure and comparatively higher temperature conditions. Various modifications of the gas law of Equation 14.9 are available, to describe the state of the gas more precisely and over a wider temperature and pressure range – the van der Waal formulation being more popular. Although the relationships change from gas to gas, when expressed in a normalized fashion, they follow a well-defined pattern with reasonable accuracy. Consider one mol of a gas. Let

$$Z = \frac{P_r V}{T_r R} \tag{14.10}$$

Where

$$P_r = \frac{P}{P_c} \tag{14.11}$$

$$T_r = \frac{T}{T_c} \tag{14.12}$$

$\Rightarrow P_c$ is the critical pressure

$\Rightarrow T_c$ is the critical temperature and

$\Rightarrow Z$ is the compressibility factor (or the volume of the gas expressed as a ratio or multiple of the volume of an 'ideal gas')

Figure 14.14 shows the nature of variation of Z with P_r; T_r is the running parameter here. These curves represent the state of the gases over a wide range of T, P and V. They are more general and comprehensive than the relationship of Equation 14.9 and hold good for most of the gases. Accuracy of the relationship varies from 2 % to 7 % over the whole range. Only in the case of hydrogen and helium, the deviation is more substantial.

Flowmeters are normally calibrated under specified conditions. When the actual operating conditions deviate from these, the necessary corrections are carried out with the help of the above universal curves. This also requires knowledge of the critical temperature and critical pressure of the concerned gas (See Table 14.1).

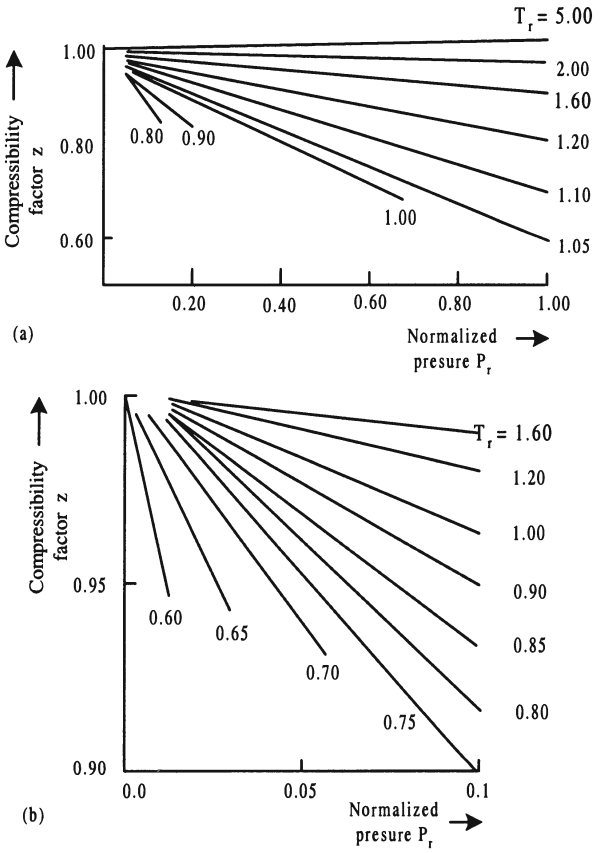


Figure 14.14 Normalized-compressibility charts for normal gases; Normalized temperature is the running parameter

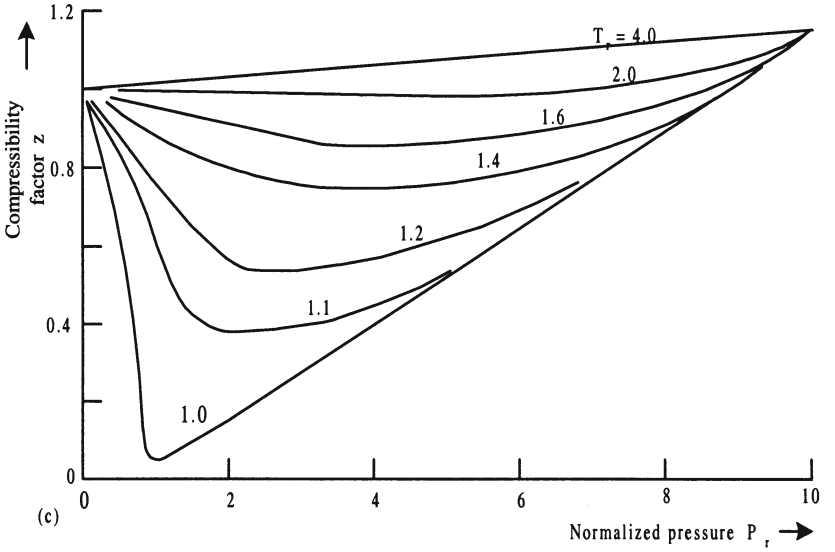


Figure 14.14 (Cont'd) Normalized-compressibility charts for normal gases; Normalized temperature is the running parameter

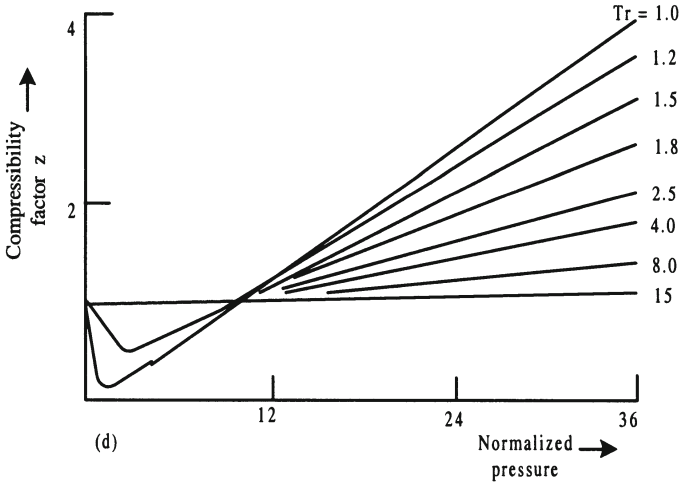


Figure 14.14 (Cont'd) Normalized-compressibility charts for normal gases; Normalized temperature is the running parameter

14.3.3 Standard Conditions

Whenever the value of any physical variable changes with atmospheric conditions, it is specified at widely-accepted standard conditions – often referred to as 'Standard Temperature and Pressure (STP)'. However, there is no universally

accepted and used unique 'Standard conditions'. Some combinations are more commonly used. In the absence of a universally accepted standard, it is good practice to specify the standard along with the concerned value of the variable. Commonly used standard conditions are

- 14 · 696 psia (101 · 325 kPa) and 15° C (59° F)	
- 14 · 7 psia, 14 · 4 psia, 4 oz pressure, 1 bar - 15° C (59° F), 60° F, 68° F, 70° F, 0° C	Combinations of these

Table 14.1 Critical constants of some common gases

Gas	P_c atm.	V_c cm^3mol^{-1}	T_cK	Z_c $[=(P_c V_c/nRT_c)]$
He	2.3	57.8	5.3	0.306
H_2	12.8	65.0	33.2	0.304
Ne	26.9	41.7	44.4	0.302
N_2	33.5	90.1	126.0	0.291
O_2	50.3	74.4	154.5	0.302
CO_2	72.7	95.0	304.2	0.275
H_2O	218.0	55.6	647.3	0.227
NH_2	112.0	72.0	405.5	0.243
CH_4	45.8	99.0	191.0	0.290
C_2H_6	48.2	139.0	305.5	0.267
C_2H_4	50.5	124.0	417.2	0.275

14.3.4 Compensation

The volume flow readings of a flowmeter obtained at specific operating temperature, and pressure conditions can be used as a base for obtaining other data. Thus, one can compute the equivalent volume flow rate at any other specified temperature and pressure. Alternately one can compute the equivalent mass flow-rate. A few specific examples are in order here.

Example 1

Nitrogen is supplied through a pipe at 10.5 atmospheres pressure and 300°C temperature. What should be the flow rate so that it reflects as 500 ft^3/min. at 60 atmospheres and 450°C?

Critical pressure of nitrogen (from Table 14.1) = 33.5 atmos

Critical temperature of nitrogen (from Table 14.1) = 126 k

$$\text{Relative pressure of measurement} = \frac{10.5}{33.5} = 0.3134$$

$$\text{Relative temperature of measurement} = \frac{273.15 + 300}{126} = 4.549$$

Corresponding z value from the chart = 1.0

$$\text{Relative pressure at desired condition} = \frac{60}{33.5} = 1.79$$

$$\text{Relative temperature at desired condition} = \frac{450+273.15}{126} = 5.74$$

$$\text{Corresponding z value from the chart} = 1.08$$

Hence the Nitrogen volume flow rate at the desired conditions, will be 8% more than the volume at the measured conditions. The flow rate at the measured conditions should be

$$\frac{500}{1.08} = 463 \text{ ft}^3/\text{min}$$

Example 2

Repeat the above for Oxygen.

$$\text{Critical pressure of Oxygen} = 50.1 \text{ atmospheres}$$

$$\text{Critical Temperature of Oxygen} = 154 \text{ k}$$

$$\text{Relative pressure of measurement} = \frac{10.3}{50.1} = 0.206$$

$$\text{Relative Temperature of measurement} = \frac{273.15+300}{154} = 3.72$$

$$\text{Relative pressure at desired condition} = \frac{60}{50.1} = 1.12$$

$$\text{Relative Temperature at desired condition} = \frac{273.15+450}{154} = 4.70$$

$$\text{Corresponding z value from the chart} = 1.05$$

$$\text{Required flow rate} = \frac{500}{1.05} = 476 \text{ ft}^3/\text{min}$$

14.4 Flowmeters

The importance of flow instrumentation in industry stems from three factors.

⇒ Fluids like natural gas, petroleum and oxygen are supplied to customers on a continuous basis through dedicated pipelines. Precise on-line measurement of quantum of supply is essential for payment purposes.

⇒ Many processes require precise proportioning of constituents to ensure optimization. Here optimization implies purity of the product desired, quantum of production, minimization of wastage, minimization of the resources used and the like.

⇒ Flow control systems require the flow to be measured, compared with a reference and the error used for control of flow rate in closed loop fashion. The reference often being an electrical voltage, precise conversion of the flow into electrical voltage is essential.

The very variety of liquids and gases used and the conditions of their use (pressure, temperature, viscocity of the fluid *etc.*), call for a corresponding variety in the methods of measurement [Benedict, Cheremisinoff, Chopey, Considine, Ginesi, Solonkhin and Afgan]. As far as the principle of operation is corncerned, possibly, flowmeters have the widest variety – each has its own area of application with some overlap.

Flow measurement is broadly of two types: Point-velocity measurement and quantum-flow measurement. Point-velocity measurement is done mainly for investigative purposes and is of limited use in an industrial environment. It is not dealt with in detail here.

14.4.1 Quantum Flow Measurement

The measurement can be in terms of mass flow rate, volume flow rate, or average velocity. Volume flow rate measurement is most common. When required, the other two are inferred by computation. Mostly the measurement itself is done in an indirect manner, from which the volume flow rate itself, is inferred.

14.4.2 Differential Pressure Measurement

About 50% of all flowmeters in use measure flow using the differential-pressure measurement approach. Here an intentional obstruction is created in the fluid flow line. There is a consequent pressure drop in the fluid. It is sensed using a differential pressure sensor and directly related to the flow rate.

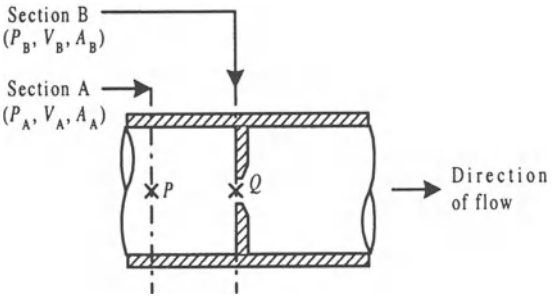


Figure 14.15 Flow of a fluid through a constriction

14.4.2.1 Principle of the Differential Pressure Flowmeter

Consider for the present, a liquid flowing through a pipe as shown in Figure 14.15. The normal section of the pipe is as shown at A. Its area of section for flow is A_a. The pipe has a constriction at section B where the area of section available for flow is reduced and equal to A_b.

$$A_b < A_a \tag{14.13}$$

Further points P and Q are taken as representative of sections A and B respectively. Referring to points P and Q, we have

⇒ P_a is the pressure of liquid at P in section A

⇒ P_b is the pressure of liquid at point Q in section B (at the orifice)

⇒ v_a is the velocity of liquid at point P

⇒ v_b is the velocity of the liquid at point Q (at the orifice)

According to Bernoulli's principle total energy of the fluid at points P and Q, must be equal. This gives for the energy of the liquid at the two sections

$$P_a + \frac{1}{2}\frac{v_a^2}{\rho} = P_b + \frac{1}{2}\frac{v_b^2}{\rho} \tag{14.14}$$

where ρ is the specific gravity of the liquid. Assuming v_a and v_b to represent the average velocities of the liquid at the two sections, the quantity of flow at the two sections can be equated as

$$Q = v_a A_a = v_b A_b \tag{14.15}$$

where

⇒ Q is the flow rate of the liquid

⇒ A_a is the area of section of the pipe at A

⇒ A_b is the area of section of the pipe at B

From Equation 14.15,

$$v_b = \frac{v_a A_a}{A_b} \tag{14.16}$$

Equation 14.14 can be rearranged as

$$v_a^2 - v_b^2 = 2\rho (P_a - P_b) \tag{14.17}$$

Substitution from Equation 14.16 and rearrangement of terms gives

$$v_a^2 = \frac{2\rho (P_b - P_a)}{[1 - (A_a / A_b)^2]} \tag{14.18}$$

$$\therefore Q = v_a A_a = A_a \sqrt{\frac{2\rho}{1 - (A_a / A_b)^2}} \sqrt{P_b - P_a} \tag{14.19}$$

$$= K\sqrt{P_b - P_a} \tag{14.20}$$

For a given pipe and given liquid in Equation 14.20, K is a constant. Equation 14.20 shows that for any fluid in motion, the flow rate is proportional to the square root of the pressure differential.

The energy balance equation is valid for laminar flow for each layer of the fluid. The crude and extended interpretation here for the 'averaged flow' of the liquid across the whole cross-section of the pipe, is also found to be valid though with some tolerance (*i.e.*, sacrifice in accuracy). The main contributors for this reduction in accuracy are

⇒ the flow is often not laminar

⇒ Viscosity and hence the temperature of the liquid, affect the value of K.

⇒ The flow rate also affects K.

⇒ Joints, valves, elbows, change in section-areas (or any other change that affects the flow structure), on either the upstream or the downstream side within close vicinity of the constriction, affect K.

To account for the imperfections, deviations *etc.*, of the above types, the flow relation of Equation 14.20 is modified as

$$Q = C_d K \sqrt{P_b - P_a} \tag{14.21}$$

where C_d is referred to as the 'Coefficient of Discharge'. Detailed literature on C_d including empirical relations and tabular values, is available [Cheremisinoff, Eckman, Liptak]. Suffice it to say here that the volume flow rate is proportional to the square root of the pressure differential. Deviations are compensated with C_d. For each geometry, C_d is obtained empirically by flow testing under simulated conditions. Let

$$P_b - P_a = \Delta P \tag{14.22}$$

Substituting in Equation14.21

$$Q = C_d K \sqrt{\Delta P} \tag{14.23}$$

If ΔP deviates by $\varepsilon\ \Delta P$ such that $\varepsilon\ \Delta P << \Delta P$, the corresponding deviation in Q designated as $\delta\ Q$ is

$$\delta Q = C_d K \sqrt{\Delta P + \varepsilon\ \Delta P} - C_d K \sqrt{\Delta P} \tag{14.24}$$

$$\approx \frac{1}{2} Q \varepsilon \tag{14.25}$$

$$\therefore \frac{\delta Q}{Q} = \frac{1}{2} \varepsilon \tag{14.26}$$

Thus the error in Q is half of that in ΔP. This gives an apparent advantage near full scale. However, at lower values of ΔP, the error in Q is more. For example a 1% error in ΔP at 10 % of the scale, reflects as a $[100\ (\sqrt{11} - \sqrt{10}\ )/\sqrt{10}\ ] = 4.5$ % error in Q. Hence, the usable range of ΔP is limited. Limiting ΔP to a 10:1 ratio limits Q to a range 10: 3.2.

Observations: -

⇒ The above derivation is valid for gases also. For gases the value of K will be different and will depend on the gas, its temperature, pressure and flow conditions. Corrections can be carried out with the universal curves of Section 14.3.2.

⇒ Neither liquid velocity, nor volume nor mass rate is directly measured here. These are inferred by indirect measurement.

⇒ Differential pressure measurement is suitable for a variety of liquids and gases.

⇒ The dynamic range of a differential pressure flowmeter rarely exceeds 3:1.

⇒ Under low or no flow conditions, small changes in differential pressure reflect as large flow changes. The sensor is said to be 'bouncy' because of its response to noise under these conditions.

⇒ When a linear relation between flow rate and output is desired, the sensor output is passed through a square-root extractor. This can be a non-linear analog processing circuit (See Section 6.3) or done digitally (See Section 9.2). In either case, the low end of the differential pressure output is to be discarded as unreliable. As discussed above, the cut-off point depends on the accuracy of the differential pressure measurement and the desired accuracy.

⇒ If the flow is fluctuating in nature, the mean value of the pressure differential does not correspond to the mean value of the flow rate.

Consider a flow rate

$$Q = Q_0 + Q_1 \sin \omega t \tag{14.27}$$

Substitution in Equation14.23 and algebraic simplification gives

$$\Delta P = \frac{1}{C_d^2 K^2}\left(Q_0^2 + \frac{1}{2}Q_1^2 - \frac{1}{2}Q_1^2 \cos 2\omega t\right) \tag{14.28}$$

Equation 14.28 yields the average value of ΔP as

$$\overline{\Delta P} = \frac{1}{C_d^2 K^2}\left(Q_0^2 + \frac{1}{2}Q_1^2\right) \tag{14.29}$$

Thus under any fluctuating conditions, ΔP indicates a larger value of average flow than the actual. The error increases with the level of fluctuations. To overcome this problem, the signal representing the pressure differential is to be linearized (using the square-root function) instantaneously and then averaged to get the average flow rate.

⇒ When flow totalization is done to get $\int Q dt$, a problem similar to the above occurs. Square-root extraction of the output representing ΔP, is to be carried out before totalization, to avoid any such error due to the non-linearity.

⇒ Mass flow rate in w kg/s, can be obtained by multiplying the volume flow rate by density. On-line measurement of density is cumbersome and rarely done. More often, the density is inferred from temperature and pressure measurements. In the case of liquids, this is done using the coefficient of volume expansion and the bulk modulus. In the case of gases, the universal curves can be used.

⇒ One of the major plus points of the differential pressure flowmeter, is the absence of any moving part. It does not call for any extra maintenance schedules or precautions. Further, the cost of the flowmeter does not increase with the pipe size.

14.4.2.2 Orifice Plate

The orifice plate is the simplest and the most commonly used constriction for differential pressure sensing. It consists of a plate obstruction normal to the flow direction. The orifice plate can have a circular hole at the centre that provides the constricted flow area.

Figure 14.16 shows the flow pattern and its alteration when an orifice plate is inserted. The pressure upstream at point A is P_i, which is the steady liquid pressure. As the liquid approaches the orifice, there is a slight increase in its pressure; subsequently the pressure drops as we pass beyond the constriction. The fluid stream offers the minimum area of flow slightly beyond the orifice plate. This section is the '*Vena Contracta*'. Beyond the *vena contracta*, the pressure increases until normal flow pattern is established. The steady pressure down stream is P_o that is slightly less than P_i due to the pressure loss or head loss across the orifice plate. Use of the pressure at the *vena contracta* in Equation 14.21, improves the accuracy in measurement. However, the position of the *vena contracta* changes with the fluid flow rate. In a practical situation, identifying the *vena contracta* and sensing the pressure there is not practical.

The ratio of the diameter of the orifice to the internal diameter of the pipe is referred to as the 'beta (β) ratio' of the orifice plate. C_d is related to β and N_R. For $N_R > 5000$ (approximately), C_d remains practically insensitive to N_R for all β values.

Hence, orifice plates are recommended for use in flow conditions where N_R is in excess of around 5000. Normally, depending on the flow conditions an orifice plate of appropriate β is selected. Manufacturers provide detailed information regarding selection of orifice plate for different flow conditions.

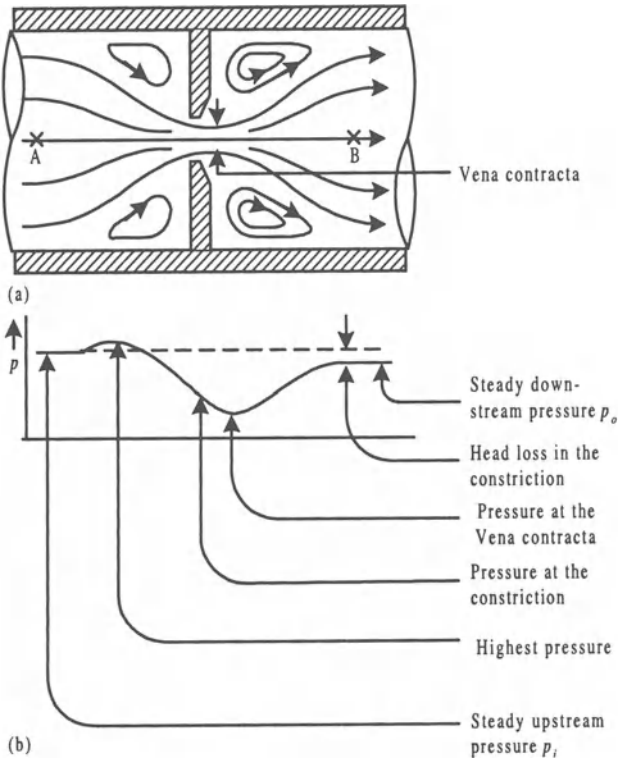


Figure 14.16 Flow of fluid through a constriction in a pipe: (a) Fluid streamlines on the upstream and the downstream sides (b) Nature of variation of fluid pressure near the constriction

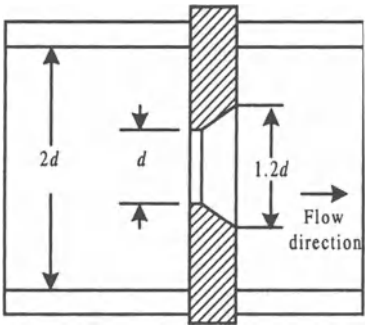


Figure 14.17 Orifice plate – typical form; proportional dimensions shown are approximate

Observations: -

⇒ The flow conditions and accuracy are said to be sensitive to the up-stream side diameter of the orifice plate as well as the effective thickness of the orifice relative to its diameter (See Figure 14.17). The orifice *per se* is made well defined and thin for this reason. Any erosion or corrosion of the up-stream diameter edge affects the accuracy markedly.

⇒ Precise positioning of the up-stream and down-stream pressure taps, can ensure measurement accuracy of 0.5 %. Indecision on this count can reflect as a corresponding loss in accuracy. In precision work, orifice plate along with (precisely laid out) pipes and flanges on either side is obtained as one unit from manufacturers.

⇒ The permanent power loss due to the introduction of the orifice plate, is ΔP $(1 - \beta^2)$ approximately. With β varying over 0.2 to 0.7, the pressure loss is in the 0.51 ΔP to the 0.96 ΔP range. Orifice plate has the maximum pressure loss amongst all the differential pressure sensors.

⇒ Bends, valves, section changes *etc.*, on either side of the orifice plate, disturb flow conditions and cause errors in measurement. This is especially true of gas flow where the associated N_R values are very high. Normally straight flow without bend, valves or change of section for 5 D length (where D is the internal diameter of the pipe) suffices on the down-stream side. A minimum of 15 D of straight run is recommended on the up-stream side. This suffices for a β of 0.1. The straight run required on the up-stream side increases as β increases. For a β of 0.75, it may go up to 50 D [Cheremisinoff].

⇒ When space constraints prevent such long lengths, flow conditioners are inserted in the pipe. Flow conditioners are honey-combed structures (Figure 14.18), which break the fluid stream into smaller segments. As the fluid emerges out of the flow conditioner, there is better uniformity of flow. However, flow conditioners do cause additional pressure loss in the line.

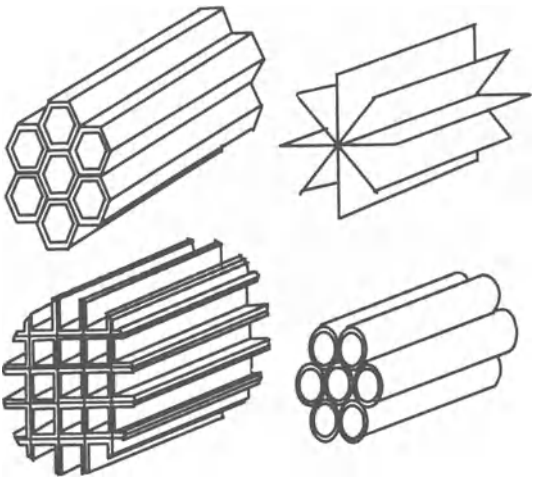


Figure 14.18 Typical flow conditioners

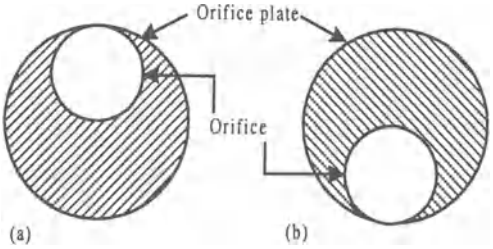


Figure 14.19 Variants of orifice plate: (a) Orifice plate for liquids with entrapped gas (b) Orifice plate for gas with traces of liquid particles

⇒ Orifice plates are normally unidirectional. Conventional industry practice is to stamp essential dimensional information of the orifice plate on the up-stream side.

⇒ When sensing the flow of a liquid with entrained gas, the gas may accumulate at the top in the up-stream side. This disturbs the flow conditions and causes error. An orifice plate with an orifice at the top is chosen for such applications [Figure 14.19 (a)]. The trace of gas present will pass through without accumulation. The pressure taps are to be provided at angles, recommended by the manufacturer.

⇒ The accuracy attainable with the modified orifice plate as above, is only of the order of 2 % to 3 % (Compare with 0.6 % with the orifice plate having concentric orifice). Alternately a small vent is provided in the flange of the tube, at the top for the gas to flow through. The vent size is negligible and does not affect the flow accuracy. However, this requires additional work in the tubing. Further if the vent is clogged, it goes unnoticed resulting in gas accumulation at up-stream end and affecting the flowmeter accuracy.

⇒ When metering gas with traces of liquid present, liquid particles may accumulate at the bottom of upstream end. This disturbs the flow conditions and causes error. An eccentric orifice plate with an orifice at the bottom, is used here [See Figure 14.19 (b)]. The liquid particles go through without accumulation.

⇒ In both the above cases, the accuracy attainable is lower at 2 % to 3 % (Compare with 0.6 % with the orifice plate having concentric orifice). Alternately one may use an orifice plate with a concentric orifice and a liquid vent at the bottom. The vent size is kept small enough to avoid its affecting the overall accuracy. However clogging of the vent may go unnoticed and cause liquid accumulation at the up-stream side leading to reading error. The pressure taps are to be provided at angles recommended by the manufacturer.

⇒ When measuring gas flow with the orifice plate, compressibility of the gas is to be considered and C_d modified accordingly. However for pressure differential of 1% or less, the gas can be considered as incompressible and C_d values specified for liquids, used. This is the case with the majority of the situations. If the differential pressure exceeds 1%, the error steadily increases with the pressure differential. One can account for the compressibility of the gas and refine accuracy.

Equation 14.19 can be modified to yield the mass flow rate as

$$W = C_d A_b \sqrt{\left[1-(A_b/A_a)^2\right]^{-1}} \sqrt{\frac{2g(P_a - P_b)}{v_a}} \qquad (14.30)$$

where

$\Rightarrow$ g is the specific gravity

$\Rightarrow$ v_a is the specific volume at state 'a' in ft^3/lbf and

$\Rightarrow$ w is the weight flow rate in lb./s.

When the differential pressure exceeds 1%, the w is modified by a factor Y to account for compressibility.

$$W = YC_d A_b \sqrt{\left[1-(A_b/A_a)^2\right]^{-1}} \sqrt{\frac{2g(P_a - P_b)}{v_a}} \qquad (14.31)$$

Where

$$Y = 1-\left(0.41+0.35\beta^4\right)\times\frac{P_a - P_b}{P_a}\times\frac{1}{k} \qquad (14.32)$$

for flange taps or vena contracta taps and

$$Y = 1-\left[0.333+1.145(\beta^2+0.75\beta^5+12\beta^{13})\right]\times\frac{P_a-P_b}{P_a}\times\frac{1}{k} \qquad (14.33)$$

for pipe taps. Here k is the ratio of specific heats (1.4 for air).

The above empirical relations are accurate to ± 0.5 % for (P_b/P_a) lying between 0.8 and 1.0. Other empirical values and expressions for Y are available in literature [Cheremisinoff].

14.4.2.3 Other Differential Pressure Schemes

The major shortcoming of the orifice plate is the high pressure-loss across the orifice. A variety of carefully engineered other flow constrictions are available. All of them have the same Q versus P relationship. C_p is available as empirically obtained and tabulated values in each case. The exact geometry used and the dimensional details are often proprietary.

14.4.2.4 Venturi Meter

Venturi meter tapers to the constriction and expands (See Figure 14.20) with a lower slope to the full diameter level. The pressure taps are provided upstream at section A and at the constriction at section B. Normally 3 or 4 taps are provided at

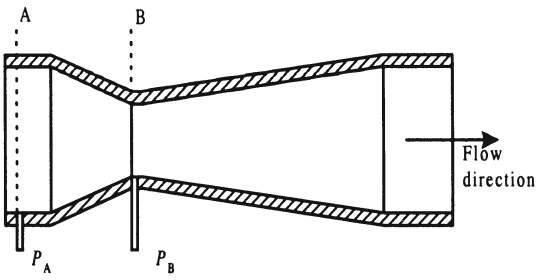


Figure 14.20 Venturi meter

the section and their average taken to represent the section pressure. The Venturi section follows the streamlines closely. The *vena contracta* can be taken to be at the section itself. The pressure loss with the Venturi pipe is lower than that with the orifice plate (It is 10 % to 15 % of ΔP for $0.2 < \beta < 0.8$). C_d ranges from 0.94 at $N_R = 10^4$ to 0.99 at $N_R = 10^6$. The Venturi meter occupies more space compared to the orifice plate. It has to be bought and installed as a total unit. It is costlier too. Venturi meter is used in situations where the pressure loss across the meter is to be kept low.

14.4.2.5 Flow Nozzle

A flow nozzle is shown in Figure 14.21. At the up-stream side, it has a bell-shaped approach. It tapers to a straight cylindrical exit section. The contour is chosen such that the contracted stream fills the throat. The smallest section of flow – the *Vena Contracta* – can be taken to be at the throat itself. For a given β, the pressure loss across the flow nozzle is lower than that across the orifice plate. However, for specified ΔP and flow rate values, β used for the orifice plate is larger compared to that of the flow nozzle. In other words, a flow nozzle and an orifice plate selected to measure the same flow conditions, have the same level of pressure loss. In precision work, the flow nozzle also uses a set of three or four pressure-taps around the periphery and takes the average pressure value. Flow nozzle is less sensitive to dirt and corrosion as compared to the orifice plate.

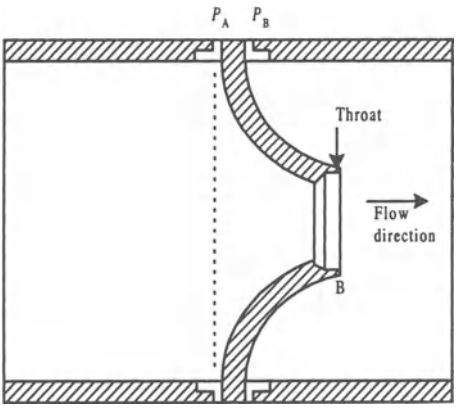


Figure 14.21 Flow nozzle

14.4.2.6 Comparison

Due to the variety of configurations available in each case, a precise comparison is not practical. However, some common factors discriminate the three types of flowmeters considered above.

Coefficient of Discharge

C_d is a function of N_R and β. With the orifice plate, for a given β, C_d decreases with N_R and attains a more or less constant value for $N_R > 10^5$ [See Figure 14.22 (a)]. For Venturi meter and flow nozzle, for a given β, C_d increases with N_R and attains a constant value for $N_R > \sim 10^5$ [Figure 14.22 (b)]. Further C_d is 40 % to 60 % more for Venturi meter and flow nozzle, as compared to the orifice plate.

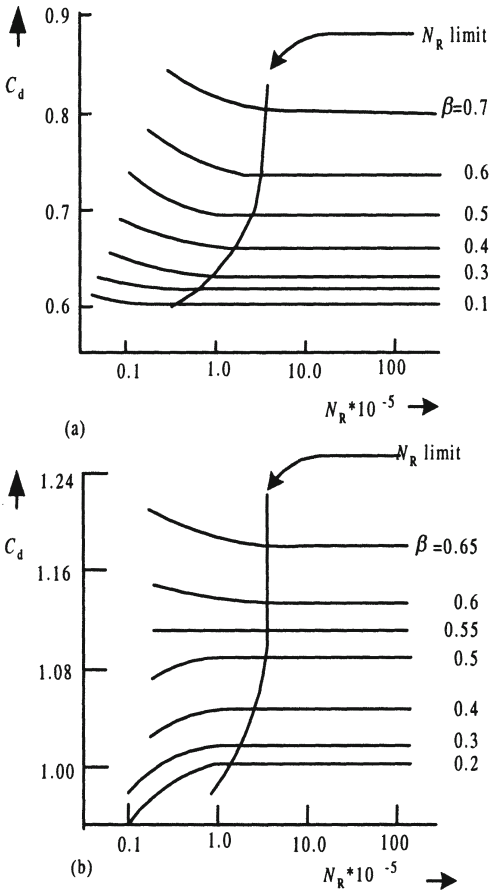


Figure 14.22 Nature of variation of C_d with N_R : (a) Venturi meter (b) Flow nozzle

Pressure Loss

Pressure loss is highest for the orifice plate and lowest for the Venturi meter. When selected to measure same flow conditions, the orifice plate and the flow nozzle, have the same level of pressure loss.

Accuracy

When properly calibrated and used, the error with the Venturi meter and the flow nozzle, are lower (~70 %) than that with the orifice plate.

Flow Conditions

Orifice plate has to be modified to suit fluids with dirt *etc.* However, flow nozzle and Venturi meter do not require such adaptation and they are less sensitive to dirt *etc.* The straight length of piping required – upstream as well as downstream – for both the flow nozzle and the Venturi meter are lower than those required with the orifice plate.

Cost and Simplicity

Orifice plate is the least costly and the simplest to use. Venturi meter is the costliest and the most sophisticated. As mentioned already, the orifice plate remains the most widely used differential pressure device for flow measurement.

14.4.2.7 Elbowmeter

The 'Elbow meter' provides a simple alternative to an intentional obstruction. When a fluid flows over a bend in a pipe, there is a pressure differential between the inside and the outside of the elbow due to the centrifugal force at the bend. This is a measure of the flow rate. Taking the elbow to be in the horizontal plane (See Figure 14.23), we have,

$$V^2 = \frac{R(P_a - P_b)}{\rho D} \tag{14.34}$$

where

- $\Rightarrow$ V is the mean velocity of flow
- $\Rightarrow$ R is the radius of bend of the elbow
- $\Rightarrow$ P_a and P_b are the pressures at the two openings and
- $\Rightarrow$ D is the pipe diameter.

From this, we get the rate of flow as

$$Q = \frac{4\pi D^2}{4}\sqrt{\frac{R(P_a - P_b)}{\rho D}} \tag{14.35}$$

The elbow meter is simple in principle and construction. Accuracy attainable is 4 %, which is low compared to the pressure differential meters considered so far. Elbow meter can be accommodated at a suitable bend in the piping; it does not require any separate installation, support and so on. This simplicity in use is its major attraction.

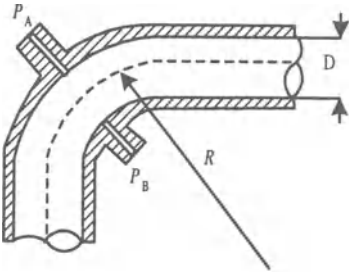


Figure 14.23 Elbow flowmeter

14.4.3 Magnetic Flowmeters

Magnetic flowmeters use the basic Faraday's law of induction to provide an electrical output proportional to flow. The principle can be understood from Figure 14.24, which shows the cross-section at the active area. The liquid of interest flows through a section of the pipe with a uniform magnetic B field normal to the direction of flow. The pipe has an insulated lining inside. The pipe can be electrically conducting. However, for the configuration shown, it should not be a

magnetic material (it can be of stainless steel) so that the magnetic flux lines will penetrate through. The fluid is taken as a conductor. Two electrodes E_1 and E_2 on two diametrically opposite sides are in contact with the liquid. They are insulated from the enclosure and brought out.

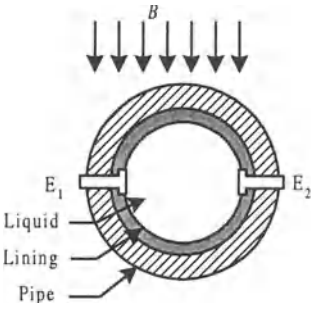


Figure 14.24 Basic scheme of the magnetic flowmeter

As the fluid flows through the pipe, an induced emf E appears across the electrodes.

$$E = BVD \tag{14.36}$$

where

⇒ B is the magnetic flux density in Tesla

⇒ V is the average fluid velocity in m/s

⇒ D is the distance between the electrodes in m.

With D as the diameter of the pipe, the volume flow rate Q is given by

$$Q = \frac{\pi}{4} D^2 V \tag{14.37}$$

and

$$V = \frac{4Q}{\pi D^2} \tag{14.38}$$

Substitution in Equation 14.36 gives

$$E = \frac{4B}{\partial D} Q \tag{14.39}$$

In practice, the liquid velocity changes across the cross-section of the pipe; it reduces as we move away from the centre of the pipe. Still the value of E can be shown proportional to the average velocity of the liquid across the section and hence the volume flowrate.

As we move in either direction away from the electrode along the line of flow, the emf induced in the liquid section reduces. Outside the region of influence of the magnetic field, the emf induced is zero. Through these areas, we get shorted current paths, which reduce the net voltage available across the diameter (See Figure 14.25). However, by extending the magnetic field spread sufficiently on either side of the electrode, the emf across E_1 and E_2 can be retained practically unaffected. There are four types of practical realizations of the magnetic flowmeter.

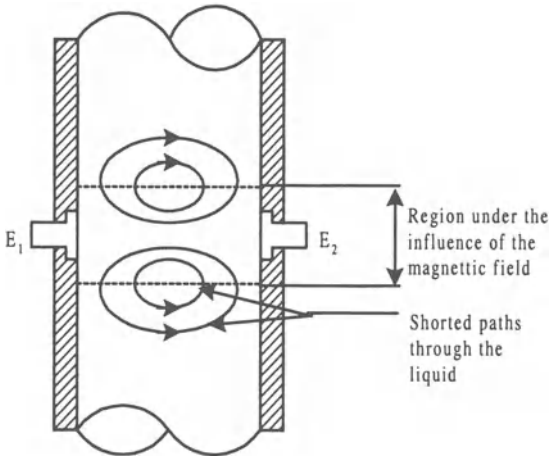


Figure 14.25 Local shorted current paths in the magnetic flowmeter reducing sensitivity

14.4.3.1 DC Magnetic Flowmeter

With a DC exciting field, a steady flux density is present across the metering region. For non-magnetic pipes like stainless steel, the exciting coil can be external to the pipe, which makes the engineering simpler. But the emf available is typically 3 mv. The magnetic field strength is to be kept constant to ensure that the sensitivity constant. Due to polarization *i.e.*, the fluid acting as an electrolyte between the electrodes, the emf available reduces with time and affects accuracy. The effect can be minimized (but not eliminated) by using non-polarizing electrodes like platinum, graphite, Calomel and the like. Being a low-level DC signal with high source impedance, amplification is cumbersome. The scheme is no longer popular.

14.4.3.2 Pulsed Magnetic Flowmeter

In principle, the scheme is the same as the DC magnetic flowmeter. The magnetic field coil is excited in a pulsed mode at 3 Hz to 8 Hz. When the excitation is absent, the emf across the electrodes is taken as spurious signal. It is sampled and subtracted from the signal when the pulse is present. The difference is taken as representing the actual output. With this, the accuracy is improved and a response time of 1s obtained.

14.4.3.3 Permanent Magnet Type Magnet Flowmeter

These use compact permanent magnets embedded inside the pipe to produce the constant magnetic field. The compactness and stability of the magnet, ensures that the field is stable and the sensitivity remains unaffected.

14.4.3.4 AC Magnetic Flowmeter

The field coils may be excited by an AC. This produces an alternating magnetic field inside. The emf induced across the electrodes is also alternating. Polarization does not affect the output emf directly. However it is equivalent to a large capacitance (~10F) in series with the signal. It attenuates the signal – especially at low frequencies. Further, the spurious output emf is far from negligible. Closeness

of the exciting field to the electrode leads and the resulting coupling is mainly responsible for this. The sensing circuit through the two electrodes forms a single turn linking the exciting winding as in a transformer. The resultant emf induced in it also adds to the spurious voltage. However, this is in quadrature to the main induced emf. The effect of the spurious voltages is reduced to some extent with the use of a phase sensitive detector. To improve the accuracy further, at regular intervals, the flow is stopped and output sensed with the meter full with the liquid. This is used for zero correction.

Observations: -

⇒ Magnetic flowmeters are used with full-scale liquid speed in the range of 1m/s to 10 m/s. Typical common value used is 3 m/s. Higher liquid velocities accelerate erosion of lining and reduce its life unduly. Depending on the lining material used, operating pressure inside can go up to 10 to 20 atmospheres and temperature can extend up to 200 °C.

⇒ Normally the minimum conductivity acceptable for the liquid is in the 1μS/cm to 5μS/cm range (Tap water has a conductivity of 200 μS/cm). Most of the liquids in use have conductivity higher than this. Organic liquids, hydrocarbons *etc.*, have much lower conductivity and the magnetic flowmeter is not suitable for them. The minimum conductivity constraint here precludes the use of magnetic flowmeter for measuring the flow rate of gases.

⇒ When measuring fluid-mixes, as a rule of thumb, if 10 % of the constituents are electrically conducting, a magnetic flowmeter can be used for the measurement.

⇒ A non-conducting pipe body is ideal for a magnetic flowmeter. Often this is not practical. A non-magnetic metal body *i.e.*, stainless steel is more common. In such cases, the pipe is to have a non-conducting lining inside. The pipe lining can be of rubber, polyurethane, polyethylene, or teflon depending on the fluid, its pressure and temperature. Stainless steel, tantalum, platinum, or some other specific alloys like Monel are commonly used for electrodes.

⇒ The miniature flowmeters of recent years use exotic materials – teflon for lining, tungsten carbide for electrodes, and zirconium or tantalum electrode holders. The meters are suitable for most fluids under adverse conditions of pressure and temperature. They have exciting coils housed inside the flowmeter pipe. With this, the flowmeter flanges can be brought closer without affecting the field pattern in the measuring area. This also contributes to the size reduction of the meter. Manufacturers claim near universality of application for such meters.

⇒ Magnetic flowmeters have no moving parts and no obstructions to flow. They are not sensitive to viscosity, liquid density, N_R value, or any flow disturbances. The requirement of straight run on either side is minimal and the meter extension on either side up to the flange itself takes care of this need. The only requirement is that the velocity profile has to be symmetric in the sensing region. They offer a wide linear-range and are suitable for bi-directional flow. Their response time is low compared to that of other flowmeter types. They are available for pipe sizes ranging from 1/10" to 96" of pipe dia. The accuracy of measurement is in the 0.5 % to the 2 % range.

14.4.4 Vortex Flowmeter

Any phenomenon associated with the flow of a fluid wherein a parameter can be identified as directly related to the flow rate, has the potential for application in flow measurement. A variety of methods has been suggested, tried and given rise to different types of flowmeters. However only a few of them have stood the test of time and proved popular. Vortex flowmeter is one of them. The principle can be understood referring to Figure 14.26.

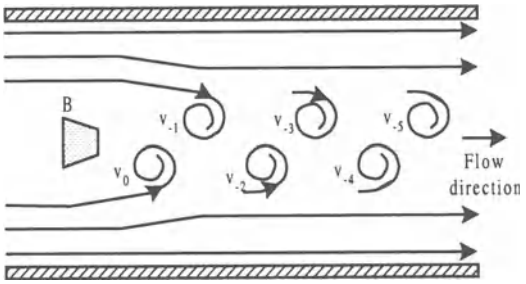


Figure 14.26 Illustration of the principle of the vortex flowmeter

Consider a straight uniform pipe through which the fluid is flowing. B is a Bluff or 'Shedder'– a symmetrical obstruction in the fluid path. At low fluid velocities, the fluid streamlines flow around the obstruction smoothly and join as one stream on the down-stream side. However as the fluid velocity increases, the fluid separates from the body and swirls to form vortices. These are formed alternately on either side. The frequency of vortex formation is directly proportional to the fluid velocity. The frequency can be sensed and used as a measure of the flow rate. The frequency and fluid velocity are related as

$$f = \frac{N_{st} V}{D} \tag{14.40}$$

where

⇒ f is the vortex shedding frequency
⇒ N_{st} is the Strouhal number
⇒ V is the fluid velocity and
⇒ D is the 'characteristic dimension' of the bluffer (shedding body).

N_{st} is an experimentally obtained non-dimensional number. For a given shedder, it changes with N_R as shown in Figure 14.27. It remains sensibly constant for all N_R lying between A and B. For flows with $N_R > 10{,}000$, f in Equation 14.40 is directly proportional to the fluid velocity and hence the flow rate. Manufacturers of vortex flowmeters use various patented shapes for the shedder and claim advantages. Vortex generation is a highly localized phenomenon with abrupt changes in fluid velocity. It is associated with corresponding pressure changes (as well as density changes). Any of these can be sensed directly or indirectly and associated frequency ascertained. The sensing procedure changes from manufacturer to manufacturer: -

⇒ The pressures on the two sides of the shedder alternate at the same frequency as the vortex generation. The two pressure changes are in anti-phase. These two pressures can be led to two sides of a diaphragm and its oscillation

sensed. In some cases a disc tied to it oscillates. The oscillation is sensed by a magnetic proximity pick-up.

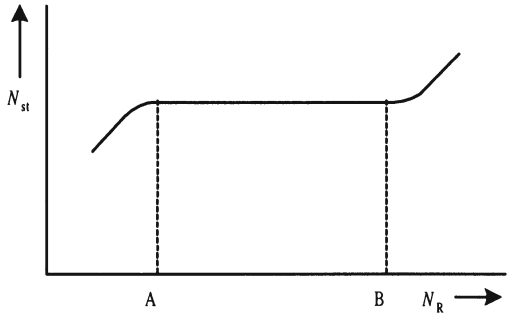


Figure 14.27 Nature of variation of N_{st} with N_R for a given vortex shedder

⇒ The alternate vortex formation on the two sides causes corresponding alternating twisting moment on the shedders. This can be sensed using semiconductor SGs. Their high sensitivity allows low sensing threshold (Note that the wide tolerance in the sensitivity of semiconductor SGs is not a constraint here).

⇒ The fluid velocity changes on either side; it can be sensed using thermistors and change in their resistance values.

⇒ The vortices can be allowed to grow in size. An ultra-sonic source and a detector kept on either side sense their presence. The received signal (Figure 14.28) is modulated at the shedding frequency. This approach is suitable only for liquids.

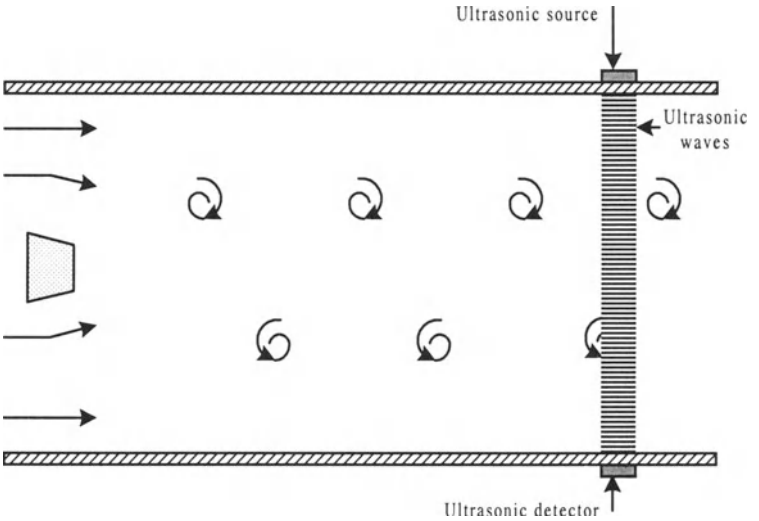


Figure 14.28 A vortex flowmeter with ultrasonic detection of vortices

Observations: -

⇒ Vortex flowmeter has a lower velocity limit on two counts. The vortex formation takes place only above a threshold velocity. Further, if the velocity is too low, the vortices and associated changes are too feeble to be sufficient to excite the sensors. The minimum velocity is in the 0.3 m/s to 0.5 m/s range. This is dependent on the fluid. Since most liquids have a ρ in the 0.8 to 1.2 range, the minimum velocity remains the same for all liquids. Gases can have a 20:1 range of ρ and a correspondingly wide range of minimum velocity.

⇒ Vortex flowmeter has no constraint on the maximum velocity. However, it is limited to 5 m/s to 10 m/s in the case of liquids. This is to avoid cavitation and to prevent any mechanical damage. With gases, manufacturers provide necessary recommendations for the maximum safe velocity.

⇒ Vortex flowmeters are available in 1" to 8" pipe sizes. Flow rates covered, range from 3 to 2700 gpm for liquids. With the compressibility of gases, the volume flow range cannot be quantified for them. With liquids, 0.5 to 1 % accuracy is achievable at full scale. Here accuracy is in the linear range where N_{st} is constant. At lower N_R values also, with the incorporation of correction, accuracy can be brought closer to these levels. Response time is typically 1.5 s.

⇒ When the fluid is at an elevated temperature, thermal expansion of the meter body reduces the vortex shedding frequency. For stainless steel body, the error on this count is 0.5 %, for every 100 °C rise in temperature.

⇒ The linear range is 15:1. The full-scale vortex shedding frequency is in the 200 Hz to 500 Hz range.

⇒ Vortex flowmeters can be used in all the situations where the minimum velocity and the N_R constraints are met. All low viscosity liquids and high-density gases under high pressure, having sufficient momentum to actuate the sensor, come under this category.

⇒ The inlet fluid pressure has to be high enough to prevent cavitation of the fluid within the meter tube. The characteristic dimension (the width of the shedder) is practically the same for all manufacturers. The pressure-drop across the meter remain the same; the minimum inlet pressure required, is also practically the same with all manufacturers. A rule of thumb to estimate the inlet pressure, is

$$P_{inlet} > 4\,\Delta P + 1.25\,P_{vapour} \qquad (14.41)$$

where ΔP is the pressure drop across the meter and P_{vapour} is the vapour pressure of the liquid.

⇒ For reliable operation of the meter, the upstream and the downstream pipes should be straight and smooth for $4D$ and $2D$ lengths respectively. The smoothness is specified by individual manufacturers. Deviations may cause eddies and false vortex-sensing.

⇒ The meter and neighbouring piping should be free from any vibration – this again is to prevent false fluid vibration being wrongly sensed as vortex shedding.

The installation cost of the vortex-shedding flowmeter is lower than that of many other traditional flowmeters. Accuracy is on par or better. This along with their versatility has carved out a *niche* for them. Vortex flowmeter can be used to measure the flow of any liquid including corrosive liquids. Models with all plastic

wetted parts are suitable to measure ultra-pure liquids. Flow of all gases as well as (dry) steam can be measured. In all cases N_R constraints are to be satisfied.

14.4.5 Turbine Flowmeter

In the turbine flowmeter, a turbine wheel inserted is in the fluid path; it rotates at a speed, which is a measure of the fluid flow rate inside. Two types of meters are in vogue.

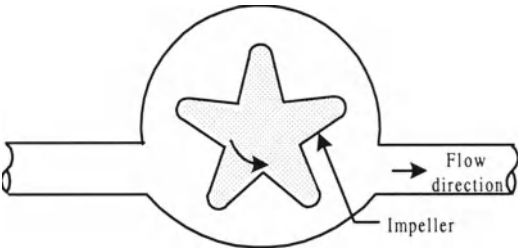


Figure 14.29 Vertical impeller type of turbine flowmeter

14.4.5.1 Vertical Impeller Type

The impeller has a set of vertical vanes around the periphery (See Figure 14.29). The fluid is directed at the impeller vane tangentially through an orifice. These are used for liquid (mostly water) flow rate measurement in the 0.15 m^3/hr to 12 m^3/hr capacity. They offer 2 % full-scale accuracy. The pressure loss in the meter is of the order of 2 psi.

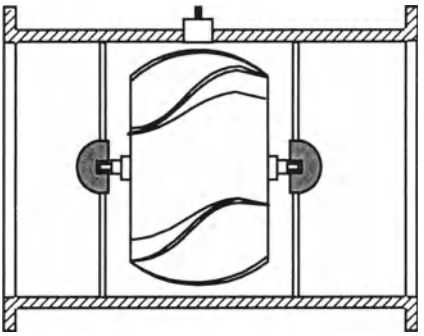


Figure 14.30 Helical-impeller type turbine flowmeter

14.4.5.2 Helical Impeller Type

These use a helical axial impeller in the flow line. The vanes are shaped in the form of a helix with a large pitch. (Figure 14.30). The rpm n of the impeller is given by

$$n = \frac{kV_{av}}{l} \tag{14.42}$$

where

⇒ n is the impeller speed in rpm

⇒ k is the proportionality constant

⇒ V_{av} is the average velocity of the fluid stream

l is the screw pitch. For high flow rates where turbulent conditions are established, the performance is practically independent of N_R and the above relation is valid. The rpm can be sensed using a magnetic proximity pick-up. Each pulse output represents a quantum of fluid displaced between adjacent vanes. Hence, the output pulse rate is proportional to the impeller speed. Often totalizers and display (cyclometer type) are also provided to indicate total volume flow.

Observations: -

⇒ The turbine flowmeter is suitable for 0.01 g/min. to 30,000 g/min. of water and 0.01 ft^3/min. to 15,000ft^3/min. of air. Some designs can work up to 70°C, though most are designed to work up to 50°C only. Pressures can go up to 10 to 15 atmospheres. Typically accuracy is 1 % over 10:1 range. Response time is 1s (reduces as flow rate increases). Full-scale pulse rate may range over 400 Hz to 1200 Hz.

⇒ Operation is satisfactory and accuracy is retained for $N_R > 20{,}000$. Some manufacturers guarantee this down to $N_R = 4{,}000$.

⇒ The accuracy depends on flow rate and viscosity. Improvement on these counts increases the pressure drop (In fact often the pressure drop is one measure of the meter quality). The pressure drop in the meter ranges from 3 psi to 10 psi for liquids and 0.2 psi to 85 psi for gases.

⇒ Normally the pressure drop across the meter is specified for water at a specified temperature. For other fluids, the pressure drop can be estimated using empirical formulae; e.g.,

$$\Delta P_2 = \Delta P_1 \left(\frac{P_2}{P_1}\right)^{0.81} \left(\frac{\mu_2}{\mu_1}\right)^{0.27} \left(\frac{Q_2}{Q_1}\right)^{1.82} \tag{14.43}$$

where

- suffix '1' refers to calibrated conditions
- suffix '2' refers to measured conditions
- P is the pressure of the fluid
- μ is the viscosity of the fluid and
- Q is the flow rate.

⇒ It is essential to align the flow direction along the axis of the impeller. Accuracy is quite sensitive to misalignment. Straight runs of $10D$ and $5D$ up-stream and down-stream are recommended by manufacturers. If the same is not possible, flow conditioners are inserted in the flow line.

⇒ Rotors are made as light as possible. This reduces the threshold of flow rate that can be sensed, as well as the response time.

⇒ Often the turbine flowmeters are self-lubricating.

⇒ Wear and tear of the bearings and the impeller affect accuracy with time. At present turbine flowmeter applications are mostly confined to water supply systems.

⇒ The' Paddle Wheel' provides a low cost alternative to the turbine flowmeter (Figure 14.31). It is tolerant of suspensions and turbid liquids. Its accuracy is of the order of 4 % only.

⇒ Different types of positive displacement pumps deliver measured quantities of fluid. They are used for fuel delivery lines. They can work over a wide temperature, pressure and viscosity range. The electronics is similar to that in the paddle or turbine flowmeter.

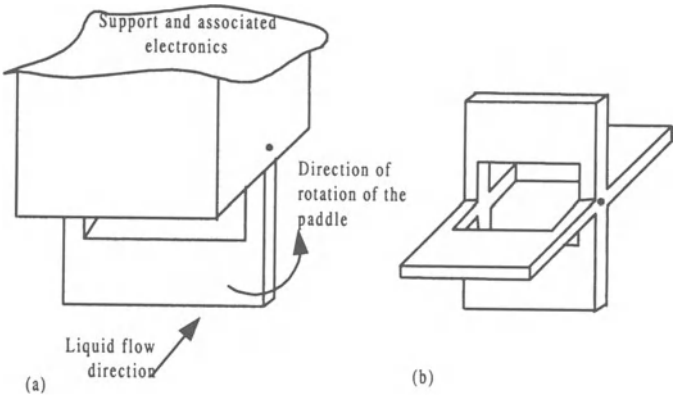


Figure 14.31 Paddle flowmeter: (a) Functional part of the meter (b) Paddle

14.4.6 Target Flowmeter

Any obstruction in the path of a fluid experiences a force. With well-dimensioned obstructions, the force is a measure of the flow rate. A simple arrangement is shown in Figure 14.32 in schematic form. The target is an obstruction symmetrically positioned in the tube. It is supported by a cantilever, which is supported on a pipe extension. SGs on the outside measure the force. With the arrangement shown, the SGs are totally isolated from the flow. If the fluid velocity is V, we have,

$$F = \frac{C_d \rho V^2 A}{2} \tag{14.44}$$

where

⇒ F is the force on the target

⇒ C_d is the drag coefficient

⇒ ρ is the density of the fluid

⇒ F is the velocity of the fluid and

⇒ A is the area of section of the obstruction or target.

The above relation is valid for flow conditions with $N_R > 4000$, *i.e.*, turbulent flow. In this region, F is independent of the N_R value as well as the viscosity of the liquid. However the square law relationship similar to that in the differential pressure flowmeters, comes into play. For flows at lower values of N_R, the force is proportional to the velocity. However, the coefficient of viscosity μ also enters the relationship at low N_R values. Being a function of temperature, the error changes with temperature. The flowmeter is not used in this range.

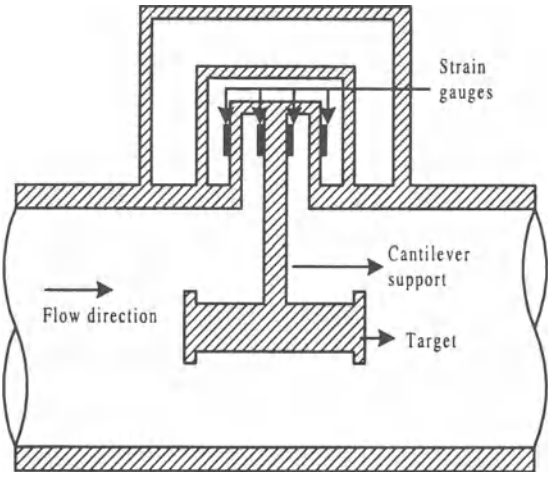


Figure 14.32 Target flowmeter

Observations: -

⇒ Target meters are available for all pipe sizes greater than 3/8". The accuracy claimed varies from 2 % to 6 %. The meter is well suited to yield a rough value of the flow rate at a low cost. The meter is economic especially for large pipes.

⇒ Due to the square law relationship, the active range is 3.5:1. Operating pressure can extend up to 600 atmospheres for the meter (Normally piping and flanges can withstand only lower pressure values.). The fluid temperature can rise up to 400 °C with some models although the electronics can withstand up to 70 °C or 85 °C only.

⇒ With a symmetric target, the flowmeter can function as a bi-directional meter.

⇒ Natural frequency of the cantilever is in the 70 Hz to the 200 Hz range. The corresponding meter output signal bandwidth is at least 10 Hz. Response time is ~ 0.3 s. On the whole, the target meter is fast in response

14.4.7 Coriolis Flowmeter

The 'Coriolis flowmeter' has the advantage of being a true mass-flowmeter with possible application for a variety of situations. It functions on the principle of the 'Coriolis Acceleration'. Figure 14.33 illustrates the principle. The fluid is made to pass through a U-tube in the flow line. Points A and B are on the two sides of the U-tube – both at the same distance from the mounting. The tube is forced to oscillate externally as a cantilever as shown in Figure 14.33 (d). This is done by a dedicated electromagnetic exciter at point C. Due to this oscillatory excitation, all fluid particles within the tube, undergo oscillation in the vertical plane. This is superimposed on the steady velocity v of the particle. At any instant let u be the oscillatory component of the velocity at point A. The effect of v and u, is a turning moment at point A as shown. In a similar manner, a turning moment appears at

point B, which is same in magnitude as that at point A but of opposite sign. The combined effect of these two moments is to twist the tube. It can be shown that the displacement of the tube is proportional to the mass flow rate (net linear mass density of the fluid). At a fixed excitation amplitude, it is also proportional to the frequency of excitation.

The external excitation frequency is selected to coincide with the natural frequency of oscillation of the U-tube or cantilever. As the density of the fluid in the tube changes, the oscillator frequency also changes. For each set of operating conditions, the excitation frequency is changed until resonance. At resonance, the excitation current is a minimum. Further, the excitation amplitude is also stabilized. Both these adjustments are carried out in an electronic closed loop feedback scheme. In one version of the meter, the time delay between the zero crossings on the two sides is measured by position sensors at zero crossings. This time delay is directly proportional to the mass flow rate and the exciter frequency does not enter the transfer function equation. As an alternative, the output amplitude is measured and corrected for the frequency change.

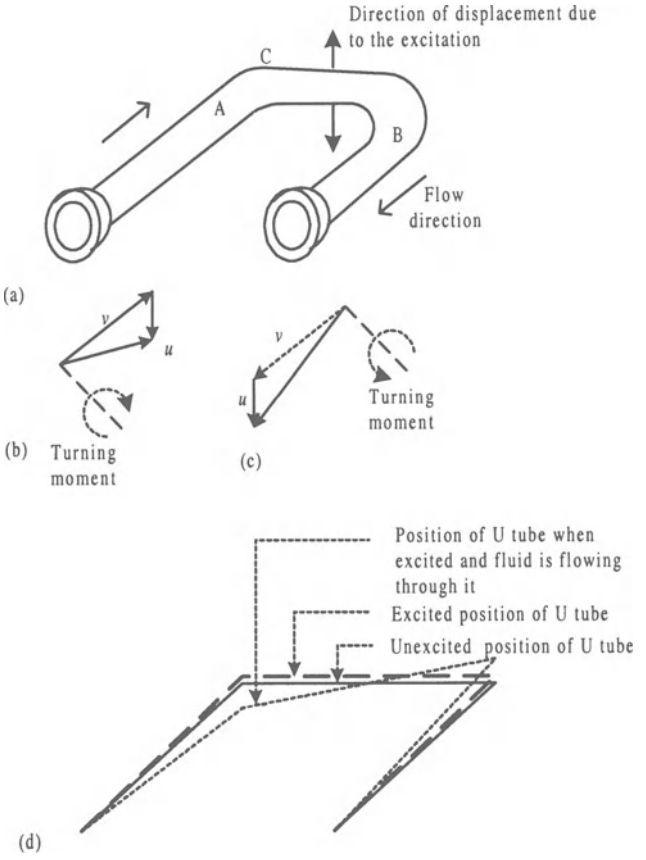


Figure 14.33 Principle of operation of the Coriolis flowmeter: (a) U-tube showing fluid flow (b) Velocities and turning moment at point A (c) Velocities and turning moment at point B (d) Tube positions at different conditions

Observations: -

⇒ The Coriolis flowmeter requires a multi-loop feedback scheme to be implemented to excite it at the natural frequency and to ensure constant frequency of oscillation. Further, the output representing the twisting of the U-tube is to be processed and translated into a signal representing mass flow rate. All these have become feasible and practically realizable with today's electronics. However, these make it perhaps the costliest of the flowmeters available.

⇒ Coriolis flowmeters are available in sizes ranging from 1/16" to 6" and cover a wide enough flow range of 0.1 lb./min to 104 lb./min. The accuracy attainable under specified conditions of operation, is 0.4 %.

⇒ The measurement is done on a cycle by cycle basis. The U-tube cantilever excitation frequency is in the 50 to 100 Hz range. This yields a typical minimum response time of 200ms.

⇒ The measurement with the Coriolis flowmeter is done without any obstructions to flow. It is insensitive to viscosity, N_R, pressure and temperature. Coriolis flowmeter can handle a variety of liquids – clean liquids, liquid mixtures, foams, slurries and liquids with entrained gases.

⇒ Versions of the Coriolis flowmeter suitable for gases use a separate thin-walled U-tube. These are suitable for gases as well as low viscosity liquids. However, application to gases is limited.

⇒ The operation is insensitive to temperature and pressure within limits. For temperature changes beyond specified limits, the error increases as the temperature deviation increases.

⇒ Normally the U-tube wall thickness is less than the piping thickness. This makes the Coriolis flowmeter to be more failure prone due to corrosion, wear and tear *etc.*, than the main piping itself.

⇒ Excitation is adjusted continuously to be at the natural frequency of the U-tube cantilever. The same changes with fluid density. This relationship can be used to extract an additional output from the instrument, as a measure of the fluid density. However the non-linear nature of the relationship between the frequency and the fluid density restricts accuracy.

⇒ The 180° bend undergone by the fluid, causes substantial head loss in the Coriolis flowmeter. This can be conspicuous with highly viscous fluids. Hence in every case, the total pressure drop in the meter and the piping as well, is to be estimated and ensured that the same is well below the available head.

⇒ With the single-tube Coriolis flowmeter, any vibration of the U-tube cantilever can cause error. To compensate for this, some versions use 2 U-tubes – one for measurement and the other to sense vibration and compensate for the same.

14.4.8 Ultrasonic Flowmeter

The ultrasonic flowmeter uses an ultrasonic pressure wave transmitted through the fluid medium for flow measurement. The effect of the fluid in motion on the wave is used in some form to measure the fluid velocity. The ultrasonic energy is coupled to the fluid through a piezo-electric crystal. The same or a similar crystal senses the

received waves. The two are correlated to yield a signal, which is a measure of the fluid velocity. For a crystal to transmit acoustic energy efficiently through the fluid, its size has to be large compared to the wavelength of the wave. With the dimensions of the crystal of around 15 mm, the wavelength can be 1.5 mm or smaller. The sonic velocity in water is 1524 m/s; for other fluids also it is of the same order. Thus, the ultrasonic sensors use frequencies above 500 kHz. Barring some exotic newer introductions [Bucci and Laudi, King-Wah and Young], the ultrasonic flowmeters are broadly of two types. One type senses the transit time of the ultrasonic wave through the fluid while the other is based on the Doppler frequency shift.

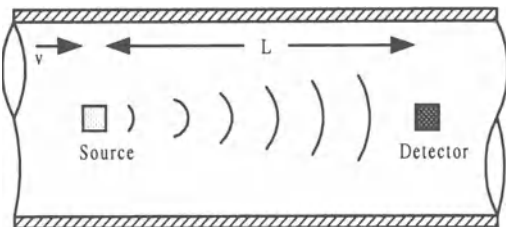


Figure 14.34 Transit time based ultrasonic flowmeter

14.4.8.1 Transit Time Based Flowmeter

Consider a liquid flowing through a straight pipe with average velocity V_{av} (See Figure 14.34). An ultrasonic transmitter source 1 and a detector 2, are kept in the line of sight of each other. The ultrasonic waves emitted by 1 travel through the liquid in motion and are received by the detector 2. If the liquid is stationary, the waves are transmitted at the sonic velocity (c m/s) of the liquid. When the liquid flows with velocity V m/s, the in the same direction as the ultrasonic waves, the transmission speed increases and the transit time reduces.

$$\text{Travel time with still fluid} = \frac{L}{c} \tag{14.45}$$

$$\text{Travel time with fluid in motion} = \frac{L}{c+V} \tag{14.46}$$

where L is the distance between the ultrasonic source and detector. From Equations 14.45 & 14.46, the difference between the two travel-times Δt_1 becomes

$$\Delta t_1 = \frac{L}{c} - \frac{L}{c+V} \tag{14.47}$$

$$\approx \frac{LV}{c^2} \tag{14.48}$$

since V << c.

For a given configuration, L is a constant. As long as c is constant, Δt_1 is proportional to V. For a given liquid, c is constant under specified conditions. If the Δt_1 changes, c also changes causing an error. Due to the presence of the c^2 term here, every 1% change in c, causes a 2% change in Δt_1. Hence, it is necessary to compensate for changes in c. If we interchange the roles of the transmitter and the receiver, we get the corresponding difference Δt_2 as

$$\Delta t_2 = \frac{L}{c-V} - \frac{L}{c} \tag{14.49}$$

$$\approx \frac{LV}{c^2} \tag{14.50}$$

since $V << c$. The difference between the above two time intervals is

$$\Delta t_2 - \Delta t_1 = \frac{L}{c}\left(\frac{1}{c-V} - \frac{1}{c+V}\right) \tag{14.51}$$

$$\approx \frac{2LV}{c^2} \tag{14.52}$$

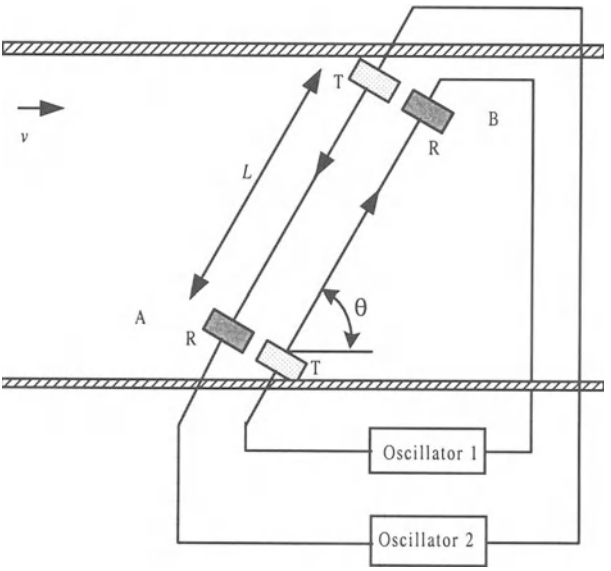


Figure 14.35 Ultrasonic-flowmeter scheme where the operation is independent of the sonic velocity through the fluid

The sensitivity has increased here but the dependence on c remains the same. The commonly used configurations of ultrasonic flowmeters adapt the above principle in a more sophisticated scheme. The principle is illustrated in Figure 14.35. Location A has an ultrasonic transmitter T. The waves transmitted by it are received by the ultrasonic receiver R at location B. These two are linked through an external oscillatory circuit - oscillator 1. The period of oscillation is decided by the transit time of the wave through the liquid. Another transmitter-receiver set functions with the ultrasonic wave transmitted in the reverse direction through oscillator 2. The two frequencies are proportional to $(1/t_1)$ and $(1/t_2)$ respectively where t_1 and t_2 are the transit times in the two cases. The difference between the two frequencies is proportional to $[(1/t_1) - (1/t_2)]$.

$$\frac{1}{t_1} - \frac{1}{t_2} = \frac{c + V\cos\theta}{L} - \frac{c - V\cos\theta}{L}$$

$$= \frac{2V\cos\grave{e}}{L} \tag{14.53}$$

With this scheme the dependence on c and the error on this count, are eliminated. The difference frequency in Equation 14.53 is obtained by classical mixing technique [See Section on 6.2.1.3] or by digital means – using up-down counters and steering pulses to it alternately from the two oscillators for equal time intervals.

Observations: -

⇒ Ultrasonic flowmeters have the transmitter and the receiver piezo-elements embedded inside sections of piping with suitable flanges on either side. The meter as a unit can be installed permanently in the piping system.

⇒ Alternately, ultrasonic flowmeters are available as compact battery operated portable units. The transmitter and receiver piezo-elements are moulded piezo-units attached external to the pipe. For efficient transmission of the ultrasonic wave, suitable coupling jelly is used at the interface. Such meters can be used for velocity and allied condition monitoring, throughout the pipe. They have the facility for manual entry of the pipe dimensions. Transit time through the pipe, affects the performance of the meter. The pipe diameter has to be large compared to the pipe thickness, or suitable correction has to be incorporated. These meters are prone to a certain amount of 'acoustic short-circuiting' due to the reflection at the inner surface of the pipe.

⇒ The velocity sensed, is the integrated average along the path of the wave. The required velocity is the average across the cross-section. The two are equal only for very large N_R *i.e.*, turbulent flow when the velocity across the cross-section is a constant. The error is a maximum for laminar flow. The 'Coefficient of Discharge' to account for this non-uniformity is (about) 0.75 for N_R<2000 (laminar flow). It varies from 0.93 to 0.96 for turbulent flow. In some versions, repeated reflections and reversal of signal paths are used between the transmitter and the receiver, to make up for this.

⇒ For the scheme to function satisfactorily, the liquid has to be a reasonable conductor of sound energy. The unit works best with clean and clear liquids without suspensions, air bubbles *etc*. Turbidity or impurities in the liquid do not affect the functioning of the meter in any way but affect its accuracy.

⇒ Build-up of deposits on the inner surface of the pipe affects accuracy over a period.

14.4.8.2 Doppler-Effect Based Flowmeter

When ultrasonic energy is coupled to a liquid, it is (partially) reflected at every interface; this breaks the homogeneity of the liquid. Such reflections take place with particles suspended in the liquid, air bubbles *etc*. If the particle is in motion, the ultrasonic wave is affected and it undergoes a shift depending on the velocity of the particles. The principle can be understood from Figure 14.36, which shows an idealized situation. T is the transmitter surface and R is the receiver surface. An ultrasonic wave emanating from T at point A is injected into the liquid at an angle of θ radians to the flow axis. The wave-peak (say) that emanates at A at a particular instant, is reflected at a particle surface at B and returns to the receiver surface R at point C. The total distance travelled by the wave is ABC. As the wave transmission continues, the particle moves with velocity V along the flow direction. The next

peak of the wave again emanates from A and continues up to point D when it encounters the same particle and is reflected. It comes to the receiver at point F. This peak traverses an extra distance of BDE compared to the last peak considered above. Correspondingly, it is received at the receiver R with a time delay, which is larger than the time-period of the transmitted wave. The net result is an increase in the wavelength (and reduction in frequency) of the received wave. This frequency shift (called the 'Doppler Shift') is a measure of the velocity of the particle or suspension or entrapped air bubble.

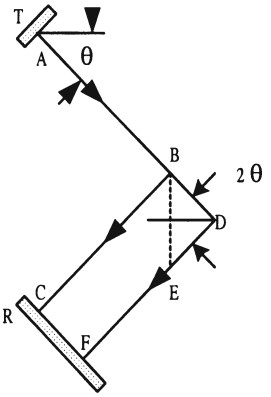


Figure 14.36 (a) Principle of operation of the Doppler effect ultrasonic flowmeter

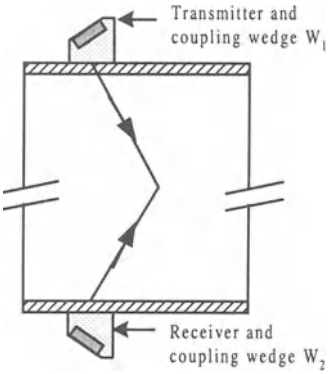


Figure 14.36 (b) Doppler effect type ultrasonic flowmeter. Use of wedges to couple waves to the liquid through the pipe

Let

x = the distance ABC

t_0 = the time of origin of the first peak at the transmitter

t_1 = the time of arrival of the first peak at the receiver

$$t_1 = t_0 + \frac{x}{c} \tag{14.54}$$

where

c is the velocity of sonic pressure waves through the liquid.

t_2, the time of origin of the next peak, is

$$t_2 = t_0 + \frac{\lambda}{c} \tag{14.55}$$

where λ is the wavelength of the Ultrasonic wave emitted.

$$\text{Additional distance travelled by the second peak} = \text{BDE} \tag{14.56}$$

$$= \frac{2V\lambda}{c\cos\theta} \ (\text{approx}) \tag{14.57}$$

From Equations 14.54, 14.55 and 14.57

$$t_3\text{, the time of reception of the second peak at the receiver} = t_0 + \frac{\lambda}{c} + \frac{2V\lambda}{c^2\cos\theta} + \frac{x}{c} \tag{14.58}$$

$$\text{Time difference between the two receiving instants} = t_3 - t_1 \tag{14.59}$$

Substitution from Equations 14.54 & 14.58 and algebraic simplification gives

$$t_3 - t_1 = \frac{\lambda}{c}\left(1 + \frac{2V}{c\cos\theta}\right) \tag{14.60}$$

$$\text{Corresponding received frequency} = \frac{c}{\lambda\left[1 + (2V/c\cos\theta)\right]} \tag{14.61}$$

$$\text{Original radiation frequency} = \frac{c}{\lambda} \tag{14.62}$$

From Equations 14.61 & 14.62 we get Δf the frequency shift as

$$\Delta f = \frac{c}{\lambda}\left[1 - \frac{1}{1 + (2V/c\cos\theta)}\right] \tag{14.63}$$

$$\approx \frac{2fV}{c\cos\theta} \tag{14.64}$$

where $V << c$
and

$$f = \frac{c}{\lambda} \tag{14.65}$$

Equation 14.64 shows that the Doppler frequency shift is directly proportional to the suspension velocity. The frequency shift can be converted into equivalent analog signal by any FM demodulation technique [See Section 6.2.2.5].

Observations: -

⇒ Equation 14.64 shows that the proportionality factor (2f/c cosθ), depends on only three factors:

- f – the ultrasonic frequency – this can be generated with a good enough level of stability
- θ – a constant for a given configuration
- c – the sonic velocity through the liquid which changes with temperature

⇒ The ultrasonic waves are coupled to the pipe through a wedge W_1 and back to the receiver through another wedge W_2 [See Figure 14.36 (b)]. Considering this, it can be shown that c cosθ for the fluid in Equation 14.64

can be replaced by a corresponding factor, which accounts for the pressure of wedges also. The sonic velocity for the wedge is much less dependent on temperature. Further, it can be corrected for a given wedge. This makes the overall sensitivity practically independent of temperature.

⇒ The method actually measures the velocity of suspension (and hence the liquid) at the point of reflection. Since under turbulent conditions, the liquid velocity can be considered the same across the cross-section, the measured velocity is taken as the average velocity. This is related to the volume flow rate of the liquid using the internal cross-sectional area of the pipe and a coefficient of discharge.

⇒ For satisfactory operation, the ultrasonic flowmeter requires a minimum amount of suspensions in the liquid. Typically, the minimum suspension level required is 25 ppm of 30 micron size suspensions. (Contrast with the transit-time measurement type flowmeter, where the suspensions should be below a minimum specified size to ensure accuracy of measurement.). Further, the particles will be in suspension only above a threshold velocity (2 m/s for solids and 0.8 m/s for bubbles) for the liquid.

⇒ These flowmeters can be battery operated and portable. They offer good repeatability at 1 % but limited accuracy of 5 %.

General Observations: -

⇒ The ultrasonic flowmeters do not offer any obstructions to flow. They have no wetted or moving parts. The sensor *per se*, is quite robust. Since the transmitter and the receiver can be fixed externally, the meter can be portable. These are easy to install and maintain. They can be used to measure the flow of any liquid without any limitation (The liquid has to conduct sonic waves). For the correlation between sensor output and the flow rate to be valid, the flow has to be axi-symmetrical.

⇒ The pipe dia. used with ultrasonic flowmeters, range from 134mm to 6m – a very wide range. They operate over –40 °C to +260 °C of temperature. Liquid velocity can range from 0.3 m/s to 30 m/s. Manufacturers claim accuracy of 1 % when calibrated for the concerned liquid. The scale is linear over the whole range. With many versions, bi-directional flow sensing is possible.

⇒ With the limited size of piezo-elements, coupling of acoustic energy to a gas and back to the receiver is not practical. Hence, the application of ultrasonic flowmeters is limited essentially to sensing of the flow of liquids.

⇒ Though manufacturers claim high accuracy and consistency, the same has not been confirmed by independent test data. Further, the ultrasonic flowmeters are yet to become popular despite their claimed advantages. Their high cost may be another one of the factors responsible for this.

14.4.9 Other Flowmeters

The flowmeters discussed so far are all of direct relevance and use or potential use to industry *vis-à-vis* instrumentation. Many other types of flowmeters are also available commercially. Some of them give direct indication of the flow rate without associated electronics. Some are for use in laboratory instrumentation while

others are purely for investigative studies. Due to their limited application in industrial instrumentation schemes, these are discussed only briefly here.

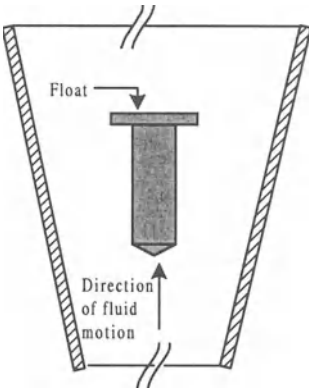


Figure 14.37 Variable area flowmeter

14.4.9.1 Variable Area Flowmeters

These are in wide use in chemical laboratories. The fluid is made to flow in an 'inverted conical tube'. The tube is transparent. A float inside takes a position, which is a measure of the flow rate of the fluid [See Figure 14.37]. The float position is such that the pressure differential across it is a constant. A graduated scale on the body of the tube indicates the position of the float and hence the flowrate. These flowmeters are more widely known as 'Rotameters'.

14.4.9.2 Capillary Type Flowmeters

These are used to measure the flow rate of fluids flowing in the laminar regime: *i.e.*, low flow rates. The pressure drop in the capillary is directly proportional to the flow rate (Contrast with the orifice plate and the like for which $\Delta P \propto Q^2$). If necessary, a number of capillaries are connected in parallel and the flow rate through each limited; with this it is ensured that $N_R < 1000$ for the flow.

14.4.9.3 Pitot Tube

Pitot tube is shown in Figure 14.38. It comprises a pair of tubes used to measure two pressures – one with an opening normal to the direction of flow, to sense the fluid pressure *per se* and the other facing the flow stream. The latter senses a pressure equal to $(p + v^2/2g)$. The difference between the two, is the pressure differential representing the fluid velocity at the point. Pitot tube is normally used to sense 'point-velocities' or to get a rough estimate of the volume flow rate from the point-velocity. It is essentially a simple laboratory device. In some cases, a few Pitot tubes are used at a fluid flow section to get an average fluid velocity at the section.

14.4.9.4 Positive Displacement Flowmeters

These deliver a fixed and measured quantum of liquid in each revolution. A number of variations are available – single position type, four-position type, nutating disc type, Helical-gearing type *etc*. The pump mechanism traps a definite amount of the

liquid and pushes it forward into the outlet area during the revolution. These may also have an associated counter to totalize and display the volume conveyed.

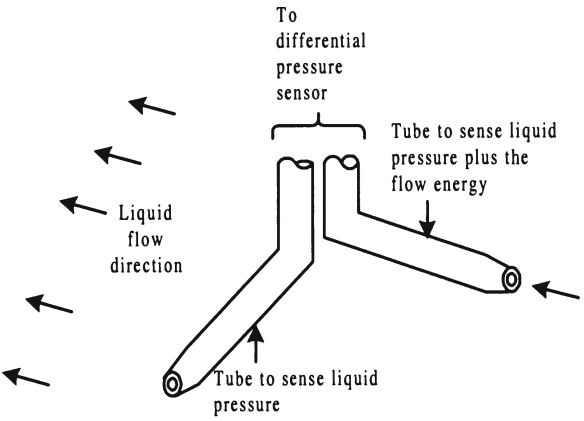


Figure 14.38 Pitot tube for point velocity measurement

14.4.9.5 Thermal Flowmeters

Different patented versions of thermal flowmeters are available. All of them are based on the relation of the fluid to carry away heat due to the fluid flow rate. One version uses two RTDs. One RTD senses the temperature of the fluid in motion. The other carries a steady current. The latter is kept close to the former but exposed to the fluid flow. Its temperature rise relative to the former is a measure of the fluid flow rate. The temperature differential is measured through a Wheatstone bridge arrangement [See Section 10.2.2] and allied electronics.

Another version uses a pair of thermistors kept at a definite distance from each other in the flow stream. A definite amount of heat energy – as a sharp pulse – is injected into the flow stream through the thermistor up-stream. By sensing the change in the temperature-profile of the thermistor down-stream, the time delay for the thermal pulse to travel to it, is ascertained. This also represents the transit time of the fluid from the first thermistor to the second.

A third version uses a heater and a pair of RTD sensors spaced at equal distances from it, on either side. In the absence of fluid flow, both the RTDs will be at the same temperature and have equal resistance values. As the fluid flows and the flow rate increases, the temperature and the resistance of the down-stream RTD increases compared to that kept up-stream. The difference between the resistances is a measure of the fluid flow rate. This difference can be measured with the help of a Wheatstone bridge.

All the above flowmeters are used essentially in the laboratories or in investigative studies. Though potentially useful, they are yet to get a foothold in industrial instrumentation schemes.

14.4.9.6 Bypass Flowmeters

There can be situations where the size of the main flow pipe, may be too big to accommodate a commercially available flowmeter. In such cases, one can have an orifice plate or the like and cause a pressure drop in the line, which is a measure of

the flow rate. A low capacity flowmeter (similar to a capillary tube or a thermal meter) can be connected in parallel to create a flow proportional to the pressure drop. This flow can be sensed and related to the flow rate in the main pipe. Due to the configuration used, the main flow has a square root relationship to the auxiliary flow measured. Thus for a 3:1 range of the main flowmeter, the auxiliary meter is to have a 10:1 range. Though commercial configurations of the scheme are being promoted, cross-verified data is not available.

14.5 Level Instrumentation

Industrial tanks containing raw materials, intermediaries as well as final products in liquid form require the level of the liquid in the tank to be sensed. The purpose can be to ascertain the feedstock level, to implement process control and / or to ensure safety. Traditionally level sensing have been crude and inaccurate. They were bulky and of questionable reliability. The tendency is to avoid level sensing if possible. As the next best alternative, upper and/or lower limits are set and the liquid level crossing the same sensed. Only when necessary, continuous level sensing has been resorted to. Among the techniques employed, level transducers using differential pressure sensors and capacitance-based sensors, are the most common.

14.5.1 Level Transducer with Differential Pressure Sensing

The scheme shown in Figure 14.39 is simple and straightforward. The pressure differential is proportional to the level of liquid inside. The sensitivity is proportional to the specific gravity of the liquid. Exact position of the taps, the position of the sensors *etc.*, are not critical. Performance, accuracy *etc.*, are essentially governed by the differential pressure transducer. Typical use is in sensing of liquid level in pressure vessels.

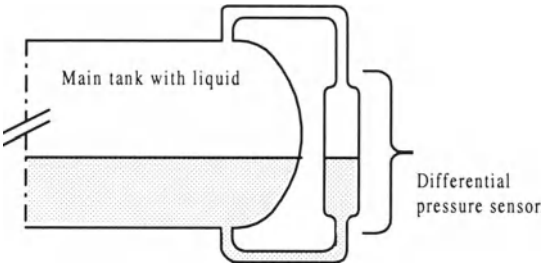


Figure 14.39 Level sensing using differential pressure principle

14.5.2 Capacitance Based Level Sensors

Capacitance type level-sensor is of two types – one for conducting liquids and the other for non-conducting liquids. Both function on the same principle.

14.5.2.1 Capacitance Sensors for Conducting Liquids

The sensor has the form shown in Figure 14.40. A cylindrical metal rod has a uniform dielectric coating on it (Teflon, PVC *etc.*). The liquid surrounds the dielectric but does not come into contact with the metal rod. The capacitance between the rod and the liquid is given by

$$C = \frac{2\pi\varepsilon_0\varepsilon_r}{\ln(r_2/r_1)} \text{ Fm}^{-1} \tag{14.66}$$

where

- ⇒ ε_0 is the permittivity of free space
- ⇒ ε_r is the relative permittivity of the dielectric sheath around the rod
- ⇒ r_1 is the diameter of the rod and
- ⇒ r_2 is the diameter of rod with sheath

The capacitance here is on a 'per metre of immersed depth' basis. If the liquid container is metallic, it is grounded. If it is non-metallic, or has a non-conducting coating by way of protection against corrosion *etc.*, a separate grounded conductor is kept immersed in the liquid – as far away from the measuring rod as possible. Normally all liquids with conductivity greater than 10 μS cm, are considered conductive. All strongly corroding acids, aqueous solutions and the like, are conducting. If the liquid wets the electrode (coats it), it can lead to erroneous reading.

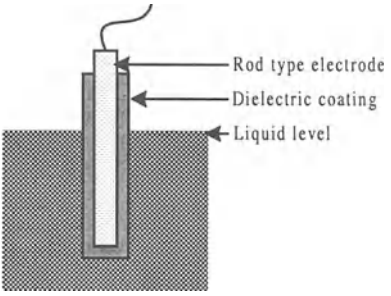


Figure 14.40 Capacitance type level sensor for conducting liquids

14.5.2.2 Capacitance Sensor for Non-conducting Liquids

Different possibilities arise here. Figure 14.41 shows the simplest case. The rod forms one electrode of a capacitor and the metallic enclosure the other electrode. The fluid is the dielectric of the capacitor. The metallic enclosure is grounded to minimize errors due to changes in the vicinity. The electrode rod and the enclosure are kept insulated from each other. The ideal outfit will be a cylindrical vessel with the electrode rod on its axis. If the length of the cylinder is large compared to its diameter, we have

$$C = \frac{2\pi\varepsilon_0}{\ln(r_2/r_1)}[\varepsilon_r x + d - x] \tag{14.67}$$

where

- ⇒ C is the capacitance between the electrodes
- ⇒ d is the depth of the vessel down to the datum point

⇒ x is the depth of the liquid from the datum point
⇒ r_1 is the diameter of the rod and
⇒ r_2 is the diameter of the cylinder

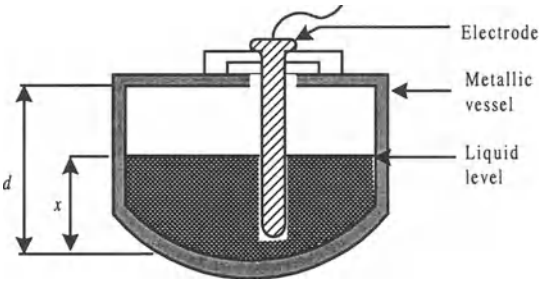


Figure 14.41 Level sensor for a non-conducting liquid in a metallic vessel

A more sensitive and reliable arrangement is to use two concentric rods as electrodes. The outer rod is connected to the enclosure and grounded; the scheme is shown in Figure 14.42. The inner rod electrode is live and insulated. Equation 14.67 for the capacitance C of the scheme is valid here also; here

⇒ r_2 is the inner radius of the outer electrode
⇒ r_1 is the radius of the rod electrode inside and
⇒ x is the depth of liquid from the datum point

This arrangement provides linear output change in C with change in depth. It is suitable for irregularly shaped vessels, non-conducting vessels as well as conducting vessels with non-conducting coating on the surface. The concentric tube scheme of the above type is less sensitive to turbulence on the liquid surface.

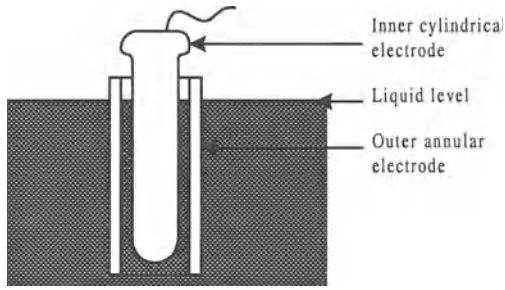


Figure 14.42 Level sensor for non-conducting liquids using concentric cylindrical electrodes

Two parallel rods with suitable non-conducting separators at regular intervals, is a simpler alternative to the concentric cylinders case. In cases where the concentriç cylinder or two parallel rod electrodes cannot be used, a single rod can be used close to the tank wall. The capacitance in this case is approximately given by

$$C = \frac{2\pi\varepsilon_0}{\ln(2g/r)}\left[\varepsilon_r x + d - x\right] \qquad (14.68)$$

where

⇒ r is the radius of the rod and

⇒ g is the shortest distance of the wall from the axis.

Liquids with conductivity less than 0.1 μS cm, can be considered insulating. All hydrocarbons, petroleum based products *etc.*, are of this category.

General Observations: -

⇒ Capacitance transducers have been dealt with in Section 10.3. The change in capacitance representing level is converted into an equivalent modulated AC signal. Frequencies used are typically in the 500 kHz to 5 MHz range.

⇒ In all capacitance type level-sensors, the tank or the outer electrode is grounded. This is to avoid any stray capacitance changes causing error.

⇒ The capacitance type level-sensor has to be calibrated *in situ*, with the liquid whose level is to be sensed. However, with the concentric electrode type sensor, calibration done with a separate container with the liquid concerned, is valid with a slightly reduced accuracy.

⇒ Level-sensors of the capacitance type are available for depths down to 12'. Manufacturers do not specify accuracy – presumably because the site conditions have a larger say on the accuracy.

⇒ Liquids, whose conductivity is in the 0.1μS cm to 10 μS cm range, cannot be termed as conductors or dielectrics – alcohol are of this category. Capacitance sensors are not directly suitable to sense their level.

⇒ The arrangement for non-conducting liquids can be used for sensing the level of powdery materials also. To ensure accuracy, the powder has to be dry and should not stick to the electrodes.

⇒ The dielectric constants of liquids are functions of temperature. Hence, change in ambient or liquid temperature can cause an error. One can compensate for this, by accounting for the temperature coefficient of ε_r (ε_r and its temperature coefficients for different liquids are published by the National Institute of Standards and Technology).

⇒ The capacitance of the electrode gland is typically 40 pF. This along with the capacitance of the sensor *in situ*, should be such that the full scale capacitance change should be at least 10 % of the standing capacitance. Further, such capacitance change should be at least 10 pF to be measured reliably. Thus the lowest capacitance values are obtained as

Gland capacitance	=	40 pF
Capacitance of sensor in position without liquid	=	60 pF
Total capacitance at zero reading	=	100 pF
Total capacitance at full scale reading	=	110 pF

Further 1nF represents 160 Ω at 1 MHz. Around 5 nF is the upper limit, that one can have for a capacitance probe type capacitor. Beyond that, the capacitive reactances become too low, to work with practical circuits.

Features of capacitance-type level sensors, types of liquids and operating environments in each case, are shown in a compact form in Table 14.2 at the end of this chapter.

14.5.3 Other Types of Level Gauges

Level sensing based on other principles, is offered by some manufacturers. The more conspicuous ones are discussed here.

14.5.3.1 Displacement Type Level Sensor

The scheme is shown in Figure 14.43. It is an extension of the float principle. A long rod of uniform section dips into the fluid extending down to the bottom. It is supported through a cantilever. The force exerted on the cantilever is measured using SGs. When the liquid level is low enough to be clear off the rod, the force experienced by the cantilever beam is the weight of the rod. However as the liquid level rises, the force experienced by the rod reduces by the amount of weight of liquid displaced. This reduction is directly proportional to the depth of the liquid.

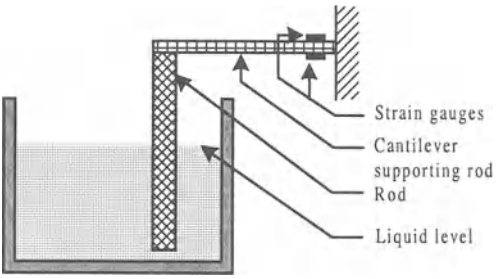


Figure 14.43 Displacement type level sensor

We have

$$F = A\,g(L\,\rho_1 - x\rho_2) \tag{14.69}$$

where

- $\Rightarrow$ F is the force experienced by the cantilever
- $\Rightarrow$ A is the area of cross-section of the rod
- $\Rightarrow$ g is the acceleration due to gravity
- $\Rightarrow$ L is the length of the rod
- $\Rightarrow$ x is the depth of the liquid to be measured
- $\Rightarrow$ ρ_1 is the equivalent density of the rod and
- $\Rightarrow$ ρ_2 is the density of the liquid.

To obtain a good sensitivity, the equivalent density of the material of the rod (mass per unit length to be more specific), has to be close to that of the liquid. The rod is kept hollow for this purpose and adjusted such that $\rho_1 \approx \rho_2$. ρ_1 may be slightly larger than the ρ of water to make it universally applicable for all fluids. The method is equally applicable for conducting as well as non-conducting liquids. Shape of the vessel does not affect the reading. The sensor has to be separately calibrated for each liquid because of the change in its ρ. Temperature changes affect ρ and cause error. This can be compensated for, by knowing the temperature coefficient of change of ρ.

14.5.3.2 Ultrasonic Level Sensor

The more common version of the ultrasonic level sensor uses a non-contact type scheme. A piezo-electric element kept above the liquid surface emits ultrasonic waves. These are reflected from the liquid surface (and the tank walls). The reflected waves are received by the piezo-sensor and the time delay (time of flight), between the time of emission and reception is estimated. From this, the liquid surface level is deduced. To ensure effective coupling of the waves into air, the

ultrasonic source has to be big in size. As its size increases, the ultrasonic wave is less 'focused' and more of it is reflected from the sides of the vessel. This causes widening of the received pulse and blurring of the signal. Further, the received pulse shape changes with the liquid level. Templates of the received pulses for different levels of the liquid are stored in a microcomputer during the calibration stage. During actual operation, the pulse received is compared with the templates for a match and the level decided based on the best match. All these require elaborate *in situ* testing and calibration. The extensive signal processing required for this, adds to the cost of the instrument.

14.5.3.3 Gamma Ray Level Sensor

The scheme is shown in simplified form in Figure 14.44. A gamma ray source and a detector are kept on either side of the container. They are oriented in such a way that the ray path is diagonal and can cover the full range of levels to be sensed. The liquid absorbs rays and the amount of absorption is related to the total amount of matter intervening.

$$I = I_0 \exp[-k\rho l] \tag{14.70}$$

where

- $\Rightarrow$ I_0 is the amount of incident radiation
- $\Rightarrow$ ρ is the density of the liquid
- $\Rightarrow$ l is the ray path length
- $\Rightarrow$ I is the intensity of radiation emerging from the liquid surface

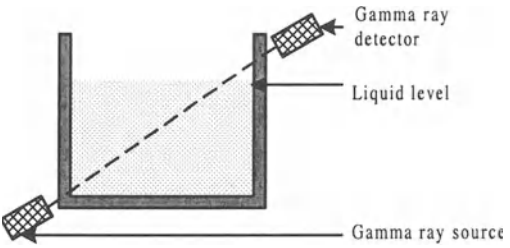


Figure 14.44 Liquid level sensor using gamma ray source and detector

Over the full range of levels to be sensed, the gamma ray path has to be partly within the liquid and partly outside. The tank surface and any other object on the ray path also absorb radiation. The unit requires expertise in installation and handling of the gamma ray source. It is to be calibrated at site. The accuracy obtainable is not high (~5%). The use of gamma gay sources and their disposal are all closely monitored by the respective Governmental Nuclear Agencies. This calls for careful handling, regular checks and reporting to the agencies. All these make the gamma ray based level gauges, unattractive for industries.

Table 14.2 Capacitance type level sensors – features and application areas

Liquid	Container	Coating of container	Sensor type	Remarks
conducting	conducting	No coating	Single bar with dielectric sheath	◊ container to be grounded ◊ liquid to be non-wetting type ◊ probe and lead to be insulated from liquid
		Insulated coating (to prevent corrosion)	Single bar with dielectric sheath	◊ container to be grounded ◊ liquid to be non-wetting type ◊ probe and lead to be insulated from liquid ◊ liquid to be grounded suitably for best accuracy; otherwise at least the container to be grounded
Non-conducting	conducting	Not Applicable	Single bar electrode	◊ container to be grounded ◊ suitable down to 10' only and only with regular tanks ◊ capacitance change depends on ε_r of the liquid
			Concentric electrodes	◊ outer electrode to be grounded ◊ suitable for any tank shape and depth ◊ capacitance change depends on ε_r of the liquid
			Two parallel rod type electrodes	◊ one electrode to be grounded ◊ suitable for any tank shape and depth ◊ capacitance change depends on ε_r of the liquid ◊ less costly and less sensitive than concentric electrodes
		Insulated coating (to prevent corrosion)	All the above three types	◊ same as with the respective types above
	Non-conducting	Not Applicable	Concentric electrodes	◊ outer electrode to be grounded ◊ suitable for any tank shape and depth ◊ capacitance change depends on ε_r of the liquid
			Two parallel rod type electrodes	◊ outer electrode to be grounded ◊ suitable for any tank shape and depth ◊ capacitance change depends on ε_r of the liquid ◊ less costly and less sensitive than concentric electrodes

15 Process Instrumentation III

Other Variables

15.1 Introduction

Instrumentation schemes for a variety of physical variables – other than temperature, pressure, flow and level – are available and in wide use in industry. The sensor characteristics of the more common ones amongst these and the constraints on related signal-processing are discussed here.

15.2 pH Instrumentation

Knowledge of the acidicity or the basicity level of liquids is necessary in many industrial processes – for monitoring as well as for control. pH value is a measure of the same. It measures the relative amount of hydrogen ions in the liquid [Glasstone].

15.2.1 Basic Ideas of pH Value

The total level of hydrogen (acidic) and hydroxyl (basic) ions in a liquid or solution or substance as the case may be, is known to be of the order of 10^{-14} /mole. If a_a and a_b represent the concentration of hydrogen and hydroxyl ions, it is known that the product $a_a\, a_b \cong 10^{-14}$/mole. This figure increases with temperature. The pH value of the substance is defined as

$$\text{pH} = -\log [a_a] \tag{15.1}$$

pH has a range of 14 extending from 0 (fully acidic) to 14 (fully basic). A fully neutral solution (like distilled water), has a pH value of 7. Figure 15.1 shows ion concentration levels, corresponding pH values and typical substances as to where they occur in the scale.

Any acidic or basic substance in contact with an electrode, develops a potential with reference to the electrode. The Nerst equation relates this potential, with respect to the electrode, to the pH value of the substance.

$$E = E_r - \frac{2.3RT}{nF}\text{p} \tag{15.2}$$

where

- $\Rightarrow$ E_r is a constant potential related to the electrode
- $\Rightarrow$ R is the universal gas constant
- $\Rightarrow$ T is the absolute temperature in K.

T. R. Padmanabhan, *Industrial Instrumentation*
© Springer-Verlag London Limited 2000

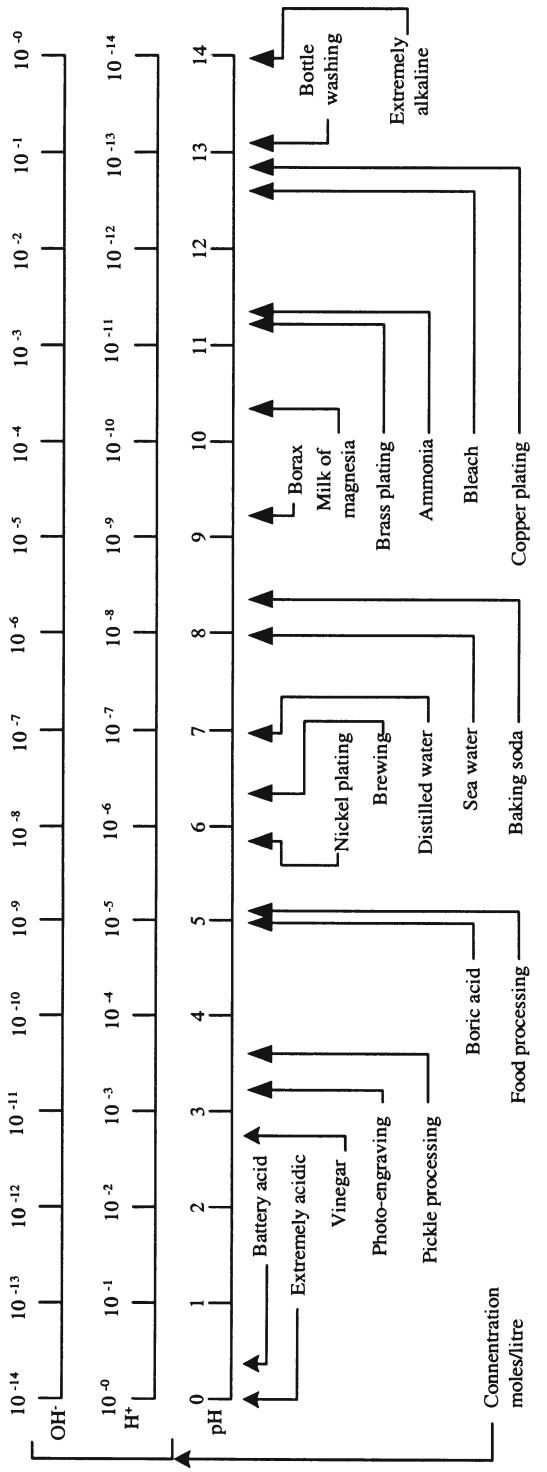


Figure 15.1 Ion concentration levels and corresponding pH values: Approximate position of different liquids and solutions used in processes are also shown

⇒ n is the charge on the ion.
⇒ F is Faraday's constant and
⇒ p is the pH value of the solution.

Often the Nerst equation forms the basis for determining the pH value of the concerned substance. A few observations are in order here: -

⇒ The pH value is linearly related to the electrode potential. At 25 °C, we get 59.16 mV/pH.
⇒ The voltage is affected by any change in the temperature of the solution. The change is taken as zero in the pH scale at 25 °C. As the temperature departs from 25 °C, the sensitivity changes. At 0 °C, it is 54.20 mV/pH and at 100 °C, it is 74.04 mV/ pH.
⇒ It is easier to measure the potential difference between a pair of electrodes rather than the absolute potential of a single one; here pH is related to the potential difference measured.

15.2.2 Measurement of Electrode Potentials

Normally any suitable pair of electrodes in contact with an electrolyte has a potential difference between them and the same can be measured. In the case of pH measurement, we require an electrode whose potential with respect to the test solution changes with the pH value and another whose potential does not change at all (in the ideal case). This calls for an elaborate arrangement. The prevalent practice is to use a scheme as shown in Figure 15.2. S_T is the solution whose pH value is to be measured. A special glass bulb G is inserted in it. The bulb has a specified and known solution S_2 within. An electrical wire L_1 is in contact with it through a suitable salt S_1. Together they form the measuring electrode. Another wire L_2 is in contact with a solution S_3 through salt S_4 around it. The solution S_3 is also of known substance and concentration. The enclosure H around S_3 separates S_T from S_3. However, it is kept porous to allow solution S_3 to continuously leak through and migrate into S_T. Thus, there is an electrical continuity between the two.

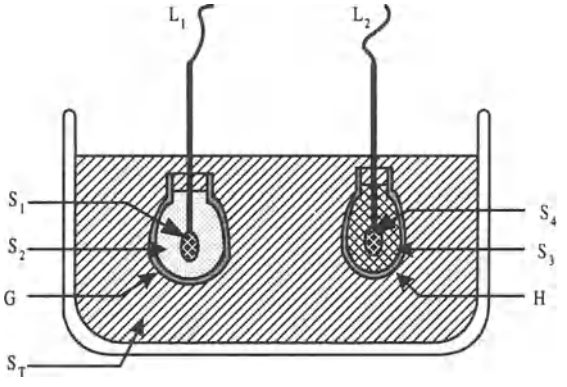


Figure 15.2 Scheme of potential measurement for pH determination

All the above together form an elaborate electrical cell. The cell develops a net voltage, which is the algebraic sum of voltages between

$\Rightarrow$ L_1 and the salt S_1
$\Rightarrow$ Salt S_1 and the solution S_2
$\Rightarrow$ Solution S_2 and the inner face of glass electrode G
$\Rightarrow$ two sides of the glass electrode
$\Rightarrow$ The outer face of the glass electrode G and the test solution S_T.
$\Rightarrow$ Test solution S_T and the known solution S_3
$\Rightarrow$ Solution S_3 and salt S_4 and
$\Rightarrow$ Salt S_4 and electrode L_2.

In the whole arrangement, we are interested in the emf developed between the outer face of the glass electrode G and the test solution S_T. Hence, all the other items should be chosen such that the respective potentials are known and they remain unchanged. This is essential from the point of view of pH measurement.

15.2.3 Glass Electrode

Glass acts as an effective electrode for pH measurement. A glass with 72 % SiO_2, 22 % Na_2O and 6 % CaO is well suited for this (Other glasses are also available). When in contact with a solution, the glass electrode develops a potential, which is a measure of the hydrogen ion concentration in the solution. This glass electrode is an effective medium to sense pH values. A typical glass electrode is shown in Figure 15.3. The special glass is formed as a thin walled bulb. It can have a 0.1 N hydrochloric acid inside with silver in silver chloride forming the electrode for connection. The silver chloride salt is coated on the silver wire. This whole combination forms the glass electrode. If immersed in the solution of interest, it forms a potential proportional to the pH value of the solution. Instead of the 0.1N HCl, any solution of known pH value (called a 'buffer' – see section 15.2.5 below) can be used, provided we account for its potential.

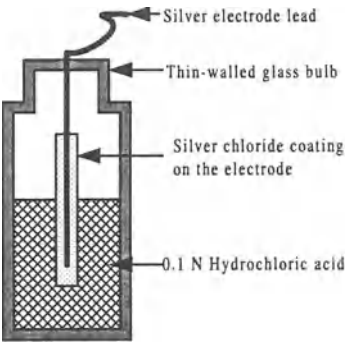


Figure 15.3 Details of typical glass electrode

15.2.4 Reference Electrode

The second electrode connected through wire L_2 is called the 'Reference electrode'. The potential associated with it has to be a constant and independent of the pH value of the solution S_T. Two reference electrodes are in common use.

15.2.4.1 Calomel Electrode

Calomel reference electrode consists of mercury in contact with a solution of potassium chloride saturated with mercurous chloride. The external connection is to mercury. The potassium chloride solution is in contact with the test solution. With the use of 0.1N KCl solution the potential developed is –0.3338 + 0.00007(t – 25)V where t is the temperature in °C. The Calomel reference electrode is suitable for all measurements at temperatures below 60 °C.

15.2.4.2 Silver- Silver Chloride Electrode

Silver in silver chloride as electrode is also used as a reference electrode. It is formed by having a vehicle with a silver coating. The surface can be converted into chloride by electrolysis on a chlorate solution. It has a constant potential of (–0.2224V). It is used for accurate work; it also forms the reference when the test solution temperature exceeds 60 °C.

Normally the reference electrode is so constructed that the reference solution in contact with it, can migrate into the test solution. This ensures electrical contact and continuity. Three methods of construction are adopted for this: -

⇒ The reference solution with the reference electrode inside is kept inside a ceramic tube or enclosure. The ceramic is porous; the reference solution leaks through the pores and migrates into the test solution.

⇒ The enclosure can be made up of fibres – woven or straight with the intervening spaces allowing migration.

⇒ The enclosure is in the form of a glass or plastic shield. Holes are ground in it and a fine sleeve inserted. Through this, the reference solution can form a junction.

15.2.5 Buffers

The emf of the overall 'cell' in Figure 15.2 is made up of a number of components – the variable component of this being due to the pH variation of the test substance. For a proper use of the set-up, the cell is normally calibrated. Calibration also corrects for errors due to the ageing of the glass electrode. Solutions of known pH values are used in place of the test substance for such calibration work. Normally calibration is carried out at 7 pH (distilled water) and a pH value close to that being measured. Solutions of known pH values, used for calibration, are called 'Buffers'. A number of buffer solutions are available (See Table 15.1). Using these and salts of respective acids, buffers of known pH can be made [Glasstone (1974)].

Table 15.1 Buffer mixtures and respective pH ranges

Mixture	PH range
Phthalic acid and potassium acid phthalate	2.2 – 3.8
Phenyl acetic acid and sodium phenyl acetate	3.2 - 4.9
Potassium acid phthalate and dipotassium phthalate	4.0 – 6.2
Sodium dihydrogen phosphate and disodium hydrogen phosphate	5.9 – 8.0
Boric acid and borax	6.8 – 9.2
Diethylbarbituric acid and sodium salt	7.0 – 9.2
Borax and sodium hydroxide	9.2 – 11.0
Disodium hydrogen phosphate and sodium hydroxide	11.0 – 12.0

15.2.6 Signal Processing

The potential difference measured between the leads L_1 and L_2 of Figure 15.2 varies linearly with the pH value of the test substance. But it has other undesirable components and characteristics: -

⇒ All the potentials referred to in Section 15.1.2, add together and form a constant bias signal. This bias has to be removed.

⇒ The sensitivity is inherently temperature dependent. For precise work, the temperature of the test substance has to be measured separately and variations due to temperature changes should compensated. In many of the microprocessor-based instruments of today, this is done automatically.

⇒ The glass electrode is specially manufactured for pH detection. It is kept thin and the exposed area is made as large as possible to keep the impedance of the glass electrode at a minimum. The low impedance here is in the 10 MΩ to the 100 MΩ range.

⇒ The reference solution used with the reference electrode has to be selected to suit the specific application. It should not react with the test substance leading to local heating. This can cause error as well as damage to the reference electrode. If it develops too high a voltage with respect to the test substance, the same may mask the signal. If it migrates out too much, the reference electrode may dry off fast. If the migration or leakage is too low, the electrical continuity may be affected.

The high levels of impedances associated with the sources and the constraints on the currents that can be drawn from them, necessitate the use of amplifiers with correspondingly higher levels of input impedances. With such high impedances, the input circuit is quite susceptible to pick up from weak interfering sources also. Low drift MOSFET opamps and low operating voltages are the choice here. Also special measures are to be taken to keep leakage effects to the minimum [See Section 4.3.3].

15.3 Humidity Sensing

Many chemical and industrial processes require the humidity to be monitored and controlled; e.g., yarn spinning requires the humidity to be maintained within limits to ensure quality and productivity. Production processes of many chemicals, photographic films, semiconductor manufacturing, PC board assembly *etc.*, are sensitive to humidity.

15.3.1 Basic Ideas of Humidity

Humidity refers to the relative amount of water vapour in atmosphere. At a specific atmospheric temperature, there is a limit to the amount of water vapour in air. This represents the 'saturated condition'. Any increase in water vapour beyond that will result in the excess vapour condensing into water. Further, as the atmospheric temperature rises, the amount of water vapour that can remain in the air rises. This gives rise to the concept of 'Relative Humidity (Rh)'.

$$\text{Relative humidity at a specified temperature} = \frac{\text{Amount of water vapour content per unit volume of air}}{\text{Maximum amount of watervapour per unit volume of air that can be contained in it (i.e., under saturated conditions)}} \quad (15.3)$$

'Dew Point' is a related concept. Consider air at a particular temperature, having a certain amount of humidity in it. As the air temperature is reduced steadily, the relative humidity rises. At a particular temperature, it becomes 100 %. Any further reduction in the temperature of air causes the excess humidity to condense and appear as dew. This is referred to as the 'Dew Point'. At any atmospheric temperature, as the relative humidity increases, the dew point temperature also increases correspondingly. The dew point temperature and the atmospheric temperature can be measured and relative humidity inferred from these. This is the classical method of determining humidity. Special charts relating the three are available (Shown reproduced in Figure 15.4). These are referred to as 'psychrometric' charts.

Apart from the relative humidity, humidity can be defined on a purely volume or mass basis. Mixing ratio (Specific humidity) is the ratio of mass of water vapour present in a gas to the mass of dry gas. Volume ratio is the ratio of parts of water vapour present per million parts of air.

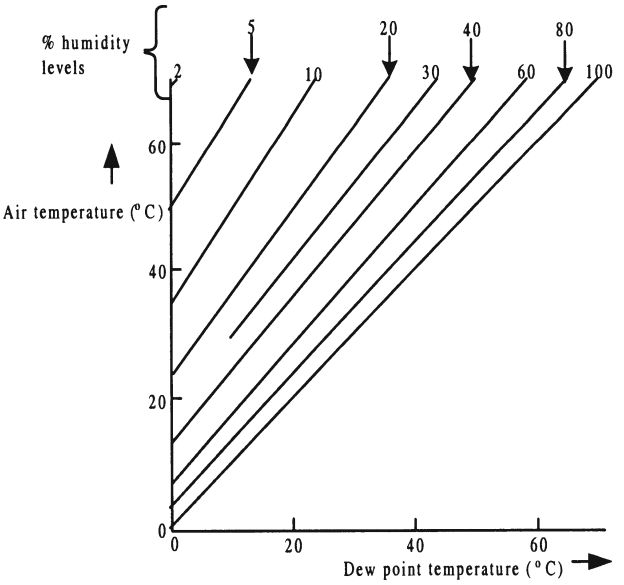


Figure 15.4 Psychrometric chart for water vapour

15.3.2 Humidity Measurement by Dew Point Sensing

'Dew point sensing' forms the most widely used but cumbersome method of relative humidity measurement. Here we measure the atmospheric temperature and

the dew point temperature. Using these two and the psychrometric chart, Rh is estimated. Conventionally the dew point determination is done using a wet bulb thermometer. The thermometer bulb is kept soaked in cotton gauze wick, which in turn is kept wet by immersing a portion of the wick in water. Further, a minimum speed of airflow is specified during measurement. With these, the thermometer bulb is ensured to be wet and the water around continuously evaporating. The wet bulb temperature measures the dew point.

An alternate procedure uses a mirror with an optical reflective photo-detector. Normally the mirror will reflect a substantial part of the incident radiation and the photo-detector will be on. As the mirror is continuously cooled, at the dew point temperature, the water vapour condenses on the mirror affecting its reflectivity substantially. The same causes the photo-detector to turn off. In the instrument proper, the photo-sensor and the cooling are arranged in a feedback scheme such that the mirror is continuously kept at the dew point temperature.

With a knowledge of both the temperatures, the Rh can be evaluated with the help of the psychrometric chart. Microprocessor based systems carry out the Rh evaluation through a series of LUTs. Two-dimensional LUTs are to be read here (See Section 9.2). Since a measurement of Rh involves the measurement of the ambient temperature also, all humidity meters have the provision to indicate the atmospheric temperature also. This is an additional information made available to the user or customer at no extra cost.

The wet and dry bulb temperature sensing method yields Rh value with 2 % accuracy – possibly the best attainable – and a resolution of 0.5 %. It is suited for Rh range of 10 to 100 %. The response time is typically 60s.

15.3.3 Humidity Measurement Using Lithium Chloride

Resistivity of lithium chloride changes with changes in atmospheric humidity in a consistent and reproducible manner. As such lithium chloride is suited to be used as a sensor. Two noble metal wires are wound on a strip of plastic with a definite spacing between them. The intervening space is coated uniformly with lithium chloride. The wires form the leads with the lithium chloride forming the bridge between them. Measured changes in resistance value between the two leads can be converted into an equivalent output using a Wheatstone bridge. Since the range of resistance variation is wide, an opamp based scheme is more common (See Section 10.2.2). The resistance variation with humidity is non-linear. Hence, typically one sensor is used over a range of about 10% of Rh only. A number of sensors are used – each for one 10 % range – in a pack forming the total sensor. The resistance of lithium chloride changes with changes in the ambient temperature. Hence, separate temperature compensation is necessary. Typical accuracy is 2 % and repeatability 0.2 %. With a small size of 30mm × 50mm × 30mm of the sensor, response time is of the order of 5s only. The sensor can function over a wide temperature range of – 40 °C to +65 °C.

15.3.4 Other Methods

Some other methods of sensing Rh value have been suggested and sensors built around them. These are yet to become popular and widely acceptable.

15.3.4.1 Pope Cell

'Pope Cell'is a patented polystyrene based ion-exchange device whose resistance changes with humidity. From a few MΩ at 0 % Rh, the resistance decreases to the kΩ range at 100% Rh. With such a wide variation in the resistance, a single sensor suffices for the full range of Rh values. It provides accuracy of the same order as the lithium chloride sensor.

Proprietary semiconductor sensors of the resistance type have also become available. Due to their porous nature, air is in continuous contact with the sensor material. Resistance decreases depending on the water absorption level. These can be adapted to function over the full 100 % Rh range. Accuracy attainable is 4 %. Their small size ensures a fast response.

15.3.4.2 Electrolytic Sensor

These function on the Faraday's electrolytic principle. A matrix similar to the lithium chloride cell above is provided and coated with a chemical (PO_5), which absorbs moisture. Atmospheric air is made to flow over the sensor at a constant rate. The sensor continuously absorbs the atmospheric moisture. A DC voltage is applied between the wires (electrodes), continuously. Due to this, the absorbed water is continuously electrolysed into H_2 and O_2. The current required for electrolysis is a function of moisture content in the air. The accuracy attainable is 3 % with a response time of 30s.

Thin film capacitors whose capacitance or loss angle, changes with humidity content in the vicinity, are also possible to be used as humidity sensors.

Table 15.2 gives typical performance and related data for Rh sensors. Note that it is customary to calibrate Rh sensors, meters, transducers etc., at 25 °C ambient. Normally the data given refers to this temperature.

Table 15.2 Typical performance data of different types of humidity sensors at 25 °C ambient temperature

Type of sensor	Rh range (%)	Rh sensing resolution (%)	Accuracy (%)	Response time (s)	Cost (relative)
Wet & dry bulb	10 - 100	0.5	2	60	10
Lithium chloride	0 -100	0.2	2	5	6
Electrolytic	0 - 100	0.2	3	30	6
Pope cell	2 - 98	1	3	30	5
Thin film cap.	5 - 95	0.2	2	10	8

15.4 Gas Sensors

Gas Sensors are used essentially to detect the presence or concentration of toxic gases (like CO), inflammable gases (like H_2) or pollutants (like CO_2) in the atmosphere. Detection range varies with the individual gas concerned. For hydrogen in air, it may range from 2 ppm to 100 ppm. For combustible gases like methane, it may range from 200 ppm to 10,000 ppm. The detection is mostly done

to ascertain whether the gas concentration has exceeded set or acceptable limits. Mainly two techniques have come into vogue – those using a sintered ceramic sensor and those based on the absorption of IR radiation.

15.4.1 Ceramic Sensors

The ceramic sensors are of the sintered tin-oxide type. The grains in the ceramic are deficient in oxygen and can be represented as SnO_{2-x}. When exposed to atmospheric oxygen, the oxygen is adsorbed at the surface. The free electrons in the grains in contact with the adsorbed oxygen molecules, are trapped by the oxygen molecules due to their high electron affinity. The resultant negative charge built-up at the boundaries causes a high potential barrier at the boundary. This hampers the free movement of the electrons across the boundary, which is reflected as a corresponding increase in the effective resistance of the sensor. Normally the resistance can decrease due to two reasons:-

⇒ Any increase in the temperature causes the electrons to acquire enough energy and cross the barrier. This continues until the effective resistance drops down to a steady level at a high enough temperature.

⇒ Any reducing gas at ppm levels in the environment reacts with the adsorbed oxygen at the boundaries. The potential barrier reduces, paving the way for easy crossing of the electrons across the boundary. This reduces the effective resistance of the sensor. As the gas concentration increases, the sensor resistance reduces. This continues until the concentration of the reducing gases is high enough to react with the adsorbed oxygen radical fully. Beyond that, the effective resistance of the sensor remains unchanged.

With combustible gases like methane, the sensor resistance may change by a factor of 3 for gas concentration up to 10,000 ppm. For a gas like hydrogen, it may change 15 times for concentrations up to 1000 ppm.

15.4.1.1 Circuit Scheme

Change in the sensor resistance can be converted into an equivalent voltage signal in many ways. Four factors are to be considered here: -

⇒ *Temperature variation*: The sensor is quite sensitive to the operating temperature. Normally it is operated at an elevated temperature maintained by a constant supply of heat through a built-in heater. This reduces sensitivity to ambient temperature changes.

⇒ *Resistance change over a wide range*: The sensor resistance changes by one order over the range of the concentration to be measured. This precludes the use of Wheatstone bridge or other schemes used with previous sensors. One can pass a constant current through the sensor and use the voltage drop across it as a measure of the resistance. Alternately, a constant voltage can be applied and the current taken as a measure of the resistance as in an inverting amplifier configuration. In both the cases, the output can be suitably biased.

⇒ *Unit to unit variation*: As with all sintered ceramic type sensors, the unit to unit variation in the resistance can be substantial (But for a given unit, the repeatability in the characteristic is more consistent). As such the scheme has to be calibrated on a unit by unit basis.

⇒ *Sensitivity to different constituents*: The sensor responds to all the gases, which react with oxygen. Individual sensitivities differ due to the difference in their affinities at different temperatures. As such the response of the sensor is the cumulative effect of changes in the concentration of all such gases in the vicinity. Sensing becomes meaningful only when the concentration of only one of the constituents changes conspicuously. In some cases, this is ensured using suitable molecular sieves or selected reagents or absorbents, which absorb the other constituents.

15.4.2 IR Sensors

Depending on the molecular structure of any gas, it absorbs IR radiation selectively. Thus, the absorption characteristics of a gas can be used as its signature to detect its presence and concentration. In a typical implementation, two source-detector pairs are kept in the gas flow stream. One set has an IR detector in the wavelength range absorbed by the target gas while the other has the IR sensor tuned to a wavelength fully transmitted by the same gas. The latter is used as a base for normalising the received radiation at the former wavelength (This is akin to the two-colour method of temperature sensing discussed in Section 13.8.7.1). The amount of IR radiation absorbed in the intervening medium, is a measure of the concentration of the target gas. With each type of gas, the two wavelengths are selected to ensure that

⇒ the absorption at the first wavelength is high and that at the second wavelength is low and

⇒ the other constituent gases do not absorb radiation at these two wavelengths.

The IR based scheme is more elaborate and costly. For each constituent gas of interest, a separate set of IR detectors is to be used. However, the performance is superior in terms of consistency and accuracy.

15.5 Gas Analysis

Analysis of gases to determine the percentage composition of individual constituents, has become an essential requirement in many industries. The basic purpose is usually one of the following: -

⇒ Efficiency of burning fuel by sensing the proportion of oxygen unburned constituents or other constituents resulting from combustion.

⇒ Gauging the quality of a process by measuring the relative level of specific constituents in the gas or the gas mixture emanating from the process.

⇒ Pollution control by measuring oxides of sulphur, nitrogen *etc.*, in the gas mixture let off to the atmosphere.

Chemical methods of analysis and chromatography are in wide use in laboratories. These are elaborate and time consuming and not suited for on-line analysis. Such on-line analysis becomes necessary when the measurement is for closed loop control or when a process is to be monitored closely. A variety of techniques is used individually or in combinations for on-line gas analysis. The most commonly used method is to measure the thermal conductivity and relate it to the quantum of the concerned gas constituent.

15.5.1 Thermal Conductivity Measurement

Thermal conductivity of some of the common gases is given in Table 15.3. The thermal conductivity of a gas mixture is a function of

⇒ the thermal conductivity of the constituents and

⇒ the % content of the constituents.

If the concentration of only one constituent varies or only two of them vary in their relative proportions, the sensed thermal-conductivity can be used as a measure of the content of the constituent or ratio of the concerned constituents respectively. Thus, a mixture of air and hydrogen has a relative thermal conductivity of 1 for 0 % of hydrogen and 7.22 for 100 % of hydrogen.

A typical 'thermal-conductivity cell' is shown in Figure 15.5. It has a glass-coated platinum filament held under constant tension. The filament is in a glass enclosure with inlet and outlet for the gas. A constant current is passed through the filament and it gets heated. Depending on the thermal conductivity of the gas inside the tube, the filament attains steady thermal conditions. Its resistance is a measure of this and hence the thermal conductivity of the gas mix. Change in the resistance of the filament is converted into an equivalent output voltage through a Wheatstone bridge or other opamp based circuits. The gas inlet and outlet are connected at the same section of the main flow pipe and normal to it. This ensures that the gas flow through the thermal-conductivity cell is solely due to convection and thus makes its operation independent of the gas flow rate.

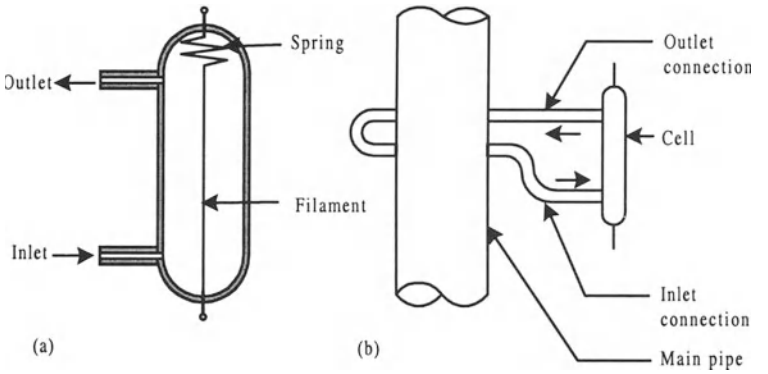


Figure 15.5 Thermal-conductivity cell (a) Cell proper (b) Connection of the cell to the main flow pipe

Observations: -

⇒ The thermal-conductivity cell can be used in a variety of ways for gas analysis. One can use a sealed reference cell in one arm of a Wheatstone bridge and the measuring cell in the adjacent arm. The deviations from a pre-set quiescent set of conditions can be sensed. One can also have thermal-conductivity cells for sensing in two arms of the bridge [See Section 10.2].

⇒ Thermal conductivity of the constituents has to be widely different for the method to be effective. From Table 15.3, we see that thermal conductivities of oxygen, nitrogen and air are sufficiently close to each other. Change in

the concentration of oxygen or nitrogen in air cannot be detected by this method. In fact, the method is best suited to sense the change in the concentration of hydrogen or helium (as far as a mixture of gases in Table 15.3 is concerned).

⇒ The cell has to be calibrated for each application with the corresponding constituents of the gas mix.

⇒ The cell output is linearly related to the change in proportion over a narrow range. Over wider ranges, the cell output change is only a rough estimate of the change in proportion. When the thermal-conductivity cell is used to sense the ratio of gases to execute a control action, often operation of the scheme is restricted to a narrow range. Hence the loss of accuracy over a wider range of operation, is not a limitation.

⇒ The thermal-conductivity cell can be combined with a variety of techniques to ascertain the levels of different constituents.

- Oxygen is a paramagnetic gas. In one class of oxygen analysers, oxygen from the main flow stream is attracted to the cell using an electromagnet. The magnet is kept at the inlet side of the cell. The oxygen-rich gas mix returns to the main pipe by natural convection. As the oxygen content in the main flow pipe increases, that through the cell also increases; this increases its thermal conductivity.
- The gas constituents can be selectively removed and the gas passed through thermal-conductivity cells repeatedly. The gas-removal can be by dissolving the gas in a solution, oxidation or by other reactions. Through such repeated measurements, changes in the proportion of more constituents can be ascertained.
- Sensitivity of the thermal-conductivity cell to changes in the water vapour content is nullified in two ways. The water vapour is completely removed by passing the gas through a dessiccator or saturating it with water vapour by passing it over a wet wick before measurement.

Table 15.3 Thermal conductivity of selected gases
(Thermal conductivity × 10^4cal ×cm^{-1}×sec^{-1}×deg^{-1}.)

Gas / vapour	at 0°C	at 100°C
air	58 (1.0)	74
Argon (Ar)	39 (0.67)	52
Carbon monoxide (CO)	53 (0.91)	-
Carbon dioxide (CO_2)	34 (0.59)	50
Hydrogen (H_2)	419 (7.22)	547
Helium (He)	343 (5.91)	408
Nitrogen (N_2)	57 (0.98)	73
Oxygen (O_2)	58 (1.0)	76
Neon (Ne)	109 (1.88)	133
Methane (CH_4)	73 (1.26)	-
Ethane (C_2H_6)	43 (0.74)	77
Propane (C_3H_8)	36 (0.62)	-
Butane (C_4H_{10})	32 (0.55)	-

15.5.2 Interferometer

The principle of the interferometer is illustrated in Figure 15.6. L is a laser source. Lens 1 produces a collimated beam. Slits S_1 and S_2 allow a narrow set of beams to pass through. The beam through S_2 passes through the reference cell lens 2 and then falls on the detector D. Similarly, the beam through S_1 passes through the measuring cell lens2 and then falls on the detector. If the gases in the reference cell and the measuring cell are identical, both the beams have identical optical path lengths and arrive at D in phase. The light intensity falling on D is a maximum under these conditions. If the content of constituents in the measuring cell changes, its refractive index changes and the optical-path length changes. This causes a phase shift between the two beams and reduces the net intensity of received radiation at D. The theoretical limit to the difference in the two optical path lengths is $\lambda/2$ when the intensity of received radiation is zero. However in practice, this can be slightly smaller. The intensity can be directly related to the phase shift through the refractive indices of the two cells.

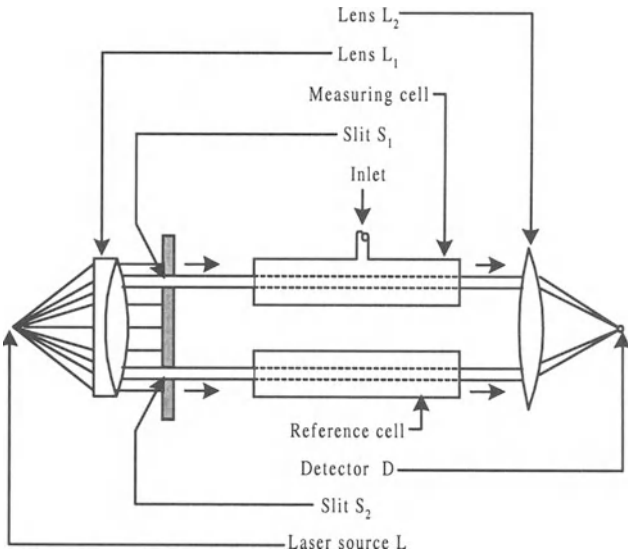


Figure 15.6 Interferometer for gas analysis

We have

$$n_1 - n_2 = \frac{\theta \lambda}{2\pi L} \tag{15.4}$$

where

- $\Rightarrow$ n_1 and n_2 are the refractive indices of the fluids in the two tubes
- $\Rightarrow$ θ is the angular equivalent of the difference in the two optical path lengths
- $\Rightarrow$ λ is the wavelength of the beam of radiation used and
- $\Rightarrow$ L is the length of the tubes.

$$\text{Total intensity of received radiation} = 2I\cos\frac{\theta}{2} \tag{15.5}$$

where I stands for the intensity of radiation received through each cell taken separately.

$$\therefore n_1 - n_2 = \frac{\lambda}{\pi L}\cos^{-1}\left(\begin{matrix}\text{fractional}\\ \text{radiation}\\ \text{received}\end{matrix}\right) \tag{15.6}$$

Despite this formula, the cell can be directly calibrated. The scheme is extremely sensitive to changes in the refractive indices. The cell is typically 100cm long for gases (The principle can be directly adapted for liquids. The cell for liquids is typically 1cm long).

Apart from the above two, a variety of other techniques is also in use. In each case, a specific property or reaction of one constituent is used to identify its content. Thus: -

⇒ When the gas mix has only one combustible gas, the mix can be burned at a filament and the rise in the filament temperature (resistance) sensed as with the thermal-conductivity cell.

⇒ A polarising cell can used to detect the amount of oxygen in a mix. The oxygen diffuses into the cell, combines with the hydrogen inside and changes the cell emf correspondingly.

15.6 Radiation Based Instrumentation

Use of radiation or 'photo-detectors' for temperature sensing has been discussed in Section [13.8.6]. These detectors are used in a variety of other applications as well. The detectors and the signal processing circuits used with them are the same or similar in all the cases. These warrant detailed attention [Saleh and Teich].

15.6.1 Photo-Detectors – Principles

Consider a p-type semiconductor material with light energy – in the UV, visible or infrared range – falling on it. We know (from Einstein's relation) that if the wavelength of radiation is sufficiently low, each quantum of incident energy may be absorbed in the material. In turn electron – hole pairs may be generated. Their minimum wavelength λ_m is governed by the equation

$$\lambda_m = \frac{1240}{E_g} nm \tag{15.7}$$

where E_g is the energy gap for the material.

For Si E_g = 1.12 eV and from Equation 15.7,
λ_m = 1100 nm
For GaAsP E_g = 1.8 eV and from Equation 15.7,
λ_m = 700 nm

A typical photo-diode formation is shown in Figure 15.7. High-resistivity n-type substrate is the starting material. A thin p-layer (1 μm or less thick), is diffused into it (boron for Si). SiO_2 mask formed around forms insulation and accurately defines the active area of the photo-diode. A silicon nitride passivation-layer on top,

is the protective layer for the device. It also forms the necessary anti-reflection coating. Contact to the p-layer is made through a photo-lithographically-defined aluminium layer. The low-resistance n^+ layer at the bottom facilitates metallization. The metallized contact below is to the n layer. The metallization also functions as a reflector for any unabsorbed radiation. This improves the sensitivity in the IR range where the absorption coefficient of the substrate is lower.

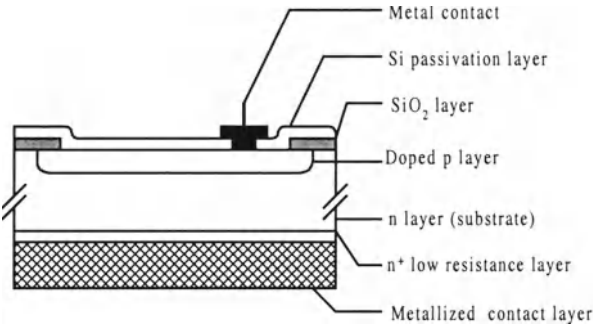


Figure 15.7 structure of a typical photo-diode

Consider radiation falling on the device on the p-layer through the passivation layer. Depending on the construction and the incident radiation, different possibilities arise (See Figure 15.8): -

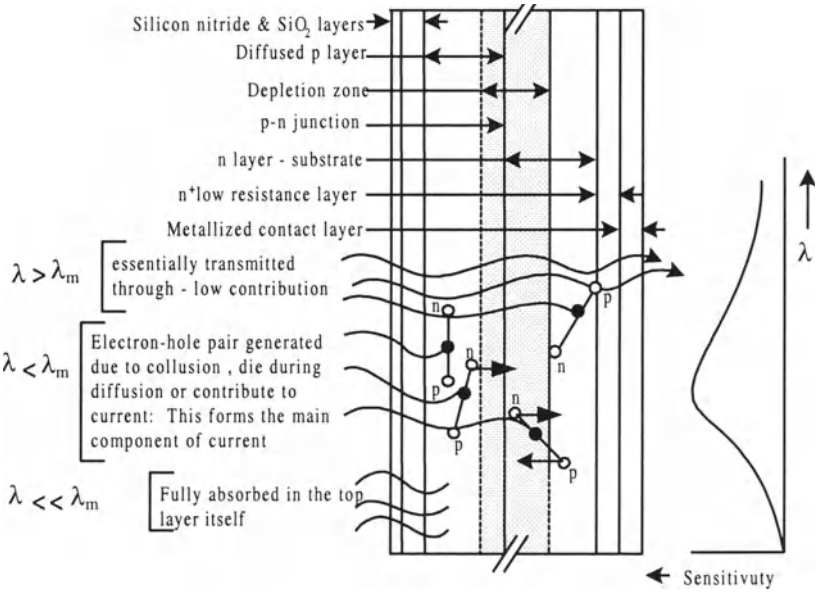


Figure 15.8 Photo-detector response at different incident wavelengths: Corresponding sensitivity curve is shown at the right

⇒ If the received radiation is such that its wavelength $\lambda > \lambda_m$ for the material, the radiation may be absorbed slightly but transmitted substantially. The detector sensitivity in this range is low

⇒ If the received radiation is such that its $\lambda << \lambda_m$, the material remains opaque to it and the radiation will be absorbed well within the p-layer itself. The detector sensitivity in this range is very low

⇒ The range where $\lambda < \lambda_m$, the detector sensitivity is definite and not negligible. This is the range of interest to us. Different possibilities arise here:-

- First consider the case when there is no externally applied voltage or field on the device; but a closed path is provided for the current flow.
- After the initial diffusion of the charges across the p-n junction, a potential difference is built-up across it. This causes a depletion layer on either side. It extends deep into the n-layer due to its low level of doping. Any majority carrier on either side faces the junction potential barrier but cannot cross over. However if minority carriers are injected and if they are sufficiently close to the junction they accelerate across the junction and constitute a current. Incident radiation can cause such current generation.
- If the wavelength of the received radiation is low, and/or its intensity is low, the same will be absorbed in the p-layer itself. Each such quantum of absorbed energy may liberate an electron-hole pair. A fraction of the electrons liberated in this manner, in the course of their drift, come to the depletion zone, cross over and constitute a current. This forms a comparatively low and slow current pulse.
- If the wavelength of radiation is larger and or its intensity is higher, more of it will pierce into the depletion zone. It may be absorbed and electron-hole pairs generated. The depletion zone in the n region, is comparatively deeper and more radiation will cause electron-hole pair generation here. The hole, which is a minority carrier (mainly in the n region), will accelerate across the barrier and constitute a current. This is the most dominant component of the photo-electric current. The corresponding current pulse is faster due to the shorter distance to be covered by the carriers.
- Comparatively larger wavelength radiation may cross over to the n side beyond the depletion zone. Part of it may cause electron-hole pair generation. As in the p region – a fraction of the minority carriers – will drift to the depletion zone, accelerate and will contribute to a current. This current forms only a small fraction of the total current and forms a slow pulse.
- Consider the case of an externally applied voltage which reverse biases the junction. This increases the electric field available for the minority carriers to accelerate, cross over and constitute a current. In effect, this increases the photo-electric current in the above three cases and also reduces the response time. Current due to the thermally generated minority carriers also increases (*i.e.*, the noise current increases).
- Consider the case of the forward biased junction. The forward bias reduces the junction potential barrier. More of majority carriers may cross over and contribute to the main current. Since this opposes the

minority carrier current above, the net current decreases. As the voltage is increased, the current becomes zero, reverses and increases in magnitude. This increase is exponentially related to the applied voltage. However, photo-diodes are rarely operated in this region.

The response of the photo-detector for the different ranges of λ, leading to the detector sensitivity characteristic is depicted in Figure 15.8.

15.6.1.1 Equivalent Circuit

Equivalent circuit of the photo-diode is shown in Figure 15.9. Current i_L represents the current injected by the incident radiation. At any specific intensity of received radiation, it is linearly related to its power. The linearity extends over 8 to 10 decades. It remains independent of the applied voltage. The ideal diode current i_d is given by

$$i_d = I_s\left[\exp\left(\frac{eV_d}{kT}\right)-1\right] \tag{15.8}$$

where

- $\Rightarrow$ I_s is the reverse saturation current,
- $\Rightarrow$ e is the charge on the electron ,
- $\Rightarrow$ V_d is the potential difference across the junction,
- $\Rightarrow$ k is Boltzman's constant and
- $\Rightarrow$ T is the absolute temperature of the junction area.

Under steady state conditions, from the equivalent circuit, we have the expression for the net current through the device as

$$i_0 = i_L - I_s\left[\exp\left(\frac{eV_d}{kT}\right)-1\right]-i_{sh} \tag{15.9}$$

where i_{sh} is the current through R_{sh} and the rest of the quantities are as in Equation 15.8.

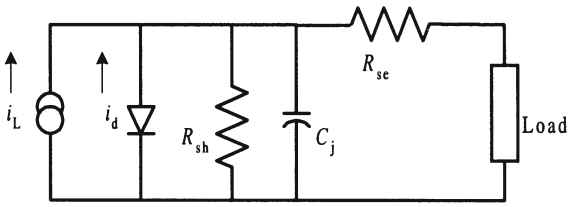


Figure 15.9 Equivalent circuit of a photo-diode

C_j is the junction capacitance. For the given photo-diode, increase in the applied reverse-voltage, increases the depletion layer depth and reduces C_j (The reduction can be by a factor of 5). Such a reduction in C_j increases the speed of response. The shunt resistance R_{sh} is in the 10MΩ to 100 MΩ range. It varies with the voltage across the device. Its effect is negligible except when the device is operated in the open circuit mode. The series resistance R_{se} is low - in the range of several ohms. The doping levels, the diffusion process and the lead resistance contribute to it. Normally its effect is negligible. The surface leakage current and the device noise current also contribute to the total current.

15.6.1.2 V – I characteristics

The $V - I$ characteristics for three different illumination levels are shown in Figure 15.10. Characteristic 'a' is for zero illumination level. It is identical to that of a normal diode. Characteristic 'b' is for one level of illumination and characteristic 'c' for twice this level. There are four distinct regions of operation – designated in Figure 15.10 as region 1, 2, 3 and 4. Operation in each region, is discussed separately.

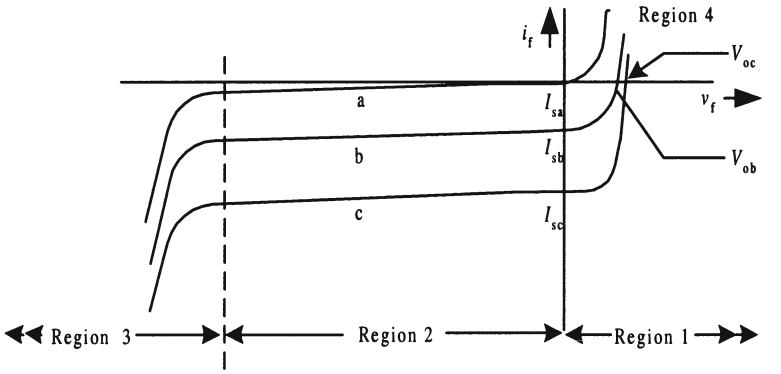


Figure 15.10 V – I characteristics of a photo-diode for three different illumination levels

Consider region 1 shown enlarged in Figure 15.11. If the photo-diode is operated in the open-circuit mode, the net current through it is zero. Operation is along the voltage axis OPQ. Neglecting i_{sh} in Equation 15.9 and imposing the condition $i_0 = 0$, we get

$$i_L = I_s\left[\exp\left(\frac{eV_d}{kT}\right) - 1\right] \tag{15.10}$$

$$\therefore V_d = \frac{kT}{e}\ln\left(\frac{i_L}{I_s} + 1\right) \tag{15.11}$$

For $i_L >> I_s$

$$V_d = \frac{kT}{e}\ln\frac{i_L}{I_s} \tag{15.12}$$

The output voltage is logarithmically related to i_L. Since i_L is linearly related to the incident light power, V_d is proportional to the logarithm of incident light power. Thus, the characteristic is highly non-linear. OP represents the output voltage for one value of the incident light intensity. As it doubles, the output increases to OQ – the increase is seen to be small.

If operated in the short-circuit mode, the voltage across the photo-diode is zero. The characteristic is along the current axis, OTU. Substituting $V_d = 0$ in Equation 15.9 we get

$$i_o = i_L - i_{sh} \tag{15.13}$$

For $i_L >> i_{sh}$

$$i_o = i_L \tag{15.14}$$

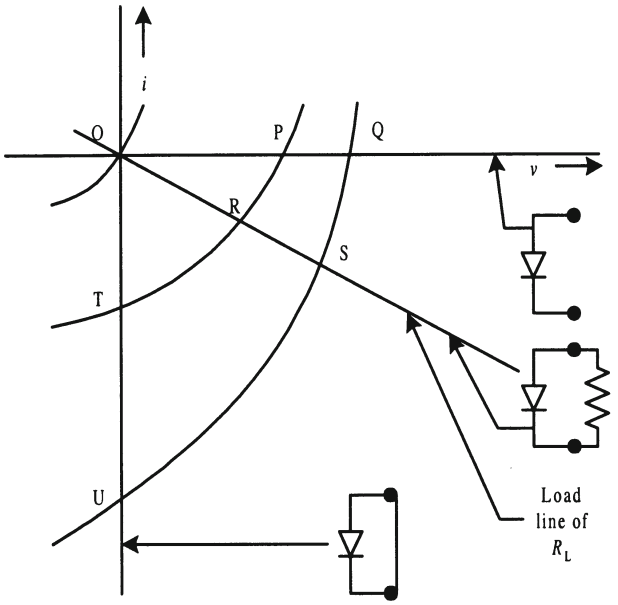


Figure 15.11 Operation of Photo-diode in region 1

If the intensity of incident radiation doubles, the current also doubles. Thus, the current characteristic is linear. As explained earlier, the linearity extends well over 8 decades. For any definite load resistance, again with zero bias voltage applied, the characteristic takes intermediate values. A typical case is represented by line ORS in Figure 15.11. The characteristic with zero-level of incident light passes through the origin O. Its slope represents R_{sh} in the equivalent circuit.

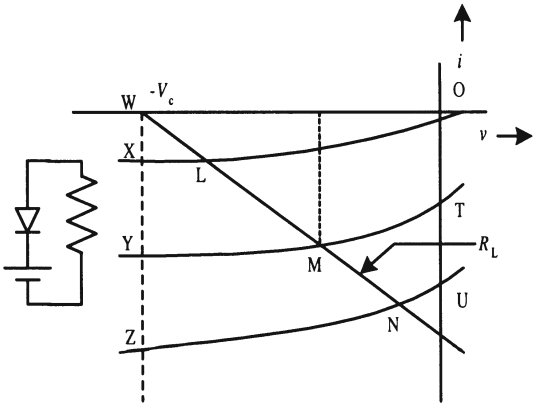


Figure 15.12 Operation of the photo-diode in region 2

In region 2 a voltage V_C is applied to the diode – the relevant portion of the characteristic is shown expanded in Figure 15.12. OW stands for the applied voltage V_C. The current WX represents the reverse current through the diode under dark conditions. WY and WZ represent currents with incident light. As explained earlier, the current increases linearly with increasing incident light power. The load

line for definite load resistance R_L is also shown. As the incident light power increases, operation shifts along line WLMN. Over the whole region the characteristics remain practically linear – linearity being better than that of the operation in region 1(4^{th} quadrant). Hence the segments YM, ZN *etc.*, representing the voltage drop across R_L, are linear with respect to the incident light power. As such we can operate with definite R_L in this region. The output versus incident light power characteristic linearly extends over 8 to 10 decades. The noise level decides the lower threshold. At the higher end, the circuit decides the limit. If the applied voltage is V_C, the maximum current I_{max} is given by

$$I_{max} = \frac{V_c + V_d}{R_{se} + R_L} \tag{15.15}$$

where V_d is the junction voltage (0.7 V for Si).

Region 3 represents operation with large applied voltages. The voltage is large enough to cause breakdown of the diode resulting in abrupt increase in the current. This region is avoided. In region 4, the diode is forward biased. Even with very small applied voltages, (~0.7V for Si), the exponential term in Equation 15.9 dominates and the majority current component far exceeds the component due to the incident radiation. Operation in this region is avoided.

15.6.1.3 Constructional Variants

The photo-diode depicted in Figure 15.7 and discussed in general so far, is of the 'planar-diffused' type. A p region (typically 1 μm deep) is diffused into the high resistivity n region to form the junction. The contact to the p region is made through the Al layer on top. The contact to the n-region underneath is made as a metallized contact to the low-resistance n^+ layer. Modifications of the basic scheme yield performance enhancement in different directions: -

- ⇒ Pure high-resistance n-type material may be used as the substrate. This increases the depth of the depletion region. It also increases sensitivity. The junction capacitance reduces and speed of response improves.
- ⇒ One can go a step further and interpose an intrinsic layer between the p and the n layers (PIN structure). This reduces the junction capacitance and the response time further. Use with a reverse bias voltage reduces the response time still further.[7]
- ⇒ Radiation at shorter wavelengths is absorbed close to the surface diffusion layer itself. This reduces sensitivity at lower wavelengths.
- ⇒ The p layer thickness can be reduced to bring the depletion layer in the p region as close to the surface as possible. This improves the sensitivity in the UV ranges. While normal photo-diodes can have sensitivity extending down to 390nm, these modified diodes are sensitive to radiation down to 190 nm.
- ⇒ Lumogen emits radiation at 550 nm when excited by radiation in the 120 – 450 nm range. Thus a thin layer of Lumogen deposited on the top, enhances the UV spectral range down to 120nm.

---

[7] The depth of penetration of radiation depends on the absorption coefficient. Typically 90% of incident radiation at 450 nm is absorbed in a depth of 1μm while radiations at 750nm and 950nm, require 10 μm and 100μm depths respectively for similar levels of absorption.

⇒ A Schottky type p-n junction can be formed by a thin sputtered gold coating on top of the n-layer. Due to the thin p-layer, the UV sensitivity improves conspicuously.

⇒ The n^+ layer diffused at the back may be made thick. This reduces the depth of the diffusion layer in the n-n^+ side. In turn the depth available for absorption is reduced. This reduces IR-sensitivity and makes the device suitable for sensing shorter wavelengths more selectively.

⇒ Avalanche type diode with a dense electric field in the depletion-region increases sensitivity. Electrons generated by incident radiation accelerate through the high field and collide with neutral atoms to cause secondary electrons to be generated. The process is akin to the photo-multiplier tube. This type of photo-diode is useful to sense low intensity light radiation.

⇒ A deep depletion layer (using high resistivity n or intrinsic layer) provides more room for penetration of IR-radiation. It increases IR sensitivity. This also increases response time for IR. However, the response time for shorter wavelengths remains small.

15.6.1.4 Spectral Response

The Quantum Efficiency (QE) of a photo-diode refers to the number of electron-hole pairs generated per photon of incident radiation. It is expressed as a percentage of the incident photons, which generate electron-hole pairs. It is of the order of 80 % for 800 nm < λ < 900nm. At shorter wavelengths, incident photons may generate more than one electron-hole pair – carrying the QE beyond the 100 % value.

Sensitivity of the photo-diode is expressed as A/W *i.e.*, amperes of photo-electric current per watt of incident radiation. It is related to QE as

$$R = \frac{\eta \lambda q}{hc'} \text{ A/W} \tag{15.16}$$

where

⇒ R is the photo- sensitivity in A/W

⇒ η is the QE

⇒ λ is the wavelength of incident radiation

⇒ q is the charge on the electron

⇒ h is the Plank's constant

⇒ c' is the speed of light through the medium

By the very nature of the definition, R increases as λ is increased. The sensitivity is shown sketched as a function of λ in Figure 15.13. The sensitivity for $\eta = 1$ (*i.e.*, 100 %) is also shown. At the most sensitive wavelength, the sensitivity is in the 0.3 A/W to 0.5 A/W range. A few features of the photo-diodes are discernible here: -

⇒ For Si at room temperature E_g = 1.12 eV with a corresponding λ_c of 100 nm. For Ge at room temperature, E_g = 1.8 eV. The corresponding λ_c =700nm. In general, materials with lower E_g are suitable for radiation in the IR range; those with higher E_g can be used (if at all) at lower values of λ only.

⇒ For $\lambda << \lambda_c$, R is low due to the high absorption in the p layer of the diode, well ahead of the depletion zone.

⇒ For $\lambda > \lambda_c$, the photon energy is not sufficient to liberate electron-hole pairs and R is low.

⇒ For $\lambda < \lambda_c$, and close to it, the value of R is definite and the device is used in this range.
⇒ As λ decreases from λ_c, R rises rapidly close to the QE = 100 % level. As λ reduces, R also reduces.
⇒ Various measures to enhance R at low λ (UV range), to reduce R in the IR range *etc.*, change the characteristic accordingly.
⇒ The absorption of borosilicate glass and plastic resin coatings is high in the IR range. They are not suitable for detectors below λ = 300nm. UV detectors are used with quartz coating.
⇒ For photo-detectors used for detection of visual spectrum, visual compensation filters are used.

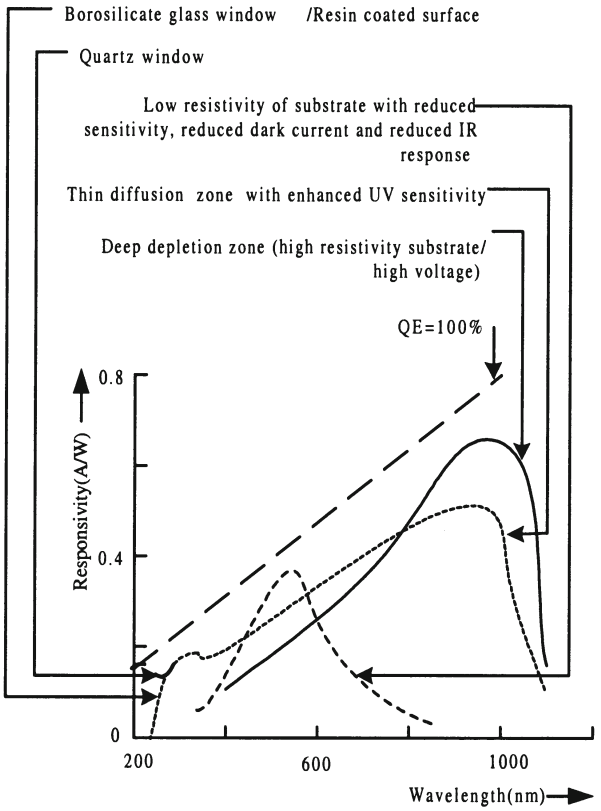


Figure 15.13 Spectral response of typical photo-diodes

15.6.1.5 Noise Characteristics

The noise generated in the photo-diode is of two types - thermal noise and shot noise (See Section 7.4).

Thermal noise: This is the noise generated in the equivalent shunt resistance of the device. The equivalent noise-current i_{nj} is given by

$$i_{nj} = \sqrt{\frac{4kTB}{R_{sh}}} \tag{15.17}$$

where

⇒ k is Boltzmann's constant
⇒ T is the temperature of the device
⇒ B is the band width
⇒ R_{sh} is the shunt resistance of the equivalent circuit.

Shot Noise: When the device carries a current i_d, the shot noise i_{ns} is given by

$$i_{ns} = \sqrt{2qi_dB} \text{ amp} \tag{15.18}$$

where

⇒ q is the charge on the electron
⇒ i_d is the current through the device
⇒ B is the bandwidth

When the device is operated with zero bias, at zero signal conditions $i_d = 0$ and shot noise component is zero. Under these conditions, mainly thermal noise is present and dominates. If the device is operated with a reverse voltage bias to increase its sensitivity, the dark current and hence the shot noise increase. Hence under biased operating conditions, shot noise dominates. Combining the two, the total noise current becomes

$$i_n = \sqrt{i_{nj}^2 + i_{ns}^2} \tag{15.19}$$

The rms. addition is due to the uncorrelated nature of the two currents. When the device has incident radiation on it, the corresponding device current i_e dominates. The corresponding shot noise is

$$i_{nl} = \sqrt{2qi_eB} \text{ amp} \tag{15.20}$$

This is more pronounced than i_{nj} or i_{ns}.

The noise current level decides the minimum incident-radiation that can be detected – *i.e.*, the threshold level. One can look upon the noise current in the device, as being generated by a hypothetical incident light power – called the 'Noise Equivalent Power (NEP)'.

$$NES = \frac{i_n}{S} \tag{15.21}$$

where S is the sensitivity of the device in A/W. NEP represents the threshold-power of incident radiation *i.e.*, the minimum incident power that can be detected.

15.6.1.6 Response Time

Response time of the device is made up of three components: -

⇒ *Transit time through the depletion zone*: The depletion zone has a potential gradient across it. Under its influence, the charges can be accelerated. The transit time here can be reduced by reducing the depth of the depletion layer and increasing the field intensity across it. Contribution of this transit time to the overall response delay is low.

⇒ *Transit time outside the depletion zone*: The time for diffusion of the electron-hole pairs generated outside the depletion zone is comparatively large. In the presence of the applied external voltage, this time reduces.

Normally incident radiation of low wavelength is absorbed close to the depletion layer. Diffusion time for the correspondingly generated electron-hole pairs is low. However, for wavelengths of lower frequencies, the absorption and the electron-hole pair generation may occur at deeper levels. When it is in the n region beyond the depletion zone, the time taken by the electron-hole pairs to diffuse and form the current is high.

⇒ *Delay with charge pairs outside the depletion zone*: Contribution of charge pairs (generated outside the depletion zone) to the main current is low. Their response times are also large. These appear as 'slowly settling tails'.

In the presence of an externally applied voltage, the transit time reduces. The charge transfer to the load is decided by the time constant C_j $(R_{se}+R_L)$ in Figure 15.9. Effect of R_{se} is negligible here. For given load conditions, the delay on this count is decided mainly by C_j. C_j increases with increase in the active area. If the depletion layer depth increases, C_j reduces. Depth of the depletion layer can be increased using a material of high resistivity or increasing the reverse voltage.

15.6.1.7 Effect of Temperature Changes

Temperature changes affect the photo-diode performance in different ways. In all cases, increase in the operating temperature affects it adversely.

⇒ As the operating temperature is increased, the number of electron-hole pairs generated by thermal agitation increases. This manifests as an increase in the dark current. The dark current approximately doubles for every 10 °C rise in temperature. In turn the thermal and shot noise levels also increase.

⇒ For $\lambda < \lambda_c$, the incident radiation is absorbed substantially at low depths. Hence, change in absorptivity does not affect response substantially. However at larger wavelengths, the absorption (and response) is poor. Any increase in the temperature of the device increases its absorption coefficient. In turn, the (90 %) depth of absorption, reduces. Probability of electron-hole pairs generated by absorption increases, increasing the sensitivity.

15.6.2 Circuits with Photo-diodes

Different circuit configurations are possible. Some of the common ones are discussed below [See Section 13.8.6]

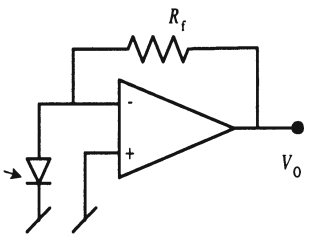


Figure 15.14 Sensing circuit with photo-diode operating in photo-voltaic mode

In the circuit of Figure 15.14, the photo-diode sees very low impedance. Operation is in short-circuit mode. This is also called the 'Photo-Voltaic' mode. The current generated is proportional to incident radiation and is i_s. As mentioned earlier, the proportionality extends over 8 decades or more. The dark current is low;

this keeps the shot noise low. The low resistance due to operation in short-circuit mode, keeps the thermal noise low. Thus, the overall noise level is low. The minimum light level that can be detected is lowest for this configuration. R_f may be shunted by a suitable capacitance C_f to limit the bandwidth (and noise outside the frequency band of interest).

If the cathode is returned to a positive potential, the photo-diode is reverse-biased as in Figure 15.15. This is the 'Photo-conductive' mode of operation. The reverse biasing improves response speed compared to the unbiased operation above. This also increases the dark current and hence the noise-level. The threshold level of incident radiation that can be detected also increases. Linearity and sensitivity remain unchanged. As above R_f may be shunted by a capacitance C_f to limit bandwidth. Photo-diodes intended to operate in this mode are provided with a guard-ring. The same may be grounded separately to minimize effects of leakage current. Any such improvement is perceptible only with reverse biased operation with 30 V to 50 V. As mentioned in Section 15.6.1.2, the photo-diode may be operated near to the open-circuit condition also. This makes V_o logarithmically related to the incident radiation and limits the range of output. The scheme is not in common use.

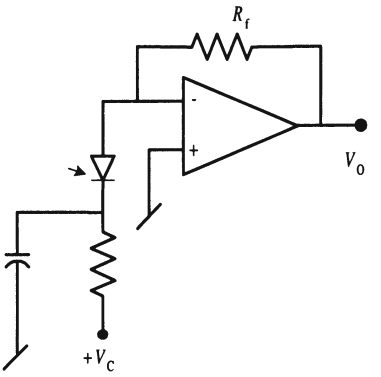


Figure 15.15 Sensing circuit with photo-diode operating in photo-voltaic mode

Observations: -

⇒ Photo-diodes that are used in precision low-threshold work, (short circuit mode), have dark currents as low as a few pA at room temperature (The exact level depends on the active area). Compatible opamps are to be used with them. FET-input opamps are best suited for this, due to their low bias current levels (~1pA).

⇒ BJT-opamps have comparatively higher i_b values and are not suited for precision work. But the relative change in i_b is low (i_b decreases as temperature increases) compared to that of the FET-input opamps (i_b doubles for every 7 °C to 10 °C rise in temperature). BJT-opamps are used when the sensing is at comparatively higher temperature or when the temperature variation expected is high.

⇒ The photo-detector is operated with a bias voltage when high speed of response is desired. The opamp has to be selected carefully to avoid oscillation and ringing at high frequencies. If necessary, frequency compensation may be provided.

⇒ In high sensitivity applications, effects of low frequency noise, drift *etc.*, are minimized by using a chopper and modulation scheme [See Section 6.2.1]. One possible arrangement is shown in Figure 15.16. The toothed wheel functions as the square-wave modulator for reference and the measuring channels. The radiation from a reference radiation source falls on detector D_2 and is amplified by opamp 2. Output of amplifier 2 is a square wave with amplitude proportional to the reference intensity. Its demodulated value (obtained through synchronous detection) represents the full-scale value. An identical channel is used for the detection of radiation also – detector D_1 followed by the amplifier with opamp 1. Its demodulated output is normalized with reference to the output of the reference channel above. The arrangement neutralizes the effects of low frequency noise (change in dark current due to drift, ambient temperature changes *etc.*). The chopping frequency is selected to be 5 to 10 times the signal bandwidth (See Section 16.3.2.4 for an application of a variant of this scheme).

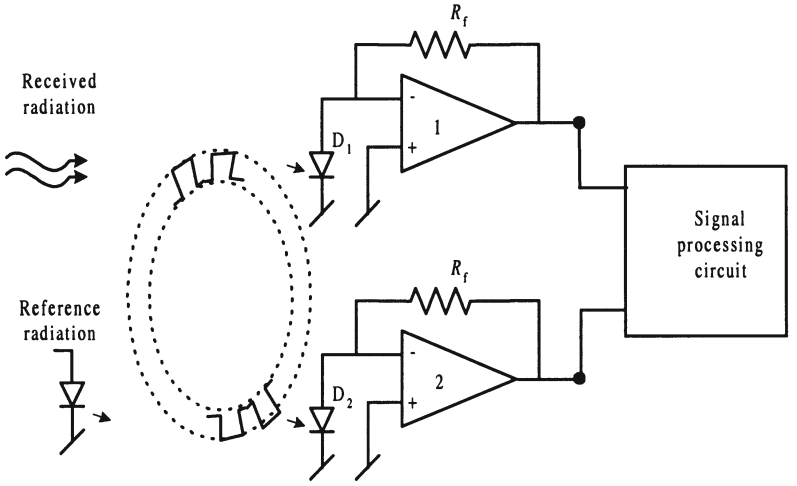


Figure 15.16 Circuit scheme for a high sensitivity application of photo-detectors

15.6.3 Radiation Sensor Arrays with CCDs

The radiation from a single source is detected by a photo-detector in terms of the intensity and spectral distribution of radiation. The concept can be extended to sense the nature of spatial variation of received radiation. This requires an array of sensors to be precisely positioned and the signal from each such position, detected. Subsequently the whole ensemble of such detected signals is to be processed together to extract necessary information from it. Such arrays of sensors find direct application in video cameras. They are also being effectively used in a variety of sensing applications.

The object to be sensed has to be sharply focussed into a small well-defined area. The individual sensors are to be precisely positioned and kept to cover the whole sensed area with sufficient resolution. Further, the signals from all such positions are to be accepted and processed sufficiently fast. The sensor array

comprising of the photo-diodes and the respective (first level) signal processing circuitry are all fabricated as one integrated circuit. The 'Charge Coupled Device (CCD)' is the primary signal-processing element.

15.6.3.1 CCD Array

A CCD array is essentially an elongated MOS transistor with a number of gates lined sequentially. Figure 15.17 shows a section of an elongated n-type Si substrate forming a CCD array. The source and drain are highly doped n+ regions at either end. Highly conducting poly-silicon islands are formed on the insulating SiO_2 layer. These islands are regularly positioned along a line. These form the gates designated as G_1, G_2 *etc.*, in the figure. Consider the unit connected as shown. If gate G_1 is taken high and held high for a sufficiently long time, free charge carrier electrons around accumulate in the depletion zone D_1 underneath the SiO_2 layer – called the 'well'. Subsequently if G_2 is taken high and then G_1 returned to low state, the electrons collected underneath G_1 get transferred to the depletion zone D_2 underneath G_2. This process can be carried through by activating all the gates in sequence one by one. Finally the charge appears as an equivalent voltage V_o. The charge transfer by shifting through successive zones is akin to the operation of a 'Bucket Brigade'. The output side MOS transistors T_1 and T_2 are a continuation of the substrate forming the bucket brigade. For convenience in understanding, they are shown separately here. Functioning of the device in this manner has the signal represented as a charge. The charge is sequentially coupled end to end. The total device is called a 'CCD'.

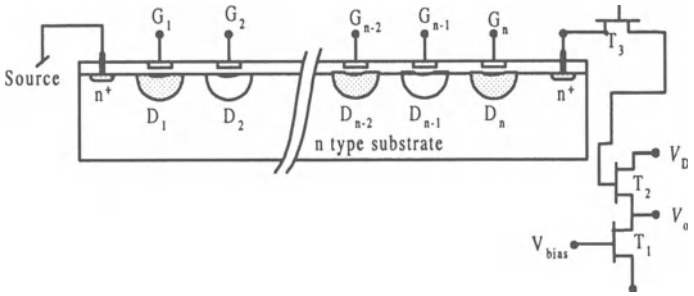


Figure 15.17 Schematic representation of a CCD array

Normal operation of a CCD takes place in a more structured fashion. In one common mode – called the 'two phase' mode – odd numbered gates are connected to one clock pulse-train ϕ_1 and the even numbered gates to a second pulse-train ϕ_2. The two clocks are 180° out of phase. The clock waveforms, the state of the CCD at successive half period ends and associated waveforms are shown in Figure 15.18. Only the portion of the CCD close to the output side is shown. Consider the instant (1). Clock ϕ_1 is in the high state and clock ϕ_2 in the low state. The depletion zones D_n, D_{n-2} *etc.*, have charges Q_1, Q_2.. *etc.*, accumulated in them. Since ϕ_2 is zero, the zones represented by D_{n-1}, D_{n-3} etc., are absent. The transistor represented as T_3 is off, since ϕ_2 is low. Hence, the output side is isolated from the bucket brigade. V_o is zero. During the next half cycle, as ϕ_2 is taken high and then taken low, the charges accumulated are shifted to the right by one 'step'. This instant is shown as (2) in Figure 15.18. Charge Q_1 that was present under the depletion zone D_n earlier, is shifted out. It appears as a corresponding output voltage V_1. The output voltage V_2

at instant (4) corresponds to charge Q_2. The charge Q_2 being high, the output voltage V_2 is also high. After one more cycle when ϕ_2 goes high again, Q_3 appears as an output voltage V_3. The operation continues in the same cyclic fashion.

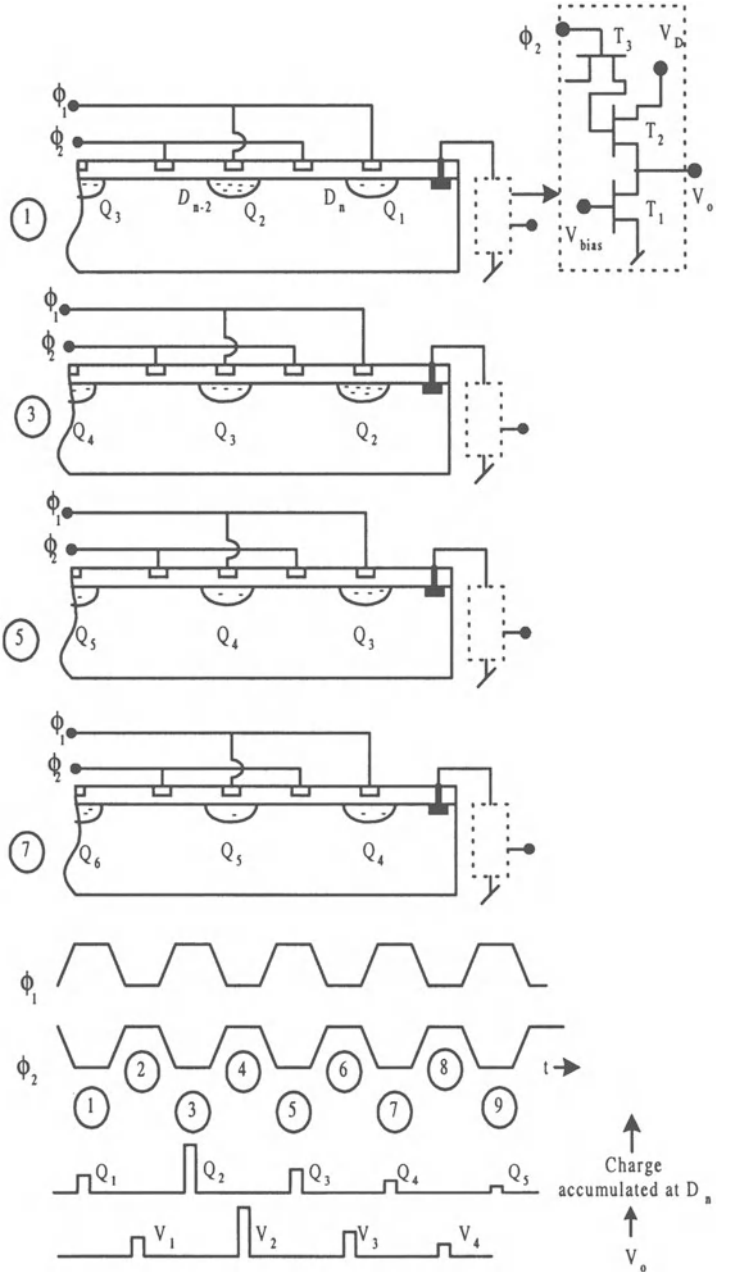


Figure 15.18 Clocking and charge-transfer scheme of CCD array

Observations: -

⇒ charges Q_1, Q_2 Q_3 *etc.*, represent analog signal sample values stored by and shifted through the CCD. In this sense, the CCD functions as an analog shift register.

⇒ Consider the time interval when ϕ_1 is high. Consider a specific depletion-zone, say D_{n-2} during this interval. Due to the thermal agitation of the atoms in the crystal lattice, electrons are generated in its vicinity. These too gravitate to the depletion zone and add to the charge stored there. It amounts to contamination of the signal by thermal noise. To keep the effect of noise low, the clock period has to be kept as low as possible. This puts a lower limit on the frequency of operation of the CCD. Thus the CCD can never operate in a static mode; it is a dynamic device.

⇒ A minimum period of overlap is necessary between ϕ_1 and ϕ_2. It ensures that all the charges in a depletion zone are fully transferred to the succeeding depletion zone. Correspondingly, there is a limit to the highest frequency of operation of the CCD. Fast rise and fall of ϕ_1 and ϕ_2, can cause ringing and feed-through errors. Hence, the rates of rise and fall are limited. Normally the rise and fall times form about $1/6^{th}$ of the pulse period. The dwell-time in the high and the low states will be about $1/3^{rd}$ of the pulse period each.

⇒ The gate width, the gate spacing and the clock voltage level are all closely inter-related. With a given CCD size, one would like to accommodate as many stages as possible. This is done by keeping the gate pitch minimum. However with a given gate voltage (the maximum safe value is 15V), one should ensure that the depletion zones are clear off each other. In case of an overlap, the electrons in one may migrate to the neighbouring depletion zones causing cross-talk.

⇒ The gate pitch should be large enough to ensure a large enough depletion zone. Restriction on the depletion zone size, restricts the signal level that the CCD may handle.

⇒ Some CCDs operate with 3 or 4 phase clocks. This improves performance at the expense of simplicity.

⇒ Only a finite time is available to transfer charge from one gate to the following one. Not all the charge is transferred during this period due to the limited time and the definite RC time constant associated with the change-over process. The impurities in the device also contribute to a certain loss of charge in transit. The effectiveness of transfer is measured by 'Charge Transfer Efficiency (CTE)' from gate to gate. Typically CTE is of the order of 99.999 % (Loss of charge at any CCD gate is less than 10 ppm).

15.6.3.2 Sensing Array

The nature of radiation distribution is sensed by an array of photo-diodes. The array used for line sensing has all the photo-diodes arranged in a straight line at a constant pitch. Each photo-diode is of the type discussed in Section 15.6.1. The response characteristic (in terms of UV enhancement, IR enhancement, IR suppression, high sensitivity, high speed and the like) is tailored to the specific application for which it is targeted. Each photo-diode has a fixed exposed or radiation capture-area. Such a photo-diode detector element with a well-defined radiation capture area is called a 'pixel' (or Pel or Pixel element). Typically, a pixel has 7 μm × 7 μm size. A linear array can have 128, 256, 512, 1024, 2048 or 4096

pixels (arrays with other number of pixel elements are also available but not so common). An array of 128 elements, has an active length of 128 × 7 = 896 μm = 0.896 mm; similarly with other arrays also. Such a pixel of 7 μm × 7 μm size has a peak sensitivity (*i.e.*, at the λ of maximum sensitivity) of 5V/μ J/cm. Arrays with pixel size 10 μm × 10 μm or 14 μm × 14 μm are also common. Some have much larger pixel width. – 7 μm × 500 μm size; such arrays are targeted at applications, which call for high sensitivity.

The photo-diode diffusion width of each pixel will be less than the pixel pitch. Figure 15.19 shows the arrangement for pixels of 7 μm pitch. The diffused area is 7 μm × 3.5 μm in each case. Electrons generated directly in the diffused zone will fully contribute to the output. Electrons generated in the non-diffused zone will gravitate to one of the adjacent pixels. On an average, the proportion of electrons gravitating to each side will vary linearly with the distance of the point-of-generation from the diffused edge. This explains the trapezoidal nature of the sensitivity curve for each pixel.

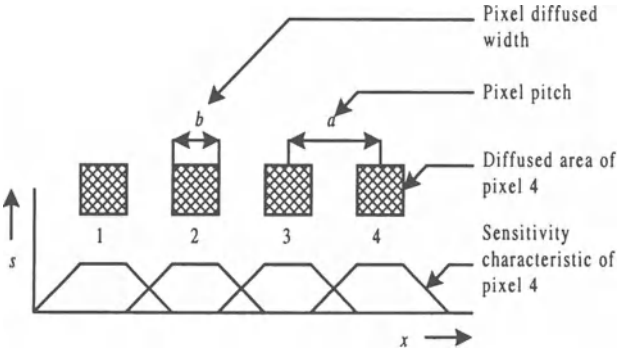


Figure 15.19 Pixel distribution and sensitivity characteristics of pixel array

15.6.3.3 Pixel Sensitivity

Pixel sensitivity is differently defined and used by different manufacturers. It can be the charge accumulated in unit active area per unit of radiation energy received. The unit of this is μC/ μJ / cm^2. The same is more commonly expressed as Amps/Watt /Cm^2 since Amps represent current in C/s and watts represent Joules/s. Some manufacturers specify sensitivity in terms of sensor output in voltage/watt/cm^2. The detector depletion zone capacitance also enters the arena here (since $V = Q/C$). When expressed in this fashion, the received radiation is implicitly taken as monochromatic and at the wavelength where the sensitivity of the detector is a maximum. Normally the received radiation power is distributed over a spectrum of frequencies. This has to be taken into account when computing actual response. Three factors are to be considered here.

- ⇒ The source of radiation itself causes a non-uniform distribution of energy over different wavelengths.
- ⇒ The detector (photo-diode) response changes with the wavelength.
- ⇒ The protective window in front of the sensor has a non-uniform transmission characteristic. It is different for glass and quartz.

15.6.3.4 *Interface with CCD*

The array of photo-diodes senses the incident radiation and signals representing radiation received at each pixel are available- on a limited time basis – as collected charges in the respective depletion zones. CCD array is capable of transferring such collected charge signals in a serial shift-register fashion. The two can be connected to form a full sensor array. Figure 15.20 shows the schematic arrangement.

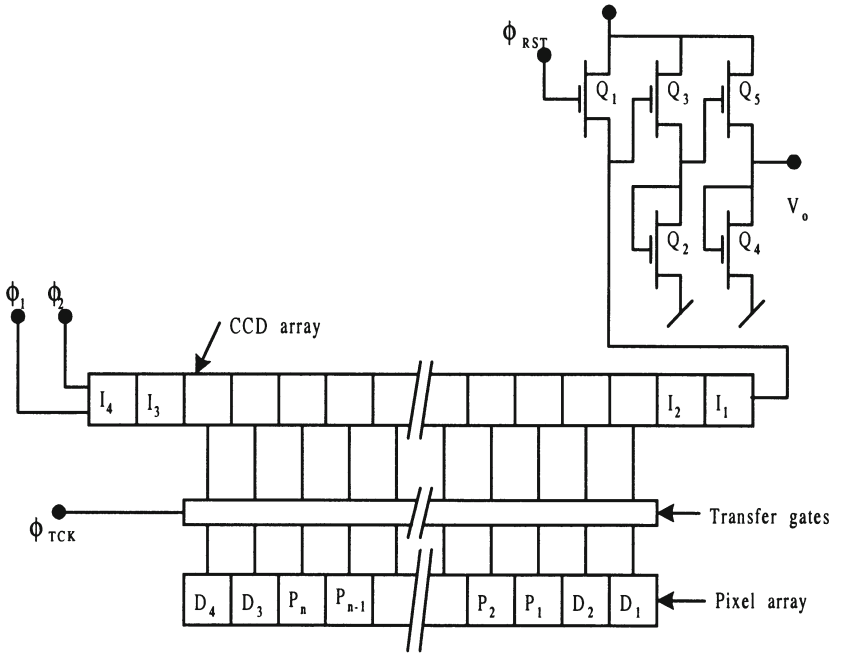


Figure 15.20 Combination of pixel and CCD arrays to form a linear sensor

The pixel array is connected to the CCD array through a set of transfer gates. Each pixel has a transfer gate and a pixel element dedicated to it. Each transfer gate is a MOS transistor. When it is turned on, the accumulated charge underneath the pixel concerned is transferred laterally to the corresponding CCD element. This is done by the clock signal ϕ_{tck}. Pulsing these elements, turns on all the transfer gates; and all the pixel-signals are transferred laterally to the respective CCD elements. Once this is done, the stored charges in the CCD elements can be shifted through the 'bucket brigade' by clocking ϕ_1 and ϕ_2 alternately. The two-stage amplifier with MOS transistors at the (right) end of the CCD array converts the charges into equivalent voltages. With the help of the timing waveforms in Figure 15.21, the operational sequence of the array can be explained as follows: -

- $\Rightarrow$ ϕ_{tck} is clocked high and then taken low. The charge accumulated under each of the pixels is transferred to the respective CCD element. As soon as the clock goes down, the pixel is isolated and is ready to receive electrons as part of the following exposure period.
- $\Rightarrow$ ϕ_{RST} is taken high. This resets the CCD output to zero state by draining off the charge at the gate zone of Q_3 through Q_1 (Figure 15.20). When ϕ_{RST} goes low, Q_1 is off and the last element of the CCD array is connected to Q_3.

⇒ ϕ_1 is high and remains high for a definite longer time. ϕ_2 is kept low. This transfers the charge 'by half of a position' in the CCD array. The output of the last stage of the CCD array is connected to Q_3. It is available as a corresponding V_o.

⇒ ϕ_1 is taken low and ϕ_2 is taken high. During this period, the charge transfer takes place through the 'second half position'. At the end of this period, the charge transfer is complete through one CCD position.

⇒ Clocking of ϕ_1 and ϕ_2 alternately in the above manner, is continued until all the charge values are shifted out as outputs. The number of pulses here is equal to the number of CCD elements. At the end of this period, ϕ_{tck} is pulsed again and pixel charges laterally transferred.

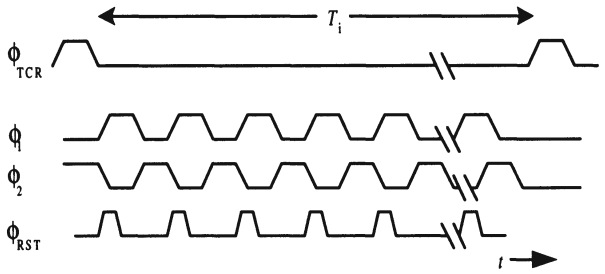


Figure 15.21 Clocking waveforms for the 2-phase CCD array

Observations: -

⇒ T_i in Figure 15.21 represents the total time for each of the pixels to be active and receive incident radiation. All the electrons generated during this interval are accumulated in the depletion zone of the photo-diode. This period is the period of integration of the pixel.

⇒ Arrays normally have a few definite numbers of dark pixel elements at either end. They are dark in the sense that the surface is fully coated and radiation does not pass through. Charge accumulated in each of them during the integration period, is due to the thermal and other noise. Analog or digital signal processing circuitry following the CCD, can subtract an equivalent value from the output of each of the active elements. This reduces the effect of thermal noise on output.

⇒ The CCD array has a few idle elements at either end. The signal processing circuitry has to account for their (zero) outputs suitably. These consistent zeros help in 'line-sync' function.

⇒ Departure from uniformity in the pixel areas, processing and waveforms cause different outputs from different pixels, under dark conditions. This is called the 'Fixed Pattern Noise (FPN)'. In precision schemes, the array output can be separately obtained under zero-illumination conditions representing the FPN. The same may be subtracted from respective signals, when under active conditions. Typically, FPN is of the order of 1 % of saturation level.

⇒ At room temperature, the dark current is of the order of 1 pA for a 14 μm × 14 μm pixel. With an integration time of 4 ms, the error due to this is of the order of 0.2 % of saturation charge. It increases proportional to the

integration time. The dark current doubles with every 7 °C rise in temperature. If necessary it is reduced by cooling of the sensor – done by a thermo-electric device, Joule-Thomson cooler or liquid nitrogen.

⇒ Some devices use an array of dummy diodes along with the active photo-diodes. The dummy diodes are also switched simultaneously with the active diodes. The signal output from the stream of dummy-diodes constitutes only the switching transients. This can be subtracted from the main output stream through a difference amplifier to get an output free from switching transients.

⇒ When high sensitivity is required, arrays with extra-wide pixels are used. As against a typical pixel size of 25 μm × 25 μm in the normal case, these may have pixel sizes of 25 μm × 250 μm. However, their response may not be as uniform as that of the 25 μm × 25 μm pixel – especially for the IR range.

15.6.3.5 Anti-Blooming and Exposure Control

Si photo-diodes operate over 8 decades of incident radiation levels in the short circuit mode (See Section 15.6.1.2). However, the pixels here accumulate charge generated due to the incident radiation. As this continues, the field and the potential differences across the diode junction change and the charge accumulation cannot continue beyond a limit. Subsequently generated charges may diffuse to the adjacent pixel zones. This spill over is called 'Blooming'. Blooming can occur due to high intensity of received radiation or long integration periods or a combination of the two. To prevent this, all pixel elements are provided with anti-blooming facilities. A separate n^+ zone is grown by the side of each pixel and a poly-silicon gate provided to bridge the pixel and the n^+ area. With a controlled potential applied to this anti-blooming gate, a fraction of the electrons accumulated in the depletion zone of the photo-diode, is diverted to this. As the potential on the anti-blooming gate is increased, more of the electrons are diverted and the pixel sensitivity reduced (the function of this diverter is similar to that of an attenuator in an amplifier). The anti-blooming gate and the associated sink can be common for the whole array. With the anti-blooming facility, the dynamic range extends up to (typically) 5000:1.

As the pixel sensitivity is reduced by control of anti-bloom gate potential, the allowable exposure time increases. This makes it possible to set integration time independent of line read-out rate.

15.6.3.6 Types of Detector Arrays

The detector array scheme described so far is the simplest possible. The pixels are all arranged in one line. The CCD shift register is on one side having a storage position corresponding to each pixel position. The pixel packing density is limited by the minimum gate size of the CCDs. Such simple linear arrays can be used in applications where a high level of performance is not expected.

A more widely used array – called the 'bilinear array' – is shown in Figure 15.22. The pixel array has one set of CCDs one side (top) and an identical CCD set on the other side (bottom). The odd numbered CCDs are connected to the pixels below and the even numbered pixels connected to the CCDs above. The CCDs on each side are half in number allowing for doubling the linear pixel density. The transfer gates for the two sides are marked TGE and TGO respectively. Normally, the two are coupled and brought out as one gate input. On a transfer

command pulse, the odd pixel outputs are transferred to the CCD array below and the even lot to the CCD array above. Subsequent serial clocking of the two outputs is identical to the single line array discussed earlier. The odd and even pixel output sequences can be processed separately or combined into a single serial output-stream at twice the speed. With odd and even outputs combined on one line, serial clocking-speeds of 80 MHz are common.

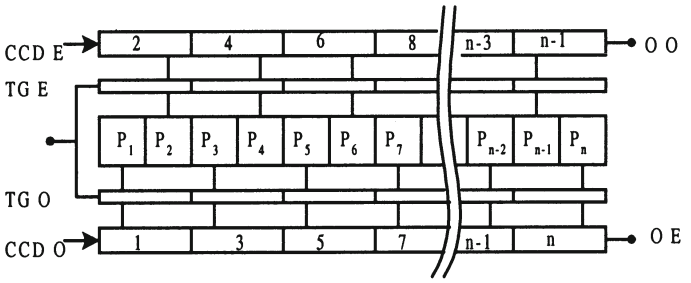


Figure 15.22 Bilinear CCD array with two-sided shift-register scheme

The concept of using 2 CCD arrays to increase the speed of operation can be extended further. One can have 4 or 8 and so on serial outputs – with each output tied to a dedicated set of pixels. Such arrays are called 'Tapped Arrays'.

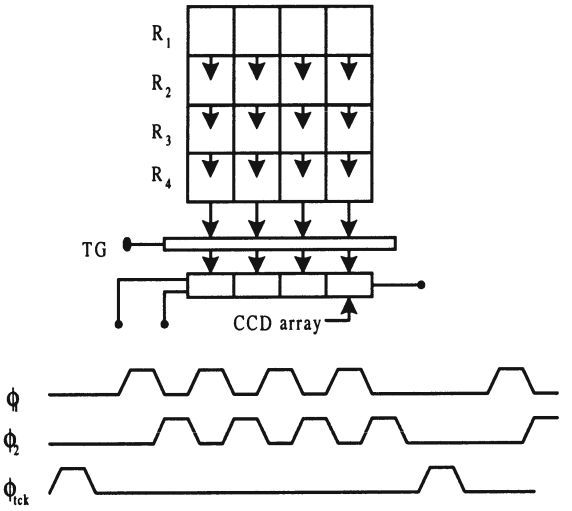


Figure 15.23 Matrix sensing array: schematic arrangement

When sensing an area two possibilities exist. Using a linear array, successive lines of an object may be sensed sequentially. Here the object or the sensing array is moved laterally in synchronism with the CCD clock. The resulting serial stream is processed to represent the object. This is the slowest mode of operation. Bilinear and tapped arrays increase speed as well as complexity. An alternative is to use an area (matrix) array of pixels. By way of illustration, a 4×4 matrix array is shown in Figure 15.23. The integration period is similar to that of the linear array. At the end of the integration period, TG is clocked. Outputs of all the pixels in R_4, are

transferred to the CCD array. Simultaneously other rows are also clocked and each row output transferred to the row below. Here the pixels themselves function as storage elements. Through the clocks ϕ_1 and ϕ_2, the CCD array output is clocked out serially at O *i.e.*, on the same lines as the linear array. At the end of this, TG is clocked a second time and the row of pixels shifted downward by one more row. Thus at the end of 16 clock periods, output of all the pixels in series, is complete. One can see that the transfer clock TG is pulsed once for every 4 periods of ϕ_1 and ϕ_2. The procedure remains the same for larger area pixels also. Total time taken to shift out all the pixel outputs in serial form ($4 \times 4 = 16$ clock periods for the case in Figure 15.24) has to be low compared to the integration time.

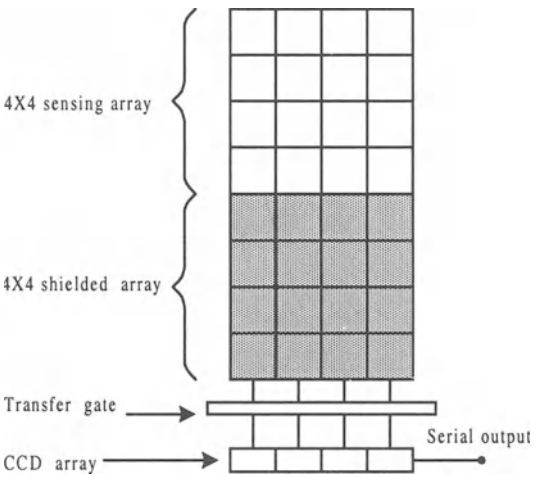


Figure 15.24 Scheme to reduce smear in area sensors

As the pixel rows are shifted downwards, each pixel information dwells in the corresponding pixel position in the following row until one full row is serially output. The radiation received during this dwell time corrupts the signal - causing 'smear'. The problem can be severe in large arrays. The smear problem can be alleviated to some extent by the scheme of Figure 15.24. The active pixel matrix is replicated below. However, the lower half is kept fully shielded; it serves only a storage function. For the 4×4 sensor array shown, through 4 successive transfer clock pulses, all the rows are fully transferred down into the storage area. Only after the row transfer is completed, the transfer to the CCD array and output in serial form are embarked upon. This reduces smear considerably but increases sensor area. The principle of operation is the same for arrays of larger sizes as well.

In many applications, the area sensors are used to sense moving objects. When the object is moving at a fast rate, the exposure time and the integration time for each pixel reduces. This also affects sensitivity adversely. The 'time delay and integration (TDI)' technique improves the sensitivity here. As the object moves, its speed is sensed and the pixel rows switched synchronously. Specifically, let a line be against the top (first) row of pixels at time t_0. As the object moves down, after time interval Δt, the line would move and be against the second row of pixels of the sensing array. Half way through *i.e.*, at time $t_0 + \Delta t/2$, the pixels are clocked and the

collected-charge (signal) at the first row of pixels, transferred to the second row (that at the second row to the third row and so on). For the next Δt time-interval, the line is against the second row. As the line movement and row shifting continues, the signal level in the pixel builds up. This is continued until the line moves out. Then the outputs at the row of pixels are transferred and horizontally serially clocked out. The scheme increases integration-time and hence array-sensitivity considerably. However, the movement of the object and the pixel switching are to be synchronised properly for satisfactory operation.

15.6.3.7 Application Example

CCD arrays can be put to use for instrumentation in a variety of ways. We consider a specific example by way of illustration - that of on-line measurement of the diameter of a wire or a cable. The schematic arrangement of the optics is shown in Figure 15.25. The laser source produces a thin pencil beam of coherent monochromatic light. Collimator 1 expands the incident beam and generates a parallel beam of required size. The size of this beam should be larger than the highest expected diameter of the object (cable or wire), which decides the size of collimator 1. The slit allows a thin uniform beam of rectangular section to pass through. The height h_1 of this beam is the same as the diameter of collimated output beam or slightly smaller. Its width is kept small. The height h_1 is greater than the maximum diameter expected of the object so that the beam incident on the object 'covers' it completely. The cable obstructs part of the incident radiation in the middle. Only that at the sides passes through and gets collimated by collimator 2; the beam emerging from it falls on the CCD array. In the absence of the object, the output of collimator 2 will be a thin beam of height h_2. h_2 is equal to or marginally smaller than the active length of the CCD array. When the object is introduced, the total number of dark pixels in the middle is a measure of the object diameter.

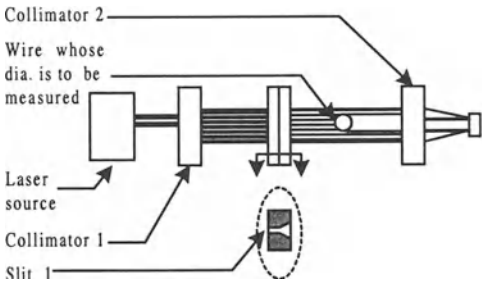


Figure 15.25 Scheme to measure the diameter of a wire using a linear CCD array

Dimensioning of Optics

For the example under discussion, the step by step procedure for dimensioning of optics, is as follows: -

- ⇒ From the desired accuracy of measurement, decide the CCD array size. For example, an array of 512 pixels gives an accuracy of 100/1024 ≈ 0.1 %.
- ⇒ The active length of the array is the product of pixel spacing and the number of pixels. With an array of 512 pixels, each of 14μm× 14μm size, the active length is 512 × 14 μm = 7.2mm. Using this and the maximum diameter of

the object, calculate the expansion ratio of the collimator C_2. If the normal diameter of the object is 2 mm, and the maximum expected variation is 20 %, the maximum diameter is 2.8 mm. Take it as 3 mm. The corresponding expansion ratio is 3/7.2 = 0.42.

⇒ The aperture of collimator C_2 has to be 3 mm. Manufacturer's data books provide lens combinations for different expansion ratios of collimation. Select a suitable combination for collimator C_2.

⇒ The slit height h_2 has to be marginally more than the maximum diameter of the object. A height of 3 mm suffices here. The slit width is selected such that the width of the radiated-beam incident on the CCD array is slightly more than the width of the pixels – 14 μm here. The expansion ratio of collimator C_2 has to be taken into account here. With an expansion ratio of 0.42 and pixel size of 14 μm, the slit width has to be greater than 33.3 μm.

⇒ From the expected signal level from the CCD and pixel sensitivity, one can estimate the laser power required.

The relevant data for a typical array are as follows: -

Diode laser wavelength = 670 nm

Responsivity of a 14μm× 14μm pixel of a CCD array at 670 nm $\approx 4V/\ \mu J/cm^2$

Saturation voltage of pixel = 0.8V

With this, maximum expected output could be taken as 0.6V.

Incident Energy density to generate 0.6Voutput $= \frac{0.6}{4}\ \mu J/cm^2$

$= 0.15\ \mu J/cm^2$ (15.22)

Pixel capture area $= 14\mu m \times 14\mu m$

$= 196\times 10^{-8}\ cm^2$ (15.23)

From Equations 15.22 & 15.23,

required incident energy per pixel $= 0.15\times10^{-6}\times196\times 10^{-8}\mu J$

$= 29.4\times10^{-14}$

Taking integration time of 0.5ms Incident power /pixel $= \frac{29.4\times10^{-14}}{0.5\times10^{-3}}\ W$

$= 588\times10^{-12}\ W$

Power incident on the whole linear array of 1024 pixels $= 588\times1024\times10^{-12}\ W$

$= 0.602\ \mu W$ (15.24)

This represents the minimum power required to be incident on the sensor array. The actual power coming out of the slit may have to be one order higher to ensure that the light energy is incident on all the pixels even under slight misalignment conditions, which can happen in practice. Assuming the laser power incident on the input-side of the slit to be confined to a circular area, from Equation 15.24 and Figure 15.26 we get

$$\text{Minimum power incident on the slit} = \frac{0.602\times\left(\frac{\pi}{4}\right)\times1024^2}{1024}$$

$$= 484\ \mu W$$

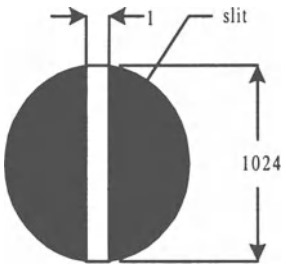


Figure 15.26 Slit through which the collimated laser beam is passed: The relative dimensions are shown

15.6.3.8 CCD Signal Processing

Estimating the diameter of the object boils down to counting the number of contiguous dark pixels in the middle and scaling it up suitably. The required hardware can be organised as shown in block diagram form in Figure 15.27. It consists of a comparator with a steady reference V_R. This represents the threshold to decide whether the pixel is dark or not. V_o = 1 for a bright pixel and 0 for a dark pixel. The 0-1 sequence represented by V_o is clocked into the microcontroller, synchronous with the CCD clock. The software in pseudo-code form is given in Figure 15.28. The steps involved in it are: -

⇒ Wait for the first high output from the comparator (to skip the few dark pixels at the head end of the pixel output sequence).
⇒ Wait for 1 to 0 transition.
⇒ Increment a counter at every clock pulse until the following 0 to 1 transition.
⇒ Read the count.

RISC type 8 bit μCs (like the PIC series of Microchip), can work at 20 MHz and execute an instruction in 200 ns. This can comfortably handle the serial data stream and compute the width with a pixel clocking frequency of 500 kHz. The pulse array from all the 512 active pixels will be received in 1024 μs. Accounting for idle pixels and other overheads, one sample of diameter will be sensed every 2ms. With a 14 μm pixel height, the cable will be fully scanned at a speed of 14μm/2ms = 7mm/ms.

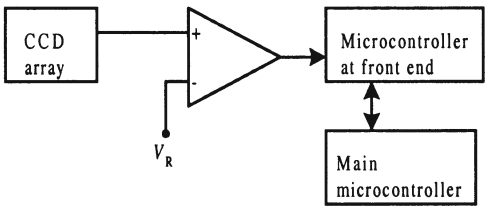


Figure 15.27 Block diagram of signal processing scheme for CCD array

Observations: -

⇒ CCD arrays with large size pixels (500μm width) are available; these can be used to increase sensitivity.

⇒ The variation of object size (cable diameter), with length can be compared to the variation of a signal with time. The size will not change significantly over small lengths (Specifically the diameter of a cable will not change significantly over 10mm). Hence, one sample may be taken for each such small length. (One diameter measurement for 10 mm length of the cable). This is analogous to sampling at a rate high compared to the signal bandwidth. Such sampling retains all the information in the 'signal' (*i.e.*, the nature of variation of the cable diameter).

⇒ From the cable diameter values, one can obtain the average diameter over definite cut-lengths, its variance, spectral components and the like – on the same lines as done with the electronic signals. The nature of variation of all such derived quantities can yield useful information regarding processing and process-related faults. All such computations and information extraction can be done by means of a μC.

⇒ The photo-sensor *per se* responds to a wide frequency spectrum. The use of a laser source ensures that the radiation of interest is restricted to a narrow wavelength range. One may use a proper colour filter in front of the detector to screen off unwanted radiation. This improves the precision of measurement.

⇒ With objects like yarn, the number and extent of hairy projections on it, are quality parameters. These too can be sensed with a linear CCD array as here. For this, successive output sequences, have to be stored in a matrix array and a two-dimensional image-processing done.

⇒ The method can be adapted to measure the size of objects wider than the practical widths of collimated beams (obtained using a beam-splitter) by sensing the two edges separately. Two sets of optics and two CCD arrays are required for this. The two source-sensor sets can be kept at known fixed distances and only the changes sensed.

⇒ The method can be adopted to measure lengths of moving objects in the form of parallel strips.

```
Start
 n = 0; shift_no = 0;
 do while shift_no < 512
 {
  Right shift bit sequence through Carry;
  Increment shift_no;
  if (Carry = 1)
    {
    (do while Carry = 0)
     {
      Right shift bit sequence through Carry;
      Increment shift_no;
       n = n + 1;
      }
      break;
     }
 }
```

Figure 15.28 Program in pseudo-code to compute the cable diameter

15.7 Instrumentation Based on Magnetics

Special magnetic cores like Mu-metal, Permalloy *etc.*, have become available in recent years. High permeability (μ_r ~ 10,000) and low saturation flux density, are characteristic of these materials. Very thin laminations of these keep down eddy current losses and permit working at kHz frequencies. A variety of instrumentation schemes has been suggested and tried using these materials [Geyger, Kraemer, Mac Martin]. Some of them are popular in specialized schemes. Two of representative applications are described here.

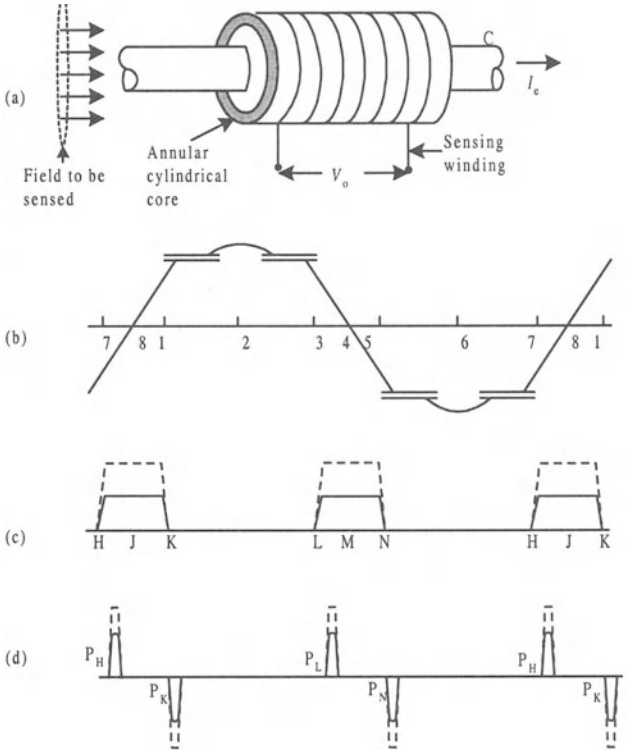


Figure 15.29 Principle of operation of flux-gate magnetometer: (a) Basic circuit (b) Exciting current waveform (c) Waveform of the axial magnetic flux component (d) Waveform of induced emf in the sense winding

15.8 Flux Gate Magnetometer

'Flux Gate Magnetometers' are used to measure weak magnetic fields- like earth's magnetic field and its local variations. Figure 15.29 illustrates the principle [Geyger]. A conductor C carries a current I_e through it. It passes through an annular cylinder of non-magnetic non-conducting material [See Figure 15.29 (a)]. The

cylinder has a thin sheet of the special magnetic material like Mumetal wrapped around it in the form of a definite closed magnetic path. The conductor carrying the current I_e provides a single turn excitation along the axis of the annular core. A sense winding of sufficient number of turns is wound on the core. The exciting winding and the sense winding have their axes normal to each other and hence the coupling between them is zero. The whole combination forms the 'Magnetometer'; it can be used to measure magnetic field strength along the axis of the annular cylinder. I_e can have a sinusoidal or triangular waveform. Even for low values of current through C, the core remains saturated, the flux being in the circumferential direction. The flux through the core reverses as I_e crosses zero. For a short interval around $I_e = 0$, the core is in the active region. During this time, the flux through the magnetic core increases in the axial direction to a level decided by the external field in the axial direction. Note that the component of such external field normal to the cylindrical axis does not produce any such net flux. As the exciting current builds up in the reverse direction, once again the core gets saturated but in the reverse direction and the axial flux due to the external field goes to zero. Figure 15.29 (b) shows the waveform of the circumferential field strength due to which the core remains saturated most of the time. However during the short intervals 7-8-1 and 3-4-5, this field and hence the corresponding core flux are close to zero. During these intervals, the axial flux builds up to the full value and reduces to zero as the circumferential flux builds up. Figure 15.29 (c) shows the corresponding axial flux waveforms, which appear as pulses H-J-K and L-M-N respectively. The peak values of these flux components at J and M in Figure 15.29 (c) occur when the circumferential flux component is zero, *i.e.*, corresponding to points 8 and 4 in Figure 15.29 (b). The changes in axial flux at points H, K, L and N induce corresponding emf pulses in the sense winding. These are designated as P_H, P_K, P_L and P_N respectively in Figure 15.29 (d). In contrast to the strength of the exciting field, that of the axial field is weak and the core remains in the active region. Hence, if the strength of the axial magnetic field increases, the flux levels at J and M in Figure 15.29 (c) increase. The magnitudes of emf pulses P_H, P_K, P_L and P_N also increase correspondingly. The waveforms of the increased axial flux component and those of the emf pulses, are shown in dotted lines in the respective figures. As long as I_e is large enough and remains reasonably constant in amplitude during an excitation cycle, we see that

- ⇒ the output voltage pulse amplitudes are proportional to the axial field strengths.
- ⇒ the output pulse strength $[\int v dt]$ is proportional to the axial field strength and
- ⇒ the output frequency is the same as the excitation frequency.

The output pulse stream from the sense-winding can be demodulated using a synchronous demodulator and used as a measure of the axial field strength.

Observations: -

- ⇒ The instrument is useful as metal detector, mine detector, for geological prospecting *etc.*
- ⇒ In principle, the Hall effect sensor can be used to form a magnetometer. Its zero drift is ~10 μT/K and uncertainty 10 mT/T. Resolution can be improved by means of ferromagnetic flux concentrators. However, they increase the effective dimensions of the sensor.

⇒ The fast saturating soft core, can be used to form other types of magnetometers also.

⇒ Giant Magneto-Resistive (GMR) materials have become available in recent years. Their resistance changes by as much as 20% when subjected to a magnetic field. Full-scale change is achieved with magnetic flux density in the 1 mT range. GMRs are offered as individual units or as compensated Wheatstone bridges. The fact that they are fabricated in IC form facilitates direct interface to the following opamp based signal processing circuitry. These sensors show promise of being more widely used to sense magnetic fields as well as related phenomena.

15.8.1 High Current Measurement

AC currents can be measured using suitable current transformers. DC and slowly varying currents up to a few amperes are measured by sensing a voltage drop across a shunt. However, as the current to be sensed increases beyond 100A, the size of the shunt and the power loss in it increase unduly. Two methods of sensing large DC currents, which do not entail such high power loss, are discussed here.

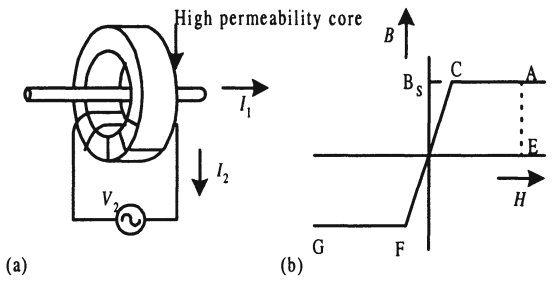


Figure 15.30 Measurement of high current using saturable reactor: (a) Scheme (b) B-H curve of the special core

Consider a high permeability core in the form of a toroid as in Figure 15.30. It has a conductor threaded through it carrying current I_1, which is the current to be measured. A second conductor is wound around the toroid and a voltage V_2 applied to it. V_2 is called the 'excitation voltage' for the core. The main circuit carrying current I_1 is assumed to be such that the emf induced in it due to the second winding, can be neglected. The H due to the current I_1 [OE in Figure 30 (b)], biases the core to operate at point A. The core is already in saturation and offers zero incremental impedance. It behaves differently for positive and negative excursions of the applied voltage V_2. When V_2 is in a direction such that the ampere-turns produced by I_2 aid those of I_1, the core continues to be in saturation. The impedance, seen by the circuit with V_2 as applied voltage, is practically zero and I_2 can increase to very high values. As V_2 changes sign, the impedance continues to be zero until point C. At this stage, the core enters the active region and the core flux reduces. Since the core permeability is large, net ampere-turns is zero.

$$I_2N_2 = I_1 \text{ (since } N_1 = 1)$$

$$I_2 = \frac{I_1}{N_2} \tag{15.25}$$

If V_2 is sustained long enough, the core flux crosses zero and it enters the saturation region beyond point F. However, V_2 is restrained to avoid operation in this zone.

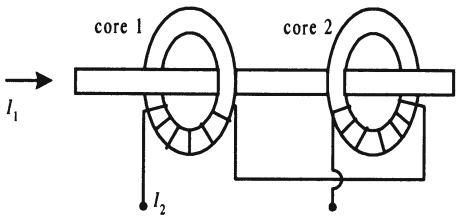


Figure 15.31 Scheme of measuring high current using two saturable reactors

Figure 15.31 shows two cores threading the primary; the secondary windings are connected in series and excited as with the single core above. In core 1, the ampereturns aid in one half cycle while in core 2, they aid in the next half cycle. In the first half cycle, core 1 is active and core 2 offers zero impedance to current I_2. Magnitude of I_2 is as given in Equation 15.25. In the second half cycle, core 1 is in saturation, and offers zero impedance to current I_2. However, core 2 is in the active region of operation and again clamps I_2 to a value given by Equation 15.25.

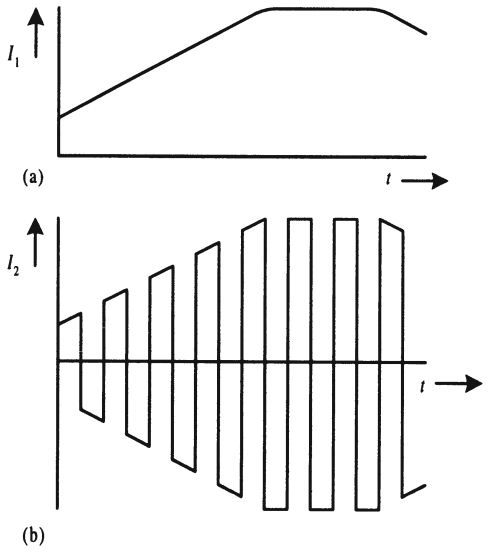


Figure 15.32 Waveforms of measuring and output currents in the scheme of Figure 15.31

Combining the two effects, I_2 is a square wave whose amplitude is proportional to I_1. We see that

$\Rightarrow$ I_2 is a square wave whose amplitude is proportional to I_1.

⇒ I_2 is independent of the magnitude of V_2 as long as V_2 is within limits, *i.e.*, the flux swing is limited to $2\phi_m$ or less where $2\phi_m$ is the saturation flux density of the cores.
⇒ I_2 represents a balanced modulated output [See Figure 15.32]. It can be demodulated by any synchronous demodulator.
⇒ The scheme operates equally well for both the directions of I_1.
⇒ The sensing is of the non-contact type.
⇒ One can use another pair of identical cores in the same fashion and thread I_1 through them in the opposite direction. With this, the net emf induced in the primary side becomes zero. Thus, the loading effect on the primary side can be limited to that of the leakage flux.
⇒ Ideally, the scheme responds satisfactorily for all changes in I_1 limited to a bandwidth of $\omega_e/2$, where ω_e is the excitation frequency. In practice this bandwidth may be more restricted - [$\omega_e/4$ to $\omega_e/10$].

With some modifications, the scheme is widely used for high current sensing [See also Ken Xu and Bingxin Jie].

15.8.2 Current Sensing Using Hall Effect Device

Consider an n-type semiconductor slice carrying a current I, kept in a magnetic field of flux density B as in Figure 15.33. The current through the semiconductor is from P to Q along the y-axis. The magnetic flux is normal to the slice, *i.e.*, in the z-direction. For the direction of current shown, the charge carriers experience a force in the direction shown and electrons crowd around face C. Thus, an emf is

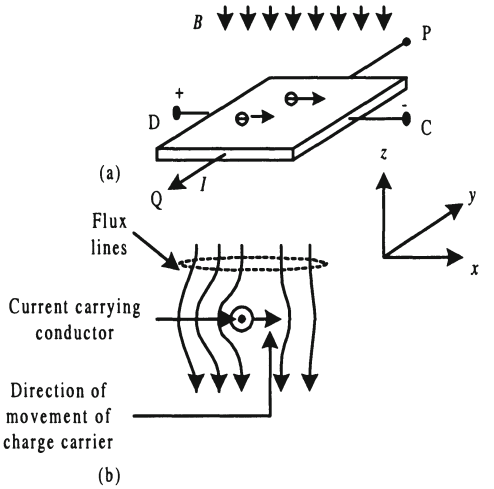


Figure 15.33 Principle of Hall sensor for current measurement

developed between D and C in the direction shown. The phenomenon is referred to as 'Hall effect' and the emf is called the 'Hall emf'. Some characteristics of the Hall emf are: -

⇒ The Hall emf V_{PQ} is proportional to the current I and the flux density B.

⇒ For a given current, V_{DC} is proportional to the flux density B over a limited range of B. (±80 mT). Beyond that, it saturates.

⇒ The Hall voltage is available over a common mode voltage. This is $V_{PQ}/2$ where V_{PQ} is the voltage drop across the device.

⇒ As the ambient temperature rises, the current I also rises (for a given V_{AB}). The sensitivity also increases.

⇒ With careful selection and circuit design, repeatability of sensitivity is ~2%.

⇒ For an n-type semiconductor, the Hall emf is in the direction shown. For a p-type semiconductor, it is of the opposite direction. For intrinsic semiconductors, the Hall emf is zero.

⇒ Specifications of a typical Hall sensor are as follows:-

V_{AB}	=	5V
I_{AB}	=	10mA
Sensitivity	=	10mV/mT (1mV/G)
Linear range	=	±80 mT (±800 G)
Settling time	≈	12μs
Change in sensitivity from 0 to 100 °C	~	5%
Sensitivity range variation (unit to unit)	=	20mV/mT to 30mV/mT.

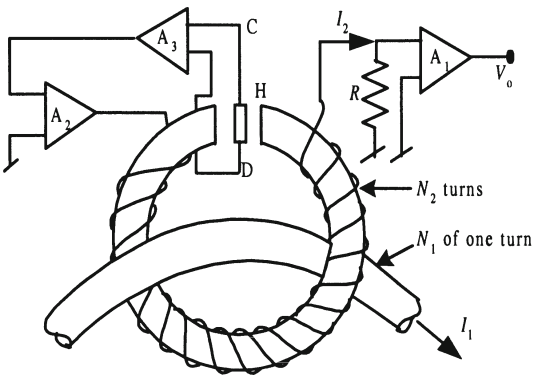


Figure 15.34 Feedback scheme of sensing current using Hall sensor

The Hall sensor *per se* has a wide variation in sensitivity. This problem can be circumvented by calibrating it on a unit by unit basis. However, the low accuracy attainable even under these conditions, prevents any effective direct use of the unit. A class of feedback type transducers built around the Hall sensor, has come into wide use to measure current. The scheme is shown in Figure 15.34. I_1 is the current to be measured. The conductor carrying the current is threaded through a laminated core of high permeability, low loss material. The feedback scheme generates a signal and an output current, which is passed through a second winding wound on the same core. The ampereturns due to the second winding N_2I_2 oppose the primary ampereturns N_1I_1. A Hall sensor is housed in a cut gap of the core. The flux through the core and that linking the sensor, are proportional to (N_1I_1 ~ N_2I_2). A steady exciting current I_e is maintained through the Hall sensor. The Hall emf V_{CD} is amplified and used to decide the current through the winding N_2. The same current is dropped across a fixed resistor R; this forms the output voltage of the sensor.

Under normal conditions, the total loop gain (A_1 and A_2 together) is of the order of 10^5. Hence, as long as I_2 is definite, the Hall sensor voltage is practically zero.

$$\therefore I_1N_1 = I_2N_2 = 0. \tag{15.26}$$

Thus, the output current is a scaled down version of the current I_1.

Typically the Hall sensor used for current measurement, has dimensions – 5 mm × 4 mm × 1 mm. It can be housed in the air gap of a core; the gap dimension can be 1.2 mm × 7 mm × 7 mm. Inductance L seen by winding N_2 (neglecting the ampereturns required by the core) is

$$L = N_2^2 \mu_0 \frac{A}{l} \tag{15.27}$$

where

⇒ N_2 is the number of turns in the winding
⇒ μ_0 is the permeability of free space
⇒ A is the air gap area and
⇒ l is the air gap length.
⇒ The L value in Equation 15.27 represents the maximum inductance attainable for a given set of A and l. Substituting for A and l from the gap dimensions considered above,

$$L = N_2^2 \times 4\pi \times 10^{-7} \times \frac{49 \times 10^{-6}}{1.2 \times 10^{-3}}$$

$$= 51.3\, N_2^2 \text{ nH}$$

With $N_2 = 300$ turns,

$$L = 4.62 \text{ mH}.$$

Let the winding N_2 be driven by an amplifier of ± 12V drive capacity. The maximum (di/dt) attainable, is decided by

$$L\frac{di}{dt} = 12 \tag{15.28}$$

This gives

$$\frac{di}{dt} = 2600 A/s \tag{15.29}$$

With 100mA as the full scale current through N_2,

Time to attain the full current value = 38.5 μs (15.30)

Full scale primary current = 30A

Let the minimum threshold signal that can be detected be equal to 100 μV

Hall sensor sensitivity = 1 mV/G

∴ Minimum detectable flux density (Residual flux density is neglected) $= \frac{100}{1000}$

$= 0.1$G

Minimum detectable secondary current $= \frac{Bl}{\mu N_2}$

$$= \frac{0.1 \times 10^{-4} \times 1.2 \times 10^{-3}}{4\pi \times 10^{-7} \times 300}$$

=32 μA

= 0.03% of full scale

This is the best accuracy attainable (0.3% of full scale accuracy is common).

Observations: -

⇒ The overall sensitivity of the scheme is (N_1/N_2). It is independent of the sensitivity of the Hall sensor. The Hall sensor sensitivity affects only the accuracy.

⇒ Accuracy of the scheme is of the order of ~(1/A) where A is the loop gain of the feedback scheme. Loop gain cannot be increased beyond a certain limit; this is to avoid instability and oscillations.

⇒ Sensors with the highest possible sensitivity are to be used to reduce the threshold level of detection. Sensor working current is of the order of 10 mA.

⇒ Calculations with the above representative scheme show that the rise time ~40 μs (Equation 15.30). The corresponding small signal bandwidth is ~20 kHz.

⇒ High permeability cores have high core loss and increase the response time. Schemes using such cores are suitable for currents at lower frequencies. On the other hand, cores suitable for high frequency of operation have comparatively lower permeability [See Table 10.2]; their use reduces loop gain and hence affects accuracy adversely. Schemes using such cores, have higher bandwidth and are suitable for high speed of operation. Their accuracy is relatively lower.

⇒ For operation in lower current ranges, the primary may have 2, 3, 4, ... *etc.*, turns. For current in the 1A range, a unit with lower value of N_2, is preferred. It offers a correspondingly increased bandwidth.

⇒ For higher current values, units can have higher values of N_2. However, the response becomes correspondingly slower.

16 Typical Instrumentation Schemes

16.1 Introduction

Instrumentation of different process variables was discussed in the preceding five chapters. In most cases, the variable is sensed, operations like amplification, compensation, corrections and filtering are carried out and the output made available directly. All such operations are carried out with electronic building blocks. With the developments in electronics, more of these building blocks are getting integrated; their cost and power consumption are reducing steadily. For example, embedded controllers are becoming more powerful, versatile and less costly. FPGAs, controllers built around DSP cores and ASICs are potential alternatives. These are being used even at the lowest level of tasks. With such improvements, there is a perceptible change in the approach to instrumentation. Many schemes have come into vogue where one or two levels of data processing are carried out in the instrumentation module itself and the information extracted therefrom made available at the output. One can go a step further and have a data fusion approach [Llinas and Waltz]. The variables that characterize a physical entity can be sensed, the entity itself modeled and its current-status inferred. This may call for a few layers of information extraction using a variety of technologies and tools.

The aim of this chapter is two-fold. Firstly, the schemes are categorized depending on the level of complexity and sophistication. Secondly practical examples of schemes – at different levels of complexity are discussed in detail.

16.2 Categorization of Instrumentation Schemes

As mentioned above, at present instrumentation schemes of different levels of complexity exist. At one extreme, there are schemes with a single sensor followed by an indicator. At the other extreme, one may have a comprehensive system comprising of a number of sensors, associated signal processing circuitry, an integrated information extraction scheme and user-friendly and interactive display at the front end. An attempt is made here to see an order in this diversity. The schemes are classified into different 'levels' depending on the level of sophistication involved in each.

16.2.1 Level 0

In the simplest of schemes, the variable is sensed and displayed [See Figure16.1]. No processing is done on the signal. The schemes are simple, rugged and cost-

T. R. Padmanabhan, *Industrial Instrumentation*
© Springer-Verlag London Limited 2000

effective. These schemes are characterized by a lack of flexibility, limited resolution, display on an 'as-is-where-is' basis and the absence of any derived information. Ammeter, voltmeter, Bourdon gauge and the old type of thermocouple with indicator are typical examples.

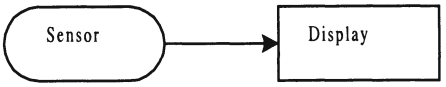


Figure 16.1 Level 0 instrumentation scheme in block diagram form

16.2.2 Level 1

A typical scheme here has a sensor and an amplifier cum filter [See Figure16.2]. The variable is sensed, transformed into an electrical form and amplified. The filter is part of the amplifier. The output is available for onward transmission or display. The schemes involve only one level of processing. Displacement sensing using potentiometers and level sensing are typical examples. The buffering provided by the amplifier allows the signal value to be transmitted over a few meters. In general the plus and minus points of the level 0 type systems hold good here also.

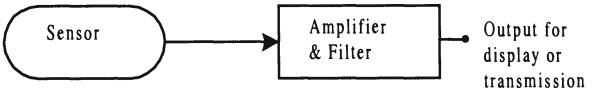


Figure 16.2 Level 1 instrumentation scheme in block diagram form

16.2.3 Level 2

Compared to schemes in level 1, these have an additional level of signal processing is present here[See Figure16.3]. This can be by way of compensation for errors due to changes in one or two environmental variables, compensation for configuration errors etc. Resolution and accuracy are one order better than those with level 1. The cost is also one order higher. Transmission over a distance without impairing signal quality is possible with these schemes. The fact that we compensate for one or two deterministic errors brings a variety of sensors into the ambit of this class. A substantial number of instrumentation schemes in use fall into this category. Strain gauges, force measurement, RTD, thermistor based sensing of temperature, most of the resistance transducer based schemes, semiconductor type temperature sensors, thermocouple, differential pressure methods for flow measurement, ionization gauges, Pirani gauge, magnetic flow meter *etc.*, are examples.

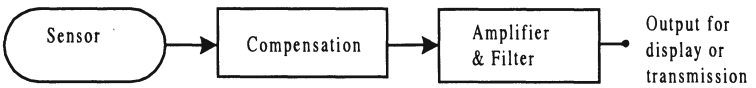


Figure 16.3 Level 2 instrumentation scheme in block diagram form

16.2.4 Level 3

The electronics and allied circuitry here are on par with those of level 2. The additional sophistication is in terms of sensor and its adaptation for different situations, skill and the expertise with the fixtures *etc* [See Figure16.4]. The performance here is on par with those of level 2 but the utility is much wider. The schemes call for expertise and care during installation. Next to the schemes of level 2, those of level 3 are the most widely used. Different types of load cells and their adaptations for weighing and torque sensing, sensing of force, tension, compression, stresses and strains on different members using SGs, pressure and flow sensing using diaphragms are typical examples of this category.

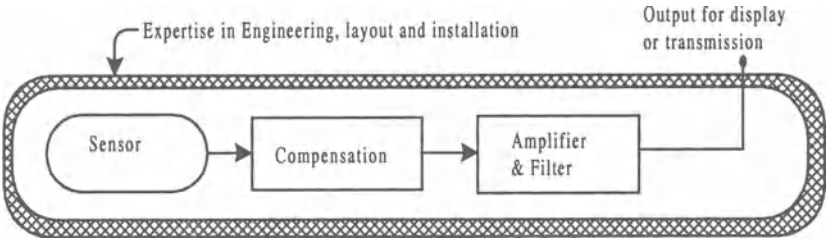


Figure 16.4 Level 3 instrumentation scheme in block diagram form

16.2.5 Level 4

Modulated schemes using synchronous detection have a modulator and a demodulator in addition to the stages in a typical scheme of level 3 [See Figure 16.5]. These offer better resolution at a higher cost. The design and manufacture call for high levels of technical expertise – this is even more true of schemes using capacitance sensors. In some instances, such expertise is required with installation, commissioning as well as regular use. Schemes using capacitance and inductance transducers are of this category. Instrumentation for displacement, thickness, humidity and level using capacitance and inductance transducers are typical examples.

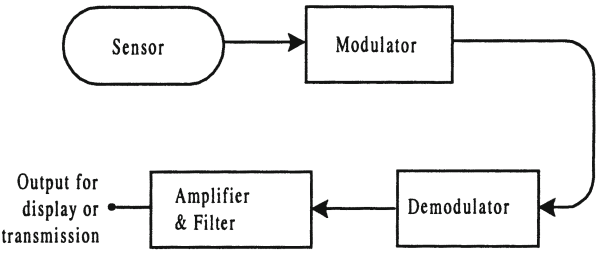


Figure 16.5 Level 4 instrumentation scheme in block diagram form

16.2.6 Level 5

Schemes that use multiple measurements to sense one variable are of this category. These have modules for compensation, amplification, filtering, ADC and computation [See Figure16.6]. The optics, engineering *etc.*, that go with these schemes also call for a high level of expertise. These schemes have become feasible and affordable only after the advent of fast and low cost processors. Humidity sensing using wet and dry bulbs, pH sensing and gas analysis are typical examples.

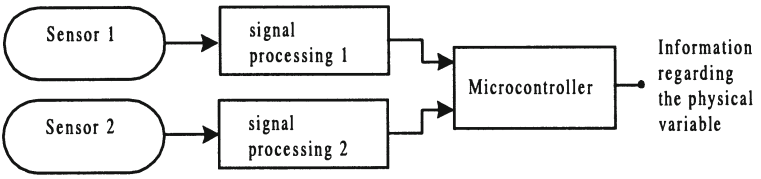


Figure 16.6 A typical level 5 instrumentation scheme in block diagram form

16.2.7 Level 6

There are varieties of schemes not conforming to any of the above patterns. They use varied principles in judicious combinations and take advantage of recent developments in electronics. Optical encoders, ultrasonic instruments, Coriolis flow meters and synchro resolvers are of this category.

16.2.8 Level 7: Schemes with Information Extraction

The role of an instrumentation scheme is to make the value of the concerned physical variable, available in an electrical form. Inferences regarding the parent process status, change and possible changes in the same – are to be made here separately by human intervention. The advent of microcontrollers and the widespread use of embedded controllers has changed the scene. One can do a substantial amount of information extraction automatically and also do it within the instrumentation scheme itself. To some extent it is done with many of the schemes at the higher levels given above. However, one can go farther and obtain information, which can be more meaningful and useful. Examples of these types of schemes are discussed in Sections 16.3.2 and 16.3.3.

16.2.9 Level 8: Specialized Schemes

In some situations, the sensed outputs of variables may not be made available directly as instrumentation signals. Physical inaccessibility (air borne vehicles), remoteness (platforms on seas), hazardous nature of the sensor environment are examples. A variety of instrumentation techniques has evolved over the last few decades for these applications. One specific type, which has become feasible in the last few years, is discussed in Section 16.3.1.

16.2.10 Level 9: Composite Instrumentation Systems

Consider a physical process or entity. We sense its different characteristics and make them available as electrical signals. Different signal values are representative of the process 'status'. Thus in a process, we may measure pressure, temperature and pH values at different points. All such measured values together represent the process status.

So far each measured variable is separately displayed, recorded or transmitted separately. Combining the information from individual sensors and extracting the 'status information' has been done conventionally by the operating personnel. As the number of sensors used to represent the status increases this becomes a daunting task. Embedded controllers, fast computers and a variety of software have added a new dimension to instrumentation schemes. It has become possible to combine the outputs of sensors of any entity or process through a model and quantify the status automatically. In many of the cases, this 'status identification' is done 'on-line' (in the sense that all the necessary computations are done on-line and very fast). The result is an instrumentation scheme, which provides the complete status information of the concerned entity or process. This widens the scope of the instrumentation scheme substantially. It calls for a coordinated information generation from the individual sensors on a continuous basis. We consider one example of this expanded role of instrumentation scheme namely 'Blast Furnace Instrumentation' in Section 16.3.4.

16.3 Typical instrumentation Schemes

Schemes up to level 5 and to some extent level 6, are fairly well established and straightforward. Various examples of these have also been discussed in the last 5 chapters. A few representative examples of the other levels are taken up for detailed discussion here.

16.3.1 Optically Powered Remote Instrumentation Scheme

Sensing of variables so far considered impractical due to their inaccessibility, their hazardous environments, the high cost of implementation or a combination of these, has become possible in recent years. The developments which have contributed to this, are: -

- ⇒ Low cost, small-sized high output laser sources
- ⇒ Improved optical fibres and connectors
- ⇒ High efficiency photovoltaic converters (GaAs based ones have efficiency > 40 %).
- ⇒ CMOS electronics with low power consumption

A typical scheme is shown in Figure 16.7. The scheme is realized through a pair of power cum signal processing units designated as U_r and U_l in Figure 16.7 [Cucci, Werthen and Andersson]. U_l is the local unit and U_r the remote unit. U_l is powered directly from the electrical mains. It has a laser source providing a definite amount

of radiation (usually ~940 nm). The optical power from the laser source – forming the power converter PC_l – is coupled to the optical cable F_l through a transmitter. At the remote end, the optical power is received through a receiver and is incident on a photo-voltaic cell – forming the power converter PC_r. PC_r forms the power source for the whole of the remote unit. The voltage regulator provides output at a stable voltage. It powers the sensor (if necessary) as well as the microcontroller. The sensor can be an RTD bridge for temperature measurement, a strain gauge bridge for measurement of pressure, flow or strain proper or any one of the other types of sensors discussed so far. Currents to be measured are made available as voltage drop across a resistor; these, thermocouples and similar sensors do not require a power source *per se* for their operation. The sensor output is amplified, converted into digital form and made available as an asynchronous serial data stream in the remote unit itself. These activities are carried out by the microcontroller at the remote unit. The opto-coupler OC_r couples the serial data into the second optic fibre F_2 through transmitter. At the local unit U_l, the data stream received through the optic-fibre F_2, is converted back into equivalent electrical form by opto-coupler OC_l. The local processor receives its output, converts it and makes it available in the desired format. The output can be in 4 mA – 20 mA analog form, bit-parallel form or in serial data form itself. It may also carry out any necessary processing on the signal, prior to making it available as output.

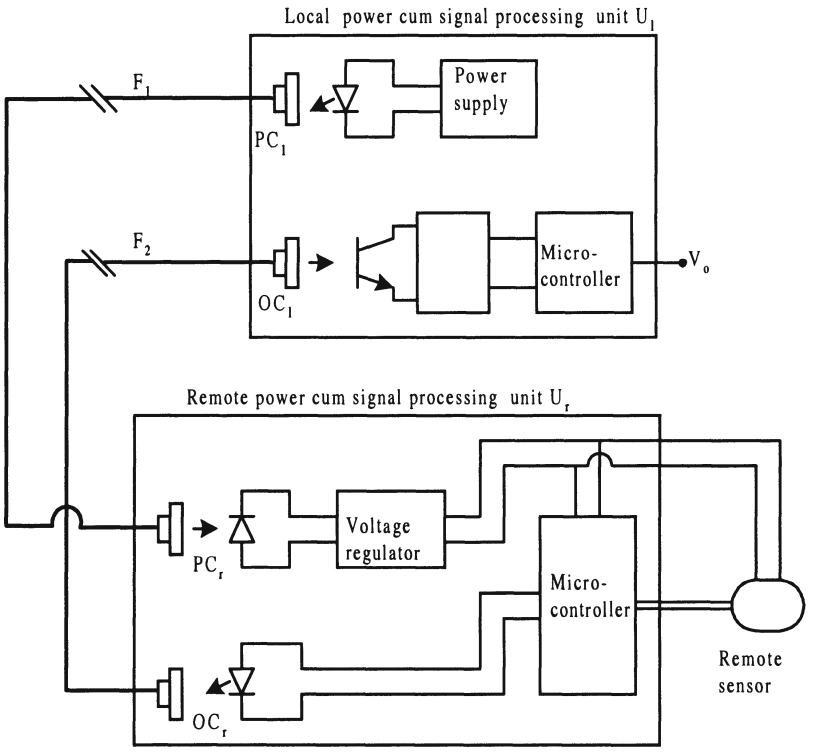


Figure 16.7 Remotely powered instrumentation scheme

Mostly signals to be handled by instrumentation schemes require bandwidths of the order of 100 Hz only. ADCs suitable for this having 10 to 12 bit resolution, consume about 2 mA. The processor in the remote unit may consume 5 mA. The sensor *per se* may consume 1mA. With all these put together, the power consumed by the remote unit is approximately 30 mW. GaAs based photovoltaic converters operate with efficiencies exceeding 40 %. With this, the optical power to be input to the remote unit is about 75 mW. Making allowance for loss in transmission, couplings *etc.,* the laser output power required here, is in the range of 120 mW. Semiconductor diode lasers of this power range have become available at reasonable prices. The optical link can comfortably extend to a few hundred meters.

Observations: -

⇒ Normally both the fibre-optic cables – the one carrying power to the remote unit and the other carrying the signal back into the local unit – are in one housing and form a single flexible cable assembly. The distance between the local and remote units ensures electrical insulation. It also keeps away any hazards associated with the environment at the remote location.

⇒ Any variable, which provides an electrical output, can be handled in this manner. However, applications with thermocouples and resistance-based sensors, are more common.

⇒ Closeness of the remote unit to the signal source precludes signal contamination substantially. To this extent, the signal processing overheads at the remote unit, are minimal. Mostly one level of amplification followed by AD conversion and transformation into the serial form, suffices.

⇒ Complete electrical isolation between the local and the remote units despite their distance, is a major advantage of the scheme.

⇒ The output can be configured to be in 4 mA – 20 mA or 0V – 5V or any other convenient format at the local unit. With this, the optical link is transparent to the user.

⇒ Diode lasers operating in the IR range (950 nm to 980 nm), have become available in the recent years. They provide long years of service and hence are preferred. The optical fibres used have 100 μm to 400 μm core and numerical aperture of 0.29 to 0.37.

⇒ Immunity to EMI, absence of ground loop, absence of failure due to corrosion *etc.*, are the other major advantages of the scheme.

Measurement of current in high-tension lines and measurement of power, temperature *etc.*, at hazardous sites, are typical attractive applications of this type of schemes.

16.3.2 Fibre Length Distribution

Quality of processing of textile fibres is governed by a number of properties of the fibre. Length of the individual fibres and their relative distribution form a set of primary criteria governing their processing and its effectiveness. In a practical environment, such length related data are to be quantified rapidly. We discuss the principles of operation and organization of such an instrument. As a prelude to this, clarifying certain related terminology is in order. This is done here with specific reference to cotton fibre [Morton and Hearle].

16.3.2.1 *Fibre Length Distribution and Related Indices*

If we observe a cotton sample – taken at random – and analyze the individual fibres for their length, we can get the 'Frequency Histogram' shown in Figure 16.8 (a).

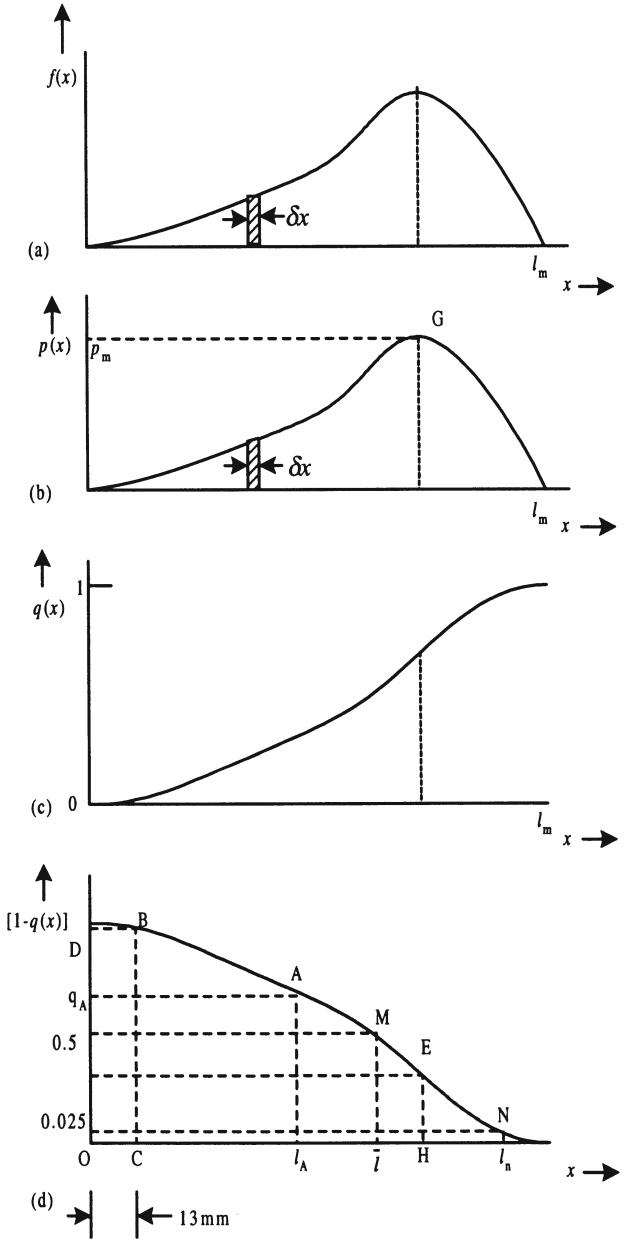


Figure 16.8 Fibre-distribution characteristics and indices: (a) Frequency histogram (b) Probability density distribution of length (c) Cumulative probability density function of length (d) Survivor diagram

For any x, $f(x)$ in the figure represents the total number of fibres of length x. Consider a width of strip δx at a distance x from the origin of the histogram; the area of the strip (shown hatched), represents the total number of fibres with lengths lying between x and $x+\delta x$. Specifically if the histogram is normalized with respect to the area under the curve, the y coordinate represents the probability density $p(x)$ of fibre length shown in Figure 16.8 (b). The integral of the probability density function, with respect to the length, is the 'Cumulative Probability Distribution' function $q(x)$ shown in Figure 16.8 (c). The probability density function $p(x)$ and the cumulative probability function $q(x)$ are formally related as

$$q(x) = \int_0^x p(x)dx \tag{16.1}$$

where

$\Rightarrow$ $p(x)$ is the probability density function of fibre length

$\Rightarrow$ $p(x)dx$ is the relative number of fibres of length lying between x and $x+dx$ and

$\Rightarrow$ $q(x)$ is the cumulative probability function.

$q(x)$ represents the relative fraction of fibres whose length does not exceed x units. Figure 16.8 (d) shows $[1\text{-}q(x)]$. It is referred to as the 'Survivor Diagram'. Consider a point A on the survivor diagram with coordinates l_A and q_A. q_A represents the fraction of fibres longer than l_A in the sample considered. The survivor diagram when represented with fibre length along y-axis is called a 'Baeer Diagram' shown in Figure 16.8 (e). The survivor diagram and Baer diagram are used to yield a variety of information regarding fibre length distribution.

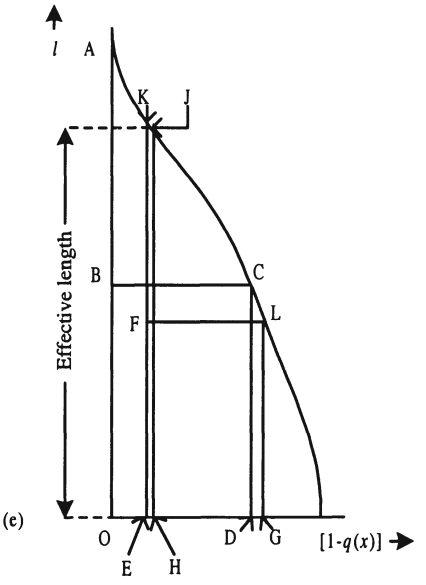


Figure 16.8 Fibre-distribution characteristics and indices (cont'd): (e) Baer diagram and geometrical construction for staple length

Short Fibre Content

In most textile applications, cotton fibres shorter than 13 mm are of no use. Their presence in the cotton affects the quality of yarn adversely. The total amount of such 'short fibres', is formally defined as the percent of weight of fibres whose length is less than 12.7 mm. The 'Short Fibre Content (SFC)' can be obtained from the survivor diagram of Figure 16.8 (d). With OC = 13 mm, draw a vertical through C to meet the curve at B. Project B to D on the y-axis. OD is the total fraction of fibres longer than 13mm. (1–OD) represents the SFC.

Modal Length

'Modal Length' is the length where the probability density is a maximum. The peak is represented by point G in Figure 16.8 (b). The corresponding point on the survivor diagram is shown as E (point of maximum slope). The length represented by OH is the modal length.

Mean Length

The point M on the survivor diagram of Figure 16.8 (d) has ordinate 0.5 and hence represents the mean length. The co-ordinate of this point – shown as $\bar{l}$ – is the mean length of fibres.

2.5% Span Length

2.5 % of the fibres are longer than this '2.5 % Span Length'. Point N represents this. The corresponding length is shown as l_n. Extending the same terminology, the mean length becomes the '50% span length'.

Staple Length

'Staple Length' is a widely used, personalized measure of the cotton quality used from the days preceding the recent methods involving qualitative measurements. A cotton sample is prepared by hand in a specific manner and the staple length decided by its appearance. However starting with a geometrical construction, an 'Effective Length' which is a quantified equivalent of the staple length, can be arrived at. Referring to the Baer diagram of Figure 16.8 (e),

$$OB = \frac{OA}{2}$$

$$= CD \tag{16.2}$$

OD represents the fraction of fibres longer than OB. In the above equation OA represents l_m, the maximum length of the fibres.

$$OE = \frac{OD}{4} \tag{16.3}$$

Mark EK

$$EF = \frac{EK}{2} \tag{16.4}$$

$$= GL \tag{16.5}$$

$$OH = \frac{OG}{4} \tag{16.6}$$

HJ is the 'Effective Length'.

Other Criteria

Some other criteria like 'Upper Quartile Length', 'Upper Half-Mean Length', 'Length Uniformity Index' *etc.*, are also in use. All these indices quantify length distribution in terms of fibre weight. These are not pursued further here.

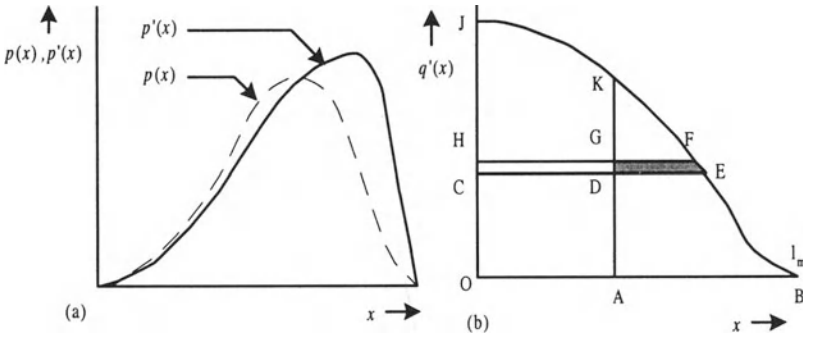


Figure 16.9 Derivation of fibre distribution from the beard diagram

16.3.2.2 Fibrogram

When cotton is processed in a textile mill, the cotton bunch is clamped at random between two rollers and moved forward to the following stage. When a bunch is clamped at random in this manner, the longer fibres have a brighter chance of being clamped. This gives a weightage to the probability proportional to length.

When the fibre is tested for its length distribution, normally the fibres are picked up at random and held in a test jig. It appears in the form of a 'beard' on one side of the jig as shown in Figure16.10 (a). With the beard also, the probability of a fibre being picked up is proportional to the fibre length. Referring to the beard,

$$\text{the probability density } p'(x) \text{ of a fibre being picked up} \propto xp(x). \qquad (16.7)$$

i.e., $p'(x)\,dx$ is the probability of fibres of length between x and $x+dx$ being picked up and appearing in the beard. This distribution is shown in Figure 16.9 (a) along with that of $p(x)$.

Let

$$p'(x) = kxp(x) \qquad (16.8)$$

where k is the constant of proportionality - yet to be determined. Since the total area under the probability density distribution curve is unity

$$\int_0^{l_m} p'(x)dx = k\int_0^{l_m} xp(x)dx$$

$$= k\bar{l}$$

$$= 1 \qquad (16.9)$$

where $\bar{l}$ is the mean length of the fibre.

$$\therefore k = \frac{1}{\bar{l}} \qquad (16.10)$$

$$p'(x) = \frac{1}{\bar{l}} xp(x) \tag{16.11}$$

By integrating $p'(x)$ with respect to x, one can get the survivor diagram for the beard as shown in Figure 16.9 (b). This is also referred to as the 'Fibrogram'. This relation is formalized as

$$q'(x) = \int_{x}^{l_m} p'(x)dx \tag{16.12}$$

q'(x) is the probability of total number of fibres of length exceeding x in the beard. Out of these, different fractions jut out to different lengths.

In the beard, a fraction of the fibres juts out longer than the length (say) OA [See Figure 16.9 (b)]. This is made up of contributions from all the fibres whose lengths are greater than OA. Consider the set of fibres whose lengths lie between CE and HF. The area CEFH represents the total number of fibres of lengths lying between CE and FH in the beard. Out of this, the fraction DEFG (shown hatched) represents the total number whose lengths jut beyond OA in the beard. Adding such areas, we get the area ABK; it represents the total number of fibres jutting out beyond OA, in the beard. Formalizing this we have r' (x) – the probability of fibres jutting out longer than x from the gripping point of the beard as

$$r'(x) = \int_{x}^{l_m} q'(x)dx \tag{16.13}$$

r'(x) represents the distribution of the fibre beard. Differentiating successively, we get,

$$\frac{dr'}{dx} = q'(x) \tag{16.14}$$

$$\frac{d^2r'}{dx^2} = \frac{dq'}{dx} \tag{16.15}$$

$$= p'(x) \tag{16.16}$$

from Equation 16.12. Substitution from Equation 16.11 gives

$$\frac{d^2r'}{dx^2} = \frac{x}{\bar{l}} p(x) \tag{16.17}$$

Equation 16.17 is the basic relation connecting the beard diagram and the fibre length distribution curve (and hence the Baer diagram), By successive differentiation of [$r'(x)$] from fibre beard diagram, we can obtain (d^2r/dx^2). From this $p(x)$ can be obtained as

$$p(x) = \frac{\bar{l}}{x} \frac{d^2r'}{dx^2} \tag{16.18}$$

In practice, one can make the beard and obtain $r(x)$ from it. Equation 16.18 gives the basic relation using which p(x) can be obtained from r(x). Here the mean length $\bar{l}$ is not known a priori. But the procedure represented by Equation 16.9 to Equation 16.11, can be carried out to obtain $\bar{l}$. Subsequently by integrating $p(x)$, from x to l_m, we get $q(x)$.

In the light of the discussions so far, the fibre characteristics and related indices, can be obtained by adopting the following step-by-step procedure: -

⇒ Form the beard and obtain the relative distribution of fibre extensions from the clamp to get the beard diagram.
⇒ Integrate the beard diagram from 0 to the maximum length l_m. Let the area obtained be A_b. Divide the ordinates by A_b (normalizing) to get $r'(x)$.
⇒ Differentiate $r'(x)$ successively with respect to x to get d^2r'/dx^2.
⇒ Get $[(d^2r'/dx^2)/x]$ and integrate with respect to x from 0 to l_m. This area is $1/\bar{l}$.
⇒ Normalize $[(d^2r'/dx^2)/x]$ and get the distribution of $p(x)$.
⇒ Integrate $p(x)$ with respect to x to get $q(x)$ as

$$q(x) = \int_x^{l_m} p(x)\,dx \tag{16.19}$$

⇒ Plot x versus q(x) to get the survivor diagram and Baer diagram.
⇒ The mean length $\bar{l}$ has already been obtained. From the survivor diagram, obtain 2.5 % span length, short fibre content and all other desired span lengths.
⇒ Carry out the geometrical construction of Section 16.3.2.1 above and obtain the staple length.

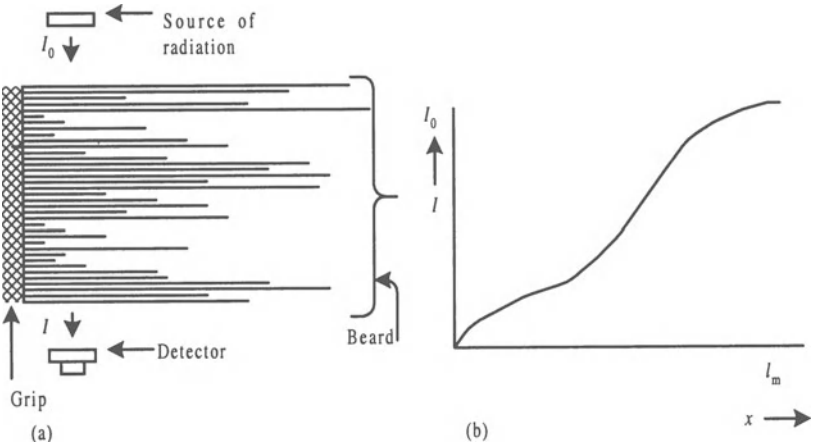


Figure 16.10 Principle of mass detection of the beard at any cross-section: (a) Beard with the source and detector (b) Nature of variation of detected light intensity with distance from the neck

16.3.2.3 Principle of Measurement

The fibre length distribution is obtained in an indirect manner. A sample of cotton is loaded into a mechanical gadget; it forms a paralleled fibre-bunch, which is gripped at a cross-section by a 'Gripper'. All the loose fibres are carefully combed off from the gripper and removed. At this stage, the gripper has fibres projecting from it to different lengths – all in parallel formation. This forms the fibre beard. If a uniform thin beam of light falls on the beard, – the line of incidence being perpendicular to the fibre orientation – part of the light falling on the beard will be absorbed. Only the rest will pass through. The amount absorbed depends on the

fibre content in the light transmission path. Referring to Figure 16.10 (a), Beer's law [Ref] relates the two through the relation

$$I_T = I_0 \exp[-aM] \tag{16.20}$$

where

⇒ I_T is the intensity of light beam transmitted
⇒ I_0 is the intensity of the incident light beam
⇒ a is the absorption coefficient of the material
⇒ M is the mass of the material in the intervening zone.

Taking logarithms on both sides and rearranging terms, we get

$$M = \frac{1}{a}(\ln I_0 - \ln I_T) \tag{16.21}$$

We can have a photo-detector to detect the total received light radiation along the line of incidence. Its output is proportional to I_T. Through another photo-detector, we can also detect I_0. Their logarithmic difference gives M, which is proportional to the total number of fibres. The process can be repeated at different cross-sections of the beard up to the maximum length. M versus length represents the beard diagram.

16.3.2.4 Circuit Scheme

The electronic circuit part of the instrument is shown schematically in Figure 16.11. It has a reference LED L_R and reference light sensor S_R. The line lighting for the beard is done through a set of LEDs L_S arranged as a closely spaced array. The same current passes through the L_R and L_S set ensuring that the respective radiations track each other. Further, the led current is switched on and off at a carrier frequency of a few kHz. The detected outputs are converted into equivalent voltages and amplified by amplifiers A_1 and A_2. The amplifier outputs S_1 and S_2 represent the respective signals amplitude-modulated on the carrier. The modulation eliminates the effect of drift and light coupling errors due to ambient light radiation falling on the detectors. Outputs of A_1 and A_2 are demodulated by demodulators D_1 and D_2. These are synchronous demodulators or detectors switched by the same source as the one that switches the current through the LEDs. The demodulator outputs are smoothened by low pass filters – LPF1 and LPF2. Their outputs – I_0 and I_T – represent the intensity of radiation received by the respective sensors S_R and S_T. I_0 and I_T are given as the inputs to the log amplifiers which give output log (I_0/I_T). The ADC converts it into equivalent digital form; the microcontroller1 does the further processing. The whole instrument is kept within an enclosure free from ambient light radiation to avoid errors due to it.

16.3.2.5 Parameters and Ranges

The maximum length of fibre to be accommodated can be taken as 70 mm (which is well above the maximum length of cotton fibres encountered). The minimum length of interest can be taken as 5mm.

Linear scanning range to be covered = 65 mm
= 65000μ m

1 mm accuracy of length measurement suffices. Taking a least count of 250μ m,

$$\text{number of steps} = \frac{65000}{250}$$
$$= 260$$

A 9 bit counter of 512 steps suffices. The beard (prepared as mentioned earlier) is interposed between the light source and the detector. It is to be moved from 5 mm at the closest to 70 mm - the distance being measured from the line of gripping of the fibres by the beard. The amount of radiation received by the detector is sensed for every 250μm movement of the beard. The displacement can be sensed using a capacitive or an optical transducer [See Section 11.5].

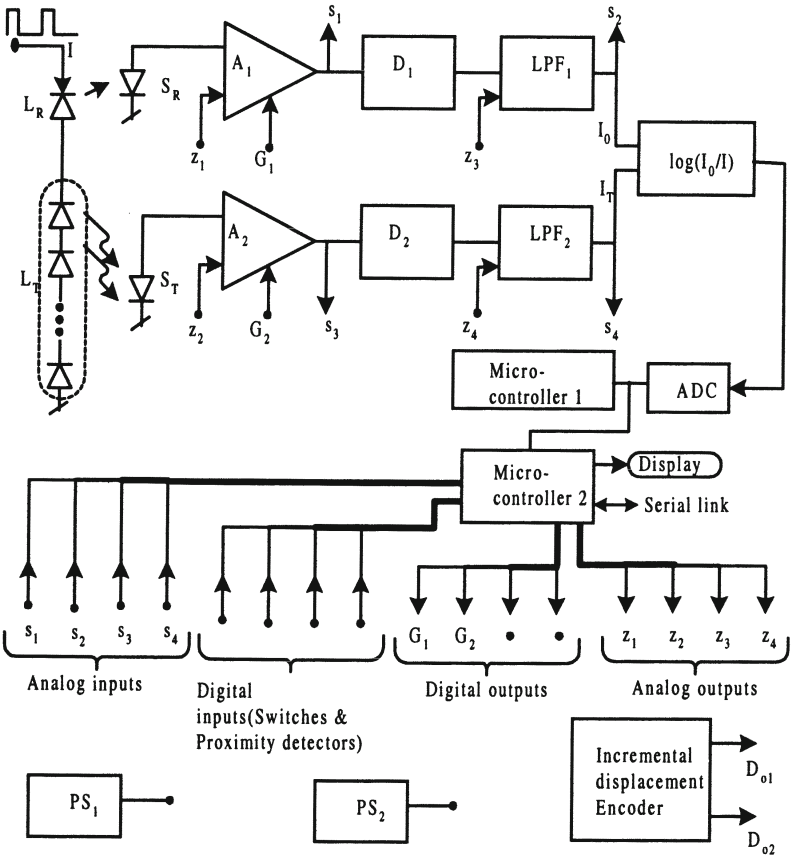


Figure 16.11 Circuit diagram of fibre testing instrument in block diagram form

16.3.2.6 Optical Source and Detection

The beard width can be taken as 60 mm. – should be as wide as possible but small enough to be accommodated in a hand-held instrument. A linear array of closely spaced LEDs can be the light source. About 15 LEDs can be accommodated within a line length of 60 mm. Such LED strip arrays are available in assembled form (in groups of 5, 7 *etc.*). Manufacturers guarantee constancy of light intensity across the whole array. The light output from the array is passed through a cylindrical lens to obtain a parallel line beam of light. The LED and the lens assembly are kept close to the beard and above it. A strip-type photo-detector is kept underneath to collect the received radiation. Taking the LEDs to be of the red colour type, a

corresponding colour acrylic filter is kept in front of the detector to filter out all radiation from extraneous sources and of other wavelengths; hence, the instrument accuracy improves.

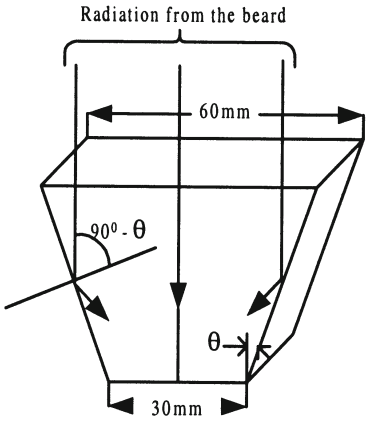


Figure 16.12 Acrylic prismatic block to direct the radiation from the beard on to the detector

Strip-type photo-detectors of 30 mm length are available. When one such detector is used to sense radiation from 60mm width, the radiation is to be fully directed on to the detector. An acrylic trapezoidal block of the type in Figure 16.12 can be used for the purpose. The taper angle is to be selected such that all the parallel rays are fully directed on to the sensor. For this, the rays falling on the side edges, are to be reflected by total internal reflection. It can happen only if $90 - \theta >$ the critical angle of refraction for acrylic. $\theta = 15°$ to $\theta = 20°$ suffices.

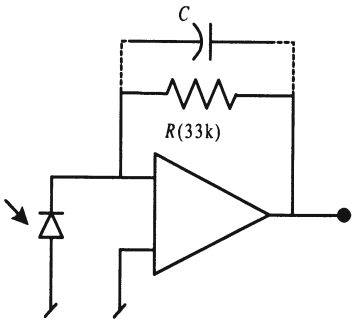


Figure 16.13 Photo-detector circuit for the fibre-length distribution scheme

The photo-detector is operated here in short-circuit mode as shown in Figure 16.13 (See Section 15.6.2) to reduce noise level. The corresponding reduction in the speed of operation is of not much consequence for an instrument of this type. Short-circuit current output of the photo-detector of this type, is in the 100 μA range. A 33 kΩ resistance in the feedback path yields 3.3 V at full illumination level. A suitable capacitor shunted across the 33 kΩ cuts off noise above the cut-off frequency. With the time for the full sweep of the beard being a few seconds, a band limit of 10 Hz is adequate. Hence, we have

$$C = \frac{1}{2\pi \times 33 \times 10^3 \times 10} F$$
$$= 48nF \text{ (say } 47nF)$$

As mentioned earlier, a reference LED of similar type with a corresponding detector is to be used for the second channel. The same (stabilized) current has to be passed through the reference Led as well as the string of LEDs forming the light or radiation source.

16.3.2.7 Sequence of Operations

The sequence of operations of the instrument, is as follows: -

⇒ An opaque 'dummy (metal) strip' is inserted in the beard slot. 'Calibrate' command is given to the instrument. The instrument adjusts the bias to the two channels so that their outputs (dark current response) are zero. The demodulated outputs as well as the outputs of the two low pass filters I_0 and I are also to be zero here. These are corrected by applying bias inputs to the two filters.

⇒ Withdraw the dummy strip. The withdrawal is sensed by checking that the sensor output exceeds set threshold levels. Adjust channel A_2 gain so that $I_0 = I$. which completes calibration.

⇒ The fibre beard is prepared, combed and cleaned. The same is inserted to the allotted slot of the instrument. 'Start test' command is given.

⇒ The microcontroller checks the presence of the beard in position. Steadily withdraw the beard. For every 250 μm incremental displacement of the beard, read ADC output and store it in memory.

⇒ Continue the above sequence until $I_0 = I$ for 40 successive readings (1 cm) or until the beard is withdrawn to 70 mm.

⇒ The measurement part is completed here. The sequence of samples obtained and stored represents respective $r(x)$ values.

⇒ Compute and obtain the cumulative sum S of all samples and normalize the sample values with S. The normalized samples represent $r'(x)$ {See Section 16.3.2.2).

⇒ Using a suitable digital filtering algorithm (See Section 9.5.1), obtain d^2r/dx^2. In general, accuracy of the computed value of d^2r/dx^2 improves as the number of samples considered for the computation is increased. With 9 successive samples we get

$$\left.\frac{dr^2}{dx^2}\right|_{x=0} = \frac{1}{h^2}\left[\frac{363}{560}r_8 - \frac{3296}{560}r_7 + \frac{120008}{5040}r_6 - \frac{1692}{30}r_5 + \frac{10365}{120}r_4 - \frac{8012}{90}r_3 + \frac{3506}{60}r_2 - \frac{5772}{210}r_1 + \frac{29531}{5040}r_0\right] \quad (16.22)$$

Here r_0, r_1, r_2, r_3, r_4, r_5, r_6, r_7 and r_8 represent samples at successive equal intervals of h units of displacement.

⇒ Divide each sample value of d^2r/dx^2 by respective x. The result represents $p(x)$ distribution as can be seen from Equation 16.16.

⇒ Get the cumulative sum of all the $(1/x)$ (d^2r/dx^2) values which gives the mean length $\bar{l}$ (50 % span length – See Equations 16.9 and 16.10).

⇒ Identify the peak of $p(x)$. The corresponding x-value is the modal length.

⇒ Integrate $p(x)$ with respect to x to get $q(x)$. A suitable digital algorithm may be used for this (See Section 9.5.2).
⇒ Get the q value for 12.7 mm of the beard displacement to get the short fibre content.
⇒ Carry out the geometrical construction explained in Section 16.2.2.1 to obtain the staple length of the fibre.
⇒ The above procedure completes all the measurements required. As in such other instruments, the measured index values can be formatted and transmitted over a serial link on call.

16.3.3 Power Analyzers

'Electrical power analyzers' have become widely available in recent years. Four factors have contributed to this development: -

⇒ Availability of the electronics gear necessary for the power analyzer, in recent years – that too at attractive prices.
⇒ The utilities, which produce and distribute power, want the power to be distributed optimally. They like to keep their load factor (average load/peak load) as high as possible. For bulk consumers they have a multi-part tariff to facilitate this. The tariff will be broadly on the following lines:-
  - A fixed rate for installed power on per kVA of installed load
  - A fixed / sliding rate for energy consumed on a per kWh basis.
  - A (punitive) payment for short term peak loads (for example, a peak load of 30 min. duration).

  Such a detailed evaluation of the load requires a continuous monitoring and detailed on-line computation. Comparatively cruder electromechanical sensing devices in use so far, are rapidly giving way to their electronics counterparts.
⇒ Power electronics equipment has proliferated in the recent years. Despite the pure sinusoidal supply voltage, they draw highly non-sinusoidal currents with steep fronts. This causes EMI and imposes a strain on the power supply system. Utilities are imposing restrictions on the waveforms of current drawn. Compliance with these requires detailed on-line analysis of the current waveforms.
⇒ PCs, networking components, cellular phones and many electronic precision equipment connected to the supply, are susceptible to EMI. Restricting the EMI, requires the current (and hence the voltage) harmonics to be kept within specified tolerances.

The overall functioning of the electric power monitor can be summarized as follows: -

⇒ Measure the line currents and voltages at the set sampling rates.
⇒ Compute power and all the desired related quantities.
⇒ Carry out the harmonic analysis of the currents and voltages, if necessary.
⇒ Display selected quantities.
⇒ Transmit selected quantities over the serial link.
⇒ Accept keyboard inputs and change the displayed as well as transmitted quantities as desired.

16.3.3.1 Schematic Arrangement

The circuit of a typical power monitor is shown in block diagram form in Figure 16.14. The scheme shown is for a three-phase four-wire system of supply. The currents and voltages are sensed by dedicated sensors C_R, C_Y, C_B and S_{RY}, S_{YB}, S_{BR} respectively [See sequel]. The sensed currents and voltages are sequentially selected by the mux and converted into digital form by the ADC. The ADC output is read by the microcontroller (In today's scenario, the ADC and the mux may be integral with the microcontroller). The microcontroller carries out the desired computations according to a structured program. The computed quantities are displayed as programmed.

The power supply can be of 50 Hz or 60 Hz as the case may be. The most general power supply is of the 3-phase 4-wire type. This requires 3 line currents and 3 line voltages to be sensed as shown in Figure 16.14. If the supply is of the 3-wire type, one can do with measurement of 2 currents and 2 voltages. However the widely accepted practice, is to go in for current measurements in each line and measurement of all the 3 voltages. The single phase supply calling for the sensing of one current and one voltage, is a simplified case.

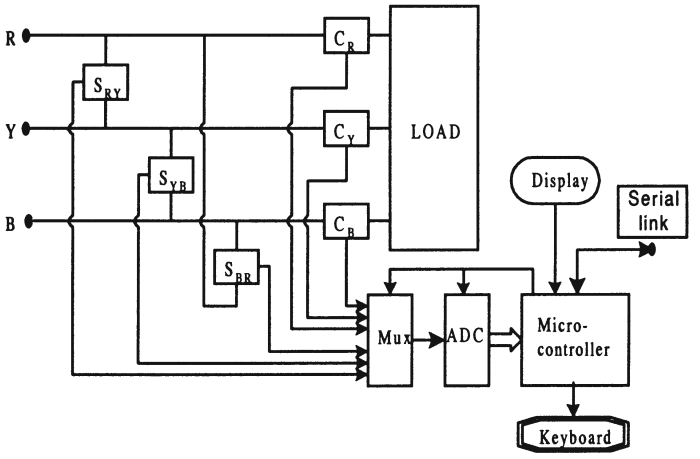


Figure 16.14 Electric power analyzer circuit in block diagram form

16.3.3.2 Electrical Quantities of Interest

The key electrical quantities to be computed are the following: -

⇒ *Amplitudes of the fundamentals of the three currents* – I_{R1}, I_{Y1} and I_{B1}. They can be obtained through FFT analysis.

⇒ *Amplitudes of the fundamentals of the three voltages* – V_{R1}, V_{Y1} and V_{B1}. These too can be obtained through FFT analysis.

⇒ *Total power consumed* – this is obtained by averaging the products $i_r v_{rb}$ and $i_y v_{yb}$.

⇒ *Average power* –

$$\text{The average power consumed} = \overline{i_r v_{rb} + i_y v_{yb}} \text{ W} \tag{16.23}$$

When the supply and the load are balanced,

$$I_{R1} = I_{Y1} = I_{B1} = I_1 \tag{16.24}$$

and

$$V_{RY1} = V_{YB1} = V_{BR1} = V_1 \tag{16.25}$$

With these

$$\text{total power consumed} = \frac{\sqrt{3}}{2} V_1 I_1 \cos\varphi \tag{16.26}$$

where cosφ is the power factor. From Equations 16.23 and 16.26, we get

$$\cos\varphi = 2\frac{\overline{i_r v_{rb} + i_y v_{yb}}}{\sqrt{3V_1 I_1}} \tag{16.27}$$

⇒ Only the fundamental components of the currents and voltages are assumed to be present in Equation 16.27.

$$\text{KVA} = \frac{\sqrt{3}V_1 I_1}{2000} \tag{16.28}$$

$$\text{KVAR} = \frac{\sqrt{3}V_1 I_1}{2000}\sin\varphi \tag{16.29}$$

Other quantities are explained in the sequel.

16.3.3.3 Sensors

Depending on the target application, two types of sensors are possible for the currents and voltages. If the unit is targeted solely at AC loads of power frequency, Potential Transformers (PT) are used for sensing voltages and Current Transformers (CT) for sensing currents. This simplifies sensing and eliminates the need for amplification prior to AD conversion.

If the sensing is to extend down to DC loads (or higher frequency loads), CTs and PTs are not functional. In such cases, Hall effect based voltage and current sensors are used (See Section 15.7.3). Typically, their bandwidth extends from DC to 10 kHz. Though as compact as CTs and PTs, they are more involved, circuit-wise – and costly. As such power analyzers with Hall sensors are used only if the application warrants the same.

16.3.3.4 Operational Details

During regular operation, the currents and voltages are sampled at regular intervals and stored in respective data files. The various quantities desired are computed from these. The main operational and computational aspects are discussed here. The discussion is with reference to the single-phase case. However, it is equally valid for the 3-phase case explained later in the sequel.

Sampling Frequency

The power supply frequency is mostly of the 50Hz or 60 Hz type. Correspondingly, the minimum sampling frequency (Nyquist rate) has to be 100Hz or 120 Hz respectively. In practice, the sampling frequency used is much higher. This is to extract information regarding the harmonic levels. Sampling at 32 samples/cycle suffices to accommodate up to the 15th harmonic. For the extreme case of obtaining components up to 10 kHz[8], 200 samples/s are to be obtained for 50 Hz supply (167

[8] This becomes necessary to compute psophometric current and to conform compliance with interference specifications of communication equipment

samples/s for 60 Hz supply). The variety of information extraction discussed here becomes practicable only at the lower sampling frequencies. When sampled at the highest frequencies, only one or two types of specific computations are carried out.

To ensure satisfactory operation, the sampling frequency is desirable to be synchronized to the supply frequency. This in turn may call for synchronizing the microcontroller clock itself to the power frequency. This is done through a PLL [See Section 6.2.2.6].

Sampling Accuracy

Accuracy of the order of 0.5 % suffices for all the computed quantities. Making allowance for the truncation errors introduced during computation, one has to have the basic current and voltage-samples converted to values which have an accuracy and resolution one order better. Ten-bit ADCs suffice here.

RMS values

The rms values of individual voltages and currents are obtained through the computation

$$x_{\text{rms}} = \sqrt{\frac{1}{n}\sum_{i=1}^{n} s_i^2} \tag{16.30}$$

where

⇒ s_i is the i^{th} sample

⇒ n is the total number of samples considered (for integral number of cycles) and

⇒ x_{rms} is the rms value of the quantity concerned.

Waveform Related Quantities

The rectified average is obtained as

$$x_{\text{av}} = \frac{1}{n}\sum_{i=1}^{n}|s_i| \tag{16.31}$$

$$\text{Form factor} = \frac{x_{\text{rms}}}{x_{\text{av}}} \tag{16.32}$$

$$\text{Crest factor} = \frac{|s_i|_{\max}}{x_{rms}} \tag{16.33}$$

where $|s_i|_{\max}$ is the largest of the sample values. The harmonics in the currents and voltages can be obtained through an FFT analysis of the respective sample sequences.

Power consumed

The power consumed

$$P = \frac{1}{n}\sum_{i=1}^{n} v_i i_i \tag{16.34}$$

where

⇒ P is the average power consumed

$\Rightarrow$ v_i is the i^{th} sample of voltage and

$\Rightarrow$ i_i is the i^{th} sample of current.

In most of the cases of interest, the supply voltage will be a pure sinusoid. As such the power will be consumed at the supply frequency only. The fundamental frequency P_f, is obtained as

$$P_f = \frac{V_1 I_1}{2}\cos(\theta_v - \theta_i) \tag{16.35}$$

where

$\Rightarrow$ V_1 is the amplitude of the fundamental of the voltage waveform

$\Rightarrow$ I_1 is the amplitude of the fundamental of the current waveform

$\Rightarrow$ θ_v is the phase angle of the fundamental of the voltage waveform and

$\Rightarrow$ θ_I is the phase angle of the fundamental of the current waveform.

V_1, I_1, θ_v and θ_I are obtained from the FFT analysis of the current and voltage waveforms.

Power Factor

$$\text{Power factor} = \cos(\theta_v - \theta_I) \tag{16.36}$$

where θ_v and θ_I are as in Equation 16.35 and are obtained from the FFT analysis.

Energy Consumed

By definition, the energy consumed E is given by

$$E = \sum_{i=1}^{n} v_i i_i \tag{16.37}$$

In practice, the energy consumed is to be evaluated over a period of days – with a resolution of (say) – 0.1 kWh. The program to compute the energy consumed is given in pseudo-code in Figure 16.15. Dimensioning of the register S is to be done such that it overflows for every 0.1 kWh of energy consumed. E represents the cumulative energy consumed.

```
          E = 0
          S = 0
recycle   I = 1
loop      S = S + vi ii
          S overflows?
                    No →    I = I+1
                            go to loop
                    Yes →   E=E +1
          go to recycle
```

Figure 16.15 Program in pseudo-code to compute the energy consumed

KVA and KVAR

$$\text{The kVA loading} = \frac{V_1 I_1}{2000} \tag{16.38}$$

where V_1 and I_1 are the amplitudes of the fundamental components of the voltage and current respectively.

$$\text{k VAR loading} = \frac{V_1 I_1}{2000} \sin(\theta_v - \theta_I) \tag{16.39}$$

Maximum Demand

It is customary to estimate the maximum demand on a 30 min basis (Any other time-interval can also be used.). Microcontrollers and DSPs offer the flexibility of computing the maximum demand in various ways (not possible with conventional rotating type maximum-demand indicators). One method is outlined here to illustrate the procedure. The corresponding routine is given in pseudo-code in Figure 16.16. Let 10s be the basic interval for demand sampling. Let d represent the power demand in the i^{th} 10s interval and S the energy consumed in the preceding 30min.

$$d = v_i i_i \tag{16.40}$$

Since the total number of demand samples in the preceding 30 min. is 180

$$S = \sum_{k=0}^{180} v_{-k}\, i_{-k} \tag{16.41}$$

R is a pointer register in the microcontroller. At any time, it stores numbers 1 to 180 - representing the serial number of the latest power sample. After every sampling of demand (at 10s intervals), R is incremented by one. The next demand sample is stored at the location pointed by P. When R content reaches 180, at the next demand sampling-instant, it is reset to one. The program sequence in the figure is executed after every ten seconds of demand sampling. At initialization, S is accumulated for 180 demand samples. Only subsequently, we enter the maximum demand routine of Figure 16.16. One can see that as long as the analyzer is on, the above routine is active. Content of register SL represents the 30min. peak demand.

```
        (SL) : SL is the register which stores the last maximum
        demand
Loop    (R) ← (R) + 1
        (S) ← (S) - ((R)); Subtract the oldest sample from S
        ((R)) ← d
        (S) ← (S) + ((R)); update S
        If (S) > (SL)
                (SL) ← (S)
        IF (R) ==180
                (R ) ← 0
        Go to loop
```

Figure 16.16 Program sequence to compute maximum demand

Peak Quantities

The peak value of the rms current, kVA, kVAR *etc.*, can be obtained by suitably modifying the above algorithm for maximum demand.

Harmonic distortion

Harmonic distortion can be computed according to any desired definition. One commonly used definition is

$$\text{Total harmonic Distortion (THD)} = \frac{\text{rms value of all harmonics}}{\text{rms value of the fundamental}} \quad (16.42)$$

Three Phase Values

All the computations have been discussed above with reference to a single-phase system. With a 3 phase balanced system (balanced supply and balanced load), all the above are directly applicable; Power, KVA, KVAR, kWh and the maximum demand are three times the respective values computed above. However, with unbalanced load, the computations require a slight modification. Consider a 3-wire 3-phase supply system. The instantaneous power supplied p, is given by

$$p = v_r i_r + v_y i_y + v_b i_b \quad (16.43)$$

where

⇒ v_r, v_y and v_b are the instantaneous values of the three line voltages with respect to neutral and

⇒ i_r, i_y and i_b are the respective currents.

At any time the currents i_r, i_y and i_b satisfy the condition

$$i_r + i_y + i_b = 0$$

Or

$$i_b = -i_r - i_b \quad (16.44)$$

Substituting in Equation 16.43, we get

$$p = (v_r - v_b)i_r + (v_y - v_b)i_y \quad (16.45)$$

Equation 16.45 shows that the power consumed is obtained in terms of two line voltages and two line currents. Let

$$v_{rb} = v_r - v_b \quad (16.46)$$

and

$$v_{yb} = v_y - v_b \quad (16.47)$$

Substitutinng from Equations 16.46 and 16.47 in Equation 16.45, equation for KW becomes

$$\text{KW} = \frac{\overline{i_r v_{rb} + i_y v_{yb}}}{1000} \quad (16.48)$$

Unbalance

The percentage unbalance in the current can be computed in the following manner [Blackburn]: -

Positive sequence current

$$I_p = \left| I_r e^{j\theta_r}\left[1 - e^{-j(2\pi/3)}\right] + I_y e^{j\theta_y}\left[e^{j(2\pi/3)} - e^{-j(2\pi/3)}\right]\right| \quad (16.49)$$

Simplification yields

$$I_P = \left|\sqrt{3}\left[\bar{I}_r e^{-j(\pi/6)} + \bar{I}_y e^{-j(\pi/6)}\right]\right| \quad (16.50)$$

where $\vec{I}_r$ and $\vec{I}_y$ are the respective current phasors.

Negative sequence current

$$I_n = \left| I_r e^{j\theta_r}\left(1 - e^{j(2\pi/3)}\right) - I_y e^{j\theta_y}\left(e^{j(2\pi/3)} - e^{-j(2\pi/3)}\right)\right| \quad (16.51)$$

Simplification yields

$$I_n = \left|\sqrt{3}\left[\vec{I}_r e^{-j(\pi/6)} - \vec{I}_y e^{j(\pi/6)}\right]\right| \quad (16.52)$$

$\vec{I}_r$ and $\vec{I}_y$ being the respective current phasors.

$$\%\ \text{unbalance in load} = \frac{I_p}{I_n} \times 100 \quad (16.53)$$

Observations: -

⇒ Power analyzers normally have the facility to function in single-phase circuits as well as three phase circuits. The three phase circuits can be of the 3-wire or the 4-wire type.

⇒ Power analyzers for AC working use good quality PTs and CTs as current and voltage sensors. The nominal voltage can be 110 V, 220 V or 440 V as the case may be. The value can be easily changed by changing the turns ratio. The CTs used are normally of the 5 A secondary type with a bar primary. It can be adapted for other lower primary current values by using multiple turns in the primary side.

⇒ Use of PTs CTs or Hall sensors, make the instrumentation scheme fully galvanically isolated from the power side circuit.

⇒ With the provision of the split core CT, the unit can be made to be of the clip-on type. This coupled with the battery-powered operation allows the instrument to operate in a stand-alone fashion without any need for external power supply.

⇒ Performance specifications of a typical unit are as follows:
Accuracy for voltage and current, ~1 % of full scale
Accuracy for energy, ~0.25 % of full scale
Accuracy of harmonic component amplitudes, ~2 % of fundamental up to the 15^{th} harmonic
Accuracy of harmonic component amplitudes, ~3 % of fundamental up to the 50^{th} harmonic
Power frequency, 50 Hz/60 Hz nominal
Fundamental frequency range, 5 Hz to 800 Hz.

⇒ If the unit can compute harmonics up to the 50^{th} with 50 Hz supply, the highest harmonic frequency that can be accommodated is 2500 Hz. This represents the frequency of the highest harmonic component that can be estimated irrespective of the fundamental frequency. In other words, as the frequency of measurement increases, the number of harmonics that can be accommodated, decreases.

16.3.4 Instrumentation for a Blast Furnace

The 'Blast Furnace' is a typical process, which calls for an elaborate and well co-ordinated instrumentation scheme. Starting with the process, we study the requirements of the instrumentation scheme for the blast furnace and examine how the same can be implemented. The focus is on the logic of selection, co-ordination of the different individual instrumentation units and exploitation of the overall scheme to extract the maximum out of it.

Iron is produced mostly by reducing the oxides of iron, available in nature in ore form. The reduction is carried out in blast furnaces. The major aims of the blast-furnace operation are: -

⇒ production of iron of the desired quality
⇒ Ensuring the consistency of quality of the iron produced
⇒ Minimization of the energy consumption on the basis per-ton of iron produced
⇒ Minimization of cost
⇒ Maximization of productivity (tons of iron produced/hr)
⇒ Operation without sacrificing the longevity of the blast furnace and allied items

Typically, a blast furnace produces 1 to 4 million tons of iron per year (114 t/hr to 456 t/hr). The blast furnace and the closely allied items occupy about 50 m × 50 m area. Operation and control of the furnace are carried out at 3 or 4 levels of elevation. Operation of this nature and magnitude calls for a variety of instrumentation schemes to be arranged at different levels and well coordinated. We review the blast furnace and its operation as a prelude to studying the instrumentation schemes [McGannon].

16.3.4.1 Blast Furnace

The essential parts of a blast furnace are shown sketched in Figure 16.17. The furnace shell is lined inside with suitable refractory bricks. The lining ensures an erosion-free surface inside. It also provides thermal insulation for the shell. The shell is continuously cooled by circulating cooling water all around through ducts. The furnace is normally packed with the 'burden' (the raw material fed from the top) and its derivatives. The hot air blast is blown through 'tuyeres' positioned near the bottom – above the hearth area. A series of tuyeres are kept distributed around the furnace. The 'bustle' pipe is the feeder of hot blast to the tuyeres. The blast furnace is operated with a gas seal. The gases emanating at the top after the reaction inside, are led through the four pipes – 'uptakes' – which join in pairs at the top and flow down through the 'down-comer'. The burden material is fed through a set of two 'skip cars', which dump the burden over a 'small bell'. After a caeful of material is dumped on the small bell, this bell opens and the fed material falls above the 'big bell' underneath. After 3 to 6 skip-cars of burden material are loaded on the big bell, it opens and dumps the burden into the furnace. With this, the furnace top level – 'stock line' – increases. The small-bell-big-bell combination of burden feeding, serves two main purposes. Firstly, the amount of blast furnace gas that escapes when material is fed into the furnace is minimized. Further, the material dumped by the skip cars, on the small-bell differs from feed to feed [See Section 16.3.4.4 below]. Hence when a few such feeds are collected together and dumped into the furnace, better uniformity of material feed is ensured.

As the reaction proceeds in the furnace, the molten iron (called the 'hot metal') accumulates at the bottom of the furnace at the 'hearth'. The liquid 'slag' with its lower density floats on the top of the hot metal. The hot metal and the slag are tapped out through respective openings – called the 'iron notches' and the 'slag notch'.

A big blast furnace of today, is 35 m in total height and 14 m in diameter at its widest part. It has a useful volume of about 4100 m^3. It can produce about 8500 t of iron per day.

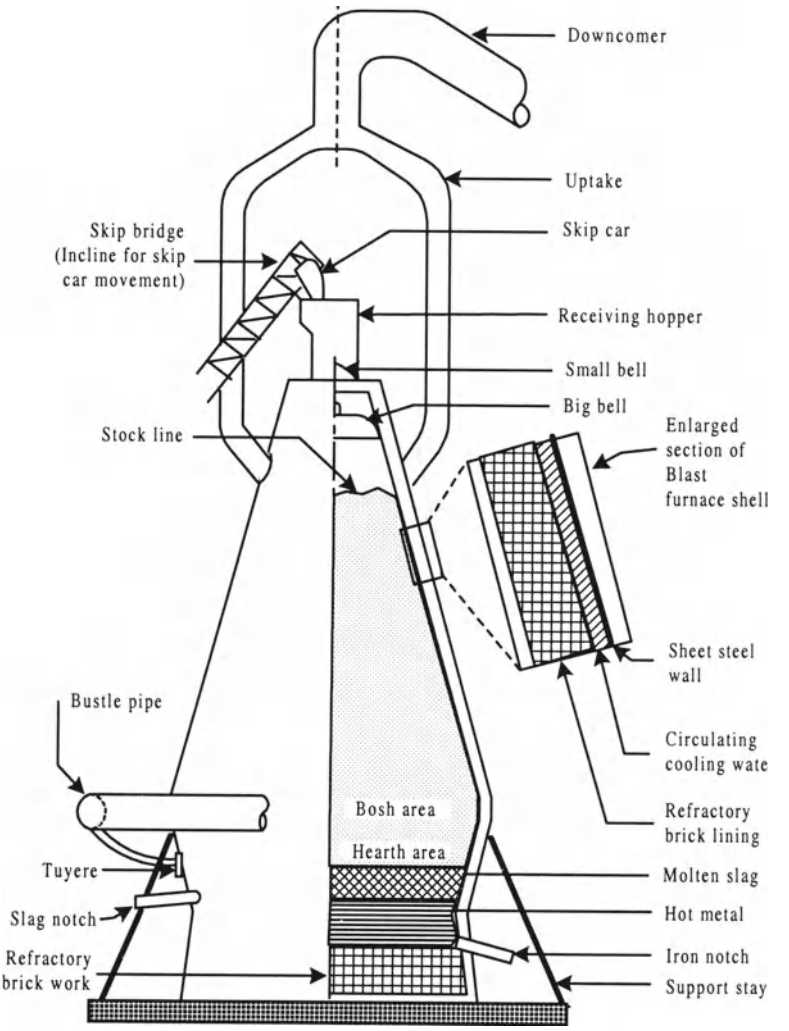


Figure 16.17 Simplified sketch of a blast furnace showing the essential parts: The external view is shown in the left and a cut-section view on the right

16.3.4.2 Blast Furnace Chemistry

The iron content in the iron ore varies from 30 to 70 % by weight. Iron is present mainly as its higher oxides and silicates. Mn, Al, P, Ca, Mg and other trace elements are also present, though at much reduced-levels. These are present mainly as compounds or as impurities in oxide form. In addition, it has water in a chemically combined form. As an iron extraction process, the blast furnace operation is essentially a reduction process. The compounds of iron are reduced to oxides and the oxides to iron in stages. Along with suitable fluxes like lime (CaO), dolomite (MnO) *etc.*, the iron ore is fed in to the blast furnace along with sufficient

amount of coke (C). The reactions proceed at different layers in the furnace in the presence of a hot blast of air and other gases as explained in the sequel. The elements fed through the flux, form compounds with the other elements present in the ore. All these compounds together form the slag and iron with a limited amount of C , Si and Mn; some other undesirable elements like P, S *etc.,* are also present in it though to a lower extent. The iron here is available in molten form – commonly called the 'hot metal'. The selection of fluxes and their proportioning with coke and air, the amount of air forced in and temperature, are all chosen to ensure the purity of iron. These also have a decided say in the aims pronounced earlier.

The main reactions taking place within the blast furnace are briefly described here. Near the blast furnace top, the temperatures are lower. CO and H_2 (though only to a limited extent), are the only reducing agents. The stoichiometric equations of reduction are

$$3Fe_2O_3 + CO \rightarrow 2Fe_3O_4 + CO_2 \quad (16.54)$$

$$\Delta H = -50.59 \text{ kJ/mol CO} \quad (16.55)$$

$$3Fe_2O_3 + H_2 \rightarrow 2Fe_3O_4 + H_2O \quad (16.56)$$

$$\Delta H = -9.42 \text{ kJ/mol } H_2 \quad (16.57)$$

$$Fe_3O_4 + CO \rightarrow 3FeO + CO_2 \quad (16.58)$$

$$\Delta H = +39.71 \text{ kJ/mol CO} \quad (16.59)$$

$$Fe_3O_4 + H_2 = \rightarrow 3FeO + H_2O \quad (16.60)$$

$$\Delta H = +80.88 \text{ kJ/mol } H_2 \quad (16.61)$$

To a certain extent, the oxides of iron are also reduced to iron at this level.

$$Fe_2O_3 + 3CO \rightarrow 2Fe + 3\,CO_2 \quad (16.62)$$

$$\Delta H = -12.87 \text{kJ/mol Fe.} \quad (16.63)$$

$$Fe_3O_4 + 4\,CO \rightarrow 3Fe + 4CO_2 \quad (16.64)$$

$$\Delta H = -3.9 \text{ kJ/mol Fe} \quad (16.65)$$

$$FeO + CO \rightarrow Fe + CO_2 \quad (16.66)$$

$$\Delta H = -16.11 \text{ kJ/mol of Fe} \quad (16.67)$$

$$Fe_2O_3 + 3H_2 \rightarrow 2Fe + 3H_2O \quad (16.68)$$

$$\Delta H = +48.95 \text{ kJ/mol of Fe} \quad (16.69)$$

$$Fe_3O_4 + 4H_2 \rightarrow 3Fe + 4\,H_2O \quad (16.70)$$

$$\Delta H = +51.04 \text{ kJ/ mol of Fe,} \quad (16.71)$$

$$FeO + H_2 \rightarrow Fe + H_2O \quad (16.72)$$

$$\Delta H = +25.10 \text{ kJ/mol of Fe} \quad (16.73)$$

In addition, the higher oxides of Mn may be reduced to MnO by CO. Thus we have

$$MnO_2 + CO \rightarrow MnO + CO_2 \quad (16.74)$$

$$\Delta H = -1476 \text{ kJ / mol} \quad (16.75)$$

$$Mn_3O_4 + CO \rightarrow 3MnO + CO_2 \quad (16.76)$$

$$\Delta H = -51.25 \text{ kJ/ mol} \quad (16.77)$$

Observations: -

⇒ At the comparatively lower temperatures prevalent at the high levels of the blast furnace, only a small fraction of the CO and H_2 present, react and reduce the oxides of iron.

⇒ The heat given out during the reactions is indicated by a negative sign. Most of the reactions here are of this type.

⇒ The oxidation of H_2 to H_2O does not liberate as much heat as that required for reduction of FeO to Fe. Hence, this reaction absorbs heat.

⇒ In general at the upper echelons of the blast furnace, the higher oxides of iron like Fe_2O_3 and Fe_3O_4, are reduced to FeO. To some extent the reduction to Fe also, may take place.

⇒ The iron oxides remaining to be reduced at lower levels are all essentially in the form of FeO. The reduction at these lower levels [Equations 16.72 & 16.73], takes place at comparatively high temperatures.

Due to the high temperatures prevalent, CO_2 is not stable and reduces to CO.

$$CO_2 + C \rightarrow 2CO \quad (16.78)$$

$$\Delta H = 172.59 kJ/mol \quad (16.79)$$

The two reactions represented by Equations 16.72, 16.73, 16.78 and 16.79, can be combined into

$$FeO + C \rightarrow Fe + CO \quad (16.80)$$

$$\Delta H = 156.48 kJ/mol \quad (16.81)$$

Similarly combining Equations 16.78 & 16.79, with

$$H_2O + C \rightarrow CO + H_2 \quad (16.82)$$

$$\Delta H = 131.38 kJ/mol \quad (16.83)$$

we have

$$FeO + C \rightarrow Fe + CO \quad (16.84)$$

$$\Delta H = 156.48 kJ/mol \quad (16.85)$$

The net reaction FeO + C→ Fe + CO absorbs a large amount of heat. The heat can come from additional oxidation of C to CO leaving behind an abundant amount of surplus CO. However, the trend is to supply air blast at 1000 °C to 1300 °C range in sufficient quantity blown in from below. The sensible heat in the air provides about 40 % of the heat required for the reduction.

Other Impurities

The oxides of Mn, Si and P are also reduced at the high temperatures prevalent at lower levels.

$$MnO + C \rightarrow Mn + CO \quad (16.86)$$

$$\Delta H = +274.47 kJ/mol \quad (16.87)$$

$$SiO_2 + 2C \rightarrow Si + 2CO \quad (16.88)$$

$$\Delta H = 658.56 kJ/mol \quad (16.89)$$

$$P_2O_5 + 5C \rightarrow 2P + 5 CO \quad (16.90)$$

$$\Delta H = +995.79 kJ/mol \quad (16.91)$$

Observations: -

⇒ The reduction of MnO to Mn takes place at temperatures greater than 1500°C.

⇒ Only 60 to 70 % of the Mn present in the raw material fed, gets reduced in this manner. It dissolves in liquid iron (hot metal). The rest goes into slag.

⇒ Reduction of SiO_2 to Si also takes place only at elevated temperatures. The amount of Si reduced increases, with increase in the temperature level of the reaction, increase in the Si content of the raw material and increase in the coke level. The reduced Si dissolves in liquid iron and the rest (unreduced) goes into slag.

⇒ Reduction of phosphorous too takes place at the higher temperatures only. However, reduction of the phosphorous in the raw material is complete and it dissolves in the hot metal. The presence of phosphorous in iron affects its properties adversely to the extent of its presence. Hence every attempt is made to keep phosphorous in the raw material as low as possible.

General Observations: -

⇒ The total height of a modern-day blast furnace is 30 m (typical). The zones corresponding to the two types of reduction reactions cannot be clearly partitioned here. They depend on the furnace temperature profile, which also changes with the operating conditions.

⇒ The ore and coke that are usually used, will have additional elements and impurities in them. Normally these are analyzed carefully and each element is identified and quantified. Based on this analysis, the contents and proportioning of the flux is done. This ensures that all such elements go into slag as compounds; thus, they are kept away from the hot metal.

⇒ In addition to the above, the fluxes are proportioned so that the flux remains basic in nature. One of the purposes of a basic slag is to see that more of sulphur reacts and gets into the slag and less into iron.

⇒ The coke that is fed, is maintained at a level, which ensures that the iron is fully reduced (maximization of productivity). Further, temperature and flow rate of the air-blast is maintained at a level, which minimizes relative coke consumption (optimization of productivity).

16.3.4.3 Flow of Materials

The raw materials comprise iron ore, selected flux materials and coke. These materials – referred to as the 'blast furnace burden' – are steadily fed from the top of the furnace in desired proportions. Raw materials in powder form clog the furnace and stand in the way of free movement of materials. Hence the raw materials of smaller sizes are well mixed together and sintered in a separate 'sinter plant'. The sintered lumps are comparatively bigger in size and are fed along with the raw materials. Simultaneously hot air is blown in from near the bottom of the furnace. Its temperature and flow-rate are controlled.

The oxygen in the hot air of the blast reacts with the carbon in the coke of the descending burden and produces CO. This in turn reacts with the FeO present and reduces it to iron. The high temperature in this zone – (>1100°C) – causes the resulting CO_2 to reduce to CO and O_2. Similar reduction reaction also takes place with MnO and other oxides. All these reactions are on the lines indicated in the preceding sub-section. Due to the high temperatures present in the furnace, the iron melts. The molten iron collects at the bottom of the furnace as 'Hot Metal'. The impurities react with oxygen and the flux material in the burden and form the 'Slag'. The molten slag collects above the molten iron. The molten hot metal and slag are tapped off regularly.

The blast composition changes substantially as it ascends. The oxygen content reduces substantially. CO and H_2 get added. Further, the blast temperature drops down abruptly. This is due to the heat consumed in the reduction of Fe, Si, and Mn, melting, and superheating of Fe and the slag. Due to these, the blast temperature reduces from 1300—1100 °C to 800—900 °C as it moves up through the bosh area. As the blast ascends further, the higher oxides of Fe and Mn are reduced to the lower oxides. Some amount of reduction of FeO to Fe may also take place here. However the blast temperature and the burden temperature change much more slowly here (*i.e.*, with respect to the height). As the gases ascend still further, the C in the coke is oxidized. The moisture in the raw material evaporates and dissociates. The resulting gases, excess CO and H_2, N_2 in the blast air and C – all these together emanate from the furnace top as 'blast furnace gas'. The upward flow of gases, the downward flow of the burden, and the continuous heat exchange between them, can be summarized as follows: -

⇒ At the top layers of the furnace, the moisture in the burden evaporates (temperature < 100 °C).

⇒ As the burden descends, the volatile material from the coke is liberated – mostly it is the residual sulphur in it (temperature 100 °C to 500 °C).

⇒ The higher oxides of Fe and Mn reduce to respective lower oxides. Limestone also decomposes (temperature 500 °C to 900 °C).

⇒ At lower levels, all FeO is reduced to Fe represented by the reaction of Equation 16.80. The temperatures in this zone extend from 900—1200 °C.

⇒ As the burden descends further, Si, Mn and P are reduced at higher temperatures. The Fe also melts fully in this zone (temperature of 1200 °C to 1300 °C).

⇒ The impurities, the ash in the coke and flux material together form the molten slag (temperature of 1300—1500 °C).

⇒ At the lowest level, above the molten metal and the slag in the furnace hearth area, C in the coke burns with the oxygen in the blast.

16.3.4.4 Blast Furnace and Accessories

The size and complexity of blast furnace operation, requires a variety of accessories for its operation. Only the main accessories – relevant for our discussion – are dealt with here.

Burden Feeding

The burden is fed into the blast furnace through a pair of skip cars (Figure 16.18). The two skip cars move on an incline over rails. The two are tied together through a rope and driven. Let the total travel length of the skip-cars be *l*m. When skip car SC_1 is at a distance of x m from the bottom of the skip-incline and it is going up, skip car SC_2 is $[l\text{-}x]$ m from the top and it is going down.

When one skip car is dumping material into the small bell, the other is in the 'pit' collecting material. Thus, operation of the two skip cars is synchronized. Depending on the furnace size, the two skip cars can carry and dump 50 t of material on each trip. The skip cars are filled with coke, ore, fluxes *etc* (Nowadays all the blast furnaces have the provision to weigh all the materials fed in.). Coke – since it is the major constituent – has a separate feeding system. Through a vibratory screening system, it is screened and the screened residue fed into the furnace after weighing. Other raw materials are fetched from the individual bins by

a 'scale car', brought above the pit and dumped into the skip car. The scale car is usually engine-powered and run by an operator. The material is collected each time on a hopper with weighing arrangement. To facilitate such movement of the scale car and collection of material by it, all the bins are lined on either side of the scale car path. The bins are filled as and when the supplies come.

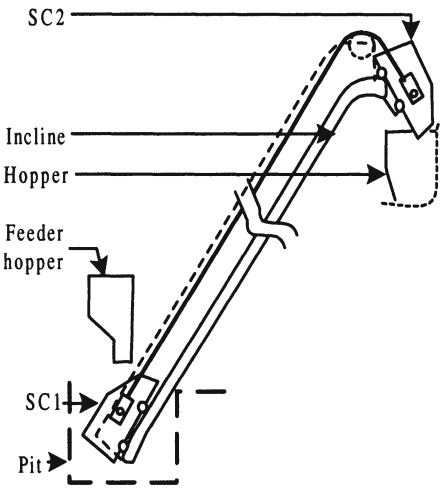


Figure 16.18 Skip cars feeding the burden to the blast furnace: They move in adjacent sets of rails. When one is in the pit receiving charge material, the other is at the top delivering material above the small bell.

Normally the scale car operator is given a charging sequence and the weights of individual charges. A typical charging sequence is Ore-Coke-Lime Stone-Ore-Coke-Coke designated as OCSOCC/. The '/' at the end indicates opening of the large bell. The charging sequence is decided by the technical personnel accountable for the furnace and its operation. Variation in the quality of the burden materials and changes in the blast furnace conditions may call for changes in the sequence and/or the weights of individual items. Sometimes two distinct successive charging sequences, may be repeated cyclically. All these are done to ensure equitable distribution of burden on the top and to avoid any abnormal operation of the furnace. Further, an associated feed monitoring system operates an interlock. This ensures that the scale car operator sticks to the feed schedule given to him. With the lumpy material, close control of weight collected for dumping into the furnace at each feeding, is difficult. Hence, whenever a material is collected for feeding, corrections for deviations in the preceding charge of the material are carried out. In this manner, it is ensured that the cumulative charge of each material over a definite period is at the desired level. The burden fed at the top is not homogeneously distributed at the top. Various factors contribute to this: -

⇒ The burden material is lumpy and of different sizes.
⇒ The size distribution of individual items, is not the same.
⇒ When dropped from a height by opening the large bell, the finer particles fall down directly while the coarser ones may roll to the side.

⇒ Since 10 t to 20 t load of each item is dumped one above the other, their mixing is not uniform.

Various innovations are in vogue to bring better uniformity of material distribution. Position of charges deposited successively is changed so that a more equitable charge distribution is attained.

All blast furnaces have two or more stock level indicators. These are mostly guided steel rods with wide horizontal plates at the bottom. They rest on top of the furnace stock (similar to a float type level-gauge). The end of the rod protruding at the top indicates the stock level. The same is converted into suitable output using a displacement transducer. The furnace filled with the burden corresponds to zero of the stock level. As the burden descends, the stock level reduces. A low enough stockline to accommodate a full burden charge is a pre-condition to charging.

Stoves

The blast of air at the tuyeres of the blast furnace is heated in the stoves. Each blast furnace may have three or four stoves attached to it. The air is heated in the stove in a regenerative manner. For this, a fuel-air mix is burned in the combustion zone of the stove; the hot flue gas from here passes over the active zone of the stove. The stove is first heated in this manner and it stores the heat energy. The cold blast of air is subsequently passed through the stove; it gets heated by absorbing the stored heat energy in the stove. The hot air from the stove is blown into the furnace. This sequence of heating the stove and transferring the heat to the blast is repeated cyclically.

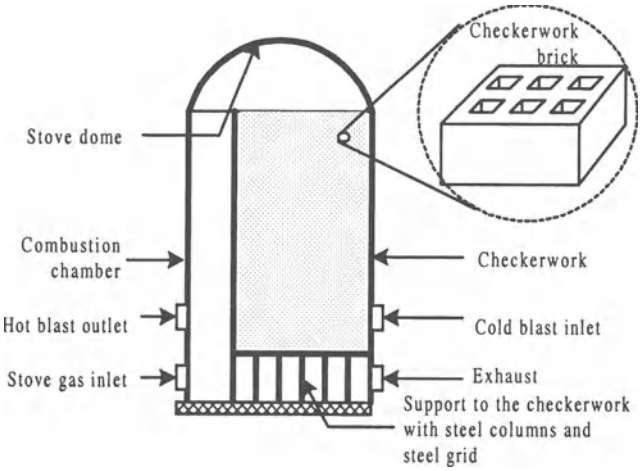


Figure 16.19 Schematic diagram of the stove for the blast furnace

Figure 16.19 shows a typical stove. It is dome shaped and size-wise almost as big as the blast furnace itself. The steel dome has a thermal insulation in the form of a suitable brick lining inside it. The combustion chamber is to a side. Rest of the dome has chequered ceramic brickwork – similar to a honeycomb. Typically, a stove operates cyclically through two phases. In the first phase (called the 'Heat Phase') the fuel-air mixture led through the inlet into the combustion zone, burns. The hot gases from the combustion chamber pass through the dome and the chequered brickwork. The zigzag passage ensures effective heat transfer to the

brickwork. Finally, the gases are led out through the exhaust. Heating of the stove in this manner continues until the dome and the checkerwork stack-area are sufficiently hot. This completes the heating phase. Then the fuel and the air mix input are turned off. The second phase is the air blast phase. The air blast to be heated is let in at the cold blast inlet. During passage through the chequerwork, the blast absorbs the heat stored in the brickwork and its temperature rises. It goes out through the hot blast outlet and to the blast furnace tuyeres. This completes the second phase – called the 'Blast Phase'.

The blast of air required is blown through a turbo-blower. Normal operation of each stove is to be controlled and operation of all stoves coordinated to ensure that the blast furnace gets a steady blast at the required rate and temperature. Figure 16.20 shows the scheme in simplified form. At any time, only one stove is 'on-blast' and the other two are 'on-heat'. Temperature of the blast into the furnace is regulated by continuously controlling the proportion of the hot air coming through the stove and the cold air bypassing it [Figure 16.20 (b)]. Consider an instant when Stove S_1 is on blast. The main valve V_{B1} is open. The hot blast valve H_1 and the cold blast valve C_1 are open in a specific proportion. V_{B2}, V_{B3}, H_2, H_3, C_2 and C_3 are closed. As soon as stove S_1 goes on blast, it is at its hottest and transfers maximum heat to the blast; the level of opening of V_{B1} will be at the lowest and that of C_1 at the highest expected. The mix will be of the desired temperature. Any deviation from the desired value of temperature is corrected by adjusting V_{B1} and C_1. Thus if the temperature is higher than desired, the opening of V_{B1} is reduced and that of C_1 increased simultaneously. As the blast proceeds, the hot blast temperature drops steadily. In turn the V_{B1} opening is increased and C_1 opening reduced. This is continued – all the time maintaining the hot blast temperature – until C_1 is closed (say) 80 %. This is the time to change over stoves. At this stage, S_2 may be put on blast. In automated systems in vogue today, the changeover will be effected in 3 to 10 minutes. Each stove will be on blast for 45 minutes to 150 minutes in turn. The rest of the time, – 1.5 hr. to 3 hr. minus the changeover time – it will be on heat.

During changeover, the sequence of valve operations, is coordinated to ensure:

⇒ undisturbed blast furnace function and

⇒ no fuel wastage or escape, to avoid hazards

A typical sequence of operations to put the stove on blast [Figure 16.20 (b)], is as follows: -

⇒ Close the fuel inlet valve

⇒ Close the air inlet valve (*i.e.*, air let in with the fuel for its burning)

⇒ Close the chimney valve

⇒ Open the cold air blast bypass valve to build up pressure in the stove without upsetting blast pressure.

⇒ Open the hot blast valve

⇒ Initiate cold/hot blast control to regulate hot blast temperature.

The sequence of valve operations to take a stove off, are: -

⇒ Shut off the cold blast valve

⇒ Shut off the hot blast valve

⇒ Depressurize the stove by opening the 'blow-off' valve.

⇒ Open air (supply to fuel gas mix) inlet valve.

⇒ Open fuel gas valve

Normally, a fraction of the blast furnace gas itself is used as the fuel for heating the stoves. The stove-dome temperature and the stack-chequer-work temperature – are monitored to ascertain stove status. If the dome gets hot faster, the fuel supply is reduced. If the stack gets hotter, the fuel is weak and requires enrichment – if necessary by external fuel injection.

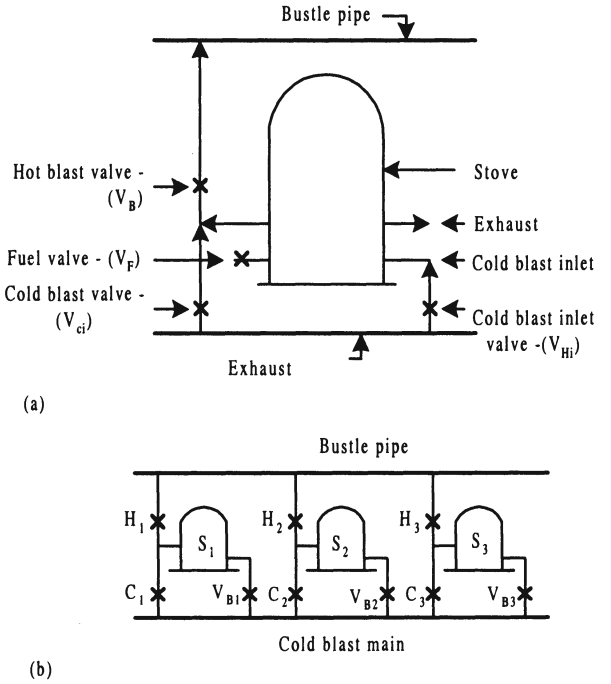


Figure 16.20 Scheme of control and co-ordination of stove operations: (a) Single stove (b) Group of 3 stoves

Blast Furnace Gas Cleaning

The gas coming out of the blast furnace through the downcomer, (Figure 16.17), has flue dust in it. Normally, it may extend up to 6 mm size (under abnormal conditions, for short time, large lumps of coke too may get in). These are to be removed to avoid the blast furnace gases clogging passages *en route* and creating other problems. The cleaning is carried out in stages. A dust catcher, where the gas flows down and turns upwards with a steady velocity, captures comparatively larger sized particles (>800 μm size). The following stage has a Venturi washer where 90 % to 95 % of the dust is removed. A following electrostatic precipitator stage cleanses the gas of particles down to the μm level.

Moisture and Oxygen Addition

In some cases, the air blast is enriched with oxygen. This increases furnace productivity. Every 1 % increase in O_2 increases the hot metal output by 2 % to 3 %. The coke rate also comes down. O_2 is added at the blower input or at the tuyeres under pressure. The amount of moisture content in the coke is varying in

nature. Measured quantity of steam is added to the blast to make the relative proportion of moisture constant.

16.3.4.5 Blast Furnace Process Description

The blast furnace along with the main accessories described can be looked upon as a multiple-input multiple-output system of the type in Figure 16.21. The basic aims are to produce hot metal of consistent quality and maintain high productivity. From past experience and operational data, the input quantities, their rates of feed and the furnace operating conditions are computed and maintained. The model of Figure 16.21 is valid for the regular operation of the furnace. The relations connecting hot metal – its quantity as well as quality to each of the inputs – will be available as quantitative data. Similar data on the changes in the hot metal as well as slag – again quantitative as well as qualitative – due to the changes in the individual constituents, will also be available. Each such relation involves a proportionality factor as well as a time-delay factor (in the simplest of models). The nature and complexity of blast furnace operation, entails a variety of time-delays. However they fall into three broad categories: -

- ⇒ Transit time of the hot blast through the furnace. This extends from 2 s to 5 s depending on the furnace operating conditions.
- ⇒ Time for burden movement from stock-line to hot metal and slag. This extends from 5 hr. to 10 hr.
- ⇒ Other quantities injected at the tuyeres. Fuel injected to increase heat input, increases the temperature above the hearth in seconds. But for the change to percolate upwards, to the top may take an hour or two. Similarly, lime may be injected to bring down the temperature. It may take an hour or two to take full effect.

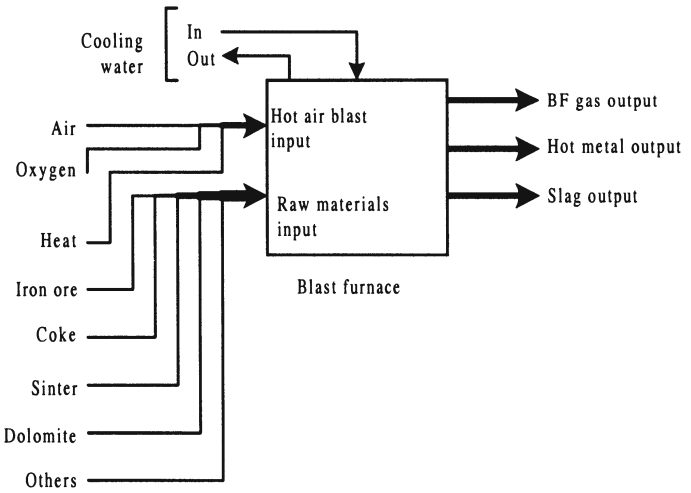


Figure 16.21 Blast furnace as a multiple-input multiple-output system

With such a well quantified model and regular observations, changes needed for each input quantity are computed; these are carried out through suitable commands and control actions. This task is one of the primary activities of the operating personnel of the furnace. As mentioned earlier, maximization of production and

minimization of coke rate without jeopardizing the furnace health, are the main criteria for decisions here. The above relate to the regular operation of the blast furnace. During starting of the furnace and its stopping or shut-down for various reasons, specific schedules are followed. The burden, the blast parameters and sequencing for each of these, are different. These too come under the purview of the furnace operating personnel.

16.3.4.6 Functions of the Instrumentation Scheme

The direct function of the blast furnace instrumentation scheme is 'status monitoring' as with any other process. This comprises of measurement of process variables, their temperature, flow, weight, pressure and chemical compositions. *Prima facie,* they are checked against expected values to confirm that the process is 'on-track'. Apart from this, a number of indirect functions are also served by the instrumentation scheme: -

On-line Corrections

A number of process variables are continuously sensed; measures to regulate them to be within restricted bands are also carried out. Most common among these are: -

- ⇒ *Stock line*: Stock level indicator shows the stock level; when low, it is corrected by resuming burden feed.
- ⇒ *Hot blast flow low or high*: Increase or decrease the same as the case may be, by changing the blower speed or otherwise. The control is at the blower stage.
- ⇒ *blast temperature high or low*: If it is cyclically repeated, increase fuel ratio. If not, control cold/ hot blast ratio.
- ⇒ *Cold blast valve position at the minimum*: Change stove.
- ⇒ *Stove dome temperature high (low)*: Increase (decrease) fuel rate.
- ⇒ *Cooling water outlet temperature too high*: Increase water flow rate. Isolate any segment that is being overheated and investigate the same.
- ⇒ *Top gas dust content too high*: Gas cleaners require attention.
- ⇒ *Indirect blast temperature*: It is controlled by adjusting the ratio of the hot and cold blasts (through respective valves).
- ⇒ *Furnace top pressure*: Controlled by controlling top pressure
- ⇒ *Hearth temperature*: Controlled mainly by controlling the blast temperature

Health Monitoring

These functions result in safety releases, alarm actuation, shut down *etc.* Some of the common ones are: -

- ⇒ *Top gas pressure too high*: Pressure is released by opening the pressure-release valve.
- ⇒ *Stock not-moving*: (Deduced by sensing the stock line). This may require more detailed investigation and corrective measures. Short-term measures are through blast while the long term measures are through the burden.
- ⇒ *Specific areas of the furnace wall getting hot*: calls for detailed investigation. Corrective steps may extend to lining the inside of the furnace by specific refractory material if erosion of the areas is detected.

Process Optimization

There are mainly three aspects to this.

⇒ *Hot metal composition*: A consistent hot metal quality has to be ensured. This is done by working back from the desired hot metal composition and arriving at individual constituents required and their feed rates. These are corrected continuously for any change in raw material composition. Maintaining slag basicity, is also part of this. Note that burden changes affect the hot metal composition with a lag of 5 hr. to 10 hr. Blast effect is much more rapid.

⇒ *Hot metal temperature*: A high and consistent value is desired. The desired value is dependent on the composition also. Once the constituents required to ensure the desired hot metal composition are decided, a heat balance is done. Blast rate and the temperature to support the same are worked out.

⇒ *Coke Rate*: Energy input from coke is secondary to its function in the reduction of iron. Hence, the blast temperature is kept as high as the system permits. This reduces the amount of coke to be fed. In turn, there is more room for feeding iron ore and increasing productivity.

Energy Balance:

As mentioned earlier the burden composition and proportioning have to ensure that the minimal energy required for the process has to be supplied. However, the actual energy supplied is more than the minimum. All sources of energy supply, energy absorbed in the process and wasted are ascertained.

Heat inputs: -

⇒ Through blast (Sensible heat of air and heat energy supplied through fuels injected)

⇒ Heat input through coke

⇒ Heat released through various oxidation reactions

Heat absorption or heat carried away: -

⇒ Heat absorbed by various reduction reactions

⇒ Heat absorbed or carried away by other reactions-forming slag

⇒ Heat carried away by the blast furnace gas – sensible heat as well as heat in CO and H_2

⇒ Sensible heat in hot metal and latent heat of melting

⇒ Sensible heat in slag and latent heat of melting

⇒ Heat carried away by the cooling water (quantity × temperature rise).

⇒ Heat given out by radiation

'Energy-Balance' computations are carried out at regular intervals by combining all the above. This has a two-fold purpose: -

⇒ Sources of energy wastage or 'leakage' are identified and remedial measures taken.

⇒ Specific energy consumption – joules/kg of hot metal – is minimized whenever possible.

16.3.4.7 Investigative Studies

Due to the size, closed nature and the high temperature of operation, the blast furnace is not amenable for precise and detailed study and analysis. The reactions, their environment and the various operational sequences involve a substantial amount of intelligent guesswork. As such, detailed investigations are carried out regularly by all plants for a better understanding of the process. Through such investigations and measures based on them, they try to improve the performance.

All these call for relevant investigative studies to be carried out. Catering to this aspect of the blast furnace working, is an important function of the installed instrumentation scheme (In contrast, majority of the industrial processes, focus attention on production, productivity and related activities. Investigative studies are done separately – if necessary – in pilot plants in R & D organizations).

16.3.4.8 Quantities for Instrumentation

Various quantities measured and displayed are given in Table 16.1. Possible uses of each are also listed. The quantities and their uses mentioned in the table, do not constitute the universal practice. There can be substantial variations from this list from unit to unit. Some general observations are in order here: -

⇒ All the temperature measurements are carried out using thermocouples fixed in respective positions. The exceptions are
- Use of thermocouple to measure the temperature of hot metal by dipping the thermocouple in the hot metal for a short time.
- Use of optical pyrometer to sense the hearth temperature – non-contact type.
- Use of thermistors or other types of sensors to sense cooling water inlet and outlet temperature separately for each segment

⇒ All gas and air flowmeters are of the differential pressure type. Cooling water flow rate measurement also can be of the differential pressure or other types.

⇒ Weighing of each of the constituents of the burden is done through load cells. Coke is weighed through a weigh hopper after screening. The hopper is supported on load cells.

⇒ All other materials are fed through scale cars mounted on load cells. Since each charge cannot conform to precise weight, the surplus or deficiency in each charge is made up in the subsequent charge.

⇒ Moisture content in coke and other burden materials is estimated by a weighing-drying-weighing sequence (loss of weight method). Cobalt based neutron moisture gauges are being tried but are to become acceptable.

⇒ Coke, ore and other materials, are analyzed chemically in the laboratory for their composition. This is carried out on samples drawn from each lot of material received. The results of analysis form the basis for burden and heat balance computations.

⇒ Flux is analyzed chemically in the laboratory to determine its constituents and their relative proportions.

⇒ Blast furnace iron is analyzed in the laboratory chemically to ascertain its composition. In addition, spectroscopic methods are also used. This gives a quick estimate – though not as accurate as the chemical analysis method. The iron (hot metal) and slag analysis is also carried out in this manner on samples drawn from each tap.

⇒ Calorific values of coke and blast furnace gas are determined in the laboratory from respective samples.

⇒ Due to the size and spread of the blast furnace and its accessories, various measurements are done at different locations. All such information is brought to the centralized Data Acquisition System (DAS). This also includes the analysis results of the blast furnace gas, coke, hot metal, flux

and the burden material. All such tests are done in the laboratories on an off-line basis. The results are communicated to the DAS through a serial link.

16.3.4.9 Computations

As shown in Table 16.1, the values of various physical variables measured are displayed close to the point of measurement wherever feasible and at points where the value is key to a process decision. These apart, these values are transmitted to a central computer. The computer essentially functions as a DAS. As part of its assigned tasks, it carries out a number of in-depth computational activities. These are briefly dealt with here: -

Heat Balance

Well-established structured-procedures are available to do heat balance calculations [Wegmann (1984)]. The steps involved in this are as follows: -

- ⇒ Compute the sensible heat in the input quantities. The heat content of the hot blast is the main contributor to this.
- ⇒ Compute the equivalent heat energy input through fuels. The calorific value of coke, mass of coke and the calorific value of any fuel injected at the tuyeres and the mass of the fuel, are the main contributors to this.
- ⇒ Compute the heat of formation of each constituent of the burden. Mostly these are negative.
- ⇒ Use all the above values and compute the net heat input.
- ⇒ Compute the sensible heat carried away by the hot metal, slag and the blast furnace gas.
- ⇒ Compute the heat energy available in the blast furnace gas (Calorific value and the mass of respective constituents.).
- ⇒ Compute the heat of formation of the output constituents – namely hot metal, slag and blast furnace gas. Account for the fact that hot metal and slag are in liquid form.

For convenience in working, all the heat quantities are reduced to a common platform – e.g., water equivalent or Kg of hot metal. Combining the three quantities above, the net heat outflow is computed. The heat input and outflow must balance. Further, the heat input must be sufficient for the reactions to take place at the appropriate locations; if not productivity will be affected adversely. Regularly, these calculations are carried out and the process corrections done.

Material Balance

Material balance calculations are carried out on the same lines as the heat balance. Broadly, this comprises of the following: -

- ⇒ Estimate productivity as kg of hot metal /hr.
- ⇒ Compute iron ore and sinter to be fed on a 'per-kg of iron per-hour' basis for the expected level of productivity. Make allowance for 0.2 to 0.8 % of FeO content (by weight in the Slag).
- ⇒ Compute the amount of coke required. This is to be based on the carbon requirement for reduction of iron. The reduction due to the amount of hydrogen in the moisture content present and the amount of carbon content in the sinter are to be accounted for here.
- ⇒ Compute the amount of hot blast at the desired temperature to be fed.

⇒ Estimate the quantitative level of each of the impurities present in the iron ore. This is to include every constituent of the ore. From the chemical balance arrived at earlier, compute the basic amount of each of the fluxes to be fed to form the slag. This may also require additional coke, which has to be added to the coke estimated earlier.

Efficiency

The heat carried away by the cooling water is computed and the heat lost by radiation estimated. The sensible heat in hot metal, slag and the blast furnace gas are also to be computed. Out of these, the sensible heat in the hot metal is recovered substantially. However, the others are lost. Using these and the heat input, the efficiency is computed.

Indices of performance

A variety of indices of performance is in use with the blast furnace operation. Most common amongst these (with the ranges) are as follows: -

⇒ Unit output (hot metal) (t/m^3 day) : 1.4 to 2.1
⇒ Specific consumption of coke (kg/ton of iron) ; 450 to 600
⇒ Slag basicity : CaO/SiO_2 : 0.85 to 1.2
⇒ % O_2 content in blast : 21 to 28
⇒ Additional fuel [$kg(m^3)$ /t of hot metal]
⇒ Yield of iron/kg of burden
⇒ Specific energy consumption - joules/kg of hot metal

These are computed regularly to ascertain process performance

Logging

The collected data and the computed indices are logged in relevant formats and databases. This facilitates the performance to be ascertained and compared with past performance on a continuing basis.

Modeling

The size of blast furnace, its closed nature of working and the high temperature of operation, prevent a point by point or instant to instant monitoring of its operations. The delay of 5hr to 10hr, in the effect of the burden being felt at the hot metal stage, adds to this. Any decisions for change or measures to counter malfunctioning of the furnace cannot be based solely on a precise knowledge of the operating conditions. Technical expertise of the operating personnel, their experience and 'intuitions' compensate for this.

Powerful PCs – computing capacity and memory-wise – have become widely available in recent years. This has also spawned effective computational algorithms and a variety of software. All these together have opened the possibility of modeling the blast furnace on-line. The simplest approach to modeling can be on the following lines: -

⇒ Consider a set of operating conditions with a steady burden and a constant blast.
⇒ Knowing the chemical reactions at different levels, the furnace can be considered as frozen.

⇒ Divide the furnace into a three dimensional grid.
⇒ Each node of the grid is to be treated as a source or sink of heat flux along with a heat capacity. Each link between two adjacent nodes has a thermal conductivity.
⇒ With the above information and assumptions, one can do a thermal modeling.
⇒ If necessary, corrections to the scheme are applied considering the surface thermal profile decided by the measurement of blast furnace surface temperatures by thermocouples.
⇒ The temperatures at different zones are determined. Hot spots are identified.

Effects of changes on operating conditions due to changes in burden and blast can be studied using the model. Predictions regarding changes in operating conditions and performance indices can be made.
One can refine the model by accounting for the changes in chemistry with temperature at different zones. Hazardous conditions can be predicted. Effects of possible remedial measures can be simulated and compared prior to a final decision. Closeness of the model to actual situations can be ascertained by comparing predicted results with actual observations. As the reliability of the model improves, it can be used to yield more information and used more effectively. These can be in terms of

⇒ performance improvement
⇒ health monitoring
⇒ process corrections and
⇒ operational projections.

16.4 User Configurable Instrumentation Scheme

PCs have become widely and universally available. They have the provision to support external circuit cards. Such circuit cards occupy specific slots in the PC. The connection is through well-established interface buses. This has opened up the possibility of configuring any instrumentation scheme around PCs. Figure 16.22 shows such a typical user configurable instrumentation scheme in block diagram form. The 'Data Acquisition Card' and the 'Signal Conditioning Unit' are standard circuit cards. In either case, the user makes a choice from among a variety available and configures the whole system.

16.4.1 Signal Conditioning Unit

The signal-conditioning unit provides the necessary amplification to the signal from the sensor and presents an output, which can be directly handled by the data acquisition card. Typically, the output is in the 0V to 5V form.
The signal-conditioning unit may do several other additional functions. Excitation for the sensor (AC or DC as the case may be), isolation, filtering, demodulation and multiplexing are the main functions. The signal-conditioning unit provides these in different combinations. These functions will be programmable.

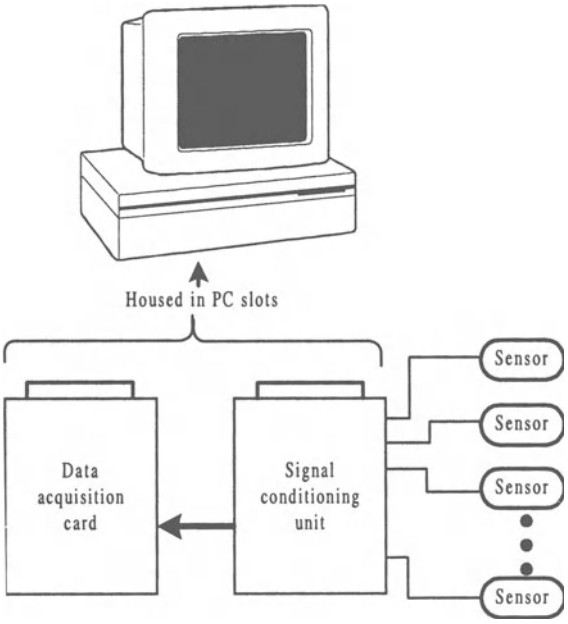


Figure 16.22 Typical user-configurable instrumentation scheme

16.4.2 Data Acquisition Card

The data acquisition card converts the signal conditioning unit output to digital form - its main function is A-D conversion. The converted output may be in parallel or serial form and directly fed to the PC. In addition, it may have timers, D-A converters and a specific number of digital outputs. These are for control and display functions.

16.4.3 Software

The instrumentation scheme configured as above is made as a workable unit through associated software. The software – at least the platform – is provided by the add-on card vendors; the software provided, are of four types: -

⇒ Drivers
⇒ Utilities
⇒ Data analysis
⇒ System analysis

16.4.4 Drivers

The driver software configures the hardware, programs the same and does debugging. The driver functions for the signal conditioning unit are as follows;-

⇒ Set the amplifier gain

⇒ Adjust the filter parameters
⇒ Carry out any corrections for ambient temperature variations or other extraneous influences.
⇒ In case the sensors are multiplexed, select each sequentially.
⇒ Carry out diagnostic tests like open thermocouple, breakage of strain gauge wire or RTD wire.
⇒ Carry out any linearization necessary

The driver functions for the data acquisition card may take various forms. The functions of direct relevance to the instrumentation schemes are as follows:-

⇒ Set the sampling rate.
⇒ Set the ADC resolution
⇒ Set the format for reading the ADC output.
⇒ Set the mode for the ADC - polled or interrupt driven and so on.
⇒ Check for lower and upper limits, crossing alarm-threshold-levels and so on.

16.4.5 Utilities

Typically the utilities configure the system to provide the output in the desired format like 4 to 20 mA, meter type of indication, function as a chart recorder and so on.

16.4.5.1 Data Analysis

The samples acquired through the data acquisition card may have to be analyzed and presented as output in a desired format. This can take the form of a simple reconstruction, filters for smoothening, checking for limits and alarm values and so on.

16.4.5.2 System Analysis

The data acquired or the signal reconstructed above may have to be processed at a higher level. This may involve modeling and associated system level studies like correlation, system analysis and the like.

Observations:-

⇒ The user can treat the dedicated instrumentation scheme as a black box and fit it into the application directly. In a PC based scheme, user expertise is called for, in the proper selection of combinations of signal conditioning units and data acquisition cards and subsequent software development.
⇒ The PC based scheme essentially provides an 'Open Architecture'. The user can choose individual circuit cards from vendors and combine them to form his application.
⇒ The scheme can be easily modified and reconfigured for other applications.
⇒ In a PC-based scheme, one trades off cost against performance; *i.e.*, if the performance is to be on par with a dedicated scheme, the cost is one order higher. Standard signal conditioning units and data acquisition boards are general in nature and are aimed at a wider clientele. They may not be optimized for a specific application on hand.

Table 16.1 Quantities normally measured with a Blast Furnace and their possible uses

Item		Sensed quantity	Remarks
Hot metal		Temperature	Carried out on a batch by batch basis The results are used for process corrections
		Composition	
Slag		Temperature	--Do --
		Composition	
Burden	Iron ore	Composition, Physical properties, Weight	Weight of every constituent is measured at the input stage Combustion analysis of coke samples are carried out for every batch Proportion of constituents is changed to yield predicted composition for hot metal and desired basicity for slag
	Coke	Same as above, Moisture content, Calorific value	
	Lime	Impurity content, Weight	
	Dolomite		
	Other items		
Blast		Temperature Moisture content	If necessary lime and moisture injection are done with the blast
Stoves		Air blast flowrate, pressure & temperature; Valve positions of hot & cold blasts; Dome &stack temperatures at selected points; Air & fuel rates (when on heat)	Blower pressure and flowrate adjusted to maintain those of blast; Relative positions of hot & cold blast valves adjusted to maintain blast temperature; Hot blast valve position used to decide changing of stoves Air-Fuel ratio (for stove on heat) adjusted for optimum efficiency

Table 16.1 (continued)

Item	Sensed quantity	Remarks
Hearth	Sense temperature	
Cooling water	Inlet temperature, outlet temperature, flow rate	The measurement is done for each segment separately Helps in identifying incipient faults to the refractory lining
Furnace wall	Temperature at regular intervals in the periphery at selected heights in the hearth, bosh & stack areas and underneath the stack	-- Do --
Stock top	Stock-line indicators – at least two numbers; temperature	Ascertain burden movement
	Temperature	Some sensors are kept above stock line; others are kept 1.5 m – 2 m below stock line; identify severe gas channelling
Blast furnace top	Top pressure	
	BF gas temperature; gas flowrate BF gas analysis	Ascertain BF gas quality, calorific value *etc.*
Electrical energy	Blast blower; Water pump; Skip car drive; Other assorted items	Account for all electrical energy consumed in carrying out energy balance

Appendix A

Basics of z - transforms

A variety of operations is done on numbers in microcomputers. When these numbers represent samples of signals at regular intervals, operations on them are effectively handled using z-transforms. Z-transform is to sampled-data, what Laplace transform is to continuous data. To this extent, there is a close parallel between the two. Our discussion here is limited to the applications of interest to us. Hence z - transform is introduced solely from a functional point of view and only properties relevant to our application, are dealt with [Oppenheim and Schafer, Rabiner and Gold].

Consider a sample sequence $[x_i]$ composed of samples x_0, x_1, x_2, x_3,.. x_n.., representing a signal.

$$[\, x_i \,] \;=\; [x_0, x_1, x_2, x_3, \ldots x_{n\ldots.}] \qquad \text{(A.1)}$$

Here $[x_i]$ may be a sequence of mere numbers, which may conform to some specific norms. Alternately $[x_i]$ may be formed by sampling a continuous signal $x(t)$ at regular intervals of T seconds. In the latter case, x_0 represents the signal at time zero seconds, x_1 that at time Ts, x_2 that at time $2T$s and so on. Using z-transform the sample sequence $[\, x_i \,]$ may be represented as

$$X(z) \;=\; x_0 z^{-0} + x_1 z^{-1} + x_2 z^{-2} + x_3 z^{-3} + \ldots\ldots \qquad \text{(A.2)}$$

Here z^{-n} represents a time delay operator of n periods, i.e., nTs. $X(z)$ represents the full sample-sequence of the signal. It is referred to as the 'z-transform' of the sequence $[x_i]$.

Properties:-

- ⇒ z-transforms possess all linearity properties - Associativity, Commutativity and the like.
- ⇒ Multiplication of a sample by z^{-k} is equivalent to delaying it by k sample periods.
- ⇒ If the z-transform of a signal sample sequence is represented by an arbitrary function $F(z)$, then the sample value at the n^{th} sampling instant, is the coefficient of z^{-n} in F(z). To obtain this, $F(z)$ is first expressed as a polynomial in z^{-1} and the coefficient of z^{-n} identified, which is the desired sample value.
- ⇒ If $\{\, x_n \,\}$ is the input sequence to a linear time invariant system, the output sequence is obtained from the relation

$$Y(z) \;=\; X(z)\, G(z) \qquad \text{(A.3)}$$

where

- $X(z)$ is the z-transform of the input sequence and
- $G(z)$ is the z-transform of the sequence $\{g_i\}$ obtained from the unit impulse response $g(t)$ of the system.

The last property warrants an elaboration. Fig.A.1, shows the linear time invariant system in block diagram form. $G(z)$ is the z-transfer function of the system. Consider $X(z)$ as a unit impulse with

$$X(z) \;=\; 1 \qquad \text{(A.4)}$$

With this, EquationA.3 becomes

$$Y(z) = G(z) \tag{A.5}$$

$G(z)$ can be represented as a polynomial in z^{-1} as

$$G(z) = g_0 z^{-0} + g_1 z^{-1} + g_2 z^{-2} + g_3 z^{-3} + \ldots\ldots \tag{A.6}$$

Substitution in EquationA.4 gives

$$Y(z) = g_0 z^{-0} + g_1 z^{-1} + g_2 z^{-2} + g_3 z^{-3} + \ldots\ldots \tag{A.7}$$

This represents the Unit Impulse Response of the system. Here g_n forms the response of the system at the n^{th} sampling instant following the unit impulse input of EquationA.4. For the case of the more general input $[x_i]$ of EquationA.2, $Y(z)$ can be obtained by substituting $X(z)$ from EquationA.2 and $G(z)$ from EquationA.6 in EquationA.5. With this we get

$$y_n = \sum_{i=0}^{n} g_i x^{-(n-i)} \tag{A.8}$$

EquationA.8 gives the value of y_n in terms of the unit impulse response of the system and the previous input samples. This is the discrete equivalent of the convolution integral for continuous linear time invariant systems. Depending on the nature of the relation between $X(z)$ and $Y(z)$, two broad cases arise.

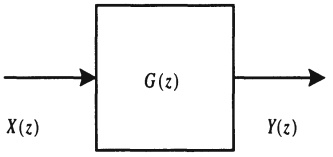


Figure A.1 Linear time invariant system in block diagram form with an input sequence

Case 1: Finite Impulse Response (FIR) system

The impulse response represented by Equation A.6 is characterized by a limited number of terms - say g_0 to g_k. With this, Equation A.8 becomes

$$y_n = \sum_{i=0}^{k} g_i x^{-(n-i)} \tag{A.9}$$

This is a restricted case of Equation A.8 where only a definite and limited number of terms is to be considered. Often the computational work to be carried out here is high. However, the scheme is inherently stable.

Case 2: Infinite Impulse Response (IIR) system

$G(z)$ can be represented here as

$$G(z) = \frac{Q(z)}{P(z)} \tag{A.10}$$

where $Q(z)$ and $P(z)$ are polynomials in z^{-1} in the form

$$P(z) = \sum_{0}^{L} p_i z^{-1} \tag{A.11}$$

$$Q(z) = \sum_{0}^{M} q_i z^{-1} \tag{A.12}$$

Here M and L are positive integers representing the degrees of the respective polynomials. Substituting in Equation A.10 and cross-multiplying, the relation to be satisfied by y_n is obtained as

$$y_n p_0 + y_{n-1}p_1 z^{-1} + y_{n-2}p_2 z^{-2} + \ldots + y_0 p_n z^{-n} + y_{-1}p_{n+1}z^{-(n+1)} + \ldots + y_{n-L}p_L z^{-L}$$
$$= x_n q_0 + x_{n-1}q_1 z^{-1} + x_{n-2}q_2 z^{-2} + \ldots + x_0 q_n z^{-n} + x_{-1}q_{n+1}z^{-(n+1)} + \ldots + x_{n-M}q_M z^{-M} \quad \text{(A.13)}$$

It is customary to take $p_0 = 1$. With this, Equation A.13 can be rearranged as

$$y_n = -\sum_{i=1}^{L} p_i y_{n-1} z^{-1} + \sum_{j=0}^{M} q_j x_{n-j} z^{-j} \quad \text{(A.14)}$$

Equation A.14 shows that y_n is obtained as a weighted linear sum of

⇒ samples of the output sequence $[y_n]$ up to the $(n\text{-}1)^{th}$ sample and

⇒ samples of the input sequence $[x_j]$ up to the n^{th}.

Equation A.14 is the difference equation counterpart of the transfer function representation of Equation A.13. Systems of this type, relate $[y_i]$ and $[x_j]$ through a recursive relationship; y_n is defined in terms of a definite number of previous samples of $[y_i]$ and a definite number of samples of $[x_j]$ up to x_n. Two characteristics of the system are

⇒ The Impulse Response of the System is composed of an infinite number of impulses. Hence, the system is called the 'Infinite Impulse Response (IIR) system'.

⇒ The system is stable only if all the roots of $P(z)$ lie within the Unit Circle around the origin.

Frequency Response

Consider the n^{th} sample of the sequence $[x_i]$. It occurs at time nT. It represents an Impulse of strength x_n at time nT. It has the Fourier Transform

$$X_n(j\omega) = x_n \exp[-jn\omega T] \quad \text{(A.15)}$$

This can also be obtained by substituting

$$z = \exp[j\omega T] \quad \text{(A.16)}$$

in the corresponding z transform. Generalising, this holds good for z-transforms of sequences as well as transfer functions. Thus the frequency spectral characteristics of sampled signal sequences and z-transfer functions of systems, filters etc., are obtained by the substitution of Equation A16. All such frequency spectra have a periodicity in the ω plane with period $(2\pi/T)$. The periodicity in the frequency domain implies two things:-

⇒ The frequency characteristics in the baseband – *i.e.*, from $(-\pi/T)$ to $(+\pi/T)$ – is repeated in all subsequent periods.

⇒ For all physically realizable systems and signals,

$$f(j\omega) = \overline{f(j\omega)} \quad \text{(A.17)}$$

or $f(j\omega)$ and $\overline{f(j\omega)}$ are complex conjugates. Combining the above two, we find that the full frequency information in the Fourier transform of any periodically sampled function, is contained in the band $(-\pi/T)$ to $(+\pi/T)$, where T is the sampling period.

Appendix B

Linear Operations with one Dimensional Discrete Variable

The following have been assumed in the relationships below:

⇒ x is the independent variable.

⇒ y is the dependent variable.

⇒ h is the sampling interval in x.

⇒ $y_0, y_1, y_2, \ldots$ .etc., are the values of y at zeroth, first, second, third, . . . *etc.*, sampling instants.

B.1 Formulae using forward differences

$$\begin{aligned}
\Delta y_0 &= y_1 - y_0 \\
\Delta y_1 &= y_2 - y_1 \\
\Delta y_2 &= y_3 - y_2 \\
\Delta y_3 &= y_4 - y_3
\end{aligned}$$

$$\begin{aligned}
\Delta^2 y_0 &= y_2 - 2y_1 + y_0 \\
\Delta^2 y_1 &= y_3 - 2y_2 + y_1 \\
\Delta^2 y_2 &= y_4 - 2y_3 + y_2 \\
&= \\
\Delta^3 y_0 &= y_3 - 3y_2 + 3y_1 - y_0 \\
\Delta^3 y_1 &= y_4 - 3y_3 + 3y_2 - y_1 \\
\Delta^4 y_0 &= y_4 - 4y_3 + 6y_2 - 4y_1 + y_0
\end{aligned}$$

B.1.1 Derivatives

$$y'(x_0) = \frac{1}{h}\left(\Delta y_0 - \frac{1}{2}\Delta^2 y_0 + \frac{1}{3}\Delta^3 y_0 - \frac{1}{4}\Delta^4 y_0 + \ldots\right) \tag{B.1}$$

Truncating EquationB.1 to 1, 2, 3, . . . etc., terms and substituting from the relevant equations above, we can get different approximations to the derivatives.

First approximation:

$$y'(x_0) = \frac{1}{h}\left(y_1 - y_0\right) \tag{B.2}$$

Second approximation:

$$y'(x_0) = \frac{1}{2h}\left(-y_2 + 4y_1 - 3y_0\right) \tag{B.3}$$

Third approximation:

$$y'(x_0) = \frac{1}{6h}\left(2y_3 - 9y_2 + 18y_1 - 11y_0\right) \tag{B.4}$$

Fourth approximation:

$$y'(x_0) = \frac{1}{12h}\left(-3y_4 + 16y_3 - 36y_2 + 48y_1 - 25y_0\right) \tag{B.5}$$

B.1.2 Interpolation and Extrapolation

$$y(x) = y_0 + x\Delta y_0 + \frac{x(x-1)}{2!}\Delta^2 y_0 + \frac{x(x-1)(x-2)}{3!}\Delta^3 y_0 + \frac{x(x-1)(x-2)(x-3)}{4!}\Delta^4 y_0 + \ldots\ldots \quad \text{(B.6)}$$

General case

$$y(x) = y_0 + \frac{x-x_0}{h}\Delta y_0 + \frac{(x-x_0)(x-x_0-h)}{h^2 2!}\Delta^2 y_0 + \frac{(x-x_0)(x-x_0-h)(x-x_0-2h)}{h^3 3!}\Delta^3 y_0 + \frac{(x-x_0)(x-x_0-h)(x-x_0-2h)(x-x_0-3h)}{h^4 4!}\Delta^4 y_0 + \ldots\ldots \quad \text{(B.7)}$$

EquationsB.6 and B.7 give the formulae to be used. Δy_0 , $\Delta^2 y_0$, $\Delta^3 y_0$, . . . are as in the above sub-section. Substituting and simplifying, we get the following.

First approximation:

$$y(x) = \frac{1}{h}\left[(1-x)y_0 + xy_1\right] \quad \text{(B.8)}$$

Second approximation:

$$y(x) = \frac{1}{h}\left[\frac{1}{2}(x^2-x)y_2 + (2x-x^2)y_1 + \frac{1}{2}(2-3x+x^2)y_0\right] \quad \text{(B.9)}$$

Third approximation:

$$y(x) = \frac{1}{h}\left[\frac{1}{6}(2x-3x^2+x^3)y_3 + \frac{1}{2}\left(-3x+4x^2-x^3\right)y_2 + \frac{1}{2}\left(6x-5x^2+x^3\right)y_1 + \frac{1}{6}(6-11x+6x^2-x^3)y_0\right] \quad \text{(B.10)}$$

Fourth approximation:

$$y(x) = \frac{1}{h}\left[\frac{1}{24}(-6x+11x^2-6x^3+x^4)y_4 + \frac{1}{6}(8x-14x^2+7x^3-x^4)y_3 + \frac{1}{4}\left(-12x+19x^2-8x^3+x^4\right)y_2 + \frac{1}{6}\left(24x-26x^2+9x^3-x^4\right)y_1 + \frac{1}{24}(24-50x+35x^2-10x^3+x^4)y_0\right] \quad \text{(B.11)}$$

B.2 Formulae using backward differences

$$\begin{aligned}
\nabla y_0 &= y_0 - y_{-1} \\
\nabla y_{-1} &= y_{-1} - y_{-2} \\
\nabla y_{-2} &= y_{-2} - y_{-3} \\
\nabla y_{-3} &= y_{-3} - y_{-4} \\
\nabla^2 y_0 &= y_0 - 2y_{-1} + y_{-2} \\
\nabla^2 y_{-1} &= y_{-1} - 2y_{-2} + y_{-3} \\
\nabla^2 y_{-2} &= y_{-2} - 2y_{-3} + y_{-4} \\
\nabla^2 y_{-3} &= y_{-3} - 2y_{-4} + y_{-5}
\end{aligned}$$

$$\nabla^3 y_0 = y_0 - 3y_{-1} + 3y_{-2} - y_{-3}$$
$$\nabla^3 y_{-1} = y_{-1} - 3y_{-2} + 3y_{-3} - y_{-4}$$
$$\nabla^4 y_0 = y_0 - 4y_{-1} + 6y_{-2} - 4y_{-3} + y_{-4}$$

B.2.1 Derivatives

$$y'(x_0) = \frac{1}{h}\left(\nabla y_0 + \frac{1}{2}\nabla^2 y_0 + \frac{1}{3}\nabla^3 y_0 + \frac{1}{4}\nabla^4 y_0 + \ldots.\right) \quad \text{(B.12)}$$

Truncating EquationB.12 to 1, 2, 3, . . . etc., terms and substituting from the relevant equations above, we can get different approximations to the derivatives.

First approximation:

$$y'(x_0) = \frac{1}{h}\left(y_0 - y_{-1}\right) \quad \text{(B.13)}$$

Second approximation:

$$y'(x_0) = \frac{1}{2h}\left(3y_0 - 4y_{-1} + 4y_{-2}\right) \quad \text{(B.14)}$$

Third approximation:

$$y'(x_0) = \frac{1}{6h}\left(11y_0 - 18y_{-1} + 9y_{-2} - 2y_{-3}\right) \quad \text{(B.15)}$$

Fourth approximation:

$$y'(x_0) = \frac{1}{12h}\left(25y_0 - 48y_{-1} + 36y_{-2} - 16y_{-3} + 3y_{-4}\right) \quad \text{(B.16)}$$

B.2.2Interpolation and Extrapolation

$$y(x) = y_0 + x\nabla y_0 + \frac{x(x+1)}{2!}\nabla^2 y_0 + \frac{x(x+1)(x+2)}{3!}\nabla^3 y_0 + \frac{x(x+1)(x+2)(x+3)}{4!}\nabla^4 y_0 + \ldots\ldots \quad \text{(B.17)}$$

General case;

$$y(x) = y_0 + \frac{x-x_0}{h}\nabla y_0 + \frac{(x-x_0)(x-x_0+h)}{h^2 2!}\nabla^2 y_0 + \frac{(x-x_0)(x-x_0+h)(x-x_0+2h)}{h^3 3!}\nabla^3 y_0 + \frac{(x-x_0)(x-x_0+h)(x-x_0+2h)(x-x_0+3h)}{h^4 4!}\nabla^4 y_0 + \ldots.. \quad \text{(B.17)}$$

Equations.B.17 and B.18 give the formulae to be used. ∇y_0, $\nabla^2 y_0$, $\nabla^3 y_0$, . . .etc., are as in the above sub-section. Substituting and simplifying, we get the following.

First approximation:

$$y(x) = \frac{1}{h}\left[(1+x)y_0 - xy_{-1}\right] \quad \text{(B.19)}$$

Second approximation:

$$y(x) = \frac{1}{h}\left[\frac{1}{2}(x^2 + x)y_{-2} - (2x + x^2)y_{-1} + \frac{1}{2}(2 + 3x + x^2)y_0\right] \quad \text{(B.20)}$$

Third approximation:

$$y(x) = \frac{1}{h}\left[\begin{array}{l} -\frac{1}{6}(2x+3x^2+x^3)y_{-3}+\frac{1}{2}\left(3x+4x^2+x^3\right)y_{-2} \\ -\frac{1}{2}\left(6x+5x^2+x^3\right)y_{-1}+\frac{1}{6}(6+11x+6x^2+x^3)y_0 \end{array}\right] \quad \text{(B.21)}$$

Fourth approximation:

$$y(x) = \frac{1}{h}\left[\begin{array}{l} \frac{1}{24}(6x+11x^2+6x^3+x^4)y_{-4}-\frac{1}{6}(8x+14x^2+7x^3+x^4)y_{-3}+ \\ \frac{1}{4}\left(12x+19x^2+8x^3+x^4\right)y_{-2}-\frac{1}{6}\left(24x+26x^2+9x^3+x^4\right)y_{-1} \\ +\frac{1}{24}(24+50x+35x^2+10x^3+x^4)y_0 \end{array}\right] \quad \text{(B.22)}$$

B. 3 Integrals

Trapezoidal rule:

$$\int_{x_0}^{x_n} y\,dx = \frac{h}{2}\left(y_0+2y_1+2y_2+2y_3+\ldots.+y_n\right) \quad \text{(B.23)}$$

The error is of the order of h^2.

Simpson's (1/3) rule:

$$\int_{x_0}^{x_n} y\,dx = \frac{1}{3}\left(y_0+4y_1+2y_2+4y_3+\ldots.+4y_{n-1}+y_n\right) \quad \text{(B.24)}$$

The number of samples has to be odd. The error is of the order of h^4.

Simpson's (3/8) rule:

$$\int_{x_0}^{x_n} y\,dx = \frac{3}{8}\left(\begin{array}{l} y_0+3y_1+3y_2+2y_3+3y_4+3y_5 \\ +2y_6\ldots.+2y_{n-3}+3y_{n-2}+3y_{n-1}+y_n \end{array}\right) \quad \text{(B.25)}$$

n has to be chosen such that n = 3m +1 where m= 1, 2, 3, . .*etc.*

Weddle's rule:

$$\int_{x_0}^{x_n} y\,dx = \frac{3}{10}\left(y_0+5y_1+y_2+6y_3+y_4+5y_5+y_6\right) \quad \text{(B.26)}$$

This is the rule with 7 samples. The rule with 13 samples is

$$\int_{x_0}^{x_n} y\,dx = \begin{array}{l} \frac{3}{10}\left(y_0+5y_1+y_2+6y_3+y_4+5y_5+y_6\right)+ \\ \frac{3}{10}\left(y_6+5y_7+y_8+6y_9+y_{10}+5y_{11}+y_{12}\right) \end{array} \quad \text{(B.27)}$$

and so on. n has to be such that n = 6m + 1, with m = 1, 2, 3, . . . *etc.*

Appendix C

Bessel Functions

Bessel functions of the first kind of order n and argument x – commonly denoted by $J_n(x)$ - is defined as

$$J_n(x) = \frac{1}{\pi}\int_0^{\pi} \cos(x\sin\theta - n\theta)d\theta \quad \text{(C.1)}$$

$J_n(x)$ can be expanded in a power series form as

$$J_n(x) = \sum_{m=0}^{\infty} \frac{(-1)^m (x/2)^{n+2m}}{m!(n+m)!} \quad \text{(C.2)}$$

Properties of Bessel Functions

$$J_n(x) = (-1)^n J_{-n}(x) \quad \text{(C.3)}$$

$$= (-1)^n J_n(-x) \quad \text{(C.4)}$$

$$J_{n-1}(x) + J_{n+1}(x) = \frac{2n}{x} J_n(x) \quad \text{(C.5)}$$

For $x << 1$

$$J_n(x) \approx \frac{x^n}{2^n n!} \quad \text{(C.6)}$$

For $x >> 1$

$$J_n(x) = \sqrt{\frac{2}{\pi x}} \cos\left(x - \frac{\pi}{4} - \frac{n\pi}{2}\right) \quad \text{(C.7)}$$

Thus for large values of x, $J_n(x)$ behaves like a sinusoid with the amplitude varying as $x^{-(1/2)}$.

$$\sum_{n=-\infty}^{+\infty} J_n^2(x) = 1 \quad \text{(C.8)}$$

for all x.

Appendix D

Basics of Stress and Strain

For an ideal elastic material, the strain is proportional to the stress (and becomes zero when the stress is made zero). This is true of tensile stresses, compressive stresses as well as shear stresses.

Let a uniform cylindrical body of material with length l and area of cross-section A be subjected to an axial load P. The stress s is the average force per unit area of cross-section

$$s = \frac{P}{A} \tag{D.1}$$

Due to the stress, the material undergoes longitudinal deformation δ where

$$\varepsilon = \frac{\delta}{l} \tag{D.2}$$

$$s = \varepsilon E \tag{D.3}$$

and

$$\delta = \frac{P}{A}\frac{l}{E} \tag{D.4}$$

where

$\Rightarrow$ ε is the strain - a non-dimensional quantity and

$\Rightarrow$ E is the proportionality constant relating stress and strain. It is called the 'Young's Modulus' or the 'Modulus of Elasticity'.

D.1 Normal Stress

Consider an infinitesimally small element of the material of sides dx, dy and dz as in Figure D.1, the material being elastic. Let the material be pulled by tensile forces of magnitude P_z along the z direction. Let s_z be the corresponding force per unit area *i.e.*, stress.

Due to its elastic nature, the material undergoes elongation in the z-direction. Let the corresponding strain be ε_z.

$$\varepsilon_z = \frac{s_z}{E} \tag{D.5}$$

The elongation of the material in the z-direction $= dz\,\varepsilon_z$ (D.6)

A tensile stress of s_z in the z direction causes an elongation in the z direction. Simultaneously the material shrinks in the x and y directions. The respective strains are

$$\varepsilon_x = \varepsilon_y - \sigma\,\varepsilon_z \tag{D.7}$$

Here σ is the 'Poisson's ratio' for the material. σ ranges from 0,0 to 0.3 for normal materials. Material under compression behaves in a similar manner with appropriate change of sign.

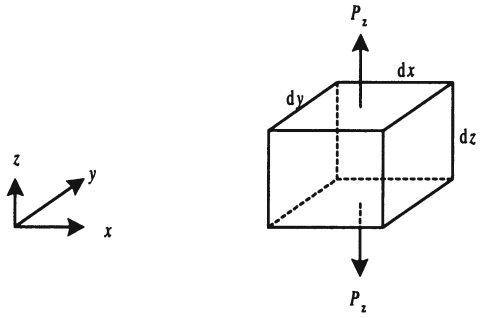


Figure D.1 An infinitesimally small element of a material stressed in the z direction

D.2 Shear Stress

Consider the same element as above, under shear stress as in Figure D.2 (a). The shear stresses appear only on 4 of the 6 faces of the element – *i.e.*, excluding faces AEFB and DHGC. s_{xy} is the shear stress acting on the area BFGC. The total force due to this is

$$F = s_{xy}\, dz\, dy \tag{D.8}$$

Similarly with forces in the other directions as well.

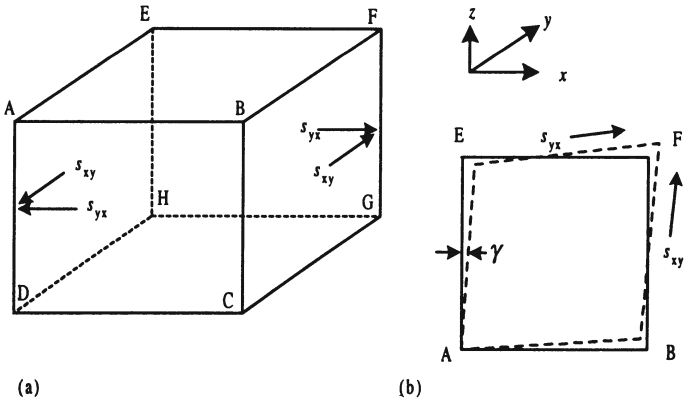


Figure D.2 An infinitesimal element under shear stress: (a) Element with stress directions (b) Top view of the element with strain directions

Since the material is under equilibrium, net moment of forces around line AD is zero. This gives

$$S_{xy}\, dx\, dy\, dz = s_{yx}\, dx\, dy\, dz \tag{D.9}$$

$$s_{xy} = s_{yx} \tag{D.10}$$

Thus, the shear-stress on the four faces are equal. Due to the shear stress, the material undergoes deformation- the corner angles of the base rectangle depart from

90° [Figure D.2 (b)]. The departure angle in radians is γ. This is the shear strain the material undergoes. The shear strain and the stress are related by

$$\frac{s}{G} = \gamma \tag{D.11}$$

where G is the 'Modulus of Elasticity' in shear. G, E and σ are related as

$$G = \frac{E}{2(1+\sigma)} \tag{D.12}$$

From Figure D.2 (b), it can be seen that the deformation of the element is such that the diagonal AF elongates to the maximum extent while the diagonal EB shortens by the maximum extent. Shear strain can be measured by measuring the linear strain along these two directions.

D.3 Combined Shear and Tension or Compression

For a more general case, we can compute the normal and shear stresses for any desired plane in a material. Consider an elemental part of the material with an arbitrary plane inclined at an angle to the y-axis as shown in Figure D.3.

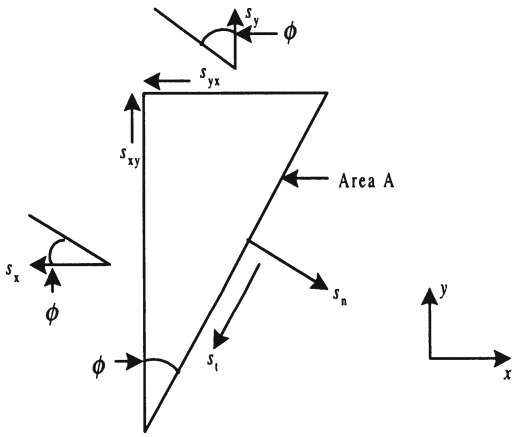


Figure D.3 Forces with combined shear and tension/compression

Referring to the figure we can see the following: -

- ⇒ s_{xy} and s_{yx} are the shear stresses,
- ⇒ s_x and s_y are the normal stresses acting on faces normal to x and y axes respectively,
- ⇒ A is the area of the arbitrary plane considered,
- ⇒ $s_n$is the stress normal to the face of area A and
- ⇒ s_t is the stress tangential to the area A – the shear stress

Since the element is in equilibrium, all the forces along the directions of s_n and s_t should balance out. This gives

$$As_n = = s_xA\cos^2\phi + s_yA\sin^2\phi + 2s_{xy}A\cos\phi\sin\phi \tag{D.13}$$

Dividing throughout by A we get

$$s_n = s_x\cos^2\phi + s_y\sin^2\phi + 2s_{xy}\cos\phi\sin\phi \tag{D.14}$$

Simplification yields

$$s_n = \frac{1}{2}(s_x + s_y) + \frac{1}{2}(s_x - s_y)\cos 2\phi + s_{xy}\sin 2\phi \quad \text{(D.15)}$$

Similarly, we get

$$As_t = s_yA\sin\phi\cos\phi - s_{xy}A\sin^2\phi + s_{xy}A\cos^2\phi - s_xA\cos\phi\sin\phi \quad \text{(D.16)}$$

Dividing throughout by A and simplifying

$$s_t = \frac{1}{2}(s_x - s_y)\sin 2\phi - s_{xy}\cos 2\phi \quad \text{(D.17)}$$

Equations D.15 and D.17 show that s_n and s_t can be obtained for any ϕ, from Mohr's circle shown in Figure D.4 where

$$OA = \frac{s_x + s_y}{2} \quad \text{(D.18)}$$

$$AB = \frac{s_x - s_y}{2} \quad \text{(D.19)}$$

$$BC = s_{xy} \quad \text{(D.20)}$$

AC is the reference radius at angle θ to the x axis where

$$\tan 2\theta = \frac{BC}{AB}$$

For any given ϕ, we can mark point F on the circle at an angle 2ϕ from the reference radius AC to get point F on the circle. The x and y co-ordinates of point F – namely OG and GF – form the effective normal stress s_n and the effective shear stress s_t respectively for the plane.

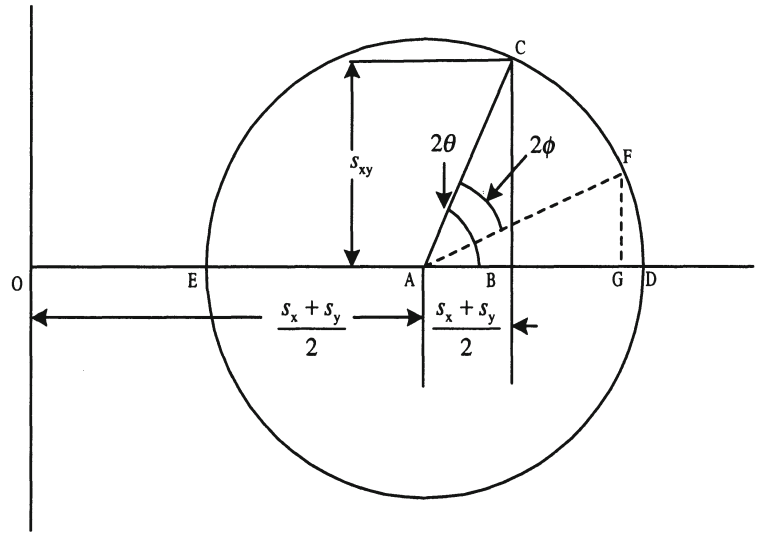


Figure D.4 Mohr circle construction to obtain the Principal axes

Referring to the Mohr's circle in Figure D.4, the normal stress is a maximum for

$$\phi = -\theta \quad \text{(D.21)}$$

s_{max} – the maximum value of s_n – is OD.

$$s_{max} = \frac{s_x + s_y}{2} + \sqrt{\left(\frac{s_x - s_y}{2}\right)^2 + s_{xy}^2} \quad \text{(D.22)}$$

The corresponding direction is a 'Principal Axis' and the stress is a principal stress. The tangential and shear stresses for this direction are zero. Similarly, s_{min} – the minimum value of stress s_n – is OE. It occurs for

$$\phi = \frac{\pi}{2} - \theta \quad \text{(D.23)}$$

We have

$$s_{min} = \frac{s_x + s_y}{2} - \sqrt{\left(\frac{s_x - s_y}{2}\right)^2 + s_{xy}^2} \quad \text{(D.24)}$$

The shear stress for this direction, is zero. This is the second 'Principal Axis'.

D.4 Cantilever with End Load

In Figure D.5 (a), ABC is a Cantilever with force F acting vertically downward at point C. M - the bending moment acting at B, -is

$$M = Fl \quad \text{(D.25)}$$

This causes tensile strain at the upper side and compressive strain at the lower side of the beam. The stresses and strains change from section to section [See Figure D.5 (b)]. They reach the maximum value at the surface. The stress and strain are zero at the 'Neutral Axis' passing through the centre of gravity of the section.

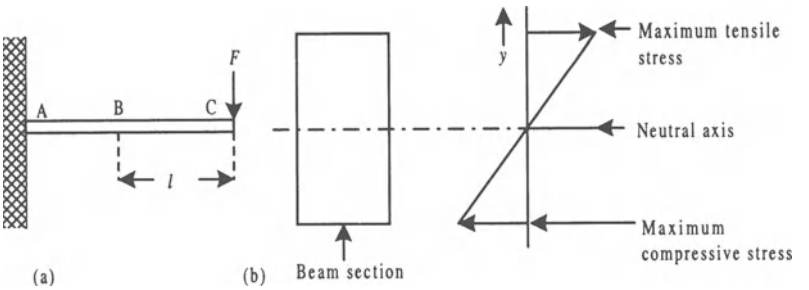


Figure D.5 (a) Cantilever with end-load (b) Nature of variation of stress at different levels from the neutral axis for a rectangular beam section

$$s_{max} = \frac{Mc}{I} \quad \text{(D.26)}$$

where

⇒ M is the moment given by Equation D.25,
⇒ I is the inertia of the section of the beam about the neutral axis and
⇒ c is the distance of the extreme layer from the neutral axis.

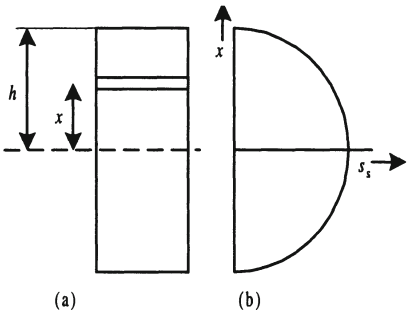


Figure D.6 Nature of variation of shear stress in rectangular beam: (a) Beam section (b) Nature of variation of shear stress along beam axis

Every layer of the beam at any section is subjected to a set of shear forces. For the specific case of the uniform rectangular section of the cantilever (Figure D.6) the shear stress s_s is given by

$$s_s = \frac{3F}{2A}\left(1-\frac{4x}{h^2}\right) \tag{D.27}$$

where

⇒ F is the force acting on the cantilever,
⇒ A is the area of section of the cantilever,
⇒ h is the height of the cantilever section and
⇒ x is the height from the neutral axis.

The shear stress is a maximum at the neutral axis and reduces on either side becoming zero at the surface.

Depending on the force, its distribution, cross-section of the beam and the type of support, the normal and shear stress distribution change. These are dealt with exhaustively in standard textbooks. In all cases, the following hold good at any section: -

⇒ Normal stress is zero at a neutral axis.
⇒ For loading in the vertical direction, normal stress is a maximum at the top and bottom surfaces.
⇒ The shear stress is a maximum at the neutral axis
⇒ For small distances from the neutral axis, the shear stress remains sensibly constant. This is more so with I sections.
⇒ When the cantilever is subjected to a single concentrated load, all the above stress values are proportional to it.
⇒ All the above generalizations are valid for beams also.

D.5 Circular Shaft with Applied Torque

Consider a uniform cylindrical shaft of length l and radius R. It is subjected to a torque T. Due to this the shaft undergoes deformation. A line AB on its surface is deformed and takes the position AC. At the right circular face, every element shifts proportionately. Thus the radius OD shifts to OE. The radial shift is denoted by angle ϕ radians. The shear strain at the surface is γ radians. We can see from Figure D.7, that

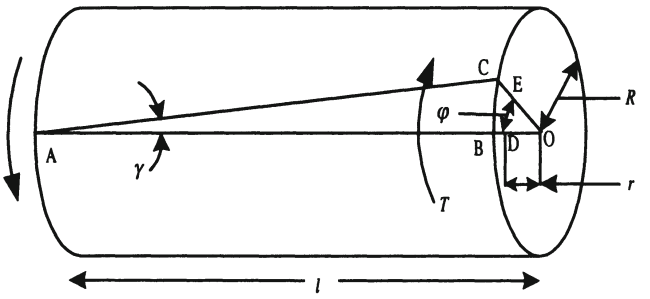


Figure D.7 Circular shaft with applied torque

$$I\gamma = R\phi \tag{D.28}$$

If s_s is the shear stress at the surface

$$s_s = \gamma G \tag{D.29}$$

where G is the modulus of elasticity in shear. Further, it can be shown that at radius r

$$S_s = \frac{Tr}{J} \tag{D.30}$$

where J is the polar moment of inertia of the shaft. Hence, s_{smax} the maximum shear stress at the surface becomes

$$s_{smax} = \frac{TR}{J} \tag{D.31}$$

Using Equation D.38 and Equation D.39 in Equation D.41, we get

$$\phi = \frac{Tl}{JG} \tag{D.32}$$

This is similar to Equation D.4 for normal stress.

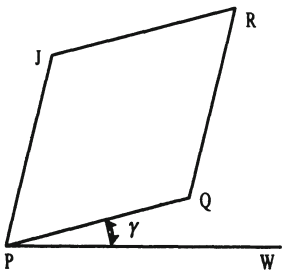


Figure D.8 A rectangular element of the shaft surface distorted due to shear

In general, the above expressions are valid only for points well away from the plane of application of the torque T. Figure D.8, shows a rectangular element PQRS on the shaft surface under stress. Line PW is parallel to the shaft axis. γ in radians represents the shear strain. As explained above the elongation along diagonal PR and shortening along diagonal TQ are maximum and minimum respectively. These two diagonals are inclined at 45° on either side of the axis. The stress and the strain of the non-cylindrical shafts subjected to similar torque, are not so easily tractable.

However, for every type of section, the stresses and strains at any point and at any element are directly proportional to the applied torque. Hence, their magnitudes can be used as a measure of the torque.

Appendix E

Tables of Properties

Table E.1 Dielectric constants of selected materials

Material	ε_r	Material	ε_r
ABS pellet	1.5 - 2.5	Acetone	20
Acrylic resin	2.7 - 6.0	Industrial alcohol	16 - 31
Aluminium sulphate	6	Asphalt	2.5 - 3.2
Liquid benzene	2.3	Calcium carbonate	1.8 -2.0
Calcium oxide	11.8	Calcium sulphate	5.6
Carbon dioxide	1.6	Epoxy resin	2.6 - 6
Ethyl alcohol	24	Glass	2.0 - 2.5
Heavy oil	2.6 - 3.0	Liquid hexane	5.8 - 6.3
Nylon	5 - 6	PE pellet	1.5
PP pellet	1.5 - 1.8	PVC powder	1.4
Rubber	2.1 - 2.7	Liquid toluene	2.0 - 2.4
Urethane	6.5 - 7.1	Water	48 - 80

Table E.2 Thermal and electrical properties of selected materials

Material	Thermal conductivity (W/in-°C)	Thermal expansion (ppm/°C)	TCR(%/°C)	Resistivity at 20°C (μΩ/°C)
Aluminium	6.02	23.9	0.429	2.66
Barium	0.468	18		50.0
Beryllium	5.10	12	2.5	5.9
Bismuth	0.201	13		106.8
Chromium	2.38	6.1	0.3	13.0
Cobalt	2.54	12	0.604	6.24
Copper	10.2	17	0.68	1.673
Gold	8.08	14.2	0.4	2.19
Iron	2.04	11.7	0.651	9.71
Lead	0.897	29.3	1.65	4.46
Magnesium	3.96	25	1.65	4.46
Nickel	2.31	13	0.69	6.84
Platinum	1.82	8.8	0.3927	9.83
Rhodium	1.48	90		12.5
Silver	10.9	19.6	0.41	1.59
Tin	1.70	23	0.47	11.5
Titanium	0.556	8.5		47.8
Tungsten	4.39	4.3	0.524	5.6
Manganin	0.564	18.7	±0.0015	44
Al_2O_3	0.53	6.7		500
BeO	6.0	8.0		10^{22}

Appendix F

Conversion Tables

Table F.1 Pressure conversion factors

	Atmos.	Bars	Dynes/ cm^2	In of Hg (0°C)	In of H_2O (4°C)	Kg/m^2	Lb/in^2 (psi)	mm of Hg (torr)	microns	Pascals
Atmos.	1	9.86923×10^{-1}	9.86923×10^{-7}	3.34207×10^{-2}	2.458×10^{-3}	9.678×10^{-5}	6.8046×10^{-2}	1.316×10^{-3}	1.316×10^{-3}	9.86923×10^{-6}
Bars	1.01325	1	10^{-6}	3.3864×10^{-2}	2.491×10^{-3}	9.8067×10^{-5}	6.8948×10^{-2}	1.333×10^{-3}	1.333×10^{-6}	10^{-6}
Dynes/cm^2	1.01325×10^{6}	10^{6}	1	3.386×10^{4}	2.491×10^{3}	9.8067×10^{1}	6.8948×10^{4}	1.333×10^{3}	1.333	10
In of Hg(0°C)	2.99213×10^{1}	2.953×10^{1}	2.953×10^{-5}	1	7.355×10^{-2}	2.896×10^{-3}	2.036	3.937×10^{-2}	3.937×10^{-5}	2.953×10^{-4}
In of water (4°C)	4.068×10^{2}	4.0148×10^{2}	4.0148×10^{-4}	1.360×10^{1}	1	3.937×10^{-2}	2.768×10^{1}	5.354×10^{-1}	5.354×10^{-6}	4.014×10^{-3}
Kg/m^2	1.033227×10^{4}	1.0197×10^{4}	1.0197×10^{-2}	3.453×10^{2}	2.54×10^{1}	1	7.0306×10^{2}	1.359×10^{1}	1.359×10^{-2}	1.019×10^{-1}
Lb/In^2(psi	1.46956×10^{1}	1.4504×10^{1}	1.4504×10^{-5}	4.912×10^{-1}	3.6126×10^{-3}	1.423×10^{-3}	1	1.934×10^{-2}	1.934×10^{-5}	1.450×10^{-4}
mm of Hg(torr)	7.60×10^{2}	7.5006×10^{2}	7.5006×10^{-4}	2.54×10^{1}	1.868	7.3558×10^{-2}	5.1715×10^{1}	1	10^{-3}	7.502×10^{-3}
microns	7.60×10^{5}	7.5006×10^{5}	7.5006×10^{-1}	2.54×10^{4}	1.868×10^{3}	7.3558×10^{1}	5.1715×10^{4}	10^{3}	1	7.502
Pascals	1.01325×10^{5}	10^{5}	10^{-1}	3.386×10^{3}	2.491×10^{2}	9.8067	6.8948×10^{3}	1.333×10^{2}	1.333×10^{-1}	1

Example: To convert pressure in atmospheres to pressure in Pascals, multiply by 1.01325×10^{5}

Table F.2 Force Conversion Factors

	Pounds	Ounces	Grams	Kgs	Newtons	Tons	Metric tons
Pounds	1	6.25×10^{-2}	2.2×10^{-3}	2.2046	2.248×10^{-1}	2×10^{3}	2.205×10^{3}
Ounces	1.6×10^{1}	1	3.527×10^{-2}	3.5242×10^{1}	3.5971	3.2×10^{4}	2.205×10^{3}
Grams	4.5359×10^{2}	2.8349×10^{1}	1	10^{3}	1.0207×10^{2}	9.080×10^{5}	10^{6}
Kgs	4.5359×10^{-1}	2.835×10^{-2}	10^{-3}	1	1.0207×10^{-1}	9.08×10^{2}	10^{3}
Newtons	4.448	2.78×10^{-1}	9.797×10^{-3}	9.797	1	8.896×10^{3}	9.807×10^{3}
Tons	5.0×10^{-4}	3.13×10^{-5}	1.101×10^{-6}	1.101×10^{-3}	1.124×10^{-4}	1	1.103
Metric tons	4.535×10^{-4}	2.838×10^{-5}	10^{-6}	10^{-3}	1.020×10^{-4}	9.067×10^{-1}	1
Example: To convert force/ weight in pounds into force/ weight in metric tons, multiply by 4.535×10^{-4}							

Table F.3 Torque conversion factors

	Pound-inch	Pound-foot	Ounce-inch	Kg-cm	kgm	Nm
Pound-inch	1	1.2×10^{1}	6.25×10^{-2}	8.681×10^{-1}	8.681×10^{1}	8.8511
Pound-foot	8.334×10^{-2}	1	5.2×10^{-3}	7.234×10^{-2}	7.234	7.375×10^{-1}
Ounce-inch	1.6×10^{1}	1.92×10^{2}	1	1.38858×10^{1}	1.38858×10^{3}	1.416×10^{2}
Kg-cm	1.152	1.3826×10^{1}	5.2×10^{-3}	1	10^{2}	1.0197×10^{1}
kgm	1.152×10^{-2}	1.38×10^{-1}	7.2×10^{-4}	10^{-2}	1	1.0197×10^{-1}
Nm	1.129×10^{-1}	1.356	7.026×10^{-3}	9.807×10^{-2}	9.807	1

Table F.4 Thermal conductivity – Conversion actors

	cal/s-cm-°C	W/cm-°C	W/in-°C	BTU/hr-ft-°F	kg-cal/hr-m-°C	W/m-°C
cal/s-cm-°C	1	4.186	10.63	241.9	360.0	418.6
W/cm-°C	0.2389	1	2.540	57.8	86.00	100
W/in-°C	0.09405	0.3937	1	22.75	33.86	39.37
BTU/hr-ft-°F	4.134×10^{-3}	0.0173	0.044	1	1.488	1.730
kg-cal/hr-m- °C	2.778×10^{-3}	0.01163	0.0295	0.672	1	1.163
W/m-°C	2.389×10^{-3}	0.01	0.0254	0.578	0.860	1

References

Ajluni C. Low Pressure Sensor Opens Wide Application Frontier. Electronic Design, Dec. 16, 1996.

Analog Devices (1996) High Speed Design Techniques. Analog Devices, Ma

Anderson KF (1997) The New Current Loop: An Instrumentation and Measurement circuit Topology. IEEE Trans Instrum Meas. Vol 46, No. 5 Oct

Antoniou A (1993) Digital Filters: Analysis, Design and Applications. 2nd Edn. McGraw-Hill, New York.

Baracchino L, Basso G, Ciofi C, Neri B(1997) Ultra Low-Noise Programmable Voltage Source. IEEE Trans Instrum Meas Vol 46 No 6 Dec

Baxter LK (1997) Capacitive Sensors - Design and Applications. IEEE, New York.

Benedict RP (1984) Fundamentals of Temperature, Pressure And Air Flow Measurement, 3rd edn. Wiley, New York

Beckwith TG Buck WL Marangoni RD (1982) Mechanical Measurements, 3rd edn. McGraw-Hill, New York

Blackburn JL (1993) Symmetrical Components for Power Systems Engineering. Marcel Dekker, New York

Broch JT (1972) Mechanical Measurement and Shock Meassurement. Bruel and Kjaer Instruments, Marlboro, MA

Bruns RW The Helix Load Cell. Sensors, May (1998)

Bucci G, Laudi C (1997) Numerical Methods for Transit Time Measurement in Ultrasonic Sensor Applications. IEEE Trans Instrum Meas Vol 46 No 6 Dec

Carlson AB (1988) Communication Systems - An Introduction to Signals and Noise in Electrical Communication, 3rd edn. McGraw-Hill, New York.

Carr JJ (1996) Elements of Electronic Instrumentation And Measurements, 3rd edn. Prentice Hall, New York

Chirlian PM (1987) Analysis and Design of Integrated Electronic Circuits, 2nd Edn. Wiley, New York

Cerni RH, Foster LE (1962) Instrumentation for Engineering Measurement. Wiley, New York.

Cheng DA (1993) Fundamentals of Engineering Electromagnetics. Addison-Wesley, New York

Cheremisinoff NP (1979) Applied Fluid Flow Measurement - Fundamentals and Technology. Marcel Dekker, New York

Chopey NP (1996) Instrumentation and Process Control. McGraw-Hill, New York

Cheney EW (1966) Introduction to Approximation Theory. McGraw-Hill, New York

Clayton AE Hancock NN (1962) Performance and Design of DC Machines. Pitman, London.

Considine DM (1993) Process/Industrial Instruments And Controls Handbook, 4th edn. McGraw-Hill, New York

Cucci GR (1996) Sensors and Transmitters Powered by Fiber Optics, Proceedings, Sensors Expo, 16-18 April

Dally J (1993) Instrumentation for Engineering Measurements, 2nd edn. Wiley, New York

Dally JW Riley WF (1978) Experimental Stress Analysis, 2nd edn. McGraw-Hill, New York

Davenport WB Root WL (1958) Random Signals and Noise. McGraw-Hill, New York

Dewitt DP Nutter GD (1988) Theory and Practice of Radiation Thermometry. Wiley, New York

Donati S Falzoni L Merlo S (1996) A PC-Interfaced, Compact Laser-Diode Feedback Interferometer for Displacement Measurements IEEE Trans Instrum Meas Vol. 45 No 6 Dec

Draper CS Walter Mcay Sidney Lees (1955) Instrument Engineering vol. 1 to 3. McGraw-Hill, New York

Eckman DP (1950) Industrial Instrumentation. Wiley, New York

Franco S (1988) Design with Operational Amplifiers and Analog Integrated Circuits. McGraw-Hill, New York

Fish PJ (1993) Electrical Noise and Low Noise Design. Macmillan, London

Geyger WA (1957) Magnetic Amplifier Circuits – Basic Principles, Characteristics and Applications, 2nd Edn. McGraw Hill New York

Giacoletto LJ (1977) Electronic Designers' Handbook. McGraw-Hill, New York

Ginesi D Flow Sensing: The Next Generation. Control Engineering, November (1997)

Glasstone S (1974) Textbook of Physical Chemistry, 2nd Edn. Nan Nostrand, New York

Graeme JG (1973) Applications of Operational Amplifiers. McGraw-Hill, New York

Gray PR Meyer RG (1992) Analysis and Design of Analog Integrated Circuits, 2nd Edn. Wiley, New York

Harris FK (1952) Electrical Measurements. Wiley, New York

Haykin S (1994) An Introduction to Analog and Digital Communications. Wiley, New York

Haus H. A (1989) Electromagnetic Fields and Energy. Prentice Hall, Engelwood Cliffs, NJ

Heerens W Chr (1986) Application of Capacitance Techniques in Sensor Design. Journal of Physics E: Scientific Instruments 19, Institute of Physics, Bristol, England.

Hix CF Alley RP (1958) Physical Laws and Effects. Wiley, New York

Holman JP Gajda WJ (1978) Experimental Methods for Engineers, 3rd edn. McGraw-Hill, New York

Hordeski M (1987) Transducers for Automation. Van Nostrand Reinhold, New York

Huelsman P (1993) Active and Passive Analog Filter Design – An Introduction. McGraw-Hill, New York

ISA (1973) Inductance Calculations - Working Formulae and Tables. Instrument Society of America, Pittsburgh

Jones RV Richards JCS (1973) The Design and Some Applications of Sensitive Capacitance Micrometers. Journal of Physics E: Scientific Instruments, 6, Institute of Physics, Bristol, England.

Ken Xu and Bingxin Jie (1997) A False-Balance-Avoidance Transductor for Measuring Large DC Currents IEEE Trans Instrum Meas Vol. 46 No 5 Oct

Kennedy G Davis B (1993) Electronic Communication Systems. McGraw-Hill, New York

Khalsa NS Ramsay R (1996) A Triaxial Fiber-Powered Acclerometer Proc Sensors Expo, 16-18 April,.

King-Wah W. Young Angle-Insensitive Flow Measurement Using Doppler Bandwidth IEEE Trans Ultra Ferro Freq Contr Vol 45 No 3

Kosel PB (1981) Capacitance Transducer for Accurate Disolacement Control. IEEE Trans Instrum Meas IM-30(2)

Kraemer W (1964) Development of the DC Instrument Transformer for the Precision Measurement of Highest Direct Current. IEEE Trans Comm Electron Vol CE-83

Lathi BP (1988) Modern Digital and Analog Communication Systems, 2nd edn. Holt, Reinhart and Winston, New York

Lion S (1959) Instrumentation in Scientific research. McGraw-Hill, New York

Liptak BG (1969, 1970) Instrument Engineers Handbook Volume I and II, Philadelphia Chilton, Philadelphia

Llinas J Waltz E (1990) Multisensor Data Fusion. Artech House, Boston MA

Ludeman LC (1986) Fundamentals of Digital Signal Processing. Harper and Row, New York

Mac Martin MP (1976) An Improved Transductor for Measuring Large Direct Currents IEEE Trans on Power App Syst Vol PAS-95 January.

Magison EC (1990) Temperature Measurement in Industry. ISA, Pittsburg

McGannon HE (1985) The Making, Shaping and Treating of Steel, 10th Edn. United States Steel Corp. Pittsburgh

McGee TD (1988) Principles and Methods of Temperature Measurement. Wiley, New York

Minorsky N (1962) Nonlinear Oscillations. Van Nostrand Reinhold, New York

Morris AS (1988) Principles of Measurement and Instrumentation. Prentice Hall, Engelwood Cliffs, NJ

Morrison R (1986) Grounding and Shielding Techniques in Instrumentation, 3rd edn.Wiley, New York

Morton WE Hearle JWS (1993) Physical Properties of Textile Fibres, 3rd Edn. The Textile Institute, Manchester

Mylroi MG Calvert G (1984) Measurement and Instrumentation for Control. Peter Peregrinus, London

Nachtigal CL (1990) Instrumentation and Control - Fundamentals and Applications. Wiley, New York

National Semiconductor (1995) National Data Acquisition Handbook.
(1995) Operational Amplifiers Data Book

NBS (1979) Thermocouple Reference Tables. Monograph 125 National Bureau of Standards, Washington DC

Neubert HKP (1963) Instrument Transducers. Oxford University Press, London
Norden KE (1993) Electronic Weighing - Fundamentals and Applications. Butterworth Heinemann,
Norton HR (1989) Handbook of Transducers for Electronic Measuring Systems. Prentice Hall, Engelwood Cliffs, NJ
Ott HW (1988) Noise Reduction Techniques in Electronic Systems, 2nd edn. Wiley, New York
Orlosky S Avolio G Basics of Rotary Optical Encoders, Control Engineering, Nov 1997.
Oppenheim AV Schafer RW (1975) Digital Signal Processing. Prentice Hall, Engelwood Cliffs, NJ
Papoulis A (1991) Probability, Random Variables and Stochastic Processes. McGraw-Hill, New York
Parks TW McClellan JH Chebyshev (1992) Approximation for Non-recursive Digital Filters with Linear Phase IEEE Trans Circuit Theory, Vol. CT-19 March
Paul CR (1979) Prediction of Crosstalk involving twisted pairs of Wires - Part I: A Transmission Line Model for Twisted Pair Wires IEEE Trans EMC, May.
Prediction of Crosstalk involving twisted pairs of Wires - Part II: A Simplified Low Frequency Prediction Model ibid.
Platt G (1994) ISA Guide to Measurement Conversion. ISA, Pittsburgh
Plonus MA (1978) Applied Electromagnetics. McGraw-Hill, New York
Preobrazhensky V (1980) Measurements and Instrumentation in Heat Engineering. Mir Publishers, Moscow.
Preston-Thomas H (1990) The International Temperature Scale of 1990 (ITS90). Metrologia 27, 3-10
Proakis JG Manolakis DG (1992) Digital Signal Processing - Principles, Algorithms and Applications. Macmillan, Engelwood Cliffs, NJ
Quinn T J (1983) Temperature. Academic, New York
Rabiner LR Gold B (1975) Theory and Applications of Digital Signal Processing. Prentice Hall, Engelwood Cliffs, NJ
Ramsay DC (1996) Principles of Engineering Instrumentation. Wiley, New York
Ed Ramsden Interfacing Sensors and Signal Processing Components Sensors,May 1998.
Rangan CS Sarma GR Mani VSV (1997) Instrumentation – Devices and Systems. Tata McGraw-Hill, New Delhi.
Remez E Ya (1957) General Computational Methods for Tchebycheff Approximation, Kiev: Atomic Energy Commission, Translation 4491
Ruehli AE Inductance Calculations in a complex Integrated circuit Environment, IBM Journal of Research and Development, Sept 1992
Saleh BEA. Teich MC (1991) Fundamentals of Photonics. Wiley, New York
Schubert Jr T Kim E (1996) Active and Non-linear Electronics. Wiley, New York
Shpak DJ Antoniou A A (1990) Generalized Remez Method for the Design of FIR Digital Filters IEEE Trans on Circuits Syst Vol 37 Feb
Smith E (1984) Principles of Industrial Measurement for Control Applications. ISA, Pittsburgh

Solonkhin RI Afgan NH (1985) Measurement Techniques in Heat and Mass Transfer. Hemisphere, New York

Stein PK (1964) Measurement Engineering. Stein Engineering Services Inc, Phoenix, Arizona

Streetman BG (1990) Solid State Electronic Devices. Prentice Hall, Engelwood Cliffs, NJ

Sze SM (1969) Physics of Semiconductor Devices. Wiley, New York

Taub H. Schilling DL (1986) Principles of Communication Systems, 2nd Edn. McGraw-Hill, New York

Terman FE (1955) Electronic and Radio Engineering, 4th Edn. McGraw-Hill, New York

Tietze U Schenk Ch Schmid E (1991) Electronic Circuits – Design and Applicatons. Springer Verlag, Berlin

Timoshenko S (1984) Strength of Materials, (Reprint) Robert E Krieger Publishing Co, Florida

Trietley HL (1986) Transducers in Electronic and Mechanical Design. Marcel Dekker

Viterbi AJ (1966) Principles of Coherent Communication. McGraw-Hill, New York

Wait JV Huelsman LP. Korn GM (1992) Introduction to Operational Amplifiers - Theory and Applications, 2nd Edn. McGraw-Hill, New York

Walker CS (1990) Capacitance, Inductance and Crosstalk Analysis. Artech House, Boston

Wegmann EF (1984) A Reference Book for Blast Furnace Operators. Mir Publishers, Moscow

Werthen JG Andersson AG Optically Powered Sensors and Transmitters for Industrial Applications Proceedings, Sensors Expo, 16 18 April, 1996.

Woebcken W (1995) Saechtling International Plastics Handbook for the Technologist, Engineer and users, 3rd Edn. Hanser, Munich.

Wolfe WL Zissis GJ (1990) The Infrared Handbook. Optical Engineering Press, Bellington WA

Yamada M Watanabe K A (1997) Capacitive Pressure Sensor Interface Using Oversampling Δ-Σ Demodulation Techniques IEEE Trans Instrum Meas Vol 46 No1 February.

Yang WQ (1996) A Self-Balancing Circuit to Measure Capacitance and Loss Conductance for Industrial Transducer Applications IEEE Trans Instrum and Meas Vol 45 No 6 Dec

Index

AC Bridge, 40-49, 347
  Analysis near balance, 43-46
  Classification, 41-42
  Mutual inductance, 49-51
  Possible configurations, 40-43
  Sensitivity, 43-46
    Conditions for maximum, 44-46
    Unbalance
      Large, 46-47
      Small, 43-46
  Wein, 48-49
Acceleration sensing, 412-416
Accelerometer, 412-416
  Piezo-electric, 414-415
  Vibration sensing, 414-415
Active filters (See Filters)
ADC (See Analog to Digital Convertor)
Amplifier
  Analysis, 78-82
  Buffer, 90
  Current to voltage convertor, 87
  Difference, 92
    Adaptations, 94
  Instrumentation, 96-102
  Inverting, 78-86
  Isolation, 102-106
    Capacitance type, 104
    Opto-coupler type, 105
    Schematic arrangement, 102
    Transformer type, 103
  Leakage error(See amplifier)
    Minimization, 85
  Noise, 82-85
  Non-ideal, 78-82
  Non-inverting, 89
  Non-linear, 189-195
    Logarithmic, 193-195
    Piece-wise linear, 189-191
    Precision rectifier, 191-193
  Operational, 56-73
    Selection, 68
  Summing, 86
Amplitude modulation, 158-174
  Demodulation, 165-174
  Double side band scheme, 162
  DSB-SC, 162-164
  Lower side band, 162
  Performance in the presence of noise, 228-230
  Principles, 158-162
  Single sideband, 162
  Upper sideband, 162
  Vestigial sideband, 162
Analog signal processing, 74-106, 157-195
  Linear (See Linear signal processing)
  Non-linear (See Non-linear signal processing)
Analog switch, 246-248
  Specifications, 248
Analog to Digital Convertor, 263-268, 274-288
  Differential quantization, 284
  Latency, 279
  Microcomputer interface, 289-290
  Over sampling ratio, 287
  Specifications, 263-269
    Accuracy, 264
    Conversion rate, 264
    Dynamic range, 267
    Gain error, 265
    Linearity error, 266
    Monotonicity, 267
    Non-linearity
      Integral, 266
      Differential, 267
    Offset error, 264
    Quantization error, 264
  Temperature coefficient, 268
  Thermometer code, 278
  Types
    Dual slope, 274-276
    Flash, 278
    Ripple, 281
    Serial, 281
    Sigma-delta, 284
    Sub-ranging, 279
    Successive approximation, 277
  Window function, 240,299

Band gap based voltage reference, 263
Bellows, 461
Blast furnace
  Accessories, 594-599
  Chemistry, 590-593
  Flow of materials inside, 593-594
  Instrumentation, 602
  Process, 599
Bourdon tube, 461
Bridge
  AC, 40-50, 347-349
  DC, 30-39, 320-327
  Inductively coupled ratio arm bridge, 49,369
  Mutual inductance, 49
  Wein, 47

Bypass flowmeter, 508

Capillary tube flowmeter, 507
CCD, 542-555
  Anti-blooming, 549
  Array, 543-545
    Tapped, 554
    TDI, 554
    Time delay integration, 554
  Blooming, 549
  Fixed pattern noise, 549
  Pixel, 546
    Smear, 546
  Pixel sensitivity, 546
Charge coupled devices (See CCD)
Compressor, 3
Convertor
  Analog to digital (See Analog to digital convertor)
  Current to voltage, 87
  Digital to analog (See Digital to analog convertor)
Coriolis flowmeter, 498
Cotton sample, 570-580
  Specifications, 571-574
Current sensing, 556-563
  Hall sensor based, 550-563

Deconvolution, 305
Diaphragm, 464-466
  bonded SG, 464
  semionductor SG, 465
Differential pressure flowmeter, 478-488
Differential transformer, 359-368
  LVDT, 359-366
  RVDT, 359-366
Differentiator, 91
Digital filter (See Digital signal processing)
Digital signal processing, 291-317
  Determination of centroid, 304
  Edge detection, 304
  Filters
    Finite impulse response, 297-302
    IIR, 306-311
      Canonical form, 309-311
    Infinite impulse response, 306-311
    Linear phase, 111, 298
  Handling LUT, 291-293
    Corrections for parametric changes, 296
    Direct reading, 292
    Indirect reading, 294
  Linear operations
    Differentiation, 313
    Extrapolation, 313
    Integration, 313
    Interpolation, 313
  Profile detection, 305
Digital system, 25-29
Digital to analog convertor, 269-272
  Current based, 269
  Microcomputer interface, 289-290
  Specifications (See Analog to digital convertor)
  Voltage based, 270-272
Displacement sensing
  Capacitance transducer, 370-371
  Differential transformer, 359-368
    Microsyn, 366
    Resolver, 364
    Signal processing, 362
  Encoder, 370-379
    Absolute, 379
    Electro-optic, 373-379
    Incremental, 374
      Design, 374
  Potentiometer, 355-358
    Conductive plastic, 357
    Magneto-resistance, 357
    Signal processing, 358
    Wire wound, 356
  Resolver, 364
    Two speed, 365
  Variable reluctance transformer, 367
Doppler effect flowmeter, 503-505
DSB-SC, 162-164
Dual slope ADC, 274-276

Elbowmeter, 488
Elimination of
  Capacitively coupled noise, 199-201
  Conducted noise, 197-198
  Inductively coupled noise, 202-204
Equivalent noise bandwidth, 213

Feedback type transducer, 54, 350
Fibre length distribution, 570-574
Filter
  All pass filters, 110
  Band pass, 110, 114, 144-148
  Band rejection, 110, 115, 149
  Bessel / Thomson (See also individual types), 121
  Butterworth (See also individual types), 118
  Characteristics
    Delay time, 113
    Overshoot, 113
    Rise time, 113
    Settling time, 113
  Chebyshev (See also individual types)
  Classification, 107-110
  Digital (See Digital signal processing)
  Elliptic (See also individual types)
  High pass, 108, 114, 135-141
  Ideal characteristics, 107-110
  Low pass, 107, 111, 117-135
  Multiple feedback, 129, 139, 146

Filter (Continued)
Narrowband, 116, 142-149
Normalised, 117-123
Notch, 150-154
Requirements in instrumentation, 111
Sallen-Key, 126, 136, 144
S-K, 126, 136, 144
Specifications, 111-116
State variable, 131, 140, 148
S-V, 131, 140, 148
Switched capacitor type, 154
Flash ADC, 278
Flowmeter
Bypass, 508
Capillary tube, 507
Coefficient of discharge, 478-481
Coriolis, 498
Differential pressure, 478-488
Doppler effect, 503
Elbowmeter, 488
Magnetic, 488-491
Nozzle, 486
Orifice plate, 481-484
Beta ratio, 481-487
Pitot tube, 507
Positive displacement, 507
Target, 497
Thermal, 508
Turbine
Helical impeller type, 495
Paddle, 496
Vertical impeller type, 495
Ultrasonic, 500-505
Variable area, 507
Rotameter, 507
Vena *contracta, 485-487*
Venturi, 485
Vortex, 492-494
Bluffer, 492
Shedder, 492
Fluid flow, 470-476
Reynold's number, 470-473
Effect of change in density, 473
Streamlined, 470-472
Turbulent, 470-472
Flux gate magnetometer, 556-557
Force balance transducer, 410
Force sensing (See also Strain gauge), 409-410
LVDT, 409
Frequency modulation, 175-188
Circuits, 181
Demodulation, 175-188
Circuits, 182
Performance in the presence of noise, 231
Phase locked loop, 184-188
Principles, 175-177

Gamma ray level gauge, 514
Gas analysis, 526-529
Interferometer, 529
Thermal conductivity based, 527
Gas concentration sensing, 524-526
Ceramic based, 525
IR based, 526
Gas law, 473-475
Universal curves, 473-475
Gauge pressure, 460-461

Hall sensor, 560-563
Current sensing, 558-563
Hold (See also sampling), 249-256
Zero order, 243-245
Aperture delay time, 249
Error, 253
Jitter error, 251
Humidity, 521-524
Dew point, 521-522
Mixing ratio, 521-522
Psychrometric chart, 521-522
Relative, 521-522
Saturated conditions, 521-522
Sensing
Dew point based, 522
Electrolytic, 524
Lithium chloride based, 523
Pope cell, 524
Specific, 521-522
Volume ratio, 521-522

IIR Filter, 306-311
Inductively coupled ratio arm bridge, 369
Infinite impulse response filter (See IIR filter)
Infrared thermometry (See IR pyrometry)
In-motion weighing, 305
Instrumentation (See individual types)
Blast furnace, 589-599
Block diagram, 21
Categorization, 564-568
Fibre length distribution, 570-577
Specifications
Accuracy, 11
Dead zone, 15
Drift, 16
Errors, 12
Correction, 12
Hysteresis, 14
Input impedance, 19
Linearity, 18
Output impedance, 19
Precision, 11
Repeatability, 17
Resolution, 15
Sensitivity, 13
Threshold, 15
Structure, 21, 564-568
User configurable, 605-607

Instrumentation(Continued)
Data acquisition, 606
Data analysis, 607
Instrumentation scheme
Generic structure, 318-354
Self-calibrating type, 327
Integrator, 87, 313
Interferometer for gas analysis, 529
Internal noise (See Noise)
Inverse transducer, 350-354
IR pyrometry, 441-459
Basics, 441
Disappearing filament, 457
Emissivity, 444
Optics, 446
Radiation detection, 449-454
Photo-conductor, 450
Photo-emissive sensor, 454
Photo-voltaic sensor, 451
Single colour method, 457
Thermal detection, 446
Thermopile, 446
Two colour method, 454
Isolation amplifier, 102-106
Capacitance coupled, 104
Opto-coupled, 105
Schematic arrangement, 102
Transformer coupled, 103

Leakage error (See Amplifier)
Level sensing, 509-515
Capacitance based, 509-511
Conducting liquids, 510
Non-conducting liquids, 510
Differential pressure, 509
Displacement based, 513
Gamma ray based, 514
Ultrasonic, 513
Linear signal processing, 74-106, 303-315
Analog (See also respective entries)
Differentiator, 91
Filter, 107-156
Integrator, 87
Linear variable differential transformer (See also Displacement sensing), 359-366
Force sensing, 409-411
Load cell, 403-406
Cantilever, 404
Column, 403
Proving ring, 400-402
Shear beam, 400-402
Logarithmic amplifier, 193-195
Lowpass filter (See filters)
LPF(See filters)
LVDT, 359-366

Magnetic flowmeter, 488-491
Magnetometer, 556-557

Minimisation of
Capacitively coupled noise, 199-201
Conducted noise, 197-198
Inductively coupled noise, 202-204
Internal noise, 220-226
Modulation systems, 157-189
Performance in the presence of noise, 227-234
Multiplexer, 257-260
Multiplexing, 257-260
Mux, 257-260
Cross talk, 257-260
Pedestal error, 257-260

Nerst equation, 516-517
Noise
External, 196-205
Conducted noise, 197-198
Elimination, 197-198
Minimisation, 197-198
Inductively coupled, 202-204
Elimination, 202-204
Minimisation, 202-204
Inside feedback loop, 221
Internal, 215-220
Contact, 219
Flicker, 218
Johnson, 217
Minimization, 220
Popcorn, 220
Schottky, 215
Shot, 215
Thermal, 217
Random (See Random noise)
Non-linearity, 18, 266-267
Non-linear signal processing, 157-195
Amplifiers, 189-195
Logarithmic, 193-195
Piece-wise linear, 189-190
Precision rectifier, 191-192
Amplitude modulation (See respective entries)
Frequency modulation (See respective entries)
Nozzle flowmeter, 486

Operational amplifier, 56-73
Bias current, 60
Characteristics, 66-67
Trade-offs, 66
Common mode input, 62
Common mode input impedance, 62
Common mode rejection, 62
Common mode rejection ratio, 62
Compensated, 56
Drift, 61-62
Gain bandwidth product, 58
Ideal, 56
Input current, 60

Operational amplifier (Continued)
Input impedance, 62
Linearity, 59
Noise, 60-65
Flicker, 64
Popcorn, 65
Schottky, 64
Shot, 64
Offset current, 62
Drift, 62
Offset voltage, 61
Drift, 61
Open loop gain, 57
Output impedance, 62
Protection against overvoltages, 74
Range of output swing, 61
Selection, 68
Slew rate, 63
Specifications, 57-65
Uncompensated, 56
Optically powered instrumentation scheme, 568-569
Orifice plate flowmeter, 481-484
Oscillator type transducer (See transducer)

pH sensing, 516-520
Calomel electrode, 520
Electrode potential, 518
Glass electrode, 519
Nerst equation, 516-517
Reference electrode, 519
Silver-silver chloride electrode, 520
Phase locked loop, 184-188
Photo-detector, 530-541
Circuits, 540-541
Constructional variants, 536
Effect of temperature changes, 540
Equivalent circuit, 533
Noise, 538
Quantum efficiency, 537
Response time, 539
Spectral response, 537
Photo-diode, 530
Conductive mode, 540
Voltaic mode, 541
Piece-wise linear amplifier, 189-191
Piezo-electric sensor, 407
Pitot tube flowmeter, 507
Pixel, 546
Integration period, 546
Smear, 546
Plastic extrusion, 3-6
Positive displacement flowmeter, 507
Potentiometer, 355-358
Power analyzer, 581-587
Precision rectifier, 191-192
Pressure
Absolute, 460
Bellows, 461
Bourdon tube, 461
Differential pressure (See also Flowmeter), 478-488
Low pressure, 467-469
Ionisation gauge, 468
Pirani gauge, 467
Thermocouple gauge, 468
Sensing, 463-469
Capacitance based, 466
Capsule, 461
Diaphragm, 464-466
With bonded SG, 464
With semiconductor SG, 465
STP conditions, 475
Units, 461
Vacuum gauge, 460
Water hammer, 466
Primary sensor, 22
Pyro-electric detector, 446

Quantization, 241-242
Differential, 284-288

Radiation
Absorbance, 441-444
Black body, 441-444
Emittance, 441-444
Gray body, 441-444
Plank's equation, 441-444
Wein's equation, 441-444
Radiation based instrumentation, 530-555
Bolometer, 446
CCD array (See also CCD), 543-546
Field of view, 446
FOV, 446
Photo-detector (See also Photo-detector), 530-541
Pyro-electric detector, 446
Thermal, 446-448
Random noise, 206-214
Amplitude characteristics, 207
Equivalent noise bandwidth, 213
Narrowband, 214
Spectral characteristics, 208
Ratio arm bridge, 369
Reaction vessel, 7
Receiver, 568
Rotational variable differential transformer, 359-366
R-2R ladder network, 269-272
RVDT, 359-366

Sample and hold, 249-256
Operation, 249
Sample-Hold circuit, 255-256
Topologies, 255-256
Sampling, 236-240
Acquisition time, 250
Aperture time, 251

Sampling (Continued)
Error, 251
Charge dumping, 251
Feedthrough, 251
Hold interval, 252
Sample to hold transition, 251
Hardware, 246
Analog switch (see Analog switch)
Ideal, 236
Over-sampling ratio, 284-288
Practical, 240
Quantization, 241-242
Reconstruction, 243
Secondary sensor, 29-55
Sensor (See entries under respective variables)
Capacitance, 328-341
Circuit configurations, 334-341
AM, 336
DC circuit, 334
Oscillator, 335
Electrode geometries, 330-333
Guard ring, 338-341
Shielding, 338-341
Signal threshold, 337
Inductance, 342-349
Circuit configurations, 347-349
Bridge, 347
Differential transformer, 349
Oscillator, 347
Sensor geometries, 346
Piezo-electric, 407
Primary, 22
Resistance, 318-327
Circuit configuration, 320
Modified Wheatstone bridge, 322
Wheatstone bridge, 320
Secondary, 23
SFDR, 267
Sigma-delta type ADC, 284-288
Signal conversion
Ideal sampling, 236
Practical sampling, 240
Quantization, 241
Reconstruction, 243
Signals from physical systems, 210-212
Signal processing
Analog, 74-106, 157-195
Digital (See digital signal processing)
Linear, 74-106
Spurious free dynamic range, 267
Standard conditions, 475
STP conditions, 475
Strain
Direct measurement, 400-402
Strain gauge, 388-409
Adhesive, 391
Backing, 391
Bonded foil, 390
Error compemsation, 396
Foil, 390
Sputter deposited, 390
Vacuum deposited, 390
Patterns, 392
Semiconductor, 390
Signal processing, 399
Unbonded, 389
Successive approximation ADC, 277
Summing amplifier, 86
Surface roughness, 381
Surface waviness, 381

Target flowmeter, 497
Temperature sensing
Conventional methods, 421
Infrared (See IR thermometry)
Resistance transducer, 422-426
Direct conversion, 423
Thermistor, 426
Wheatstone bridge, 422
RTD (See also resistance transducer), 422-425
Copper, 424
Nickel, 425
Platinum, 425
Semiconductor based, 427
Thermocouple based (See thermocouple), 429-440
Tension sensing, 411
Thermal conductivity based gas analysis, 427-428
Thermal flowmeter, 508
Thermocouple, 429-440
Basics, 429-430
Burn-out, 436
Cold junction, 429-430
Cold junction compensation, 433-435
Compensating cable, 436
Extension wires, 436
Gauge for low pressure sensing, 468
Hot junction, 429-430
Laws, 429-430
Minerally insulated, 439-440
Sheath, 439-440
Signal processing, 436-440
Types, 431
Thermo-emf, 429-430
Torque sensing, 416-418
Direct sensing, 418
Reaction force, 417
Transducer (See also respective entries)
AC bridge type, 40-49
Acceleration, 412-415
Capacitance, 328-341
Current, 558-563
Displacement, 355-379
Feedback type, 350-354
Flow, 477-508

Transducer (Continued)
Force, 409-410
Force balance type, 410
Frequency, 51-54
Gas concentration, 526-529
Humidity, 521-524
Inductance, 342-349
Inverse, 350-354
Magnetic field, 556-557
Moisture, 521-524
Oscillator type, 51-54
pH value, 516-521
Position, 355-379
Pressure, 460-469
Resistance, 318-327
Sensitivity, 13
Speed, 380
Strain, 399
Stress, 388-408
Temperature, 420-459
Tension, 411
Torque, 416-419
Wein bridge, 47-48
Wheatstone bridge type, 29-39
Transmitter, 24
Turbine flowmeter, 495-496
Twin-T network, 150-152

Ultrasonic flowmeter, 500-505

Vacuum gauge, 467-469
Variable area flowmeter, 507
Vena contracta, 485-487
Venturi flowmeter, 485
Vibration sensing, 414-415
Voltage reference, 261-263
Band gap based, 263
Zener based, 262
Vortex flowmeter, 492

Water hammer, 466
Snubber, 466
Wheatstone bridge, 29-39
Adjacent sensing arms, 37-38
All four sensing arms, 39
Assumptions, 30
Diagonally opposite sensing arms, 36
Large unbalance, 33
Near balance, 30
One sensing arm, 30-33
Transducer, 30-39
Unbalanced, 30-39
Window functions, 240,299

Zener based voltage reference, 261-263